Oceanologia

Official Journal of the Polish Academy of Sciences: Institute of Oceanology and Committee on Maritime Research

This journal is supported by the Ministry of Science and Higher Education, Warsaw, Poland

Indexed in: ISI Journal Master List, Science Citation Index Expanded, Scopus, Current Contents, Zoological Record, Thomson Scientific SSCI, Aquatic Sciences and Fisheries Abstracts, DOAJ

IMPACT FACTOR ANNOUNCED FOR 2017 IN THE 'JOURNAL CITATION REPORTS' IS 1.614; 5-year IF is 1.585

Publisher
Elsevier Sp. z o.o.
22, Jana Pawła II Avenue
00-133 Warsaw, Poland

Associate Publisher
Justyna Kasprzycka
j.kasprzycka@elsevier.com
+31 20 485 3846

ISSN 0078-3234

Oceanologia (2019) 61, 1—16

Available online at www.sciencedirect.com

ScienceDirect

journal homepage: www.journals.elsevier.com/oceanologia/

ORIGINAL RESEARCH ARTICLE

Distributions of photosynthetic and photoprotecting pigment concentrations in the water column in the Baltic Sea: an improved mathematical description

Joanna Stoń-Egiert [a,*], Roman Majchrowski [b], Mirosława Ostrowska [a]

[a] *Institute of Oceanology, Polish Academy of Sciences, Sopot, Poland*
[b] *Institute of Physics, Pomeranian University in Słupsk, Słupsk, Poland*

Received 30 January 2018; accepted 20 August 2018
Available online 12 September 2018

KEYWORDS
Phytoplankton pigments;
Marine photosynthesis;
Baltic

Summary Mathematical formulas are given to describe the changes with depth of concentrations of chlorophylls *b*, *c*, and photosynthetic and photoprotecting carotenoids in Baltic phytoplankton resulting from the adaptation of algal cells to ambient conditions. They take into account the spectral variability and differences in intensity, characteristic of the Baltic, in the irradiance penetrating the water, and also the spectral similarities among the spectra of different groups of phytoplankton pigments. The formulas were derived and validated on the basis of an extensive set of empirical data acquired from different parts of the Baltic Sea in 1999—2016. The standard error factor *x* of these formulas ranges from 1.32 to 1.73. These values are lower than those obtained for formulas derived for ocean waters, in which the influence of allogenic constituents on optical properties is negligibly small: 1.44 and 1.52 respectively in the case of chlorophyll *c*, and 1.32 and 1.47 respectively for photoprotecting carotenoids. With these formulas, overall levels of the main groups of pigments can be calculated from known irradiance conditions and chlorophyll *a* concentrations at any depth in a layer equal to one and a half thicknesses of the euphotic layer (i.e. to an optical depth of τ = 7) in the Baltic. The accuracy of these approximations is close to that of estimates of other bio-optical characteristics in this sea. This was confirmed by a validation based on an independent dataset (*x* from 1.27 to 1.84).

* Corresponding author at: Institute of Oceanology Polish Academy of Sciences, Powstańców Warszawy 55, 81-712 Sopot, Poland. Tel.: +48 58 7311816.
E-mail address: aston@iopan.gda.pl (J. Stoń-Egiert).
Peer review under the responsibility of Institute of Oceanology of the Polish Academy of Sciences.

https://doi.org/10.1016/j.oceano.2018.08.004

1. Introduction

Solar radiation in the visible range (VIS) is a major factor governing the photosynthetic production of organic matter in the sea. The intensity and spectral composition of this radiation in different depths in seawater depends on the autogenic and allogenic substances dissolved or suspended in it. Having diverse physicochemical properties, they absorb and scatter solar radiation with varying intensity in different parts of the spectrum, thereby giving rise to a set of optical properties characteristic of a particular basin.

Phytoplankton are an important group of suspended particles absorbing light for primary production. In some types of water, they are estimated to be responsible for more than 90% of the total absorption of visible light (Woźniak and Dera, 2007). Phytoplankton cells contain VIS-absorbing pigment-proteinaceous complexes, i.e. photosynthetic pigments — chlorophylls, carotenoids and phycobilins. Their roles and functions in the mechanisms of marine biophysical processes utilising solar radiation have been analysed in numerous papers (see Babin et al., 1996; Scheer, 1991; Woźniak et al., 1999; Woźniak and Dera, 2007; and the references therein). The composition and mutual proportions of these pigments are unique taxonomic features of the various classes of algae (Jeffrey and Vesk, 1997; Roy et al., 2011; Wright et al., 1991). Nevertheless, under given, often stressful, growing conditions, the amounts and types of pigments in cells can change. These variations make use of the absorption properties of each compound in order to establish a composition and concentration of pigments optimal for a given set of ambient irradiance conditions. Above all, such changes are an adaptation to the intensity and spectral distribution of the underwater irradiance, which varies in accordance with a season and the area where the phytoplankton are growing.

The high intensity of irradiance in the short-wave part of the visible light spectrum, which can cause the photodestruction of the photosynthetic centre, invokes photoprotecting mechanisms in algae that involve the enhanced production of photoprotecting pigments, chiefly carotenoids like diadinoxanthin, lutein, β-carotene, alloxanthin and zeaxanthin (Bricaud et al., 2004; Demmig-Adams, 1990; Henriksen et al., 2002; Schlüter et al., 2000; Staehr et al., 2002; Stramski et al., 2002; Sukenik et al., 1990; Woźniak and Dera, 2007). Having absorption maxima in this spectral range, they enable the safe utilisation of absorbed energy by algae. In contrast, the narrow spectral ranges of the irradiances prevailing in deeper waters do not always coincide with the absorption range of chlorophyll *a*, the basic photosynthetic pigment. This energy is absorbed by pigments additionally synthesised in algal cells (carotenoids: fucoxanthin, echinenone, peridinin and phycobiliproteins) with absorption maxima in the relevant spectral ranges and then transferred to the chlorophyll *a* molecule for subsequent use in the photosynthesis of organic matter.

The processes by which algal cells adapt to ambient irradiance conditions directly affect the vertical distributions of pigment levels in the water column. The concentrations of photoprotecting pigments relative to the chlorophyll *a* level are higher at the sea surface and decrease with depth. Near the sea surface, this is due to the intensity adaptation elicited by high irradiances in the short-wave part of the spectrum. Deeper in the water column, however, the relative concentrations of photosynthetic pigments increase: this results from the chromatic adaptation of algal cells, which, in turn, is due to the variable spectral distributions of irradiance at different depths (Majchrowski and Ostrowska, 2000, 2009; Woźniak et al., 1997b; Uitz et al., 2006, 2015; Trees et al., 2000).

The variability of pigment concentrations with depth in the context of the photo- and chromatic acclimation occurring in phytoplankton cells has been studied for a long time (Babin et al., 1996; Berner et al., 1989; Bricaud et al., 1983; Dera and Woźniak, 2010; Falkowski and LaRoche, 1991; Harrison and Platt, 1986; Hoffmann and Senger, 1988; Mitchell and Kiefer, 1988; Morel et al., 1987; Sathyendranath et al., 1987; Schlüter et al., 2000; Sosik and Mitchell, 1991; Staehr et al., 2002; Stramski et al., 2002; Sukenik et al., 1990; Woźniak et al., 2003; Woźniak and Dera, 2007). This research has yielded relationships describing these processes in the form of a function dependent on the trophic type of waters, a corresponding function of spectral adaptation (in the case of chromatic acclimation) and a function accounting for the amount of photodestructive radiation propagating in the sea (with respect to intensity photo-adaptation) with satisfactory accuracy for ocean waters, in which optical properties are determined solely by the phytoplankton organisms present in them (Majchrowski and Ostrowska, 2000, 2009; Woźniak et al., 2003; Woźniak and Dera, 2007).

In contrast, the optical properties of Baltic Sea waters are governed not only by phytoplankton, but also by other optically significant, allogenic particles and quite frequently by large amounts of CDOM, which can have a major effect on the transmission of irradiance down into the water (Harvey et al., 2015; Kowalczuk et al., 2005; Levin et al., 2013; Meler et al., 2016; Simis et al., 2017; Stedmon et al., 2000). Within such a context, the adaptation and acclimation of phytoplankton cells to the irradiance conditions prevailing in the Baltic are affected by far more factors than in the case of phytoplankton in ocean waters, in which the influence of allogenic constituents on optical properties is negligibly small (Dera, 1995; Mobley, 1994; Prieur and Sathyendranath, 1981; Woźniak et al., 2013). Formulas describing photo- and chromatic acclimation processes in ocean waters, if applied to waters like those in the Baltic Sea, area consequently encumbered with a substantial error (Majchrowski et al., 2007).

Our analyses aimed to find relationships for estimating pigment concentrations at different depths in the Baltic Sea analogous to those for ocean waters. They revealed patterns of vertical distributions of different groups of pigments characteristic of Baltic waters. Even so, we considered the accuracy of those formulas to be less than satisfactory (Majchrowski et al., 2007; Stoń-Egiert et al., 2012). The levels of error of the simplified model for the Baltic, enabling vertical profiles of phytoplankton pigment concentrations to be determined, were acceptable only for the formulas derived separately for summer and winter. The approximations of that model took into account the influence of irradiance conditions in the water on pigment concentrations in phytoplankton via the statistical link with this trophic type of basin, represented by the surface level of chlorophyll *a* (according to Woźniak and Pelevin, 1991) and the optical depth τ (Majchrowski and Ostrowska, 2009; Majchrowski et al., 2007).

There is no relationship describing how the pigment composition varies in response to the irradiance conditions prevailing in the Baltic with an accuracy approaching that of other estimated photosynthetic characteristics in these

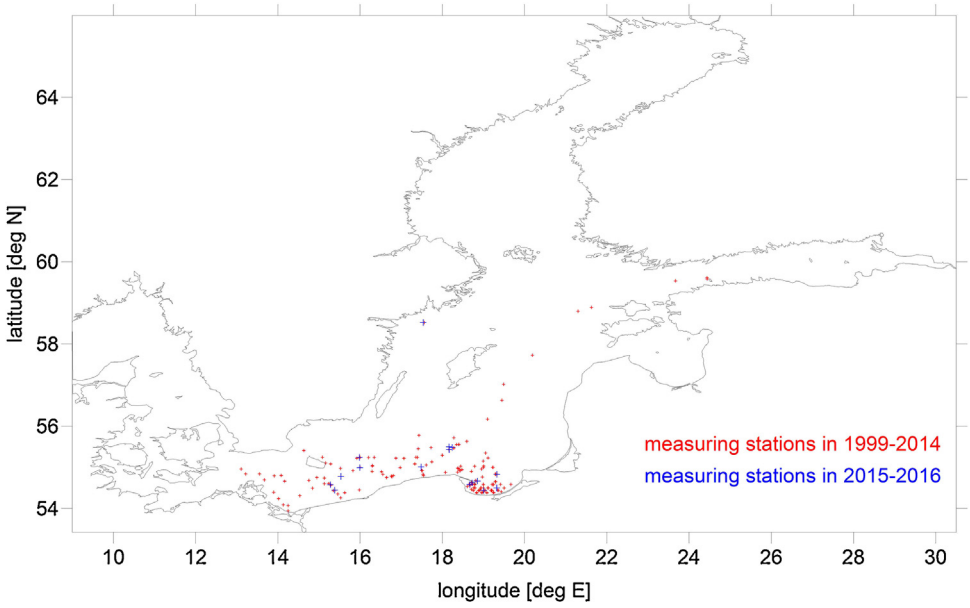

Figure 1 Distributions of stations, at which vertical distributions of pigment concentrations and the relevant characteristics of physical fields were measured in 1999—2016. The red dots indicate the positions of the stations where water samples were taken in 1999—2014 for determining levels of the pigments used for deriving the formulas; the blue dots show the positions of the stations where empirical material was gathered in 2015—2016 and used to validate the formulas.

waters. It was this fact that lay behind the decision to study this aspect of the functioning of Baltic plant communities in greater detail.

The aims of the current analyses were:

1. to extend knowledge on how Baltic plant communities function by analysing the qualitative and quantitative changes in chlorophyll and carotenoid levels taking place as a result of adaptation to the spectrally and intensity variable irradiance conditions obtaining in the Baltic;
2. to derive new model formulas describing how the concentrations of these groups of pigments vary with depth in the Baltic Sea with an accuracy approaching that of the formulas derived for ocean waters.

The achievement of these aims will enable the relationships obtained to be applied in algorithms for determining a range of characteristics of the marine environment at the level of remotely measurable parameters. In particular, they can be used in existing satellite algorithms derived for the Baltic Sea, such as the DESAMBEM[1] algorithm employed in the SatBałtyk System.[2] This allows a range of characteristics of the Baltic ecosystem, including the magnitude of primary production in the euphotic layer and at other depths, to be determined on the basis of remote sensing data (Darecki et al., 2008; Ostrowska et al., 2015a; Woźniak et al., 2004, 2008, 2011).

2. Material and methods

The formulas in this paper were derived on the basis of the following empirical datasets gathered during measurement campaigns in 1999—2016, mainly in the southern Baltic Sea (Fig. 1):

- total concentrations of groups of phytoplankton pigments [mg m^{-3}] measured using RP-HPLC in seawater sampled from the surface and at different depths: chlorophylls *a* (allomer, epimer, chlorophyllide *a*, div chlorophyll *a*, pheophytin *a*, pheophorbide *a*), chlorophylls *b* and their optical isomers, chlorophylls *c* (chlorophylls *c1* + *c2* and *c3*), photosynthetic carotenoids PSC (fucoxanthin, peridinin, prasinoxanthin, 19′but-fucoxanthin, 19′hex-fucoxanthin, echinenon and α-carotene) and photoprotecting carotenoids PPC (antheraxanthin, alloxanthin, diadinoxanthin, diatoxanthin, lutein, neoxanthin, violaxanthin, β-carotene, myxoxanthophyll and zeaxanthin).
- spectral distributions of underwater irradiance fields measured at specific depths in the sea (using MER2040 irradiance meters [Biospherical Inc., Hyperspectral-Ramses, Trios]), or indirectly using the bio-optical model in the DESAMBEM algorithm (Woźniak et al., 2008).

Methodical details on both parameters are described in the following subsections.

2.1. Sample collection

During the cruises, the water was sampled for pigment content analysis. The samples (0.5—2 dm^3) were taken with an SBE 32 bathometer. The sampling depth was chosen with respect to the shape phytoplankton biomass profiles determined based on fluorimetric indications, usually from three

[1] DESAMBEM — Development of a Satellite Method for Baltic Ecosystem Monitoring.
[2] SatBałtyk — Satellite Environment Monitoring of the Baltic Sea.

to ten depths taking into account the surface layer, the maximum fluorescence depth, and below the euphotic zone and indirect depths. The sea water samples were immediately filtered through Whatman GF/F glass-fibre filters (φ = 25 mm) under a gentle vacuum (<0.4 atm). The filtration time did not exceed one hour. The samples were stored in liquid nitrogen (−196°C) until laboratory analysis to improve extraction efficiency and minimise pigment alterations (Mantoura et al., 1997).

2.2. Extraction of pigments from phytoplankton cells

Extraction of chlorophylls and carotenoids from phytoplankton samples were conducted by use of water solution of 90% acetone (Parsons et al., 1984). Technics of isolation of pigments from algae cells were based on mechanical grinding and sonication (2 min, 20 kHz, Cole Parmer, 4710 Series) in the darkness conditions at 4°C during 2 h. Such prepared extracts were centrifuged (20 min, 5°C, 3210 × *g*, Beckman, GS-6R) to remove the filters and cellular debris and then subjected to the chromatographic analysis.

2.3. Quantification and qualification of pigments during chromatographic analysis

Two types of appropriately calibrated chromatographic systems were used for pigments separations by RP-HPLC in presented data sets: Agilent Technologies HP1050 (in 1999—2010) and HP1200 (2010—2016), equipped with diode array detectors (HP1100 and HP1200 respectively), fluorescence detectors (HP1046 and HP1200 respectively) and type C18 chromatographic columns (LichroCART™ Hypersil ODS — to separate the samples collected in 1999—2001, LichroCART, Lichrospher 100 RP18e — to separate samples collected in 2002—2016) with the same dimensions parameters: 250 × 4 mm, particle size: 5 μm, pore size 100 Å (Merck). Both systems were intercalibrated and comparable results were obtained. Method of pigments isolation and separation was introduced by Mantoura and co-workers (Mantoura and Llewellyn, 1983), adopted and modified in later years by other researchers (Barlow et al., 1993; Stoń and Kosakowska, 2002; Stoń-Egiert and Kosakowska, 2005). The pigments were separated in a gradient mixture of methanol, 1 M ammonium acetate and acetone. Pigment detection was based on absorbance measurements at λ = 440 nm. The fluorescence measurements with extinction at λ_{ex} = 431 nm and emission at λ_{em} = 660 nm were taken parallel during analysis in order to confirm the presence of chloropigments in the sample.

Calibration of chromatographic systems was based on commercially available chlorophylls and carotenoids (The International Agency for 14C Determination DHI Institute for Water and Environment in Denmark). The pigment standards were subjected to chromatographic analysis in order to obtain calibration curves, detection limits and absorption spectra. Qualitative analysis was based on a comparison of the retention times, the absorbance spectra of eluting peaks with those of the standards (Wright and Shearer, 1984) and on individual response factor obtained during calibration procedure conducted for each pigment and parameters obtained during chromatographic resolution of samples. Identification was confirmed by co-injection and on-line diode array spectra. The quantitative characteristics of the pigments occurring in natural samples were based on the external standardisation equation (Mantoura and Repeta, 1997).

The measurement precision was 2.9 ± 1.5% and a recurrence error was 9.7 ± 6.4% (Stoń-Egiert et al., 2010). The chlorophyll *a* concentrations determined with this method stand in agreement with the corresponding concentrations obtained spectrophotometrically in ethanol extracts (Ostrowska et al., 2015b).

The pooled concentrations of pigments included levels of unidentified derivatives and their degradation products estimated on the basis of their similar spectral properties. Their presence in the samples is due mainly to the physiological condition of the phytoplankton, the state of their growth and the degree of development of the plant community, and only minimally to the measurement procedures (Jeffrey, 1997; Louda et al., 1998; Porra et al., 1997; Repeta and Bjørnland, 1997). The highest estimated levels of derivatives and unidentified pigments come from after-bloom periods when the current phytoplankton population consists mainly of ageing and dead cells. The unidentified pigments and derivatives in our database comprise on average from 1 to 7% chlorophylls, 16% PSCs and 10% PPCs. Taking into account the derivatives and degradation products of a specific group of compounds will ensure that the mathematical formulas we shall be deriving are universally applicable in time, regardless of the seasonal cycle of phytoplankton growth and development in the Baltic.

2.4. Spectral distributions of underwater irradiance fields

During the cruise on r/v 'Oceania' the spectral distribution of solar radiation in the water column were measured by spectrophotometer MER 2040 (Biospherical Inc.). The measurements of spectral distribution of light were performed just above, below surface layer and in water column in eight spectral bands (412, 443, 490, 510, 550, 665, 683 and 710 nm). Also, the continous measurements of summarise downward radiation reaching the surface were performed by set of piranometers (Eppley Laboratory Inc.) equipped with Schotta filters (395 and 695 nm). Based on these measurements, using appropriate calculation methods (described in the works of, for example, Woźniak and Montwiłł, 1973, Woźniak et al., 1983), the doses of photosynthetically available radiation PAR (400—700 nm) [Ein m^{-2}] was obtained for selected depth levels (1, 2, 3, 5, 7, 10, 15, 20, 25 and 30 m).

The empirical material acquired in 1999—2016 comprises 339 depth profiles of pigments and their corresponding irradiance distributions. The collected set of data was divided into two sets: data collected in 1999—2014 (313 complete profiles of vertical distributions of pigments and the corresponding irradiances) and data collected in 2015—2016 (26 complete profiles of pigments vertical distributions and the corresponding irradiances). The first more extensive set of data was used to obtain the mathematical relationships presented in this work, while the second set of data was used as independent to validate the relationships obtained. Table 1 lists the characteristics of both sets of empirical pigment concentrations.

The range of variability of chlorophyll *a*, the most important pigment in photosynthesis, recorded in 1999—2014, covered four orders of magnitude (0.068—95.598 mg m^{-3}). This therefore

Table 1 Overall concentrations [mg m^{-3}] of the groups of pigments identified in the analysed database.

Group of pigments	Number of measurements	Concentration [mg m^{-3}]			Median [mg m^{-3}]	Standard deviation [mg m^{-3}]
		Min	Max	Mean		
Measuring years 1999–2014						
Chlorophyll *a* C_a	1372	0.068	95.6	4.30	2.17	7.11
Chlorophyll *b* C_b	1187	0.004	7.63	0.304	0.182	0.481
Chlorophyll *c* C_c	1365	0.005	11.8	0.514	0.208	0.956
Photosynthetic carotenoids C_{PSC}	1368	0.005	28.4	1.02	0.364	2.21
Photoprotecting carotenoids C_{PPC}	1372	0.005	19.5	0.949	0.567	1.441
Measuring years 2015–2016						
Chlorophyll *a* C_a	181	0.069	4.90	2.02	1.86	1.04
Chlorophyll *b* C_b	181	0.008	0.523	0.163	0.140	0.127
Chlorophyll *c* C_c	181	0.005	1.78	0.261	0.184	0.248
Photosynthetic carotenoids C_{PSC}	181	0.015	2.04	0.434	0.385	0.348
Photoprotecting carotenoids C_{PPC}	181	0.030	1.52	0.463	0.435	0.267

embraces 9 trophic types of water[3] (according to the classification of Woźniak and Pelevin, 1991), from oligotrophic (type O2, chlorophyll *a* levels from 0.05 to 0.10 mg m^{-3}) to eutrophic (type E5, concentrations $>$ 20 mg m^{-3}. The 2015–2016 dataset was also gathered from waters with a wide trophic range, i.e. from oligotrophic to eutrophic, except when surface chlorophyll *a* was very high during seasonal increases in phytoplankton biomass.

The content of pigments from different groups was governed by the current state of the growing Baltic phytoplankton, the species composition of which varies seasonally; consequently, the characteristic indicator pigments vary likewise. Levels of accessory pigments were up to 14 times lower than those of chlorophyll *a*, with absolute levels of chlorophyll *b* being the lowest. The relatively high levels of carotenoids were due to the spring blooms of diatoms and dinoflagellates; this is confirmed by numerous studies on the taxonomic composition of Baltic plant communities (Stoń-Egiert et al., 2010; Thamm et al., 2004; Wasmund et al, 1996; Wasmund and Uhlig, 2003).

3. Results

As already mentioned, there are two main groups of pigments (PSC and PPC) absorbing visible solar radiation in phytoplankton cells. The intracellular content of photosynthetic and photoprotecting pigments is governed by the irradiance conditions in the immediate environment of the phytoplankton, as a result of processes adapting them to the intensity and spectral composition of the irradiance. The adaptation to irradiance intensity is controlled above all by the quantitative and qualitative composition of pigments protecting the photosynthetic apparatus from destruction by excessive intensities of short-wave light. On the other hand, chromatic adaptation in phytoplankton establishes the composition of pigments enabling the entire PAR to be utilised in photosynthesis. We therefore performed our analyses separately for pigments directly involved in photosynthesis and for photoprotecting pigments.

3.1. Photosynthetic pigments

Relative levels of photosynthetic pigments increase with depth because chromatic adaptation of phytoplankton cells intensifies the production of pigments with absorption properties that effectively utilise the spectral distributions of irradiances at the depths where the algae are at any given instant. Hence, in the photosynthetic apparatus of phytoplankton, there is an increase in the proportion of those pigments, the light absorption ranges of which include bands present in underwater irradiance fields in which chlorophyll *a* does not absorb (Babin et al., 1996; Woźniak et al., 2003).

How the absorption properties of the individual pigments are matched to the ambient irradiance conditions can be defined by the spectral fitting function $F_j(z)$, also known as the chromatic adaptation factor (Majchrowski and Ostrowska, 1999, 2000; Woźniak et al., 1997a, 1997b, 2003). The spectral fitting functions were determined for three main groups of photosynthetic pigments: chlorophylls *b* and *c* and photosynthetic carotenoids on the basis of their known spectral shape of absorbance coefficients (Ficek et al., 2004) and irradiance at characteristic sampling depths. They are defined by the following equation:

$$F_j(z) = \frac{1}{a^*_{j,max}} \int_{400\,nm}^{700\,nm} \frac{E_d(\lambda, z)}{PAR(z)}\, a^*_j(\lambda)\, d\lambda, \qquad (1)$$

where j – the type of pigment's group: PSC – photosynthetic carotenoids, a – chlorophyll *a*, b – chlorophylls *b* and c – chlorophylls *c*, a^*_j (λ) – specific coefficient of absorption for the jth group of pigments [m^2 (mg pigment)$^{-1}$] (Ficek et al., 2004), $a^*_{j,max}$ – maximum specific absorption coefficient for the jth group of pigments [m^2 (mg pigment)$^{-1}$], $E_d(\lambda,z)$ – spectral distribution of downward irradiance at depth z [Ein m^{-2} s^{-1} nm^{-1}], PAR (z) – photosynthetic available radiation at depth z [Ein m^{-2} s^{-1}].

[3] In accordance with the convention used by our research team, the trophic index (trophicity) is defined as the surface concentration of chlorophyll *a* Ca(0). Depending on the concentration Ca(0) [mg tot. chl m^{-3}], the following trophic types of waters can be distinguished: oligotrophic: O1 –Ca(0) = 0.02–0.05; O2 –Ca(0) = 0.05–0.10; O3 –Ca(0) = 0.10–0.20; mesotrophic: M –Ca(0) = 0.2–0.5; intermediate: I –Ca(0) = 0.5–1.0; eutrophic: E1 –Ca(0) = 1–2; E2 –Ca(0) = 2–5.

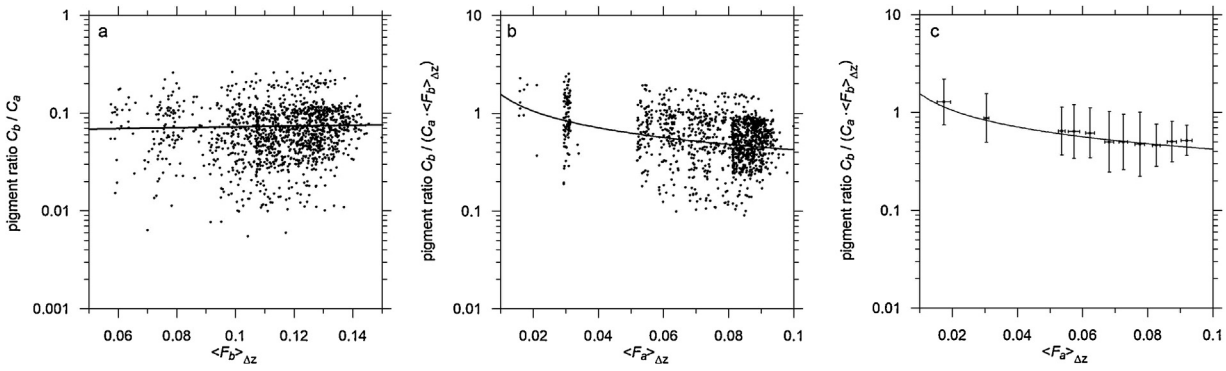

Figure 2 Relationships between the relative concentration of chlorophyll *b* (referred to the concentration of chlorophyll *a*) C_b/C_a and the mean spectral fitting functions of chlorophyll *b* $<F_b>_{\Delta z}$ in the mixing layer (see Eq. (1a)) for empirical data obtained in 1999–2014 (a); the relationship between relative chlorophyll *b* concentrations expressed by the formula $C_b/(C_a<F_b>_{\Delta z})$ and mean spectral fitting functions of chlorophyll *a* $<F_a>_{\Delta z}$ (b) and their averaged values (c).

This function depends mainly on the relative spectral distribution of irradiance in the sea $f(\lambda, z) = E_d(\lambda, z)/PAR(z)$ but only minimally on its absolute values. It can take values from 0 to 1. If the spectral distribution of the absorption coefficient of a given pigment or groups of pigments does not coincide anywhere with the underwater irradiance spectrum, the spectral matching function is 0. If, on the other hand, the spectral distribution of underwater irradiance coincides exactly with the absorption spectrum of a given group of pigments, then the spectral matching function takes the value of 1.

In order to take account of mixing in the water column, the consequent vertical movements of phytoplankton cells, and how the "history" of these movements affect pigment levels, the spectral matching function in a water layer was averaged for the purposes of the statistical analyses. The best results were obtained for water layer thicknesses of $\Delta z = z_2 - z_1$, where:

$$z_2 = z + 15\,\text{m} \text{ and } z_1 = \begin{cases} 0 \text{ if } z < 15\,\text{m} \\ z - 15\,\text{m} \text{ if } z \geq 15\,\text{m} \end{cases}, \quad (1a)$$

This means that the concentration of each pigment at depth *z* has been determined using F_j averaged for a layer of 30 m ($z \pm 15$ m), or less, for depths of 0–15 m.

It is well known that the overall absorption of light by phytoplankton is the superposition of the absorption of all groups of pigments present in phytoplankton cells capable of absorbing light in a given region of the spectrum (Woźniak and Dera, 2007). So, bearing in mind the similarities of the light absorption spectra of the different varieties of chlorophyll with maxima in roughly the same spectral areas, we analysed the statistical dependence of the relative concentrations of chlorophylls *b* and *c* not only on their individual spectral matching functions but also on the spectral matching function of chlorophyll *a* (see Figs. 2 and 3). In this figures are presented the relationships, obtained for empirical data collected in 1999–2014, between the relative concentration of chlorophylls *b* and *c* (referred to the concentration of chlorophyll *a*) and the mean spectral fitting functions of particular photosynthetic chlorophylls group: chlorophyll b $<F_b>_{\Delta z}$ and c $<F_c>_{\Delta z}$ in the 30 m mixing layer (Figs. 2a and 3a). The dependences of these relationships on additional parameters such as the spectral matching function of chlorophyll *a* $<F_a>_{\Delta z}$ are clearly visible in Figs. 2b, c and 3b,c. In the case of PSCs, the analyses covered entire groups of pigments and exhibited a dependence of their relative concentration only on the average matching functions determined for that group, $<F_{PSC}>_{\Delta z}$ (Fig. 4).

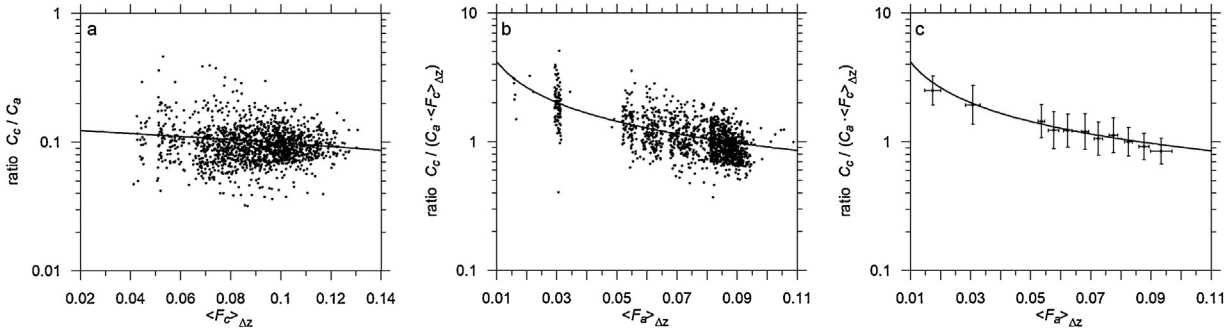

Figure 3 Relationships between the relative concentration of chlorophyll *c* (referred to the chlorophyll *a* concentration) C_c/C_a and the mean spectral fitting functions of chlorophyll *c*, $<F_c>_{\Delta z}$ in the mixing layer (see Eq. 1a) for empirical data (a); the relationship between relative chlorophyll *c* concentrations expressed by the formula $C_c/(C_a<F_c>_{\Delta z})$ and mean spectral fitting functions of chlorophyll *a* $<F_a>_{\Delta z}$ (b) and their averaged values (c).

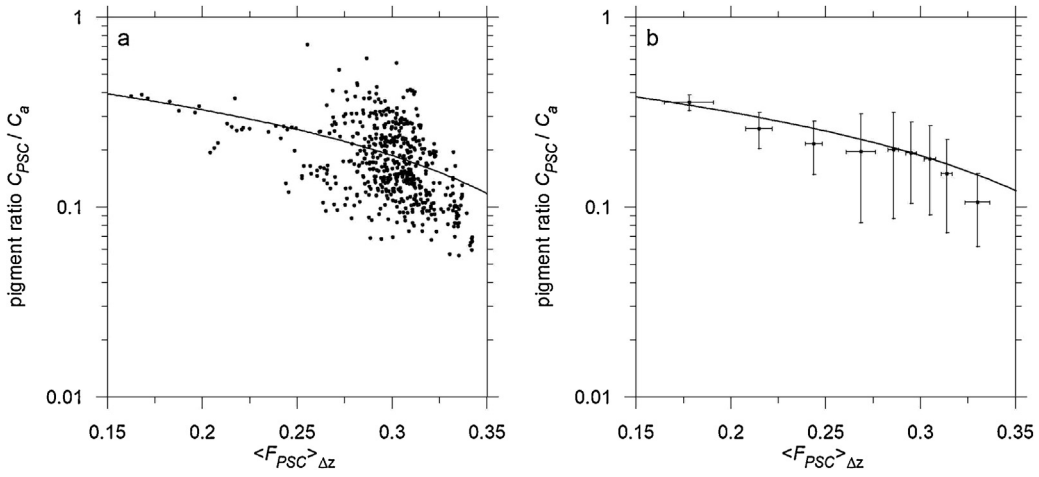

Figure 4 Relationships between the relative concentration of photosynthetic carotenoids (referred to the chlorophyll *a* concentration) C_{PSC}/C_a and their mean spectral fitting functions $<F_{PSC}>_{\Delta z}$ in the mixing layer (see Eq. 1a) for empirical data (a) and their averaged values (b).

Hence, using the least squares method, statistical dependences were derived enabling depth changes in photosynthetic pigments levels, presented in Fig. 2b, c, 3b, c and 4a as a solid line, in phytoplankton cells to be determined with respect to the ambient irradiance conditions in the form:

$$C_b/C_a = 0.115\langle F_a\rangle_{\Delta z}^{-0.567} \times \langle F_b\rangle_{\Delta z}, \quad (2)$$

$$C_c/C_a = 0.198\langle F_a\rangle_{\Delta z}^{-0.663} \times \langle F_c\rangle_{\Delta z}, \quad (3)$$

$$C_{PSC}/C_a = 0.576 - 1.30\langle F_{PSC}\rangle_{\Delta z}, \quad (4)$$

where $\langle F_j\rangle_{\Delta z}$ – mean chromatic adaptation factor in the 30 m layer for particular groups of pigments, $\langle F_j\rangle_{\Delta z} = 1/z_2 - z_1 \int_{z_1}^{z_2} F_j(z)dz$, j – the type of pigment's group: PSC – photosynthetic carotenoids, a – chlorophyll a, b – chlorophylls b and c – chlorophylls c, C_a, C_b, C_c, C_{PSC} – concentrations of groups of pigments: chlorophylls a, chlorophylls b, chlorophylls c, photosynthetic carotenoids PSC [mg m^{-3}].

Table 2 and Fig. 5 list the errors of these approximations. These errors show the accuracy with the developed formulas describing the analyzed set of empirical data. As one can see, the proposed formulas describe vertical variations in concentrations of photosynthetic pigments in 1999–2014 with satisfactory accuracy. The PCS concentration is encumbered with the highest systematic error with PSC while the best approximation of measured concentrations was obtained for chlorophyll *c*.

3.2. Photoprotecting pigments

The part played by photoprotecting carotenoids PPCs in the surface water layer is crucial: chlorophyll *a*, the fundamental pigment in photosynthesis, is vulnerable to photo-oxidation because of the direct action of excessive quantities of radiation in the 400–480 nm range – this is known as Potentially Destructive Radiation (PDR). This is reflected in the depth profile of averaged relative PPC concentrations. These levels are the highest at the surface, where, as a result of intensity adaptation processes, phytoplankton cells contain pigments in abundance to protect chlorophyll *a* molecules from the excessive absorption of PDR (Majchrowski and Ostrowska, 1999, 2000; Woźniak et al., 1999, 2003).

The presence of PPCs in phytoplankton at a given depth is thus due directly to the intensity of radiation from the shortwave part of the PAR spectrum reaching that depth:

$$PDR^*(z) = \int_{400\,nm}^{480\,nm} a_a^*(\lambda)\langle E_0(\lambda, z)\rangle_{day}\, d\lambda, \quad (5)$$

Table 2 Errors of concentrations of pigment groups estimated using formulas 2–4 based on an analysis of data collected from 1999 to 2014.

Group of pigments	Arithmetic statistics		Logarithmic statistics			
	Systematic error	Statistical error	Systematic error	Standard error factor	Statistical error	
	$<\epsilon>$ [%]	σ_ϵ [%]	$<\epsilon>_g$ [%]	x	σ_- [%]	σ_+ [%]
C_b	12.0	± 76.7	−4.45	1.73	−42.3	73,2
C_c	7.29	± 41.9	0.340	1.44	−30.4	43.8
C_{PSC}	18.1	± 47.44	−9.60	1.50	−33.5	50.4

Where $\epsilon = (C_{i,C} - C_{i,M})/C_{i,M}$ – arithmetic error; $<\epsilon>$ – mean arithmetic error, $\langle\epsilon_g\rangle$ – mean logarithmic error, $\langle\epsilon\rangle_g = 10^{[\langle\log(C_{i,C}/C_{i,M})\rangle]} - 1$, $<\log(C_{i,C}/C_{i,M})>$ – mean of $\log(C_{i,C}/C_{i,M})$, σ_ϵ – standard deviation (statistical error), $\sigma_{\log}$ – standard deviation of $\log(C_{i,C}/C_{i,M})$, $x = 10^{\sigma_{\log}}$ – standard terror factor, $\sigma_+ = x - 1$ i $\sigma_- = \frac{1}{x} - 1$.

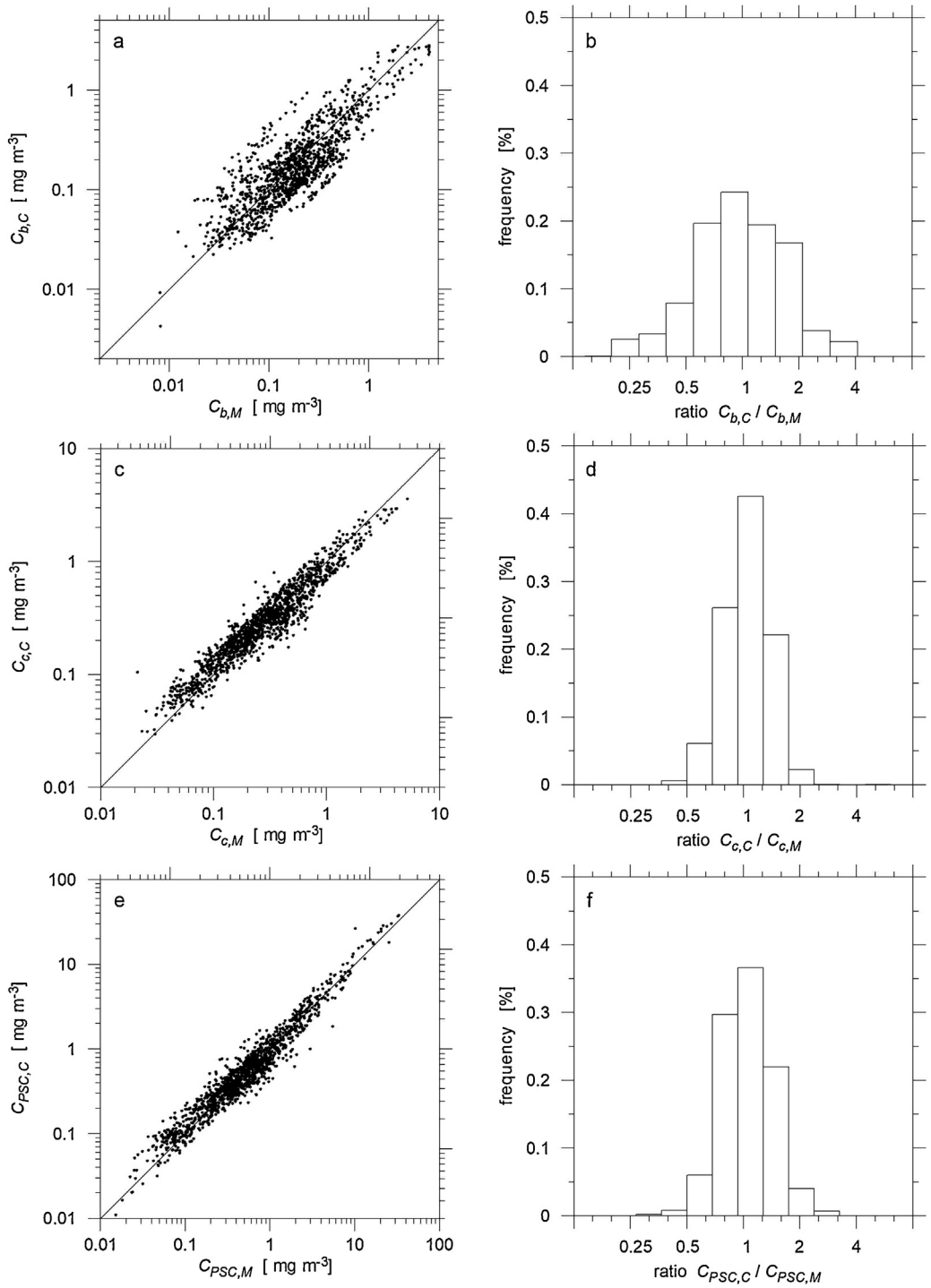

Figure 5 Comparison of concentrations of various groups of pigments C_b (a), C_c (c) and C_{PSC} (e) determined empirically (subscript M) and using formulas 2—4 (subscript C) for a dataset on the basis of which the relationships were derived; histograms of the relative errors in these formulas $C_{b,C}/C_{b,M}$ (b), $C_{c,C}/C_{c,M}$ (d), $C_{PSC,C}/C_{PSC,M}$ (f).

where PDR^* — potentially destructive radiation per unit mass of chlorophyll *a* [μEin (mg chla)$^{-1}$ s^{-1}] (also known as the acclimation factor), $<E_0(\lambda,z)>_{day}$ — mean daily scalar irradiance in the sea at a given depth *z* [Ein m^{-2} s^{-1} nm^{-1}], $a^*_a(\lambda)$ — specific coefficient of light absorption by chlorophyll *a* [m^2 (mg pigment)$^{-1}$].

Using collected database a statistical analysis of the changes in relative PPC concentrations with respect to the irradiance conditions prevailing at different depths in the sea was performed for averaged values of potentially destructive radiation in short part of light spectrum (400—480 nm) per unit mass of chlorophyll *a* PDR* in layers Δ*z*:

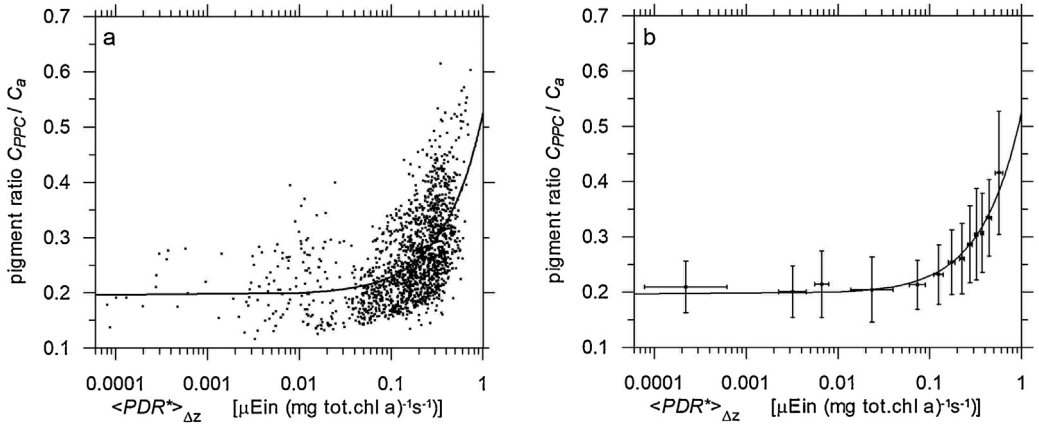

Figure 6 Relationship between the relative concentration of photoprotecting pigments (referred to chlorophyll *a*) C_{PPC}/C_a and the function of Potentially Destructive Radiation PDR* averaged in the 30 m layer $<PDR^*>\Delta_z$ for empirical data (a) and their averaged values (b).

$$\langle PDR^* \rangle_{\Delta z} = \frac{1}{z_2 - z_1} \int_{z_1}^{z_2} PDR^*(z)dz, \tag{6}$$

where z_1 and z_2 are defined in Eq. (1).

As in the case of PSCs, the best results were obtained for a water thickness of 30 m.

Fig. 6 illustrates the dependence of PPC concentration referred to chlorophyll *a* on averaged PDR* functions. The evident increase in the relative level of PPCs for values of $<PDR^*>\Delta_z$ greater than 0.1 [µEin (mg tot chl *a*)$^{-1}$ s^{-1})] indicates that their presence in the pigment composition depends strongly on the irradiance conditions in which phytoplankton live.

Eq. (7), derived from statistical analyses, describes the dependence of the relative PPC concentration in a given set of irradiance conditions at any depth in the sea:

$$C_{PPC}/C_a = 0.328\langle PDR^* \rangle_{\Delta z} + 0.196, \tag{7}$$

where $\langle PDR^* \rangle_{\Delta z}$ – mean *PDR** function in the 30 m layer; C_{PPC} – PPC concentration [mg m^{-3}].

The errors encumbering this formula are listed in Table 3 and Fig. 7 compares PPC levels determined (using Eq. 7 presented in Fig. 7 as a solid line) with empirical values. Values of errors indicate that the developed formula corresponds well to the data set on the basis of which it was

Table 3 Errors of concentrations of photoprotecting carotenoids PPC estimated using Eq. (7) based on an analysis of data collected from 1999 to 2014. The errors were determined using the formulas given in Table 2.

Group of pigments	Arithmetic statistics		Logarithmic statistics			
	Systematic error	Statistical error	Systematic error	Standard error factor	Statistical error	
	$<\epsilon>$ [%]	σ_ϵ [%]	$<\epsilon>_g$ [%]	x	σ_- [%]	σ_+ [%]
C_{PPC}	6.58	± 22.9	2.68	1.32	−24.1	31.7

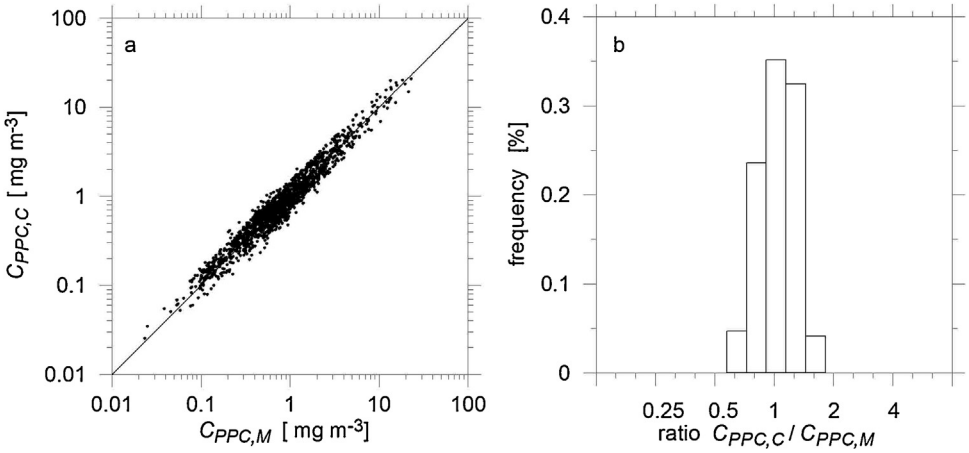

Figure 7 Comparison of concentrations of photoprotecting pigments determined empirically ($C_{PPC,M}$) and based on formula 7 ($C_{PPC,C}$) (a); histograms of the relative errors in this formula (b).

determined. Approximation errors show similar values as in the case of approximations developed for photosynthetic pigments.

4. Discussion

Composition and concentration of phytoplankton pigments, particular in the surface layer of different sea regions have been the subject of investigations by many authors (e.g. Ho et al., 2015; Araujo et al., 2017; Wulff and Wängberg, 2004). This is the base for further analyzing differences in the spatial and seasonal distribution of pigments in different seas (Smith et al., 2010; Wänstrand and Snoeijs, 2006; Zhang et al., 2017) or determining the phytoplankton composition using CHEMTAX (Mendes et al., 2011; Swan et al., 2016).The composition of the pigments can be recognized on the basis of the radiation signal of the sea surface recorded by the satellite radiometer. Global and local satellite algorithms to determine the concentration of chlorophyll in the surface layer of the sea are now widely used (Zheng and DiGiacomo, 2017; Kim et al., 2017) methods for determining other phytoplankton pigments are intensively developed (Pan et al., 2010; Soja-Woźniak et al., 2018). However, the satellite observes only the surface layer, while the pigments compositions and concentrations change with depth. Complete information can only be obtained by knowing the depth profiles of pigments in combination with satellite observations. For this purpose, an accurate mathematical description of the distribution of pigment depth profiles is necessary. The development of mathematical formulas describing such distributions with satisfactory accuracy is complex and requires a comprehensive representative data bank from various regions and seasons in the water body under investigation. In many research teams are developed mathematical descriptions the dependences of bio-optical processes in the sea on environmental conditions in different regions (Cherukuru et al., 2016; Dickey et al., 1993; Strutton et al., 2011). The vertical variation of phytoplankton pigments has been described so far in the clean waters of open oceans (Majchrowski and Ostrowska, 2000), but there are no reports of similar formulas that have been worked and calibrated for shelf seas and coastal areas. Only in the case of the Baltic Sea, the authors attempted to develop such a dependence taking into account the specific optical properties of this basin (Majchrowski et al., 2007; Stoń-Egiert et al., 2012).

This work was inspired by the lack of statistical analyses and physically justified formulas for estimating pigment compositions in phytoplankton cells in the Baltic Sea with an accuracy comparable to that of formulas applicable to ocean waters.

The dependencies used hitherto (see Table 4) enabled pigment concentrations in Baltic waters to be estimated from their statistical dependences on optical depth and surface concentration of chlorophyll *a*, determined separately for summer and winter (Majchrowski et al., 2007), or else did not take into account the mutual influence of pigments with similar absorption properties on their total concentration and relative proportions in the photosynthetic apparatus (Stoń-Egiert et al., 2012). Table 4 also sets out the error factors *x* of all the formulas derived to date: one can thus assess which of the approximations best reflects the modelled dataset.

The formulas derived for ocean waters (Majchrowski and Ostrowska, 2000) yield modelled values closer to measured values than is the case with the formulas so far derived for Baltic waters. As already mentioned, however, absorption properties in open ocean waters are governed mainly by phytoplankton. Therefore, ocean formulas, if applied to the determination of relative pigment concentrations in the optically far more complex waters of the Baltic, are encumbered with major errors (Majchrowski et al., 2007).

By introducing the spectral matching function to the mathematical description of changes in phytoplankton pigment levels with depth (Stoń-Egiert et al., 2012), we were able to derive formulas that retain temporal continuity and are of a form that is independent of the season when analyses are carried out. These formulas thus fulfil the requirements for continuous, long-term observations of changes in plant communities. However, there is no statistically significant improvement in the accuracy of estimates, and in the case of chlorophyll *b*, the error factor *x* actually increased from 1.77 to 2.34 with respect to the statistical relationships.

Our analyses show that a mathematical description of the adaptation of photosynthetic pigments: chlorophyll *c* and *b* to ambient conditions must take into account the presence of other groups of pigments with similar spectral features. The formulas derived in accordance with this assumption give far better estimates of a dataset than the statistical relationships derived earlier. The error factors *x* are then approximately the same as those obtained for ocean waters. The results of our analyses can thus be deemed satisfactory, particularly in the case of chlorophyll *c* (where error factors *x* are 1.44 for the Baltic and 1.52 for ocean waters) and PPCs (1.32 and 1.47 respectively).

The estimation accuracy of depth profiles of pigments in the Baltic Sea using new formulas was analysed on the basis of independent dataset collected in the years 2015—2016 not used for deriving any of these new relationships (see Table 1). The errors are presented in Table 5 section 1. A compelling argument justifying the use of formulas based on physical premises instead of purely statistical relationships is provided by the comparison (see Table 5 section 2) of errors in determining pigment concentrations using statistical formulas (Majchrowski et al., 2007), so far encumbered with the smallest error, and the new formulas derived in this paper. Those errors were determined for the same independent set of data gathered in 2015—2016. Table 5 shows that the inclusion in the mathematical description of the concentrations of chlorophylls *b* and *c* $<F_a>$ improved the accuracy of determining these pigments: this is confirmed by the magnitudes of both the systematic errors $<\epsilon>_g$ and the standard error factor *x*. In the case of both PSCs and PPCs, the accuracy is similar to or only slightly less than in the case of the statistical formulas. Since, however, the relationships used to date required an arbitrary separation into two seasons, the result can be regarded as satisfactory. It is worth noting that the accuracy of these formulas approaches that of similar statistical relationships for estimating other characteristics describing the state and functioning of Baltic plant communities (Stramska and Zuzewicz, 2013; Meler et al., 2017).

These dependencies make it possible at the euphotic zone to track changes with depth of the relative concentrations of

Table 4 Comparison of statistical formulas describing the vertical distributions of relative pigment concentrations in samples of the Baltic Sea and ocean waters.

No	Authors	Group of pigments	Equations	Standard error factor x
1	obtained in this work – for the Baltic Sea	chl *b*	$C_b/C_a = 0.1146\langle F_a\rangle_{\Delta z}^{-0.5673} \times \langle F_b\rangle_{\Delta z}$	1.73
		chl *c*	$C_c/C_a = 0.1976\langle F_a\rangle_{\Delta z}^{-0.6627} \times \langle F_c\rangle_{\Delta z}$	1.44
		PSC	$C_{PSC}/C_a = 0.5760 - 1.2961\langle F_{PSC}\rangle_{\Delta z}$	1.50
		PPC	$C_{PPC}/C_a = 0.3279\langle PDR^*\rangle_{\Delta z} + 0.1962$	1.32
2	Majchrowski et al. (2007) – for the Baltic Sea	chl *b*	winter $x = \log(Ca(0))$	1.77
			$C_b/C_a = 10^{-1.0703-0.1599\tau+0.04312\tau^2-0.30871x-0.040076x\tau-0.074687x^2}$ summer	
			$C_b/C_a = 10^{-0.8808+0.075078\tau-0.023728\tau^2-0.54886x+0.046307x\tau+0.20785x^2}$	
		chl *c*	winter $x = \log(Ca(0))$	1.64
			$C_c/C_a = 10^{-1.2314+0.14836\tau-0.031219\tau^2+0.051019x-0.0093837x\tau+0.053311x^2}$ summer	
			$C_c/C_a = 10^{-1.1330+0.1146\tau-0.020600\tau^2-0.011478x+0.0037213x\tau-0.0082814x^2}$	
		PSC	winter $x = \log(Ca(0))$	1.82
			$C_{PSC}/C_a = 10^{-1.1436+0.064027\tau-0.0054346\tau^2+0.29550x-0.0065549x\tau+0.015895x^2}$ summer	
			$C_{PSC}/C_a = 10^{-0.82451+0.072685\tau-0.014871\tau^2+0.016015x-0.010256x\tau+0.029283x^2}$	
		PPC	$C_{PPC}/C_a = 0.164\langle PDR^*\rangle_{\Delta z} + 0.164$	1.73
3	Stoń-Egiert et al. (2012) – for the Baltic Sea	chl *b*	$C_b/C_a = 90.01\langle F_b\rangle_{\Delta z}^{4.2825} + 0.0751$	2.34
		chl *c*	$C_c/C_a = -0.2024\langle F_c\rangle_{\Delta z} + 0.1110$	1.53
		PSC	$C_{PSC}/C_a = -0.4810\langle F_{PSC}\rangle_{\Delta z} + 0.3175$	1.83
		PPC	$C_{PPC}/C_a = 0.0623\langle PDR^*\rangle_{\Delta z} + 0.2251$	1.62
4	Majchrowski and Ostrowska (2000) – for ocean waters	chl *b*	$C_b/C_a = 54.068\langle F_b\rangle_{\Delta z}^{5.157} + 0.091$	1.68
		chl *c*	$C_c/C_a = 0.0424\langle F_c\rangle_{\Delta z}\langle F_a\rangle_{\Delta z}^{-1.197}$	1.52
		PSC	$C_{PSC}/C_a = 1.348\langle F_{PSC}\rangle_{\Delta z} - 0,093$	1.32
		PPC	$C_{PPC}/C_a = 0.1758\langle PDR^*\rangle_{\Delta z} + 0.176$	1.47

the main pigment groups in Baltic waters over the whole range of irradiances and trophic conditions prevailing in this sea. Columns 1 and 2 in Fig. 8 exemplify model profiles of relative pigment concentrations (to the concentration of chlorophyll *a* at given depth) determined using these relationships for an irradiance of 500 μEin m^{-2} s^{-1}. They cover a layer of about 1.5 euphotic zones for trophic types from meso- to eutrophic (for surface chlorophyll *a* levels from 0.2 to >50 mg m^{-3}). The modelled vertical changes in relative concentrations of the various groups of pigments are shown for both the real depth z (column 1) and the optical depth τ (column 2) characterising the changes in irradiance conditions with depth in the water. Column 3 in this figure shows some empirical profiles for trophic type E1, with surface chlorophyll levels from 1 to 2 mg m^{-3}.

Table 5 Systematic errors $<\epsilon>_g$ [%] and error factors x, determined for an independent dataset from 2015 to 2016, defining the accuracy of pigment concentrations calculated using the formulas obtained in this work and also those applied hitherto in models describing the optical properties of the Baltic Sea.

No	Authors	Group of pigments	Systematic error $<\epsilon>_g$ [%]	Standard error factor x
1	obtained in this work – for the Baltic Sea	chl *b*	2.19	1.84
		chl *c*	−3.82	1.46
		PSC	1.87	1.54
		PPC	13.3	1.26
2	Majchrowski et al., 2007 – for the Baltic Sea	chl *b*	49.6	2.12
		chl *c*	−30.4	1.60
		PSC	−27.1	1.59
		PPC	−9.4	1.24

With respect to each group of pigments, these formulas take into account the spectral and intensity differentiation in irradiance in waters of different trophic types; they also characterise well the course of chromatic and intensity adaptation in phytoplankton In the case of all trophic types, the changes in the relative levels all pigment groups with depth in the Baltic differ in comparison with such changes in open ocean waters (Majchrowski and Ostrowska, 2000). As already mentioned, this is due to the presence in these waters of allogenic suspended particulate matter and dissolved substances, which give rise to spectral and intensity distributions of irradiance in ocean waters different from

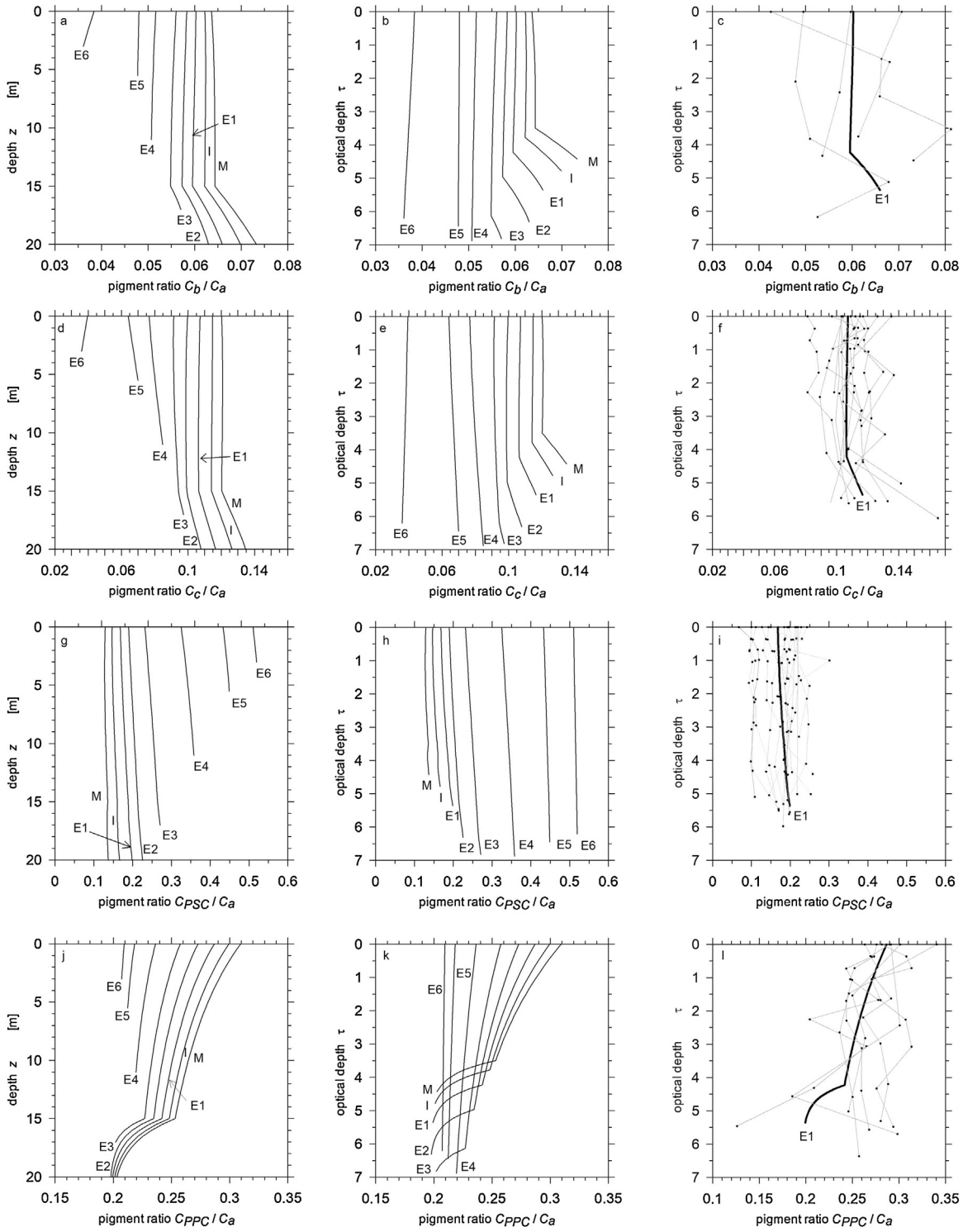

Figure 8 Vertical profiles of relative accessory pigment concentrations to a depth of 1.5 euphotic zone (i.e. optical depth = 7) in different trophic type of waters: modelled according to formulas 2, 3, 4, 7 with respect to the real depth z (column 1) and the optical depth τ (column 2); comparison of profiles — empirical (grey) and modelled (black) — in waters with a surface chlorophyll concentration from 1 to 2 mg m^{-3} (column 3). The modelled profiles are for an irradiance 500 μEin m^{-2} s^{-1} and characteristic trophic types of Baltic waters defined on the basis of the surface concentration of chlorophyll a. The symbols denote the trophic type according to the classification of Woźniak and Pelevin (1991).

those in shelf waters and enclosed seas (Dera, 1995; Woźniak and Dera, 2007).

Column 3 in Fig. 8 exemplifies profiles of the relative contents of the pigment groups within a particular range of chlorophyll *a* concentrations together with the modelled profile corresponding to these conditions. Clearly, the formulas described in this work quantitatively and qualitatively fit into the range of variability of the relative pigment levels

recorded in the Baltic Sea. Any discrepancies are the greatest in the case of the relationship describing changes in chlorophyll *b*, the concentrations of which are lower than those of the other accessory pigments. In addition, this pigment is present mainly in cells of algae from the classes chlorophytes, prasinophytes and euglenophytes, which make up just a small percentage (from 0.01 to 3.40%) of the phytoplankton biomass and no more than 30% during blooms (Stoń-Egiert et al., 2010).

5. Summary

The formulas presented in this work enable changes with depth in concentrations of chlorophylls *b* and *c*, PSCs and PPCs to be determined in the Baltic Sea on the basis of known irradiance characteristics and the concentration of chlorophyll *a*, the principal photosynthetic pigment, with an accuracy no worse than that of formulas derived for ocean waters. The errors ensuing from applying these formulas for calculating chlorophyll, PSC and PPC levels are in all cases smaller than with the formulas used to date.

The achieved accuracy of estimation is sufficient for assessing the spatial variability of pigment concentrations on the basis of remote measurements made during research cruises or by satellite. This will considerably speed up the accumulation of information on the environment; it will also enable water sampling sites and areas to be selected on a continuous basis and detailed laboratory analyses to be carried out in line with research objectives.

An important aspect of these relationships is that they are independent of season. This will ensure continuity in the estimates of depth profiles of pigment concentrations for analyses and monitoring of their annual and seasonal variabilities. Reliable information on the quantitative and qualitative composition of pigments in phytoplankton cells at any depth obtained on the basis of known levels of chlorophyll *a* and the spectral distribution of irradiance in the water may underpin a range of analyses for assessing the state and functioning of Baltic plant communities. Of no mean significance, moreover, is the fact that the data essential for calculating these concentrations can be measured remotely without time-consuming and often costly laboratory studies having to be performed; this will substantially accelerate the acquisition of the relevant data.

With remote sensing techniques for measuring surface chlorophyll *a* and the irradiance conditions, one can also quite quickly determine phytoplankton pigments levels in a whole basin, and even, if the necessary satellite data are available, for the whole Baltic Sea. The formulas presented in this paper describe vertical distributions of pigments in the water column, so analyses can cover the entire euphotic zone.

These mathematical physically justified formulas have been incorporated into the DESAMBEM multi-component light-marine photosynthesis model used in the SatBałtyk system. They further improve the accuracy of the SatBałtyk spatial and depth profiles of various characteristics describing the Baltic ecosystem and the photosynthesis of organic matter in its waters, such as the absorption of solar radiation by phytoplankton, quantum yields of photosynthesis and chlorophyll *a* fluorescence, either global or estimated at various levels of primary productivity, to name but a few.

Acknowledgements

This work was carried out within the framework of the SatBałtyk project funded by the European Union through the European Regional Development Fund (contract No. POIG.01.01.02-22-011/09 entitled 'The Satellite Monitoring of the Baltic Sea Environment'), project NCN DEC-2017/01/X/ST10/00168 and also as part of IO PAS's statutory research.

References

Araujo, M.L.V., Mendes, C.R.B., Tavano, V.M., Garcia, C.A.E., Baringer, M.O., 2017. Contrasting patterns of phytoplankton pigments and chemotaxonomic groups along 30°S in the subtropical South Atlantic Ocean. Deep-Sea Res. Pt. I 120, 112—121, http://dx.doi.org/10.1016/j.dsr.2016.12.004.

Babin, M., Sadoudi, N., Lazzara, L., Gostan, J., Partensky, F., Bricaud, A., Veldhuis, M., Morel, A., Falkowski, P.G., 1996. Photoacclimation strategy of *Prochlorococcus* sp. and consequences on large scale variations of photosynthetic parameters, Ocean Optics 13. Proc. SPIE 2963, 314—319, http://dx.doi.org/10.1117/12.266462.

Barlow, R.G., Mantoura, R.F.C., Gough, M.A., Fileman, T.W., 1993. Pigment signatures of the phytoplankton composition in the northeastern Atlantic during the 1990 spring bloom. Deep-Sea Res. Pt. II 40 (1/2), 459—477.

Berner, T., Dubinsky, Z., Wyman, K., Falkowski, P.G., 1989. Photoadaptation and the 'package effect' in *Dunaliella tertiolecta* (Chlorophyceae). J. Phycol. 25 (1), 70—78, http://dx.doi.org/10.1111/j.0022-3646.1989.00070.x.

Bricaud, A., Morel, A., Prieur, L., 1983. Optical efficiency factors of some phytoplankters. Limnol. Oceanogr. 28 (5), 816—832, http://dx.doi.org/10.4319/lo.1983.28.5.0816.

Bricaud, A., Claustre, H., Ras, J., Oubelkheir, K., 2004. Natural variability of phytoplanktonic absorption in oceanic waters: influence of the size structure of algal populations. J. Geophys. Res. 109, C11010, http://dx.doi.org/10.1029/2004JC002419.

Cherukuru, N., Davies, P.L., Brando, V.E., Anstee, J.M., Baird, M.E., Clementson, L.A., Doblin, M.A., 2016. Physical oceanographic processes influence bio-optical properties in the Tasman Sea. J. Sea Res. 110, 1—7, http://dx.doi.org/10.1016/j.seares.2016.01.008.

Darecki, M., Ficek, D., Krężel, A., Ostrowska, M., Majchrowski, R., Woźniak, S.B., Bradtke, K., Dera, J., Woźniak, B., 2008. Algorithms for the remote sensing of the Baltic ekosystem (DESAMBEM). Part 2: Empirical validation. Oceanologia 50 (4), 509—538.

Demmig-Adams, B., 1990. Carotenoids and photoprotection in plants: a role of xanthophyll zeaxanthin. Biochim. Biophys. Acta 1020 (1), 1—24, http://dx.doi.org/10.1016/0005-2728(90)90088-L.

Dera, J., 1995. Underwater irradiance as a factor affecting primary production. Diss. and monogr, 7. IO PAN, Sopot, 110 pp.

Dera, J., Woźniak, B., 2010. Solar radiation in the Baltic Sea. Oceanologia 52 (4), 533—582, http://dx.doi.org/10.5697/oc.52-4.533.

Dickey, T., Granata, T., Marra, J., Langdon, C., Wiggert, J., Chai-Jochner, Z., Hamilton, M., Vazquez, J., Stramska, M., Bidigare, R., Siegel, D., 1993. Seasonal variability of bio-optical and physical properties in the Sargasso Sea. J. Geoph. Res. Oceans 98 (C1), 865—898, http://dx.doi.org/10.1029/92JC01830.

Falkowski, P.G., LaRoche, J., 1991. Acclimation to spectral irradiance in algae. J. Phycol. 27 (1), 8—14, http://dx.doi.org/10.1111/j.0022-3646.1991.00008.x.

Ficek, D., Kaczmarek, S., Stoń-Egiert, J., Woźniak, B., Majchrowski, R., Dera, J., 2004. Spectra of light absorption by phytoplankton pigments in the Baltic; conclusions to be drawn from a Gaussian analysis of empirical data. Oceanologia 46 (4), 533—555.

Harrison, W.G., Platt, T., 1986. Photosynthesis-irradiance relationships in polar and temperate phytoplankton populations. Polar Biol. 5 (3), 153—164, http://dx.doi.org/10.1007/BF00441695.

Harvey, E.T., Kratzer, S., Andersson, A., 2015. Relationships between colored dissolved organic matter and dissolved organic carbon in different coastal gradients of the Baltic Sea. AMBIO 44 (Suppl. 3), S392—S401, http://dx.doi.org/10.1007/s13280-015-0658-4.

Henriksen, P., Riemann, B., Kaas, H., Sorensen, H.M., Sorensen, H.L., 2002. Effects of nutrient-limitation and irradince on marine phytoplankton pigments. J. Plankton Res. 24 (9), 835—858, http://dx.doi.org/10.1093/plankt/24.9.835.

Ho, T.-Y., Pan, X., Yang, H.-H., Wong, G.T.F., Shiah, F.-K., 2015. Controls on temporal and spatial variations of phytoplankton pigment distribution in the Northern South China Sea. Deep Sea Res. II 117, 65—85, http://dx.doi.org/10.1016/j.dsr2.2015.05.015.

Hoffmann, B., Senger, H., 1988. Kinetics of photosynthesis apparatus adaptation in *Scenedesmus obliquus* to change in irradiance and light quality. Photochem. Photobiol. 47 (5), 737—739, http://dx.doi.org/10.1111/j.1751-1097.1988.tb02773.x.

Jeffrey, S.W., 1997. Structural relationships between algal chlorophylls. In: Jeffrey, S.W., Mantoura, R.F.C., Wright, S.W. (Eds.), Phytoplankton Pigments in Oceanography: Guidelines to Modern Methods, UNESCO Publishing, Paris. 566—571.

Jeffrey, S.W., Vesk, M., 1997. Introduction to marine phytoplankton and their pigment signatures. In: Jeffrey, S.W., Mantoura, R.F.C., Wright, S.W. (Eds.), Phytoplankton Pigments in Oceanography: Guidelines to Modern Methods. UNESCO Publishing, Paris, 37—84.

Kim, H.-C., Son, S., Kim, Y.H., Khim, J.S., Nam, J., Chang, W.K., Lee, J.-H., Ryu, J., 2017. Remote sensing and water quality indicators in the Korean West coast: Spatio-temporal structures of MODIS-derived chlorophyll-a and total suspended solids. Mar. Pollution Bull. 121, 425—434, http://dx.doi.org/10.1016/j.marpolbul.2017.05.026.

Kowalczuk, P., Olszewski, J., Darecki, M., Kaczmarek, S., 2005. Empirical relationships between coloured dissolved organic matter (CDOM) absorption and apparent optical properties in Baltic Sea waters. Int. J. Remote Sens. 26 (2), 345—370, http://dx.doi.org/10.1080/01431160410001720270.

Levin, I., Darecki, M., Sagan, S., Radomyslskaya, T., 2013. Relationships between inherent optical properties in the Baltic Sea for application to the underwater imaging problem. Oceanologia 55 (1), 11—26, http://dx.doi.org/10.5697/oc.55-1.011.

Louda, J.W., Li, J., Liu, L., Winfree, M.N., Baker, E.W., 1998. Chlorophyll-a degradation during senescence and death. Org. Geochem. 29 (5—7), 1233—1251, http://dx.doi.org/10.1016/j.orggeochem.2011.03.018.

Majchrowski, R., Ostrowska, M., 1999. Modified relationships between the occurrence of photoprotecting carotenoids of phytoplankton and Potentially Destructive Radiation in the sea. Oceanologia 41 (4), 589—599.

Majchrowski, R., Ostrowska, M., 2000. Influence of photo- and chromatic acclimation on pigment composition in the sea. Oceanologia 42 (2), 157—175.

Majchrowski, R., Ostrowska, M., 2009. Mathematical description of vertical algal accessory pigment distributions in oceans — a brief presentation. Oceanologia 51 (4), 561—580, http://dx.doi.org/10.5697/oc.51-4.561.

Majchrowski, R., Stoń-Egiert, J., Ostrowska, M., Woźniak, B., Ficek, D., Lednicka, B., Dera, J., 2007. Remote sensing of vertical phytoplankton pigment distributions in the Baltic: new mathematical expressions. Part 2: Accessory pigment distribution. Oceanologia 49 (4), 491—511.

Mantoura, R.F.C., Llewellyn, C.A., 1983. The rapid determination of algal chlorophyll and carotenoid pigments and their breakdown products in natural waters by reverse-phase high-performance liquid chromatography. Anal. Chim. Acta 151, 297—314.

Mantoura, R.F.C., Repeta, D.J., 1997. Calibration methods for HPLC. In: Jeffrey, S.W., Mantoura, R.F.C., Wright, S.W. (Eds.), Phytoplankton Pigments in Oceanography: Guidelines to Modern Methods. UNESCO Publ., Paris, 407—428.

Mantoura, R.F.C., Wright, S.W., Jeffrey, S.W., Barlow, R.G., Cummings, D.E., 1997. Filtration and storage of pigments from microalgae. In: Jeffrey, S.W., Mantoura, R.F.C., Wright, S.W. (Eds.), Phytoplankton Pigments in Oceanography: Guidelines to Modern Methods. UNESCO Publ., Paris, 283—305.

Meler, J., Kowalczuk, P., Ostrowska, M., Ficek, D., Zabłocka, M., Zdun, A., 2016. Parameterization of the light absorption properties of chromophoric dissolved organic matter in the Baltic Sea and Pomeranian lakes. Ocean Sci. 12, 1013—1032, http://dx.doi.org/10.5194/os-12-1013-2016.

Meler, J., Ostrowska, M., Stoń-Egiert, J., Zabłocka, M., 2017. Seasonal and spatial variability of light absorption by suspended particles in the southern Baltic: A mathematical description. J. Mar. Sys. 170, 68—87, http://dx.doi.org/10.1016/j.jmarsys.2016.10.011.

Mendes, C.R., Sá, C., Vitorino, J., Borges, C., Garcia, V.M.T., Brotas, V., 2011. Spatial distribution of phytoplankton assemblages in the Nazaré submarine canyon region (Portugal): HPLC-CHEMTAX approach. J. Mar. Sys. 87, 90—101, http://dx.doi.org/10.1016/j.jmarsys.2016.10.011.

Mitchell, B.G., Kiefer, D.A., 1988. Chlorophyll a specific absorption and fluorescence excitation spectra for light-limited phytoplankton. Deep-Sea Res. 35, 639—663, http://dx.doi.org/10.1016/0198-0149(88)90024-6.

Mobley, C.D., 1994. Light and Water, Radiative Transfer in Natural Waters. Acad. Press, San Diego, USA, 592 pp.

Morel, A., Lazzara, L., Gostan, G., 1987. Growth rate and quantum yield time response for a diatom to changing irradiances (energy and color). Limnol. Oceanogr. 32 (5), 1066—1084, http://dx.doi.org/10.4319/lo.1987.32.5.1066.

Ostrowska, M., Darecki, M., Krężel, A., Ficek, D., Furmańczyk, K., 2015a. Practical applicability and preliminary results of the Baltic environmental satellite remote sensing system (SatBałtyk). Polish Mart. Res. 3 (22), 43—49, http://dx.doi.org/10.1515/pomr-2015-0055.

Ostrowska, M., Stoń-Egiert, J., Woźniak, B., 2015b. Modified methods for defining the chlorophyll concentration in the sea using submersible fluorimeters — Theoretical and quantitative analysis. Cont. Shelf Res. 109, 46—54, http://dx.doi.org/10.1016/j.csr.2015.09.009.

Pan, X., Mannino, A., Russ, M.E., Hooker, S.B., Harding Jr., S.B., 2010. Remote sensing of phytoplankton pigment distribution in the United States northeast coast. Remote Sens. Environ. 114, 2403—2416, http://dx.doi.org/10.1016/j.rse.2010.05.015.

Parsons, T.R., Maita, Y., Lalli, C.M., 1984. A Manual of Chemical and Biological Methods for Seawater Analysis. Pergamon Press, Oxford, 173 pp.

Porra, R.J., Pfündel, E.E., Engel, N., 1997. Metabolism and function of photosynthetic pigments. In: Jeffrey, S.W., Mantoura, R.F.C., Wright, S.W. (Eds.), Phytoplankton Pigments in Oceanography: Guidelines to Modern Methods. UNESCO Publ., Paris, 85—126.

Prieur, L., Sathyendranath, S., 1981. An optical classification of coastal and oceanic waters based on the specific spectral absorption curves of phytoplankton pigments, dissolved organic matter, and other particulate materials. Limnol. Oceanogr 26 (4), 671—689, http://dx.doi.org/10.4319/lo.1981.26.4.0671.

Repeta, D.J., Bjørnland, T., 1997. Preparation of carotenoids standards. In: Jeffrey, S.W., Mantoura, R.F.C., Wright, S.W. (Eds.), Phytoplankton Pigments in Oceanography: Guidelines to Modern Methods. UNESCO Publ., Paris, 239—260.

Roy, S., Llewellyn, C.A., Egeland, E.S., Johnsen, G., 2011. Phytoplankton Pigments, Characterization, Chemotaxonomy and Applications in Oceanography. Cambridge Univ. Press, 845 pp.

Sathyendranath, S., Lazzara, L., Prieur, L., 1987. Variations in the spectral values of specific absorption of phytoplankton. Limnol. Oceanogr. 32 (2), 403—415, http://dx.doi.org/10.4319/lo.1987.32.2.0403.

Scheer, H., 1991. Structure and occurrence of chlorophylls. In: Scheer, H. (Ed.), Chlorophylls. CRC Press, Boca Raton, 3—30.

Schlüter, L., Mohlenberg, F., Havskum, H., Larsen, S., 2000. The use of phytoplankton pigments for identifying phytoplankton groups in coastal areas: testing the influence of light and nutrients on pigment/chlorophyll *a* ratios. Mar. Ecol.-Prog. Ser. 192, 49—63, http://dx.doi.org/10.3354/meps192049.

Simis, S.G.H., Ylöstalo, P., Kallio, K.Y., Spilling, K., Kutser, T., 2017. Contrasting seasonality in optical-biogeochemical properties of the Baltic Sea. PLoS ONE 12 (4), e0173357, http://dx.doi.org/10.1371/journal.pone.0173357.

Smith Jr., W.O., Dinniman, M.S., Tozzi, S., DiTullio, G.R., Mangoni, O., Modigh, M., Saggiomo, V., 2010. Phytoplankton photosynthetic pigments in the Ross Sea: Patterns and relationships among functional groups. J. Mar. Sys. 82, 177—185.

Soja-Woźniak, M., Darecki, M., Wojtasiewicz, B., Bradtke, K., 2018. Laboratory measurements of remote sensing reflectance of selected phytoplankton species from the Baltic Sea. Oceanologia 60 (1), 86—96, http://dx.doi.org/10.1016/j.oceano.2017.08.001.

Sosik, H.M., Mitchell, B.G., 1991. Absorption, fluorescence, and quantum yield for growth in nitrogen-limited *Dunaliella tertiolecta*. Limnol. Oceanogr. 36 (5), 910—921, http://dx.doi.org/10.4319/lo.1991.36.5.0910.

Staehr, P.A., Henriksen, P., Markager, S., 2002. Photoacclimation of four marine phytoplankton species to irradiance and nutrient availability. Mar. Ecol. Prog. Ser. 238, 47—59, http://dx.doi.org/10.3354/meps238047.

Stedmon, C.A., Markager, S., Kaas, H., 2000. Optical properties and signatures of chromophoric dissolved organic matter (CDOM) in Danish coastal waters. Est. Coast. Shelf Sci. 51, 267—278, http://dx.doi.org/10.1006/ecss.2000.0645.

Stoń, J., Kosakowska, A., 2002. Phytoplankton pigments designation — an application of RP-HPLC in qualitative and quantitative analysis. J. Appl. Phycol. 14 (3), 205—210, http://dx.doi.org/10.1023/A:1019928411436.

Stoń-Egiert, J., Kosakowska, A., 2005. RP-HPLC determination of phytoplankton pigments — comparison of calibration results for two columns. Mar. Biol. 147 (1), 251—260, http://dx.doi.org/10.1007/s00227-004-1551-z.

Stoń-Egiert, J., Łotocka, M., Ostrowska, M., Kosakowska, A., 2010. The influence of biotic factors on phytoplankton pigment composition and resources in Baltic ecosystems: new analytical results. Oceanologia 52 (1), 101—125, http://dx.doi.org/10.5697/oc.52-1.101.

Stoń-Egiert, J., Majchrowski, R., Darecki, M., Kosakowska, A., Ostrowska, M., 2012. Influence of underwater light fields on pigment characteristics in the Baltic Sea — results of statistical analysis. Oceanologia 54 (1), 7—27, http://dx.doi.org/10.5697/oc.54-1.007.

Stramska, M., Zuzewicz, A., 2013. Comparison of primary productivity estimates in the Baltic Sea based on the DESAMBEM algorithm with estimates based on other similar algorithms. Oceanologia 55 (1), 77—100, http://dx.doi.org/10.5697/oc.55-1.077.

Stramski, D., Sciandra, A., Claustre, H., 2002. Effects of temperature, nitrogen, and light limitation on the optical properties of the marine diatom Thalassiosira pseudonana. Limnol. Oceanogr. 47 (2), 392—403, http://dx.doi.org/10.4319/lo.2002.47.2.0392.

Strutton, P.G., Martz, T.D., DeGrandpre, M.D., McGillis, W.R., Drennan, W.M., Boss, E., 2011. Bio-optical observations of the 2004 Labrador Sea phytoplankton bloom. J. Geoph. Res. 116, C11037.

Sukenik, A., Bennett, J., Mortain-Bertrand, A., Falkowski, P.G., 1990. Adaptation of photosynthetic apparatus to irradiance in *Dunaliella tertiolecta*. Plant Physiol. 92 (4), 891—898, http://dx.doi.org/10.1104/pp.92.4.891.

Swan, C.M., Vogt, M., Gruber, N., Laufkoetter, C., 2016. A global seasonal surface ocean climatology of phytoplankton types based on CHEMTAX analysis of HPLC pigments. Deep-Sea Res. Pt. I, 109, 137—156, http://dx.doi.org/10.1016/j.dsr.2015.12.002.

Thamm, R., Schernewski, G., Wasmund, N., Neumann, T., 2004. Spatial phytoplankton pattern in the Baltic Sea. In: Schernewski, G., Wielgat, S. (Eds.), Baltic Sea Typology Coastline Reports 4, Warnemünde, 85—109.

Trees, C.C., Clark, R.D.K., Bidigare, R., Ondrusek, M.E., Mueller, J. L., 2000. Accessory pigments versus chlorophyll A concentrations within the euphotic zone: A ubiquitous relationship. Limnol. Oceanogr. 45 (5), 1130—1143, http://dx.doi.org/10.4319/lo.2000.45.5.1130.

Uitz, J., Claustre, H., Morel, A., Hooker, S.B., 2006. Vertical distribution of phytoplankton communities in open ocean: an assessment based on surface chlorophyll. J. Geophys. Res. 111 (C8), C08005, http://dx.doi.org/10.1029/2005JC003207.

Uitz, J., Stramski, D., Reynolds, R.A., Dubranna, J., 2015. Assessing phytoplankton community composition from hyperspectral measurements of phytoplankton absorption coefficient and remote-sensing reflectance in open-ocean environments,. Remote Sens. Environ. 171, 58—74, http://dx.doi.org/10.1016/j.rse.2015.09.027.

Wasmund, N., Breuel, G., Edler, L., Kuosa, H., Olsonen, R., Schultz, H., Pys-Wolska, M., Wrzołek, L., 1996. Pelagic biology. In: Third periodic assessment of the state of marine environment of the Baltic Sea, 1989—93, Balt. Sea Environ. Proc. No. 64B, HELCOM Background doc. 89—93.

Wasmund, N., Uhlig, S., 2003. Phytoplankton in large river plumes in the Baltic Sea,. ICES J. Mar. Sci. 56, 23—32.

Wänstrand, I., Snoeijs, P., 2006. Phytoplankton community dynamics assessed by ships-of-opportunity sampling in the northern Baltic Sea: A comparison of HPLC pigment analysis and cell counts. Est. Coast. Shelf Sci. 66 (1—2), 135—146, http://dx.doi.org/10.1016/j.ecss.2005.08.003.

Woźniak, B., Bradtke, K., Darecki, M., Dera, J., Dudzińska-Nowak, J., Dzierzbicka-Głowacka, L., Ficek, D., Furmańczyk, K., Kowalewski, M., Krężel, A., Majchrowski, R., Ostrowska, M., Paszkuta, M., Stoń-Egiert, J., Stramska, M., Zapadka, T., 2011. SatBałtyk — A Baltic environmental satellite remote sensing system — an ongoing project in Poland. Part 1: Assumptions, scope and operating range. Oceanologia 53 (4), 897—924, http://dx.doi.org/10.5697/oc.53-4.897.

Woźniak, B., Dera, J., 2007. Light Absorption in Sea Water. Springer, New York, 454 pp.

Woźniak, B., Dera, J., Ficek, D., Majchrowski, R., Kaczmarek, S., Ostrowska, M., Koblentz-Mishke, O.J., 1999. Modelling the influence of acclimation on the absorption properties of marine phytoplankton. Oceanologia 41 (2), 187—210.

Woźniak, B., Dera, J., Ficek, D., Majchrowski, R., Ostrowska, M., Kaczmarek, S., 2003. Modelling light and photosynthesis in the marine environment. Oceanologia 45 (2), 171—245.

Woźniak, B., Dera, J., Majchrowski, R., Ficek, D., Koblenz-Mishke, O. J., Darecki, M., 1997a. 'IOPAS initial model' of marine primary production for remote sensing application. Oceanologia 39 (4), 377—395.

Woźniak, B., Dera, J., Majchrowski, R., Ficek, D., Koblentz-Mishke, O.J., Darecki, M., 1997b. Statistical relationships between photosynthesis and abiotic conditions in the ocean — the IO PAS initial model for remote sensing application. SPIE vol. 3222, 516—528.

Woźniak, B., Hapter, R., Maj, B., 1983. The inflow of solar energy and the irradiance of the euphotic zone in the region of Ezcurra Inlet during the Antarctic summer of 1977/78. Oceanologia 15, 141—174.

Woźniak, B., Krężel, A., Darecki, M., Woźniak, S.B., Majchrowski, R., Ostrowska, M., Kozłowski, Ł., Ficek, D., Olszewski, J., Dera, J., 2008. Algorithm for the remote sensing of the Baltic ecosystem (DESAMBEM). Part 1: Mathematical apparatus. Oceanologia 50 (4), 451—508.

Woźniak, B., Krężel, A., Dera, J., 2004. Development of a satellite method for Baltic ecosystem monitoring (DESAMBEM) — an ongoing project in Poland. Oceanologia 46 (3), 445—455.

Woźniak, B., Montwiłł, K., 1973. Methods and techniques of optical measurements in the sea. Stud. i Mater. Oceanol. 7, 71—108, (in Polish).

Woźniak, B., Pelevin, V.N., 1991. Optical classifications of the seas in relation to phytoplankton characteristics. Oceanologia 31, 25—55.

Woźniak, S.B., Meler, J., Lednicka, B., Zdun, A., Stoń-Egiert, J., 2013. Inherent optical properties of suspended particulate matter in the southern Baltic Sea. Oceanologia 53 (3), 691—729, http://dx.doi.org/10.5697/oc.53-3.691.

Wright, S.W., Jeffrey, S.W., Mantoura, R.F.C., Llewellyn, C.A., Bjørnland, T., Repeta, D., Welschmeyer, N., 1991. Improved HPLC method for the analysis of chlorophylls and carotenoids from marine phytoplankton. Mar. Ecol.-Prog. Ser. 77, 183—196.

Wright, S.W., Shearer, J.D., 1984. Rapid extraction and high-performance liquid chromatography of chlorophylls and carotenoids from marine phytoplankton. J. Chromatogr. 294, 281—295.

Wulff, A., Wängberg, S.-A., 2004. Spatial and vertical distribution of phytoplankton pigments in the eastern Atlantic sector of the Southern Ocean. Deep-Sea Res. Pt. II, 51, 2701—2713, http://dx.doi.org/10.1016/j.dsr2.2001.01.002.

Zhang, D., Lavender, S., Muller, J.P., Walton, D., Karlson, B., Kronsell, J., 2017. Determination of phytoplankton abundances (Chlorophyll-*a*) in The optically complex inland water — The Baltic Sea. Remote Sci. Tot. Environ. 601—602, 1060—1074, http://dx.doi.org/10.1016/j.scitotenv.2017.05.245.

Zheng, G., DiGiacomo, P.M., 2017. Remote sensing of environment remote sensing of chlorophyll-a in coastal waters based on the light absorption coefficient of phytoplankton,. Remote Sens. Environ. 201, 331—341, http://dx.doi.org/10.1016/j.rse.2017.09.008.

Oceanologia (2019) 61, 17—25

Available online at www.sciencedirect.com

ScienceDirect

journal homepage: www.journals.elsevier.com/oceanologia/

ORIGINAL RESEARCH ARTICLE

Influence of environmental factors on the population dynamics of key zooplankton species in the Gulf of Gdańsk (southern Baltic Sea)

Maja Musialik-Koszarowska [a], **Lidia Dzierzbicka-Głowacka** [b,*], **Agata Weydmann** [a]

[a] *Institute of Oceanography, University of Gdańsk, Gdynia, Poland*
[b] *Institute of Oceanology, Polish Academy of Sciences, Sopot, Poland*

Received 16 November 2017; accepted 4 June 2018
Available online 30 June 2018

KEYWORDS
Copepoda;
Environmental factors;
Acartia spp.;
Temora longicornis;
Pseudocalanus sp.;
Biomass

Summary We studied the influence of abiotic environmental factors on the seasonal population dynamics' of *Acartia* spp., *Temora longicornis* and *Pseudocalanus* sp. in the southern Baltic Sea in the period of 2006—2007 and 2010—2012. Zooplankton samples were being collected monthly at 6 stations located in the western part of the Gulf of Gdańsk with a WP2 net (100 µm mesh sizes) and then analyzed according to the HELCOM guidelines. Although the sampling stations did not significantly differ from each other in the terms of variability of abiotic environmental factors, the biomass of copepods developmental stages differed between them, apart from the shallow stations in both, Gulf of Gdańsk and in its inner part — Puck Bay. According to redundancy analysis, 26.1% of the total variability observed in the biomass of the copepod species has been explained by water temperature, salinity, air temperature, cloudiness, wind speed and direction and station's depth, with the first variable having the greatest power, alone explaining 13.7%. ANOSIM revealed that sampling stations in the Gulf of Gdańsk were significantly different from one another in terms of copepods' biomasses. Generalized Additive Models fitted for water temperature and salinity were significant for all ontogenetic stages of *Acartia* spp. and *Temora longicornis* and for the majority of stages of *Pseudocalanus* sp. (apart from the C1 for both and the males for salinity).

* Corresponding author at: Institute of Oceanology, Polish Academy of Sciences, Sopot, Poland. Tel.: +48 58 523 68 46.
E-mail address: dzierzb@iopan.gda.pl (L. Dzierzbicka-Głowacka).
Peer review under the responsibility of Institute of Oceanology of the Polish Academy of Sciences.

Production and hosting by Elsevier

https://doi.org/10.1016/j.oceano.2018.06.001

1. Introduction

At present, the Baltic Sea ecosystem raises a major concern in the fishery sector of the Polish economy.

Over the last hundred years, this ecosystem has been subject to various transformations resulting from both, the climate fluctuations and the anthropogenic pressure (BACC II). So far the observed climate-driven changes in the Baltic Sea environmental conditions included *inter alia*: the increase in both, the sea surface temperature and in the atmospheric precipitation, as well as river discharge (causing a significant drop in a seawater salinity), and a reduction of the seasonal ice cover. Despite the fact that the biggest warming has been recorded in the northern Baltic Sea, the ecosystem of its southern part — more productive and diverse — is much more susceptible to the negative effects of the climate change.

The latest computer simulations indicated that the Baltic Sea warming will continue (Meier et al., 2012), therefore investigating the reactions of marine organisms to the ongoing transformation of the environment is a particularly important task. The Baltic Sea is relatively sensitive to changes in the environmental conditions, due to its inland location, a large catchment area and a limited exchange of sea waters with the Atlantic Ocean.

Zooplankton are bioindicators of the climate change for many reasons (Richardson, 2008). Their physiological processes such as ingestion, respiration and reproductive development are highly sensitive to temperature (Mauchline, 1998). Additionally, most zooplankton species have a short life cycle and a fast reproduction rate so they are highly associated with both climate and population dynamics (Hays et al., 2005).

In terms of biomass and abundance, the key zooplankton taxa of the southern part of the Baltic Sea are copepods such as *Acartia* spp., *Pseudocalanus* sp. and *Temora longicornis*, then Rotifera, mainly *Synchaeta* spp. and *Keratella quadrata*, and amid Cladocera, which are dominated by *Evadne nordmanni*, *Eubosmina maritima* and *Pleopis polyphemoides*. The less important are euryhaline freshwater and typical freshwater species, found mainly in estuaries (*Eurytemora* sp.) (Lemieszek, 2013).

Copepods are part of the pelagic trophic chain and therefore they play an important role in the transfer of energy between producers and consumers from higher levels, acting as a food source for much pelagic fish (Dippner et al., 2000; Möllmann et al., 2000; Vuorinen et al., 1998). Being the organisms feeding on phytoplankton, copepods indirectly indicate changes in the trophic status of the water body, such as eutrophication, reflecting changes in the structure of phytoplankton. They also indicate climate changes, predation, contamination with synthetic compounds and the impact of alien species (Richardson, 2008).

The most important copepods species in the Gulf of Gdańsk, such as *Acartia* spp. (i.e. *A. bifilosa*, *A. longiremis* and *A. tonsa*), *Temora longicornis* and *Pseudocalanus* sp. are the main food components of commercial fish, like, *Clupea harengus* and *Sprattus sprattus* (Möllmann et al., 2003), hence any anomalies in the copepod biomass negatively affect fish populations (Dzierzbicka-Głowacka et al., 2013). In the Baltic Sea, *Pseudocalanus* sp. is the food for large larvae of cod (*Gadus morhua*) (Hinrichsen et al., 2002; Möllmann et al., 2003) and for the adult pelagic fish such as sprat (*Sprattus sprattus*) or herring (*Clupea harengus*) (Flinkman et al., 1992; Möllmann and Köster 1999, 2002). *Temora longicornis* is primarily the food for sprat (*Sprattus sprattus*) which abundance in the Baltic Sea has begun to decrease since the 1990s (Möllmann and Köster, 1999). *Acartia* spp. is a brackish species, adapted to lower salinity and common in the Baltic Sea (Ackefors, 1969; Fransz et al., 1991). It occurs in the upper part of the water column where, due to the food availability, growth conditions are presumably better compared to the ones in the deeper regions. The same may hold for the neritic, euryhaline species *Temora longicornis*, which can be found in the waters spanning over a wide salinity range but which is less strongly confined to shallow water than *Acartia* spp. Both copepods are described as thermophilic species (Chojnacki and Antończak, 2008; Hansen et al., 2006; Möllmann et al., 2000, 2003). In contrast, *Pseudocalanus* sp. prefers lower temperatures and higher salinities (Hansen et al., 2006).

Although sampled regularly during monitoring programs, the detailed knowledge on the copepod seasonal distribution and production patterns in the coastal area of the southern Baltic Sea is still insufficient. The Baltic Monitoring Programme (HELCOM) provided zooplankton data mostly with a very low spatiotemporal resolution. Apart from these studies, data on the copepod distribution in the southern Baltic Sea are available only sporadically or from the coastal areas (Bielecka et al., 2000; Chojnacki et al., 1975; Chojnacki and Drzycimski, 1976; Józefczuk et al., 2003; Mudrak and Żmijewska, 2006; Otto et al., 2014).

The aim of this study was to investigate how seasonal changes in abiotic environmental conditions such as hydrographic water properties as well as wind speed and direction or cloudiness, influence population dynamics and distribution of the copepods, important to fisheries. Another goal was to describe an average monthly distribution of the key copepod species observed in the southern Baltic Sea during the following research periods: 2006—2007 and 2010—2012.

2. Material and methods

2.1. The study area

The Study area covers the Gulf of Gdańsk and its inner basin — Puck Bay, located in the southern Baltic Sea. The Gulf of Gdańsk is a system of estuaries in which there is a mix of brackish and marine waters that is typical for this type of a basin. All zooplankton samples were being collected at six stations, out of which five (S1, S2, S3, S4, J23) were located along a depth gradient in the Gulf of Gdańsk and one (M2) was located in Puck Bay (Fig. 1) (Table 1). Puck Bay is a semi-enclosed area, isolated from the rest of the Gulf of Gdańsk by the presence of the shoal.

2.2. Sampling

Zooplankton was sampled monthly in the periods from January 2006 to December 2007 and from March 2010 to December 2012 with a WP2 net (100 μm mesh size), equipped with

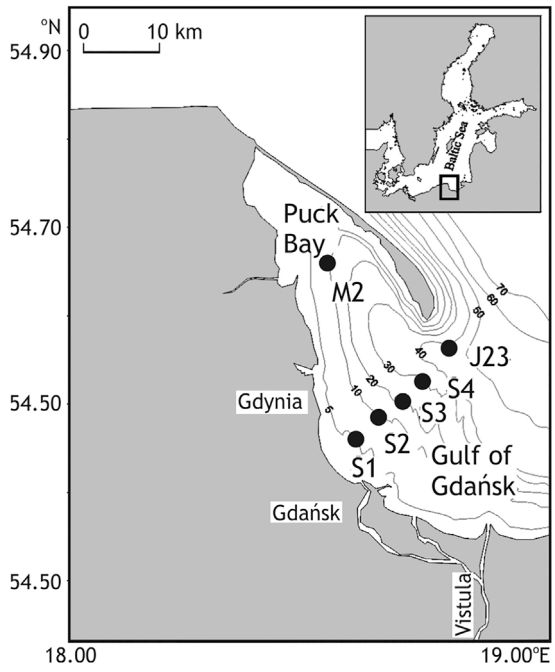

Figure 1 Study area and location of the sampling stations.

Table 1 Location of the sampling stations in the western part of the Gulf of Gdańsk.

Station	Lat.	Long.	Depth [m]
M2	N 54°39′0″	E 18°33′8″	10
J23	N 54°32′0″	E 18°48′2″	40
S4	N 54°30′7″	E 18°46′0″	30
S3	N 54°29′7″	E 18°43′7″	20
S2	N 54°27′7″	E 18°36′7″	10
S1	N 54°27′0″	E 18°34′8″	5

Hydro-Bios Mechanical Flow Meter. At the shallow stations, S1, S2, M2, vertical hauls were conducted from the bottom to the surface. At deeper stations, J23, S4, S3 (>10 m), samples were collected from the water column every 10 m. All samples were collected during the daytime (mainly between 11 am and 2 pm) so the diurnal vertical migrations were not taken into account. Water salinity and temperature were measured each time after collecting zooplankton samples, with a handheld WTW Cond 3110. In addition, the air temperature, cloudiness, wind speed and direction were also being noted. Qualitative and quantitative zooplankton laboratory analysis was performed in accordance with the Manual for Marine Monitoring in the COMBINE (Cooperative Monitoring in the Baltic Marine Environment) Programme of HELCOM (Helsinki Commission) (Annex C-7) (HELCOM, 2015).

2.3. Statistical analyses

Statistical analyses were run on the square root transformed biomass data of copepods' development stages for sampling layers integrated at the stations [mg C m^{-3}]. To reveal differences between particular sampling locations for the biomasses of the main copepod taxa, significance tests for differences between ordered groups of samples were performed using one-way Analysis of Similarities (ANOSIM). Similarly, ANOSIM has been used to reveal differences between sampling stations — in terms of biotic environmental factors such as water temperature, salinity, air temperature, cloudiness, wind speed and direction, which were normalized prior to the analysis. Above analyses were performed in PRIMER version 7 (Plymouth Marine Laboratory, Plymouth, UK) (Clarke and Warwick, 1994).

To study the relationship between environmental variables (water temperature, salinity, air temperature, cloudiness, wind speed and direction, station depth) and biomasses of developmental stages of the studied calanoid copepods, redundancy analysis (RDA) was performed in CANOCO 5 (Ter Braak and Šmilauer, 2012). The environmental variables were ranked, according to their quantitative importance, by manual selection based on the Monte Carlo permutation test adjusted for temporal autocorrelation (Ter Braak and Šmilauer, 2012). Then, Generalized Additive Model (GAM, Poisson distribution, 4 df) was used to examine responses of individual developmental stages separately against water temperature and salinity, hence to illustrate non-parametric relationships between copepods' life stages and significant environmental variables.

3. Results

3.1. Hydrology

The temperature was characterized by a very similar distribution throughout the study period (Fig. 2). In the period of 2006–2007 the average water temperature ranged from 1°C in March 2006 to 17°C in July 2007. From June to September 2007, the average temperature was above 15°C. In the period of 2010–2012 the average temperature fluctuated between 1°C in March 2010 and 18°C in August 2010. Temperature above 10°C has been observed from June to September 2010, June–October 2011 and 2012. Differences in salinity were even less distinguished, with the annual variations between 5.8 and 7.6.

Interestingly, according to ANOSIM test for differences, the sampling stations did not differ significantly, in the terms of biotic environmental factors such as water temperature, salinity, air temperature, cloudiness, and neither of wind speed nor of its direction (p = 0.999, global R = −0.017).

3.2. Seasonal changes in biomass

The average biomass of investigated copepods showed a seasonal variability for each species. The highest biomass in the water column for *Acartia* spp. and *Temora longicornis* has been recorded during the summer months, while the highest biomass for *Pseudocalanus* sp. has been noted in winter. The minimal average biomass has been observed for *Acartia* spp. in December (2.05 mg C m^{-3}) and for *Temora longicornis* in January (4.33 mg C m^{-3}). The minimal biomass values for *Pseudocalanus* sp. have been observed in the spring and in the autumn months (Fig. 3).

During the study period, a bimodal biomass of Copepoda distribution has been observed. For *Acartia* spp., the first

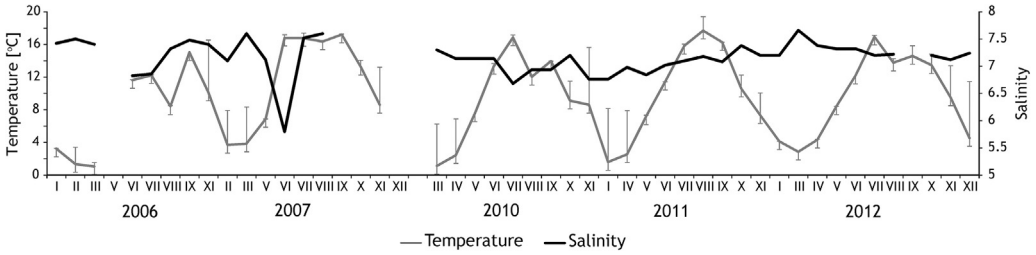

Figure 2 Water temperature with SD and salinity in the Gulf of Gdańsk.

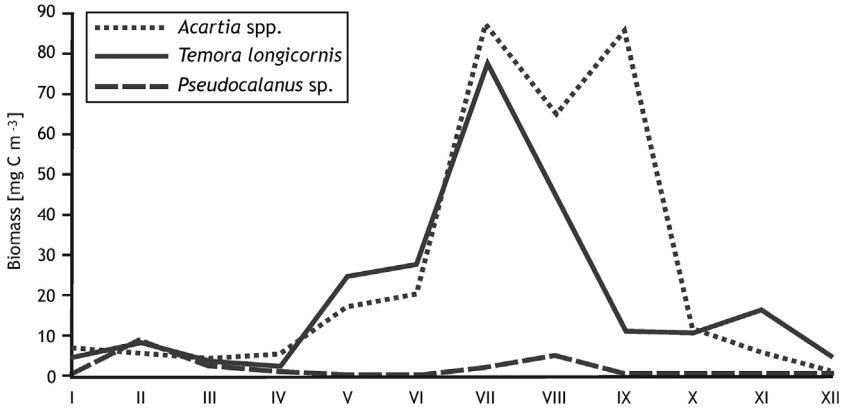

Figure 3 The average value of biomass in the Gulf of Gdańsk in 2006—2007 and 2010—2012.

biomass peak was recorded in July with the value of 86.45 mg C m^{-3}, then in September — 85.80 mg C m^{-3}. In July, the first biomass peak for *Temora longicornis* (76.95 mg C m^{-3}) was also observed, while the second, much lower, was recorded in November (16.11 mg C m^{-3}). *Pseudocalanus* sp. was characterized by the first, higher biomass peak in February with the value of 7.61 mg C m^{-3}, and the second peak in August — 4.19 mg C m^{-3}.

ANOSIM revealed that the sampling stations in the Gulf of Gdańsk were significantly different from one another in terms of copepods' biomasses ($p = 0.001$, global $R = 0.056$). According to the following pairwise tests, no similarities have been noted between the S2 and M2 stations, the S1 and M2 stations, and also not between S1—S4 stations. The highest similarity has been noted between the S4 and S3 stations (over 84%). The analysis also showed the lower similarity between the S3 and S2 (24%), S4 and S2 (18%) stations. The shallower stations S2, S1 and M2 were similar to each other in ca. 12%.

3.3. Influence of environmental factors on copepods

The model based on the species-environment relationships in RDA ($p = 0.001$, pseudo-$F = 7.6$) explained 26.1% of the total variability observed in the population composition and biomass of the three copepod species in the Gulf of Gdańsk during the study period. The environmental variable with the greatest explanatory power was water temperature, which explained 13.7% of the total variability. The air temperature (3.2%), cloudiness (2.5%), station depth (2.4%), and salinity (2.2%) were of secondary importance. The wind speed and direction were responsible for 1.2% and 0.8%, respectively (Table 2).

The RDA analysis revealed that the higher biomass of *Acartia* spp. corresponded with the higher water and air temperatures (Fig. 4). The older stages of *Pseudocalanus* sp. and the females of *Temora longicornis* were strongly correlated with the wind direction in the southern part of the Baltic Sea. The presence of nauplii and the females of both *Acartia* spp. and *Temora longicornis* as well as young copepodids of *Pseudocalanus* sp. was correlated with both salinity and cloudiness.

Generalized Additive Models fitted for the water temperature and salinity were significant for all ontogenetic stages of *Acartia* spp. and *Temora longicornis* ($p \leq 0.00001$), and for the majority of stages of *Pseudocalanus* sp., apart from C1 for both (temperature $p = 0.84325$, salinity $p = 0.60031$) and the males for salinity ($p = 0.3372$) (Fig. 5). For the first two mentioned species, the nauplii responded strongly to the temperature around 16—17°C, with the remaining stages peaking in slightly lower temperatures in case of *Acartia* spp., or in higher temperatures for *Temora longicornis*. However, the latter species mentioned, show a bi-modal distribution with the less intense, primary peak around 10°C for most of its stages. The females, C4 and C5 of *Pseudocalanus* sp. peaked in the lowest temperatures, while C2, C3 and nauplii have also shown a bi-modal biomass distribution, with the second peak in similar temperatures as in case of the species mentioned before. In case of salinity, all copepods clearly preferred the highest measured values, peaking above 7.5.

Table 2 Environmental variables that best explained the variability of biomasses of ontogenetic stages of the three dominant Baltic calanoid copepods. These variables are significant, according to the Monte Carlo permutation test applied during forward selection in the redundancy analysis (RDA).

Variable	Explains [%]	Contribution [%]	pseudo-*F*	*p*
Temperature	13.7	47.7	34.5	0.001
Air temperature	3.2	11.2	8.3	0.001
Cloudiness	2.5	8.6	6.6	0.001
Station depth	2.4	8.4	6.6	0.001
Salinity	2.2	7.5	6.1	0.001
Wind speed	1.2	4.3	3.5	0.005
Wind direction	0.8	2.9	2.3	0.042

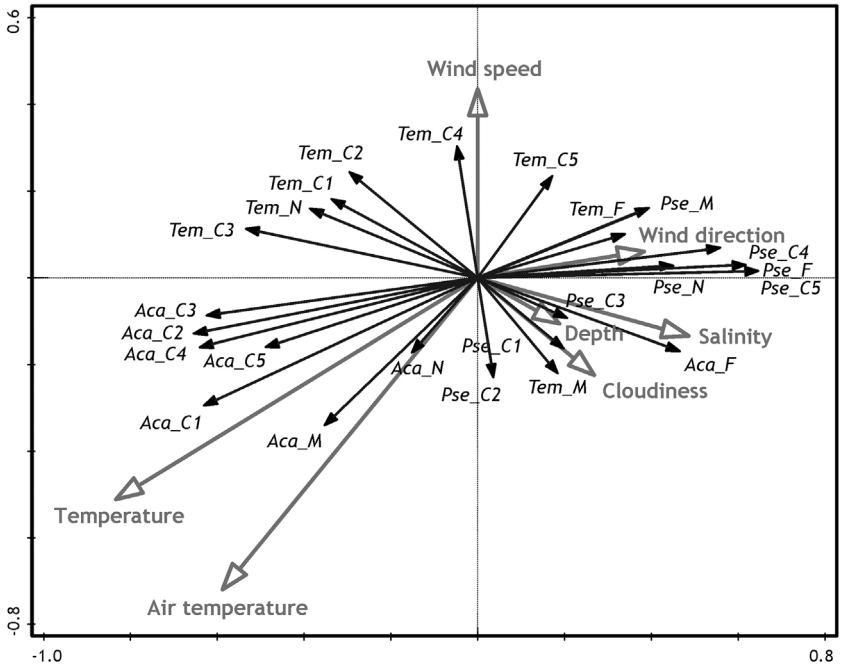

Figure 4 Ordination plot from redundancy analysis (RDA) on biomasses of development stages of *Acartia* spp., *Temora longicornis* and *Pseudocalanus* sp. (N — nauplii, F— females, M — males, C1—C5 copepodids of respective stage) monthly sampled in the Gulf of Gdańsk (black arrows) and their relation to abiotic environmental variables (grey arrows).

4. Discussion

Our studies indicate that the Gulf of Gdańsk is a specific reservoir of brackish water where temperature determines the occurrence of copepods. The Generalized Additive Models (GAM) were used to determine the relationship between temperature and biomass of the studied copepods. Similarly to Möllmann et al. (2000), the GAM results obtained for *Acartia* spp. reflect a positive correlation between the biomass and temperature. This confirms the fact that *Acartia* spp. is classified as a thermophilic organism and also that the increase in biomass of this copepod follows the increase of temperature (Möllmann et al., 2000). The sudden increase in the biomass of this taxon began when the water temperature exceeded the level of 10°C, and the maximum for all stages was observed at the temperature level of 17—18°C. According to Dzierzbicka-Głowacka et al. (2010) and the parabolic function of temperature, a decrease occurs at the level of above 18°C as a result of physiological depression. The results obtained for *Temora longicornis* also indicate the correlation between temperature and biomass. The rapid growth of biomass began at the temperature of 13°C, and the optimum temperature for this species was 18°C. This result is consistent with the results obtained by Mudrak (2004). Based on all the data obtained, we can conclude that the temperature in the Gulf of Gdańsk determines the biological processes, affects variability, including distribution, abundance and biomass of Copepoda. Therefore, any temperature anomalies may have a direct effect on phenology, community structure or on trophic interactions in the Baltic ecosystem.

The gradual increase in water temperature related to the global warming may, on one hand, accelerate copepods metabolism and life cycle, thus reducing the total time of transition from the stage of nauplii into the stage of adult forms (Weydmann et al., 2015, 2018), but on the other hand, may have a negative impact on psychrophilic species such as *Pseudocalanus* sp. The research conducted by Holste in the Baltic Sea (Holste et al., 2008) has revealed that the water

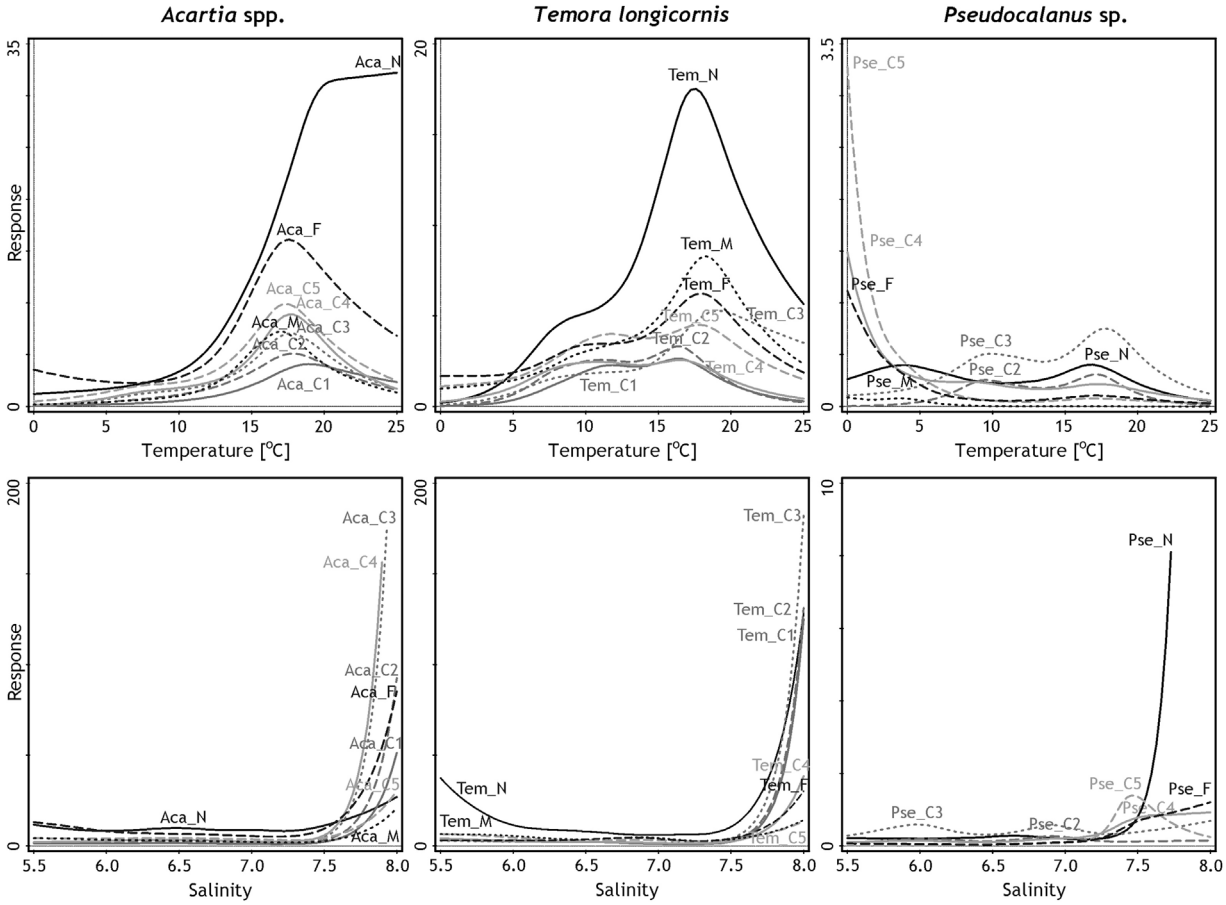

Figure 5 Generalized Additive Models (GAM) of ontogenetic stages (N — nauplii, F — females, M — males, C1 — C5 copepodids of respective stage) of *Acartia* spp., *Temora longicornis* and *Pseudocalanus* sp. biomasses versus water temperature and salinity. The models are presented only for significant relationships ($p \leq 0.05$).

temperature is an important factor affecting the reproductive process of *Temora longicornis*. At the temperature of 16°C, the production of eggs by females of this copepod reached the maximum, and at the level of 24°C — all of the examined organisms have died. The research indicates that the temperature rise cannot be unlimited. There is a "T0" value (optimum temperature) for every species, the exceeding of which, negatively affects the development of organisms, i.e. either inhibits the growth of organisms or leads to their death (Dzierzbicka-Głowacka et al., 2010).

Additionally to the temperature effect on copepods, which has been observed directly, it seems worth to discuss the impact of the climate change on the functioning of the trophic structure in the pelagic ecosystem. Concurrently, apart from the biomass decline in primary producers, and/or the displacement of phenological phases of protozoa, the consequence of warming in the marine ecosystems is the change in a size structure towards nanoplankton domination, including flagellates (Gardner et al., 2011; Polovina and Woodworth, 2012). The high-calorie microplankton diatoms, which are a food base favored by zooplankton, are being gradually replaced by less nutritive nanoplankton flagellates. As a consequence, the energy flow through the ecosystem is less efficient (Legendre, 1990), copepods which are feeding on ciliates, contribute to a food chain elongation, as well as to the derivation of carbon from heterotrophic rather than autotrophic sources (Dahlgren et al., 2011). As a result, the trophic transfer of essential compounds being produced by algae to upper trophic levels, may become limited.

Moreover, the omission or overlapping of protozoa and zooplankton peaks may determine the change of energy transfer direction, both along the sea and along the land ecosystem food webs (Thackeray, 2012). In the case of the Baltic Sea, the restructuring of unicellular plankton is currently being observed (Suikkanen et al., 2007). Moreover, it includes a significant increase in the proportion of planktonic cyanobacteria, especially the toxic species (Allen et al., 2006). Even though recent studies indicate that cyanobacteria may be an important component of zooplankton food base (Hogfors et al., 2014), their massive development is widely recognized as a negative phenomenon for planktonic Metazoa. The adverse impact of cyanobacteria on zooplankton manifests itself in difficulty to get food, reducing their fertility and high mortality rate (Śliwińska-Wilczewska and Latała, 2017).

The Generalized Additive Models (GAM) for *Acartia* spp., *Temora longicornis* and *Pseudocalanus* sp. showed no clear relationship between copepods and salinity, what was also confirmed by the redundancy analysis (RDA), where this factor explains only 2.2% of the variation in the studied species. This relationship does not correspond to the research conducted by Möllmann et al. (2000). Möllmann

et al. (2000) showed that the biomass of the main species in the Baltic Sea in 1959–1997 was partly determined by the hydrography of the water body. The strongest correlation has been obtained for *Pseudocalanus elongatus*, which shows the strong affinity with higher salinity at low temperature (Möllmann et al., 2000). The discrepancy in the results and the lack of correlation between salinity and biomass of *Pseudocalanus sp*. may result from the small depth of the Gulf of Gdańsk and the rarity of this taxon in the region. *Pseudocalanus* sp. prefers salinity of about 12 and, therefore, it occurs in small numbers in the coastal waters such as the Gulf of Gdańsk. Due to a small amount of data available for this taxon, our analysis does not provide a clear answer on whether a complete generation of *Pseudocalanus* sp. develops in the Gulf of Gdańsk. However, the species is common in the Gdańsk Deep where the life cycle of this taxon includes only one generation per year (Mudrak, 2004). In the North Sea, due to a high water temperature during summer, higher salinity and sufficient concentration of food in months between March and August, three or four generations of *Pseudocalanus elongatus* have been observed in the German South Bay (Dippner et al., 2000) during the annual cycle and three generations have been noted in its northern part (Bossicart, 1980). Evans (1977) has described four to six generations of *Pseudocalanus elongatus* in the coastal waters of Northumberland (the North Sea) (Renz and Hirche, 2005).

The variability of copepods in the Gulf of Gdańsk is also affected by meteorological factors. The air temperature is connected with seasonality what in a temperate climate has a considerable impact on the variability of zooplankton species, thereby directly affecting the water temperature in the sea area. According to the RDA analysis, the cloud cover accounts for 2.5% of the variation in copepods and appears to affect the vertical migrations in the water column, as well as the occurrence of the studied organisms – in the areas being closer to the water surface during cloudy days. Copepods are planktonic organisms, passively floating in the pelagic zone and are not capable to resist the sea currents. Therefore, the wind direction and velocity affect the variability, carrying these organisms along with the water masses. The wave displaces water organisms within the water column and influences the local communities of mesozooplankton, which are additionally affected by the tidal range and currents. The topography of the shallow coastal waters affects the water circulation and relevant water properties (temperature, oxygen, turbidity), and thus can be mainly responsible for the space-time variation of mesozooplankton (Pineda, 2000).

The obtained results confirm that zooplankton of the Baltic Sea is subject to the seasonal biomass changes. The seasonality is a pronounced reason for a structural variability in plankton communities of temperate regions like the Baltic Sea. It is associated with the species demands' for food availability and specified temperature levels. Literature data often indicate that seasonality of zooplankton is directly related to seasonality and productivity of phytoplankton, development of which is being primarily regulated by the lighting cycle (Chiba et al., 2008). However, studies conducted in the offshore waters of the Baltic Sea indicate that the composition and abundance structure of zooplankton were not related to the occurrence and abundance of phytoplankton (Lennuk et al., 2016). So the seasonal dynamics of copepods is probably caused mainly by the temperature, in our research area. In the area of the temperate waters of the Baltic Sea, the structural variability of the plankton communities is also observed (Józefczuk et al., 2003; Mudrak and Żmijewska, 2006). Copepoda were recorded in the Baltic zooplankton samples throughout the year, and according to Lemieszek, they are the main component of zooplankton in the water column for the most months (Lemieszek, 2013), while Rotifera and Cladocera are being observed in the highest abundances, particularly in the summer time (Mudrak and Żmijewska, 2006). Rotifera typically dominate in May (*Synchaeta* spp.) and in August (*Keratella* spp.) when their parthenogenetic reproduction mode allows utilizing the optimal food conditions within a short period.

We have noticed that the biomass of *Pseudocalanus* sp. in the Gulf of Gdańsk, in comparison with the research conducted on the Gdańsk Deep in 2010, was very low. *Pseudocalanus* sp. has been accounted for over 50% of the share as a component of zooplankton in the spring and autumn seasons. This difference may be the result of a small tolerance to low salinity, which limits the occurrence of this copepod in the Gulf of Gdańsk. The species is a stenohaline organism, which is the main component of plankton in deeper waters and is one of the most important zooplankton taxa in the Baltic Sea (Ojaveer et al., 2000). Analyzing the seasonal biomass distribution, we can conclude that *Acartia* spp. dominated in terms of biomass, and *Temora longicornis* was a subdominant species in the Gulf of Gdańsk. In addition to the investigated copepods species in the southern Baltic *Centropages hamatus* also appears, with its largest share in biomass is being recorded in the summer season with the maximum average biomass in July (7 mg C m^{-3}) and in the autumn season (about 2 mg C m^{-3}) (Mudrak, 2004). *Eurytemora* species is present rather rarely but with a negligible share in biomass (Lemieszek, 2013).

The quantity and taxonomic composition of zooplankton resources have an influence on growth and survival of fish in early development stages (Cushing, 1995). According to Sparholt (1994), reduction of *Pseudocalanus* sp. biomass in the Baltic Sea, as the main component of food, has undoubtedly contributed to the herring population decline (*Clupea harengus*) since the early 1980s. Möllmann et al. (2003) showed that condition of the herring population (*Clupea harengus*) depends on the amount of *Pseudocalanus* sp. biomass, in the central Baltic. Another species of Baltic fish, which population has been declining since the 1990s, was sprat (*Sprattus sprattus*). The food of this pelagic fish is primarily *Temora longicornis* (Möllmann and Köster, 1999). The decrease of *Sprattus sprattus* population may be caused by the competition between *Sprattus sprattus* and *Clupea harengus*, and which, with the absence of a sufficient amount of *Pseudocalanus* sp., had to include other copepods species, such as *Temora longicornis*, in their diet.

5. Conclusions

The environmental variable in the Gulf of Gdańsk, with the greatest explanatory power of the total variability in the copepods population composition and biomass, was the water temperature. Therefore, we contend that it is the controlling factor in the Gulf of Gdańsk.

Generalized Additive Models fitted for water temperature and salinity were significant for all ontogenetic stages of the *Acartia* spp. and *Temora longicornis* and also for most stages of *Pseudocalanus* sp., apart from the C1 for both and the males — for salinity.

ANOSIM has revealed that the sampling stations in the Gulf of Gdańsk were significantly different from one another in the terms of copepods' biomasses.

Copepoda taxa composition has changed seasonally in the Gulf of Gdańsk. *Acartia* spp. and has reached the highest values in the summer months, while, *Temora longicornis* dominated in biomass in the spring and autumn seasons. The maximum value of biomass for *Pseudocalanus* sp. has been observed in the winter time.

Acknowledgements

Partial support for this study has been provided by the project: WaterPUCK (No. BIOSTRATEG3/343927/3/NCBR/2017) founded by the National Centre for Research and Development within the BIOSTRATEG III program.

We express our gratefulness to the anonymous reviewers for valuable comments on the earlier versions of the manuscript.

We are also thankful for the substantive support which has been provided by Prof. Dr hab. M.I. Żmijewska.

References

Ackefors, H., 1969. Seasonal and vertical distribution of zooplankton in the Askö area (Northern Baltic proper) in relation to hydrographical conditions. Oikos 20 (2), 480—492, http://dx.doi.org/10.2307/3543210.

Allen, J.L., Anderson, D., Burford, M., Dyhrman, S., Flynn, K., Gilbert, P.M., Grane'li, E., Heil, C., Sellner, K., Smayda, T., Zhou, M., 2006. Global ecology and oceanography of harmful algal blooms in eutrophic systems. GEOMA Breport 4. IOC and SCOR, Paris, Baltimore, MD, 1—74.

Bielecka, L., Gaj, M., Mudrak, S., Żmijewska, M.I., 2000. The seasonal and short term changeability of zooplankton taxonomic composition in the shallow coastal area of the Gulf of Gdańsk. Oceanol. Stud. 29 (1), 57—76.

Bossicart, M., 1980. Population dynamics of copepods in the Southern Bight of the North Sea (1977—1979), use of a multicohort model to derive biological parameters. In: Coun. Meet. Explor. Sea C.M.-ICES/L:24 ICES CM L:24. .

Chiba, S., Aita, M.N., Tadokoro, K., Saino, T., Sugisaki, H., Nakata, K., 2008. From climate regime shifts to lower-trophic level phenology: synthesis of recent progress in retrospective studies of the western North Pacific. Prog. Oceanogr. 77, 112—126, http://dx.doi.org/10.1016/j.pocean.2008.03.004.

Chojnacki, J., Antończak, E., 2008. Seasonal changes in the neritic zone mesozooplankton of Pomeranian Bay in 2000. Electron. J. Polish Agric. Univ. 11 (4), 29.

Chojnacki, J., Drzycimski, I., 1976. The southern Baltic zooplankton in spring and summer 1974. Ann. Biol. Cons. Perm. Int. Explor. Mer, Copenhagen 31, 72—73.

Chojnacki, J., Drzycimski, I., Maslowski, J., Radziejewska, T., Strzelichowski, M., 1975. Zooplankton of the southern Baltic in 1972—1973. Ann. Biol. Cons. Perm. Int. Explor. Mer, Copenhagen 30, 73—74.

Clarke, K.R., Warwick, R.M., 1994. Changes in Marine Communities: An Approach to Statistical Analysis and Interpretation. Natural Environment Research Council, UK, 144 pp.

Cushing, D.H., 1995. The long-term relationship between zooplankton and fish. ICES J. Mar. Sci. 52 (3—4), 611—626, http://dx.doi.org/10.1016/1054-3139(95)80076-X.

Dahlgren, K., Eriksson Wiklund, A.-K., Andersson, A., 2011. The influence of autotrophy, heterotrophy and temperature on pelagic food web efficiency in a brackish water system. Aquat. Ecol. 45, 307—323, http://dx.doi.org/10.1007/s10452-011-9355-y.

Dippner, J.W., Kornilovs, G., Siedrevics, L., 2000. Long-term variability of mesozooplankton in the central Baltic Sea. J. Mar. Syst. 25 (1), 23—31, http://dx.doi.org/10.1016/S0924-7963(00)00006-3.

Dzierzbicka-Głowacka, L., Żmijewska, M.I., Mudrak, S., Jakacki, J., Lemieszek, A., 2010. Population modelling of *Acartia* spp. in a water column ecosystem model for the South-Eastern Baltic Sea. Biogeosciences 7 (7), 2247—2259, http://dx.doi.org/10.5194/bg-7-2247-2010.

Dzierzbicka-Głowacka, L., Kalarus, M., Żmijewska, M.I., 2013. Interannual variability in the population dynamics of the main mesozooplankton species in the Gulf of Gdańsk (southern Baltic Sea): seasonal and spatial distribution. Oceanologia 55 (2), 409—434, http://dx.doi.org/10.5697/oc.55-2.409.

Evans, F., 1977. Seasonal density and production estimates of the commoner planktonic copepods of Northhumberland coastal waters. Estuar. Coast. Mar. Sci. 5 (2), 233—241, http://dx.doi.org/10.1016/0302-3524(77)90019-6.

Flinkman, J., Vuorinen, I., Aro, E., 1992. Planktivorous Baltic herring (*Clupea harengus*) prey selectively on reproducing copepods and cladocerans. Can. J. Fish. Aquat. Sci. 49 (1), 73—77, http://dx.doi.org/10.1139/f92-008.

Fransz, H.G., Colebrook, J.M., Gamble, J.C., Krause, M., 1991. The zooplankton of the North Sea. Neth. J. Sea Res. 28 (1—2), 1—52, http://dx.doi.org/10.1016/0077-7579(91)90003-J.

Gardner, J.L., Peters, A., Kearney, M.R., Joseph, L., Heinsohn, R., 2011. Declining body size: a third universal response to warming? Trends Ecol. Evol. 26, 285—291, http://dx.doi.org/10.1016/j.tree.2011.03.005.

Hansen, J., Sato, M., Ruedy, R., Lo, K., Lea, D.W., Medina-Elizade, M., 2006. Global temperature change. PNAS 103, 14288—14293, http://dx.doi.org/10.1073/pnas.0606291103.

Hays, G.C., Richardson, A.J., Robinson, C., 2005. Climate change and plankton. Trends Ecol. Evol. 20, 337—344, http://dx.doi.org/10.1016/j.tree.2005.03.004.

HELCOM, 2015. Manual for Marine Monitoring in the COMBINE Programme of HELCOM. http://helcom.fi/action-areas/monitoring-and-assessment/manuals-and-guidelines/combine-manual/, (accessed 10.09.16).

Hinrichsen, H.H., Möllmann, C., Voss, R., Köster, F.W., Kornilovs, G., 2002. Biophysical modeling of larval Baltic cod (*Gadus morhua*) growth and survival. Can. J. Fish. Aquat. Sci. 59 (12), 1858—1873, http://dx.doi.org/10.1139/f02-149.

Hogfors, H., Motwani, N.H., Hajdu, S., El-Shehawy, R., Holmborn, T., Vehmaa, A., Engström-Öst, J, Brutemark, A, Gorokhova, E., 2014. Bloom-forming cyanobacteria support copepod reproduction and development in the Baltic Sea. PLOS ONE 9 (11) e112692, eCollection 2014, https://doi.org/10.1371/journal.pone.0112692.

Holste, L., St John, M., Peck, M.A., 2008. The effects of temperature and salinity on reproductive success of *Temora longicornis* in the Baltic Sea: a copepod coping with a tough situation. Mar. Biol. 156 (4), 527—540, http://dx.doi.org/10.1007/s00227-008-1101-1.

Józefczuk, A., Guzera, E., Bielecka, L., 2003. Short-term and seasonal variability of mesozooplankton at two coastal stations (Gdynia, Sopot) in the shallow water zone of the Gulf of Gdańsk. Oceanologia 45 (1), 317—336.

Legendre, P., 1990. Quantitative methods and biogeographic analysis. In: Evolutionary Biogeography of the Marine Algae of the North Atlantic. Springer-Verlag, Berlin Heidelberg, 9—35.

Lemieszek, A., 2013. The Population Dynamics of *Temora longicornis* in the Southern Baltic Sea. (PhD Thesis). Univ. Gdańsk, Gdynia, (in Polish).

Lennuk, L., Kotta, J., Lauringson, V., Traits, K., Jänes, H., 2016. Which environmental scales and factors matter for meso zooplankton communities in a shallow brackish water ecosystem? J. Plankton Res. (38), 1—15, http://dx.doi.org/10.1093/plankt/fbv111.

Mauchline, J., 1998. The biology of calanoid copepods. In: Advances in Marine Biology. Acad. Press 33, 710 pp.

Meier, H.E.M., Hordoir, R., Andersson, H.C., Dieterich, C., Eilola, K., Gustafsson, B.G., Schimanke, S., 2012. Modelling the combined impact of changing climate and changing nutrient loads on the Baltic Sea environment in an ensemble of transient simulations for 1961—2099. Clim. Dyn. 39, 2421—2441, http://dx.doi.org/10.1007/s00382-012-1339-7.

Mudrak, S., 2004. Short- and Long-Term Variability of Zooplankton in Coastal Baltic Waters: Using the Gulf of Gdańsk as an Example. (PhD Thesis). Univ. Gdańsk, Gdynia, (in Polish).

Mudrak, S., Żmijewska, M.I., 2006. Spatio-temporal variability of mesozooplankton from the Gulf of Gdańsk (Baltic Sea) in 1999—2000. Oceanol. Hydrobiol. St. 36 (2), 3—19, http://dx.doi.org/10.2478/v10009-007-0007-4.

Möllmann, C., Köster, F.W., 1999. Food consumption by clupeids in the central Baltic: evidence for top-down control. ICES J. Mar. Sci. 56, 110—113, http://dx.doi.org/10.1006/jmsc.1999.0630.

Möllmann, C., Kornilovs, G., Sidrevics, L., 2000. Long-term dynamics of main mesozooplankton species in the central Baltic Sea. J. Plankton Res. 22 (11), 2015—2038, http://dx.doi.org/10.1093/plankt/22.11.2015.

Möllmann, C., Köster, F.W., 2002. Population dynamics of Calanoid copepods and the implications of their predation by clupeid fish in the Central Baltic Sea. J. Plankton Res. 24, 959—978.

Möllmann, C., Köster, F.W., Kornilovs, G., Sidrevics, L., 2003. Interannual variability in population dynamics of calanoid copepods in the central Baltic Sea. ICES Mar. Sci. 219, 220—230.

Ojaveer, H., Simm, M., Lankov, M., Lumberg, A., 2000. Consequences of invasion of a predatory cladoceran. ICES International Council for the Exploration of the Sea, C.M. 2000/U:16.

Otto, S.A., Kornilovs, G., Llope, M., Möllmann, C., 2014. Interactions among density, climate, and food web effects determine long-term life cycle dynamics of a key copepod. Mar. Ecol. Prog. Ser. 498 (73), U408, http://dx.doi.org/10.3354/meps10613.

Pineda, J., 2000. Linking larval settlement to larval transport: assumptions, potentials, and pitfalls. Oceanogr. East. Pac. 1, 84—105.

Polovina, J., Woodworth, P.A., 2012. Declines in phytoplankton cell size in the subtropical oceans estimated from satellite remotely-sensed temperature and chlorophyll, 1998—2007. Deep-Sea Res. Pt. II 77, 82—88.

Renz, J., Hirche, H.J., 2005. Life cycle of *Pseudocalanus acuspes* Giesbrecht (Copepoda, Calanoida) in the Central Baltic Sea: I. Seasonal and spatial distribution. Mar. Biol. 248, 567—580, http://dx.doi.org/10.1007/s00227-005-0103-5.

Richardson, A.J., 2008. In hot water: zooplankton and climate change. ICES J. Mar. Sci. 65, 279—295, http://dx.doi.org/10.1093/icesjms/fsn028.

Sparholt, H., 1994. Fish species interactions in the Baltic Sea. Dana 10, 131—162.

Suikkanen, S., Laamanen, M., Huttunen, M., 2007. Long-term changes in summer phytoplankton communities of the open northern Baltic Sea. Estuar. Coast. Shelf Sci. 71, 580—592, http://dx.doi.org/10.1016/j.ecss.2006.09.004.

Śliwińska-Wilczewska, S., Latała, A., 2017. Oddziaływania allelopatyczne sinic i mikroglonów w środowisku wodnym. Kosmos 66 (2), 217—224.

Ter Braak, C.J.F., Šmilauer, P., 2012. Canoco Reference Manual and User's Guide: Software for Ordination, Version 5.0. Microcomputer Power, Ithaca, USA.

Thackeray, S.J., 2012. Mismatch revisited: what is trophic mismatching from the perspective of the plankton? J. Plankton Res. 34, 1001—1010, http://dx.doi.org/10.1093/plankt/fbs066.

The BACC II, Author Team, 2008. Second Assessment of Climate Change for the Baltic Sea Basin. Regional Climate Studies. Springer Int. Publ., 1—22, http://dx.doi.org/10.1007/978-3-319-16006-1.

Vuorinen, I., Hänninen, J., Viitasalo, M., Helminen, U., Kuosa, H., 1998. Proportion of copepod biomass declines with decreasing salinity in the Baltic Sea. ICES J. Mar. Sci. 55 (4), 767—774, http://dx.doi.org/10.1006/jmsc.1998.0398.

Weydmann, A., Zwolicki, A., Muś, K., Kwaśniewski, S., 2015. The effect of temperature on egg development rate and hatching success in *Calanus glacialis* and *C. finmarchicus*. Polar Res. 34 (1), 23947, http://dx.doi.org/10.3402/polar.v34.23947.

Weydmann, A., Walczowski, W., Carstensen, J., Kwaśniewski, S., 2018. Warming of Subarctic waters accelerates development of a key marine zooplankton Calanus finmarchicus. Glob. Change. Biol. 24, 172—183, http://dx.doi.org/10.1111/gcb.13864.

Oceanologia (2019) 61, 26—37

Available online at www.sciencedirect.com

ScienceDirect

journal homepage: www.journals.elsevier.com/oceanologia/

ORIGINAL RESEARCH ARTICLE

Role of macrophytes in structuring littoral habitats in the Vistula Lagoon (southern Baltic Sea)

Krzysztof Pawlikowski *, **Ryszard Kornijów**

Department of Fisheries Oceanography and Marine Ecology, National Marine Fisheries Research Institute, Gdynia, Poland

Received 10 January 2018; accepted 26 May 2018
Available online 18 June 2018

KEYWORDS
Submerged and emergent vegetation;
Oxygenation;
Temperature;
Insulation;
Sediments

Summary The objective of the research conducted in the years 2011—2014 in the near-shore zone of the Vistula Lagoon was the verification of the hypothesis that in the coastal lagoon, similarly as in inland waters, habitat conditions can be substantially modified by macrophytic vegetation, depending on the represented life form and its abundance. The research was conducted in the zone of emergent plants (reed rush composed of *Phragmites australis*) and in the zone of submerged plants occurring as scattered patches of *Potamogeton perfoliatus* and *Stuckenia pectinata*. The hypothesis was supported only in the case of the reed rush which substantially modified water insolation, temperature, and oxygenation, as well as the grain size composition of sediments, and concentration of organic matter contained in the sediments. Patches of submerged vegetation had insufficient surface area and were too scarcely overgrown by plants to considerably affect the habitat conditions and weaken the strong mechanical effect of waves and rate of water exchange between the littoral and open water zone.

1. Introduction

The littoral is a zone of a water body above the compensation point (Odum, 1971). The most important biotic characteristic of the zone is macrophytic vegetation (vascular flora, stoneworts, bryophytes). It usually occurs in the form of more or less interwinding belts and clusters. The area nearest to the shore is usually occupied by the assemblage of emergent

* Corresponding author.
E-mail address: k.pawlikowski@mir.gdynia.pl (K. Pawlikowski).
Peer review under the responsibility of Institute of Oceanology of the Polish Academy of Sciences.

Production and hosting by Elsevier

https://doi.org/10.1016/j.oceano.2018.05.003

plants (helophytes), deeper areas by vegetation with floating leaves (nympheids), and the deepest – vegetation with submerged leaves (elodeids). The presence of such plants indicates the richness of animal communities related to them in various ways (in trophic and paratrophic terms), both invertebrates (epiphytic fauna) and vertebrates (amphibians, reptiles, fish, and birds). In shallow water bodies where the majority of the bottom surface is insolated, the role of macrophytes in the functioning of the entire ecosystem can be sufficiently significant to provide the basis for the designation of one of the alternative regimes – macrophyte-dominated state (Scheffer et al., 1993).

Many papers discuss the impact of different abiotic factors on aquatic vegetation. Considerably fewer publications concern the opposite relations, i.e. the effect of plants on the habitat conditions occurring in the littoral. So far, the issue has been mainly investigated in inland water bodies, and particularly in shallow lakes (Barko and James, 1998; Carpenter and Lodge, 1986; Chen and Barko, 2011; Horppila and Nurminen, 2005; Miranda et al., 2000; Moller and Sand-Jensen, 2012), but very rarely in the conditions of coastal lagoons (Viaroli et al., 1996). It may be caused by among others the popular opinion that in the littoral of lagoons, the habitat conditions are primarily determined by physical parameters, including wave action (Perez-Ruzafa et al., 2011; Viaroli et al., 2008). This paper presents a hypothesis that in a coastal lagoon, like in inland waters, habitat conditions can also be substantially modified by macrophytic vegetation, depending on the represented life form (helophytes, elodeids) and its abundance. The thesis was verified by four years of research in the near-shore zone of the Vistula Lagoon.

2. Study area

The Vistula Lagoon is a brackish lagoon separated from the Gdańsk Bay (Baltic Sea) by the Vistula Spit. The exchange of water masses between the Lagoon and open sea is possible through the Baltijsk Strait. The Vistula Lagoon has an area of 838 km^2 and is divided approximately in half between Poland (south-western part) and Russia (north-eastern part). The lagoon is a shallow water body with a depth usually not exceeding 4 m. The length of the shoreline of the Vistula Lagoon on the Polish side is 92.3 km. Homogenous assemblages of emergent vegetation (EMV) occur along the shoreline, particularly including *Phragmites australis* (Cav.) Trin. ex Steud, and patches of submerged vegetation (SUV), composed mainly of *Potamogeton perfoliatus* L. The greatest degree of vegetation cover occurs in the western part of the lagoon (Fig. 1) (Gajewski, 2010).

Bottom sediments are primarily composed of silt and sand (Zachowicz et al., 1995). The concentrations of total nitrogen and phosphorus in the water are high, and amount to 1.1–4.4 mg dm^{-3} and 0.06–0.19 mg dm^{-3}, respectively. The most frequently recorded water transparency (measured as Secchi disc depth) is approximately 40 cm (Kornijów, 2018). The Vistula Lagoon is classified as a eutrophic water body (Kruk et al., 2012; Nawrocka & Kobos, 2011), and from the viewpoint of alternative stable states theory, the majority of its basin is phytoplankton-dominated, with chlorophyll-*a*

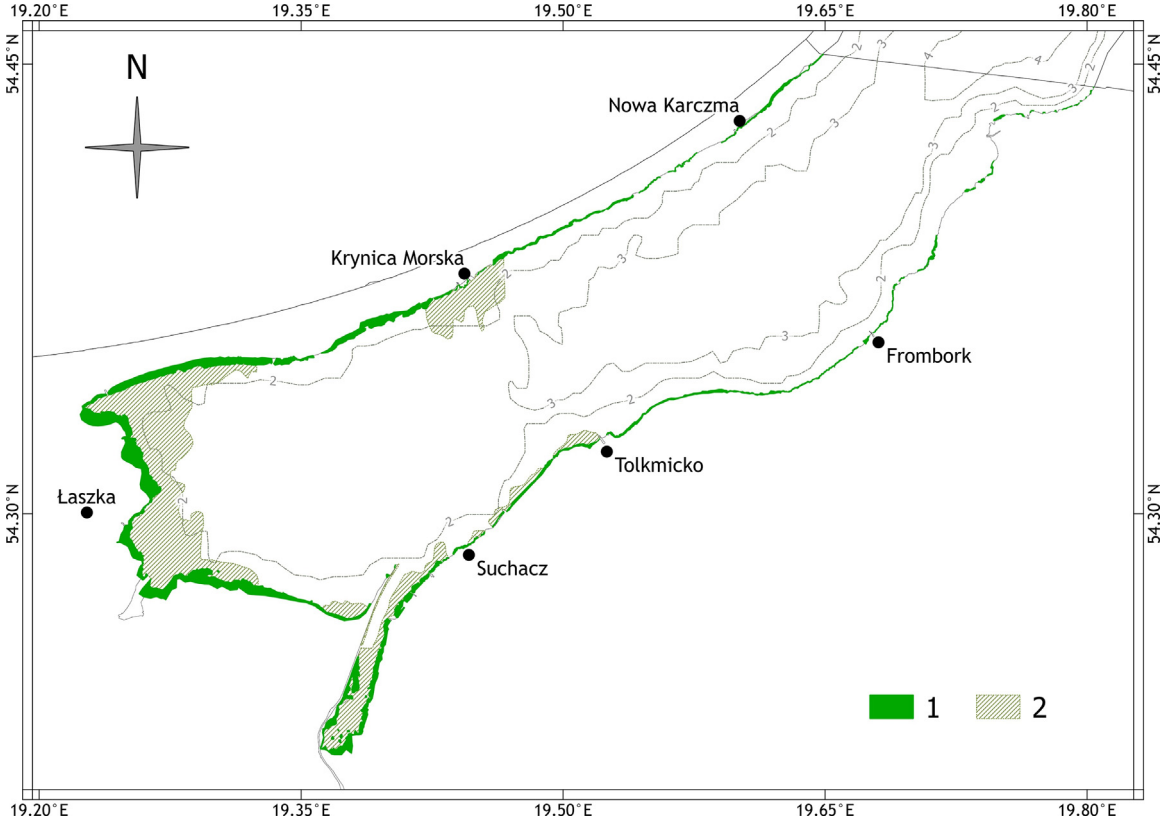

Figure 1 Map of distribution of emergent (1) and submerged vegetation (2) in the Polish part of the Vistula Lagoon. Based on maps elaborated by Gajewski (ed., 2010). Bathymetry adapted from Chubarenko (2008).

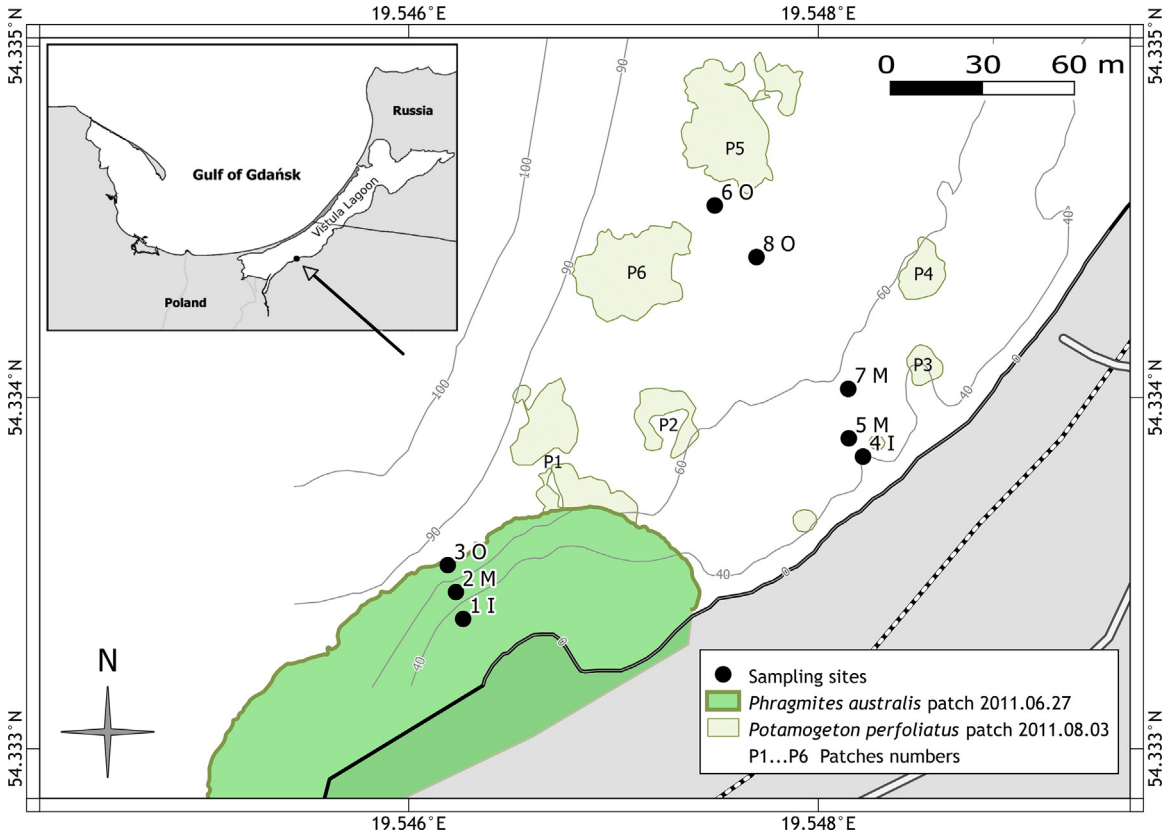

Figure 2 Map of the littoral section studied. For explanation of the site symbols see Table 1.

concentrations between 13 and 107 mg m^{-3} (Kornijów, 2018).

The studied fragment of the littoral (Fig. 2) was located 2 km north-east of the port in Tolkmicko and had a length of approximately 500 m and width of 110 m. A patch overgrown by common reed (*Phragmites australis*) occurred there, with a length of 200 m, as well as a 300 m long section of sandy bottom (psammolitoral) with several patches of submerged vegetation dominated by perfoliate pondweed *Potamogeton perfoliatus*, and more rarely by sago pondweed *Stuckenia pectinata* (L.) Börner. The research was performed at 14 sites selected based on the criterion of depth and occurrence of vegetation (Fig. 2, Table 1). Three sites were located in the zone of emergent vegetation (EMV) overgrown by reed rush, five on the adjacent sandy bare bottom between the patches of SUV macrophytes (herein treated as control), and six within SUV patches (*P. perfoliatus*). The littoral belt was divided into three zones: inner littoral (depth 0–40 cm,

Table 1 Characteristics of the sampling sites: location within the research area, depth, type of sediment, and exposure to wave action. EMV – emergent vegetation, SUV – submerged vegetation.

Site	Zone	Location	Distance from shore [m]	Depth [m] (range in brackets)	Bottom sediment	Exposure to wave action
Site 1 I	EMV (inside the patch)	inner	32	0.25 (0.11–0.51)	silt	weak
Site 2 M	EMV (inside the patch)	mid	40	0.50 (0.26–0.66)	silt	medium
Site 3 O	EMV (inside the patch)	outer	50	0.70 (0.64–0.97)	sand	strong
Site 4 I	SUV (between patches)	inner	13	0.40 (0.23–0.57)	sand	strong
Site 5 M	SUV (between patches)	mid	20	0.50 (0.33–0.67)	sand	strong
Site 6 O	SUV (between patches)	outer	103	0.72 (0.61–0.95)	sand	strong
Site 7 M	SUV (between patches)	mid	31	0.58 (0.36–0.65)	sand	strong
Site 8 O	SUV (between patches)	outer	82	0.71 (0.54–0.78)	sand	strong
Patch P1	SUV (inside patches)	outer	60	0.70	sand	strong
Patch P2	SUV (inside patches)	outer	54	0.70	sand	strong
Patch P3	SUV (inside patches)	inner	22	0.34 (0.17–0.41)	sand	strong
Patch P4	SUV (inside patches)	mid	40	0.59 (0.35–0.66)	sand	strong
Patch P5	SUV (inside patches)	outer	111	0.78 (0.57–0.85)	sand	strong
Patch P6	SUV (inside patches)	outer	103	0.81 (0.67–0.88)	sand	strong

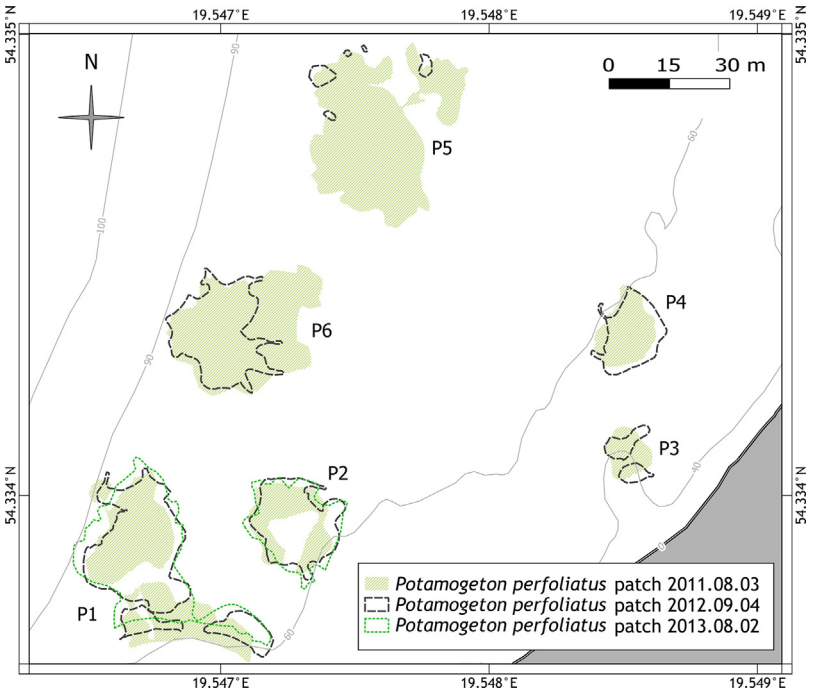

Figure 3 Changes in the surface area occupied by vegetation patches in the period 2011—2013. P1...P6 — numbers of patches.

distance from the shore of approximately 0—40 m), mid-littoral (depth 40—60 cm, distance from the shore of 20—50 m), and outer littoral (depth 60—90 cm, distance from the shore of 50—111 m).

3. Methods

The research was conducted in the years 2011—2014. The estimation of the length of the phytolittoral in the Polish part of the Vistula Lagoon occupied by emergent vegetation (EMV) was performed by means of Google Earth software (Google Inc., 2014—2016). Belts of emergent vegetation were identified, and their length was measured along the shoreline. The length of the shoreline free from reed rush (i.e. belts of artificially altered psammolittoral and littoral) was measured the same way. The identification of vegetation also applied aerial and satellite photographs publicly available online [http://geoportal.gov.pl (Geoportal, 2014), http://www.yandex.ru/maps/ (Yandex, 2014)].

Measurements of the outline of vegetation patches near Tolkmicko were performed by means of a GPS receiver (Garmin GPSMAP 60CSx) by wading along the boundary of vegetation on the water side. Results of the records were preliminarily processed in Garmin MapSource software. The resulting GIS layers were then loaded to Quantum GIS software for final processing and visualisation (Figs. 2 and 3). A density of plants was determined by counting reed stems per 0.25 m^2 plot, designated by means of a wooden frame without one side, which allowed for sliding the device into the thicket of vegetation (Bernatowicz, 1960). At each site, plant measurements were performed on 10 fields located at a distance of several metres from each other.

Research on the vegetation was also conducted along the entire shoreline on the Polish side of the lagoon. While paddling in a boat, the presence of submerged vegetation patches was recorded, and their surface area was estimated. Due to the dispersed character of the patches and their scarce degree of cover, quantitative measurements of density were not performed. Such measurements were performed in reference to reed assemblages at six selected sites (Table 2).

Bathymetric measurements in the littoral near Tolkmicko were performed by means of a ranging rod with accuracy to 1 cm on 2014.09.04. Depth was measured in 154 points with geographic coordinates determined by means of a GPS receiver (Garmin GPSMAP 60CSx). The memory of the receiver also recorded the course of the shoreline (zero depth). The data matrix was loaded to Surfer 10 software in which a detailed bathymetric map of the studied water body was generated by means of the kriging method. The map was then visually processed by means of Quantum GIS software (Figs. 2 and 3).

Water level was measured at study sites: 1I, 2M, 3O, 4I, 5M, and 6O in the years 2011—2012 by means of a gauge with a centimetre scale. In order to demonstrate full water level amplitude, six situations with extreme water levels were selected from maps generated by the hydrodynamic model of the Institute of Oceanography of the University of Gdańsk (Ecohydrodynamic Model, 2016). Readings from the model provided the basis for the calculation of the probable water level at measurement sites. Two sites were selected for the visualisation of water level fluctuations, namely the shallowest site 1I in EMV and one of the deepest ones in SUV — site 6O.

Continuous measurements of water temperature fluctuations at 10-min intervals were performed by means of temperature loggers Seamon Mini in the periods from 2011.07.20 to 2011.10.03 (sites 1I and 2M) and from 2012.04.21 to 2012.09.12 (site 1I). Single temperature and salinity measurements were performed by means of a sonde Saiv A/S STD-CTD model SD-202 or SD-204 at sites 1—6 in four terms in 2011. On 2—3.08.2011, daily water temperature and

Table 2 Density of *Phragmites australis* stems (±SD standard deviation) at sites around the Polish part of the Vistula Lagoon in 2014. Location of the sites in the vicinity of the mentioned municipalities are marked in Fig. 1. Sites sharing the same letter do not differ statistically (post hoc Friedman test).

Name of location near sampling site	Stems density [N m^{-2}] ± SD	Significant difference
Frombork	104 ± 27	c
Tolkmicko	70 ± 11	ac
Suchacz	76 ± 21	ac
Łaszka	62 ± 22	ac
Krynica Morska	56 ± 22	ab
Nowa Karczma	55 ± 17	ab

oxygenation fluctuations were also traced. The measurements were performed by means of a portable sonde at 21:30, 3:30, 9:30, and 14:45 at three sites in EMV (Sites: 1–3) and at three sites in SUV (Sites: 4–6). Measurements of solar radiation were performed in the EMV zone at site 2. They involved the application of two pyranometers of type LI-COR LI-200SA connected to a LI-COR datalogger. One pyranometer was placed on a mast above plant canopies, at a height of 2.73 m above the water surface, and the other at the base of plants, 0.14 m above the water surface. Solar radiation values [Wh m^{-2}] for a 48 h period were recorded between 2012.08.06 at 14:00 and 2012.08.08 at 14:00. Data were logged with 10 min intervals.

For the purpose of determination of the type of bottom sediments and their grain size composition, sediment cores were sampled in both zones (EMV and SUV) by means of a core sampler with a diameter of 4.4 cm, pushed into the bottom to a depth of 25 cm. At the laboratory, the sediments were dried and manually ground in a mortar, and then sieved on a set of geological sieves with the mesh of 2 mm, 1 mm, 0.5 mm, 0.25 mm, 0.125 mm, and 0.063 mm. The obtained data were processed with the application of GRADISTAT software version 8 (Blott and Pye, 2001). Organic matter content in sediment was determined by the direct method of mass losses on ignition at a temperature of 500°C.

Statistical analyses were performed by means of Statistica 10 software (StatSoft Inc, 2011). ANOVA Friedman and Wilcoxon tests were used in order to determine statistical differences (Sokal and Rohlf, 1995).

4. Results

4.1. Vegetation

Particular sections of the Polish shoreline of the Lagoon are occupied by EMV to different degrees: the northern section along the Vistula Spit, from the border to Skowronki, is occupied in 85%, the western section between Skowronki and Suchacz in 99%, and the southern section from the border to Suchacz in 74%.

The density of *P. australis* stems at six sites around the Polish part of the Vistula Lagoon varied from 55 stems m^{-2} ± 17 SD to 104 stems m^{-2} ± 27 (Table 2). The density statistically differed only between the site near Frombork and two sites (near Krynica Morska and Nowa Karczma) on the opposite side of the lagoon at the Vistula Spit [post hoc, ANOVA Friedman test: χ^2 (N = 10, df = 5, p = 0.00613) = 16.26437].

The ranges of the EMV patch, monitored near Tolkmicko, practically did not change in the years 2011–2013, as opposed to the ranges and sizes of SUV patches (Fig. 3). The surface area of *P. perfoliatus* patch 16P in the period 2011–2012 decreased approximately by half, and patch 15P practically entirely declined in 2012. In 2013, all patches inconsiderably increased their surface area.

Seasonal changes in plant density involved a gradual increase in the number of stems during the vegetative season. In the EMV zone, the highest (and relatively even) values of reed density were observed in late summer (132–158 stems m^{-2} in 2011) (Fig. 4).

The density of *P. perfoliatus* stems in the period from June to August only increased in deeper located patches in the mid- and outer littoral zones, and remained unchanged in the inner littoral (Fig. 5). In September, the commencement of the rapid process of dying-off of plants and disappearance of the patches was observed.

4.2. Water level fluctuations

Water level fluctuations were characterised by high dynamics with an amplitude of approximately 40 cm (Fig. 6). Data from the hydrodynamic model show that the performed field measurements did not reflect the full annual amplitude of changes, which could be much greater, leading to periodical exposure of the bottom at the shallowest site.

4.3. Salinity — seasonal changes

Water salinity varied from 1.4 PSU to 3.0 PSU (Fig. 7). Seasonal salinity dynamics, with an evident maximum

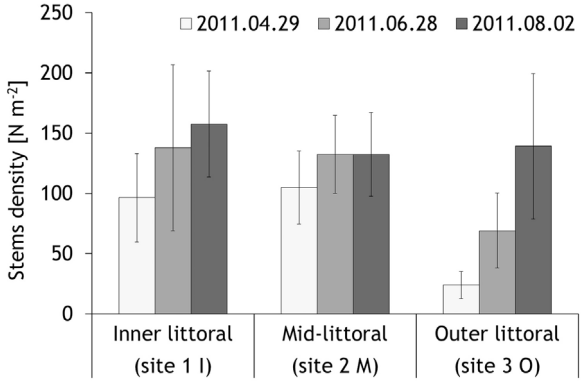

Figure 4 Seasonal changes in the density of *Phragmites australis* stems ± SD in the EMV zone. N — number of stems.

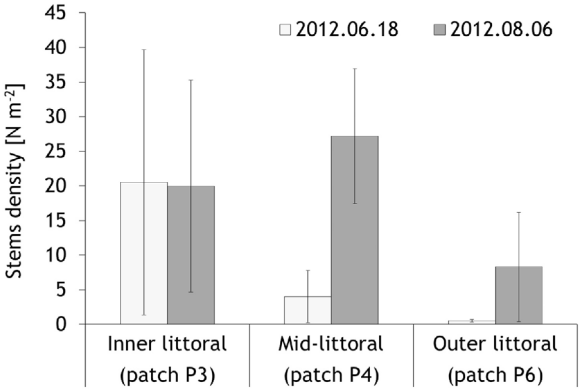

Figure 5 Seasonal changes in the density of *Potamogeton perfoliatus* stems ± SD in the SUV zone. Patch P5 in the outer littoral was not considered due to the very low stem density in June 2012 (0.07 stems m^{-2}) and its later complete disappearance.

recorded in autumn, showed a similar course at all sites, irrespective of the analysed zone, without significant statistic differences [ANOVA Friedman test: χ^2 (N = 3, df = 5, p = 0.095) = 9.37].

4.4. Temperature — seasonal changes

Water temperature changed seasonally [ANOVA Friedman test χ^2 (N = 6, df = 3, p = 0.00094) = 16.89; post hoc]. A greater amplitude of temperature fluctuations was recorded in the EMV zone (15.2—22.0°C) than in the SUV zone (16.4—21.7°C) (Fig. 8). In the EMV zone, water temperature developed differently at the shallowest sites (inner- and mid-littoral) than at the remaining ones, where the temperature distribution had a similar pattern [differences statistically non-significant [ANOVA Friedman test χ^2 (N = 4, df = 3, p = 0.91) = 0.53]. In the elodeid zone (SUV), where the spatial distribution of temperatures was even, no such dependency was observed [ANOVA Friedman test χ^2 (N = 4, df = 5, p = 0.078) = 9.89].

4.5. Temperature — diurnal changes

Water temperature in summer in a diurnal cycle varied from 19.4 to 22.8°C (Fig. 9). Diurnal changes in water temperature at two shallowest sites (shaded, and isolated from the open water zone, located in the reed belt (EMV)) had a different course from the remaining ones in the SUV zone, where they

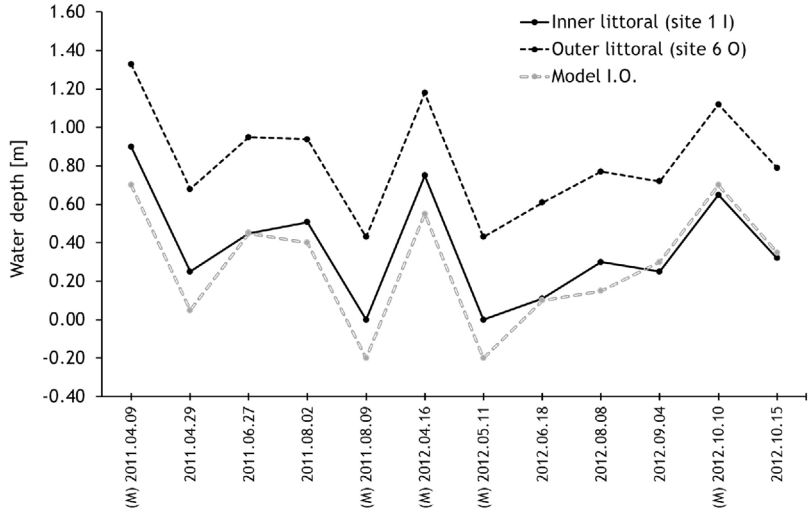

Figure 6 Changes in water depth in the period from 2011.04 to 2012.10 in the EMV zone — inner littoral and in the SUV zone — outer littoral based on field measurements. Additional data (dates marked with letter M) were obtained from the Ecohydrodynamic Model (Model I.O.) developed at the University of Gdańsk, Institute of Oceanography (Ecohydrodynamic Model, 2016).

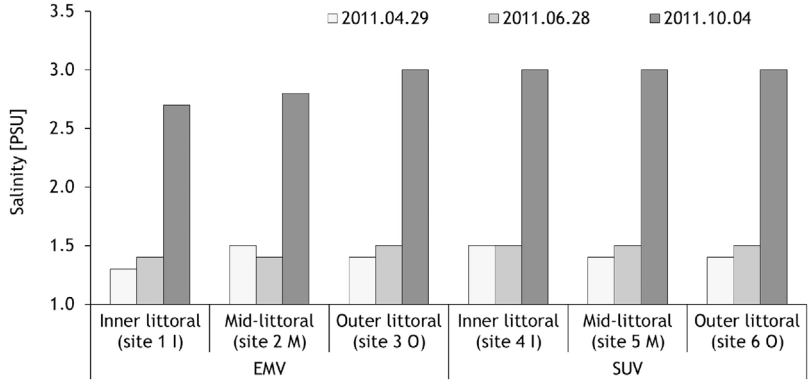

Figure 7 Seasonal changes in salinity in EMV and SUV zones. Numbers of sampling sites in brackets.

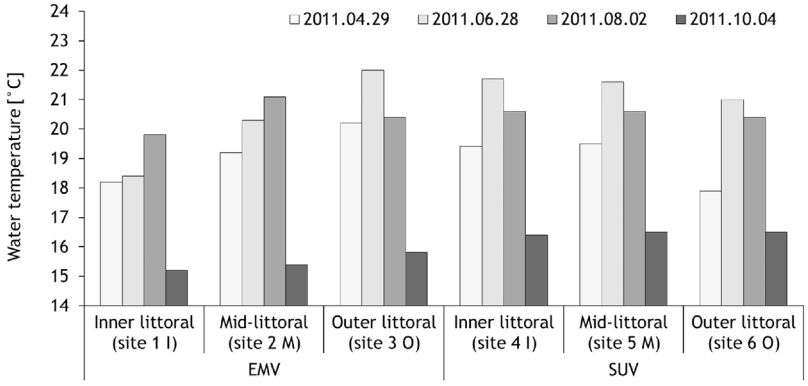

Figure 8 Seasonal changes in water temperature in EMV and SUV zones. Numbers of sites in brackets.

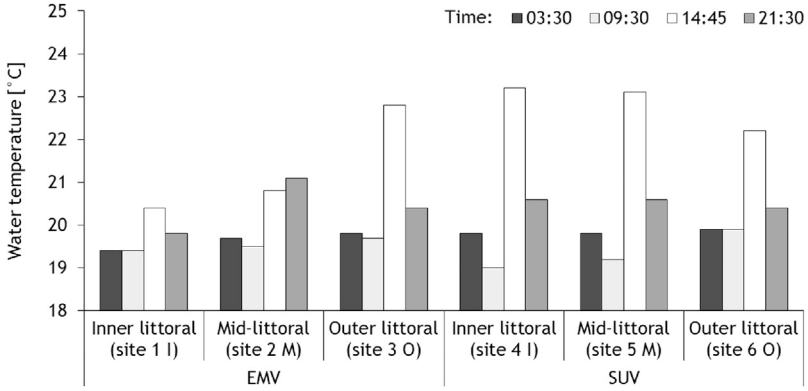

Figure 9 Diurnal changes in water temperature in EMV and SUV zones. Measurements performed on 1.08.—2.08.2011.

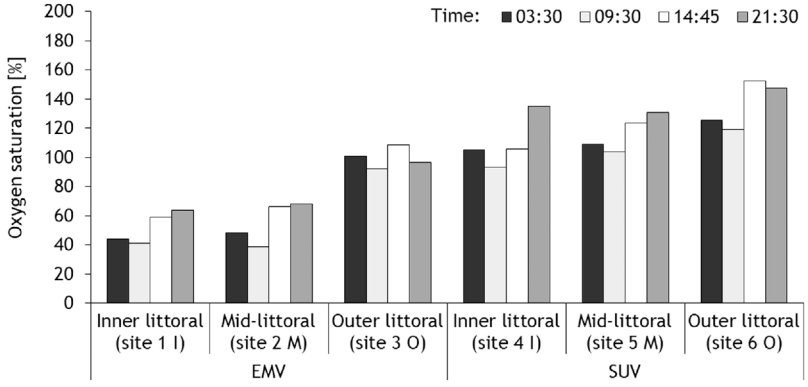

Figure 10 Diurnal changes in oxygen saturation in EMV and SUV zones. Measurements performed on 1.08.—2.08.2011.

developed in a similar way. The differences particularly concerned afternoon hours, when water temperature had relatively low values in the inner- and mid zone of EMV, and considerably higher values at the remaining sites. In the outer littoral zone of EMV, the diurnal amplitude of temperature fluctuations was similar to that at sites in the SUV zone.

4.6. Oxygen — diurnal changes

In summer, in a diurnal cycle, water saturation with oxygen varied from 39% to 152% in the EMV zone, and from 110% to 136% in the SUV zone (Fig. 10). The lowest values of oxygen saturation during the entire day were recorded at two shallowest sites (inner and mid-littoral) in the EMV zone. The course of oxygen saturation in the diurnal cycle was similar at all the sites, irrespective of the zone, with the lowest values in morning hours, and the highest in the evening.

4.7. Solar radiation — diurnal changes

Insolation in the analysed zone changed substantially in the diurnal cycle (Fig. 11). Maximum mean hourly solar radiation

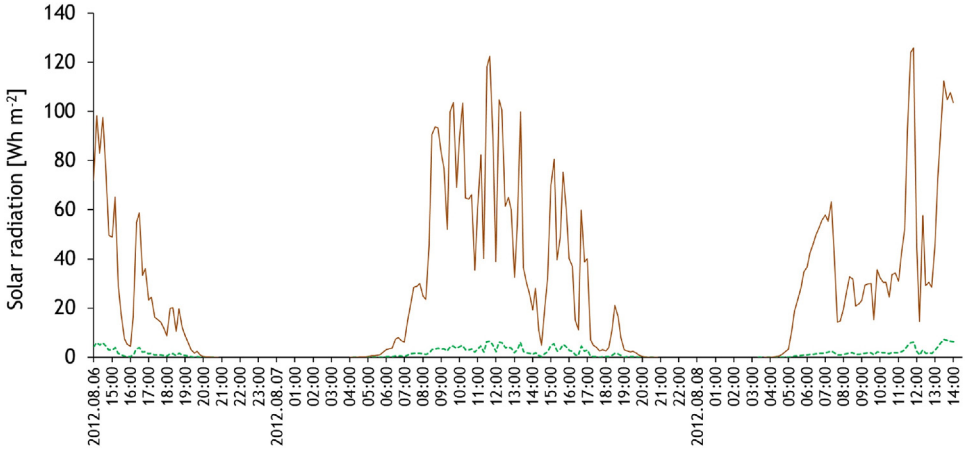

Figure 11 48-hour record of changes in solar radiation reaching the EMV and SUV zones (solid line), and water surface under plant canopies inside EMV (dotted line). Measurements performed on 2012.08.06–08.

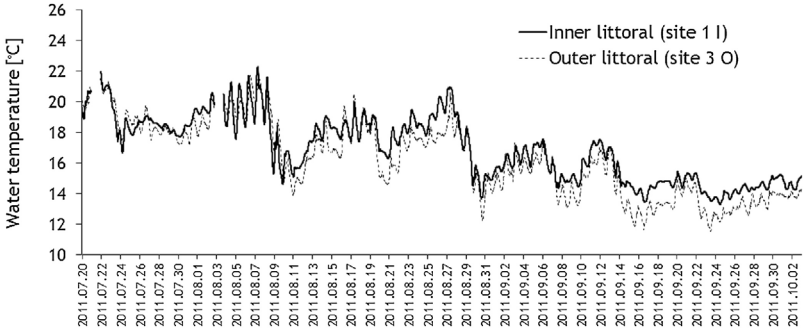

Figure 12 Results of continuous measurements of water temperature fluctuations in the inner- and outer littoral in the EMV zone (2011.07.20–2011.10.02).

amounted to 86.2–104.6 Wh m^{-2}. Under canopies of EMV, right above the water surface, it amounted to (4.7–6.6 Wh m^{-2}) and was considerably lower [Wilcoxon Test: T ($Z = 12.354$, $N = 203$, $p < 0.01$) = 0], constituting only approximately 6% of the total supplied solar radiation.

4.8. Temperature — continuous measurements of energy accumulation

Water temperatures in the majority of terms in the inner littoral zone of EMV near the shore were higher than in the outer littoral zone bordering on the open water zone (Fig. 12). Also mean temperature in the inner littoral (16.92°C) was significantly higher than in the outer littoral zone (16.24°C) [Wilcoxon Test: T ($Z = 70.285$, $N = 10\,597$, $p < 0.01$) = 5 941 811].

4.9. Sediments

In the EMV zone, bottom sediments were primarily composed of fine fractions (very fine sand, very coarse silt) (Fig. 13). In the SUV zone, sediments with coarser grains occurred, in particular, fine sand and medium sand were present. Both zones showed a tendency for increasing contribution of coarse-grained fractions with growing depth and distance from the shore.

Organic matter content in bottom sediments was highest in the inner littoral of the EMV zone (3.1%), and lowest in the mid-littoral of SUV zone (0.4%) (Fig. 14). With growing depth, the recorded values showed a decreasing tendency in EMV and an increasing one in SUV.

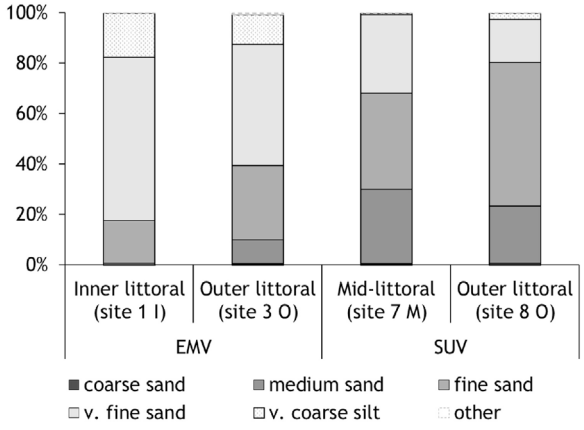

Figure 13 Percentage of particular fractions of bottom sediments in EMV and SUV zones (2012.08.08).

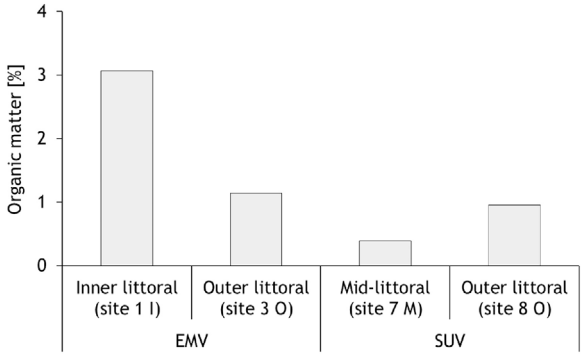

Figure 14 Organic matter content in bottom sediments in EMV and SUV zones (2012.08.08).

5. Discussion

5.1. Impact of vegetation on physical water properties

The research revealed that submerged vegetation has no substantial effect on the habitat conditions in the analysed littoral area. Irrespective of distance from shore, depth, and place within patches, physical water parameters in the SUV zone were similar. This may result from a relatively small surface area of the patches and low plant density, as well as from the observed substantial changes in ranges of the patches in particular years (Fig. 3). The conclusion concerning lack of evident effect of SUV on habitat conditions can be probably transposed to the entire northern and southern shore of the lagoon, where the occurrence of submerged macrophytes is very scarce. A different situation can be expected in the western part of the lagoon, where dense submerged vegetation covers extensive areas (Fig. 1). This is suggested by frequently observed even three times higher water transparency (Różańska and Więcławski, 1978; Szarejko-Łukaszewicz, 1959; Żmudziński and Szarejko, 1955), and approximately a dozen times lower chlorophyll concentrations (Latała, 1978) in the western part of the lagoon than in the remaining areas in spite of similar nutrient concentrations. The dependencies were often associated with the different degree of development of submerged macrophytes (Kornijów, 2018; Latała, 1978; Pliński and Simm, 1978; Renk et al., 2001; Ringer, 1959; Żmudziński and Szarejko, 1955).

Mean density of reed stems determined in the Vistula Lagoon (74 stems $m^{-2} \pm 18$) corresponded with the top values determined in local channels (Boszke et al., 2005), as well as in freshwater and brackish ecosystems of the North America, where reed is an invasive species (Meyerson et al., 2000). It was within the lower range of maximum density values (60–250 m^{-2}) reported from different aquatic environments of Europe by Haslam (1973).

Unlike SUV, the extensive patches of densely growing EMV had a considerable modifying effect on certain physical water parameters (Fig. 15). The effect particularly involved the diversification of lighting conditions and temperature. The energy of solar radiation reaching the reed patch (EMV) was largely reflected and dispersed on the surface of plants, as confirmed by other studies (Grant, 1987; Ondok, 1973). The photosynthetically useful part of the spectrum (PAR) is absorbed by plants and used for photosynthesis (McCree, 1981). The remaining part of the radiation is transformed into heat. Such transformations probably resulted in the observed higher than average water temperature values in the EMV zone.

Differences in temperatures along sections at different distances from the shore and with different depths suggest the variable intensity of water mixing, related to the suppression of the kinetic energy of wave action by densely

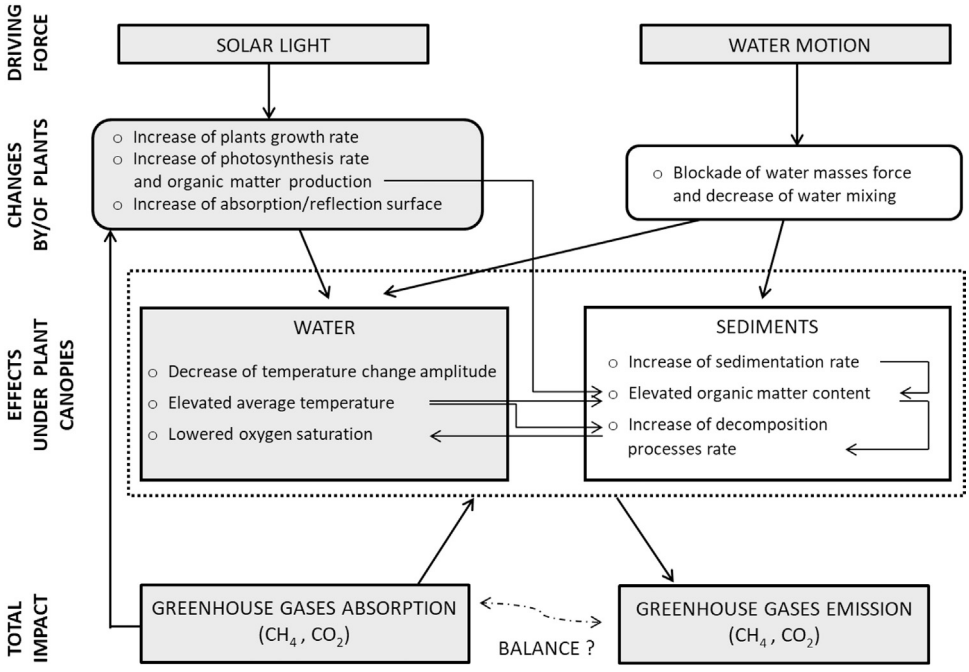

Figure 15 Simplified ideogram of some dependencies and processes related to the presence of macrophytic assemblages in the analysed area. Grey fields concern both SUV and EMV, white fields — only EMV.

growing plant stems. According to Kornijów (2018), the crucial driver regulating the structure and processes occurring in the Vistula Lagoon is wave exposure. Therefore, low rate of water exchange between the littoral and open water zone, and attenuation of the mechanical effect of waves by near-shore vegetation are very important in terms of protection of shores against destructive wave action and erosion (Moller et al., 2011; Rupprecht et al., 2017). Near-shore vegetation is also known to play an important role as a filter for nutrients and organic material flushed from the catchment (Berthold et al., 2018; McGlathery et al., 2007). Moreover, it creates a habitat not only for water organisms, but also for those associated with land, namely amphibians, waterfowl, and mammals.

Due to its high heat capacity, water is a good indicator of energy accumulation in a longer term. The comparison of several months of temperature measurements within EMV and at the boundary of the zone showed that as a result of both a decrease in water mixing and absorption of solar radiation causing air heating within EMV, mean water temperature in summer amongst the reed rush was higher than in the remaining area of the water body. In spring and autumn, the pattern was opposite.

The summer diurnal amplitude of temperature fluctuations in the EMV zone was also lower than in other zones, probably due to the effect of shading by plant canopies and heat inertia of water. It is very likely, that the shading effect by reed stems results in the inhibition of development of other plants in reed rush patches. In consequence, in the Vistula Lagoon, it is primarily composed of a monoculture of *P. australis*, which is interpreted as a manifestation of good condition of the plant assemblage (Haslam, 1973).

Uniform diurnal water oxygenation in the inner and mid-littoral of EMV zone was probably the effect of intensive decomposition processes, as well as a decrease in the intensity of photosynthesis due to very limited access of sunlight to the water surface, as also emphasised by Viaroli et al. (1996). It can also be related to limited water exchange between the rush patch and the open water. In the outer littoral of EMV zone, water oxygenation was considerably higher throughout the day, but it was also uniform in time. This could be determined by continuous mixing with the well-aerated deeper water. Considerable oxygenation drops below 40% can substantially limit the occurrence of animals, both invertebrates and fish (Able and Hagan, 2000; Warren et al., 2001).

No significant differences were observed in salinity within the EMV patch. Water salinity in the Vistula Lagoon is probably not sufficient for a considerable salinity gradient to develop as a result of limiting water mixing by vegetation.

In conclusion, the stated hypothesis in reference to water parameters proved supported only in the case of the reed rush which considerably modified lighting conditions, temperature, and water oxygenation, particularly in warm seasons of the year when reed density was high.

5.2. Impact of vegetation on sediments

Within the SUV zone, no considerable differences were observed in the composition of bottom sediments. This was probably caused by the fact that processes occurring in sediments are largely determined by the mechanical movement of water masses and strong and even insolation the intensity of which could not be affected by macrophytes showing a low degree of cover and density.

In the EMV zone, limited mixing of water masses could favour sediment deposition and permit sedimentation of finer fractions of dead organic matter. This probably led to the observed shallowing and occurrence of sediments with an increased contribution of organic matter. Organic matter content in bottom sediment in the EMV zone, next to limited water mixing, is undoubtedly also determined by the presence of plants dying in masses in autumn (Kuehn et al., 2000).

The stated hypothesis in reference to bottom sediments was supported only in the case of the reed rush which considerably modified the grain size composition of sediments and content of organic matter.

5.3. Total impact

Wetlands are among the most ecologically valuable environments (Mitsch et al., 2013). The key importance of wetlands for the ecosystem, involving e.g. their contribution in primary production, in matter circulation, or water storage, was described by many authors (among others: Kuehn et al., 2000; Mitsch et al., 2013). A particular role in the littoral-wetland environment is played by emergent plant assemblages (Wetzel and Hough, 1973). Their presence influences a number of biochemical processes such as production and decomposition of organic matter (Kuehn et al., 2000), and physical and chemical processes such as release of greenhouse gases: methane (Ding et al., 2005; Olsson et al., 2015) and carbon dioxide (Kuehn and Suberkropp, 1998). Wetlands are among ecosystems absorbing CO_2 (Bekele et al., 2016; Bernal and Mitsch, 2012) and CH_4 (Olsson et al., 2015). The balance of absorption and release of greenhouse gases differs, however, depending on the characteristics of particular wetlands (Bekele et al., 2016; Bernal and Mitsch, 2012; Ding et al., 2005), including the species composition of the vegetation (Kim et al., 1998; Olsson et al., 2015). Plants from genus *Phragmites* belong to the most common plants in wetlands, and rapidly expand the area of its occurrence all over the word (Able and Hagan, 2000; Haslam, 1973; Lelong et al., 2007; Meyerson et al., 2000; Próchnicki, 2005; Warren et al., 2001; Weisner, 1991), also as a result of human activities aimed at limiting areas under agricultural use (Huryna and Pokorny, 2016). Results of the cited studies permit stating the hypothesis that also in the marshy environment of the littoral of the Vistula Lagoon, abundantly covered with vegetation, as well as others lagoons of the Baltic Sea, analogical processes occur that may have a specific impact on climatic changes. The scale of such impact, however, requires further research aimed at among others the determination of the production balance, and release and absorption of greenhouse gases.

Acknowledgements

The research was conducted as a part of statutory activities of the Department of Fishery Oceanography and Marine Ecology of the National Marine Fisheries Research Institute, project number: DOT16/Vistula.

References

Able, K.W., Hagan, S.M., 2000. Effects of common reed (*Phragmites australis*) invasion on marsh surface macrofauna: Response of fishes and decapod crustaceans. Estuaries 23 (5), 633—646, http://dx.doi.org/10.2307/1352890.

Barko, J.W., James, W.F., 1998. Effects of submerged aquatic macrophytes on nutrient dynamics, sedimentation, and resuspension. In: Jeppesen, E., Søndergaard, M., Søndergaard, M., Christoffersen, K. (Eds.), The structuring role of submerged macrophytes in lakes. Ecol. Stu. An., Vol. 131. Springer, New York 197—214, https://doi.org/10.1007/978-1-4612-0695-8_10.

Bekele, T., Lemma, B., Mengistou, S., 2016. Carbon sequestration potentials of selected wetlands at Lake Ziway, Ethiopia. J. Environ. Earth Sci. 6 (9), 1—9.

Bernal, B., Mitsch, W.J., 2012. Comparing carbon sequestration in temperate freshwater wetland communities. Glob. Change Biol. 18 (5), 1636—1647, http://dx.doi.org/10.1111/j.1365-2486.2011.02619.x.

Bernatowicz, S., 1960. Methods of examination of vascular vegetation in lakes. Roczniki Nauk Rolniczych 77 (B-l), 61—78, (in Polish).

Berthold, M., Karstens, S., Buczko, U., Schumann, R., 2018. Potential export of soluble reactive phosphorus from a coastal wetland in a cold-temperate lagoon system: Buffer capacities of macrophytes and impact on phytoplankton. Sci. Total Environ. 616—617, 46—54, http://dx.doi.org/10.1016/j.scitotenv.2017.10.244.

Blott, S.J., Pye, K., 2001. GRADISTAT: A grain size distribution and statistics package for the analysis of unconsolidated sediments. Earth Surf. Proc. Land. 26 (11), 1237—1248, http://dx.doi.org/10.1002/esp.261.

Boszke, P., Bociag, K., Szmeja, J., 2005. Population structure and regeneration of *Phragmites australis* (Cav.) Trin. ex Steud in flood control ditches in the depression wetland (Żuławy Wiślane, Northern Poland). Pol. J. Ecol. 53 (1), 3—12.

Carpenter, S.R., Lodge, D.M., 1986. Effects of submersed macrophytes on ecosystem processes. Aquatic Botany 26, 341—370, http://dx.doi.org/10.1016/0304-3770(86)90031-8.

Chubarenko, B.V., 2008. The Vistula Lagoon. In: Chubarenko, B.V. (Ed.), Transboundary waters and basins in the south-east Baltic, Terra Baltica, Kaliningrad, 37—57, ISBN 978-5-98777-031-3.

Chen, R.L., Barko, J.W., 2011. Effects of fresh-water macrophytes on sediment chemistry. J. Freshwater Ecol. 4 (3), 279—289, http://dx.doi.org/10.1080/02705060.1988.9665177.

Ding, W., Cai, Z., Tsuruta, H., 2005. Plant species effects on CH_4 emissions from freshwater marshes. Atmos. Environ. 39 (18), 3199—3207, http://dx.doi.org/10.1016/j.atmosenv.2005.02.022.

Ecohydrodynamic Model, 2016. Ecohydrodynamic Model. The Gulf of Gdańsk including the Vistula Lagoon. Inst. Oceanograph. Univ. Gdańsk. http://model.ocean.univ.gda.pl/ (accessed 05.11.16.).

Gajewski, L. (Ed.), 2010. Research of the Vistula Lagoon bottom (including the Elbląg Bay).Final Report. Rep. No. 334 by the Maritime Institute in Gdańsk for the Maritime Office in Gdynia, 1—96, (in Polish).

Geoportal, 2014. Geoportal, http://geoportal.gov.pl/, (accessed 2014).

Google Inc., 2014—2016. Google Earth computer software, (accessed 2014).

Grant, L., 1987. Diffuse and specular characteristics of leaf reflectance. Remote Sensing of Environment 22 (2), 309—322, http://dx.doi.org/10.1016/0034-4257(87)90064-2.

Haslam, S.M., 1973. Some aspects of the life history and autecology of *Phragmites communis* Trin. — A review. Pol. Arch. Hydrobiol. 20, 79—100.

Horppila, J., Nurminen, L., 2005. Effects of different macrophyte growth forms on sediment and P resuspension in a shallow lake. Hydrobiologia 545 (1), 167—175, http://dx.doi.org/10.1007/s10750-005-2677-9.

Huryna, H., Pokorny, J., 2016. The role of water and vegetation in the distribution of solar energy and local climate: A review. Folia Geobot. 51 (3), 191—208, http://dx.doi.org/10.1007/s12224-016-9261-0.

Kim, J., Verma, S.B., Billesbach, D.P., Clement, R.J., 1998. Diel variation in methane emission from a midlatitude prairie wetland: Significance of convective through flow in *Phragmites australis*. J. Geophys. Res. — Atmos. 103 (D21), 28029—28039, http://dx.doi.org/10.1029/98JD02441.

Kornijów, R., 2018. Ecosystem of the Polish part of the Vistula Lagoon from the perspective of alternative stable states concept, with implications for management issues. Oceanologia 60 (3), 1—15, http://dx.doi.org/10.1016/j.oceano.2018.02.004.

Kruk, M., Rychter, A., Mróz, M. (Eds.), 2012. The Vistula Lagoon. Environment and its research in the VISLA project. PWSZ, Elbląg, 1—178.

Kuehn, K.A., Suberkropp, K., 1998. Diel fluctuations in rates of CO_2 evolution from standing dead leaf litter of the emergent macrophyte *Juncus effusus*. Aquat. Microbial Ecol. 14 (2), 171—182, http://dx.doi.org/10.3354/ame014171.

Kuehn, K.A., Lemke, M.J., Suberkropp, K., Wetzel, R.G., 2000. Microbial biomass and production associated with decaying leaf litter of the emergent macrophyte *Juncus effusus*. Limnol. Oceanogr. 45 (4), 862—870, http://dx.doi.org/10.4319/lo.2000.45.4.0862.

Latała, A., 1978. Chlorophyll concentration in the waters of the Vistula Lagoon. Stud. Mater. Oceanol. 4 (21), 81—94, (in Polish).

Lelong, B., Lavoie, C., Jodoin, Y., Belzile, F., 2007. Expansion pathways of the exotic common reed (*Phragmites australis*): A historical and genetic analysis. Divers. Distrib. 13 (4), 430—437, http://dx.doi.org/10.1111/j.1472-4642.2007.00351.x.

McCree, K.J., 1981. Photosynthetically active radiation. In: Lange, O.L., Nobel, P.S., Osmond, C.B., Ziegler, H. (Eds.), Physiological plant ecology I. Encyclopedia of plant physiology (New Series) 12/A. Springer, Berlin, Heidelberg, 41—55, http://dx.doi.org/10.1007/978-3-642-68090-8_3.

McGlathery, K.J., Sundback, K., Anderson, I.C., 2007. Eutrophication in shallow coastal bays and lagoons: The role of plants in the coastal filter. Mari. Ecol. Progr. Ser. 348, 1—18, http://dx.doi.org/10.3354/meps07132.

Meyerson, L.A., Saltonstall, K., Windham, L., Kiviat, E., Findlay, S.A., 2000. A comparison of *Phragmites australis* in freshwater and brackish marsh environments in North America. Wetl. Ecol. Manag. 8 (2—3), 89—103, http://dx.doi.org/10.1023/A:1008432200133.

Miranda, L.E., Driscoll, M.P., Allen, M.S., 2000. Transient physicochemical microhabitats facilitate fish survival in inhospitable aquatic plant stands. Freshwater Biol. 44 (4), 617—628, http://dx.doi.org/10.1046/j.1365-2427.2000.00606.x.

Mitsch, W.J., Bernal, B., Nahlik, A.M., Mander, Ü., Zhang, L., Anderson, L., Jørgensen, S.E., Brix, H., 2013. Wetlands, carbon, and climate change. Landscape Ecol. 28 (4), 583—597, http://dx.doi.org/10.1007/s10980-012-9758-8.

Moller, I., Mantilla-Contreras, J., Spencer, T., Hayes, A., 2011. Microtidal coastal reed beds: Hydro-morphological insights and observations on wave transformation from the southern Baltic Sea. Estuar. Coastal Shelf Sci. 92 (3), 424—436, http://dx.doi.org/10.1016/j.ecss.2011.01.016.

Moller, C.L., Sand-Jensen, K., 2012. Rapid oxygen exchange across the leaves of *Littorella uniflora* provides tolerance to sediment anoxia. Freshwater Biol. 57 (9), 1875—1883, http://dx.doi.org/10.1111/j.1365-2427.2012.02849.x.

Nawrocka, L., Kobos, J., 2011. The trophic state of the Vistula Lagoon: An assessment based on selected biotic and abiotic parameters according to the Water Framework Directive. Oceanologia 53 (3), 881—894, http://dx.doi.org/10.5697/oc.53-3.881.

Odum, E.P., 1971. Fundamentals of ecology. W.B. Saunders Co., Philadelphia, London, Toronto, 1—574.

Olsson, L., Ye, S., Yu, X., Wei, M., Krauss, K.W., Brix, H., 2015. Factors influencing CO_2 and CH_4 emissions from coastal wetlands in the Liaohe Delta, Northeast China. Biogeosciences 12 (16), 4965–4977, http://dx.doi.org/10.5194/bg-12-4965-2015.

Ondok, J.P., 1973. Some basic concepts of modeling freshwater littoral ecosystems with respect to radiation regime of a pure *Phragmites* stand. Pol. Arch. Hydrobiol. 20 (1), 101–109.

Perez-Ruzafa, A., Marcos, C., Perez-Ruzafa, I.M., Perez-Marcos, M., 2011. Coastal lagoons: "Transitional ecosystems" between transitional and coastal waters. J. Coast. Conserv. 15 (3), 369–392, http://dx.doi.org/10.1007/s11852-010-0095-2.

Pliński, M., Simm, A., 1978. Seasonal fluctuations in the composition, distribution and quantity of phytoplankton in the Vistula Lagoon in 1974 and 1975. Stud. Mater. Oceanol. 4 (21), 53–80.

Próchnicki, P., 2005. The expansion of common reed (*Phragmites australis* (Cav.) Trin. ex Steud.) in the anastomosing river valley after cessation of agriculture use (Narew River Valley, NE Poland). Pol. J. Ecol. 53 (3), 353–364.

Renk, H., Ochocki, S., Zalewski, M., Chmielowski, H., 2001. Environmental factors controlling primary production in the Polish part of the Vistula Lagoon. Bull. Sea Fish. Inst. 1 (152), 77–95.

Ringer, Z., 1959. An attempt to estimate the biomass of the littoral flora of the Vistula Lagoon based on the studies carried out in 1955. Prace Morskiego Instytutu Rybackiego w Gdyni 10 (A), 193–214.

Różańska, Z., Więcławski, F., 1978. Study of environmental factors of the Vistula Lagoon under human pressure. Studia Mat. Oceanol., Biologia Morza 4 (21), 9–36, (in Polish).

Rupprecht, F., Moller, I., Paul, M., Kudella, M., Spencer, T., Van Wesenbeeck, B.K., Wolters, G., Jensen, K., Bouma, T.J., Miranda-Lange, M., Schimmels, S., 2017. Vegetation–wave interactions in salt marshes under storm surge conditions. Ecol. Eng. 100, 301–315, http://dx.doi.org/10.1016/j.ecoleng.2016.12.030.

Scheffer, M., Hosper, S.H., Meijer, M.L., Moss, B., Jeppesen, E., 1993. Alternative equilibria in shallow lakes. Trends Ecol. Evol. 8 (8), 275–279, http://dx.doi.org/10.1016/0169-5347(93)90254-M.

Sokal, R.I., Rohlf, J., 1995. Biometry: The principle and practice of statistics in biological research. Freeman & Co, New York, 1–887.

StatSoft Inc., 2011. STATISTICA (data analysis software system), version 10. Available from www.statsoft.com.

Szarejko-Łukaszewicz, D., 1959. Hydrographic research on the Vistula Lagoon in 1953–1954. Prace Morskiego Instytutu Rybackiego w Gdyni 10 (A), 215–228, (in Polish).

Viaroli, P., Bartoli, M., Bondavalli, C., Christian, R.R., Giordani, G., Naldi, M., 1996. Macrophyte communities and their impact on benthic fluxes of oxygen, sulphide and nutrients in shallow eutrophic environments. Hydrobiologia 329 (1–3), 105–119, http://dx.doi.org/10.1007/BF00034551.

Viaroli, P., Bartoli, M., Giordani, G., Naldi, M., Orfanidis, S., Zaldivar, J.M., 2008. Community shifts, alternative stable states, biogeochemical controls and feedbacks in eutrophic coastal lagoons: A brief overview. Aquat. Conserv. 18 (S1), 105–117, http://dx.doi.org/10.1002/aqc.956.

Warren, R.S., Fell, P.E., Grimsby, J.L., Buck, E.L., Rilling, G.C., Fertik, R.A., 2001. Rates, patterns, and impacts of *Phragmites australis* expansion and effects of experimental Phragmites control on vegetation, macroinvertebrates, and fish within tidelands of the lower Connecticut River. Estuaries 24 (1), 90–107, http://dx.doi.org/10.2307/1352816.

Weisner, S.E.B., 1991. Within-lake patterns in depth penetration of emergent vegetation. Freshwater Biol. 26 (1), 133–142, http://dx.doi.org/10.1111/j.1365-2427.1991.tb00515.x.

Wetzel, R.G., Hough, R.A., 1973. Productivity and role of aquatic macrophytes in lakes: An assessment. Polish Archive of Hydrobiology 20, 9–19.

Yandex, 2014. Yandex — Maps, https://www.yandex.ru/maps/, (accessed 2014).

Zachowicz, J., Uścinowicz, Sz., Anolik, P., Zaleszkiewicz, L., Krzymińska, J., Jegliński, W., 1995. Geological survey of the Vistula Lagoon area. Archiwum OGM, PIG, Gdańsk, (in Polish).

Żmudziński, L., Szarejko, D., 1955. Hydrographic and biological studies of the Vistula Lagoon. Prace Morskiego Instytutu Rybackiego w Gdyni 8, 284–312, (in Polish).

Oceanologia (2019) 61, 38—49

Available online at www.sciencedirect.com

ScienceDirect

journal homepage: www.journals.elsevier.com/oceanologia/

ORIGINAL RESEARCH ARTICLE

Effects of atmospheric circulation on water temperature along the southern Baltic Sea coast

Józef Piotr Girjatowicz, Małgorzata Świątek *

Unit of Hydrology and Water Management, Faculty of Geosciences, University of Szczecin, Szczecin, Poland

Received 11 May 2017; accepted 5 June 2018
Available online 10 July 2018

KEYWORDS
Circulation patterns;
Water temperature;
Correlation;
Regression;
Relationship;
Coastal zone

Summary The relationships between atmospheric circulation patterns and water surface temperature along the coast of the southern Baltic Sea were studied. Seasonal water temperature values for Świnoujście, Międzyzdroje, Kołobrzeg, Władysławowo, Hel and Gdynia stations measured during the period of 1951—2010 were used. The methods of correlation and regression were applied to determine the relationships between water temperature and the number of days of atmospheric circulation patterns.

It was demonstrated that the strongest relationships occur in winter, chiefly on account of intense atmospheric circulation activity and weaker effects of solar radiation. The relationships with western circulation are slightly stronger than that associated with the eastern circulation. During the remaining seasons, those dependencies are clearly weaker. Asynchronous relationships between water temperature and atmospheric circulation are less pronounced than the synchronous ones. Despite being weaker, the asynchronous relations are still statistically significant, mainly in the spring season and as such, they may have a prognostic significance.

1. Introduction

The surface water temperature along the southern coast of the Baltic Sea depends mostly on the solar radiation and thermal properties of air masses as well as on the water circulation. In general, the SST depends on the heat transfer between air mass and water surface — the exchange that includes the processes of convection and turbulence movements, phase transitions, thermal conductivity and radiation. However, it is the atmospheric circulation that is the

* Corresponding author at: Unit of Hydrology and Water Management, Faculty of Geosciences, University of Szczecin, Ul. Mickiewicza 16, 70—383 Szczecin, Poland
E-mail addresses: jozef.girjatowicz@usz.edu.pl (J.P. Girjatowicz), malgorzata.swiatek@usz.edu.pl (M. Świątek).
Peer review under the responsibility of Institute of Oceanology of the Polish Academy of Sciences.

ELSEVIER Production and hosting by Elsevier

https://doi.org/10.1016/j.oceano.2018.06.002

principal climate-shaping factor affecting water thermal conditions in the cold season (Leppäranta and Myrberg, 2009; Omstedt et al., 2014). In turn, during the warm season (spring, summer) solar radiation has a dominant influence on the water thermal conditions (Miętus, 1999). In addition, Stramska and Białogrodzka (2015) showed significant correlations between the NAO index value and the Baltic Sea SST in winter, with a simultaneous lack of significant relations between the average annual values.

The relations between the Baltic Sea SST and atmospheric circulation were also studied by, i.a. Siegel et al. (2008). Strong relationships have been demonstrated between the atmospheric circulation during January–March period and the water temperature in March. In case of the Arkona Basin, the SST in March correlated with monthly North Atlantic Oscillation (NAO) index for three cold months (January–March) and the determination coefficient amounted to 0.84, while for the analogous correlations with Arctic Oscillation (AO) index, the coefficient amounted to 0.6. Additionally, the correlation with the Baltic Winter Index (WIBIX) introduced by Hagen and Feinstel (2005) was calculated as 0.86.

As for the southern coasts of the Baltic Sea, the relationships between the NAO index and SST in winter months (December–February) were weaker (Girjatowicz, 2008). The determination coefficients fluctuated in the range of 0.41–0.56.

The NAO and AO are the phenomena related to the hemispherical atmospheric circulation, whereas WIBIX is related to the regional circulation. The relations of SST in the Bornholm Basin showed respective determination coefficients of 0.8, 0.61 and 0.77. Atmospheric circulation (defined by NAO, AO and WIBIX) has the strongest impact on the minimum temperature and ice range in March. On that account, the index values during January–March period (JFM) demonstrate the strongest correlations with March surface water temperature (Hagen and Feinstel, 2005). According to the study of Siegel et al. (2006), the WIBIX index is correlated with the minimum water temperature during winter in the Arkona Basin, i.e. a site located relatively close to the area analysed in the study.

In literature, the influence of atmospheric circulation on the air temperature was analysed far more frequently than its influence on the water temperature. The variability and values of both variables for the southern Baltic Sea demonstrate substantial convergence (Siegel et al., 1999; Stramska and Białogrodzka, 2015), e.g. water temperature in both the Arkona Basin as well as the Danish Straits shows, more or less, a monthly delay in relation to air temperature value in Warnemünde (Siegel et al., 1999). The highest average SST value can be observed in August and the lowest in February–March (Bradtke et al., 2010), due to a slower reaction of the water temperature to the solar radiation inflow compared to the air temperature reaction. The research conducted by Stramska and Białogrodzka (2015) showed significant correlations between the NAO index value and SST for the Baltic Sea in winter with a simultaneous lack of significant relations between average annual values.

The influence of directions of air masses advection on surface water temperature distribution in the Baltic Sea was also analysed on the basis of satellite data by Kozlov et al. (2012) and Siegel et al. (1996, 1999). Satellite data analyses were used to determine the time and place of the water temperature decrease alongside the coast in the summer months caused by upwelling (Gurova et al., 2013; Lehmann et al., 2012; Uiboupin and Laanemets, 2009).

Currently, at the SatBałtyk system site (satbaltyk.iopan.gda.pl), ongoing hydrometeorological characteristics of the Baltic Sea are posted four times daily. The SST satellite observations are one of the fundamental SatBałtyk products complemented by model data of the cloud-covered regions. The principles of functioning and the characteristics of the products obtained within the framework of the SatBałtyk project were described in the publications of Paszkuta and his team (Paszkuta et al., 2012) as well as in the publications of Woźniak and his team (Woźniak et al., 2008, 2011a, 2011b).

A difference of surface water temperature between the littoral zone and open waters of the southern Baltic Sea is noticeable. The average annual water temperature is slightly higher in the littoral zone. Greater differences are evident in individual seasons. In spring, the water temperature in the littoral zone is higher by 4°C on average, than that at the open sea. Similar differences, although lower in value, are observed in summer. In winter and autumn, the waters of the open southern Baltic Sea are warmer than the waters in the littoral zone by approximately 2°C (Cyberska, 1994). This difference is most visible in the region of Pomeranian Bay, chiefly due to the local conditions, such as bathymetry and the inflow of river waters.

In this work, atmospheric circulation was described with the use of the circulations types defined in accordance with Lityński's method. The first analytic surveys regarding the impact of atmospheric circulation types on water temperature (based on Lityński's method (1969)), were undertaken in 1999 (Girjatowicz, 1999). It was found that during the six cold months (October, November, December, January, February and March) those relationships become statistically significant; even at the level of α = 0.01, when individual circulation types are combined into sectors, and individual months into periods of several months. However, the research referred only to Międzyzdroje and Władysławowo during the colder seasons (October–March) between the years 1951 and 1990. The problem that still needs to be examined concerns Lityński's individual atmospheric circulation types occurrence and their influence on the water temperature of the southern Baltic Sea coast. The following questions remain: What are the strength and statistical significance of such relationships? Does the strength of those relationships vary in terms of space and season? Which of the non-circulation factors can affect such variations?

The purpose of the paper is to determine and examine the correlations between the atmospheric circulation patterns (specified in accordance with Lityński's classification) and surface water temperature along the southern coast of the Baltic Sea, using the data from possibly the longest timespan (1951–2010), encompassing all seasons of the year (December–February, March–May, June–August, September–November). In addition, the spatial and seasonal variability of the strength of the relationships, as well as the contribution of non-atmospheric factors, were investigated.

2. Material and methods

In this study, average seasonal values of surface water temperature on the southern coast of the Baltic Sea were used for individual seasons: winter (December–February), spring

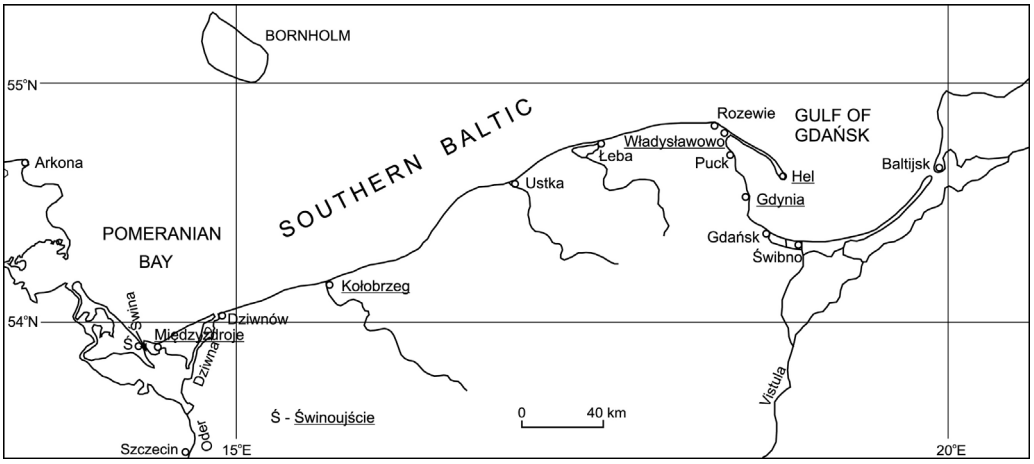

Figure 1 Location of hydrometeorological stations on the south coast of the Baltic Sea.

(March—May), summer (June—August) and autumn (September—November), mainly from the period of 1951—2010. Data were gathered by the Institute of Meteorology and Water Management — National Research Institute (IMGW-PIB) at Świnoujście, Międzyzdroje, Kołobrzeg, Władysławowo, Hel and Gdynia stations (Figure 1). As far as Kołobrzeg is concerned, the data refer to the years 1957—2010. The longest-running study of water temperature has been conducted for these 6 aforementioned stations. Average monthly water temperatures, calculated on the basis of daily values, were published in IMGW's materials (Cyberska et al., 1986—1998; *Hydrographic...*, 1950—1970; *Hydrological...*, 1961—1990; Krzymiński et al., 1999—2001; Miętus et al. 2002—2010). Using the monthly values, seasonal means from individual years were calculated. Means, extreme means and their amplitudes as well as standard deviations of seasonal surface water temperature for those regions are presented in Table 1. The mean amplitude was calculated as a difference between the mean maximum, i.e. maximum seasonal mean temperature averaged over all stations, and mean minimum seasonal water temperature values.

Water temperature measurements were taken outside the harbour breakwater in Władysławowo, Hel and Gdynia, from the pier — in Kołobrzeg and Międzyzdroje, and in the harbour canal in Świnoujście. The measurements were taken with mercurial thermometers, with the accuracy of 0.1°C, in the surface water layer at the depth of 0.5 m at 06:00 UTC. The location of water temperature measurement did not change in the course of the analysed period. The measurement points analysed in the paper are representative of the littoral zone of the southern Baltic Sea. Further away from the coast, in the open waters of the southern Baltic Sea, water temperature is different, particularly during the transitional seasons (Cyberska, 1994).

It was decided not to use the data obtained from satellite measurements, taking into consideration their imprecision and that they are available for much shorter periods than measurements collected at coastal stations. The statistical

Table 1 Mean, extreme, amplitude (A) and standard deviations (B) of water temperature (°C) in individual seasons (1951—2010).

Season		Świnoujście	Międzyzdroje	Kołobrzeg	Władysławowo	Hel	Gdynia	Mean	Mean amplitude
A									
Dec.—Feb.	min	0.4	0.0	0.1	0.4	1.0	0.4	0.4	
	mean	1.7	1.7	2.2	1.9	2.5	2.1	2.0	4.3
	max	4.0	4.5	5.3	4.5	5.0	4.6	4.7	
Mar.—May	min	5.5	4.6	4.8	4.2	3.3	3.7	4.4	
	mean	7.7	6.9	6.5	5.9	5.5	6.2	6.5	4.8
	max	9.9	10.4	9.1	8.3	8.2	9.0	9.2	
Jun.—Aug.	min	16.3	15.9	15.1	13.8	14.4	14.9	15.1	
	mean	18.5	17.8	16.6	16.0	16.7	17.4	17.2	4.0
	max	20.0	20.0	18.3	17.9	18.7	19.2	19.0	
Sep.—Nov.	min	9.8	8.4	9.7	8.6	9.4	8.6	9.1	
	mean	11.2	11.1	11.0	10.6	11.8	11.3	11.2	3.9
	max	13.1	13.2	12.3	12.5	13.5	13.5	13.0	
B									
Dec.—Feb.		0.76	0.89	1.02	0.89	0.90	0.88	0.9	
Mar.—May		1.07	1.28	1.04	0.99	1.17	1.23	1.1	
Jun.—Aug.		0.82	0.93	0.83	0.95	0.94	1.08	0.9	
Sep.—Nov.		0.77	0.80	0.65	0.71	0.73	0.73	0.7	

error of 1.2°C (expressed as a standard deviation of the differences between the temperature determined with the use of a retrieval algorithm and the temperature measured *in situ*) was demonstrated through a comparison of the satellite data (even after the application of so-called data assimilation process) with water temperature obtained from the coastal stations. An additional shortcoming of the data obtained from the satellite model is the fact, that it works by assimilating inflowing satellite data concerning SST only for cloudless areas (Kowalewski, 2016).

Atmospheric circulation data come from "Calendar of atmospheric circulation patterns" (Pianko-Kluczyńska, 2006) devised in line with Lityński's method (Lityński, 1969). More recent data (2006—2010) were obtained directly from IMGW-PIB. Lityński (1969) used an equiprobable, three-class, numerical classification to define atmospheric circulation while determining frequency distribution curves. He defined an atmospheric circulation pattern with three numerical parameters: zonal circulation index (Ws), meridional circulation index (Wp) as well as pressure index at the point coinciding with the location of Warsaw (Cp). Zonal and meridional circulation indices, defining the advection direction of air masses, were determined for the area limited by 40°N and 65°N parallels as well as 0°E and 35°E meridians. The atmospheric pressure was read from the same weather charts from which atmospheric circulation indices were calculated.

Lityński (1969) calculated the zonal circulation index, in accordance with Rossby's definition (after Lityński, 1969), from a formula that contains averaging latitudinal component of the geostrophic wind:

$$Ws = \frac{4.8\overline{\Delta p}}{\sin\overline{\varphi}\Delta n},$$

where Ws — zonal index in m/s,

$\frac{\overline{\Delta p}}{\Delta n}$ — average pressure gradient in hPa per 1° longitude,

$\overline{\varphi}$ — average latitude.

Once the figures resulting from the determined zone of index calculation are entered, the formula assumes the following form (Lityński, 1969):

$$Ws = 6.1\,\frac{P_{40}-P_{65}}{25},$$

where P_{40} — average pressure at the section of 40°N latitude in 0—35°E zone,

P_{65} — average pressure at the section of 65°N latitude in 0—35°E zone.

In order to compute the meridional circulation index, Lityński (1969) adopted an analogous formula, taking into account the fact that 1° at a parallel is of smaller length than 1° at a meridian:

$$Wp = 10.0\,\frac{P_{35}-P_0}{35},$$

where Wp — meridional index in m/s,

P_{35} — average pressure at the section of 35°E longitude in 40—65°N zone,

P_0 — average pressure at the section of 0° longitude in 40—65°N zone.

Lityński (1969) defined Ws index with the following classes: E (eastern), 0 (zero), W (western), and Wp index — N (northern), 0 (zero), S (southern). In turn, Cp atmospheric pressure was defined by him with the following classes: c (cyclonic), 0 (zero — close to normal) and a (anticyclonic). He thus arrived at a total of 27 circulation patterns: Nc, N_0, Na, NEc, NE_0, NEa, Ec, E_0, Ea, SEc, SE_0, SEa, Sc, S_0, Sa, SWc, SW_0, SWa, Wc, W_0, Wa, NWc, NW_0, NWa, 0c, 0_0, 0a.

Dominant circulation types of each day in the period from 1951 to 2010 used in this work originate from "Calendar of atmospheric circulation patterns" (Pianko-Kluczyńska, 2006) as well as from the materials obtained directly from IMGW-PIB. The authors summed up the numbers of days with particular circulation types.

In order to obtain stronger relationships, the authors combined individual circulation patterns into sectors. Generally, sectors were adopted from zonal directions that exert the greatest impact on water temperature. These are chiefly sectors of eastern directions, such as: NE + E (23°—112°), NE + E + SE (23°—157°), E + SE + S (68°—202°) and western directions, such as: SW + W (203°—292°), SW + W + NW (203°—337°), W + NW + N (248°—22°). Except for summer, seasonal atmospheric circulation patterns were not differentiated in terms of pressure indexes (c, 0, a).

Subsequently, the number of days for given atmospheric circulation patterns were calculated in previously mentioned sectors (NE + E, NE + E + SE, E + SE + S, SW + W, SW + W + NW and W + NW + N) yearly for each individual season, from 1951 to 2010. As opposed to monthly relationships, seasonal relationships provide greater averaging of variable values, the reduction of their extremes and smaller deviations of empirical points in the Cartesian coordinate system from the regression line, which strengthens the correlation. However, in transition periods between two different regimes, the averaging may reduce correlations.

The analysis methods of correlation and regression were applied in order to determine and examine statistical dependency between seasonal water temperatures (dependent variable) and the number of days with a given atmospheric circulation type in the studied sectors (independent variable; Łomnicki, 1999; *Time...*, 2010). Statistical significance of these relationships was analysed with Fisher—Snedecor test (F) at significance levels of $\alpha = 0.05$, $\alpha = 0.01$ and $\alpha = 0.001$ (risk of error amounted to 5%, 1% and 0.1% respectively). The null hypothesis of the test was formulated under an assumption that the regression coefficient value is equal to zero, i.e. in the considered population (in the study period) one of the variables does not exert influence on the other variable. Statistical significance less than, or equal to, the adopted levels (0.05, 0.01 and 0.001) showed grounds for rejection of the null hypothesis claiming lack of influence of the number of days in the given circulation type on the SST near the Baltic Sea coast, i.e. accepting a hypothetical existence of a correlation between the analysed variables.

The strength of relationships between the examined variables was defined with a correlation coefficient (r), while the degree of their dependency — with a determination coefficient ($r^2 \times 100\%$). The determination coefficient is the proportion of the variance in the dependent variable that is predictable from the independent one. Moreover, mean values and standard deviation values were computed for seasonal water temperatures, constituting a measure of dispersion (the information on the dispersion of the values of the variables around their mean value).

Table 2 Correlation coefficients between the number of days with selected atmospheric circulation patterns and water temperature in individual seasons (1951—2010).

Circulation	Świnoujście	Międzyzdroje	Kołobrzeg	Władysławowo	Hel	Gdynia
Winter						
NE + E	−0.57[c]	−0.55[c]	−0.58[c]	−0.61[c]	−0.57[c]	−0.60[c]
NE + E + SE	−0.64[c]	−0.58[c]	−0.65[c]	−0.69[c]	−0.63[c]	−0.70[c]
E + SE + S	−0.54[c]	−0.44[c]	−0.53[c]	−0.56[c]	−0.50[c]	−0.58[c]
SW + W	0.62[c]	0.57[c]	0.62[c]	0.66[c]	0.62[c]	0.64[c]
SW + W + NW	0.68[c]	0.62[c]	0.67[c]	0.72[c]	0.64[c]	0.70[c]
W + NW + N	0.49[c]	0.40[b]	0.46[c]	0.49[c]	0.42[c]	0.52[c]
Spring						
NE + E	−0.32[a]	−0.35[b]	−0.37[b]	−0.34[b]	−0.38[b]	−0.39[b]
NE + E + SE	−0.34[b]	−0.40[b]	−0.41[c]	−0.37[b]	−0.42[c]	−0.41[c]
E + SE + S	−0.11	−0.28[a]	−0.27[a]	−0.23	−0.14	−0.10
SW + W	0.09	0.19	0.24	0.13	0.25	0.20
SW + W + NW	0.22	0.31[a]	0.44[c]	0.30[a]	0.32[a]	0.23
W + NW + N	0.35[b]	0.44[c]	0.47[c]	0.39[b]	0.36[b]	0.28[a]
Summer						
NE + E	0.48[c]	0.29[a]	−0.03	−0.03	0.12	0.27[a]
NE + E + SE	0.54[c]	0.34[b]	−0.13	−0.09	0.19	0.33[b]
E + SE + S	0.49[c]	0.35[b]	−0.11	−0.12	0.32[a]	0.37[b]
SW + W	−0.27[a]	−0.10	0.14	0.16	−0.06	−0.26[a]
SW + W + NW	−0.50[c]	−0.25	0.07	0.04	−0.22	−0.42[c]
W + NW + N	−0.51[c]	−0.41[c]	0.00	−0.02	−0.27[a]	−0.46[c]
Autumn						
NE + E	−0.21	−0.28[a]	−0.09	−0.13	−0.19	−0.24
NE + E + SE	−0.09	−0.20	−0.24	−0.31[a]	−0.29[a]	−0.35[b]
E + SE + S	0.19	0.04	−0.26[a]	−0.40[b]	−0.13	−0.23
SW + W	0.08	0.08	0.19	0.24	0.24	0.28[a]
SW + W + NW	−0.12	0.03	0.21	0.27[a]	0.15	0.20
W + NW + N	−0.27[a]	−0.04	0.11	0.25	−0.02	0.09

[a] Values significant at the level α = 0.05.
[b] Values significant at the level α = 0.01.
[c] Values significant at the level α = 0.001.

3. Results

3.1. Synchronous relationships between water temperature and atmospheric circulation patterns

When examining the relationship between the number of days with given type of atmospheric circulation (combined into sectors from zonal directions) and water surface temperatures in the individual seasons, it was found that stronger relationships occur during the winter season. For nearly all of the studied regions, those relationships are statistically significant even at a level of α = 0.001 (Table 2). The relationships between water temperature and the number of days with a circulation from the western sector (SW + W, SW + W + NW) are slightly stronger than that related to the eastern sector (NE + E, NE + E + SE). For SW + W + NW circulation correlation coefficients range from 0.62 in Międzyzdroje to 0.72 in Władysławowo. The strongest seasonal relationship with the correlation coefficient of 0.72 occurs in winter in Władysławowo. As demonstrated by the determination coefficient of average winter (from three winter months), water temperature variability can be explained by the variability of the number of days with SW + W + NW circulation in 51% of the cases. The increase in the number of days by 1 with SW + W + NW circulation will result in an increase by an average of 0.036°C in the winter water temperature in Władysławowo. The same circulation pattern explains winter water temperature in Gdynia in 50%, and in Międzyzdroje, in 39% of the cases. In summer, the diversification of determination coefficients is greater along the southern Baltic Sea coast. Values for the SST association with the number of days featuring SW + W + NW circulation amount to 0—25% and with NE + E + SE circulation to 1—30%. In the Pomeranian Bay (Świnoujście, Międzyzdroje) and in the Gdańsk Bay (Gdynia) the relations of water temperature in summer, both with the number of days featuring NE + E + SE as well as SW + W + NW circulation, are statistically significant even at levels α = 0.01 and α = 0.001. However, these relations are not statistically significant alongside open (unshielded) shores.

The differentiation in the strength of correlation coefficients during individual seasons, in the region that is exposed the most to the sea influences, is presented for Władysławowo (Figure 2). In winter, correlation coefficients are the strongest and these relationships are statistically significant even at a level of α = 0.001. During transitory seasons, i.e. in spring and autumn, the relationships are evidently weaker, but still statistically significant, typically at a level of α = 0.05. The correlations of water temperatures and the number of days with atmospheric circulation during summer

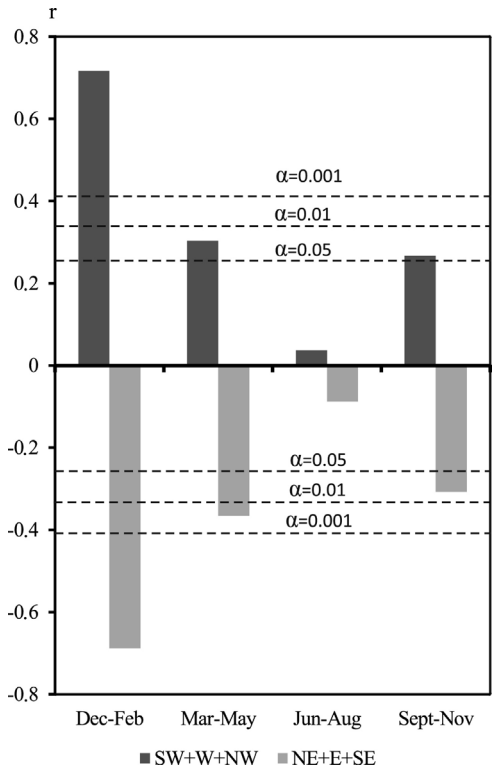

Figure 2 Correlation coefficients (r) of the water temperatures at Władysławowo and number of days with atmospheric circulation (SW + W + NW, NE + E + SE) in individual seasons (1951—2010).

seasons are statistically insignificant (Figure 2). In this season, anticyclonic types of circulation have an impact on water temperature. However, the correlation coefficients between water temperature and the number of days featuring an eastern anticyclonic (NEa + Ea + SEa), cyclonic (NEc + Ec + SEc) and zero (NE0 + E0 + SE0) circulation patterns for Władysławowo amount to 0.06, —0.12 and —0.19 and are statistically insignificant, respectively. In turn, certain relations concerning bays, particularly the Pomeranian Bay, appeared to be statistically significant. The relations that are significant (at the level of at least α = 0.05) were found in Świnoujście — with the number of days featuring NEa + Ea + SEa (r = 0.49) and NEc + Ec + SEc (r = 0.30) circulation, and in Międzyzdroje — with the number of days featuring NEa + Ea + SEa (r = 0.37) circulation, in Kołobrzeg — with the number of days featuring NE0 + E0 + SE0 (—0.30) circulation, and in Gdynia — with the number of days featuring NEa + Ea + SEa circulation (r = 0.31).

It can further be observed, that the studied correlations considering SW + W + NW as well as the NE + E + SE circulation pattern give similar absolute values and they differ only with a direction (indicated a positive linear relationship or the negative one) (Figure 2). It was found that the fraction of a total number of days with (SW + W + NW) + (NE + E + SE) circulation patterns in an individual season is not too high and it varies from 65% in summer to 67% in winter. The yearly variability of the number of days with the circulation from the western and eastern sectors (defined by the variation coefficient) is the same in spring, summer and autumn, and amounts to 0.14. In winter, it is significantly greater — the variation coefficient is equal to 0.17.

More detailed analyses demonstrated that in the examined multiyear period in Władysławowo (at the level of α = 0.001) the water temperature in February and May is significantly correlated with spring (March—May) and summer (June—August) water temperature, respectively, with the spring relations being stronger (r = 0.83) than the ones observed in summer (r = 0.52). The relations between water temperature in November and August and respectively winter (December—February) as well as autumn (September—November) water temperatures appeared to be statistically insignificant. The study also comprised the relations between average water temperature values in Władysławowo in individual seasons of the year and the respective average seasonal air temperatures in Gdynia. It was found that these dependencies are stronger than the relation between the water temperature and the number of days with a given atmospheric circulation type. The strongest relations occurred in winter (r = 0.91) and in spring (r = 0.84), while the weakest ones were observed in summer (r = 0.43) and in autumn (r = 0.65). In summer, correlation coefficients between the average water temperature and the number of days with western or eastern atmospheric circulations are statistically insignificant at stations exposed to sea (unsheltered) shores (Kołobrzeg, Władysławowo).

Figure 3 demonstrates some empirical points clearly outlying from the regression line. This figure shows the relationship between the average water temperature in Władysławowo and the number of days with the atmospheric circulation types — western (A) and eastern (B) in winter (December—February). The regression coefficients are 0.036 (A) and 0.045 (B), while the determination coefficients are 0.51 and 0.47, respectively. Such point distribution from the regression line refers to atypical cases, chiefly very mild winters. The points that are most distant from the regression line are the ones with coordinates referring to the winter of 2006/2007. In the winter of 2006/2007 very high water temperature was observed in Władysławowo (4.5°C) in comparison to the average value (2.0°C). The number of days with the circulation bringing warmer weather (SW + W + NW) amounted to 54 (Figure 3A). Both December 2006 and January 2007 featured particularly high water temperatures. The deviations from an average SST for the multiyear period of 1950—2010 during these two months were equal to 3.4°C and 3.5°C, respectively. Thermal water inertia affected a relatively high water temperature in February (as well as additional deviation from the average value amounting to 1°C) despite distinct dominance of the number of days featuring NE + E + SE circulation (9 days, 32% days in month) over the number of days featuring SE + W + NW circulation (2 days, merely 7% days in the month).

In order to explain a substantial deviation of the average surface water temperature (SST) in the winter of 2006/2007 from a regression line (Figure 3A), only the winters (11 cases) with the similar number of days (from 49 to 59) featuring SW + W + NW atmospheric circulation were analysed. The analysis, with a focus placed on deviations from the average value and relations with SST, concerned the following factors of the selected winters: water temperature in November, winter insolation in Gdynia, average air temperature in winter in Gdynia and the number of days featuring N, S, 0, SW, S + SW, SE + S and NE + E + SE circulation patterns. It

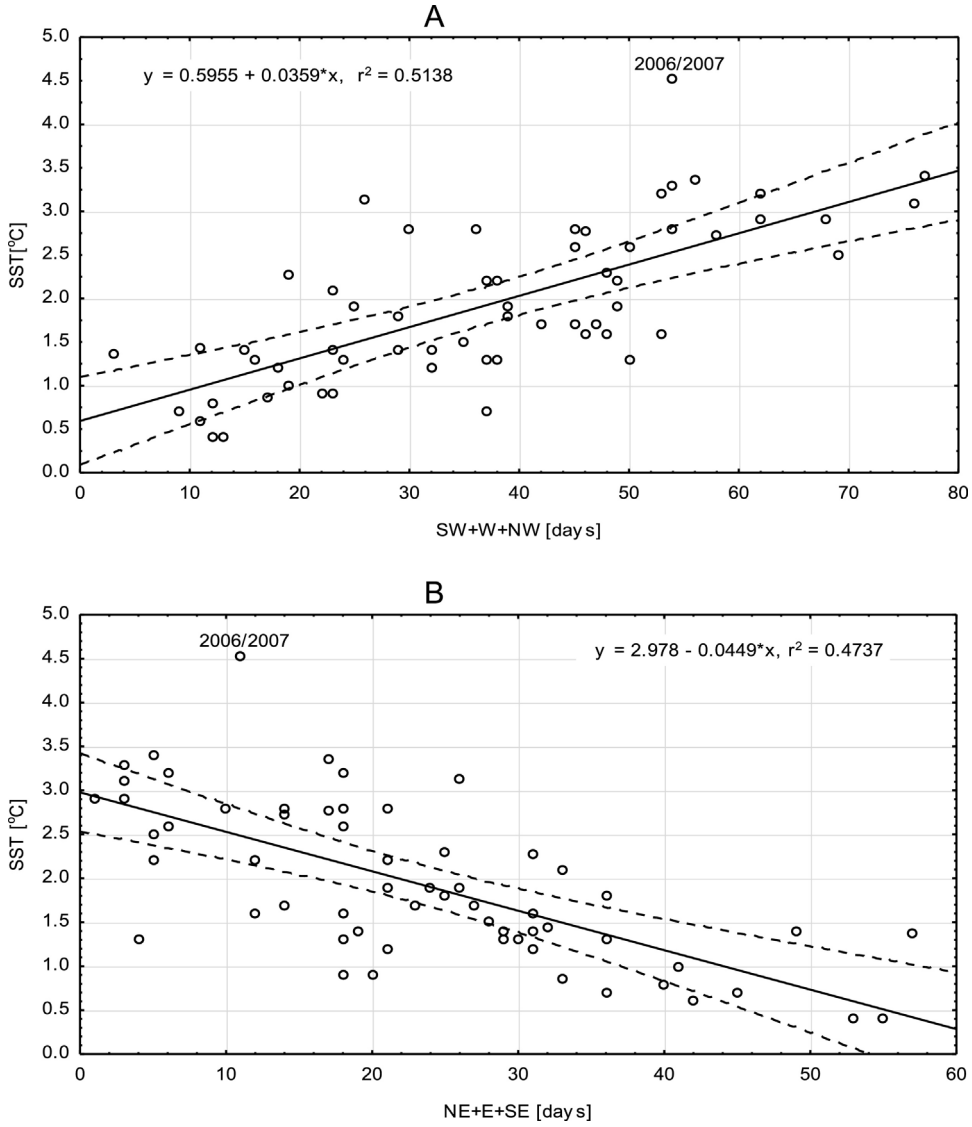

Figure 3 Linear regression estimated for the relationship between water temperature at Władysławowo with the number of days with atmospheric westerly circulation patterns for (A) and easterly ones (B) during December—February (1951—2010). Curves presented 99% confidence interval.

was found, that in the selected group of 11 atypical winters the one of 2006/2007 had the highest deviations from average values among the group, regarding such factors as: air temperature (deviation from the average air temperature of the selected winters was 1.7°C), water temperature in November (deviation from the selected winters average value was equal to 2.0°C), and the number of days with S circulation (deviation from the group's average value amounted to 4 days). For that group, correlation coefficients between SST and the air temperature, the water temperature in November as well as the number of days with S circulation amounted to 0.94, 0.45 and 0.56, respectively, and were statistically significant only with air temperature (α = 0.001). It was also observed that an increase in air temperature in Gdynia by 1°C resulted in an increase in SST in Władysławowo by an average of 0.713°C. Summing up, it can be assumed that the relatively high air temperatures in the winter of 2006/2007 and in November 2006 are responsible for a significant deviation of the actual water temperature from the value obtained from the regression equation.

3.2. Asynchronous relationships between water temperature and atmospheric circulation patterns

Relationships between surface water temperatures and the number of days with atmospheric circulation patterns were studied. Both the western (SW + W + NW) and the eastern (NE + E + SE) circulation patterns were considered, preceded by one, two or three seasons during which water temperature (SST) was analysed. It was found that asynchronous relationships are weaker than simultaneous (synchronous) relationships. The strength of such relationships decreased as time intervals increased, within the interval of just two seasons they were typically statistically insignificant (Table 3). The strongest relationships are the ones regarding the relation

Table 3 Correlation coefficients between the number of days with selected atmospheric circulation pattern SW + W + NW and NE + E + SE with lagged water temperature (SST) one (A), two (B) and three (C) seasons (1951–2010).

Variables	Świnoujście	Międzyzdroje	Kołobrzeg	Władysławowo	Hel	Gdynia
A						
$SW + W + NW_{winter}, SST_{spring}$	0.54[c]	0.62[c]	0.64[c]	0.67[c]	0.63[c]	0.62[c]
$SW + W + NW_{spring}, SST_{summer}$	0.35[b]	0.52[c]	0.39[b]	0.30[a]	0.44[c]	0.56[c]
$SW + W + NW_{summer}, SST_{autumn}$	−0.29[a]	−0.23	−0.22	−0.26[a]	−0.27[a]	−0.24
B						
$SW + W + NW_{winter}, SST_{summer}$	−0.07	0.20	0.25	0.41[b]	0.14	0.14
$SW + W + NW_{spring}, SST_{autumn}$	0.23	0.19	0.17	0.20	0.35[b]	0.29[a]
C						
$SW + W + NW_{winter}, SST_{autumn}$	−0.06	−0.01	0.01	−0.03	0.05	−0.07
A						
$NE + E + SE_{winter}, SST_{spring}$	−0.54[c]	−0.53[c]	−0.62[c]	−0.60[c]	−0.60[c]	−0.57[c]
$NE + E + SE_{spring}, SST_{summer}$	−0.12	−0.30[a]	−0.26[a]	−0.24	−0.39[b]	−0.50[c]
$NE + E + SE_{summer}, SST_{autumn}$	0.20	0.25	0.22	0.24	0.16	0.13
B						
$NE + E + SE_{winter}, SST_{summer}$	0.01	−0.18	−0.18	−0.26[a]	−0.17	−0.20
$NE + E + SE_{spring}, SST_{autumn}$	−0.04	−0.06	−0.14	−0.20	−0.34[b]	−0.29[a]
C						
$NE + E + SE_{winter}, SST_{autumn}$	0.01	−0.07	−0.08	−0.05	−0.11	0.00

[a] Values significant at the level $\alpha = 0.05$.
[b] Values significant at the level $\alpha = 0.01$.
[c] Values significant at the level $\alpha = 0.001$.

between water temperature in spring (SST_{spring}) and the number of days with atmospheric circulation in winter. These relationships were slightly stronger for the days with SW + W + NW_{winter} circulation than for days with the NE + E + SE_{winter} circulation. All of them were, however, statistically significant, even at a level of $\alpha = 0.001$. The strongest relationship of water temperature in spring (SST_{spring}) and the number of days with western atmospheric circulation (SW + W + NW_{winter}) in winter occurred in Władysławowo, resulting in a correlation coefficient of 0.67. The determination coefficient of 0.45 means, that water temperature variability in spring can be explained by the variability of the number of days with western circulation in winter in 45%. As demonstrated by a regression coefficient, an increase in the number of days with western circulation in winter by 1 day will cause a rise of water temperature in spring in Władysławowo by an average of 0.04°C.

The coefficients determining the relationship between the number of days with western circulation (SW + W + NW_{winter}) in winter and water temperature in spring (SST_{spring}), summer (SST_{summer}) and autumn (SST_{autumn}) are weaker (Table 3). The determination coefficients of the number of days with eastern circulation (NE + E + SE_{winter}) in winter with subsequent seasonal water temperatures (SST_{spring}, SST_{summer} and SST_{autumn}) decrease in a similar fashion (Table 3). Such drop in strength of asynchronous relationships can be explained by the sea water masses thermal inertia. The thermal conditions of water masses strengthened by the atmospheric conditions in winter are still being reflected in the following seasons. The thermal effects of winter circulation encoded in water masses die down with time, while asynchronous relationships become statistically insignificant.

4. Discussion

The water temperature variability depends on the thermal properties of the incoming air masses, especially in winter. In this paper, the atmospheric circulation patterns developed by Lityński (1969) constitute the measure of air mass advection. The numbers of days with circulation patterns were added up for chiefly two sectors: SW + W + NW and NE + E + SE as they influenced water temperature variability the most. The proper generalisation of circulation patterns, involving their combination into sectors, provides a better reflection of their occurrence real frequency since there are sometimes unjustified significant differences in their occurrence between neighbouring patterns. On the other hand, excessively wide sectors deteriorate the relationship, because they may contain the conflicting circulation patterns with an opposite effect on water thermal conditions (Girjatowicz, 2001).

Comparing previous studies by Girjatowicz (2008) regarding the impact of the NAO index on the SST along the southern Baltic Sea shores, with this work, one can notice some differences in the statistical significance of the compounds. The NAO index (reflecting the intensity of the polar-marine air masses advection) corresponds to the SW + W + NW type of atmospheric circulation according to the Lityński's classification. The SST compounds with the NAO index and the number of winter and autumn SW + W + NW circulation days. Furthermore, both are characterized by similar statistical significance. However, these relationships clearly differ for summer and even more so for spring. In spring, the SST associations with the SW + W + NW atmospheric circulation were usually statistically significant, while for the NAO index none of them was. A similar situation occurs for the NE + E + SE circulation days and the NAO index association

with SST. The Lityński's classification provides more detailed and precise information about the relationship between atmospheric circulation and SST than the NAO index, thus it has been used in this work.

It was determined that directions of air masses advection significantly influence water temperature along the southern coast of the Baltic Sea. The strongest relationships occurred in winter, which may be explained by more intensive atmospheric activity (resulting from stronger baric gradients over Europe during the winter season (Löptien et al., 2008; Sepp et al., 2005) and by the limited influence of solar radiation (low real insolation — Koźmiński and Michalska, 2005). One must remember, that the European thermal conditions in winter are determined by the heat coming from lower latitudes, transported by the Gulf Stream and accumulated in the northern Atlantic. Above all, oceans feature high thermal inertia ("thermal memory"), characterised by a gradual heat transfer in thermal exchange processes (e.g. through latent heat) between water and atmosphere (Marsz, 1999). The heated air mass is, in turn, carried from Atlantic to the east through the proper atmospheric circulation (western flow), the most intensive in temperate geographic latitudes during winter (Andersson, 2002; Lamb, 1978). Similarly, in the Gulf of Gdańsk, where the heat accumulated during spring, as a result of atmospheric circulation, particularly in the deeper water layers, influences water temperature in certain regions of the southern Baltic Sea coast in autumn. It can be explained by the greater thermal inertia of deeper water layers of the Bay of Gdańsk in comparison to the remaining regions of the southern Baltic Sea coast. In the water masses of the Bay of Gdańsk, the effects of earlier atmospheric circulation are better "remembered", which are later manifested.

The conducted research confirmed, that winter thermal features are related to the atmospheric circulation activity over northern Europe and the Baltic Sea (cf. Leckebusch and Ulbrich, 2004; Löptien et al., 2008; Sepp et al., 2005). At this time of the year, the frequency of deep low-pressure systems over the Baltic Sea increases (Bengtsson et al., 2006; Brayshaw, 2005; Walther and Bennartz, 2006). In the subsequent seasons, the atmospheric circulation activity is weaker, as is the strength of the studied correlational relationships. At the same time, the influence of the solar radiation differentiation depending on the sunshine duration (cloudiness) increases, reaching its maximum in summer.

During summer, especially the eastern (NE + E + SE) circulation is frequently accompanied by high pressure, cloudless weather or the weather with little cloudiness. Days with western anticyclonic circulation may also be relatively sunny, however, the most solar energy arrives during the eastern anticyclonic circulation, mainly in the spring and summer (Rozwadowska, 1992). In such circumstances, solar radiation has a significant impact on water temperature. According to Miętus (1999), summer water temperature is determined by anticyclonic forms of atmospheric circulation, which are contributing to the increased amount of direct sun radiation to the surface of the sea. Thus, in summer the relationships of water temperature with atmospheric circulation are weak and typically statistically insignificant.

In summer, during western circulation, inflowing polar-sea air masses are colder than the continental air mass (cf. Kożuchowski and Marciniak, 1988; Marsz and Styszyńska (eds.), 2002). In turn, during eastern circulation, warm, polar-continental air masses arrive over the southern Baltic Sea region (Miętus (ed.), 1997).

The factors interfering with the relationships of water temperature with atmospheric circulation are the solar radiation described earlier and a phenomenon of upwelling. The upwelling is an upward current caused by the wind blowing parallel to the coast located on its left (Bychkova and Victorov, 1987; Gidhagen, 1987; Leppäranta and Myrberg, 2009). Along the southern coastline of the Baltic Sea, it is mostly the eastern wind that gives rise to the upwelling, most strongly manifested during the warm season (May—September), occurring with the frequency of approximately 30% (Krężel, 1997; Urbański, 1995). In the warm season, water temperature rise is generated during eastern circulation, which is accompanied by cloudless weather or the weather with little cloudiness, and the high solar radiation inflow. The eastern circulation corresponds approximately to similar wind directions giving rise to an upwelling. Siegel et al. (2008) noticed that along the German and Polish Baltic Sea coasts (with the exclusion of the Oder estuary zone) upwelling occurs when eastern winds blow at speeds higher than 15 m/s. The greatest negative anomalies of surface water temperature caused by upwelling occur alongside the Hel Peninsula (at the side of the open sea) and in the most northern part of the Polish coast (Kowalewski and Ostrowski, 2005). In summer, cooler water coming to the surface from deeper sea layers reduces the surface water temperature. Consequently, upwelling weakens the relationships between water temperature and atmospheric circulation. In the region of Hel, Kołobrzeg and Łeba, the upwelling phenomena are more frequent than in the other regions of the Polish Baltic Sea coast (Lehmann et al., 2012). The maximum water-temperature difference between the centre of upwelling and water surrounding it was observed. It amounted to 14°C in Hel, 12.5°C in Łeba and 8.9°C in Kołobrzeg (Krężel et al., 2005). Inflows of cool water from the deeper layers (upwellings) do not occur in bays due to their shallow depths (cf. Kowalewska-Kalkowska and Lejman, 2002/2003). Downwellings appear far more frequently than upwellings along the Baltic Sea southern coast (Kowalewski and Ostrowski, 2005; Myrberg and Andrejev, 2003), a result of the western and south-western winds domination in that part of the Baltic Sea (Miętus (ed.), 1997). However, downwellings do not have a greater impact on the variability of the surface water temperature.

An upwelling may slightly weaken the influence of atmospheric circulation on water temperature in the cold season as well. However, owing to a lower vertical gradient of water temperature than in summer, the impact is slightly weaker. In winter, during eastern circulation, frosty and dry polar-continental air masses arrive, causing a decrease of water temperature. Similarly, sea-surface wind directions accompanying this circulation pattern cause warmer waters to resurface from deeper sea layers causing the slight surface water temperature rise (cf. Girjatowicz, 1987; Łomniewski, 1960).

5. Conclusions

The objective of this work was to analyse the influence of western (SW + W + NW) and eastern (NE + E + SE) atmospheric circulation patterns during individual seasons of

the year (December—February, March—May, June—August, September—November) on the surface water temperature of the Baltic Sea southern coast. The focus was also placed on the strength difference of those relationships in this particular geographical region for each season separately. Long-term (1951—2010) water temperature data from the following stations: Świnoujście, Międzyzdroje, Kołobrzeg, Władysławowo, Hel and Gdynia were used. Circulation types were adopted from "Calendar of atmospheric circulation patterns" prepared by IMGW-PIB according to Lityński's method. In order to examine the strength of these relationships, the analytical methods of correlation and regression were employed. Statistical significance of the relationships was analysed with Fisher-Snedecor test.

The relationships obtained for winter seasons demonstrate the high statistical significance (α = 0.001). The correlation and regression coefficients of the SST and a number of days with SW + W + NW circulation are positive, indicating that an increase of SW + W + NW circulation frequency corresponds to a rise in the water temperature. This circulation has an opposite effect on water temperature during summer, however, these relationships are usually statistically insignificant. The relationships that are statistically significant have a negative correlation and regression coefficients. A rise in the frequency of the SW + W + NW circulation pattern, which is accompanied by an advection of cool air masses from the Atlantic and cloudiness, results in water temperature drop.

Strong relationships in winter can be explained by the thermal influence of the air masses incoming from the west or east. The westerly air masses (coming from the Atlantic), mostly the polar-sea air masses, are much warmer, while the easterly ones (from the Eurasian continent) the polar-continental air masses, are much cooler compared to the coastal waters of the southern Baltic Sea. A clear thermal difference between the westerly and easterly air masses distinctly affects the respective increases and decreases of water temperatures, which are reflected by the strong correlational relationships between these variables.

The relationships of the water temperature with the NE + E + SE circulation in winter are slightly weaker than with the SW + W + NW circulation, but they are also statistically significant at a level of α = 0.001. An upwelling (the inflow of warmer waters) may weaken these relationships, especially under the NE + E + SE circulation in winter. The correlations and regression coefficients are negative, which indicates that a greater frequency of the NE + E + SE circulation in winter corresponds to the water temperature decrease. That circulation has the opposite effect on the water temperature in summer. During the summer season, relatively small thermal differences between the incoming air masses are observed, and thereby small water temperature variations are present, which may affect weak relationships. Simultaneously, a significant influence of the eastern anticyclonic circulation (NEa + Ea + SEa) on the water temperature in bays is noticeable, particularly in the relatively shallow Pomeranian Bay. The NEa + Ea + SEa circulation is frequently accompanied by cloudless weather or weather with low cloud cover, favouring an increase of the solar radiation inflow affecting the water temperature rise.

Atmospheric circulation of a different type than SW + W + NW or SE + E + SE occurs during approximately 34% (i.e. 31) of days. On these days, with circulation 0 (14%, 13 days), N (10%, 9 days) and S (10%, 9 days) the advection of air with a distinctly different temperature can happen. Advection from the N direction brings cold air masses, while from the S direction — warm ones. This will have an effect on the weakening correlations between the average water temperature and the number of days with SW + W + NW or with NE + E + SE circulation.

The water temperature in February and May has a significant impact on the water temperature in spring (March—May) and summer (June—August). In other words, the water temperature in the months directly preceding a given season (spring or summer) directly influences the water temperature of that season. At the same time, the influence of atmospheric circulation on the water temperature weakens in those two seasons. In turn, the water temperature in winter and autumn is not significantly affected by the water temperature in the months preceding those seasons. The atmospheric circulation is of greater influence at the time (particularly in winter). It affects both air and water temperature. Average seasonal air temperatures exert a significant influence on the seasonal water temperatures, and the correlation coefficient is the highest in winter and spring. Average water temperature values in individual seasons and appropriate seasonal average air temperatures show stronger relationships than between average water temperature values and the number of days with SW + W + NW or NE + E + SE circulation.

No distinct spatial differentiation of the correlation coefficient value was found in winter, with the number of days of both the SW + W + NW and NE + E + SE circulation patterns alongside the southern Baltic Sea coast. Still, the correlation coefficients on the eastern coast, particularly in Władysławowo and in Gdynia, are slightly higher (in these stations variabilities of average water temperature in winter are explained by the number of days with SW + W + NW circulation in 51% and 50% respectively). That coefficient variability could have been caused by increases of continentalism and the degree of winter severity in the eastern direction. The influence of continentalism on the strength of relationships is most visibly demonstrated in the relation between the number of days with NE + E + SE circulation pattern and the accompanying intensity of the cooler weather in winter, in the eastern direction. However, a differentiation of these coefficients (SST and circulation) between sheltered waters (bays) and non-sheltered waters in summer is evident. During this season, in Pomeranian Bay and the Bay of Gdańsk, the relationships are statistically significant, whereas alongside the open (unsheltered) Baltic Sea coast they are statistically insignificant. The difference in strength is chiefly affected by local conditions, such as upwellings and the inflows of river waters. Upwellings reducing surface water temperature occur alongside the open shores during eastern circulation in summer. The influence of an upwelling on water temperature is, thus, opposite to the influence exerted by circulation factors. In summer the upwelling, next to poor atmospheric circulation activity and strong insolation, is one of the factors weakening the relationships of water temperature with the number of days with NE + E + SE circulation. The phenomenon of upwelling does not occur in Pomeranian Bay and the Bay of Gdańsk, therefore, it does not disturb the correlational relationships. At the same time, the inflow of river waters to those bays has a positive effect on the

relationships. In summer, during NE + E + SE circulation (especially of the anticyclonic types), accompanied by the weather with the cloudless sky (or with a little cloud cover) and high solar radiation, the water temperature rises. At the same time, a discharge from rivers brings warm water masses into the bays. Conversely, during the SW + W + NW circulation pattern, when cold air masses from the ocean come in accompanied by cloudy weather (especially during the cyclonal circulation), water temperature decreases. Concurrently, colder river waters flow in. Hence, atmospheric circulation factors together with the river water inflow have a similar effect on the water temperature of the bays. Consequently, it translates to statistically significant correlational relationships, despite the poor circulation activity in summer.

Asynchronous relationships between water temperature and the number of days with atmospheric circulation may offer a certain prognostic possibility. It is based on winter and spring correlations of water temperature with the number of days with atmospheric circulation, and averaged water temperature of the preceding season. These are all statistically highly significant relationships (α = 0.001) for both circulation patterns — NE + E + SE and SW + W + NW — presented in a number of days. As time intervals (seasonal intervals) increase between the variables, their relationships weaken. However, two-season intervals continue to be significant, i.e. between the number of days with spring circulation and water temperature in autumn in the stations located closer to deeper regions of the Baltic Sea (Hel, Gdynia).

Statistical significance of asynchronous relationships may be affected by ongoing atmospheric circulation, i.e. occurring while the seasonal temperature data is gathered. The circulation synchronised time-wise with water temperature may either improve or deteriorate correlation relationships. Other factors, both meteorological and hydrological ones, can have a similar effect.

Many other factors, aside from atmospheric circulation, can affect the statistical significance of synchronous and asynchronous relationships. Those relationships would be stronger if circulation patterns accounted for advection intensity. As it is, the significance of such relationships depends on, inter alia: intensity of solar radiation, air temperature, upwelling or river water inflow of differing thermal properties. However, the examination of the impact of those factors on water temperature was omitted, as it would exceed the envisaged scope of the paper.

Acknowledgements

Authors would like to express their gratitude to anonymous referees for their efforts in improving the manuscript.

References

Andersson, H., 2002. Influence of long-term regional and large-scale atmospheric circulation on the Baltic sea level. Tellus A 54 (1), 76—88, http://dx.doi.org/10.1034/j.1600-0870.2002.00288.x.

Bengtsson, L., Hodges, K.I., Roeckner, E., Brokopf, R., 2006. On the natural variability of the pre-industrial European climate. Clim. Dynam. 27 (7—8), 743—760, http://dx.doi.org/10.1007/s00382-006-0168-y.

Bradtke, K., Herman, A., Urbański, J., 2010. Spatial and interannual variations of seasonal sea surface temperature patterns in the Baltic Sea. Oceanologia 52 (3), 345—362, http://dx.doi.org/10.5697/oc.52-3.345.

Brayshaw, D., 2005. Storm Tracks Under Climate Change. rdg.ac.uk.

Bychkova, I.A., Victorov, S.V., 1987. Use of satellite data for identification and classification of upwelling in the Baltic Sea. Oceanology 27 (2), 158—162.

Cyberska, B., 1994. Water temperature. In: Majewski, A., Lauer, Z. (Eds.), Atlas of the Baltic Sea, Wyd. IMGW, Warszawa, 214 pp., (in Polish).

Cyberska, B., Launer, Z., Trzosińska, A (Eds.), 1986. Environmental conditions of the Polish zone of the southern Baltic Sea, Mater. IMGW, Gdynia, (in Polish).

Gidhagen, L., 1987. Coastal upwelling in the Baltic Sea — satellite and in situ measurements of sea-surface temperatures indicating coastal upwelling. Estuar. Coast. Shelf. Sci. 24, 449—462.

Girjatowicz, J.P., 1987. Hydrological and meteorological causes of the occurrence of ice cover inversion in the southern Baltic. Ann. Sci. Stetinenses 2 (2), 45—51, (in Polish).

Girjatowicz, J.P., 1999. The influence of atmospheric circulation on water temperature at the Polish Baltic in cold half-year, Inż. Mor. Geotech. 1, 4—7, (in Polish).

Girjatowicz, J.P., 2001. Effects of atmospheric circulation on ice conditions in the Southern Baltic coastal lagoons. Int. J. Climatol. 21 (13), 1593—1605, http://dx.doi.org/10.1002/joc.698.

Girjatowicz, J.P., 2008. The relationships of the Nord Atlantic Oscillation to water temperature along the southern Baltic Sea Coast. Int. J. Climatol. 28, 1071—1081, http://dx.doi.org/10.1002/joc.1618.

Gurova, E., Lehmann, A., Ivanov, A., 2013. Upwelling dynamics in the Baltic Sea studied by a combined SAR/infrared satellite data and circulation model analysis. Oceanologia 55 (3), 687—707, http://dx.doi.org/10.5697/oc.55-3.687.

Hagen, E., Feinstel, R., 2005. Climatic turning points and regime shifts in the Baltic sea region: the Baltic winter index (1659—2002). Boreal Environ. Res. 10, 211—224.

Hydrographic Yearbook of the Baltic Sea, 1950-1970, Wyd. Komunik. Łącz., Warszawa, (in Polish).

Hydrological and Meteorological Marine Bulletin, 1961-1990, Wyd. IMGW, Warszawa, (in Polish).

Kowalewska-Kalkowska, H., Lejman, J., 2002/2003. Changes of water physical features as indicators of the convection movements in the Coastal Zone of the Pomeranian Bay. Baltic Coast. Zone (7), 5—20.

Kowalewski, M., 2016. Water Temperature (PM3D model). www.satbaltyk.pl.

Kowalewski, M., Ostrowski, M., 2005. Coastal up- and downwelling in the southern Baltic. Oceanologia 47 (4), 453—475.

Kozlov, I., Kudryavtsev, V., Johannessen, J., Chapron, B., Dailidiene, I.I., Myasoedov, A., 2012. ASAR imaging for coastal upwelling in the Baltic Sea. Adv. Space Res. 50 (8), 1125—1137, http://dx.doi.org/10.1016/j.asr.2011.08.017.

Koźmiński, Cz., Michalska, B., 2005. Sunshine in Poland. Akad. Rol., Szczecin 110 pp., (in Polish).

Kożuchowski, K., Marciniak, K., 1988. Variability of mean monthly temperatures and semi-annual precipitation totals in Europe in relation to hemispheric circulation patterns. J. Climatol. 8 (2), 191—199, http://dx.doi.org/10.1002/joc.3370080206.

Krężel, A., 1997. Recognition of mesoscale hydrophysical anomalies in a shallow sea using broadband satellite teledetection methods. Uniw. Gdańsk., Gdańsk, 173 pp., (in Polish).

Krężel, A., Ostrowski, M., Szymelfenig, M., 2005. Sea surface temperature distribution during upwelling along Polish Baltic coast. Oceanologia 47 (4), 415—432.

Krzymiński, W, Łysiak-Pastuszak, E, Miętus, M (Eds.), 1999. Environmental conditions in the Polish Zone of the southern Baltic Sea, Mater. IMGW, Gdynia, (in Polish).

Lamb, H.H., 1978. Climate: Present, Past and Future. Methuen, London, 825 pp.

Leckebusch, G.C., Ulbrich, U., 2004. On the relationship between cyclones and extreme windstorm events over Europe under climate change,. Global Planet. Change 44 (1—4), 181—193, http://dx.doi.org/10.1016/j.gloplacha.2004.06.011.

Lehmann, A., Myrberg, K, Höflich, K., 2012. A statistical approach to coastal upwelling in the Baltic Sea based on the analysis of satellite data for 1990—2009. Oceanologia 54 (3), 369—393, http://dx.doi.org/10.5697/oc.54-3.369.

Leppäranta, M., Myrberg, K., 2009. Physical Oceanography of the Baltic Sea. Springer and Praxis Publishing, Berlin, 371 pp.

Lityński, J., 1969. A numerical classification of circulation patterns and weather types in Poland. Prace Państwowego Instytutu Hydrologiczno-Meteorologicznego, 3—15, 97 pp., (in Polish).

Löptien, U., Zolina, O., Gulev, S., Latif, M., Soloviov, V., 2008. Cyclone life cycle characteristics over the Northern Hemisphere in coupled GCMs. Clim. Dynam. 31 (5), 507—532, http://dx.doi.org/10.1007/s00382-007-0355-5.

Łomnicki, A., 1999. Introduction to Statistics for Naturalists. Wydawnictwo Naukowe PWN, Warszawa, 263 pp. (in Polish).

Łomniewski, K., 1960. Thermohaline relations in the coastal zone of the southern Baltic Sea, Zeszyty Geograficzne 2. Wydawnictwo Wyższej Szkoły Pedagogicznej, Gdańsk, 45—74, (in Polish).

Marsz, A., 1999. The North Atlantic Oscillation and the thermal regime of waters in the area of north—west Poland and the Polish coast of the Baltic Sea. Przegl. Geogr. 71 (3), 225—245, (in Polish).

Marsz, A.A., Styszyńska, A. (Eds.), 2002. North Atlantic Oscillation and its role in shaping of variability of climate and hydrological conditions in Poland. Akad. Mor., Gdynia, 222 pp., (in Polish).

Miętus, M (Ed.), 1997. The climate of the Baltic Sea basin, WMO/TD-No. 933. IMGW, Gdynia, 185 pp.

Miętus, M., 1999. The role of atmospheric circulation over Europe and north Atlantic in forming climatic and oceanographic conditions in the Polish coastal zone, Mater. Bad., ser. Meteorologia 29. IMGW, Warszawa, 157 pp., (in Polish).

Miętus, M, Łysiak-Pastuszak, E, Zalewska, T., Krzymiński, W (Eds.), 2002—2010. Southern Baltic Sea — environmental conditions, Mater. IMGW, Gdynia, (in Polish).

Myrberg, K., Andrejev, O., 2003. Main upwelling regions in the Baltic Sea — a statistical analysis based on three-dimensional modelling,. Boreal Environ. Res. 8, 97—112.

Omstedt, A., Elken, J., Lehmann, A., Leppäranta, M., Meier, H.E.M., Myrberg, K., Rutgersson, A., 2014. Progress in physical oceanography of the Baltic Sea during the 2003—2014 period. Prog. Oceanogr. 128, 139—171, http://dx.doi.org/10.1016/j.pocean.2014.08.010.

Paszkuta, M., Stoń-Egiert, J., Stramska, M., Zapadka, T., 2012. Practical applicability and preliminary results of the Baltic Environmental Satellite Remote Sensing System (SatBaltic), Geophys. Res. Abstracts 14, EGU2012-12987.

Pianko-Kluczyńska, K., 2006. New calendar of types of atmospheric circulations according to J. Lityński. IMGW, Warszawa, 123 pp., (in Polish).

Rozwadowska, A., 1992. The variability of solar energy inflow to the southern Baltic Sea, typescript of PhD dissertation, IO PAS, Sopot. 140 pp., (in Polish).

Sepp, M., Post, P., Jaagus, J., 2005. Long-term changes in the frequency of cyclones and their trajectories in Central and Northern Europe. Nord. Hydrol. 36 (4—5), 297—309.

Siegel, H., Gerth, M., Schmidt, T., 1996. Water exchange in the Pomeranian Bight investigated by satellite data and shipborne measurements. Cont. Shelf Res. 16 (14), 1793—1817, http://dx.doi.org/10.1016/0278-4343(96)00012-X.

Siegel, H., Gerth, M., Tiesel, R., Tschersich, G., 1999. Seasonal and interannual variation in satellite derived sea surface temperature of the Baltic Sea in the 1990s. German J. Hydrogr. 51 (4), 407—422, http://dx.doi.org/10.1007/BF02764163.

Siegel, H., Gerth, M., Tschersich, G., 2006. Sea surface temperature development of the Baltic Sea in the period 1990—2004. Oceanologia 48 (S), 119—131.

Siegel, H., Gerth, M., Tscherisich, G., 2008. Satellite-derived sea surface temperature for the period 1990-2005. In: Feistel, R., Nausch, G., Wasmund, N. (Eds.), State and evolution of the Baltic Sea. Wiley Interscience, Warnemünde, 207—217.

Stramska, M., Białogrodzka, J., 2015. Spatial and temporal variability of sea surface temperature in the Baltic Sea based on 32-years (1982—2013) of satellite data. Oceanologia 57 (3), 223—235, http://dx.doi.org/10.1016/j.oceano.2015.04.004.

Time Series Analysis. Section III, 2010, Department of Statistics, Univ. Oxford, Oxford, 47 pp.

Uiboupin, R., Laanemets, J., 2009. Upwelling characteristics derived from satellite sea surface temperature data in the Gulf of Finland, Baltic Sea,. Boreal Environ. Res. 14, 297—304.

Urbański, J., 1995. Upwellings along the Polish coast of the Baltic Sea. Przegl. Geofiz. 40 (2), 141—153, (in Polish).

Walther, A., Bennartz, R., 2006. Radar-based precipitation type analysis in the Baltic area. Tellus A 58 (3), 331—343, http://dx.doi.org/10.1111/j.1600-0870.2006.00183.x.

Woźniak, B., Bradtke, K., Darecki, M., Dera, J., Dudzińska-Nowak, J., Dzierzbicka-Głowacka, L., Ficek, D., Furmańczyk, K., Kowalewski, M., Krężel, A., Majchrowski, R., Ostrowska, M., Paszkuta, M., Stoń-Egiert, J., Stramska, M., Zapadka, T., 2011a. SatBałtyk — a Baltic environmental satellite remote sensing system — an ongoing project in Poland, Part 1: Assumptions, scope and operating range. Oceanologia 53 (4), 897—924, http://dx.doi.org/10.5697/oc.53-4.897.

Woźniak, B., Bradtke, K., Darecki, M., Dera, J., Dudzińska-Nowak, J., Dzierzbicka-Głowacka, L., Ficek, D., Furmańczyk, K., Kowalewski, M., Krężel, A., Majchrowski, R., Ostrowska, M., Paszkuta, M., Stoń-Egiert, J., Stramska, M., Zapadka, T., 2011b. SatBałtyk — a Baltic environmental satellite remote sensing system — an ongoing project in Poland, Part 2: Practical applicability and preliminary results. Oceanologia 53 (4), 925—958, http://dx.doi.org/10.5697/oc.53-4.925.

Woźniak, B., Krężel, A., Darecki, M., Woźniak, S., Majchrowski, R., Ostrowska, M., Kozłowski, Ł., Ficek, D., Olszewski, J., Dera, J., 2008. Algorithm for remote sensing of the Baltic ecosystem (DESAMBEN). Part 1: Mathematical Apparatus. Oceanologia 50 (4), 451—508.

Oceanologia (2019) 61, 50—59

Available online at www.sciencedirect.com

ScienceDirect

journal homepage: www.journals.elsevier.com/oceanologia/

ORIGINAL RESEARCH ARTICLE

Driving forces of sandy sediment transport beyond the surf zone

Magdalena Stella [a,*], **Rafał Ostrowski** [a], **Piotr Szmytkiewicz** [a], **Jarosław Kapiński** [b], **Tomasz Marcinkowski** [b]

[a] *Institute of Hydro-Engineering, Polish Academy of Sciences (IBW PAN), Gdańsk, Poland*
[b] *Maritime Institute in Gdańsk, Gdańsk, Poland*

Received 2 November 2017; accepted 12 June 2018
Available online 2 July 2018

KEYWORDS
Wind-induced current;
Wave—current interactions;
Apparent roughness;
Sediment transport rates

Abstract The paper deals with experimental and theoretical investigations of forces that drive sediment motion beyond the surf zone of the southern Baltic Sea. The study site is located in the sandy coastal zone at Lubiatowo (Poland). Field surveys were carried out by the Institute of Hydro-Engineering of the Polish Academy of Sciences (IBW PAN) and the Maritime Institute in Gdańsk (IMG). The measurements comprise parameters of wind, waves and currents. The wind velocities and directions were recorded at the IBW PAN Coastal Research Station (CRS) in Lubiatowo, while the wave and current data were collected near CRS Lubiatowo, ca. 1.5 Nm from the shoreline, at a depth of 17 m. Theoretical investigations concern wind-induced currents, nearbed wave-induced oscillatory velocities and wave-current interactions. The concept of the apparent roughness related to the wave bed boundary layer is used in the description of wind-induced steady flow. A theoretical model of the wind-induced current is proposed in two variants, depending on the predominance of wave or current impact. The wind-induced flow model is successfully verified using measured current velocity profiles. Previously developed at IBW PAN, a three-layer sediment transport model is adapted to the study site and applied in calculations of sediment transport rates.

* Corresponding author at: Institute of Hydro-Engineering, Polish Academy of Sciences (IBW PAN), ul. Kościerska 7, 80-328 Gdańsk, Poland.
E-mail address: m.stella@ibwpan.gda.pl (M. Stella).
Peer review under the responsibility of Institute of Oceanology of the Polish Academy of Sciences.

ELSEVIER Production and hosting by Elsevier

https://doi.org/10.1016/j.oceano.2018.06.003

1. Introduction

In coastal areas, wave-induced orbital velocities together with wave-induced steady currents are the dominant driving forces of sediment transport. The farther in the seaward direction, the weaker the influence of these factors. Beyond the surf zone, wave-driven currents do not occur, and the impact of wave oscillatory flows becomes less important. The seaward boundary beyond which no sediment movement occurs is theoretically defined by the so-called depth of closure (h_c). The depth of closure describes a maximum depth at which bed changes are noticeable, and there is no measurable evolution of the bottom deeper in the sea. The value of the depth of closure h_c can be obtained in two ways. First, there is a theoretical method based on wave parameters, namely an effective wave height H_e (i.e. a significant wave height that is exceeded 12 h during a year, or 0.137% of the time considered) and the corresponding wave energy peak period T_p. Here, two simple formulas can be used, derived by Birkemeier (1985) or earlier by Hallermeier (1978, 1981). The second method is based on the analysis of bathymetric data. Having processed deep-water wave parameters measured at the IBW PAN Coastal Research Station (CRS) in Lubiatowo in 2006-2015, Cerkowniak et al. (2015a) determined H_e = 3.8 m and T_p = 9.75 s. These quantities yielded a depth of closure h_c equal to 7.6 m. Some research investigations, however, show that there are many examples of sediment motion at even greater depths. For example, large bed forms have been observed at depths of 15–30 m along the shores of the southern Baltic Sea, especially on the Polish coast from Hel to Karwia, from Rowy to Ustka and near Kołobrzeg. The bathymetry measured near Rozewie (also in Poland) shows the asymmetry of sand waves (with one steep and one mild slope) that are about 4 m high, see Rudowski et al. (2008) and Kubacka et al. (2016). The most interesting aspect of this finding is that such bed forms are typical of tide-dominated basins, and the formation genesis of such features in a non-tidal sea such as the Baltic Sea is unknown. It should also be highlighted that the analysis of cross-shore profiles near CRS Lubiatowo (Cerkowniak et al., 2015a, 2015b) reveals seabed changes between two measurements at depths greater than the calculated depth of closure. Sediment movement beyond the surf zone is also evidenced by sedimentation found in post-dredging pits at depths of 14–17 m and by the disappearance of traces left by a trailing suction hopper dredger after 11 months. In addition, it is mentioned in the literature that a 0.4–0.8 m thick sand layer moved under storm conditions at depths of 15–20 m (Uścinowicz et al., 2014).

Conventionally (see e.g. Ostrowski, 2004), seabed changes are modelled as resulting from the spatial variability

Figure 1 Measurement location near CRS Lubiatowo.

of net sediment transport rates. The distinct morphodynamic effects observed in the transitional region between the surf zone and the deep sea, where the nearbed hydrodynamic forcing is very weak, probably result from long-term lithodynamic processes of low intensity. Therefore, it seems almost impossible or very difficult to carry out successful quantitative theoretical modelling of the appearance and movement of sandy bed forms or sedimentation in underwater excavations. It is possible, however, to try to identify sediment transport mechanisms at particular water depths. The objective of this paper is to provide a theoretical explanation of nearbed sediment transport and to assess transport rates under storm wave—current conditions in the coastal region beyond the surf zone.

2. Study site

The analysis in the present study is based on theoretical investigation supported by wind, wave and current measurements in the period from April 26, 2014 to June 30, 2014. The field data was recorded by the Institute of Hydro-Engineering of the Polish Academy of Sciences (IBW PAN) and the Maritime Institute in Gdańsk (IMG). The current and waves were measured in the vicinity of CRS Lubiatowo, where wind data was recorded. The study site lies about 70 km NW of Gdańsk (see Figure 1), and its hydrodynamics, lithodynamics and morphodynamics are typical of the south Baltic sandy coast (see Ostrowski et al., 2015). The seashore is mildly sloped (with an inclination of 1—2%) and consists of quartz sand having a grain diameter d_{50} in the range from 0.1 to 0.4 mm (mostly 0.15—0.25 mm). The seabed soil density amounts to ρ_s = 2650 kg/m^3, see Pruszak et al. (2008). In addition, to determine whether the grain diameter differed further away from coast, two samples of surface seabed soil were taken near the wave—current measuring point, at a depth of 17 m.

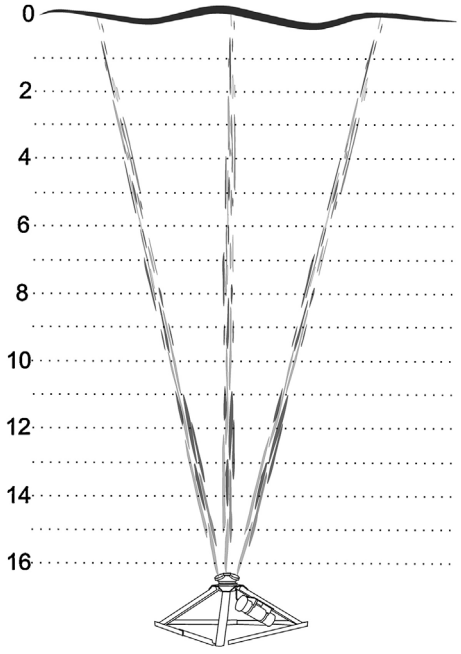

Figure 2 Scheme of wave and flow measurements.

3. Methods of field measurements

Waves and current were measured using an acoustic current profiler with an attached surface wave measurement module AWAC (produced by Nortek) operating at a 600 kHz transmit frequency. The device was installed on a bottom-resting frame (see Figure 2) at a distance of about 1.47 Nm (i.e. 2.72 km) from the coastline, where the mean water depth amounted to 17 m, at coordinates 54°50.48′N and 17°53.09′E. The device collected data on wave height, period and direction, as well as on current velocity and direction. Wave parameters were measured continuously once an hour for about 17 min (2048 samples recorded with a frequency of 2 Hz) and then averaged. Water flows were measured in 1-m-thick layers once an hour, and they were averaged for 2-min recordings registered with a 1 Hz frequency. Current measurements were not performed in the nearbed layer (about 1 m thick), because of technical reasons (height of the frame on which the instrument was mounted and the so-called blanking distance i.e. direct water body thickness to transducers where the accuracy of measurements

Figure 3 Anemometer on top of a mast at CRS Lubiatowo.

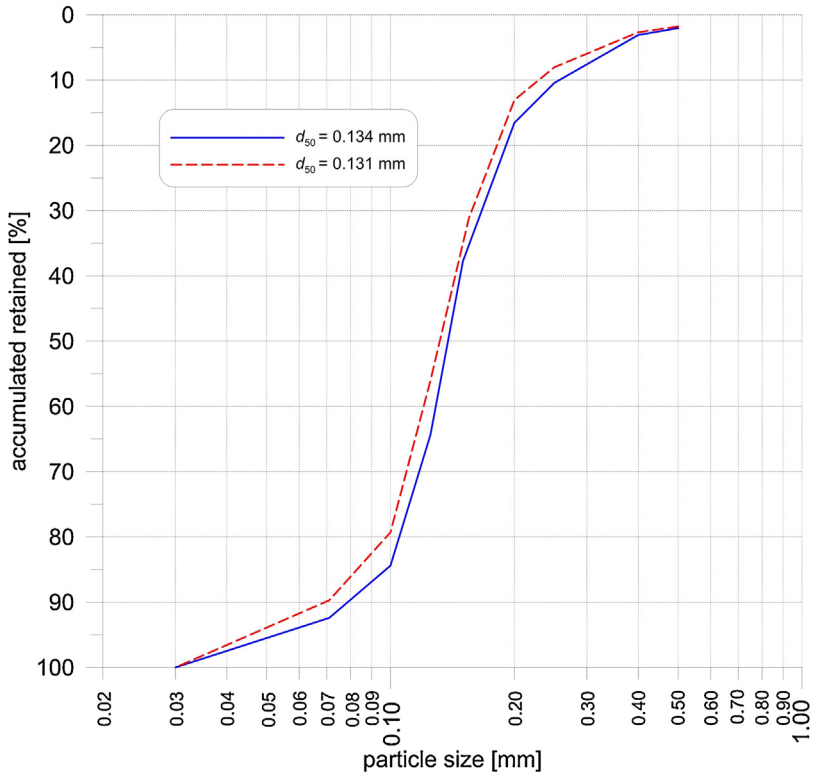

Figure 4 Grain size distributions based on samples taken on October 10, 2014.

is not acceptable). Additionally, the results of current measurements in the surface water layer (from 5 to 10% of the total depth) have limited reliability due to side-lobe interference. This layer should, therefore, be analysed with some care. Raw and processed wave data were collected in the internal memory of the instrument and retrieved for analysis during maintenance cruises.

The wind data were collected by a cup anemometer SW-48 (produced by MORS, Poland) installed on a mast 22 m high. The mast is located on land close to CRS Lubiatowo (54°48.70′N, 17°50.43′E), at a distance of about 150 m from the shoreline. The anemometer stands out about 4 m above the top branches of the nearby trees (Figure 3).

The measurements are slightly biased by the nearby trees. It is possible to recalculate the "land" wind velocity recorded at CRS Lubiatowo to obtain the wind velocity at sea. This was done in the present study by a method proposed by Ostrowski et al. (2017).

4. Measured data

4.1. Grain size analysis

Grain size distribution analysis based on two samples taken on October 10, 2014 (Figure 4) showed that the sediment was well sorted, and the grain diameter d_{50} was equal to 0.131 mm and 0.134 mm (an approximate value of 0.13 mm was subsequently used in the theoretical modelling of sediment transport). The first sample contained fine sand, and the second sample contained fine sand with an admixture of silt. The seabed soil density of the samples amounted to ρ_s = 2650 kg/m^3 and ρ_s = 2645 kg/m^3, respectively (Table 1).

4.2. Wave and flow velocity measurements

The measurements of current, wind and wave parameters (Table 2) revealed that the dominant direction for all factors

Table 1 Results of grain size analysis for samples taken on October 10, 2014.

	Sample 1	Sample 2
Seabed soil	Fine sand	Fine sand with silt admixture
Grain percentage of diameter > 2 mm	0%	0%
Grain percentage of diameter 2–0.05 mm	96%	92.5%
Grain percentage of diameter 0.05–0.002 mm	4%	7.5%
Grain percentage of diameter < 0.002 mm	0%	0%
Seabed soil density ρ_s	2.65 g/cm^3	2.645 g/cm^3
d_{50}	0.134 mm	0.131 mm

Table 2 Dominant direction, mean and maximum values of measurements of flow velocity, wind speed and significant wave height for the period from April 26, 2014 to June 30, 2014.

	Flow (averaged over water column)	Wind	Significant wave
Dominant direction	From N and NW (46%)	From N and NW (36%)	From N and NW (49%)
Mean	0.13 m/s	6.3 m/s	0.67 m
Maximum	0.44 m/s	16.6 m/s	2.76 m

was alike, i.e. from N and NW sectors. Further analysis and modelling, however, was performed for all directions. The maximum current velocity averaged over the water column amounted to 0.44 m/s, and the mean value was 0.13 m/s. The maximum wind speed amounted to 16.6 m/s, whereas the mean wind speed during the measurement period was equal to 6.3 m/s. The maximum significant wave height amounted to 2.76 m, and the mean wave height was equal to 0.67 m.

5. Velocity profile

In the formulation of the wind-induced flow model, aside from the wind velocity being the major input, wave–current interaction is taken into account. In addition, the effect of the wave bed boundary layer on the steady current is considered. The procedure comprises 4 major stages described below. Stage 1 has recently been proposed by Ostrowski et al. (2017), and it is briefly presented here to make the reasoning complete and comprehensible.

6. Stage 1: logarithmic velocity distribution

The first stage is based on the assumption that the shear stresses τ in the water column, where the wind-driven current occurs, satisfy the Boussinesq hypothesis as follows:

$$\tau = \rho \nu_t \frac{du(z)}{dz}, \tag{1}$$

where ν_t is the kinematic turbulent viscosity in the vertical direction z, and $u(z)$ is the velocity of stationary water flow.

It is further assumed that turbulent viscosity increases linearly from the bottom, being proportional to von Karman's constant κ and the friction velocity u_f, so that

$$\nu_t = \kappa u_f z. \tag{2}$$

With the shear stress defined as $\tau = \rho u_f^2$, it is possible to obtain the logarithmic vertical distribution of the flow velocity $u(z)$:

$$u(z) = \frac{u_f}{\kappa} \ln\left(\frac{z}{z_0}\right), \tag{3}$$

in which z_0 denotes the ordinate at which the velocity u equals zero.

The quantity z_0 can be regarded as a theoretical seabed level from which the logarithmic profile of the velocity $u(z)$ starts. In this paper, this level is defined as the bottom roughness height $z_0 = k_f/30$, where k_f is the bed form height, assumed to be equal to 0.1 m. The bed form height is the mean magnitude of seabed forms observed at the study site.

The wind-driven current speed in the surface layer equals 2–5% of the wind speed w at the 10 m height above the sea level (see e.g. Kim et al., 2010). Analysis of the wind data and surface current velocity measurements showed that for wind speeds averaged over 12 h exceeding 8 m/s, the magnitude of the surface current (in a 1-m-thick layer) was about 3.5% of the wind speed, and for winds below 8 m/s, the surface velocity was around 3% of the wind speed. Thus, the empirical formula proposed e.g. by Kim et al. (2010) is assumed as follows:

$$\begin{aligned} u_{surface} &= 0.035w \text{ for } w > 8\,\text{m/s}, \\ u_{surface} &= 0.03w \text{ for } w < 8\,\text{m/s}. \end{aligned} \tag{4}$$

It was found by Ostrowski et al. (2017) that mean flow velocities measured in the entire water column had almost the same direction as the local wind. Hence, it appears that at the limited depths of the Baltic Sea the wind-driven current velocity profile can be described by a directionally invariable distribution.

The wind-driven flow velocity in the surface layer (from the mean water level to 1 m depth, namely for z = 16.5 m) is calculated by Eq. (4). With the assumed bed roughness and with the resulting value of z_0, one can easily determine the friction velocity u_f from Eq. (3) if only the flow velocity u at any level z is known. The velocity calculated by Eq. (4) is assumed to satisfy the logarithmic distribution given by Eq. (3). Thus, on the basis of Eq. (3), the sought friction velocity u_f reads

$$u_f = \frac{\kappa \cdot u(z = 16.5\text{m})}{\ln((z = 16.5\text{m})/z_0)}. \tag{5}$$

It is visible from the form of Eqs. (1)–(3) that both the friction velocity u_f and the shear stress τ are independent of the ordinate z (constant in the entire water column).

After the friction velocity u_f has been calculated, the vertically averaged velocity u_{mean} is determined using the integrated logarithmic velocity distribution of Eq. (3) as follows:

$$\begin{aligned} u_{mean} &= \frac{1}{h}\int_0^h u(z)dz = \frac{1}{h}\int_0^h \left[\frac{u_f}{\kappa}\ln\left(\frac{z}{z_0}\right)\right]dz \\ &= \frac{u_f}{\kappa}\left[\ln\left(\frac{h}{z_0}\right) - 1\right]. \end{aligned} \tag{6}$$

7. Stage 2: wave influence on wind-driven current

In order to include the effect of wave propagation accompanied by the wind-driven current, represented by the vertically averaged velocity u_{mean}, the dispersion relationship in the following form is applied:

$$gk\tanh kh = (\omega - ku_{mean}\cos\alpha)^2, \tag{7}$$

where ω is the angular frequency in wave motion, $k = 2\pi/L$ is the wave number (L stands for the wave length), and α denotes the angle between the wind-induced flow velocity u_{mean} (having the same direction as the local wind) and the wave propagation direction.

It is also necessary to include an additional hydrodynamic effect that appears as a larger roughness for the steady flow due to the occurrence of waves (see e.g. Nielsen, 2009), which is called the apparent bottom roughness k_a:

$$k_a = \frac{30z_{max}}{\exp(V\kappa/u_{fc})}. \tag{8}$$

In the above equation, z_{max} denotes the upper limit of the wave bed boundary layer, and V is the mean velocity at the ordinate z_{max}, while the friction velocity u_{fc} is calculated from the values of the wave-induced friction velocity $u_f(t)$ according to the following formula (see Ostrowski, 2004):

$$u_{fc} = \sqrt{\frac{1}{T}\int_0^T |u_f(t)|u_f(t)\cos\varphi(t)d\omega t}, \tag{9}$$

where $\cos\varphi(t)$ is an instantaneous angle between the steady current and the direction of wave-induced nearbed oscillatory flow during the wave period T.

Time series of water surface elevation are rarely available from field measurements. The field wave data usually comprise representative wave parameters, namely wave height (e.g. root-mean-square wave height H_{rms}), period (e.g. wave energy peak period T_p) and direction (e.g. wave energy peak direction), as well as water depth. Nearbed wave-induced velocities (variable over wave period) can be calculated from these parameters according to a wave theory — linear or nonlinear. A bed shear stress model should then be applied to determine the time-variable friction velocity u_f, needed to obtain u_{fc} from Eq. (9).

Developed by Kaczmarek and Ostrowski (2002), the model of intensive near-bed sand transport under wave–current flow has been adapted to the case of the open sea (beyond the surf zone). The time-variable friction velocity u_f related to bed shear stresses generated jointly by waves and the wind-driven current, as well as the friction velocity u_{fc} and the apparent roughness k_a were determined iteratively. The wave parameters H_{rms} and T_p were taken from the analysis of the wave data collected from April 26, 2014 to June 30, 2014 in the study area constituted the input data for these calculations. The initial mean velocity was obtained by the method described in stage 1.

After all the above necessary quantities, including the effects of wave–current interaction, had been determined, the steady flow velocity was obtained as follows:

$$u(z) = \frac{u_{fc}}{\kappa}\ln\left(\frac{30z}{k_a}\right). \tag{10}$$

8. Stage 3: dependence of flow distribution on dominant force

After confrontation of the theoretical values of flow velocity profiles with the measured ones, it appeared that not every measured case met the logarithmic distribution. This depends largely on the dominant force acting under conditions at the time. The data analysis together with the results from stages 1 and 2 made it possible to assume that the

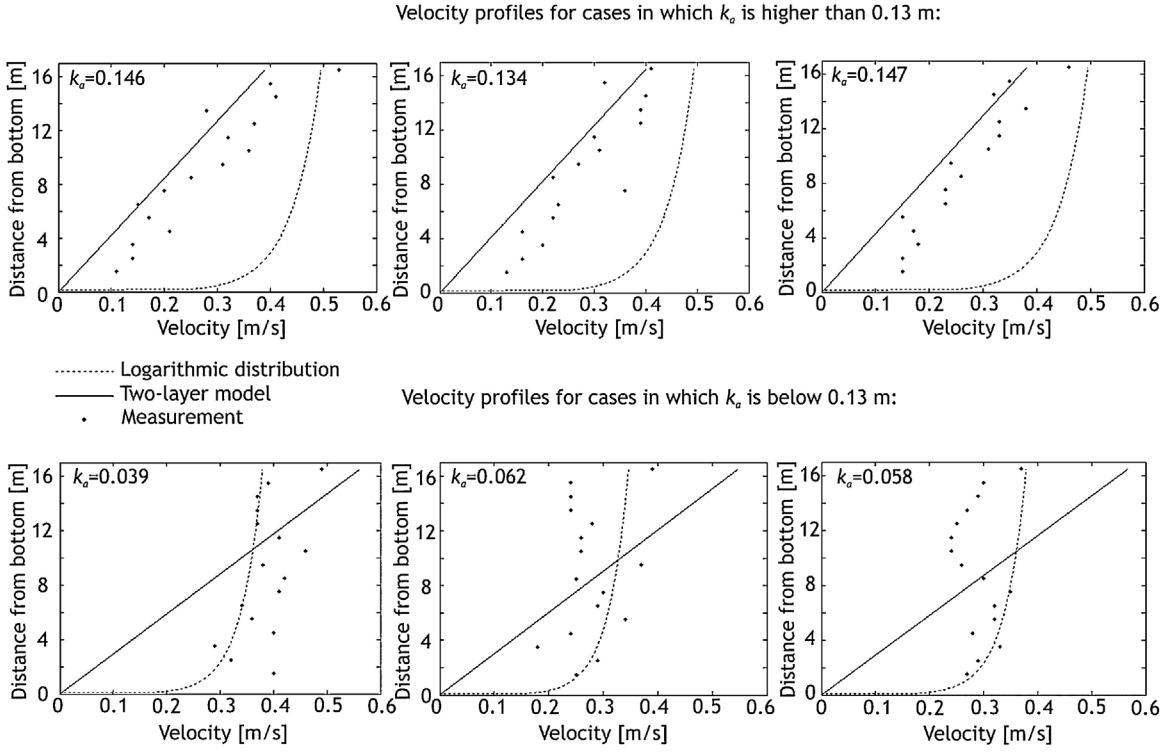

Figure 5 Examples of flow velocity distribution for different apparent roughness values.

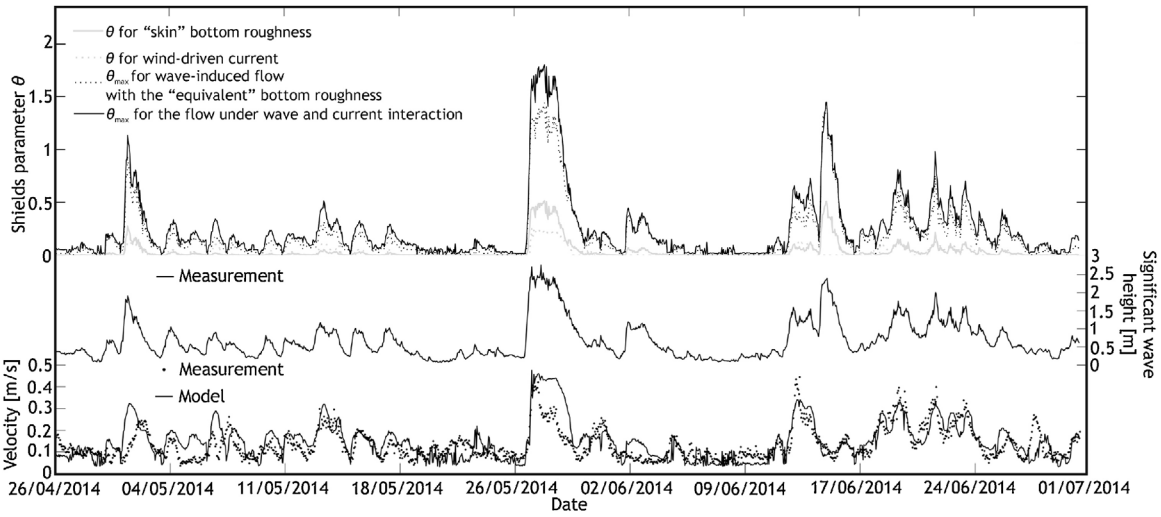

Figure 6 Hourly time series of measured wave height and mean flow velocity for the time period from April 26, 2014 to June 30, 2014 versus mean flow velocity u_{mean} calculated by the method described in stage 3 and Shields parameter calculated for different kinds of flow.

distinction between wave- and current-dominated flows can be made using the value of apparent roughness. Then it is possible to divide the solution of flow distribution into two methods, depending on which phenomenon is predominant.

The analysis has shown that the wave flow is dominant under conditions in which the apparent roughness k_a is bigger than 0.13 m. In such a case, the following two-layer distribution of turbulent viscosity ν_t and velocity u is assumed:

$$\begin{aligned} \nu_t &= \kappa u_f z \quad u = \frac{u_f}{\kappa}\ln\frac{z}{z_0} \quad \text{for} \quad z<\delta, \\ \nu_t &= \kappa u_f \delta \quad u = \frac{u_f}{\kappa}\left(\frac{z}{\delta}+\ln\frac{\delta}{z_0}-1\right) \quad \text{for} \quad z>\delta, \end{aligned} \tag{11}$$

where δ denotes the wave–current boundary layer thickness in the phase of wave crest, determined using the integral momentum model of Fredsøe (1984).

The analysis has shown that the wind current is dominant when the apparent roughness k_a is below 0.13 m. In such a case, the flow velocity profile in the water column is calculated by the method described in stage 2, using Eq. (10).

Examples of flow velocity distribution for different apparent roughness values k_a are shown below (Figure 5).

The turbulent viscosity distribution described by Eq. (11) yields a logarithmic velocity profile in a thin nearbed layer only and a linearly variable velocity in the water column. This is visible in the upper part of Figure 5, where the linear velocity distributions match the measured velocities for $k_a < 0.13$ m. The lower part of Figure 5 implies that for $k_a > 0.13$ m the logarithmic velocity profiles (resulting from the linearly variable turbulent viscosity distribution given by Eq. (2)) match the experimental data better than the linear velocity profiles.

9. Stage 4: result verification

The last stage consists in verifying the modelled mean flow velocity u_{mean} from stage 3 by the measured one. The results of calculations versus measurements, together with the dimensionless bed shear stresses θ (Shields parameter) determined as described by Ostrowski et al. (2017), are shown in Figure 6.

It can be seen in Figure 6 that the agreement between measured and modelled velocities varies from good in some time segments to poor in others. Distinct underestimations by the model are seen for the beginning of May 2014, when both high and moderately high waves occur. A similar underestimation is visible for a storm that occurred in the end of May. Considerable overestimations can be seen only for a storm of middle June 2014 and for 28 June, while slight overestimations occur for a series of weak storms in the period from 20 to 23 June.

The statistical analysis of the measured mean flow velocities for the period from April 26, 2014 to June 30, 2014 versus those calculated by the method described in stage 3 shows a relatively good correlation, with a correlation coefficient r of 0.71 (Figure 7).

10. Sediment transport

Sediment transport rates were calculated by the three-layer model of Kaczmarek & Ostrowski (2002), adapted to the study site conditions. The model consists of different theoretical descriptions in each of three layers: the bedload layer

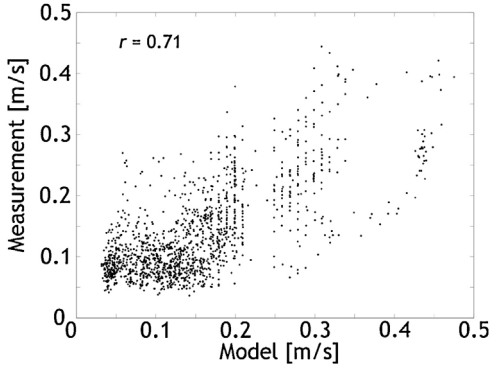

Figure 7 Scatterplot of measured mean flow velocity against modelled velocities u_{mean} for the period from April 26, 2014 to June 30, 2014.

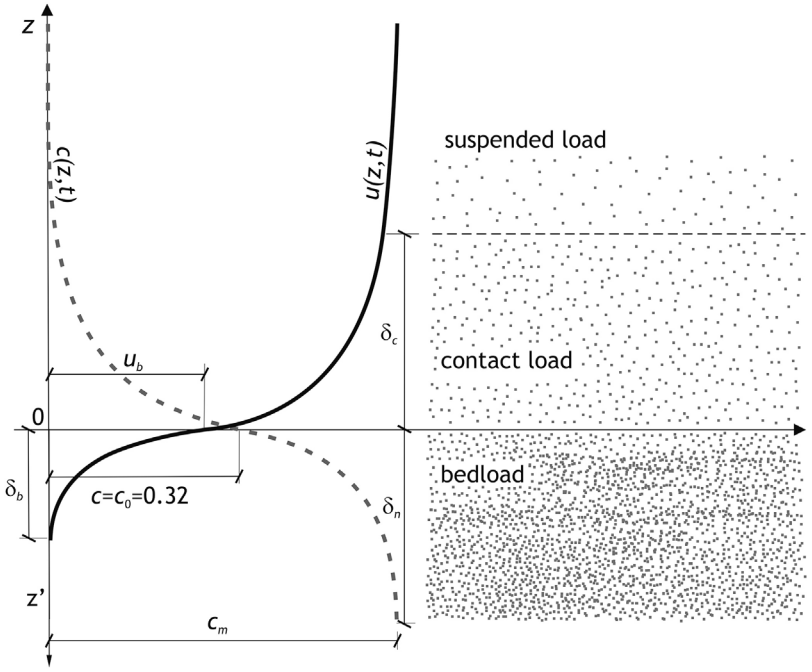

Figure 8 Three-layer sediment transport model.

(below the theoretical bed level) and two layers of suspension, namely the contact load layer (nearbed suspension of sediment) and the outer layer (suspension higher in the water column), as shown in Figure 8.

The bedload layer consists of a moveable dense water-sand mixture, while the contact load layer consists of water with suspended sand grains. Close to the bedload layer, the concentration of suspended sediment in the contact load layer is very high and corresponds to sand liquidity, with $c = c_0 = 0.32$. On the boundary between the bedload layer and the contact load layer, the liquefied sand moves with the velocity $u = u_b$. On the basis of the input friction velocity, this quantity is obtained from the solution of the bedload layer and then used as a boundary condition in the solution of the contact load layer. Deeper in the seabed, the concentration is assumed to represent moderately closely packed sand grains ($c = c_m$). The details of the phase-resolving models of the bedload layer and the contact load layer can be found in the publication of Kaczmarek and Ostrowski (2002).

Sediment transport rates are quantified separately for each layer. In the contact load layer and in the bedload layer, they are obtained from calculated instantaneous distributions of velocity and the concentration of water-soil mixture in the following way:

$$q_b(t) = \int_0^{\delta} u(z',t)\cdot c(z',t)dz', \tag{12}$$

$$q_c(t) = \int_0^{\delta_c} u(z,t)\cdot c(z,t)dz, \tag{13}$$

where δ_b is the thickness of the bedload layer, and δ_c is the thickness of the contact load layer.

In the suspended load layer (beyond the nearbed layer), the sediment transport rate is determined in a simplified way, using time-averaged velocity and concentration:

$$q_{out} = \int_{\delta_c}^{h} \overline{u}(z)\cdot\overline{c}(z)dz. \tag{14}$$

The results of sediment transport calculations are presented in Figure 9, which shows sediment transport rates (separately for each layer) obtained on the basis of the measured and modelled flow velocities.

The largest rates of sediment transport were obtained for conditions of strong wind-driven current accompanied by high (stormy) waves, generating high shear stresses (represented by Shields parameter), cf. Figure 6. It should be pointed out that high waves or strong current alone can generate some sediment transport, but not as intensive as the one when these phenomena occur simultaneously. This is visible in Figure 9 where long periods of no transport or very low transport predominate.

In addition, [the comparison of sediment transport rates obtained from the modelled mean flow velocity and those obtained from the measured values within the three layers shows a strong correlation, with the correlation coefficient r amounting to 0.88, 0.93 and 0.9 for q_{out}, q_s and q_b, respectively (Figure 10).

Although strong correlations exist for all sediment transport components, it can be seen in Figure 10 that the transport rates determined for the modelled flow velocities are overestimated with respect to the rates determined using the measured velocities. This certainly results from an overestimation of flow velocities, cf. Figure 7. The overestimation concerns all components of sediment transport and is particularly visible for high transport rates, occurring under intensive hydrodynamic conditions.

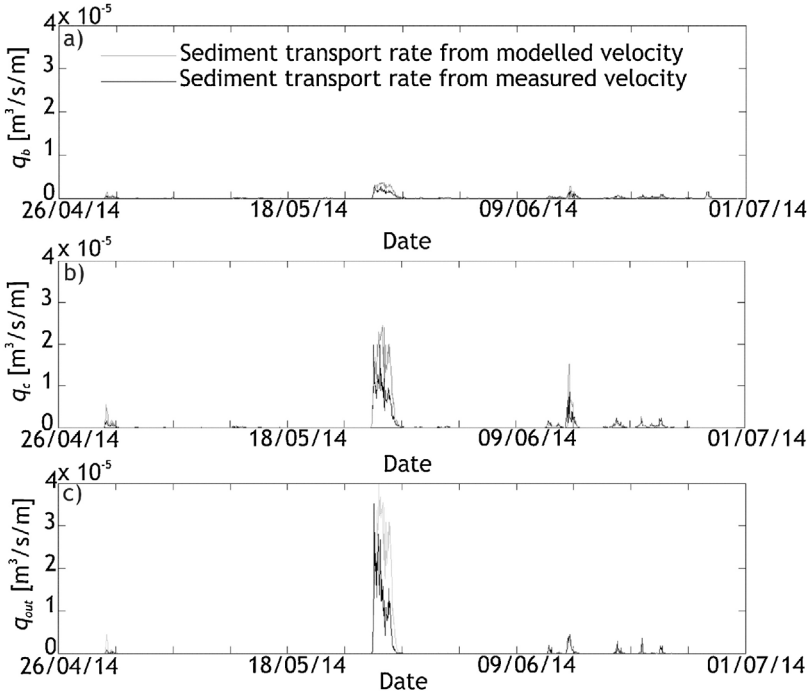

Figure 9 Sediment transport rates in bedload (a), contact load (b) and suspended load (c) layers obtained by three-layer sediment transport model on the basis of modelled and measured mean flow velocities from Figure 6.

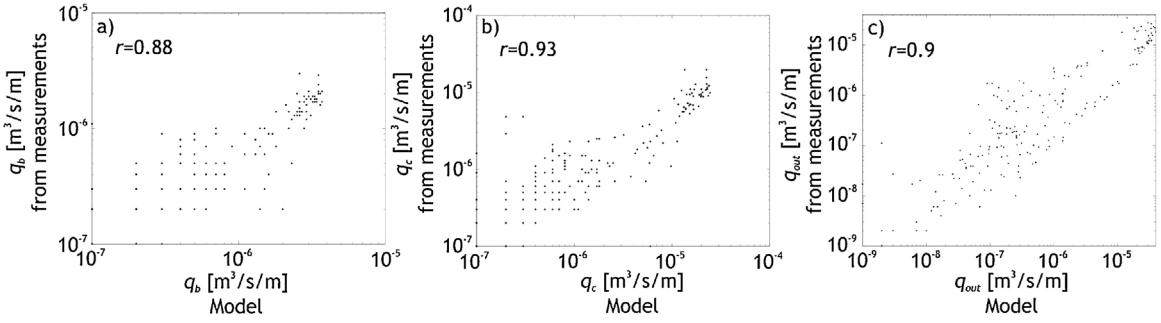

Figure 10 Scatterplot of sediment transport rates in bedload (a), contact load (b) and suspended load (c) layers obtained by three-layer sediment transport model on the basis of modelled and measured mean flow velocities.

11. Discussion

The sediments at the study site, namely fine quartz sand (see Table 1 and Figure 4), are susceptible to movement even under mild hydrodynamic forcing. Sediment motion near the bottom is frequently associated with the appearance and evolution of sandy bed forms. Interesting information on the presence of bed forms in the study area was provided by a survey carried out with a multi-beam echo-sounder and a sonar in the period from November 7 to 8, 2017. The measurements covered a rectangular area of 2.6 km × 0.53 km, with the base lying parallel to the shoreline, about 2.5 km offshore. The surveyed sea bottom was mostly smooth. In some regions, however, two kinds of bed forms were observed. There were ripple marks with approximate heights from 5 cm to 20 cm and a crest-to-crest distance (i.e. sand wave length) of about 1—2 m, as well as larger sand waves having a length of 5—10 m.

The present study is not aimed at theoretical modelling of the appearance and evolution of the sandy bed forms observed. Sediment transport rates obtained for extreme wave—current conditions can, however, constitute evidence of motion of sandy material at depths that are conventionally believed to lie beyond the depth of closure, delimiting the region where seabed dynamics is assumed to be intensive.

The sediment transport rates modelled for stormy wave—current conditions, extreme in the period of measurements, at the end of May 2014 attain the values of about 0.3×10^{-5}, 2×10^{-5} and 3×10^{-5} m^3/s/m for bedload (q_b), contact load (q_c) and suspended load (q_{out}), respectively. The rate of sediment motion suspended beyond the nearbed layer (q_{out}) distinctly predominates over the nearbed transport rates (q_b and q_s). This is due to the very fine sand grains of the seabed (d_{50} = 0.13 mm). The situation would be opposite for coarser sand, with d_{50} = 0.2 mm or more (Ostrowski, 2004).

In order to realize the accumulative potential of the above rates, let us imagine a 1-m-wide sand trap in the sea bottom. Under the extreme hydrodynamic conditions considered, such a virtual sand trap would accumulate 0.19 m^3 of sediment per hour.

Under conditions of simultaneous strong wind-induced current and high waves, the driving forces of intensive sediment transport are triggered. These driving forces are represented by high values of the dimensionless shear stress (Shields parameter θ). However, one should bear in mind that there could be another factor responsible for sediment movement and generation of sand waves. One can suppose that this factor becomes predominant under calm conditions when the impact of waves and wind-driven currents is smaller. As already mentioned, bed forms observed in the south Baltic beyond the surf zone have a shape typical of tide conditions. Thus the idea arises that a phenomenon like internal waves could also play an important role in the formation of those subaqueous sand dunes. This is an interesting and still unexplored hypothesis for further research.

12. Conclusions

The results of measurements and modelling presented in this paper were helpful in identifying sediment transport mechanisms at water depths greater than the conventionally defined depth of closure. The investigations concerned a coastal location with a water depth of 17 m. Even during heavy storms, the wave-induced nearbed oscillatory water motion is not capable of causing noticeable sediment transport. Similarly, a wind-driven steady current alone does not generate bed shear stresses sufficient to move the bottom sand. It turns out that under strong storm conditions the stresses represented by Shields parameter resulting from the wave—current flow are higher than the sum of stresses for stationary and wave flows separately. The stronger the storm conditions, the stronger the impact of wind current on the sediment movement seems to be. Only synergic nonlinear interaction of waves and wind-induced currents under extreme stormy conditions can result in distinct nearbed sediment motion. This hypothesis was supported by the computations of sediment transport rates in the three-layer model.

The proposed simple two-variant model of wind-induced current was successfully tested versus field wind and current data. The model was then used to simulate joint wave—current nearbed shear stresses, being the driving forces of sand motion.

The sediment transport rates obtained for the stormiest period of measurements appeared sufficiently high to represent a considerably intensive movement of fine sand grains constituting the sea bottom. It can be expected that seabed dynamics under such conditions will result in the emergence and evolution of bed forms. This process, however, lies beyond the scope of the study.

References

Birkemeier, W.A., 1985. Field data on seaward limit of profile change. J. Waterw. Port. C-ASCE 111 (3), 598—602, http://dx.doi.org/10.1061/(ASCE)0733-950X(1985)111:3(598).

Cerkowniak, G.R., Ostrowski, R., Stella, M., 2015a. Depth of closure in the multi-bar non-tidal nearshore zone of the Baltic Sea: Lubiatowo (Poland) case study. Bull. Maritime Inst. Gdańsk 30 (1), 180—188, http://dx.doi.org/10.5604/12307424.1185577.

Cerkowniak, G.R., Ostrowski, R., Stella, M., 2015b. Wave-induced sediment motion beyond the surf zone: case study of Lubiatowo (Poland). Arch. Hydro-Eng. Environ. Mech. 62 (1—2), 27—39, http://dx.doi.org/10.1515/heem-2015-0017.

Fredsøe, J., 1984. Turbulent boundary layer in combined wave—current motion. J. Hydraul. Eng. ASCE 110 (8), 1103—1120, http://dx.doi.org/10.1061/(ASCE)0733-9429(1984)110:8(1103).

Hallermeier, R.J., 1978. Uses for a calculated limit depth to beach erosion. In: Proceedings, 16th Coastal Engineering Conference, Amer. Soc. Civil Eng. 1493—1512.

Hallermeier, R.J., 1981. A profile zonation for seasonal sand beaches from wave climate. Coast. Eng. 4 (3), 253—277.

Kaczmarek, L.M., Ostrowski, R., 2002. Modelling intensive near-bed sand transport under wave—current flow versus laboratory and field data. Coast. Eng. 45 (1), 1—18, http://dx.doi.org/10.1016/S0378-3839(01)00041-2.

Kim, S.Y., Cornuelle, B.D., Terrill, E.J., 2010. Decomposing observations of high-frequency radar derived surface currents by their forcing mechanisms: locally wind-driven surface currents. J. Geophys. Res. 115 (C12), C12046, http://dx.doi.org/10.1029/2010JC006223.

Kubacka, M., Rudowski, S., Wróblewski, R., Szefler, K., Gajewski, Ł., 2016. Giant Subaqueous dunes on a tideless Sea Bottom, Rozewie Bank, Southern Baltic. In: Van Landeghem, K.J.J., Garlan, T., Baas, J.H. (Eds.), MARID 2016. Fifth International Conference on Marine and River Dune Dynamics, Caernarfon, United Kingdom, 4 — 6 April 2016. Bangor University and SHOM, 216 pp.

Nielsen, P., 2009. Coastal and estuarine processes. Adv. Ser. Ocean Eng., Vol. 29. World Sci. Publ., Singapore, 343 pp.

Ostrowski, R., 2004. Morphodynamics of a Multi-Bar Coastal Zone, DSc Thesis. IBW PAN, Gdańsk, 163 pp.

Ostrowski, R., Schönhofer, J., Szmytkiewicz, P., 2015. South Baltic representative coastal field surveys, including monitoring at the Coastal Research Station in Lubiatowo. Poland. J. Mar. Syst. 162, 89—97, http://dx.doi.org/10.1016/j.jmarsys.2015.10.006.

Ostrowski, R., Stella, M., Szmytkiewicz, P., Kapiński, J., Marcinkowski, T., 2017. Coastal hydrodynamics beyond the surf zone of the south Baltic Sea. Oceanologia 60 (3), 264—276, http://dx.doi.org/10.1016/j.oceano.2017.11.007.

Pruszak, Z., Szmytkiewicz, P., Ostrowski, R., Skaja, M., Szmytkiewicz, M., 2008. Shallow-water wave energy dissipation in a multi-bar coastal zone. Oceanologia 50 (1), 43—58.

Rudowski, S., Łęczyński, L., Gajewski, Ł., 2008. Sand waves on the bottom of the deep nearshore and their role in shore formation. Landf. Anal. 9, 214—216, (in Polish).

Uścinowicz, S., Jegliński, W., Miotk-Szpiganowicz, G., Nowak, J., Pączek, U., Przezdziecki, P., Szefler, K., Poręba, G., 2014. Impact of sand extraction from the bottom of the southern Baltic Sea on the relief and sediments of the seabed. Oceanologia 56 (4), 857—880, http://dx.doi.org/10.5697/oc.56-4.857.

Oceanologia (2019) 61, 60—67

Available online at www.sciencedirect.com

ScienceDirect

journal homepage: www.journals.elsevier.com/oceanologia/

ORIGINAL RESEARCH ARTICLE

Impact of artificial coastal protection structures on Ascidians settlement along the Tamil Nadu coast, India

Jebarathanam Prince Prakash Jebakumar[a,*], Ganesan Nandhagopal[a], Bose Rajan Babu[a], Shunmugavel Ragumaran[a], Chokalingam Muthiah Ramakritinan[b], Abdul Jaffar Ali[c], Mohammed Kaleem Arshan[c], Vijaya Ravichandran[a]

[a] *Coastal Environmental Engineering Division, National Institute of Ocean Technology, Pallikaranai, Chennai, India*
[b] *Department of Marine and Coastal Studies, Madurai Kamaraj University, Madurai, India*
[c] *Department of Biotechnology, Islamiah College, Vaniyambadi, India*

Received 5 February 2018; accepted 18 June 2018
Available online 6 July 2018

KEYWORDS
Artificial structures;
Novel niche;
Ascidian;
Native;
Introduced;
Cryptogenic

Summary Ascidians are one of the dominant marine sedentary filter feeders recorded more frequently as introduced species than other taxa. It is renowned that artificial structures offer novel niches to the non-native species. A yearlong investigation was carried out to understand the role of ascidian colonization on various artificial structures located along 84 stations stretched on the 1076 km long Tamil Nadu coast of South India. It revealed the occurrence of 26 ascidian species, among these18 specimens were identified to species level, 8 were identified to genus level based on morphological characters. As on origin and nativity, out of the total 26, 3 species were classified as introduced, 8 species were classified as native and 15 as cryptogenic species. Interestingly, *Polyclinum isipingense* and *Diplosoma variostigmatum* were reported first time in Indian waters. The cryptogenic and colonial forms of ascidians are dominant in the artificial structures. There were significant differences observed between artificial structure type, geographic locations ($p = 0.0071$) and between ascidians forms as well as geographic areas ($p = 0.00375$). This study also confirms the artificial structures offer new niches for non-native ascidian colonization. The influence of the substrate (structure type) as well as geographic locations on the biotic assemblage was also observed.

* Corresponding author at: Coastal Environmental Engineering Division, National Institute of Ocean Technology, Pallikaranai, Chennai 600100, India. Tel.: +91 6678 3465; fax: +91 6678 3336.
E-mail address: prince@niot.res.in (P.P.J. Jebarathanam).
Peer review under the responsibility of Institute of Oceanology of the Polish Academy of Sciences.

https://doi.org/10.1016/j.oceano.2018.06.005

1. Introduction

The urban sprawl near the coasts is one of the most extreme and widespread human impacts (Mckinney, 2006). It leads to severe landscape changes, species extinctions, homogenization of biota at local, regional and global scales (Mckinney and Lockwood, 1999). The anthropogenic impact on coastal areas occurs in the form of coastal structures for erosion prevention, which offer novel niches to the introduced species. However, their role in the subsequent invasions into native habitat remains unknown (Dumont et al., 2011). The enduring effect of artificial structures on the diversity of coastal biota at the regional level has started to increase along with the controversies of the lower diversity of native species and higher diversity of non-native species on these structures (Airoldi et al., 2015).

The colonization of artificial structures by native species was influenced by many factors — such as structural types, environmental factors etc. In some areas, colonization of the artificial structures by non-indigenous organisms exceeds the native forms (Dafforn et al., 2009; Firth et al., 2015; Glasby et al., 2007). Even though maritime activity distributes non-native species all around the globe, the triggering factor inducing the invasive nature ascertained between the prime entry point and the adaptability to the favorable new environment remains unclear (Hewitt et al., 2009). After a successful invasion, the local fishing and recreational boating activities potentially facilitate further expansion (Davidson et al., 2010). Thus, the harbors and marinas play a crucial role from the initial inoculation to the successful establishment by spreading to adjacent places (Forrest et al., 2009). Interestingly, there are limited reports available on further expansion of non-native organisms to the natural habitats.

It is well documented that introduced species were more frequently found on the artificial hard substrate in estuaries and bays than on the open coasts (Wasson et al., 2005). The occurrences of numerous cracks and gaps on these structures act as a shelter and protection from predation, desiccation, wave action and other stresses for the animals. Hence, non-indigenous species are more abundant on the artificial structures than in the natural rocky systems. Since the world is connected by the growing transport networks and infrastructure, the spread of the non-indigenous species (NIS) became a common problem (Minchin and Gollasch, 2003). Moreover, these artificial hard networks are considered to be the biggest threat to biodiversity after a habitat loss (Wilcove et al., 1998). Significant investment in reducing invasion opportunities in the form of managing the transport vectors or border control were found to be ineffective and lead to an upsurge in the eradicating cost (Hulme, 2009).

The ascidians are the common sessile filter feeders often recorded as introduced species, mostly occupying the artificial coastal defense structures and (Aldred and Clare, 2014; Lambert and Lambert, 2003). Their successful proliferation is based on flexibility to survive in varying temperature, salinity (Nagar and Shenkar, 2016) and pollution (Beiras et al., 2003). Some of the invasions have deleterious economic (McKindsey et al., 2007) and ecological (Lutz-Collins et al., 2009) impact on the surrounding environment.

Short-lived, non-feeding, low-dispersal larval stageofascidians are considered an indicator of invasion if found miles from its known habitat and are spreading through ballast water transport and hull fouling dispersion (Lambert, 2007). These invasive ascidians are acting as strong spatial competitors by frequently displacing native anemones, mussels, algae and other fouling community, where the mechanism of eradication is complicated (Lindeyer and Gittenberger, 2011). They foul various artificial structures like jetties, ship hulls, floating docks, buoys, floats, cables and other human-made structures (Lambert, 2005). Hence, the study of the ascidians communities is necessary for monitoring the non-indigenous species.

Numerous researches have been carried out worldwide to ascertain the negative impacts of ascidians colonization on the artificial structures but few studies concerned species conservation (Ferrario et al., 2016; Firth et al., 2014). In India, sporadic studies on location-specific non-indigenous ascidians species on certain structures and harbor were carried out (Ali et al., 2009; Jaffar et al., 2016). Hence, an extensive survey along the entire stretch of the Tamil Nadu coast was conducted to comprehend the distribution of the ascidians species on various types of artificial coastal defense structures.

2. Material and methods

The 1076 km coastal stretch of Tamil Nadu is located in the southeastern part of the Indian Peninsula and it forms a part of the Coromandel Coast on the Bay of Bengal and the Indian Ocean. This coastal corridor comprises 15 marinas and harbors. The entire coastline is occupied by numerous artificial structures and protective groins that provide habitat for a wide variety of marine organisms. Based on utility, these structures were classified into four types. (1) The artificial structures in the fishing harbor, such as breakwaters, groins, etc. are organized under “Fishing”. (2) The structures with function in the fish farming, salt pan, are categorized under “Commercial”. (3) The structures with a role in the development of tourism (surfing, boat riding, etc.) are organized under “Recreational”. (4) The artificial structures like sea wall and groins used for the shoreline armoring and urban coastal protection are classified under the “Coastal armoring” category

Series of field surveys were conducted through SCUBA diving and Snorkelling at low tide, at depths ranging from 1 to 5 m (Jebakumar et al., 2015) at seven sampling zones during January, May, and September 2016. Each zone included 8 to 18 sampling stations (total of 84 stations) along the Tamil Nadu coast (Fig. 1). Investigated habitats comprised artificial substrates such as boulder piles, groins, caissons, tetrapods, fishery jetties, pipeline trestles, and harbor breakwaters along the entire shoreline of Tamil Nadu. The entire structure at each station was surveyed completely to collect the ascidian samples. Hand tools were employed to remove animals from solid surfaces of the artificial structures.

Representative ascidians were photographed in situ. In the case of large colonial ascidians, a portion of the colony was collected after inspecting the structure and dimension of the whole colony. In the case of ascidians, after collecting representative specimens identified in the field, others were transported to the laboratory for detailed study. The

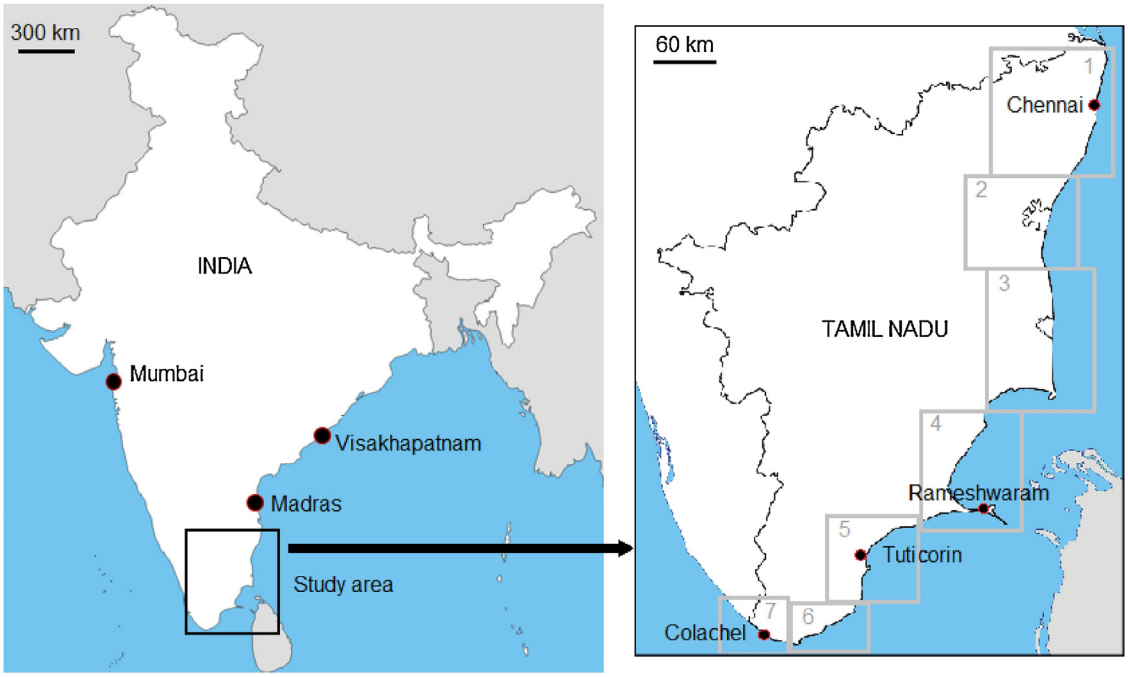

Figure 1 Study Area: The Tamil Nadu coast in southern India; grey squares indicate the seven sampling zones where the 84 sampling stations were placed (see supplementary material Table S1 for coordinates).

collected samples were narcotized in menthol crystals up to two hours for colonial ascidians and three hours for solitary ascidians. After narcotization, the specimens were fixed separately by quickly adding one part of 40% formaldehyde to nine parts of fresh sea water, and preserved in 70% ethanol. The samples were sorted and identified up to species, or the lowest possible taxa by observing all the taxonomical characters using various microscopes, e.g. Olympus, (Germany), compound (Labomode, Vision 2000) and stereo microscopes (Micros, Austria). The taxonomical keys and all the observed characters were compared with previously published data (Kott, 1985; Millar, 1975; Monniot and Monniot, 1996; Renganathan, 1986; Tokioka, 1967). Voucher specimens were deposited to Zoological Survey of India, Chennai.

To compare the ascidian diversity and structure types, the results were visualized with the help of the non-metric multidimensional scaling (nMDS) plot. The analyzes were carried out using the software PRIMER v7.0 (Clarke et al., 2014). The Bray-Curtis similarity matrices were transformed to the distance for input into the PRIMER v7.0. to perform a nMDS plot (no transformation to the original data was applied, as it was semi- quantitative). The analyses were carried out by comprising all the species (native, introduced and cryptogenic) obtained from each structure. The nMDS performs 20 different random starts and compares them to find a stable solution. Additionally, the non-parametric Kruskal–Wallis test was also performed using the software PAST 3 (Hammer et al., 2001), to find the significant correlation between the structure types and the abundance of native, introduced and cryptogenic ascidian species. The same datasets were also analyzed using the single factor ANOVA to test for the difference between the structure types and ascidian species abundance in detail.

3. Results

An extensive survey on the presence of ascidian species was carried out in 84 stations comprising the artificial coastal defense structures along the 1076 km coastal stretch of Tamil Nadu (the south-eastern coast of India) three times a year (January, May, and September). During the survey, 26 different ascidian samples belonging to 8 families under three orders were collected and identified (Table 1). Out of 26 samples, 18 were identified at the species level, and the remaining eight specimens identified at genus level due to invisible key morphological characters. Among the surveyed artificial structures, the highest species richness was observed in the Colachel fishing harbor (CFH) (n = 13) followed by Punnaikayal left arm (PKLA) (n = 11), Muttam fishing harbor (MFH) (n = 11) and Thondi (TDMV) (n = 10). There are almost 57 artificial structures out of the 84 surveyed with zero ascidian species recorded (Table S1). The artificial structures used in fishing harbor recorded the highest species richness (n = 24) followed by the Recreational (n = 8), Armor (n = 6) and Commercial (n = 2) (Fig. 2).

After identification of the ascidian samples, each species was classified into one of the following groups: native, cryptogenic and invasive, depending on their origin (Carlton, 1996). If the species' origin, distributional and genetic data exists, it can be classified as Introduced. The species endemic to Indian subcontinent was classified as Native. Finally, when supportive data of nativity or geographic origin was not available, it was classified as cryptogenic species (Jaffar et al., 2016). In the artificial coastal defense structures cryptogenic species were highly abundant (n = 15), followed by native (n = 8) and invasive (n = 3) species (Fig. 3). The species abundance pattern along the geographical locations is represented in Fig. 4. Further, out of 26 ascidian species, 24 species were

Table 1 Distribution of Ascidian species along the study area.

Sl.No	Order	Species	Origin	Accession number	Structure type
1	Aplousobranchia	*Polyclinum indicum*	Native		1
2		*Polyclinum isipingense**	Cryptogenic	NZC/MBRC/M.327	1
3		*Didemnum psammatodes*	Cryptogenic	NZC/MBRC/M.328	1, 3
4		*Lissoclinum fragile*	Cryptogenic		1, 3
5		*Didemnum vexiculum*	Cryptogenic		1, 3
6		*Tridemnum miniatum*	Cryptogenic	NZC/MBRC/M.319	1
7		*Aplidium* sp.	Native		1, 2, 4
8		*Eudistoma sluiteri*	Native	NZC/MBRC/M.326	2, 3
9		*Eudistoma tumidum*	Native	NZC/MBRC/M.322	1
10		*Diplosoma variostigmatum**	Cryptogenic	NZC/MBRC/M.323	3
11		*Synoicum* sp.	Native		1
12		*Aplidium multiplicatum*	Native	NZC/MBRC/M.325	1
13	Phlebobranchia	*Corella eumyota*	Invasive		1
14		*Phallusia nigra*	Invasive		1
15		*Ascidia gemmata*	Cryptogenic	NZC/MBRC/M.320	1
16		*Ecteinascidia* sp.	Native		1
17		*Ecteinascidia venue*	Native	NZC/MBRC/M.329	1
18	Stolidobranchia	*Symplegma brakenhielmi*	Cryptogenic	NZC/MBRC/M.321	1, 3
19		*Styela canopus*	Invasive	NZC/MBRC/M.324	1, 3
20		*Symplegma* sp.	Cryptogenic		1
21		*Symplegma* sp.-2	Cryptogenic		3
22		*Herdmania momus Savigny*	Cryptogenic		1
23		*Botrylloides nigrum*	Cryptogenic		1
24		*Botryllus* sp.3	Cryptogenic		1
25		*Botryllus* sp.2	Cryptogenic		3
26		*Botrylloides* sp.1	Cryptogenic		1

* indicates the organisms reported first time in Indian waters.
Fishing — 1, Commercial — 2, Recreational — 3 and Armour — 4.

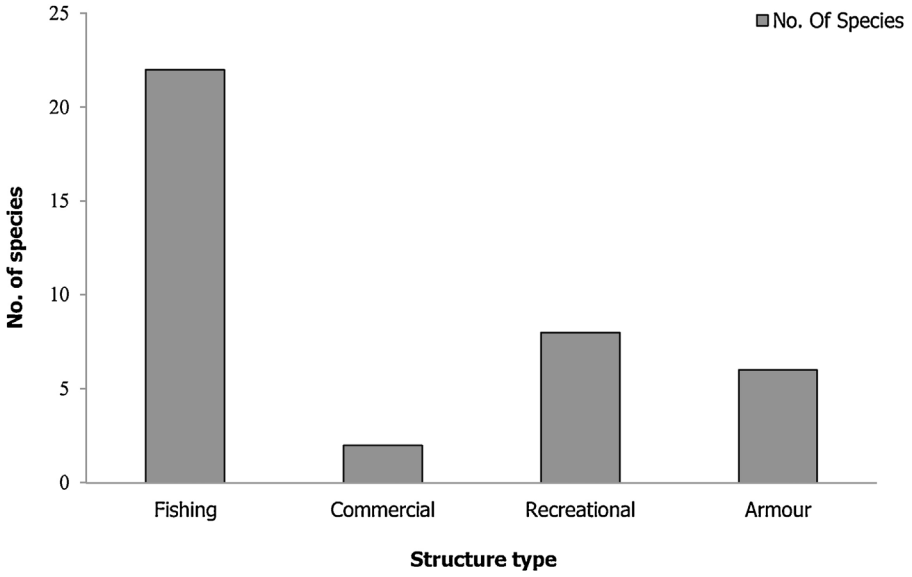

Figure 2 Number of Ascidian Species recorded at each structure type.

reported earlier in Indian sub-continent and, the remaining two species, namely *Diplosoma variostigmata* and *Polyclinum isipingense*, were reported for the first time in Indian waters. The two newly recorded species were confirmed and submitted to Zoological Survey of India to obtain accession numbers (Accession No. NZC/MBRC/M.323 & NZC/MBRC/M.327).

The population densities of native and cryptogenic species were the most dominant and prevailing in all types of artificial structures. Low density of population represented the invasive species and was limited to the specific areas. The number of ascidians species present in the fishing harbor structures was high, with an average of 3.35 species/structure, followed

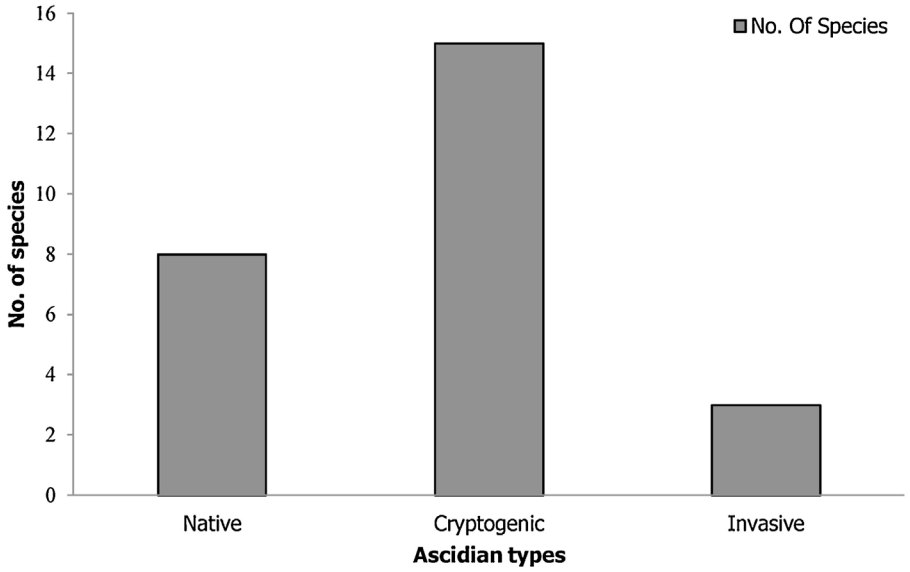

Figure 3 Total Number of Ascidian Species recorded as per type of species (Native, Cryptogenic and Introduced).

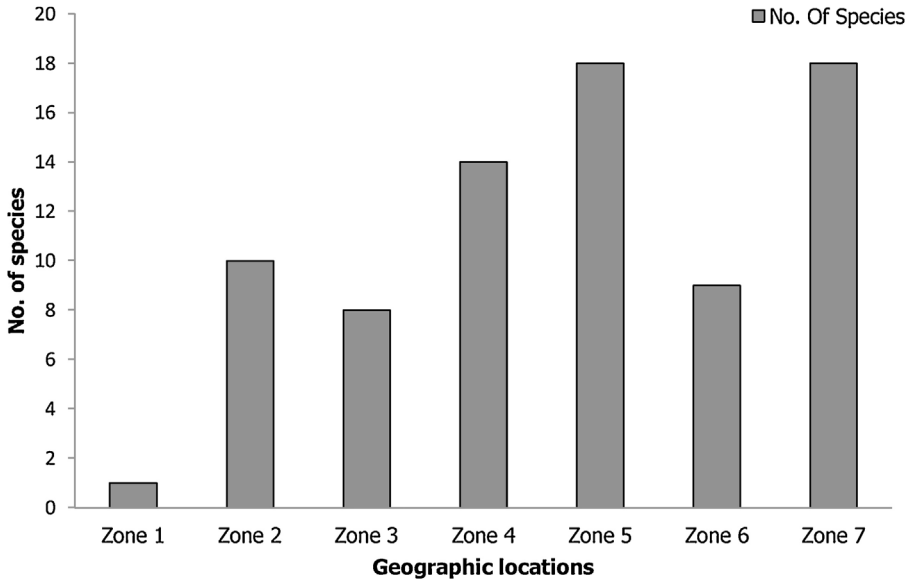

Figure 4 Total number of Ascidian species recorded at each sampling zone, Tamil Nadu.

by commercial (0.2 species/structure), armor (0.588 species/structure) and recreational (0.5 species/structure). Among widely distributed colonial and solitary forms of ascidians, the colonial forms dominated the artificial structures during the entire study period. Also, most of the cryptogenic species belonged to the colonial forms, whereas the invasive belonged to the solitary type. Further, there was no significant correlation observed between the types and forms of ascidians. The *D. passamodes*, *L. fragile* and *D. vexiculum* were the most common colonial ascidians to occupy the several artificial structures. Of the *L. fragile* recorded in the 15 structures, *D. passamodes* recorded in the 14 structures and the *D. vexiculum* was recorded on 12 structures. Surprisingly, the solitary ascidians such as *C. eumyte* was observed on three structures, *P. nigra* and *H. savingy* were observed on four structures.

When the permutational analysis was done considering the geographical location (zone wise), and structural types (Fishing, Armor, Commercial and Recreational), results showed a significant effect of both factors on the ascidian community structures ($p = 0.0071$). Likewise, the Kruskal–Wallis test also showed a substantial difference in ascidian community, with geographical locations and structure types ($p = 0.00064$).

Similarly, significance ($p = 0.00375$) was observed between geographic location (zone wise) and the ascidian types (Native, Cryptogenic, and Introduced) when permutational analysis of the community structures with the location only was performed. In addition, Kruskal–Wallis test was carried out, and this result proved a significant difference between the geographical location and ascidian type ($p = 0.00495$).

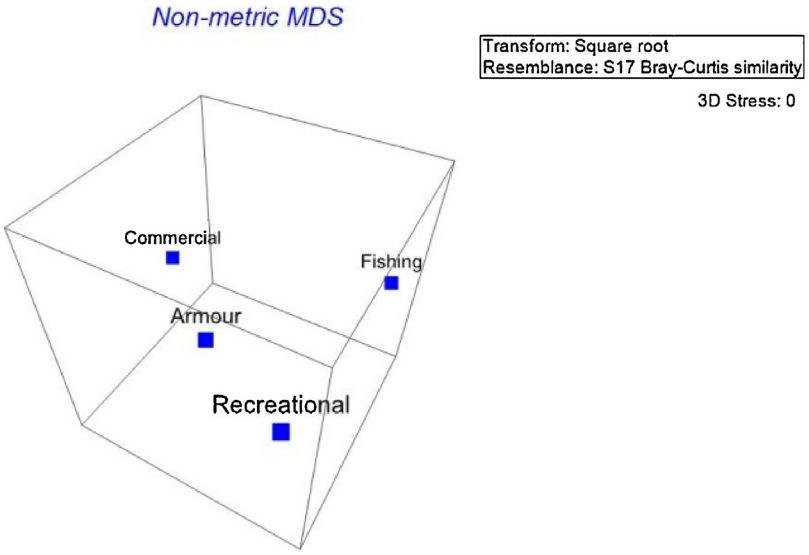

Figure 5 Non-metric MDS plot obtained from the Bray-Curtis similarity index for the whole dataset (structure types and ascidian abundance in each type).

The non-metric MDS plot constructed from relative abundance data (using Bray-Curtis index) showed improved differentiation among the types of structures (Fig. 5). The significant difference observed in ANOVA, and Kruskal–Wallis test between the different structures and the geographical locations (zone wise) is represented graphically with the separation of structures. By considering the four types of structures alone for statistical treatment, the Recreational, Commercial and Armoring structures showed linearity, whereas the Fishing structure was apart from the other three in the graph.

4. Discussion

The present study was a pioneering attempt to compile an up-to-date list of ascidian species along with the Non-Indigenous species (NIAs) found on the various artificial coastal defense structures along the 1076 km coast of Tamil Nadu, India. Among the 84 artificial coastal defense structures surveyed, 26 different types of ascidian species were recorded. Among them, 18 species were identified at the species level and the remaining were identified at the genus level. The two species, namely *Polyclinum isipengense* and *Diplosoma variostigma* were reported for the first time in the Indian waters. These newly recorded species were observed only on the Fishing and Recreational types of structures. It leads to the conclusion that the introduction of the species happened through hull fouling and was followed by spreading through the local vessel movement. The *D. variostigma* was observed in Japan (Hirose and Oka, 2008), whereas the *P. isipengense* was observed at South Africa (Sluiter, 1898). However, the nativity of these species remains unclear. Therefore, these two species observed in the present study were categorized as cryptogenic species, though they are non-native to Indian waters. In general, the cryptogenic species dominated the native and introduced forms along the artificial structures, with the maximum record of 15 species. In the case of introduced species, the artificial structures sheltered only three species, whereas eight native ascidian forms have also been recorded. During the past systematic fauna studies, the ascidian species attracted little attention, hence the lacuna in nativity records for most of these species (Ali et al., 2009). Thus the cryptogenic species outnumbered the non-indigenous species (López-Legentil et al., 2015). This applies the general understanding that the artificial structures are not a suitable habitat for the native ascidian species. Among the different types of structures, the lowest number of 2 ascidian species was recorded on the Commercial structures, followed by six species on the Armoring structures, eight species on the Recreational structures and the maximum of 24 species were recorded on the Fishing harbor structures. The abundance of the ascidian settlements on the Fishing harbor structure was due to the occurrence of exclusively cryptogenic and introduced species. The observed preference of the non-native ascidians for the Fishing harbors structures, which are considered a hotspot for exotic species, was also reported by Murray et al. (2012) and López-Legentil et al. (2015).

The permutational analysis and Kruskal–Wallis test showed the significant difference when the comparison is done between the abundance of ascidians types (native, introduced and cryptogenic) with the geographic locations (zone wise). The significant difference might be due to the presence of fishing harbors at some zones – the harbors are considered to be a hotspot for non-indigenous species. The frequent ship movement along the Fishing harbor structures facilitated the settlement of the non-native ascidian species from the hulls of vessels. Furthermore, the Zones 5, 6 and 7 contained a higher number of non-native ascidian species (Table S1) than the native species. It has been confirmed by the permutational analysis and revealed that the structure types had significant effects on the ascidian settlements. The structure types and ascidian types showed the significant difference, which was further confirmed by Kruskal–Wallis test. The overall results evidently show that the fishing harbor structures are supporting the non-native species more than the native species. In general, the colonial ascidian

forms outnumbered the solitary forms whereas most of the cryptogenic ascidians observed are colonial forms. It has been established that several colonial species were introduced worldwide through hull fouling and aquaculture (Lambert, 2002).

Further, reduction in the vessel movement around the Commercial, Recreational and Armoring structures lead to a deficiency of non-native species. The distance from the fishing harbor and the sparse movement of the vessels along the other three type of structures limited the secondary spread. This result supports the hypothesis that non-indigenous species (NIAs) thriving on artificial structures in the proximity to vector but failing to spread on other structures (Lambert, 2002).

The n-MDS plot constructed by using the Bray-Curtis Index showed, that the structure types mostly drove the settlement of ascidian types and forms. Among the various types of structures studied, fishing harbor structures were distinct and stood out compared to the other structures (Fig. 5). The separation of the fishing structures from the remaining structures was explained by the presence of some exclusive species such as *Botrylloides nigrum, Herdmania momus saving* and *Symplegma* sp. or the most exclusive species like *Polyclinum isipingense, Synocium* sp., *Corella eumyota* and *Phallusia nigra*. The current scenario of augmented recreational sailing and the proliferation of marinas and artificial marine structures in recent decades provided additional sites for the colonization of non-indigenous species (NIAs), even those with low dispersal abilities (Shenkar and Loya, 2009). Many studies substantiated that the artificial coastal defense structures serve as an asylum for the NIAs (Airoldi et al., 2015; Shenkar and Loya, 2009). The observations in the present study are comparable with the earlier researches. However, the artificial coastal defense structures proved to be a novel niches for the colonization of marine organisms and developed unique ecosystems (Ferrario et al., 2016; Firth et al., 2014). The study clearly depicted that the distribution and diversity of the ascidian species largely depend on the type of structure and a proximity between them. This detailed study also put forth the idea, that the artificial coastal defense structures can help in the development of the coastal ecosystem. Therefore, the better understanding, proper planning and appropriate utilization of the artificial structures along the coast will reduce the settlement of the non-native species and will also help enhance the presence of native species.

5. Conclusion

Despite the variations in structures, the ascidians species (Native, Cryptogenic, and Introduced) occupied almost all types of structures. The artificial structures hold all three varieties of ascidians forms of both solitary as well as colonial types. The cryptogenic species was more dominant than the native and introduced species. However, the diversity of the native species was similar to the abundance of the cryptogenic form. In the results, it was apparent that the structures with substantial vessel traffic harbor non-native species and vice versa in the case of structures with the fewer or no vessel traffic. It necessitates continuous monitoring of the non-native species on these artificial coastal defense structures, which should be considered a hotspot for bio-pollution monitoring. This study warrants in-depth studies on physiology, life spawn, larval settlement pattern, prey-predation and fouling efficiency, which would help prepare a proper management plan for the artificial coastal defense structures.

Acknowledgments

This study was carried out under the 'Sustainable Shoreline Management' program of the National Institute of Ocean Technology (NIOT), funded by the Ministry of Earth Sciences, Government of India.

Appendix A. Supplementary data

Supplementary material related to this article can be found in the online version at https://doi.org/10.1016/j.oceano.2018.06.005.

References

Airoldi, L., Turon, X., Perkol-Finkel, S., Rius, M., 2015. Corridors for aliens but not for natives: effects of marine urban sprawl at a regional scale. Divers. Distrib. 21, 755—768, http://dx.doi.org/10.1111/ddi.12301.

Aldred, N., Clare, A.S., 2014. Mini-review: impact and dynamics of surface fouling by solitary and compound ascidians. Biofouling 30 (3), 259—270, http://dx.doi.org/10.1080/08927014.2013.866653.

Ali, H.A.J., Sivakumar, V., Tamilselvi, M., 2009. Distribution of alien and cryptogenic ascidians along the Southern Coasts of Indian Peninsula. World J. Fish. Mar. Sci. 1 (4), 305—312.

Beiras, R., Bellas, J., Fernández, N., Lorenzo, J.I., Cobelo-Garcıa, A., 2003. Assessment of coastal marine pollution in Galicia (NW Iberian Peninsula); metal concentrations in seawater, sediments and mussels (*Mytilus galloprovincialis*) versus embryo—larval bioassays using *Paracentrotus lividus* and *Ciona intestinalis*. Mar. Environ. Res. 56 (4), 531—553, http://dx.doi.org/10.1016/S0141-1136(03)00042-4.

Carlton, J.T., 1996. Biological invasions and cryptogenic species. Ecology 77 (6), 1653—1655.

Clarke, K.R., Gorley, R.N., Somerfield, P.J., Warwick, R.M., 2014. PRIMER-E, Plymouth. In: Change in Marine Communities: An Approach to Statistical Analysis and Interpretation. 3rd edn. 260 pp.

Dafforn, K.A., Johnston, E.L., Glasby, T.M., 2009. Shallow moving structures promote marine invader dominance. Biofouling 25 (3), 277—287.

Dumont, C.P., Harris, L.G., Gaymer, C.F., 2011. Anthropogenic structures as a spatial refuge from predation for the invasive bryozoan *Bugula neritina*. Mar. Ecol. Prog. Ser 427, 95—103.

Davidson, I.C., Zabin, C.J., Chang, A.L., Brown, C.W., Sytsma, M.D., Ruiz, G.M., 2010. Recreational boats as potential vectors of marine organisms at an invasion hotspot. Aquat. Biol. 11, 179—191, http://dx.doi.org/10.3354/ab00302.

Ferrario, F., Iveša, L., Jaklin, A., Perkol-Finkel, S., Airoldi, L., 2016. The overlooked role of biotic factors in controlling the ecological performance of artificial marine habitats. J. Appl. Ecol. 53 (1), 16—24, http://dx.doi.org/10.1111/1365-2664.12533.

Firth, L.B., Mieszkowska, N., Grant, L., Bush, L., Davies, A.J., Frost, M.T., Cunningham, P.N., Moschella, P., Hawkins, S.J., 2015. Historical comparisons reveal multiple drivers of decadal change of an ecosystem engineer at the range edge. Ecol. Evol. 5 (15), 3210—3222, http://dx.doi.org/10.1002/ece3.1556.

Firth, L.B., Schofield, M., White, F.J., Skov, M.W., Hawkins, S.J., 2014. Biodiversity in intertidal rock pools: informing engineering criteria for artificial habitat enhancement in the built environment. Mar. Environ. Res. 102, 122—130, http://dx.doi.org/10.1016/j.marenvres.2014.03.016.

Forrest, B.M., Gardner, J., Taylor, M.D., 2009. Internal borders for managing invasive marine species. J. Appl. Ecol. 46 (1), 46—54, http://dx.doi.org/10.1111/j.1365-2664.2008.01544.x.

Glasby, T.M., Connell, S.D., Holloway, M.G., Hewitt, C.L., 2007. Nonindigenous biota on artificial structures: could habitat creation facilitate biological invasions? Mar. Biol. 151 (3), 887—895.

Hammer, Ø., Harper, D.A.T., Ryan, P.D., 2001. Paleontological statistics software: package for education and data analysis. Palaeontol. Electron. 4, 9.

Hewitt, C.L., Gollasch, S., Minchin, D., 2009. The vessel as a vector — biofouling, ballast water and sediments. In: Rilov, G, Crooks, JA (Eds.), Biological Invasions in Marine Ecosystems. Ecol. Stud., Vol. 204. Springer, Berlin, Heidelberg, 117—131, http://dx.doi.org/10.1007/978-3-540-79236-9_6.

Hirose, E., Oka, A.T., 2008. A new species of photosymbiotic ascidian from the Ryukyu Archipelago, Japan, with remarks on the stability of stigma number in photosymbiotic Diplosoma species. Zool. Sci. 25 (12), 1261—1267, http://dx.doi.org/10.2108/zsj.25.1261.

Hulme, P.E., 2009. Trade, transport and trouble: managing invasive species pathways in an era of globalization. J. Appl. Ecol. 46 (1), 10—18, http://dx.doi.org/10.1111/j.1365-2664.2008.01600.x.

Jaffar, H.A., Akram, A.S., Arshan, M.K., Sivakumar, V., Tamilselvi, M., 2016. Distribution and invasiveness of a colonial ascidian, *Didemnum psammathodes*, along the southern Indian coastal water. Oceanologia 58 (3), 212—220, http://dx.doi.org/10.1016/j.oceano.2016.04.002.

Jebakumar, J.P.P., Nandhagopal, G., Ragumaran, S., Rajanbabu, B., Ravichandran, V., 2015. First record of alien species Eualetestulipa (Rousseau in Chenu, 1843) from the Royapuram fishing harbour at Chennai, India. Bioinvasions Rec. 4 (3), 201—204, http://dx.doi.org/10.3391/bir.2015.4.3.08.

Kott, P., 1985. The Australian Ascidiacea part 1, Phlebobranchia and Stolidobranchia. Mem. Qd. Mus. 23, 1—440.

Lambert, G., 2002. Nonindigenous ascidians in tropical waters. Pac. Sci. 56 (3), 291—298, http://dx.doi.org/10.1353/psc.2002.0026.

Lambert, G., 2005. Ecology and natural history of the protochordates. Can. J. Zool. 83 (1), 34—50, http://dx.doi.org/10.1139/Z04-156.

Lambert, G., 2007. Invasive sea squirts: a growing global problem. J. Exp. Mar. Bio Ecol. 342 (1), 3—4.

Lambert, C.C., Lambert, G., 2003. Persistence and differential distribution of nonindigenous ascidians in harbors of the Southern California Bight. Mar. Ecol. Prog. Ser. 259, 145—161.

Lindeyer, F., Gittenberger, A., 2011. Ascidians in the succession of marine fouling communities. Aquat. Invasions 6 (4), 421—434, http://dx.doi.org/10.3391/ai.2011.6.4.07.

López-Legentil, S., Legentil, M.L., Erwin, P.M., Turon, X., 2015. Harbor networks as introduction gateways: contrasting distribution patterns of native and introduced ascidians. Biol. Invasions. 17 (6), 1623—1638, http://dx.doi.org/10.1007/s10530-014-0821-z.

Lutz-Collins, V., Ramsay, A., Quijón, P.A., Davidson, J., 2009. Invasive tunicates fouling mussel lines: evidence of their impact on native tunicates and other epifaunal invertebrates. Aquat. Invasions 4, 213—220.

McKinney, M.L., 2006. Urbanization as a major cause of biotic homogenization. Biol. Conserv. 127 (3), 247—260, http://dx.doi.org/10.1016/j.biocon.2005.09.005.

McKinney, M.L., Lockwood, J.L., 1999. Biotic homogenization: a few winners replacing many losers in the next mass extinction. Trends Ecol. Evol. 14 (11), 450—453, http://dx.doi.org/10.1016/S0169-5347(99)01679-1.

Mckindsey, C.W., Landry, T., O'Beirn, F.X., Davies, I.M., 2007. Bivalve aquaculture and exotic species: a review of ecological considerations and management issues. J. Shellfish Res. 26 (2), 281—294.

Millar, R.H., 1975. Ascidians from the Indo-West-Pacific region in the Zoological Museum, Copenhagen (Tunicata, Ascidiacea). Steenstrupia 3 (20), 205—306.

Minchin, D., Gollasch, S., 2003. Fouling and ships' hulls: how changing circumstances and spawning events may result in the spread of exotic species. Biofouling 19 (S1), 111—122, http://dx.doi.org/10.1080/0892701021000057891.

Monniot, F., Monniot, C., 1996. New collections of ascidians from the western Pacific and southeastern Asia. Micronesia 29, 133—279.

Murray, C.C., Therriault, T.W., Martone, P.T., 2012. Adapted for invasion? Comparing attachment, drag and dislodgment of native and nonindigenous hull fouling species. Biol. Invasions 14 (8), 1651—1663, http://dx.doi.org/10.1007/s10530-012-0178-0.

Nagar, L.R., Shenkar, N., 2016. Temperature and salinity sensitivity of the invasive ascidian *Microcosmus exasperatus* Heller, 1878. Aquat. Invasions 11 (1), 33—43, http://dx.doi.org/10.3391/ai.2016.11.1.04.

Renganathan, T.K., 1986. Studies on the Ascidians of South India. (PhD Thesis). Madurai Kamaraj University, Madurai, India.

Shenkar, N., Loya, Y., 2009. Non-indigenous ascidians (Chordata: Tunicata) along the Mediterranean coast of Israel. Mar. Biodivers. Rec. 2, http://dx.doi.org/10.1017/S1755267209990753.

Sluiter, C.P., 1898. Beitrage zur kenntnis der fauna von Sud-Afrika. Ergebnisse einer Reise von Prof. Max Weber im Jahre 1894. II. Tunicaten von South-Africa. Zool. Jahrb. Syst. 11, 1—64.

Tokioka, T., 1967. Pacific Tunicata of the United States National Museum. Bull. US Nation Museum 251, 1—242.

Wasson, K., Fenn, K., Pearse, J.S., 2005. Habitat differences in marine invasions of central California. Biol. Invasions 7 (6), 935—948, http://dx.doi.org/10.1007/s10530-004-2995-2.

Wilcove, D.S., Rothstein, D., Dubow, J., Phillips, A., Losos, E., 1998. Quantifying threats to imperiled species in the United States. BioScience 48 (8), 607—615.

Oceanologia (2019) 61, 68—77

Available online at www.sciencedirect.com

ScienceDirect

journal homepage: www.journals.elsevier.com/oceanologia/

ORIGINAL RESEARCH ARTICLE

Surface layer desalination of the bays on the east coast of Novaya Zemlya identified by shipboard and satellite data

Dmitry I. Glukhovets [a,b,*], **Yury A. Goldin** [a]

[a] *Shirshov Institute of Oceanology, Russian Academy of Sciences, Moscow, Russia*
[b] *Moscow Institute of Physics and Technology, Moscow Region, Russia*

Received 16 February 2018; accepted 3 July 2018
Available online 17 July 2018

KEYWORDS
Surface layer;
Continental runoff;
High-resolution satellite data;
Salinity;
Fluorescence

Summary This study examined the influences of continental and island river runoff as well as glacial meltwater runoff on the water surface layers of the Kara Sea in different bays on the eastern coast of Novaya Zemlya, an archipelago off the coast of Russia. High-resolution satellite and shipboard data obtained in 2015 were used to determine the sources of desalination (glacial meltwaters and river waters), which can be distinguished by the type of correlation (positive, negative, or none) seen between salinity and the coloured dissolved organic matter fluorescence intensity. Examples of the various situations that can occur in the bays are provided and discussed.

1. Introduction

In recent years, interest in Arctic sea exploration has been growing. International scientific groups have performed numerous studies that have produced significant advances in our understanding of the on-going processes (Amon, 2003; Carmack et al., 2016; Flint, 2010; Granskog et al., 2015; Lisitzyn and Vinogradov, 1994; Matsuoka et al., 2017; Nummelin et al., 2016). Particular attention is being paid to the Kara Sea, where the hydrological regime is significantly determined by the influence of runoff from Siberian rivers (Amon, 2003; Fichot et al., 2013; Kubryakov et al., 2016; Osadchiev et al., 2017; Zatsepin et al., 2010, 2015).

* Corresponding author at: Shirshov Institute of Oceanology, Russian Academy of Sciences, 36 Nahimovskiy pr., Moscow, 117997, Russian Federation. Tel.: +7 (499) 129-27-36.
E-mail address: glukhovets@ocean.ru (D.I. Glukhovets).
Peer review under the responsibility of Institute of Oceanology of the Polish Academy of Sciences.

ELSEVIER Production and hosting by Elsevier

https://doi.org/10.1016/j.oceano.2018.07.001

Summer runoff from the Ob and Yenisei rivers carries fresh water (continental runoff) with a high dissolved organic carbon (DOC) content into the Kara Sea (Belyaev et al., 2010; Drozdova et al., 2017; Fichot et al., 2013). These waters form a surface desalinated layer (SDL) that occupies a significant portion of the water area (Burenkov and Vasilkov, 1994; Carmack et al., 2016; Polukhin and Makkaveev, 2017; Zatsepin et al., 2010, 2015). In some years, when there is a western distribution of the SDL, its waters can reach the shores of Novaya Zemlya (Kubryakov et al., 2016; Zatsepin et al., 2015). In addition to reduced salinity, increased DOC concentration is an indicator of this SDL (Amon, 2003; Burenkov et al., 2010a; Gonçalves-Araujo et al., 2016). Within the SDL, a strong negative correlation exists between the salinity and DOC concentration (Amon, 2003) and between the DOC concentration and coloured dissolved organic matter (CDOM) fluorescence intensity (Pugach et al., 2018), meaning measurements of the CDOM fluorescence intensity (I_{fl}) can be used as a proxy for the DOC concentration (Gonçalves-Araujo et al., 2016; Kowalczuk et al., 2010; Pugach et al., 2018). As a consequence, there is a strong anti-correlation between salinity and the CDOM fluorescence intensity at the 373 nm excitation wavelength (Glukhovets and Goldin, 2014).

A number of studies have been devoted to investigating desalination processes in the Arctic and northern sea waters, which were conducted using various methods: hydrological, using conductivity-temperature-depth (CTD) profiles (Granskog et al., 2015; Zatsepin et al., 2010, 2015); hydro-chemical (Dai and Martin, 1995; Makkaveev et al., 2015; Polukhin and Makkaveev, 2017); optical (Burenkov et al., 2010a; Gonçalves-Araujo et al., 2016; Sagan and Darecki, 2017); satellite (Burenkov et al., 2010a, 2010b; Fichot et al. 2013; Kubryakov et al., 2016; Matsuoka et al., 2017; Osadchiev et al., 2017; Pozdnyakov et al., 2005; Zatsepin et al., 2015); hydro-biological (Demidov et al., 2018); geological (Bröder et al., 2016; Kravchishina et al., 2015; Politova et al., 2012); and modelling (Kubryakov et al., 2016; Nummelin et al., 2015; Nummelin et al., 2016). Fluorescent methods (Kowalczuk et al., 2010), including excitation — emission matrices or EEMs (Amon, 2003; Coble, 2007; Drozdova et al., 2017) and lidars (Pelevin et al., 2017), also play an important role. The relative simplicity of measuring fluorescence intensity allows the development of express methods that can be implemented in flow-through fluorimeters. These instruments can quickly gather large amounts of data with a high spatial resolution along the vessel's route (Burenkov et al., 2010a; Lorenzen, 1966).

The overwhelming majority of studies in the Kara Sea are performed in open water areas. However, there is also great interest in studying the mesoscale processes occurring in the bays on Novaya Zemlya due to the presence of an additional factor influencing the desalination — island runoff, in the form of small rivers and thawed glacial water.

In a recently published paper (Sagan and Darecki, 2017), the inherent optical properties and distributions of suspended matter in two fjords of Spitsbergen are reported. The authors showed that despite the different hydrological conditions in the two fjords, the glacial and small river runoff had a decisive influence. They found distinct differences in the suspended matter composition of the two fjords. The mineral fraction dominated in the first fjord, while in the second, the mineral and organic contributions were approximately equal. Their study demonstrated the high variability in the optical properties that can be found in the waters of the closely situated fjords and the efficiency of using optical methods for their investigation. Murray et al. (2015) and Stedmon et al. (2015) have similarly reported interesting

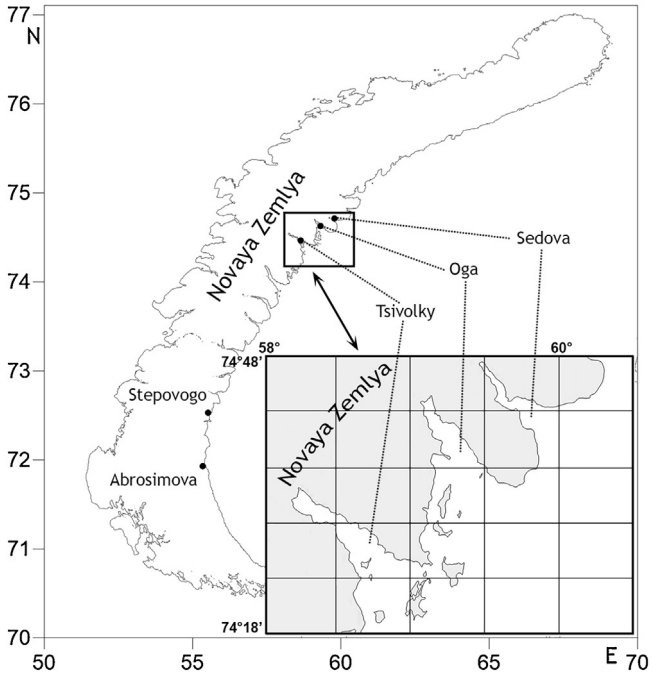

Figure 1 Location of the bays (represented by points) on the east coast of Novaya Zemlya. Inset: an enlargement of the North Island bays.

results on the effect of thawed glacial waters in Greenland bays.

There are also glaciers on the northern island of the Novaya Zemlya Archipelago, and their impact can be significant. Their thawed waters are characterized by a high amount of suspended matter originating from the shores of Novaya Zemlya (Kravchishina et al., 2015). Thus, in the bays having glaciers, a high concentration of suspended matter is a marker for glacial meltwater. These traits make it possible to effectively record the areas they occupy by both contact and remote sensing methods (Gordon and Morel, 2012).

In contrast to the Spitsbergen fjords and Greenland bays, the bays on the east coast of Novaya Zemlya have one more factor that affects the water structure. In addition to island runoff, the surface layer can be affected by waters from the continental SDL, which under certain conditions can reach the eastern coast of the Archipelago and penetrate into the bays. Because of the relatively small size of these bays (width is ~10 km), an additional requirement for the research methods to investigate them is a high spatial resolution of the shipboard and satellite methods. Their joint use makes it possible to obtain a detailed picture of the spatial structure of these local desalinated regions.

Performing this work became possible thanks to a unique combination of circumstances. In a fairly short period of time, we had an opportunity to obtain shipboard data in five of the bays in the Novaya Zemlya Archipelago. Meanwhile, a new Multispectral Instrument ocean-colour scanner installed on the Sentinel-2 satellite was launched shortly before the research began, allowing us to use its data in our study. During this period in 2015, there was also a strong western transfer of the SDL that coincided with quite rare cloudless conditions over the areas of the bays being investigated, allowing us to obtain satellite data close to the same period as the shipboard studies.

Hence, this study examined the combined influences of continental runoff from the Ob and Yenisei rivers and island runoff from small rivers and glacial meltwater on the desalination of the surface waters in the bays of east coast of Novaya Zemlya using continuous shipboard measurements and high-resolution satellite ocean-colour data.

2. Material and methods

2.1. Research area

Shipboard data were collected during the 63rd cruise of the r/v 'Akademik Mstislav Keldysh' from August to October 2015. Underway measurements were made both in open areas of the Kara Sea and in Sedova, Oga, Tsivolky, Stepovogo, and Abrosimova Bays on the east coast of Novaya Zemlya (Fig. 1). Satellite data from the same period were also analysed for these bays.

This area is available for research using satellite data for only a short period each year, with the beginning (July to early August) determined by the discharge of the Kara Sea from the ice cover, and the end (late September to October) marked by the presence of continuous cloud cover, which prevents the use of the ocean-colour scanners.

2.2. Shipboard data collection

A flow-through system developed at the Ocean Optics Laboratory of the Shirshov Institute of Oceanology (Goldin et al., 2015) was used to conduct the shipboard measurements. It consists of a two-channel flow-through fluorimeter (FTF-2) with high-brightness LEDs and a thermosalinograph (Expert-002). The complex provides continuous measurements of the fluorescence intensities of the CDOM and chlorophyll *a* in the near-surface layer along the ship's route, as well as the seawater's salinity (S) and temperature (T). The chlorophyll fluorescence intensity was not used in this work.

The fluorescence intensity is measured in a fixed spectral range that includes the maxima of the fluorescence band. A high-brightness LED (373 nm, $FWHM_{CDOM}$ = 15 nm) working in continuous mode was used as the source of excitation in the FTF-2, and a photomultiplier was used to record the fluorescence radiation. The emission detection range was determined by a coloured glass optical filter (transmittance maxima — 480 nm, $FWHM_{CDOM}$ = 150 nm). The device provides the I_{fl} measurements in relative units. The combination of excitation wavelength and registration method used allows the instrument to primarily register the fluorescence of the terrestrial humic-like DOC component (Coble, 2007).

The water-intake system ensured the water flow over the instrument was at depth of 1—2 m. The data-averaging interval was 15 s, and the relative error in the I_{fl} measurements was <1%. The random error did not exceed 0.01 PSU in determining the salinity or 0.01°C in recording the temperature. The calibration of the thermosalinograph was corrected based on the probe CTD measurements at the stations.

2.3. Satellite data collection

The satellite images shown are based on high-resolution data from the Multispectral Instrument ocean-colour scanner installed on the Sentinel-2 satellite (https://scihub.copernicus.eu). Averaging during image processing provided a spatial resolution of 40 m. Due to frequent cloudiness over the areas of the bays being investigated, the quantity of available satellite data at the required quality was very limited. Therefore, all available data for the given regions and times were analysed. No atmospheric corrections were performed, as it was not necessary for solving the set tasks.

Local areas desalinated with glacial meltwater contain an increased concentration of suspended matter (Kravchishina et al., 2015). For instance, Blagopoluchiya Bay, located on the North Island of the Novaya Zemlya Archipelago, is relatively close to those in our study and has a similar structure. When it was investigated, the direct determinations of the suspended matter concentrations showed the thawed glacial waters contained 9.8 mg/L of suspended matter, whereas the surface layer of the inner waters of the bay contained only 1.3—2.3 mg/L. The lowest concentrations of suspended matter (0.2—0.5 mg/L) are found in the western (near Novaya Zemlya) and northern parts of the Kara Sea (Burenkov et al., 2010b). This raised concentration of particles can be sensed by satellite data because it leads to increased backscattering (Burenkov et al., 2010b; Sagan and Darecki, 2017) brings to an increase in the water-leaving radiance. Because the satellite data was processed in a graphics editor, the

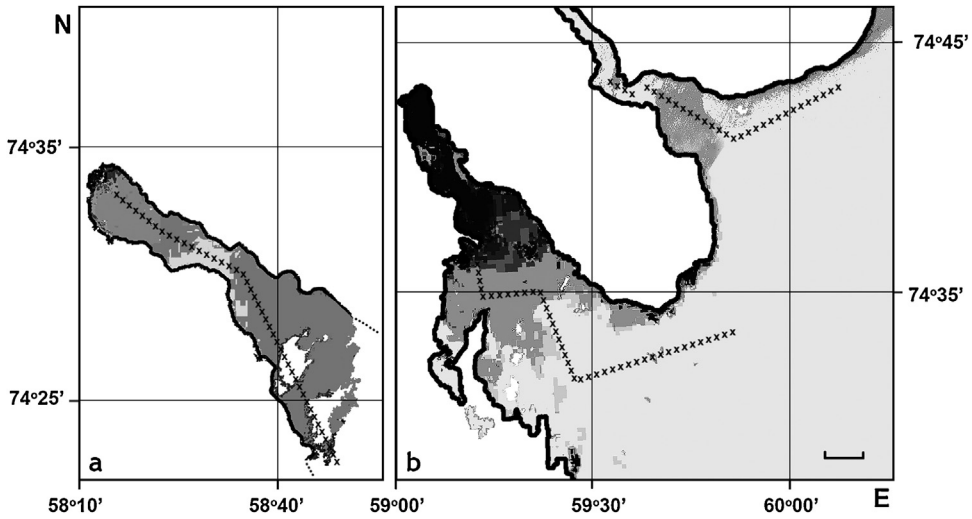

Figure 2 Images constructed from the Sentinel-2 data: (a) Tsivolky Bay, 24 September 2015; (b) Oga (left) and Sedova (right) Bays, 22 September 2015. Black crosses indicate scheme of the sections of the route (transects) for which correlations between the salinity and fluorescence intensity of the coloured dissolved organic matter were calculated. Scale bar = 3 km.

areas of increased brightness (i.e., increased particle concentration) corresponding to the position of locally desalinated regions due to glacial meltwater runoff are identified in grey-scale.

Maps of the CDOM absorption spatial distribution were used to show the propagation of the SDL caused by continental river runoff reaching the shores of Novaya Zemlya. Those maps are based on data from the Moderate Resolution Imaging Spectrometer (MODIS) ocean-colour scanner using the regional algorithm (Vazyulya et al., 2014). This semi-analytical algorithm for solving the inverse problem uses the R_{RS} MODIS data for the wavelength range $\geq$488 nm; $R_{RS}(412)$ and $R_{RS}(443)$ are not used, as the probability of atmospheric correction errors for them is high.

The satellite values for $R_{RS}(\lambda)$ and the water-leaving reflectance $\rho(\lambda)$ values, which are determined during the shipboard measurements, are connected by formulas derived by Lee et al. (1998), where $R_{RS}(\lambda) = 0.518\ \rho(\lambda)/(1 - 1.562\ \rho(\lambda))$. The formula $\rho(\lambda) = 0.0922\ \pi\ b_b(\lambda)/a(\lambda)$ was used for the relation between the spectral values of the reflectance $\rho(\lambda)$, seawater absorption $a(\lambda)$, and backscattering $b_b(\lambda)$ coefficients (Morel and Gentili, 1993). The inverse problem of finding $a(\lambda)$ and $b_b(\lambda)$ is solved using low-parametric models in which these seawater coefficients are represented as a superposition of the contributions of the main components. The absorption coefficient $a(\lambda)$ is defined as the sum of the absorption values of pure sea water, CDOM, and the phytoplankton pigments, while $b_b(\lambda)$ is defined as the superposition of the backscattering by pure sea water and the suspended particles. The contribution of chlorophyll is accounted for by using a regional algorithm (Kuznetsova et al., 2013). An iterative approach was used to improve the accuracy when estimating the slope of the absorption spectrum. As a result of solving the inverse problem, two parameters are defined: $a_g(443)$ and $b_{bp}(555)$.The development and validation of the algorithm was performed with the shipboard measurement data, which contain no errors from atmospheric correction; the algorithm was tested on both the shipboard and satellite data and showed acceptable results.

In the regional algorithm (Kuznetsova et al., 2013), the chlorophyll concentration was calculated with the formula $\ln(Chl) = -3.07\ \ln[R_{RS}(531)/R_{RS}(547)] + 0.148$. This formula was derived based on the satellite data for R_{RS} that directly measured the chlorophyll concentrations in the Kara Sea in 2007 and 2011.

All MODIS satellite data processing was performed in the SMCS software package (Sheberstov, 2015), which is a system for the acquisition, processing, storage, and analysis of satellite and field bio-optical data developed at the Ocean Optics Laboratory of the Shirshov Institute of Oceanology.

Due to frequent dense clouds over the Kara Sea, the satellite maps were averaged over a time interval corresponding to the same period as the in situ measurements. The L2 satellite data was retrieved from the NASA website (http://oceancolor.gsfc.nasa.gov), and the L3 maps were produced by averaging the L2 data over a grid with 3×3 km bins. This relatively low resolution can eliminate the gaps that arise due to clouds.

Data from the INTERIM reanalysis (Dee et al., 2011) were used to estimate the effect of surface wind on the distribution of the desalinated waters.

3. Results and discussion

The shipboard studies of the three bays (Sedova, Oga, and Tsivolky) on the east coast of North Island in Novaya Zemlya (shown in Fig. 1) were conducted successively from 25 to 29 September 2015. The Sentinel-2 data closest in time (22 and 24 September 2015) to those of the expedition were selected for the analysis. Due to clouds, only pairs of bays were exposed on the satellite images from those dates. However, Oga Bay, located in the centre, was visible on both images, which allowed us to correlate the results of the processing.

The maps of the total upwelling radiance shown in Fig. 2 were constructed with data from the B2—B4 channels. The intensity of the total upwelling radiance is shown in grey-

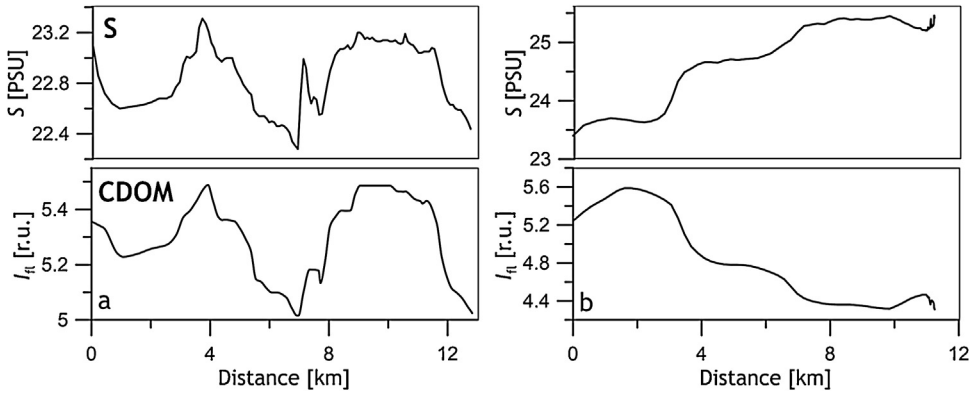

Figure 3 Distributions of the salinity (S) and fluorescence intensity (relative units) of the coloured dissolved organic matter (CDOM) along a section of the transect where it crosses desalinated areas in (a) Oga Bay and (b) Sedova Bay. See Fig. 2 for the transect routes.

scale, with the darker tones corresponding to a greater intensity. These darker areas correspond to the more intensive backscattering caused by the increased concentration of suspended matter in local areas desalinated by glacial meltwater. As mentioned previously, Kravchishina et al. (2015) recorded a similar increase in the concentration of suspended matter in the nearby Blagopoluchiya Bay. Likewise, an increase in the concentration of suspended matter due to the influence of thawed glacial waters has also been reported in the fjords of Spitsbergen (Sagan and Darecki, 2017). These authors recorded an increase in the light attenuation coefficient (from 5.81 m^{-1} up to 26.5 m^{-1}), with a significantly smaller increase in the coefficient of light absorption by particles (from 0.1 m^{-1} up to 0.22 m^{-1}). Importantly, the changes in the values of the light attenuation coefficient were much larger for the fjord with the dominant mineral suspension contribution. These data confirm there is increased suspended matter content in thawed glacial waters.

The analysis of the surface wind maps (1—2 days preceding and coinciding with the high-resolution satellite data and shipboard data) showed a low wind speed of less than 7 m/s that varied greatly in its direction. Therefore, the wind had no influence on the spatial distribution of the suspended matter and the propagation of the SDL in the bays during the data collection period.

Glacier tongues directly contact the waters of the Oga and Tsivolky Bays, while the waters in Sedova Bay do not interact with a glacier. The satellite image processing made it possible to rank the volumes of glacial meltwater in the bays. The largest runoff came from the 'Goluboy' glacier into Oga Bay, while a much smaller volume came into Tsivolky Bay from the 'Serp i Molot' glacier (the darkest areas inside the bays in Fig. 2). Sedova Bay does not receive any glacial meltwater, but a small island river (tens of kilometres in length) flows into it. This river's influence is manifested in the form of a darkened area in the middle of the bay (Fig. 2).

The salinity and CDOM fluorescence intensity distributions along the Oga Bay transect were derived from the shipboard data. The distributions shown in Fig. 3a are where the transect crosses an area desalinated by the waters from glacial meltwater runoff (Fig. 2). The salinity distribution confirms the presence of a small amount of desalination (~1 PSU) in the Oga Bay waters. The freshly melted glacial waters in the Novaya Zemlya North Island bays contain no DOM (Drozdova et al., 2017). Therefore, the positive correlation between the S and I_{fl} indicates that the desalination of this region was due to glacial meltwater. An example of another type of relation that is characteristic for desalinated terrestrial runoff waters forming a SDL (Glukhovets and Goldin, 2014) is shown in Fig. 3b.

In 2015, there was a western distribution of the SDL. Fig. 4 shows the spatial distribution of the CDOM absorption [a_{CDOM} (443)] that characterized the location of the SDL at the time. The map was drawn using MODIS data averaged over the period from 28 August to 28 September 2015. To better fill the map, we used 3 × 3 km spatial averaging. As can be seen from the map, the waters of the SDL formed by the waters of the continental river runoff reached most of the eastern shore of Novaya Zemlya. In particular, the three North Island bays investigated in this study were under the influence of the SDL.

Data from the array of shipboard measurements were used to produce scatter diagrams of the salinity and CDOM fluorescence intensity in Sedova, Oga, and Tsivolky Bays (Fig. 5). It should be noted that the amount of desalination in the bays was relatively small (1—3 PSU). Different types of relations were found in the three bays. First, S and I_{fl} were negatively correlated (R^2 = 0.91) in Sedova bay. This type of relation is usual for SDL waters in the open portion of the Kara Sea. In Oga Bay, there was a positive correlation (R^2 = 0.83) between S and I_{fl}. This type of relation is due to the dominant influence being glacial meltwater, which as mentioned earlier, does not contain CDOM. As can be seen in Fig. 2, the local desalinated region occupies a significant portion of the bay. No correlation (R^2 = 0.22) was seen between S and I_{fl} in the eastern part of Tsivolky Bay (east of 58.6°E). The lack of correlation in this case resulted from the magnitude of the impacts by the thawed glacial and river water runoffs being comparable. The thawed glacial waters entered the eastern part of Tsivolky Bay from its southern shore near the entrance.

Additional information to identify the sources of desalination in the surface layer is provided by the water temperature. Fig. 6 shows scatter diagrams for the bays investigated on the northern island of Novaya Zemlya, with the colours representing the seawater temperature. Frames highlight

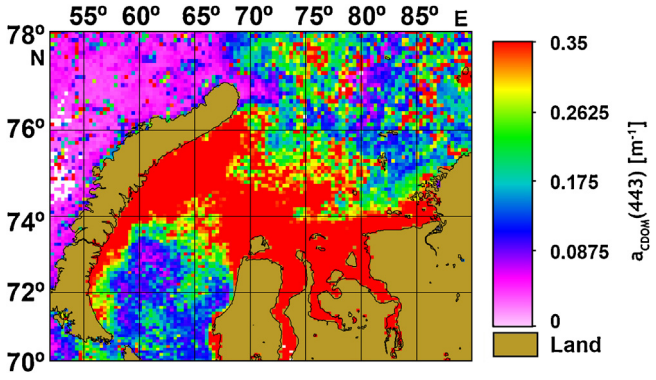

Figure 4 Spatial distribution of the coloured dissolved organic matter absorption in the Kara Sea region (MODIS data averaged from 28 August to 28 September 2015).

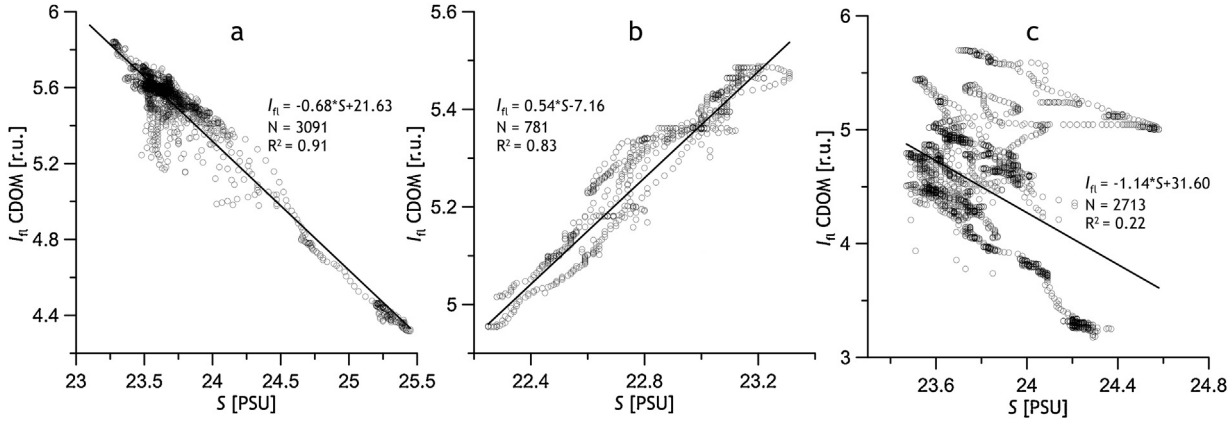

Figure 5 Scatter diagrams of the salinity (S) and coloured dissolved organic matter (CDOM) fluorescence intensity (relative units) in Novaya Zemlya bay waters (Kara Sea) based on shipboard data collected with a flow-through system in 2015: (a) Sedova Bay, 25—26 September; (b) Oga Bay, 26—27 September; and (c) Tsivolky Bay, 28—29 September.

the waters corresponding to the different bays. The temperature variability can be seen as the vessel moves from the entrance of the bay towards the interior (direction of arrows). It should be noted that all of the transects began in sections corresponding to warmer waters with a range of initial temperatures that correspond to temperatures typical of SDL waters in the open areas of the Kara Sea. As the vessel progressed forward into the bays, the temperatures decreased monotonically.

The transect into Sedova Bay (Fig. 6a) began in warm, relatively salty water with average CDOM fluorescence intensities. These waters correspond to the SDL. Inside the bay, the waters became colder and less salty, and the fluorescence signal increased. This appears to be due to the influence of runoff from a small river on Novaya Zemlya, which is clearly visible in Fig. 2. Its waters contain significantly less suspended matter than the thawed glacial waters in the neighbouring Oga Bay.

The temperature distribution in the Oga Bay (Fig. 6a) confirms that the source of desalination in this bay is thawed glacial waters. When moving into the bay, the values of T, S, and I_{fl} all decreased.

Based on the shipboard data for Tsivolky Bay, two different regions were distinguishable for the eastern and western portions of the bay (Fig. 6b). The border between them is located at approximately 58.6°E. The temperatures of the waters east of this border were lower than the temperature of the SDL waters and close to the temperature of the waters in Oga Bay. This is apparently due to the contribution of thawed glacial waters in this region. The western area is located in the heart of the bay and occupied by colder saltier waters. Presumably, these waters entered further into the Bay at the beginning of the summer season before the SDL arrived. The available data is insufficient for a more detailed analysis of these waters' origin. According to the satellite data for the western part directly near the glacier tongue (there were no shipboard measurements for that area) exposed a local area that is affected by thawed glacial waters (the dark area in Fig. 2). A similar distribution was recorded in a Greenland fjord (Murray et al., 2015), where the concentration of suspended matter in the immediate proximity of the glacier was almost four times higher than is typical for most of the fjord.

The main feature of the South Island of Novaya Zemlya is the absence of glaciers. As a consequence, there are no

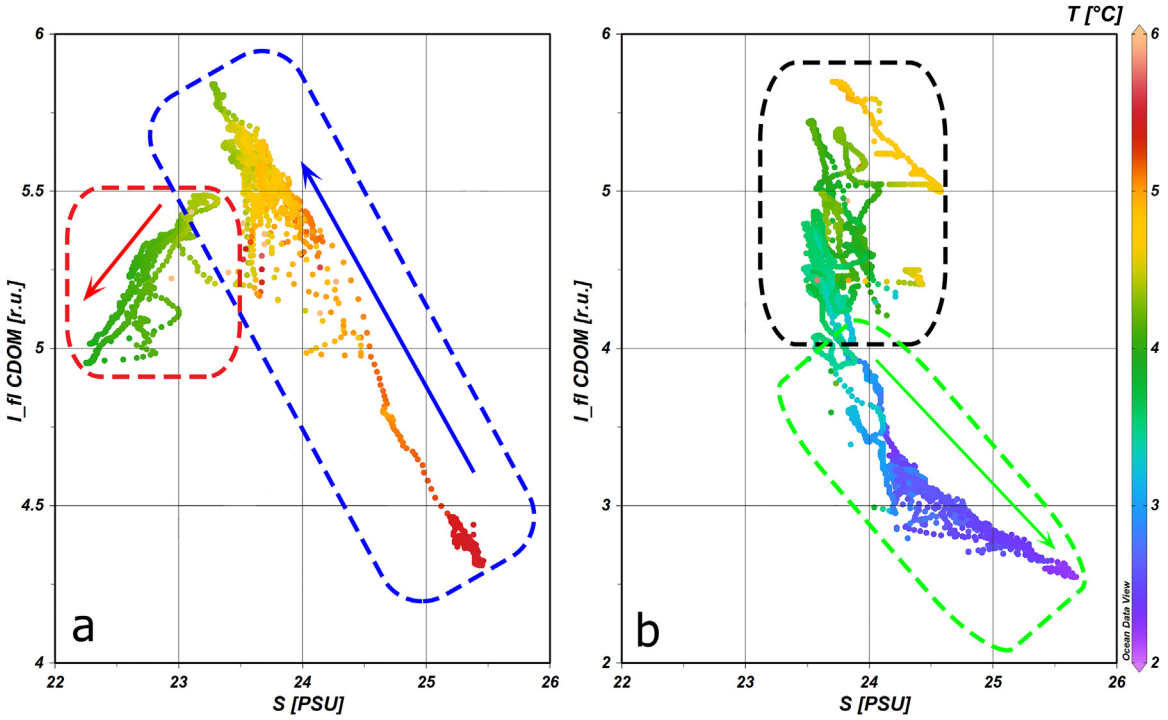

Figure 6 Scatter diagrams of the salinity (S) and coloured dissolved organic matter (CDOM) fluorescence intensity. Colour represents temperature as shown in the scale on the right. Frames indicate the waters: Sedova Bay (blue), Oga Bay (red), eastern Tsivolky Bay (black), and western Tsivolky Bay (green). Arrows correspond to the direction of travel for the transects into the bays. The figure was drawn using ODV (Schlitzer, 2017).

thawed glacial waters desalinating the waters of the bays. Therefore, the only possible desalination factor is caused by river runoff, both island and continental. It is known that the island rivers dry up in the summer once the snow thaw has ended (Coulson et al., 2014). The ship measurements were performed in the eastern parts of the two South Island bays from 30 September to 5 October 2015. Thus, only two types of relations between the S and I_{fl} are possible in the South Island bays: a negative correlation or the absence of a correlation.

The results of the shipboard measurements in Stepovogo Bay showed the presence of a strong anti-correlation between S and I_{fl} ($R^2 > 0.92$). At the same time, the surface water temperature (3–5°C) corresponded to those typical for SDL waters, and a 4 PSU desalination of the water was registered. It follows from Fig. 4 that during the shipboard research period, the Stepovogo Bay was inside the SDL area. Together, these features indicate that the desalination of the surface layer of the eastern part of the Stepovogo Bay was caused by the influence of continental runoff.

In contrast, there was no correlation between S and I_{fl} ($R^2 < 0.04$) in Abrosimova Bay. In this case, low water temperatures (1–3°C), a lack of desalination (S = 31–32 PSU), and low I_{fl} values (<1 r.u.) were recorded. The spatial distribution of $a_{CDOM}(443)$ seen in Fig. 4 indicates that the Abrosimova Bay was near the southern boundary of the SDL. Thus, the absence of a correlation is explained not by the combined effect of glacial melt and river waters, as in the eastern part of Tsivolky Bay, but by a lack of influence by either source of desalination. The bay is occupied by cold salty seawater with a low CDOM content.

Table 1 Characteristics of the markers and sources of desalination in the bays investigated on Novaya Zemlya. The second column shows the types of correlations found between S and I_{fl} that were specific to each bay. The ranges provided for T, S, and I_{fl} correspond to the changes as the vessel moved into the bay.

Bay	Corr. type	T change [°C]	S change [PSU]	I_{fl} change [r.u.]	b_b [m^{-1}]	Dominant source
Sedova	Negative	5.5–4.5	25.5–23.3	4.5–6	Upper middle	SDL and a small island river
Oga	Positive	4.5–4	23.5–22.2	5.5–5	High	Glacial meltwater
Tsivolky (E)	None	5–3	~24	5.6–4	No data	None (mixture)
Tsivolky (W)	Negative	3–2	24–25	4–2.5	Medium	Marine waters
Stepovogo	Negative	3–5	31–27	1–2	No data	SDL
Abrosimova	None	3–1	31–32	<1	No data	Marine waters

The marker characteristics and concluded sources of desalination in the specific bay water surface layers are summarized in Table 1.

4. Conclusions

This study examined the desalination processes that influence the surface water layers in five bays on the east coast of the Novaya Zemlya Archipelago. The surface desalination layer results in a density stratification that prevents vertical mixing, effectively shielding the underlying water column from interacting with the atmosphere, which has a significant effect on the ecosystem. Several sources of desalination are possible: continental river runoff, which can reach the eastern shores of Novaya Zemlya as a SDL that penetrates into the bays; glacial meltwater from the glaciers on the North Island of Novaya Zemlya; and runoff from small rivers on the islands of the Archipelago.

The ratio of the contributions of the different freshwater sources entering the seawater can cause different situations: the dominance of glacial meltwater, the dominance of water desalinated by river runoff, a comparable influence by both, or an absence of desalination. All of these possible situations were detected in the bays investigated. In Sedova Bay, the desalination was due to the dominant influence of continental river runoff with an admixture of island river runoff, while the source of desalination in Oga Bay was thawed glacial water. In the eastern part of Tsivolky Bay, comparable contributions of continental runoff and glacial meltwater were recorded, while in the western extremity of the bay directly near the glacier tongue, a local area was occupied by thawed glacial waters. The only source of desalination in Stepovogo Bay was the continental river runoff, while desalination in Abrosimova Bay was absent.

It is important to note that the influence of the different desalination processes in each of the bays was distinctly individualized. Thus, each bay requires its own study.

A similar pattern was recorded for the Norwegian fjords of Spitsbergen (Sagan and Darecki, 2017), where research in two fjords found the quantitative and qualitative composition of the suspended particles and the light absorption and attenuation coefficient distributions differed significantly.

It is interesting that the continental river runoff, which is a source 500—600 km away from the bays we investigated, plays such a significant role in the desalination processes, dominating in two of the bays and providing a noticeable contribution in a third.

It is also noteworthy that it was the use of correlations between salinity and CDOM fluorescence intensity to identify the sources of desalination that allowed us to effectively divide the influences of the river runoff and thawed glacial waters. Another effective tool was the high-resolution MSI ocean colour scanner on the Sentinel-2 satellite for determining the position and size of areas affected by the glacial meltwater. In most cases, this combination of ship and satellite methods allowed us to identify the dominant source of desalination.

It would be further advisable to supplement the complex of shipboard methods with spectral fluorescence measurements (EEMs), which have been used to successfully determine the origin of other waters in the Arctic basin (Coble, 2007; Drozdova et al., 2017; Gonçalves-Araujo et al., 2016).

Our measurements were performed in 2015, when there was a significant western transfer of the SDL from continental runoff. In other years with other types of transfer, these waters may not reach the shores of Novaya Zemlya, and the resulting desalination processes in the bays will be substantially different from those obtained in this work. This emphasizes the importance of continuing this study to understand the inter-annual variability of the desalination processes in the bays on the east coast of Novaya Zemlya.

Acknowledgements

The shipboard data analysis was obtained in the framework of the state assignment of FASO Russia (theme No. 0149-2018-0002). The shipboard data acquisition, satellite data processing and analysis with their comparison were obtained within the RSF grant (project No.14-50-00095).

References

Amon, R.M.W., 2003. The role of dissolved organic matter for the organic carbon cycle in the Arctic Ocean. In: Stein, R., MacDonald, R. (Eds.), The Organic Carbon Cycle in the Arctic Ocean. Springer, Berlin, 83—99, http://dx.doi.org/10.1007/978-3-642-18912-8_4.

Belyaev, N.A., Peresypkin, V.I., Ponyaev, M.S., 2010. The organic carbon in the water, the particulate matter, and the upper layer of the bottom sediments of the west Kara Sea. Oceanology 50 (5), 706—715, http://dx.doi.org/10.1134/S0001437010050085.

Bröder, L., Tesi, T., Salvadó, J.A., Semiletov, I.P., Dudarev, O.V., Gustafsson, Ö., 2016. Fate of terrigenous organic matter across the Laptev Sea from the mouth of the Lena River to the deep sea of the Arctic interior. Biogeosciences 13 (17), 5003—5019, http://dx.doi.org/10.5194/bg-13-5003-2016.

Burenkov, V.I., Goldin, Y.A., Artem'ev, V.A., Sheberstov, S.V., 2010a. Optical characteristics of the Kara Sea derived from shipborne and satellite data. Oceanology 50 (5), 675—687, http://dx.doi.org/10.1134/S000143701005005X.

Burenkov, V.I., Goldin, Y.A., Kravchishina, M.D., 2010b. The distribution of the suspended matter concentration in the Kara Sea in September 2007 based on ship and satellite data. Oceanology 50 (5), 798—805, http://dx.doi.org/10.1134/S0001437010050164.

Burenkov, V.I., Vasilkov, A.P., 1994. Influence of river discharge on spatial-distribution of hydrological characteristics in the Kara Sea. Oceanology 34 (5), 652—661.

Carmack, E.C., Yamamoto-Kawai, M., Haine, T.W., Bacon, S., Bluhm, B.A., Lique, C., Melling, H., Polyakov, I.V., Straneo, F., Timmermans, M.L., Williams, W.J., 2016. Freshwater and its role in the Arctic Marine System: sources, disposition, storage, export, and physical and biogeochemical consequences in the Arctic and global oceans. J. Geophys. Res. Biogeosci. 121 (3), 675—717, http://dx.doi.org/10.1002/2015JG003140.

Coble, P.G., 2007. Marine optical biogeochemistry: the chemistry of ocean color. Chem. Rev. 107 (2), 402—418, http://dx.doi.org/10.1021/cr050350+.

Coulson, S.J., Convey, P., Aakra, K., Aarvik, L., Ávila-Jiménez, M.L., Babenko, A., Biersma, E.M., Boström, S., Brittain, J.E., Carlsson, A.M., Christoffersen, K., 2014. The terrestrial and freshwater invertebrate biodiversity of the archipelagoes of the Barents Sea; Svalbard, Franz Josef Land and Novaya Zemlya. Soil Biol. Biochem. 68, 440—470, http://dx.doi.org/10.1016/j.soilbio.2013.10.006.

Dai, M.H., Martin, J.M., 1995. First data on trace metal level and behaviour in two major Arctic river-estuarine systems (Ob and Yenisey) and in the adjacent Kara Sea, Russia. Earth Planet. Sci. Lett. 131 (3—4), 127—141.

Dee, D.P., Uppala, S.M., Simmons, A.J., Berrisford, P., Poli, P., Kobayashi, S., Andrae, U., Balmaseda, M.A., Balsamo, G., Bauer, D.P., Bechtold, P., 2011. The ERA-Interim reanalysis: configuration and performance of the data assimilation system. Q. J. R. Meteor. Soc. 137 (656), 553—597, http://dx.doi.org/10.1002/qj.828.

Demidov, A.B., Gagarin, V.I., Vorobieva, O.V., Makkaveev, P.N., Artemiev, V.A., Khrapko, A.N., Grigoriev, A.V., Sheberstov, S.V., 2018. Spatial and vertical variability of primary production in the Kara Sea in July and August 2016: the influence of the river plume and subsurface chlorophyll maxima. Polar Biol. 41 (3), 563—578, http://dx.doi.org/10.1007/s00300-017-2217-x.

Drozdova, A.N., Patsaeva, S.V., Khundzhua, D.A., 2017. Fluorescence of dissolved organic matter as a marker for distribution of desalinated waters in the Kara Sea and bays of Novaya Zemlya archipelago. Oceanology 57 (1), 41—47, http://dx.doi.org/10.1134/S0001437017010039.

Fichot, C.G., Kaiser, K., Hooker, S.B., Amon, R.M.W., Babin, M., Bélanger, S., Walker, S., Benner, R., 2013. Pan-Arctic distributions of continental runoff in the Arctic Ocean. Sci. Rep. 3, 1053, http://dx.doi.org/10.1038/srep01053.

Flint, M.V., 2010. Cruise 54th of the research vessel Akademik Mstislav Keldysh in the Kara Sea. Oceanology 50 (5), 637—642, http://dx.doi.org/10.1134/S0001437010050012.

Glukhovets, D.I., Goldin, Y.A., 2014. Study of bio-optical characteristics of waters of the Kara Sea by using data of satellite and ship measurements. Curr. Probl. Remote Sens. Earth Space 11 (4), 346—350, http://jr.rse.cosmos.ru/article.aspx?id=1359&lang=eng.

Goldin, Y.A., Shatravin, A.V., Levchenko, V.A., Ventskut, Y.I., Gureev, B.A., Kopelevich, O.V., 2015. Analysis of spatial variability of fluorescent intensity of seawater in western part of the Black Sea. Fundam. Prikl. Gidrofiz 7 (1), 11—20.

Gonçalves-Araujo, R., Granskog, M.A., Bracher, A., Azetsu-Scott, K., Dodd, P.A., Stedmon, C.A., 2016. Using fluorescent dissolved organic matter to trace and distinguish the origin of Arctic surface waters. Sci. Rep. 6, 33978, http://dx.doi.org/10.1038/srep33978.

Gordon, H.R., Morel, A.Y., 2012. Springer Sci. & Business Media. Remote Assessment of Ocean Color for Interpretation of Satellite Visible Imagery: A Review, vol. 4, http://dx.doi.org/10.1029/LN004.

Granskog, M.A., Pavlov, A.K., Sagan, S., Kowalczuk, P., Raczkowska, A., Stedmon, C.A., 2015. Effect of sea-ice melt on inherent optical properties and vertical distribution of solar radiant heating in Arctic surface waters. J. Geophys. Res.-Oceans 120 (10), 7028—7039, http://dx.doi.org/10.1002/2015JC011087.

Kowalczuk, P., Zabłocka, M., Sagan, S., Kuliński, K., 2010. Fluorescence measured in situ as a proxy of CDOM absorption and DOC concentration in the Baltic Sea. Oceanologia 52 (3), 431—471, http://dx.doi.org/10.5697/oc.52-3.431.

Kravchishina, M.D., Lein, A.Y., Sukhanova, I.N., Artem'ev, V.A., Novigatsky, A.N., 2015. Genesis and spatial distribution of suspended particulate matter concentrations in the Kara Sea during maximum reduction of the Arctic ice sheet. Oceanology 55 (4), 623—643, http://dx.doi.org/10.1134/S000143701503008X.

Kubryakov, A., Stanichny, S., Zatsepin, A., 2016. River plume dynamics in the Kara Sea from altimetry-based lagrangian model, satellite salinity and chlorophyll data. Remote Sens. Environ. 176, 177—187, http://dx.doi.org/10.1016/j.rse.2016.01.020.

Kuznetsova, O.A., Kopelevich, O.V., Sheberstov, S.V., Burenkov, V.I., Mosharov, S.A., Demidov, A.B., 2013. Assessment of chlorophyll concentration in the Kara Sea based on the data of satellite scanner MODIS—AQUA. Curr. Probl. Remote Sens. Earth Space 5, 21—31.

Lee, Z., Carder, K.L., Mobley, C.D., Steward, R.G., Patch, J.S., 1998. Hyperspectral remote sensing for shallow waters. I. A semianalytical model. Appl. Opt. 37 (27), 6329—6338.

Lisitzyn, A.P., Vinogradov, M.E., 1994. International high-altitude expedition in the Kara Sea during 49 cruise of R/V Dmitry Mendeleev. Oceanology 34 (5), 737—747.

Lorenzen, C.J., 1966. A method for the continuous measurement of in vivo chlorophyll concentration. Deep Sea Res. Oceanogr. Abstracts 13 (2), 223—227.

Makkaveev, P.N., Melnikova, Z.G., Polukhin, A.A., Stepanova, S.V., Khlebopashev, P.V., Chultsova, A.L., 2015. Hydrochemical characteristics of the waters in the western part of the Kara Sea. Oceanology 55 (4), 485—496, http://dx.doi.org/10.1134/S0001437010050061.

Matsuoka, A., Boss, E., Babin, M., Karp-Boss, L., Hafez, M., Chekalyuk, A., Proctor, C.W., Werdell, P.J., Bricaud, A., 2017. Pan-Arctic optical characteristics of colored dissolved organic matter: tracing dissolved organic carbon in changing Arctic waters using satellite ocean color data. Remote Sens. Environ. 200, 89—101, http://dx.doi.org/10.1016/j.rse.2017.08.009.

Morel, A., Gentili, B., 1993. Diffuse reflectance of oceanic waters. II. Bidirectional aspects. Appl. Opt. 32 (33), 6864—6879.

Murray, C., Markager, S., Stedmon, C.A., Juul-Pedersen, T., Sejr, M. K., Bruhn, A., 2015. The influence of glacial melt water on bio-optical properties in two contrasting Greenlandic fjords. Estuar. Coast. Shelf Sci. 163, 72—83, http://dx.doi.org/10.1016/j.ecss.2015.05.041.

Nummelin, A., Ilicak, M., Li, C., Smedsrud, L.H., 2016. Consequences of future increased Arctic runoff on Arctic Ocean stratification, circulation, and sea ice cover. J. Geophys. Res. Oceans 121 (1), 617—637, http://dx.doi.org/10.1002/2015JC011156.

Nummelin, A., Li, C., Smedsrud, L.H., 2015. Response of Arctic Ocean stratification to changing river runoff in a column model. J. Geophys. Res. Oceans 120 (4), 2655—2675, http://dx.doi.org/10.1002/2014JC010571.

Osadchiev, A.A., Izhitskiy, A.S., Zavialov, P.O., Kremenetskiy, V.V., Polukhin, A.A., Pelevin, V.V., Toktamysova, Z.M., 2017. Structure of the buoyant plume formed by Ob and Yenisei river discharge in the southern part of the Kara Sea during summer and autumn. J. Geophys. Res. Oceans 122 (7), 5916—5935, http://dx.doi.org/10.1002/2016JC012603.

Pelevin, V.V., Zavjalov, P.O., Belyaev, N.A., Konovalov, B.V., Kravchishina, M.D., Mosharov, S.A., 2017. Spatial variability of concentrations of chlorophyll *a*, dissolved organic matter and suspended particles in the surface layer of the Kara Sea in September 2011 from lidar data. Oceanology 57 (1), 165—173, http://dx.doi.org/10.1134/S0001437017010131.

Politova, N.V., Shevchenko, V.P., Zernova, V.V., 2012. Distribution, composition, and vertical fluxes of particulate matter in Bays of Novaya Zemlya Archipelago, Vaigach Island at the end of summer. Adv. Meteorol. 2012, Art. ID 259316, 15 pp., http://dx.doi.org/10.1155/2012/259316.

Polukhin, A.A., Makkaveev, P.N., 2017. Features of the continental runoff distribution over the Kara Sea. Oceanology 57 (1), 19—30, http://dx.doi.org/10.1134/S0001437017010143.

Pozdnyakov, D.V., Korosov, A.A., Pettersson, L.H., Johannessen, O. M., 2005. MODIS evidences the river run-off impact on the Kara Sea trophy. Int. J. Remote Sens. 26 (17), 3641—3648, http://dx.doi.org/10.1080/01431160412331330266.

Pugach, S.P., Pipko, I.I., Shakhova, N.E., Shirshin, E.A., Perminova, I. V., Gustafsson, Ö., Bondur, V.G., Ruban, A.S., Semiletov, I.P., 2018. Dissolved organic matter and its optical characteristics in the Laptev and East Siberian seas: spatial distribution and interannual variability (2003—2011). Ocean Sci. 14 (1), 17 pp., https://doi.org/10.5194/os-14-87-2018.

Sagan, S., Darecki, M., 2017. Inherent optical properties and particulate matter distribution in summer season in waters of Hornsund

and Kongsfjordenen, Spitsbergen. Oceanologia 60 (1), 65—75, http://dx.doi.org/10.1016/j.oceano.2017.07.006.

Schlitzer, R., 2017. Ocean Data View. odv.awi.de.

Sheberstov, S.V., 2015. System for batch processing of oceanographic satellite data. Curr. Probl. Remote Sens. Earth Space 12 (6), 154—161, (in Russian), http://d33.infospace.ru/d33_conf/sb2015t6/154-161.pdf.

Stedmon, C.A., Granskog, M.A., Dodd, P.A., 2015. An approach to estimate the freshwater contribution from glacial melt and precipitation in East Greenland shelf waters using colored dissolved organic matter (CDOM). J. Geophys. Res.-Oceans. 120, 1107—1117, http://dx.doi.org/10.1002/2014JC010501.

Vazyulya, S.V., Kopelevich, O.V., Sheberstov, S.V., Artemiev, V.A., 2014. Satellite estimation of the coefficients of CDOM absorption and diffuse attenuation in the White and Kara seas. Curr. Probl. Remote Sens. Earth Space 11 (4), 31—41, http://jr.rse.cosmos.ru/article.aspx?id=1348&lang=eng.

Zatsepin, A.G., Kremenetskiy, V.V., Kubryakov, A.A., Stanichny, S.V., Soloviev, D.M., 2015. Propagation and transformation of waters of the surface desalinated layer in the Kara Sea. Oceanology 55 (4), 450—460, http://dx.doi.org/10.1134/S0001437015040153.

Zatsepin, A.G., Zavialov, P.O., Kremenetskiy, V.V., Poyarkov, S.G., Soloviev, D.M., 2010. The upper desalinated layer in the Kara Sea. Oceanology 50 (5), 657—667, http://dx.doi.org/10.1134/S0001437010050036.

Oceanologia (2019) 61, 78—88

Available online at www.sciencedirect.com

ScienceDirect

journal homepage: www.journals.elsevier.com/oceanologia/

ORIGINAL RESEARCH ARTICLE

Canthaxanthin in recent sediments as an indicator of heterocystous cyanobacteria in coastal waters

Magdalena Krajewska [a], Małgorzata Szymczak-Żyła [a], Justyna Kobos [b], Małgorzata Witak [c], Grażyna Kowalewska [a,*]

[a] *Institute of Oceanology PAN, Marine Pollution Laboratory, Sopot, Poland*
[b] *University of Gdańsk, Faculty of Oceanography and Geography, Division of Marine Biotechnology Gdynia, Poland*
[c] *University of Gdańsk, Faculty of Oceanography and Geography, Division of Marine Geology, Gdynia, Poland*

Received 15 May 2018; accepted 10 July 2018
Available online 31 July 2018

KEYWORDS
Cyanobacteria;
Carotenoids;
Canthaxanthin;
Gulf of Gdańsk (southern Baltic);
Oslofjord

Summary The mean share of heterocystous cyanobacteria in total chlorophyll-*a* production in coastal waters, based on cyanobacterial marker carotenoid and chloropigments preserved in recent sediments (0—5 cm, ca 30 years), has been studied in the Gulf of Gdańsk (southern Baltic) and for comparison in the Oslofjord/Drammensfjord (southern Norway). First of all, Baltic cyanobacteria, both from laboratory cultures and field samples, were analysed to select marker heterocysteous cyanobacteria carotenoids for sediments. The pigment relation to diatom percentages of different salinity preferences has been tested, to confirm origin of cyanobacteria. The results indicate that canthaxanthin is the best marker of heterocystous cyanobacteria in the southern Baltic Sea. These filamentous cyanobacteria inflow to the Gulf of Gdańsk from the open sea and their abundance has increased in the last thirty years, in comparison with previous time. In that period they made up ca 4.6% of the total chlorophyll-*a* production in the Gulf of Gdańsk. The estimate for Oslofjord, at the same assumptions, suggests that heterocystous cyanobacteria occurred there also (up to 5.8% of the total chlorophyll-*a* production), were of marine origin, but their abundance has decreased during the last thirty years. Such an estimate may be used in environmental modelling and can be applied to other coastal areas, once the marker pigments of the main cyanobacteria species have been identified, and the percentage of total chlorophyll-*a* produced in a basin, preserved in sediments, has been determined for such area.

* Corresponding author at: Institute of Oceanology, Polish Academy of Sciences, ul. Powstańców Warszawy 55, 81-712 Sopot, Poland. Tel.: +48 587311615.
E-mail addresses: mkrajewska@iopan.pl (M. Krajewska), szymczak@iopan.gda.pl (M. Szymczak-Żyła), justyna.kobos@ug.edu.pl (J. Kobos), ocemaw@univ.gda.pl (M. Witak), Kowalewska@iopan.pl (G. Kowalewska).
Peer review under the responsibility of Institute of Oceanology of the Polish Academy of Sciences.

Production and hosting by Elsevier

https://doi.org/10.1016/j.oceano.2018.07.002

1. Introduction

Cyanobacteria (blue-green algae) blooms are presently a serious problem in the Baltic, a brackish, semi-enclosed sea (Kahru and Elmgren, 2014), as in many other coastal zones and lakes (Bianchi et al., 1993; Carstensen et al., 2015; Cook et al., 2016; Paerl et al., 2003). Some cyanobacteria species can produce toxins, so the blooms are often not only a nuisance but also pose a danger to marine life and humans (Karlson et al., 2005; Mazur-Marzec and Pliński, 2009; Sivonen et al., 1989). The cyanobacteria massive blooms which develop in the Baltic each summer may be transferred by waves and water currents to far distances. They are composed of atmospheric nitrogen-fixing (diazotrophic) cyanobacteria, of three planktic taxa: *Nodularia spumigena*, *Aphanizomenon flos-aquae* and *Dolichospermum* sp., classified as heterocystous cyanobacteria (Mazur-Marzec et al., 2013). All three taxa can produce toxins, though there are no reports on toxic *Aphanizomenon flos-aquae* from the Baltic — only on its freshwater strains (Lehtimäki et al., 1997). The most abundant of those three taxa in the southern Baltic — *N. spumigena* — produces the toxin nodularin (NOD) (Laamanen et al., 2001; Mazur-Marzec and Pliński, 2009; Stal et al., 2003). It forms blooms also in estuaries and brackish lakes of coastal zones in Australia, New Zealand, inland waters of the USA, South Africa and a saline lake in Turkey (Cook et al., 2016; Henriksen, 2005; Sahindokuyucu Kocasari et al., 2015), as well as off the North Sea coast (Nehring, 1993). *N. spumigena* needs higher salinities than *A. flos-aquae* for optimal growth, so the latter is more abundant than the former in freshwater lakes and the northern Baltic (Laamanen et al., 2002; Lehtimäki et al., 1997; Mazur-Marzec et al., 2005).

In order to determine the intensity of cyanobacteria blooms, microscopic analysis of phytoplankton samples is mostly used. Such an analysis provides only temporary information, not always relevant, since the cyanobacteria distribution in water can change very quickly in time and space (Kowalewska et al., 2014; Stal et al., 2003). Satellite detection methods (Kahru and Elmgren, 2014) give a much larger picture than the above-mentioned discrete, point monitoring, although it is still a two-dimensional, fleeting image, encumbered with such impediments like clouds, high costs, etc.

To supplement the above techniques it is worth analysing pigments in sediments. Concentrations and relative compositions of pigments in sediments depend on such factors as primary production, phytoplankton composition, sedimentation/accumulation rate, hydro-meteorological and post-depositional conditions (Jeffrey et al., 1997). Pigments differ in stability and can be degraded by both abiotic and biotic factors e.g. oxygen, light, herbivore grazing or microorganism activity (Leavitt, 1993). In consequence, studies on parent pigments and their derivatives in sediments provide information about time-averaged primary production, phytoplankton taxa and the environmental conditions (Jeffrey et al., 1997). Zeaxanthin is known as a major carotenoid, characteristic of cyanobacteria occurring in an aquatic environment (Jeffrey et al., 1997; Roy et al., 2012); echinenone and canthaxanthin are also mentioned (Henriksen, 2005; Roy et al., 2012). Zeaxanthin has been considered a universal cyanobacteria marker in the Baltic water (Stoń et al., 2002) and sediments (Bianchi et al., 2000; Łotocka, 1998). A 4-keto-myxoxanthophyll-like pigment was proposed as a marker of *N. spumigena* in seawater — the major toxic cyanobacteria species forming blooms in the Baltic Sea (Schlüter et al., 2004).

The aim of this paper was to estimate the mean contribution of heterocystous cyanobacteria to total chlorophyll-*a* production in coastal waters, based on biomarker carotenoids and chloropigments preserved in recent sediments. Such estimate may be used in environmental modelling. Sediments originated from the Gulf of Gdańsk and for comparison from the Oslofjord/Drammensfjord (southern Norway). It is a part of Skagerrak strait, connecting the North Sea and the Kattegat sea area, which leads to the Baltic Sea. Both the Gulf of Gdańsk and Oslofjord are under human impact and of restricted seawater exchange, but differ in natural conditions (salinity, water depth, geomorphology, hydrology, etc.). The sediment results were related to the Baltic cyanobacteria in laboratory cultures and seawater samples collected during summer cyanobacteria blooms to select marker carotenoids characteristic for heterocysteous cyanobacteria in this area. Correlation of cyanobacterial marker carotenoids in sediments with diatom percentage of different salinity preferences has been tested, to confirm marine/brackish origin of cyanobacteria.

2. Material and methods

2.1. Study areas

2.1.1. Gulf of Gdańsk

The Gulf of Gdańsk (area — 4940 km^2, water volume — 291 km^3 (Majewski, 1994)) is situated in the south-eastern part of the Baltic Sea and is part of the Gdańsk Basin. It has an average depth of 59 m and a maximum of 110 m (Gdańsk Deep). The input of nutrients from the waters of the Wisła (Vistula), the largest Polish river (~39 km^3 yr^{-1}), leads to a high level of primary production (up to 225 g C^{-1} yr^{-1}) (Pastuszak and Witek et al., 2012). High sedimentation/accumulation rates and limited water exchange favour intensive blooms of algae and cyanobacteria (including species producing toxins) (Conley et al., 2011). The Gdańsk Deep is a sink for particulate matter both autochthonous (originating from marine primary production) (Maksymowska et al., 2000) and allochthonous (carried by the Wisła). The salinity varies between 7 and 8 in the surface water, except for an area close to the Wisła mouth. The salinity of deeper water is higher, ca 10—15. At depth 60—80 m a halocline is formed resulting in hypoxic/anoxic conditions in the bottom waters (IMGW, 2013). The sediments in the Gulf of Gdańsk are diverse: from sand near the coast to silty clay in the Gdańsk Deep. Stations P110, P116, M1 and P1 were situated along the pathway of Wisła water inflow into the Gulf. Stations BMPK10 and P104 were located in the shallow, western part of the basin (Puck Bay), the latter near the shore but also close to the open sea.

2.1.2. Oslofjord/Drammensfjord

Oslofjord/Drammensfjord, the northward extension of the Skagerrak, lies at the entrance to the Baltic. The two main, inner and

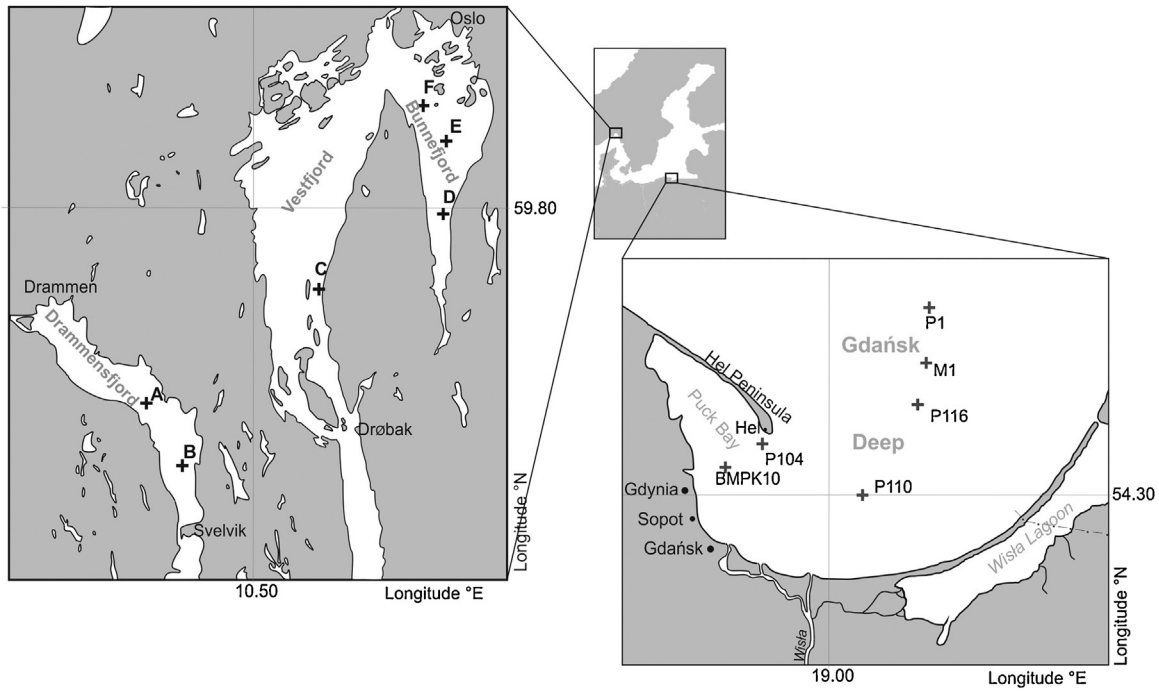

Fig. 1 Location of the sediment sampling sites.

outer fjord basins are separated by a sill at 19.5 m depth (Drobak Sound). Stations A and B were located in Drammensfjord, separated from the Greater Oslofjord by a sill at Svelvik. The other four stations were located in the inner Oslofjord: station C in the deepest, southernmost part of the Vestfjord, and stations D, E, F in the Bunnefjord. The water depths were from 113 to 152 m at stations A—D, and 77—78 m at stations E and F. The surface salinity ranged from 0 (stations A, B) to nearly 20 (Oslofjord). The halocline lay at depth 10—20 m at all stations.

2.2. Sample collection

Sediment samples were collected at six stations in the Gulf of Gdańsk and at six in the Oslofjord/Drammensfjord (Fig. 1). Sediments were collected with a Niemistö core sampler (Φ = 10 cm) during a cruise of r/v 'Oceania' in April 2014 (Gulf of Gdańsk) and in June 2014 (Oslofjord/Drammensfjord). Immediately after collection, the cores were divided into layers (0—1, 1—5, 5—10, 10—15, 15—20 cm) and frozen at −20°C on board ship and next preserved frozen until pigment and diatom analyses.

Phytoplankton samples were collected from the surface seawater at the Sopot pier during the exceptionally intensive cyanobacteria bloom in August 2015 and a much less intensive one in July 2016. The seawater samples were passed through Whatman GF/F filters, which were then stored at −20°C until HPLC analysis. The water samples were analysed under the microscope in order to identify cyanobacteria taxa.

2.3. Cyanobacteria cultures

The strains originated from the Culture Collection of Northern Poland (CCNP) at the Institute of Oceanography University of Gdańsk. The cyanobacteria had been isolated from the littoral and pelagic zones of the Baltic Sea (Table 1). Additionally, one strain of *Aphanizomenon flos-aquae* (CCAP 1401/2), isolated from a freshwater lake in the U.K., was analysed. The cyanobacteria cultures were passed through a Whatman GF/F glass-fibre filter and next analysed for pigment content.

2.4. Pigment analysis

Pigments (carotenoids and chloropigments) were analysed in sediment samples, cyanobacteria cultures and seston samples. Extraction and analysis of pigments were carried out by HPLC, according to the procedures described in detail elsewhere (Krajewska et al., 2017a; Szymczak-Żyła and Kowalewska, 2007, Szymczak-Żyła et al., 2017).

2.5. Diatom analysis

Samples for diatom analyses (ca 0.1—0.2 g dry sediment) were prepared following the standard procedure for diatom observation under a light microscope (Battarbee, 1986). The diatom samples were treated with 10% HCl to remove calcium carbonate. Next, the organic matter was digested using 30% H_2O_2, after which mineral matter was removed by decantation. To estimate the concentration of siliceous microfossils per unit weight of dry sediment (absolute abundance), a random settling technique was used (Bodén, 1991). Permanent diatom preparations were mounted in Naphrax® (refractive index n_D = 1.73). The analysis was performed with a NIKON microscope under a 100× oil immersion objective; 500 to 800 valves were counted in each sample to estimate the percentage abundance of particular taxa. The raw counts were transformed into relative abundance of the total frustules counted. The taxonomy and ecological information with respect to habitat and salinity preferences was based primarily on Krammer and Lange-Bertalot (1986), Denys (1991), Hasle and Syvertsen (1996).

Table 1 Marker cyanobacteria carotenoids in laboratory cultures and field samples.

Cyanobacteria	Myxo	Zea	Cantha	Echin
Nostocales — planktic				
Nodularia spumigena CCNP1401 (a)	myxo-like (16.4 min)	–	+	+
Nodularia spumigena CCNP 1401 (b)	–	–	+	+
Nodularia spumigena CCNP 1403	myxo-like (16.7 min)	–	+	+
Nodularia spumigena CCNP 1430	–	–	+	+
Nodularia spumigena CCNP 1440	–	–	+	+
Aphanizomenon flos-aqua CCAP1401/2[a]	+	–	+	+
Nostocales — benthic				
Anabaena sp. CCNP1417 (a)	myxo-like (17.1 min)	–	+	+
Anabaena sp. CCNP 1417 (b)	myxo-like (17.3 min)	–	+	+
Trichormus variabilis CCNP 1404	myxo-like (17.4 min)	–	+	+
Chroococcales				
Synechocystis sp. CCNP1108 (a)	myxo-DHI standard (20.1 min)	+	–	+
Synechocystis sp. CCNP 1108 (b)	myxo-DHI standard (20.1 min)	+	–	+
Synechocystis salina CCNP1104 (a)	myxo-DHI standard (20.2 min)	+	–	+
Synechocystis salina CCNP 1104 (b)	myxo-DHI standard (20.1 min)	+	–	+
Cyanobium sp. CCNP 1109	–	+	–	+
Synechococcus sp. CCNP 1110	–	+	–	+
Microcystis aeruginosa CCNP1101 (a)	myxo-like (17.5 min)	+	–	+
Microcystis aeruginosa CCNP 1101 (b)	myxo-like (17.1 min)	+	–	+
Pseudoanabaenales				
Pseudoanabaena galeata CCNP1313 (a)	myxo-DHI standard (20.1 min)	+	–	+
Pseudoanabaena galeata CCNP 1313 (b)	–	+	–	+
Oscillatoriales				
Lyngbya aestuari CCNP 1315	myxo-like (18.6 min)	+	–	+
Blooms — Gulf of Gdańsk				
Cyanobacteria bloom — August 2015 (Nostocales)	myxo-like (17.4 min)	+	+	+
Cyanobacteria bloom — July 2016 (Nostocales)	myxo-like (17.3 min)	+	+	+

[a] The UK National Culture Collection (UKNCC).

2.6. Statistical analysis

The results were statistically processed using STATISTICA 12.5 software (StatSoft, Poland); correlation analysis was used. A non-parametric method (R-Spearman correlation analysis) was applied as the basic conditions necessary for using parametric methods were not fulfilled. A correlation of $p < 0.05$ was regarded as significant.

3. Results

3.1. Carotenoid distribution in sediments

The highest concentration of sum of carotenoids (Σ11Cars) in the Gulf of Gdańsk was in the first (0—1 cm) sediment layer at each station, and varied from minimum concentration 15 nmol/g at station BMPK10 (5—10 cm) to ~860 nmol/g dw of sediment, at station P1 (0—1 cm) and were higher at the Deep of Gdańsk than at the coastal stations; the corresponding results from Oslofjord were from ~11 nmol/g at station F (15—20 cm) to 500 nmol/g at station D (5—10 cm) (Fig. 2a). The carotenoid content was the highest at stations D and E. Moreover, the carotenoid content in the 0—1 cm layer of the cores from all the fjord stations was not the highest: in fact it was sometimes even lower than in the deeper core layers.

Besides β-carotenes in sediments, there were markers of the main phytoplankton groups occurring in the southern Baltic: zeaxanthin (Zea), canthaxanthin (Cantha) and echinenone (Echin) — cyanobacteria; lutein (Lut) — green algae; alloxanthin (Allo) and α-carotene (α-Car) — cryptomonads; fucoxanthin (Fuco) and diatoxanthin (Diato) — diatoms and dinoflagellates. The percentage of three cyanobacteria pigments (zeaxanthin, echinenone and canthaxanthin) in the sum of 11 carotenoids was the lowest in the 0—1 cm layer owing to the high percentage of fucoxanthin, an unstable pigment (Appendix 1). In the deeper layers it was around 20% of the sum at all stations, although both the amounts and proportions of particular cyanobacteria carotenoids differed between stations and with depth in sediments (Fig. 2b, Appendix 2). Generally, all three carotenoids were present in distinctly higher concentrations in the sediments of the Gdańsk Deep stations than in the coastal ones. In particular, the zeaxanthin concentration rose towards the Deep and was highest in the sediments at P1. Canthaxanthin was very similarly distributed in the sediments of the four stations P1—P110, although there were differences in particular layers, while echinenone occurred in lower concentrations than zeaxanthin and canthaxanthin (Appendix 2). The three carotenoids were present in the following percentages of their sum: zeaxanthin (57—85%), canthaxanthin (10—30%) and echinenone (2—18%) (Fig. 2b). The average percentage of zeaxanthin in the sum ranged from 70 to 80% in the Gdańsk

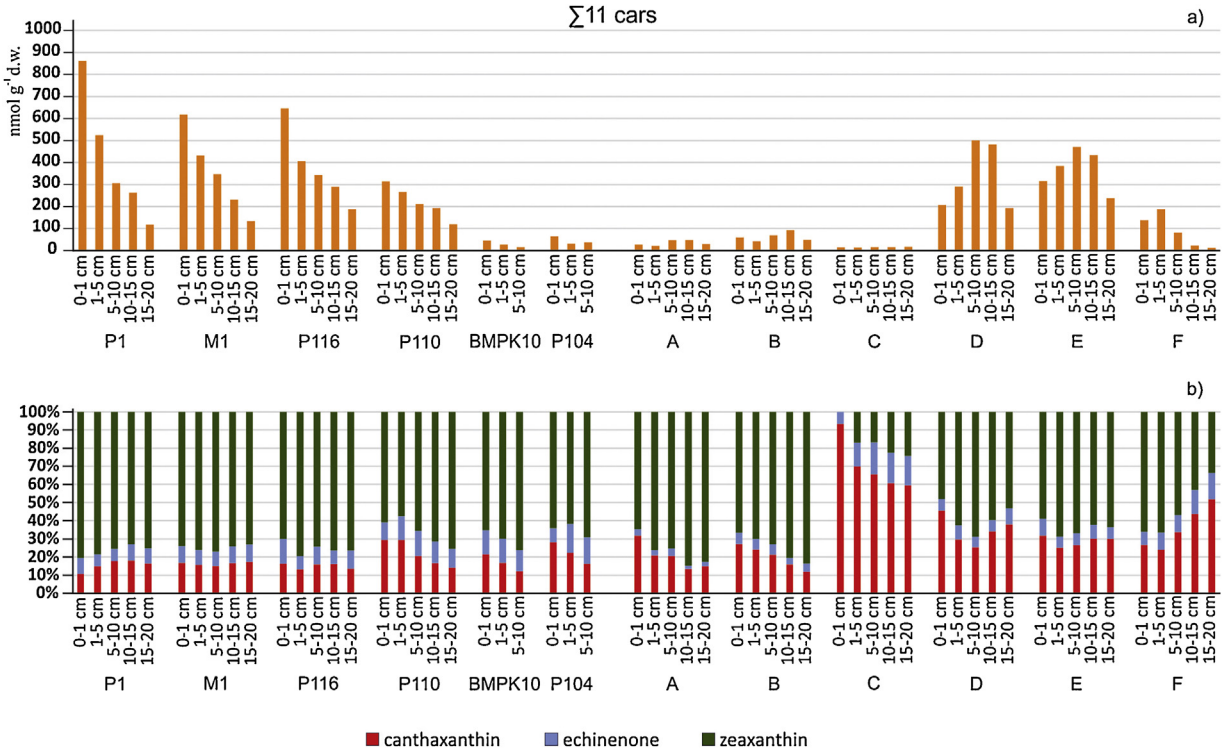

Fig. 2 (a) Sum of 11 carotenoids in recent sediments from the Gulf of Gdańsk and Oslofjord/Drammensfjord (in nmol/g). (b) Percentage of three cyanobacteria carotenoids in their sum.

Deep to 60—75% in the Oslofjord. Station C had the smallest zeaxanthin percentage and an exceptionally high percentage of canthaxanthin, ca 60%. The percentage of canthaxanthin was higher in the Oslofjord than in the Gulf of Gdańsk, while that of echinenone was lower in the Oslofjord compared to the Gulf of Gdańsk.

3.2. Diatoms

The results of the diatom analysis indicate that the sum of valves was about ten times higher in the Gulf of Gdańsk than in the Oslofjord and rarely highest in the 0—1 cm layer. At stations C and F the valves occurred only in the surface layers (0—1 and 0—5, respectively). The percentage of marine diatoms in the sum of all diatom valves in the Gulf of Gdańsk was the highest at station P110 and the lowest at station P116, generally lower in the Deep of Gdańsk sediments than in the coastal ones (Fig. 3). In the fjord sediments the content of marine planktic diatoms was much higher in the inner Oslofjord than in Drammensfjord.

3.3. Baltic cyanobacteria laboratory cultures and field samples

In order to elucidate the results for sediments, nineteen cyanobacteria cultures were analysed to determine their carotenoid composition (Table 1). Eight were of the order *Nostocales*: five of planktic *Nodularia spumigena*, three of the benthic *Anabaena* sp. and *Trichormus variabilis*, isolated from the Baltic Sea, and one of *Aphanizomenon flos-aquae* — isolated from a lake. The cyanobacteria cultures of the order *Nostocales* contained canthaxanthin and echinenone (Table 1). These cultures contained also different myxol glucoside carotenoids. The next cultures analysed were non-colonial cyanobacteria of the order *Chroococcales*: *Synechocystis*, *Synechococcus* and *Cyanobium* sp. (all non-toxic). The *Synechocystis*, *Synechococcus* and *Cyanobium* are included in the planktic picocyanobacteria which, according to literature data, may constitute as much as 80% of the cyanobacteria biomass in the Baltic Sea (Stal et al., 2003). The next one culture was also included in *Chroococcales* a freshwater toxic strain of the nanocyanobacteria *Microcystis aeruginosa* CCNP1101, isolated from the Wisła Lagoon, although *M. aeruginosa* occurs in the Gulf of Gdańsk and other parts of the Baltic coastal zone where the salinity is low (Belykh et al., 2013; Łotocka, 1998; Stoń et al., 2002). The last cultures were *Pseudanabaena*, a benthic cyanobacteria of the order *Pseudoanabaenales* and a representative of *Oscillatoriales* — *Lyngbya aestuari*. The analyses indicated that *Chroococcales*, *Pseudanabaena* sp. and *Oscillatoriales* contained echinenone and zeaxanthin but did not contain canthaxanthin. Different myxoxanthophyll-type carotenoids occurred in majority of cultures (Table 1).

The seawater samples collected from the Sopot pier during cyanobacteria blooms contained mainly canthaxanthin and echinenone of the three cyanobacteria carotenoids, characteristic of *Nostocales* (Fig. 4, Appendix 3). Microscopic analysis showed that during the blooms one cyanobacteria taxa, of the order *Nostocales*, *Nodularia* was predominant (ca 90%), *Aphanizomenon* and small amounts of *Dolichospermum* were also present. These samples contained small quantities of zeaxanthin and myxox-

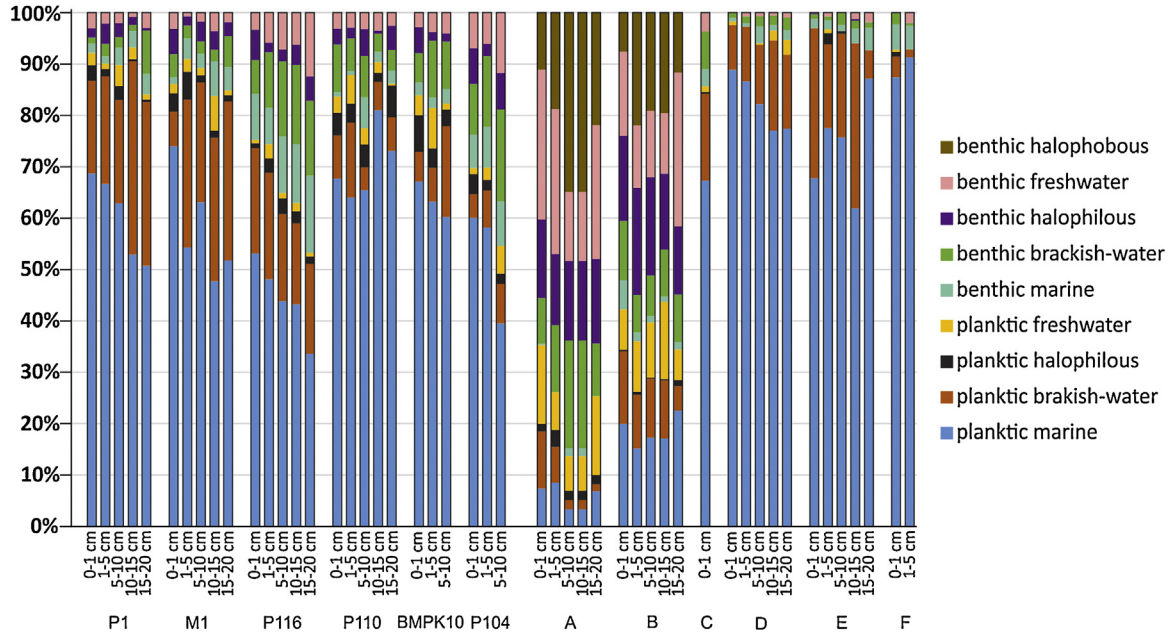

Fig. 3 Percentage of diatoms of different salinity groups.

anthin-type pigments; the letter were under limit of detection in sediments (Fig. 4, Appendix 3).

4. Discussion

4.1. Cyanobacteria marker carotenoids

Based on the laboratory culture and field sample analyses, one may infer that canthaxanthin is a marker of heterocystous cyanobacteria in the Gulf of Gdańsk. Of course, there are different cyanobacteria species in the Baltic and its coastal zone and even more numerous strains, some of which may have other sets of marker carotenoids. Nevertheless, when looking for markers of the most abundant species of filamentous diazotrophic cyanobacteria forming massive blooms in Baltic seawater, canthaxanthin seems to be the best. This carotenoid has already been considered as a marker of filamentous heterocystous cyanobacteria for Baltic seawater (Henriksen, 2005; Schlüter et al., 2004; Wojtasiewicz and Stoń-Egiert, 2016), Baltic coastal lakes (Freiberg et al., 2011), and also other aquatic basins in the world, such as an urban lake in Canada (Desphande et al., 2014). The present results disagree with those of Bianchi et al. (2000) for the Baltic, who showed that zeaxanthin is a marker of atmospheric nitrogen-fixing cyanobacteria. However, those authors stated also that zeaxanthin occurred in minor amounts in *Aphanizomenon* sp. and was absent in *Nodularia spumigena* (Bianchi et al., 2000, 2002), and they did not determine canthaxanthin. In those papers zeaxanthin and echinenone were presented as markers of filamentous atmospheric nitrogen-fixing cyanobacteria; like other authors (Desphande et al., 2014), we did not observe this. Wojtasiewicz and Stoń-Egiert (2016) also confirmed that zeaxanthin was absent in the toxic *N.spumigena* and in *Anabaena* sp.

Zeaxanthin, in turn, appears to be the best marker of picocyanobacteria which contain higher ratio Zea/ ΣChlns-*a* than other cyanobacteria (Appendix 3) and are most abundant among cyanobacteria (Stal et al., 2003). In fact, zeaxanthin has already been used as a marker of non-colonial cyanobacteria for sediments from a Canadian lake (Desphande et al., 2014). Although some authors have described the occurrence of zeaxanthin in *Nostocales* samples and from the Baltic Sea, e.g. in small amounts, in some laboratory cultures of *Nodularia spumigena* (Schlüter et al., 2008) or the sole available Baltic strain culture of *Apanizomenon flos-aquae* — KAC15 (Schlüter et al., 2004; Wojtasiewicz and Stoń-Egiert, 2016), one should treat these reports with caution. Such samples are not axenic cultures and may contain an admixture of other species, e.g. picocyanobacteria, which contain zeaxanthin. The seawater samples collected during filamentous cyanobacteria blooms on the Sopot coast also contained small amounts of zeaxanthin (Fig. 4, Appendix 3), besides small amounts of diatom and green algae markers. Moreover, zeaxanthin has a very similar structure to lutein (it differs in the location of just one double bond); because of this, it is often co-eluted with lutein in HPLC (Tse et al., 2015). Finally, not only genetic traits but also environmental conditions can considerably influence the carotenoid pattern. Intensive irradiation, light spectrum change, can enhance production of canthaxanthin and zeaxanthin as photo-protective carotenoids or convert other carotenoids to zeaxanthin (Grant and Louda, 2010; Jeffrey et al., 1997; Schlüter et al., 2000). This is very probably why *Nostocales* strains in field samples and laboratory cultures differ in their zeaxanthin content. In addition, zeaxanthin may originate from green phytoplankton algae, macroalgae or higher plants (Hall et al., 1997), but in the southern Baltic their input in total primary production is rather small and concentrating at the seashore, due to turbidity caused by eutrophication (HELCOM, 2009); in coastal Baltic waters it may also be derived from *Microcystis* sp.

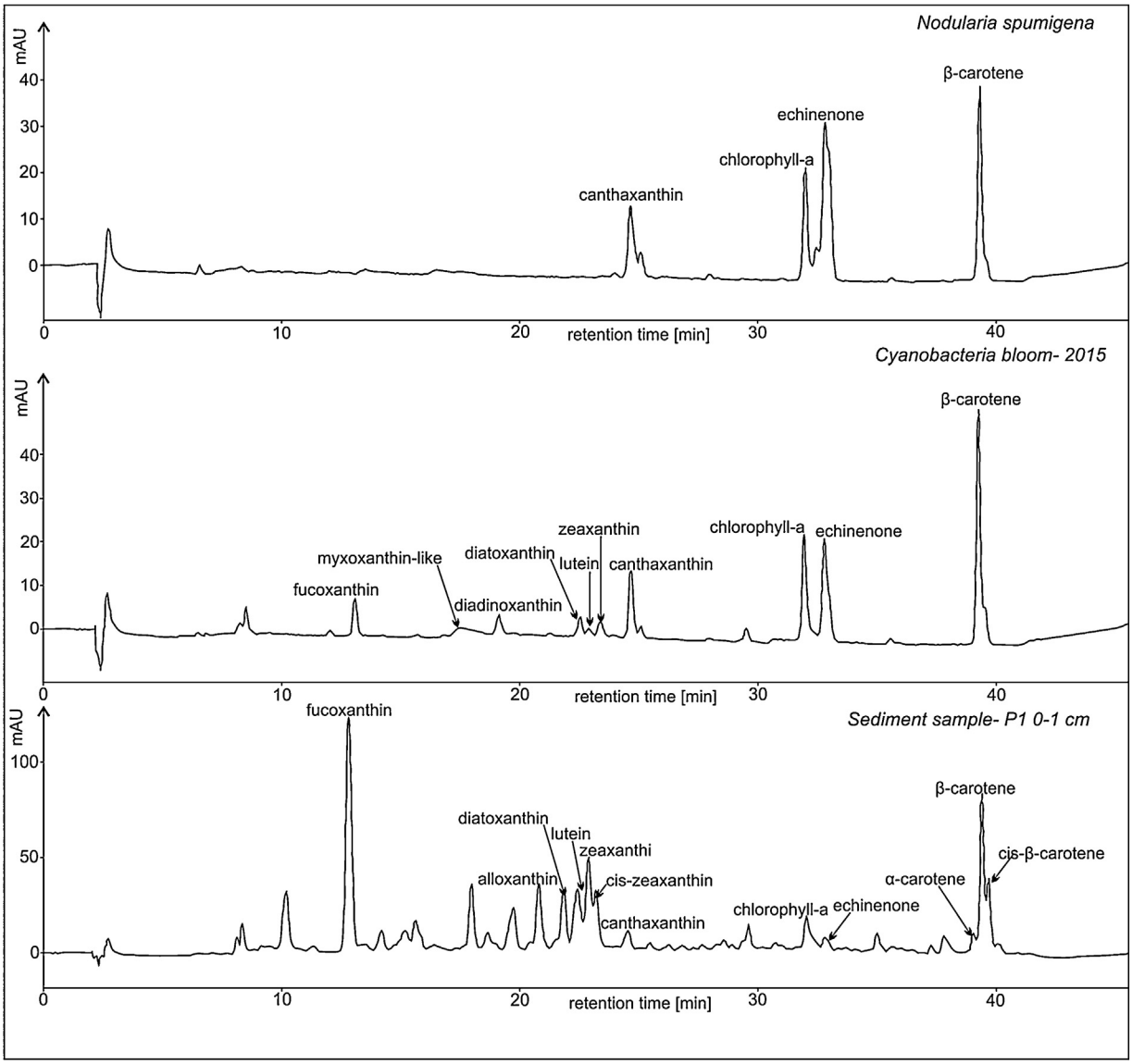

Fig. 4 HPLC chromatograms at 450 nm of (a) *Nodularia spumigena* culture, (b) Cyanobacteria bloom — 2015, at the Sopot coast, (c) sediment sample from the Gulf of Gdańsk.

Finally, it can be inferred from the culture analysis that echinenone in sediments could be a marker of all cyanobacteria, as was proposed for Baltic (Henriksen, 2005), providing that there is hypoxia, as it is evidently the least stable of the three cyanobacteria marker carotenoids even though it has been included, along with canthaxanthin and zeaxanthin, in the first pigment stability class (Leavitt and Hodgson, 2001). This is clear in the surface sediments at stations P116 and P1, where the level of hypoxia was the highest and echinenone occurred in the largest concentration. It may decompose already in water column as its ratio to chloropigment-a in laboratory cultures was evidently higher than in sediments. When deposited in sediments, canthaxanthin and zeaxanthin can remain stable for millennia, preserved in spite of very harsh environmental conditions (Watts and Maxwell, 1977).

As a 4-keto-myxoxanthophyll-like carotenoid was suggested as a specific marker of toxic Baltic cyanobacteria (Schlüter et al., 2004), it should be highlighted that myxol glucoside carotenoids, generally referred to as myxoxanthophylls (Roy et al., 2012), make up a whole group of compounds, some of which are even strain-specific (Schlüter et al., 2008). Analysis of these compounds in a culture extract or even an extract from monoclonal bloom in lakes is a much simpler task than their identification in coastal marine sediments. Above all, they are less stable than the other cyanobacteria marker carotenoids (zeaxanthin, canthaxanthin and echinenone) (Leavitt and Hodgson, 2001). Myxoxanthophylls were determined mainly in lake water samples in the past, often by thin-layer chromatography (TLC) (Hickman and Schweger, 1991). This implies that they might have been mistaken for other carotenoids or their derivatives. In HPLC analysis, separation of the particular glucoside derivatives requires chromatographic mobile and stationary phases different from those used for non-glycoside carotenoids. We extract these pigments from the sediments using method (Krajewska et al., 2017a), which gives a very high yield (98%), as can be judged from

Table 2 Concentration of canthaxanthin (Cantha), sum of chloropigments-*a* (ΣChlns-*a*) and estimated percentage of heterocystous cyanobacteria in the total chlorophyll-*a* production (Chl-a_{CYAN}) in the Gulf of Gdańsk (P1-P110) and Oslofjord (E), averaged over the last 30 years.

Station	Cantha [nmol/g]	∑Chlns-*a* [nmol/g]	Chl-a_{CYAN} [%]	Averaged Chl-a_{CYAN} [%]
P1 0–1 cm	12.09	794.60	4.01	4.64
P1 1–5 cm	16.03	345.70		
M1 0–1 cm	15.87	604.86	4.98	
M1 1–5 cm	14.85	266.87		
P116 0–1 cm	16.07	616.36	3.75	
P116 1–5 cm	10.96	271.48		
P110 0–1 cm	12.31	353.98	5.82	
P110 1–5 cm	16.23	253.27		
E 0–1 cm	11.80	324.71	5.75	5.75
E 1–5 cm	15.63	248.65		

tests with the myxoxanthin DHI standard. However, natural myxoxanthin-type pigments in marine samples are difficult to quantify because they have a variety of structures (analogues) and there are no standards for all of them. The HPLC retention time of this group of compounds was between 16 and 20 min (Fig. 4, Table 1); Rt of the available myxoxanthin standard (DHI) was 20.1 min.

4.2. Cyanobacteria origin

Correlation of cyanobacteria carotenoids in sediments with diatoms (Appendix 4) let us conclude on cyanobacteria origin. A positive correlation with planktic marine and brackish diatom percentage suggests that they are of marine not of freshwater origin. This is in agreement with the statements that *N. spumigena* can grow at salinities between 5 and 20 (Lehtimäki et al., 1997), and the fact that the surface salinity is around 7–8 in the Gulf of Gdańsk and <20 in the Oslofjord (Szymczak-Żyła et al., 2017) and they inflow to the Gulf of Gdańsk from the open sea, where very intensive blooms are observed (Stal et al., 2003).

The concentrations of particular carotenoids in sediments depend not only on their sources but also on their stability (Leavitt and Hodgson, 2001). However, the very high percentage of zeaxanthin in sum of the three cyanobacteria carotenoids (Fig. 2b), much higher than in algae cultures of both colonial and non-colonial species (Fig. 2b, Appendix 3), suggests that zeaxanthin in sediments originates not only from cyanobacteria. Zeaxanthin correlated well with echinenone and canthaxanthin (r = 0.90 and 0.83, respectively, $p < 0.05$), but the best correlation was with lutein (r = 0.96, $p < 0.05$), a marker of green algae (zeaxanthin also occurs in green algae including macroalgae) (Hall et al., 1997; Krajewska et al., 2017b) or may be formed as a photo-protective pigment at intensive irradiation (Chen et al., 2015). The comparatively low percentage of echinenone supports the hypothesis presented above regarding the lower stability of this carotenoid than canthaxanthin and zeaxanthin.

4.3. Estimation of heterocystous cyanobacteria share in total chlorophyll-*a* production

Based on marker cyanobacterial carotenoid (canthaxanthin) and chloropigment-*a* results the percentage of heterocystous cyanobacteria in the total chlorophyll-*a* production in the Gulf of Gdańsk (Chl-a_{CYAN}), averaged over the last 30 years, was calculated from the following formula (Table 2):

$$\mathrm{Chl}a_{\mathrm{CYAN}} = \frac{\mathrm{Car}_{0-5}/R_{\mathrm{CULT}}}{\sum \mathrm{Chlns}a_{0-5}/F_d} \times 100\%,$$

where Chl-a_{CYAN} – percentage of heterocystous cyanobacteria in the total chlorophyll-*a* production; Car_{0-5} – concentration of canthaxanthin (in nmol) in the 0-5 cm sediment layer; $\sum \mathrm{Chlns}\text{-}a_{0-5}$ – concentration of the sum of chloropigments-*a* (in nmol) in the 0–5 cm sediment layer; R_{CULT} = 0.10 – canthaxanthin/sum of chloropigments-*a* mean ratio in *N. spumigena* cultures; F_d = 0.1 – coefficient of chlorophyll-*a* preservation in sediments of the Gulf of Gdańsk.

The assumptions underlying the above are: 1) the sum of chloropigments-*a* (in nmol) is equal to the initial amount of chlorophyll-*a*, both in sediments and in laboratory cultures; 2) canthaxanthin does not decompose during organic matter sedimentation and burial in sediments; 3) 90% of the initial amount of chlorophyll-*a* produced in the Gulf of Gdańsk decomposes to colourless products and only 10% is preserved in sediments (Szymczak-Żyła and

Kowalewska, 2007); 4) 0—5 cm layer of sediments in the Deep of Gdańsk, was accumulated during the last ca 30 years, as the sediment accumulation rate for the four stations P1—P110 was about 0.16 cm/a (Szymczak-Żyła et al., 2017).

The calculated value, averaged for the four stations where laminated sediments occurred (P1—P110) was 4.6%. This means that on average 4.6% of chlorophyll-*a* production in the Gulf of Gdańsk during the last 30 years originated from heterocystous cyanobacteria. An estimate based on the same assumptions, done for station E in Oslofjord, where there were also laminated sediments and a similar accumulation rate as that in the Deep of Gdańsk (0.17 cm/year by Szymczak-Żyła et al., 2017) yielded 5.8% for heterocystous cyanobacteria. We realize, of course, that this is only a very rough estimate. However, it is of a similar order as the cyanobacteria species composition of blooms determined for estuarine and coastal sites in Europe and North America by Carstensen et al. (2015). The occurrence of diazothrophic cyanobacteria *Nodularia spumigena* in Oslofjord is quite probable, as this species was discovered at the North Sea coast (Nehring, 1993), in the Lindaspollene fjord near Bergen, western Norway, in the Kattegat (Henriksen, 2005; Lehtimäki et al., 1997) and in the Baltic entrance area (Henriksen, 2005). One can imagine, therefore, that as a result of the periodic great abundance of *Nodularia*, this species could be transferred from the Baltic by water currents via the Danish Sound and Skagerrak to Oslofjord, where the surface salinity is between 10 and 20 (they grow best at salinities from 7 to 18) (Lehtimäki et al., 1997). In Oslofjord, picocyanobacteria (*Synechococcus* sp.) were also found to be one of the most common groups (Ypma and Throndsen, 1996).

5. Conclusions

Summing up, zeaxanthin in sediments cannot be used as a universal marker of cyanobacteria in the Baltic Sea. Instead, echinenone may serve as a universal marker of cyanobacteria, though not quantitative as is less stable than zeaxanthin and canthaxanthin. Myxoxanthophylls are even less stable than these three carotenoids and are strain-specific, occur also in *Chroococcales* and other cyanobacteria, so are not good markers for sediments of cyanobacteria groups. It is canthaxanthin, a very stable compound, that is a best marker of heterocystous cyanobacteria. These filamentous cyanobacteria flow into the Gulf of Gdańsk from the open sea and their abundance has increased in the last thirty years comparing to the previous time. In the Gulf of Gdańsk, they made up to ca 4.6% of phytoplankton chlorophyll-*a* production. Similar estimate done for Oslofjord, on the same assumptions, suggests that heterocystous cyanobacteria also occurred there (ca 5.8% of total chlorophyll-*a* production in the inner Oslofjord), and were also of marine origin, but their abundance, in contrast to the Gulf of Gdańsk, has decreased during the last thirty years. Such an estimate can be applied to other coastal areas of enhanced sedimentation and laminated sediments, once the marker pigments of the major cyanobacteria species occurring there have been identified and the percentage of total chlorophyll-*a* produced in a basin, which is preserved in sediments, has been determined for such area.

Acknowledgements

This work was carried out within the framework of the Polish-Norwegian Research programme operated by the National Centre for Research and Development under the Norwegian Financial Mechanism 2009—2014, grant CLISED no 196128, M. Krajewska received a fellowship from the Leading National Research Centre (KNOW), Centre for Polar Studies 2014—2018. The authors would like to thank to Dr Anna Filipkowska and Dr Ludwik Lubecki of the Institute of Oceanology, PAN, Sopot, Poland, and Dr Tomasz Ciesielski from NTNU, Trondheim, Norway, for their help in organizing cruises and for their assistance in sample collection, Dr Gijs D. Breedveld and Amy M.P. Oen of NGI, Oslo, Norway, for their help in organizing the cruise to Oslofjord/Drammensfjord. Finally, we thank the crew of 'Oceania' for their assistance during cruises to the Gulf of Gdańsk and Oslofjord/Drammensfjord. We are grateful to Prof. Hanna Mazur-Marzec for her comments to the manuscript.

Appendix A. Supplementary data

Supplementary material related to this article can be found, in the online version, at doi: https://doi.org/10.1016/j.oceano.2018.07.002.

References

Battarbee, R.W., 1986. The eutrophication of Lough Erne inferred from changes in the diatom assemblages of 210Pb- and 137CS-dated sediment cores. Proc. R. Irish Acad. Sect. B 86 B (6), 141—168.

Belykh, O.I., Dmitrieva, O.A., Gladkikh, A.S., Sorokovikova, E.G., 2013. Identification of toxigenic cyanobacteria of the genus Microcystis in the Curonian Lagoon (Baltic Sea). Oceanology 53 (1), 71—79, http://dx.doi.org/10.1134/S0001437013010025.

Bianchi, T.S., Dibb, J.E., Findlay, S., 1993. Early diagenesis of plant pigments in Hudson River sediments. Estuar. Coast Shelf S. 36 (6), 517—527, http://dx.doi.org/10.1006/ecss.1993.1031.

Bianchi, T.S., Engelhaupt, E., Westman, P., Andrèn, T., Rolf, A., Elmgren, R., 2000. Cyanobacterial blooms in the Baltic Sea: natural or human-induced? Limnol. Oceanogr. 45 (3), 716—726, http://dx.doi.org/10.4319/lo.2000.45.3.0716.

Bianchi, T.S., Rolff, C., Widbom, B., Elmgren, R., 2002. Phytoplankton pigments in Baltic Sea seston and sediments: seasonal variability, fluxes and transformations. Estuar. Coast Shelf. S. 55 (3), 369—383, http://dx.doi.org/10.1006/ecss.2001.0911.

Bodén, P., 1991. Reproducibility in the random settling method for quantitative diatom analysis. Micropaleontology. 37 (3), 313—319, http://dx.doi.org/10.2307/1485893.

Carstensen, J., Klais, R., Cloern, J.E., 2015. Phytoplankton blooms in estuarine and coastal waters: seasonal patterns and key species. Estuar. Coast Shelf S. 162, 98—109, http://dx.doi.org/10.1016/j.ecss.2015.05.005.

Chen, Q., Nie, Y., Liu, X., Xu, L., Emslie, S.V., 2015. An 800-year ultraviolet radiation record inferred from sedimentary pigments in the Ross Sea area, East Antarctica. Boreas 44 (4), 693—705, http://dx.doi.org/10.1111/bor.12130.

Conley, D.J., Cartensen, J., Aigars, J., Axe, P., Bonsdorff, P., Eremina, T., Haahti, B.M., Humborg, C., Jonsson, P., Kotta, J., Lännegren, C., Larsson, U., Maximov, A., Rodriguez Medina, M., Łysiak-Pastuszak, E., Remeikaitè-Nikienè, N., Walve, J.,

Wilhelms, S., Zillèn, L., 2011. Hypoxia increasing in the coastal zone of the Baltic Sea. Environ. Sci. Tech. 45 (16), 6777—6783, http://dx.doi.org/10.1021/es201212r.

Cook, P.L.M., Jennings, M., Holland, D.P., Beardall, J., Briles, C., Zawadzki, A., Doan, P., Mills, K., Gell, P., 2016. Blooms of cyanobacteria in a temperate Australian lagoon system post and prior to European settlement. Biogeosciences 13 (12), 3677—3686, http://dx.doi.org/10.5194/bg-13-3677-2016.

Denys, L., 1991. A check-list of the diatoms in the Holocene deposits of the western Belgian coastal plain with a survey of their apparent ecological requirements. I. Introduction, ecological code and complete list. Profession. Paper Belgium Geol. Surv. 246, 1—41.

Desphande, B.N., Tremblay, R., Pienitz, R., Vincent, W.F., 2014. Sedimentary pigments as indicators of cyanobacterial dynamics in hypereutrophic lake. J. Paleolimnol. 52 (3), 171—184, http://dx.doi.org/10.1007/s10933-014-9785-3.

Freiberg, R., Nõmm, M., Tõnno, I., Alliksaar, T., Nõges, T., Kisand, A., 2011. Dynamics of phytoplankton pigments in water and surface sediments of a large shallow lake. Est. J. Earth Sci. 60 (2), 91—101, http://dx.doi.org/10.3176/earth.2011.2.03.

Grant, C.S., Louda, J.W., 2010. Microalgal pigment ratios in relation to light intensity: implications for chemotaxonomy. Aquat. Biol. 11, 127—138, http://dx.doi.org/10.3354/ab00298.

Hall, R.I., Leavitt, P.R., Smol, J.P., Zirnhelt, N., 1997. Comparison of diatoms, fossil pigments and historical records as measures of lake eutrophication. Freshw. Biol. 38 (2), 401—417, http://dx.doi.org/10.1046/j.1365-2427.1997.00251.x.

Hasle, G.R., Syvertsen, E.E., 1996. Marine diatoms. In: Tomas, C.R. (Ed.), Identifying marine diatoms and dinoflagellates. Academic Press, San Diego, 5—385.

HELCOM, 2009. Eutrophication in the Baltic Sea, Baltic Sea Environ. Proc. Np 115B, 45—52.

Henriksen, P., 2005. Estimating nodularin content of cyanobacterial blooms from abundance of *Nodularia spumigena* and its characteristic pigments-a case study from Baltic entrance area. Harmful Algae 4 (1), 167—178, http://dx.doi.org/10.1016/j.hal.2004.02.003.

Hickman, M., Schweger, C.E., 1991. Oscillaxanthin and myxoxanthophyll in two cores from Lake Wabamun, Alberta, Canada. J. Paleolimnol. 5 (2), 127—137, http://dx.doi.org/10.1007/BF00176874.

IMGW — Instytut Meteorologii I Gospodarki Wodnej, Miętus, M., Łysiak-Pastuszak, E., Zalewska, T., Krzymiński, W., 2013. Bałtyk Południowy w 2012 r. Charakterystyka wybranych elementów środowiska. IMGW, PIB, Warszawa, 196 pp.

Jeffrey, S.W., Mantoura, R.F.C., Wright, S.W., 1997. Phytoplankton pigments in oceanography. SCOR-UNESCO Publ., Paris, 661 pp.

Kahru, M., Elmgren, R., 2014. Multidecadal time series of satellite-detected accumulations of cyanobacteria in the Baltic Sea. Biogeosciences 11 (13), 3619—3633, http://dx.doi.org/10.5194/bg-11-3619-2014.

Karlson, K.M., Kankaanpaa, H., Huttunen, M., Meriluoto, J.A.O., 2005. First observation of microcystin LR in pelagic cyanobacterial blooms in the northern Baltic Sea. Harmful Algae 4 (1), 163—166, http://dx.doi.org/10.1016/j.hal.2004.02.002.

Kowalewska, G., Lubecki, L., Szymczak-Żyła, M., Bucholc, K., Filipkowska, A., Gogacz, R., Zamojska, A., 2014. Eutrophication monitoring system near the Sopot beach (southern Baltic). Ocean Coast. Manage. 98, 51—61, http://dx.doi.org/10.1016/j.ocecoaman.2014.06.007.

Krajewska, M., Szymczak-Żyła, M., Kowalewska, G., 2017a. Carotenoid determination in recent marine sediments — practical problems during sample preparation and HPLC analysis. Curr. Chem. Lett. 6, 91—104, http://dx.doi.org/10.5267/j.ccl.2017.4.003.

Krajewska, M., Szymczak-Żyła, M., Kowalewska, G., 2017b. Algal pigments in Hornsund (Svalbard) sediments as biomarkers of Arctic productivity and environmental conditions. Pol. Polar Res. 38 (4), 423—443, http://dx.doi.org/10.1515/popore-2017-0025.

Krammer, K., Lange-Bertalot, H., 1986. Bacillariophyceae. 1. Teil: Naviculaceae. In: Ettl, H, Gerloff, J, Heynig, H, Mollenhauer, D (Eds.), Süsswasser flora von Mitteleuropa, Band 2/1. Gustav Fischer Verlag, Stuttgart, New York, 876 pp.

Laamanen, M.J., Forsström, L., Sivonen, K., 2002. Diversity of Aphanizomenon flos-aquae (cyanobacterium) populations along a Baltic Sea salinity gradient. Appl. Environ. Microb. 68 (11), 5296—5303, http://dx.doi.org/10.1128/AEM.68.11.5296—5303.2002.

Laamanen, M.J., Gugger, M.F., Lehtimäki, J.M., Haukka, K., Sivonen, K., 2001. Diversity of toxic and nontoxic nodularia isolates (cyanobacteria) and filaments from the Baltic Sea. Appl. Environ. Microb. 67 (10), 4638—4647, http://dx.doi.org/10.1128/AEM.67.10.4638-4647.2001.

Leavitt, P.R., 1993. A review of factors that regulate carotenoid and chlorophyll deposition and fossil pigment abundance. J. Paleolimnol. 9 (2), 109—127, http://dx.doi.org/10.1007/BF00677513.

Leavitt, P.R., Hodgson, D.A., 2001. Sedimentary pigments. In: Smol, J.P., Birks, J.B., Last, W.M. (Eds.), Tracking Trends Environmental Changes Using Lake Sediments. Kluwer Academy Publisher, Dordrecht, 295—325.

Lehtimäki, J., Moisander, P., Sivonen, K., Kononen, K., 1997. Growth, nitrogen fixation, and nodularin production by two Baltic Sea cyanobacteria. Appl. Environ. Microb. 63 (5), 1647—1656.

Łotocka, M., 1998. Carotenoid pigments in Baltic Sea sediments. Oceanologia 40 (1), 27—38.

Majewski, A., 1994. Naturalne warunki środowiskowe Zatoki Gdańskiej i jej obrzeża. In: Majewski, A (Ed.), Zatoka Gdańska. IMGW Wyd., Geologiczne, Warszawa, 10—19.

Maksymowska, D., Richard, P., Piekarek-Jankowska, H., Riera, P., 2000. Chemical and isotopic composition of the organic matter sources in the Gulf of Gdansk (Southern Baltic Sea). Estuar. Coast Shelf S. 51 (5), 585—598, http://dx.doi.org/10.1006/ecss.2000.0701.

Mazur-Marzec, H., Żeglińska, L., Pliński, M., 2005. The effect of salinity on the growth, toxin production, and morphology of *Nodularia spumigena*. J. Appl. Phycol. 17 (2), 171—179, http://dx.doi.org/10.1007/s10811-005-5767-1.

Mazur-Marzec, H., Pliński, M., 2009. Do toxic cyanobacteria blooms pose a threat to the Baltic ecosystem? Oceanologia 51 (3), 293—319, http://dx.doi.org/10.5697/oc.51-3.293.

Mazur-Marzec, H., Sutryk, K., Kobos, J., Hebel, A., Hohlfeld, N., Błaszczyk, A., Toruńska, A., Kaczkowska, M.J., Łysiak-Pastuszak, E., Kraśniewski, W., Jasser, I., 2013. Occurrence of cyanobacteria and cyanotoxin in the Southern Baltic Proper. Filamentous cyanobacteria versus single-celled picocyanobacteria. Hydrobiologia 701 (1), 235—252, http://dx.doi.org/10.1007/s10750-012-1278-7.

Nehring, S., 1993. Mortality of dogs associated with a mass development of *Nodularia spumigena* (cyanophyceae) in a brackish lake at the German North Sea coast. J. Plankton. Res. 15 (7), 867—872, http://dx.doi.org/10.1093/plankt/15.7.867.

Paerl, H.W., Valdes, L.M., Pinckney, J.L., Piehler, M.F., Dyble, J., Moisander, P.H., 2003. Phytoplankton photopigments as indicators of estuarine and coastal eutrophication. Biosciences 53 (10), 953—964, http://dx.doi.org/10.1641/0006-3568(2003)053[0953:PPAIOE]2.0.CO;2.

Pastuszak, M., Witek, Z., 2012. Discharges of water and nutrients by the Vistula and Oder rivers draining Polish territory. In: Pastuszak, M., Igras, J. (Eds.), Temporal and Spatial Differences in Emission of Nitrogen and Phosphorus from Polish Territory to the Baltic Sea. National Mar Fisher Res/Fertilizer Research Institute (INSOL), Gdynia/Puławy, 311—353.

Roy, S., Llewellyn, C.A., Egeland, E.S., Johnsen, G., 2012. Phytoplankton Pigments. Cambridge Univ. Press, Cambridge, 845 pp.

Sahindokuyucu Kocasari, F., Gulle, I., Kocasari, S., Pekkaya, S., Mor, F., 2015. The occurrence and levels of cyanotoxin nodularin from *Nodularia spumigena* in the alkaline and salty Lake Burdur, Turkey. J. Limnol. 74 (3), 530—536, http://dx.doi.org/10.4081/jlimnol.2015.1097.

Schlüter, L., Møhlenberg, F., Havskum, H., Larsen, S., 2000. The use of phytoplankton pigments for identifying and quantifying phytoplankton groups in coastal areas: testing the influence of light and nutrients on pigment/chlorophyll a ratios. Mar. Ecol. Prog. Ser. 192, 49—63.

Schlüter, L., Garde, K., Kaas, H., 2004. Detection of the toxic cyanobacteria *Nodularia spumigena* by means of a 4-keto-myxoxanthophyll-like pigment in the Baltic Sea. Mar. Ecol. Prog. Ser. 275, 69—78, http://dx.doi.org/10.3354/meps275069.

Schlüter, L., Lutnæs, B.F., Liaaen-Jensen, S., Garde, K., Kaas, H., Jameson, I., Blackburn, S., 2008. Correlation of content of hepatotoxin nodularin and glycosidic carotenoids, 4-ketomyxol-2′-fucoside and novel 1′-O-methyl-4-ketomyxol-2′-fucoside, in 20 strains of the cyanobacterium *Nodularia spumigena*. Biochem. Syst. Ecol. 36 (10), 749—757, http://dx.doi.org/10.1016/j.bse.2008.08.002.

Sivonen, K., Kononen, K., Carmichael, W.W., Rinehart, K., Kivitanta, J., Niemela, S.I., 1989. Occurrence of the hepato-toxic cyanobacterium *Nodularia spumigena* in the Baltic Sea and structure of the toxin. Appl. Environ. Microb. 55 (8), 1990—1995.

Stal, L.J., Albertano, P., Bergman, B., von Bröckel, K., Gallon, J.R., Hayes, P.K., Sivonen, K., Walsby, A.E., 2003. BASIC: Baltic Sea cyanobacteria. An investigation of the structure and dynamics of water blooms of cyanobacteria in the Baltic Sea-responses to a changing environment. Cont. Shelf Res. 23 (17—19), 1695—1714, http://dx.doi.org/10.1016/j.csr.2003.06.001.

Stoń, J., Kosakowska, A., Łotocka, M., 2002. Pigment composition in relations to phytoplankton community structure and nutrient content in the Baltic Sea. Oceanologia 44 (4), 419—437.

Szymczak-Żyła, M., Kowalewska, G., 2007. Chloropigmnents-a in the Gulf of Gdańsk (Baltic Sea) as markers of the state of this environment. Mar. Pollut. Bull. 55 (10—12), 512—528, http://dx.doi.org/10.1016/j.marpolbul.2007.09.013.

Szymczak-Żyła, M., Krajewska, M., Winogradow, A., Zaborska, A., Breedveld, G.D., Kowalewska, G., 2017. Tracking trends in eutrophication based on pigments in recent coastal sediments. Oceanologia 59 (1), 1—17, http://dx.doi.org/10.1016/j.oceano.2016.08.003.

Tse, T.J., Doig, L.E., Leavitt, P.R., Quinones-Rivera, Z.J., Codling, G., Lucas, B.T., Liber, K., Giesy, J.P., Wheater, H., Jones, P.D., 2015. Long-term spatial trends in sedimentary algal pigments in a narrow river-valley reservoir, Lake Diefenbaker, Canada. J. Great Lakes Res. 41 (2), 56—66, http://dx.doi.org/10.1016/j.jglr.2015.08.002.

Watts, C.D., Maxwell, J.R., 1977. Carotenoid diagenesis in a marine sediment. Geochim. Cosmochim. Acta 41 (4), 493—497, http://dx.doi.org/10.1016/0016-7037(77)90287-3.

Wojtasiewicz, B., Stoń-Egiert, J., 2016. Bio-optical characterization of selected cyanobacteria strains present in marine and freshwater ecosystem. J. Appl. Phycol. 28 (4), 2299—2314, http://dx.doi.org/10.1007/s10811-015-0774-3.

Ypma, J.E., Throndsen, J., 1996. Seasonal dynamics of bacteria, autotrophic picoplankton and small nanoplankton in the inner Oslofjord and the Skagerrak in 1993. Sarsia 81 (1), 57—66, http://dx.doi.org/10.1080/00364827.1996.10413611.

Oceanologia (2019) 61, 89—102

Available online at www.sciencedirect.com

ScienceDirect

journal homepage: www.journals.elsevier.com/oceanologia/

ORIGINAL RESEARCH ARTICLE

Spectral structure of surface waves and its influence on sediment dynamics

Boris V. Divinsky *, **Ruben D. Kosyan**

Shirshov Institute of Oceanology RAS, Moscow, Russia

Received 9 April 2018; accepted 11 July 2018
Available online 28 August 2018

KEYWORDS
Sand bottom dynamics;
JONSWAP spectra;
Acoustic backscatter measurements;
Concentration profiles;
Frequency domain

Summary Analysis of the influence of wave energy frequency distribution on the dynamics of suspension over the sea-bottom is the main objective of this study. We revealed the differences between the response of the eroded sea-bottom to external disturbances represented by irregular surface waves with permanent integral characteristics (significant wave height and frequency of the spectrum peak) and variable frequency of the wave energy distribution.

1. Introduction

The dynamics of sea-bottom sediments plays an important role in the formation of foreshore morphological features. Many models exist for the analysis and the quantitative prognosis of sediment suspension and sediment transport by wave; these have been reviewed and compared by Davies et al. (2002). The hydrodynamic impact of waves (and currents) on the sea bottom is complex as in addition to the suspension of sediment from the bed there is also the impact on the sea-bed morphology via the formation and evolution of bed-forms. These bed-forms have the feedback on the hydrodynamics through bed friction and processes such as vortex ejection. In this paper, we use waves generated in a very large wave flume over a sandy bed to examine some of the processes and physical mechanisms important for the resuspension and transport of sand by waves.

Currents and wind-driven surface waves are very important for the sea-bottom sediment suspension and transport processes. The irregularity of waves is an important feature of wind-generated waves as irregular waves produce quite different patterns of suspension and bed-form dimensions from regular waves (Vincent and Hanes, 2002). Significant wave height and spectrum peak period are the main wave parameters. Generally, the surface wave spectrum can be described by the JONSWAP approximation, which is widely used in the engineering practice.

* Corresponding author at: Shirshov Institute of Oceanology RAS, 117997, 36 Nahimovskiy pr., Moscow, Russia. Tel.: +7 918 4567922.
E-mail address: divin@ocean.ru (B.V. Divinsky).
Peer review under the responsibility of Institute of Oceanology of the Polish Academy of Sciences.

Production and hosting by Elsevier

https://doi.org/10.1016/j.oceano.2018.07.003

The JONSWAP spectrum was developed in 1973 as a result of field observations in the North Sea (Hasselmann et al., 1973). It is presented in a general form as follows:

$$S(f) = \frac{\alpha g^2}{(2\pi)^4} f^{-5} exp \times \left(-\frac{5}{4}\left(\frac{f}{f_m}\right)^{-4}\right)^{\gamma} exp\left(-\frac{1}{2\sigma^2}\left(\frac{f}{f_m}-1\right)^2\right), \quad (1)$$

where f is the frequency, g is the acceleration of gravity, α is the Philip's constant (α = 0.0081) and f_m is the spectrum maximum frequency.

The same spectrum is presented in the parameterized form:

$$S(f) = \beta h_s^2 f_m^4 f^{-5} exp \times \left(-\frac{5}{4}\left(\frac{f}{f_m}\right)^{-4}\right)^{\gamma} exp\left(-\frac{1}{2\sigma^2}\left(\frac{f}{f_m}-1\right)^2\right), \quad (2)$$

where $\beta \approx \frac{0.0624}{0.230+0.0336\gamma-\left(\frac{0.185}{1.9+\gamma}\right)}$, γ is the peak enhancement coefficient, and σ takes one of two values

$$\sigma_l \approx 0.07\ (f \leq f_m) \text{ or } \sigma_r \approx 0.09\ (f \leq f_m). \quad (3)$$

Hence, the JONSWAP spectrum is determined by three main parameters: the significant wave height h_s, the spectrum peak frequency f_m, and the shape parameter γ. Generally, γ is taken to be equal to 3.3 in the sea-bottom sediment dynamics studies, which corresponds to the moderate wave formation conditions (Hasselmann et al., 1973). γ controls the spectrum form and characterizes to a great extent the wave energy frequency distribution. The surface wave spectra and their JONSWAP approximations, obtained by Divinsky (2003) using a Datawell Waverider buoy in the Black Sea, are shown in Fig. 1 as illustrations of JONSWAP spectra with various shape parameters.

The use of formula (2) requires the specification of three parameters, two of which are known and determined from the experimental spectrum: the significant wave height h_s and the frequency of the maximum of the spectrum f_m. Setting the third parameter (γ), we achieve the coincidence of the maxima of the spectra. In this case, the parameter that regulates the shape of the side lobes (σ in formula (2)) does not change.

In the spectra shown here (Fig. 2), the significant wave height is approximately 2.6 m, while the spectrum peak frequency is 0.15 Hz. However, although their spectral energy densities are almost equal there are considerable differences in the frequency distribution of the spectral energy. It is defined by the proportion of the wave energy concentration in the main peak of the irregular wave spectrum and is quantified by the γ parameter. Does this variation in wave irregularity significantly influence the suspension processes and the mobilization of sand from the sea-bed? An important objective of this work is to investigate the degree to which the suspension processes and sea-bottom matter redistribution are affected by irregularity of the surface waves with constant integral characteristics (the same values of significant wave height and spectrum peak frequency) and variable frequency distribution of the spectral wave energy (variable value of parameter γ).

The influence of the surface waves spectral structure on bottom sediment suspension was earlier addressed in the SISTEX99 experiments (Dohmen-Janssen et al., 2000; Vincent

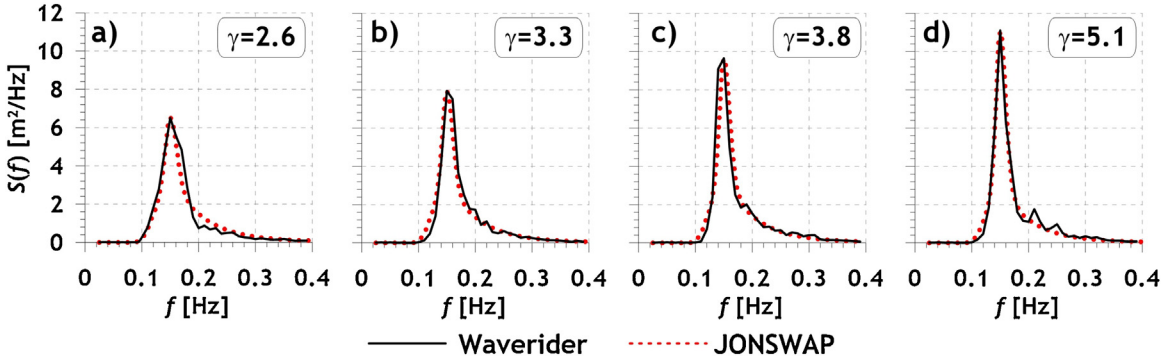

Figure 1 Wind-driven wave experimental spectra and their approximations by the JONSWAP spectrum.

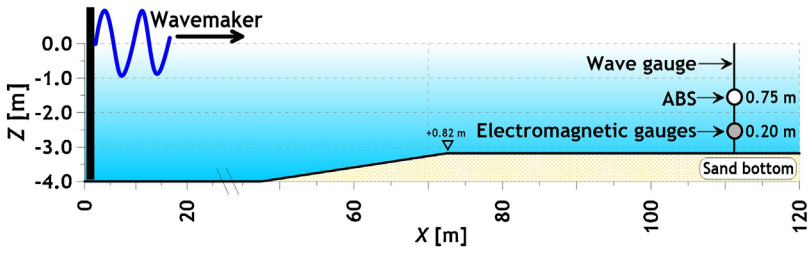

Figure 2 Scheme of the experiment.

and Hanes, 2002) using monochromatic waves, waves with a pronounced group structure, and random waves. The main conclusions of these studies concerned the dependence of the characteristics of suspension on the intensity of the waves, characterized by the height of the waves.

In our case study, we analyse a series of observations carried out at constant wave heights (and periods) under conditions of a wave spectral composition transformation which are the continuation of a previous work presented in Grüne et al. (2007) and Kos'yan et al. (2010).

In 2014, a paper was published (Divinsky et al., 2014). Both works (2014 and the present), based on the same experimental data, share a common goal, namely the study of the effect of the spectral composition of the wave on the regularities of suspension. However, these two studies set completely different objectives. The paper of 2014 focused on the dynamics of bottom-microforms (ripples). In this paper: (1) physical conditions and techniques of the experiment are described in detail (in 2014 this was not possible due to limitations on the format of the article); (2) important issues of data processing and interpretation are discussed; (3) the influence of the surface waves spectral structure on the redistribution of the bottom material is investigated; (4) the features of suspension in the frequency domain are analyzed. Thus, the present work can be considered as a further step in the study of the sand suspension regularities under the conditions of real irregular surface waves.

2. Material and methods

2.1. Experimental conditions

Experiments were conducted in 2008, led by Russian and German scientists, in the Large Wave Channel (LWC) of the Coastal Research Centre in Hannover, Germany. They included setting-up the laboratory channel and the control and production of the external hydrodynamic environment parameters to provide the specific laboratory wave conditions.

The LWC is the biggest wave channel in Europe and can be used for prototype-scale engineering and scientific experiments to study the shoreline dynamic processes. The LWC is 307 m long, 5 m wide, with 7 m high sides. Depending on the waves being produced and the depth of the sediment in the channel, this limits the maximum water depth to around 5 m. Surface waves with given statistical and spectral properties are generated by a program-controlled segmented paddle at one end of the channel. The LWC was equipped with string wave recorders located at known distances from the wave generator. At the far end of the channel, waves are absorbed by a sandy beach or a series of absorbing grids. In the course of these experiments, the bottom of the LWC was covered with a sand layer ~0.8 m thick; the median sand particle size d_{50} was 0.225 mm. Our measuring instruments were set at a distance of 111.45 m from the wave generator, at an initial still-water depth of 3.18 m (Fig. 2) close to the location of one of the LWC string wave recorders, which recorded water level at 40 Hz.

The two used instruments were: (1) an Aquascat 1000 multi-frequency profiling acoustic backscattering system (ABS) which was installed with the acoustic sensors 'looking' vertically downwards at a distance of 0.75 m from the initial sand bed and (2) a Stromungssensor Type S electromagnetic velocity meter mounted at 0.2 m from the initial bed which was used for measuring the longitudinal U and transverse V components of the water flow velocity. The ABS operating frequencies were 1, 2 and 3.84 MHz.

2.2. The processing of ABS data

The task is to determine the time-series of the profiles of suspended sediment mass concentration from the backscattered acoustic signal power from the ABS sensors (Thorne et al., 1991; Thorne and Hanes, 2002). The backscattered voltage V_{rms} measured by an ABS transducer from a mass concentration of scatterers M at a distance r from the transducer can be described by

$$V_{rms} = \frac{k_s k_t}{\psi r} M^{1/2} e^{-2r(\alpha_w + \alpha_s)}, \tag{4}$$

where

$$k_s = \frac{\langle f \rangle}{\sqrt{\langle a_s \rangle \rho_s}} \tag{5}$$

and

$$\alpha_s = \frac{3}{4r\rho_s} \int_0^r \frac{\langle \chi \rangle M}{\langle a \rangle} dr. \tag{6}$$

Here, k_t is the system calibration factor, $\langle a_s \rangle$ is the mean particle size, ρ_s is the density of sediment, α_w is the attenuation due to absorption by sound in the water column, α_s is absorption due to the presence of the sediment, ψ is a correction factor. The most important acoustic terms in Eqs. (5) and (6) are the two functions: $\langle f \rangle$, describing the scattering power of suspended particles, and $\langle \chi \rangle$ which determines the nature of the passage and attenuation of the acoustic signal in the water column in the presence of suspended solids.

Using Eq. (4) with known scattering properties of the medium it is possible to build a vertical power profile of the backscattered signal. The inverse task is to use Eq. (4) to determine the mass concentration of suspended sediment. When using a single frequency ABS to determine the concentration of suspended solids there is a need for repeated determination of the granulometric composition of suspended matter. In most wave-dominated environments, the mean size of the particles and concentration of particles in suspension have complex spatial-temporal variations. External dynamic effects (currents, wave motion, turbulence, gravity) create a spatially inhomogeneous field (gradient) of suspended particles. On this basis, the measurement results were processed by the implicit method involving data from all three working frequencies.

In the case of multiple ABS operating at different frequencies, in addition to the concentration profile of suspended sediment it is possible to estimate the profile of the mean size of the particles: the mean diameter of the particles is taken from the sediment diameter which minimizes the differences between the concentrations values of suspended solids (Thorne and Meral, 2008).

The multi-frequency acoustic signals from a suspension are converted, using Eqs. (4)–(6), into values of suspended sediment concentrations M and the mean particle size $\langle a \rangle$. Expressions for $\langle f \rangle$ and $\langle \chi \rangle$, included in Eqs. (5) and (6), have the form (Thorne and Meral, 2008):

$$\langle f(x_0)\rangle = \left(\frac{\int_0^\infty aP(a)da \cdot \int_0^\infty a^2 f(x)^2 P(a)da}{\int_0^\infty a^3 P(a)da} \right)^{1/2}, \quad (7)$$

$$\langle \chi(x_0)\rangle = \frac{\int_0^\infty aP(a)da \cdot \int_0^\infty a^2 \chi(x) P(a)da}{\int_0^\infty a^3 P(a)da}, \quad (8)$$

$$\langle a\rangle = \int_0^\infty aP(a)da,$$

where a is the radius of the sand particles, $P(a)$ is the distribution function of suspended particle sizes, $x = ka$, k is the wave number ($k = 2\pi/\lambda$, λ – length of acoustic wave), $x_0 = k\langle a\rangle$.

To determine the suspended particles concentration from Eqs. (7) and (8), which is required, the assignment functions f and χ should be accordingly defined. In the paper Thorne and Meral (2008) empirical approximations, based on the analysis of numerous data from field observations, have been proposed. For the functions f and χ they have the form:

$$f = \frac{x^2\left(1 - d_1 5e^{-((x-d_2)/d_3)^2}\right)\left(1 + d_4 e^{-((x-d_5)/d_6)^2}\right)\left(1 + d_7 e^{-((x-d_8)/d_9)^2}\right)}{d_{10} + d_{11}x^2}, \quad (9)$$

$$\chi = \frac{c_1 x^4}{c_2 + c_3 x^2 + c_4 x^4}. \quad (10)$$

The coefficients c_n and d_n, included in Eqs. (9) and (10), were determined experimentally for a real sandy bottom (Thorne and Meral, 2008). Moate and Thorne (2011) studied the acoustic scattering properties of typical marine sediments materials (quartz, rakusa, aragonite, mica, olivine, zircon, and magnetite) and for each material identified the coefficients c_n and d_n. A conclusion about significant differences in the behavior of the dispersion functions, and the necessity of taking into account the mineralogical composition of suspended matter was made.

In order to establish the distribution function of sand particle sizes, which is included in Eqs. (7) and (8), a grain size composition analysis was performed on the sediments forming the bottom of the experimental channel. Fig. 3 shows the graphs of the probability density and distribution function of particle sizes of sand. The size histogram is shown at the top of Fig. 3, and the percentage exceedance distribution is shown below; experimental data are in red. The blue curves show a lognormal distribution fitted to the data, indicating the bottom sediments conform approximately to a lognormal distribution (Kolmogorov–Smirnov test = 0.096, $p < 0.01$, Chi-square test = 93.51). In this case, the median sand

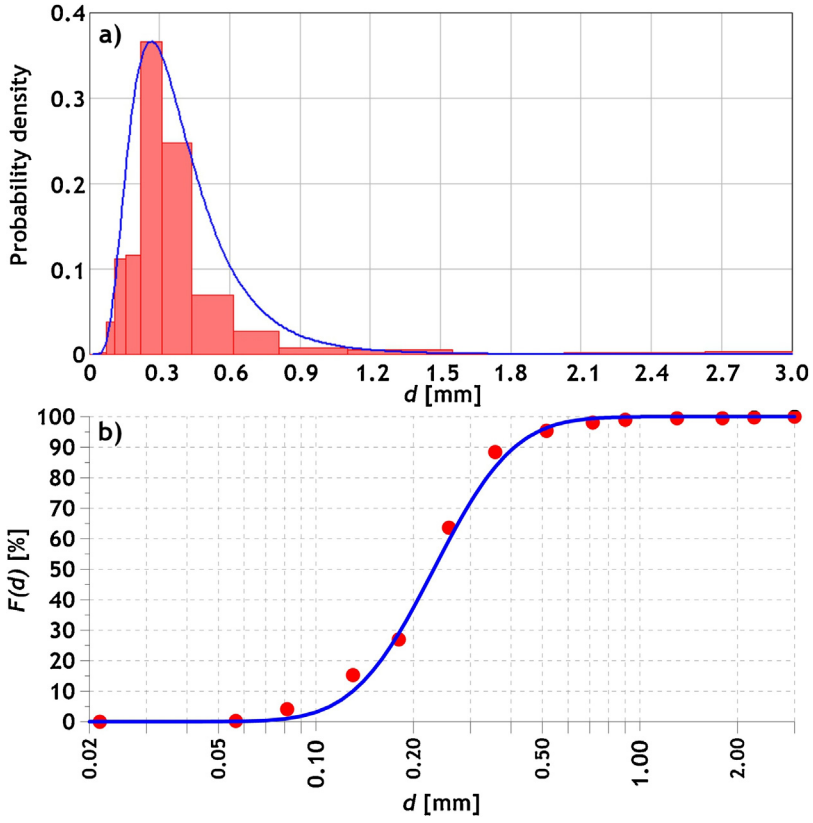

Figure 3 The probability density (a) and distribution function (b) of sand particle sizes. The blue line is an approximation to the lognormal distribution law.

Table 1 Characteristics of acoustic emitters.

Frequency, MHz	1.00	2.00	3.84
The radius of the emitter [mm]	9.00	4.80	4.85
The system calibration factor k_t	0.02259	0.00915	0.00880

particle size d_{50} is equal to 0.225 mm, with a σ_d geometric standard deviation, defined as $(d_{84}/d_{16})^{0.5}$, of 0.338 mm.

The lognormal distribution function $F(d)$ is a function in the form of:

$$F(d) = 0.5\left[1 + erf\left(\frac{\log(d/d_{50})}{\sqrt{2}\log\sigma_d}\right)\right], \quad (11)$$

where *erf* is the error function.

In summary, the processing of the acoustic signals, scattered by suspended sand particles, is as follows:

1. The bottom is a layer of quartz river sand with a median particle size d_{50} equal to 0.225 mm and a standard deviation of 0.338. The distribution of particle size corresponds to the lognormal one with the distribution function in the form of Eq. (11).
2. The characteristics of the acoustic transmitters are given in Table 1.
3. The function $\langle f \rangle$, describing the scattering power of suspended particles, and $\langle \chi \rangle$, responsible for the nature of the passage and attenuation of the acoustic signal in the water column in the presence of suspended particles, are approximated by using expressions (9) and (10), respectively.

2.3. Experimental data

Sequences of the free surface waves, described by a JONSWAP spectrum, were generated in the LWC, with characteristics described below, and random phases. The investigated experimental conditions correspond to the following set of spectral parameters of the initial wave field:

- significant wave height h_s = 0.8, 1.0, 1.2 m;
- spectrum peak frequency f_m = 0.2 Hz;
- peak enhancement parameter γ = 1.0, 1.5, 2.0, 2.5, 3.0, 3.3, 4.0, 6.0, 8.0, 9.9,

making a total of 30 wave sequences of irregular surface waves (each series duration was about 33 min). Suspended sediments concentrations were measured using the ABS for each sequence.

The ABS data processing resulted in the generation of time series data of suspended sand concentrations and mean grain diameters in the water column, as well as in the detection of the local sand bed surface location based on the sharp intensification of the sonar echoes records. Examples of the processed ABS data are given in Figs. 4–6. The time interval between profiles is 0.25 s, and the vertical spatial resolution is 1 cm. The figures show the mean diameter of the sand grains, the concentrations of the suspended sediments, and the free surface elevations. The periods of suspension and redistribution of the sand from the bed are clearly seen, both at the scale of single waves and for wave packets (groups).

Before proceeding to the discussion of the results, we wish to emphasize the following important points.

First, although the reconstruction of the suspended sediment concentration profiles and the mean sand grains diameters from the analysis of the acoustic power of the multifrequency ABS echo signals is not a trivial task, the main objective of this paper is to estimate the influence of the peak enhancement factor of the surface wave spectral structure on the sea-bottom sediments dynamics. We assume that the errors of measuring and interpretation of the acoustic signals in all observation series are the same.

Second, the shape of the JONSWAP wind-driven wave spectra approximation is determined by the γ and σ parameters in Eqs. (1) and (2). Parameter σ specifies the shape JONSWAP spectrum on either side of the spectral peak (σ_l defines the shape of the low-frequency part of the spectrum while σ_r defines the high-frequency part). The values of σ, in Eq. (3) as shown in Hasselmann et al. (1973), are estimated when the peak γ parameter value is equal to 3.3. The work represents a sufficient approximation for the other values of γ obtained when the σ-parameter is equal to the other values. In this case, Hasselmann's values for σ, σ_l = 0.07 and σ_r = 0.09, were used for all γ values. The forms of the

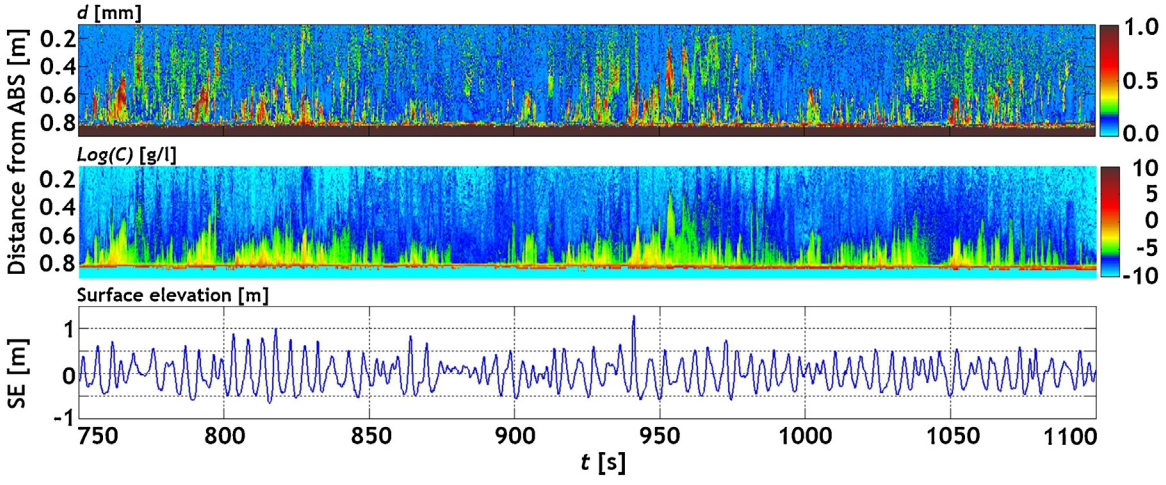

Figure 4 From top to bottom: distribution of the mean diameters of sand particles, concentrations of suspended sediments, and free surface elevation in the experiments with the following parameters: h_s = 1.2 m, f_m = 0.2 Hz, γ = 2.5.

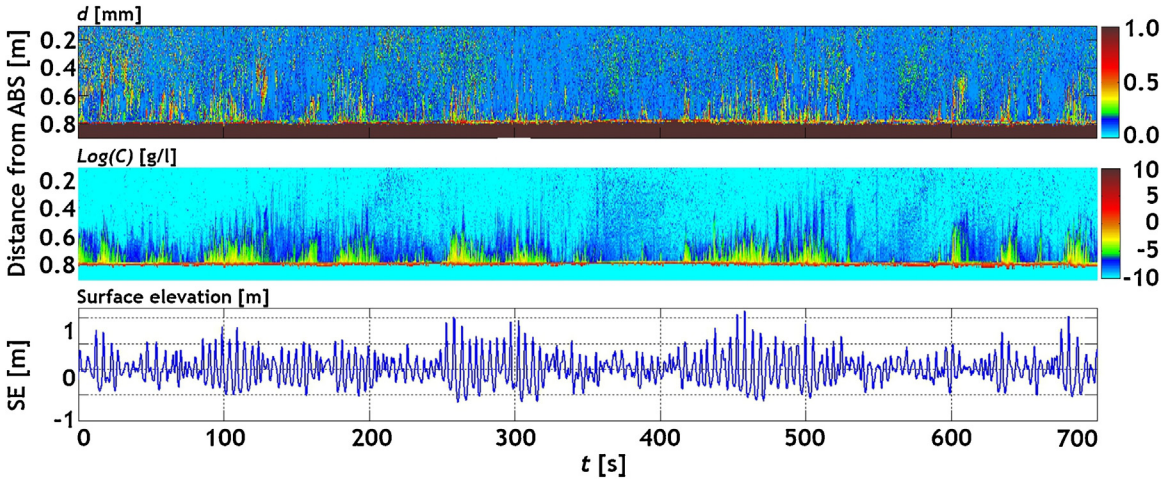

Figure 5 From top to bottom: distribution of the mean diameters of sand particles, concentrations of suspended sediments, and free surface elevation in the experiments with the following parameters: h_s = 1.0 m, f_m = 0.2 Hz, γ = 6.0.

JONSWAP spectra represented in Fig. 1, were obtained using these values. The same constants (σ_l and σ_r) were specified in the experimental generation of the free surface elevation series by the wave generator. We believe that this assumption of constant σ does not have a strong influence on the final results.

Third, the JONSWAP parameterisation is available only for a spectrum with a dominant single-peak. Transformations in the wave spectrum can be a result of bottom friction, wave breaking, or non-linear wave interactions. We estimated the variation in the γ parameter of our surface waves along the LWC from the generation region to the observation point. An example of the parameter γ transformation for the case of h_s = 1.2 m, f_m = 0.2 Hz is shown in Fig. 7.

The data used in our estimates were obtained using string wave recorders located along the LWC generator. The γ parameters were determined at the points located at the distances of 50, 79, 102, and 111 m from the wave generator. Fig. 7 shows how γ changes along the channel; the initial γ is defined as the value at the wave generator, indicated by the $\gamma_{\text{Wavemaker}}$ values on the left of Fig. 7. Table 2 shows the measured γ.

The results show a strong transformation of the surface wave spectra, associated with the wave profile transformation and partial dissipation of the wave energy, which takes place as the significant wave height increases.

The wave energy transfer is observed from the region of the main maximum together with the flattening of the spectrum, which is associated with a decrease in the γ parameter. The spectral densities of surface waves at the location of the ABS (111.45 m from the wave generator) generally differ from the initial spectral densities. Analysis of waves at the location of ABS shows that for all series of observations the frequency of the maximum of the spectrum is unchanged (0.2 Hz) while the significant wave heights varied within the range of 5–6% (Table 3).

The data in Tables 2 and 3 show that surface waves in the LWC propagate practically without loss of energy and the rearrangement of the wave field is related to the interaction between the spectral components, which makes it possible to

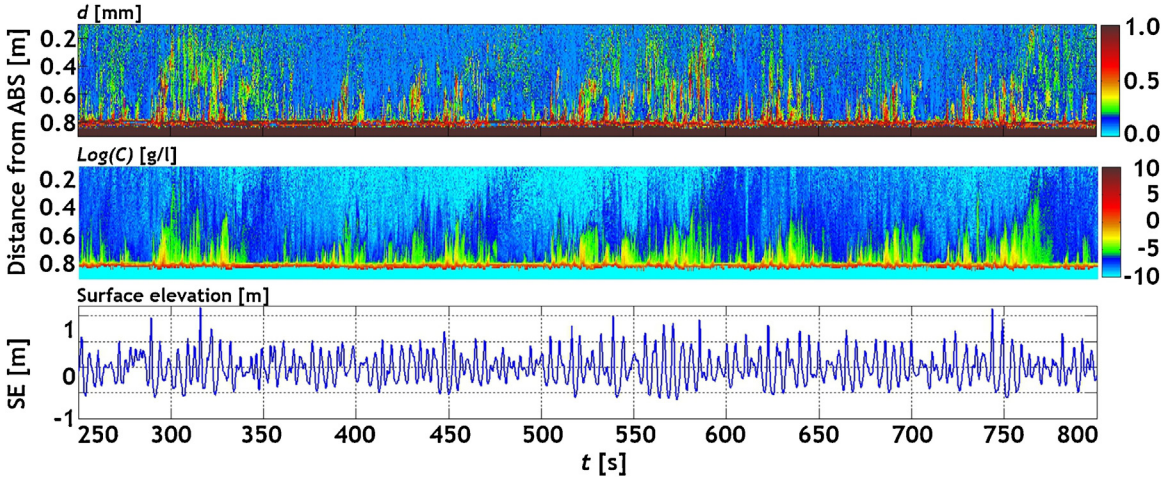

Figure 6 From top to bottom: distribution of the mean diameters of sand particles, concentrations of suspended sediments, and free surface elevation in the experiments with the following parameters: h_s = 1.2 m, f_m = 0.2 Hz, γ = 4.0.

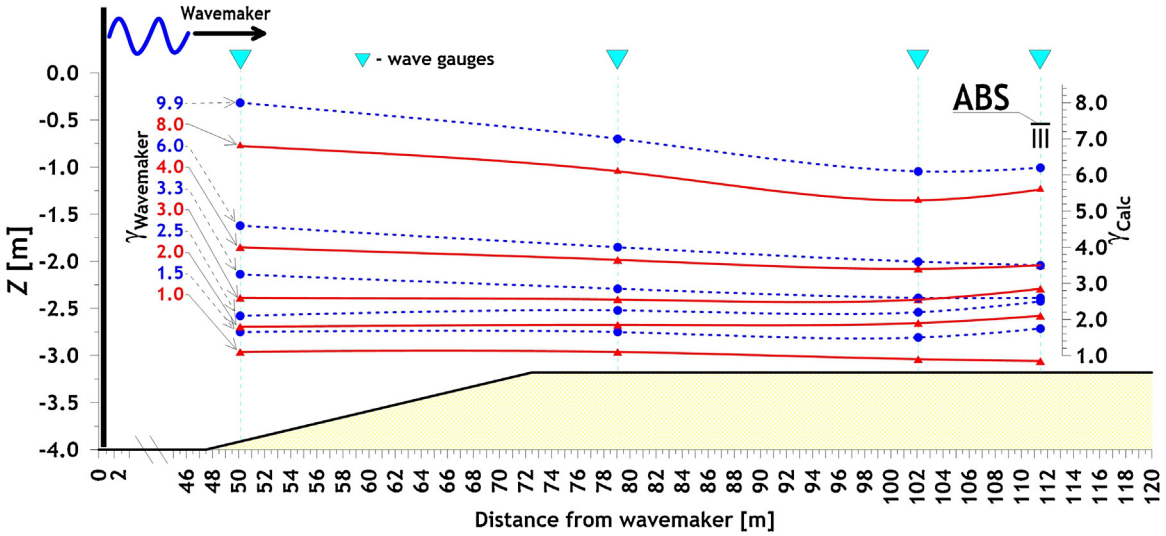

Figure 7 Variation in the γ parameter related to the propagation of waves in the experimental channel (h_s = 1.2 m).

analyze the influence of the features of spectral structure of the surface wave on the regularities of suspension of bottom material.

Furthermore, a few important remarks should be made. The effect of irregular surface waves on sediment is the formation of a characteristic profile of the bottom. The profile structure is defined by the balance between the hydrodynamic forces acting in the flow and the characteristics of the bottom material. In our laboratory experiment, the amount of material constituting the bottom remains constant, although the sand may be redistributed along the channel profile.

A mathematical model was developed to simulate and thus clarify the mechanisms controlling the redistribution of bottom material in the wave channel by irregular waves. It is phase-resolving, based on the numerical solution of the Boussinesq equations, and describes the behavior of individual waves as they propagate along the channel. The geometry of the computational channel fully corresponds to the Hannover Large Wave Channel: with length 300 m, width 5 m, smooth vertical walls, a horizontal layer of sand with a thickness of 0.82 m with an up-wave slope of 1:25, and water depth of 4 m. The surface waves in the model corresponded to those measured over a 20-min time period close to the wave-generator and had the following integral parameters of the JONSWAP spectrum: significant wave height h_s = 1.0 m, peak frequency of the spectrum of f_m = 0.2 Hz, γ = 3.3.

The simulation result is shown in Fig. 8. The software wave maker, generating a number of elevations of the free surface, was located at the position of10 m in the *x*-axis. The figure shows:

(a) the instantaneous elevation of the free surface;
(b) the component of the wave energy in the direction of wave propagation *P*;
(c) the transverse component of wave energy *Q*;
(d) the underwater profile of the channel, including areas of hard bottom and sand layer.

As can be seen from Fig. 8, the horizontal heterogeneity of the irregular wave flow lies in the fact that the wave action vector randomly deviates from the longitudinal axis of the channel. The proportion of wave energy transmitted in the transverse direction can reach 15—20% of the total wave energy. Such horizontal heterogeneity is caused by the interaction of waves with the bottom and with the channel walls. Ultimately, the process of formation of zones of erosion or accumulation of bottom material becomes essentially random. In addition, during the generation of irregular surface wave, the initial phase is set at random. The randomness of the initial phase of the waves determines the randomness of the sequence of elevations of the free surface and, as a result, the coincidence effect.

Table 2 Initial $\gamma_{Wavemaker}$ and calculated γ_{Calc} values of the JONSWAP enhancement factor.

h_s [m]	$\gamma_{Wavemaker}$									
	1.0	1.5	2.0	2.5	3.0	3.3	4.0	6.0	8.0	9.9
	γ_{Calc}									
0.8	1.02	1.34	1.71	2.37		3.04	3.41	5.15	6.68	7.57
1.0	1.13	1.85	2.12	2.55	2.89	2.67	3.91	3.95	6.51	7.61
1.2	0.85	1.75	2.11	2.51	2.85	2.60	3.47	3.51	5.60	6.20

Table 3 Significant wave heights at the observation point.

h_s [m]	$\gamma_{Wavemaker}$									
	1.0	1.5	2.0	2.5	3.0	3.3	4.0	6.0	8.0	9.9
	h_s in point of measurements [m] (111.45 m from wave generator)									
0.8	0.80	0.78	0.80	0.80	0.81	0.79	0.76	0.82	0.82	0.82
1.0	0.98	1.01	0.99	1.02	1.01	0.99	1.04	1.02	1.06	1.06
1.2	1.18	1.18	1.15	1.17	1.17	1.17	1.21	1.20	1.23	1.25

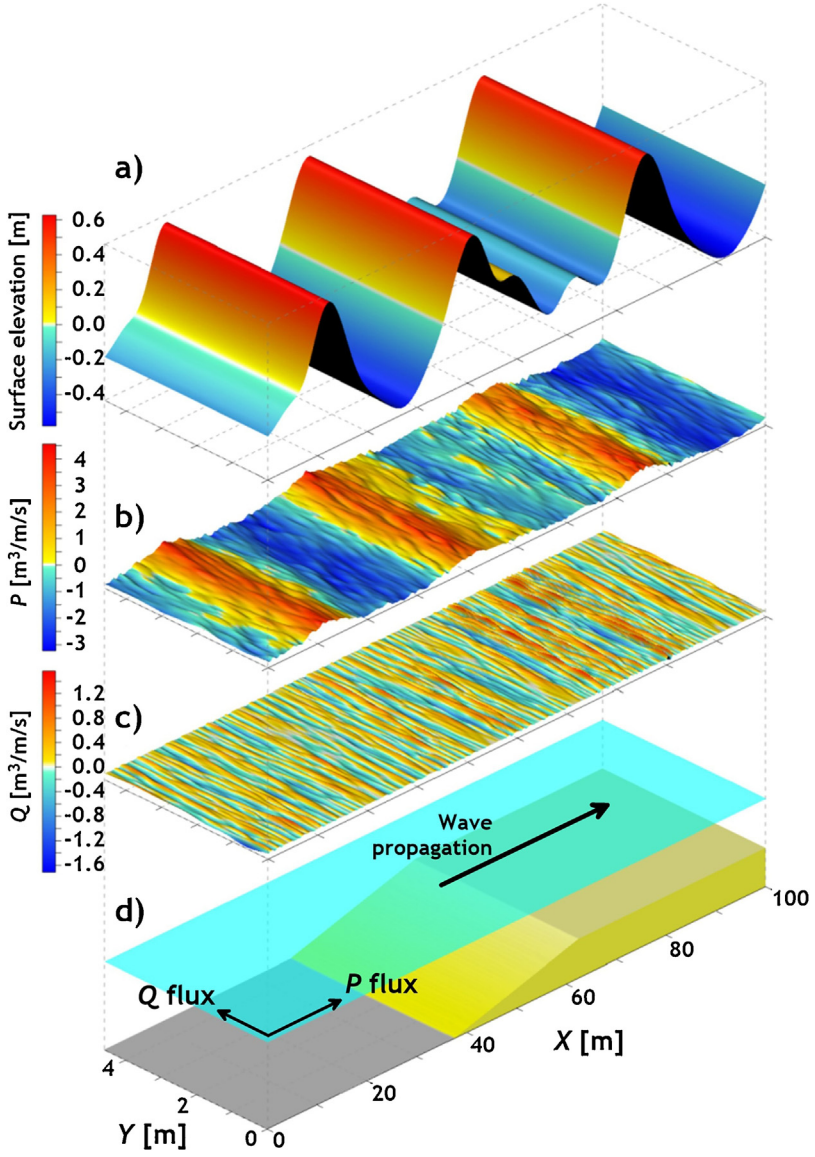

Figure 8 One-dimensional irregular waves propagation in a wave channel: (a) the elevation of the free surface, m; (b) *P*-component of the horizontal wave energy flux, $m^3/s/m$; (c) *Q*-component of horizontal wave energy flux, $m^3/s/m$; (d) the schematic presentation of the bottom profile.

3. Discussion

3.1. Sea-bed dynamics

Acoustic transducers make possible detecting the location of the hard sea bottom, which is determined as the point on the vertical profile with sharp echo signal intensification. On the profiles, this is clearly for the pair of adjacent points at which measurements have been performed and within a short distance of the spatial discreteness of the measurements (1 cm): the sediment concentrations at the point lying below are 10–20 times higher than the concentrations in the neighboring point located 1 cm above. The vertical coordinate for the point with a high concentration is taken as the position of the solid bottom.

The transformation of the sea bottom during the experiment is shown in Fig. 9. Note that Fig. 9 illustrates also the stages of the whole experiment; for this reason, the enhancement factor is indicated in the form of the initial value $\gamma_{Wavemaker}$.

The data used to plot Fig. 9 were smoothed by a low-frequency filter to demonstrate the general trend in the depth variation under the acoustic transducers. According to the conditions of the experiment, the 30-min consecutive observation series correspond to the specified initial spectral parameters of the surface wave ($\gamma_{Wavemaker}$ = 1, h_s = 0.8 m), ($\gamma_{Wavemaker}$ = 1, h_s = 1.0 m), ($\gamma_{Wavemaker}$ = 1, h_s = 1.2 m), ($\gamma_{Wavemaker}$ = 1.5, h_s = 0.8 m), ($\gamma_{Wavemaker}$ = 1.5, h_s = 1.0 m), ..., ($\gamma_{Wavemaker}$ = 9.9, h_s = 1.2 m). Usually, sea-bottom fluctuations were smaller than 2–3 cm during the period of each series. Nevertheless, an increase in the deformation of one sign (erosion or accumulation) indicates that significant potential sea-bed displacements are possible.

Fig. 9 is based on the data obtained from a 3.84 MHz transducer. The existing operational frequencies of the device

(1, 2 and 3.84 MHz) interact differently with suspended and organic matters, bubbles, or sea-bottom sediment layers. The conditions of each experiment are unique so that optimal results on the concentration profiles can be obtained from the comparison of the data received using individual frequencies or averaging different frequencies, for example, 2 and 3.84 MHz. All three frequencies are used to obtain the profile of the particle mean sizes, because, in this case, the minimum dispersion of the scattered signal is important.

The irregularity of accumulation processes together with sea-bottom matter erosion are the consequences of the surface wave influence on the eroded seabed. For example,

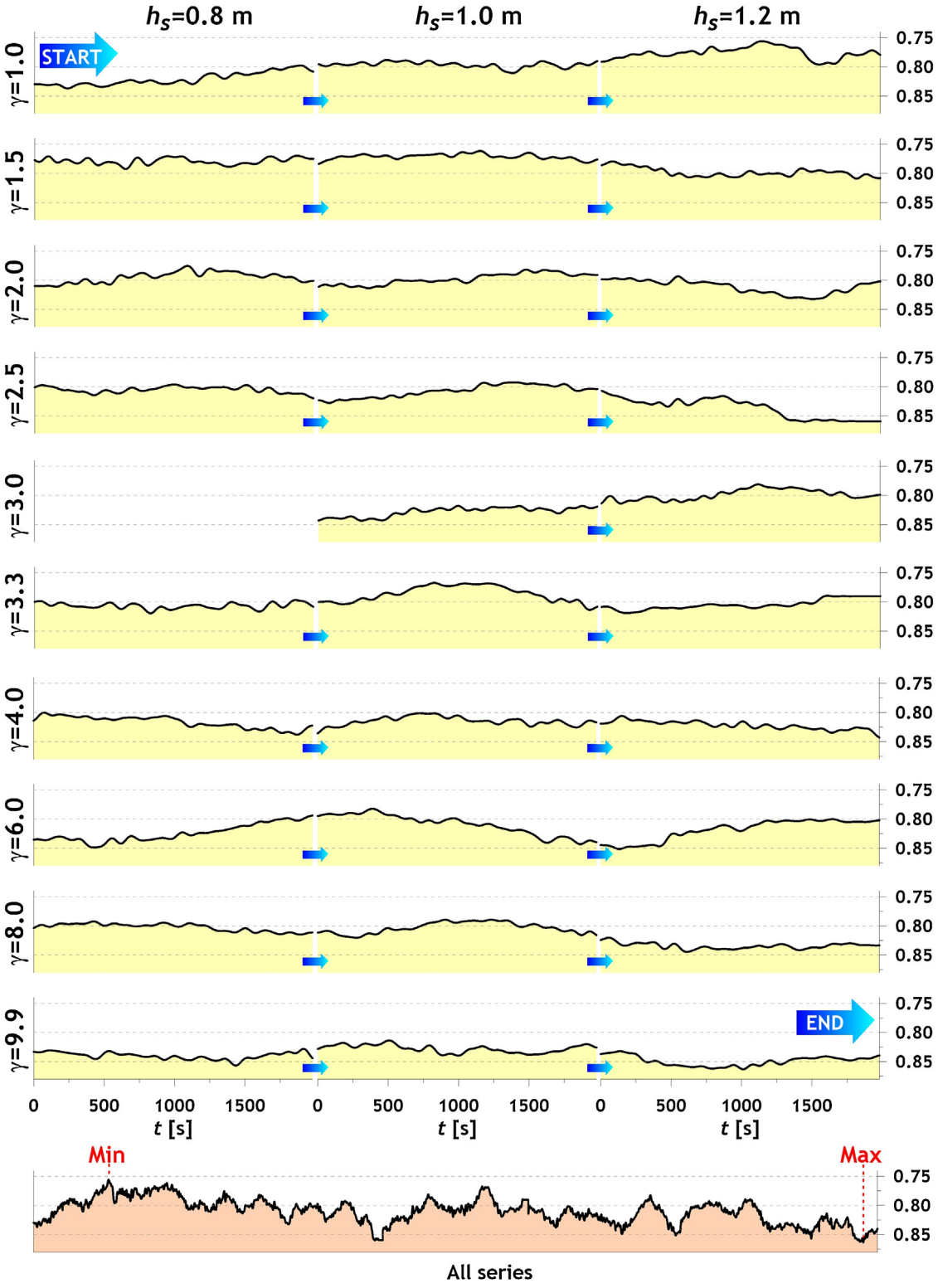

Figure 9 Location of the sand-bottom based on the results of individual sequential observation series.

according to Fig. 9, the experimental set with parameters [h_s = 0.8 m, $\gamma_{Wavemaker}$ = 6.0] is characterized by substantially permanent sand accumulation at the point of observation; erosion consistently dominates in the conditions of parameters [h_s = 1.0 m, $\gamma_{Wavemaker}$ = 6.0]; while permanent alteration of the sea-bottom deformation mark takes place in the case of the set of parameters [h_s = 1.0 m, $\gamma_{Wavemaker}$ = 4.0]. At the same time, statistical data processing allowed us to reveal regularities in the sea-bottom configuration variations.

The statistical values of the estimates of the sea bottom location depend on the parameters of the initial wave field (mean, 25% and 75% quintiles, minimum, and maximum) shown in Fig. 10.

It should be highlighted that the results shown in Fig. 10 were obtained not for single measurements of the position of the solid bottom, but they are the statistical processing of thirty experimental series of observations. The duration of each series is 1980s (~33 min), the discreteness is 0.25 s. Even though that at any given moment under the ABS sensors there can be one or another feature of the microrelief, the averaging of the observational data makes it possible to estimate the average character of the surface waves effect on the eroded bottom. In addition, taking into account the surface waves transformation along the path from the point of the wave generation, the results are given in dependence on the parameters calculated at the ABS setting point enhancement factors.

As it follows from Fig. 10, the statistical characteristics of the solid bottom position for each series of experiments undergo considerable fluctuations. This is indicated by the interquartile range and the position of the minima and maxima. Nevertheless, the mean values have an obvious tendency indicating an increase in the local depth with the increase in the enhancement factor.

Thus, there is a reason to believe that this conclusion is based on (the gain of washout) location-specific observations. Instead of the conclusion about the strengthening of the local erosion of the values of the parameter γ, it would be probably correct to point out to a noticeable trend of an increasing impact on a sandy bottom with the parameter γ growth. The summary conclusion would be: the obtained result (shown in Fig. 8) clearly indicates a possible influence of the shape of the spectrum of the irregular surface waves on the dynamics of sediments.

3.2. Vertical profiles of the suspended particle concentrations and mean sizes

We estimated how important were the differences in the vertical distributions of the suspended particles when a surface wave propagated over an eroded sea bottom. The profiles of the suspended particle concentrations and the profiles of the mean sand sizes for the observation sets at h_s = 1.2 m, f_m = 0.2 Hz, and the variable γ parameter are shown in Fig. 11.

Actually, the near-bottom averaging is not informative because the transformation of the sea-bottom profile is very strong (Fig. 9). Correspondingly, the region in Fig. 11 with light brown colour generally shows the sea-bottom. It is seen from Fig. 11 that the vertically suspended particle field becomes more homogeneous as the γ parameter increases. The decrease in the mean particle diameters vertically is related to the low γ value. The grain-size composition does not change strongly above the sea bottom when the peak parameter increases. Large values of the mean diameter in the erosion layer may appear owing to the influence of the physical factors (erosion of light fraction) as well as due to the uncertainties in the interpretation of the reflections of the acoustic signal.

Microforms of the bottom topography may be shaped depending on the condition of the sea bottom and the dynamic characteristics of the water flow. These microforms in their turn affect the suspension processes and the vertical redistribution of the sea-bed material. The size of the vortices becomes larger as the linear size of the ripples increases. This facilitates sand transport in the vertical direction. The geometric size of ripples strongly influences the general process of suspension. Further, we investigate whether the γ parameter increase affects the ripple characteristics.

3.3. Regularities of the bottom sediments suspension in the frequency domain

As a result of the experiment, synchronous time series of suspended sediment concentrations and water flow velocity were obtained, which makes it possible to evaluate their interrelations in the frequency domain. The bottom series of concentrations have been selected corresponding to a level of 0.03 m from the current bottom. The speed sensor, recall, has been located at a distance of 0.20 m from the bottom.

It is worth emphasizing that an important condition for the purity of the experiment is, of course, the idle run of the wave with the specified characteristics, at which the bottom surface is adjusted to new hydrodynamic conditions. After that, the recording of the parameters of interest begins. Preliminary estimates showed that in this particular case, the truncation of the existing 33-min records (for example, 20 min for overclocking, 13 min for analysis) did not signifi-

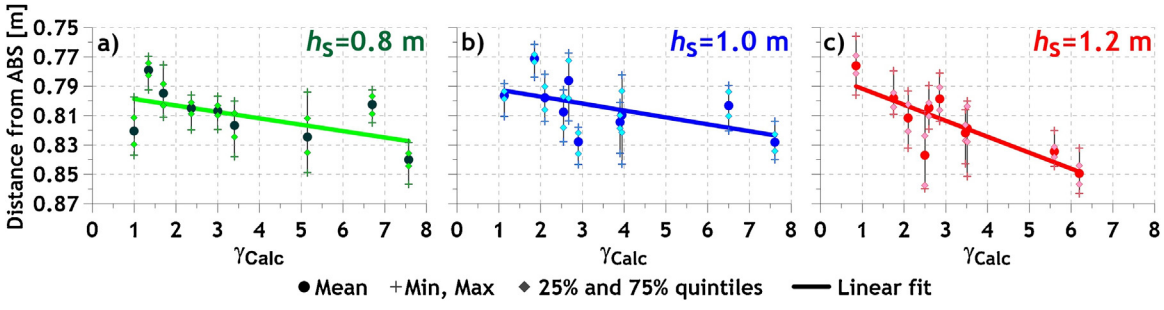

Figure 10 Statistical characteristics of the sand bottom location in the different observation series.

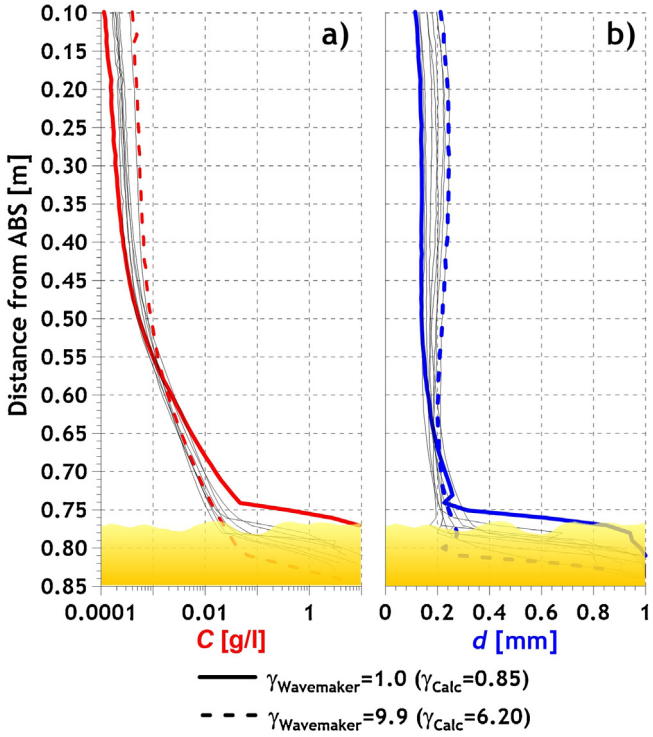

Figure 11 Vertical profiles of concentration (a) and mean diameter of suspended particles (b).

cantly affect the final results, so we used the full-length records (1980s) in further estimates.

To identify the features associated with the time structure of the velocity and concentration series, we applied the well-known Welch method. All further calculations using the periodogram method of Welch spectral analysis were carried out in the Matlab environment.

We should point out two characteristic features of the Welch method:

- use of the weighting function. It largely prevents the spreading of the spectrum and reduces the bias of the obtained assessment of the spectral components at the cost of a slight deterioration in the resolving power;
- splitting the signal into overlapping fragments. It allows increasing the total number of segments and thus reduces the variance of the estimate.

To study the frequency structure of the relationship between the velocity and concentration oscillations, we used the function of the mutual spectral density, namely the cospectrum, i.e. the real part of the cross-periodogram $Co(f)$. Cospectrum is a measure of the correlation of the same phase frequency components of two time series and is, therefore, a measure of the mutual energy of synchronous oscillations.

An example of processing of the velocity and concentration rows for the experimental series with initial parameters (h_s = 1.2 m, f_m = 0.2 Hz, γ = 8.0) is given in Fig. 12.

The distribution of the spectral density of fluctuations of the normal to shore component of the near-bottom water velocity S_U is characterized by the presence of two peaks: the main peak at 0.2 Hz and the low frequency peak (0.031 Hz) associated with the group structure of waves (Fig. 12a). Three local maxima clearly appear in the S_{SSC} concentration spectrum (Fig. 12b): at the fundamental frequency of the peak of the wave spectrum (0.2 Hz), its doubled frequency (0.4 Hz), since the sediment suspension occurs twice during the wave period, and also the low-frequency (0.031 Hz). The maximum energy of synchronous fluctuations in water velocity and concentration is collected at two frequencies: 0.2 Hz and 0.031 Hz (Fig. 12c).

The sign of the cospectrum indicates the direction of transfer of the bottom material. In our case, in almost the whole range of variability, sand moves from the shore.

For further analysis (and comparison) of the suspension features under different initial conditions, we defined some parameters characterizing the energy properties of the processes:

- Energies of low E_U(low), E_{SSC}(low) and high-frequency E_U(high), E_{SSC}(high) oscillations of water velocity and concentrations (Fig. 12a, b). The division of the spectrum into low- and high-frequency components is made from the velocity spectrum. In the example shown in Fig. 12 the separating frequency is 0.1 Hz. The energy of high-frequency E_{SSC} (high) concentration fluctuations includes the entire range from the separation frequency, since the spectral peak at the doubled frequency of the maximum is not clearly visible for all series of observations;
- the magnitudes of the cospectra (Fig. 12c) are corresponding to two frequencies: the main peak of the speed Co (f_{high}) and the low-frequency maximum $Co(f_{low})$.

The results of processing of all series of observations are shown in Fig. 13 and include the dependencies on the enhancement factor of:

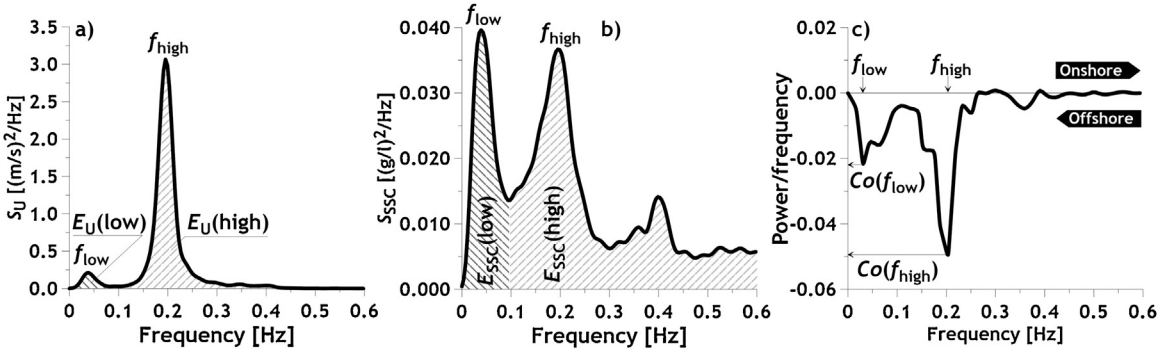

Figure 12 Autospectra *U*-velocity components (a) and suspended sediment concentrations (b), with their cospectrum (c). Initial waves parameters: h_s = 1.2 m, f_m = 0.2 Hz, γ = 8.0.

- ratios of energies of low and high-frequency oscillations of water velocity (Fig. 13a);
- ratios of energies of low and high-frequency oscillations of near bottom suspended sediment concentrations (Fig. 13b);
- ratios of absolute cospectra values at low and high frequencies (Fig. 13c);
- values of cospectra at high frequencies (Fig. 13d).

Note that the enhancement factor in Fig. 13 is not the initial but the really observed one, calculated in the measuring point.

As it follows from Fig. 13a, with the parameter γ increases, the ratio E_U(low)/E_U(high) diminishes, the more intense the greater the significant wave height is. In case of a narrow spectrum (large values of γ), the energy of the low-frequency oscillations of the E_U(low) velocity is 5–6% of the energy of the high-frequency components of the E_U(high), with the ratio practically independent of the values of h_s of the passing wave. In general, with increasing γ, the main energy of the flow velocity oscillations is concentrated in the high frequency range.

The pattern of suspension of the bottom material is influenced by a variety of hydro- and lithodynamic factors. For this reason, the dependence of the relation E_{SSC}(low)/E_{SSC}(high) on the enhancement factor cannot be unambiguous. With a relatively weak wave (h_s = 0.8 m), the E_{SSC}(low)/E_{SSC}(high) ratio is fairly stable irrespective of the enhancement factor (Fig. 13b). With an increase in both the enhancement factor and the significant wave heights, the contribution of the low-frequency oscillations associated with the group structure of the waves decreases, and for $\gamma > 5$ the energy of the low-frequency oscillations is 30–50% of the oscillation energy of the high-frequency range. We also

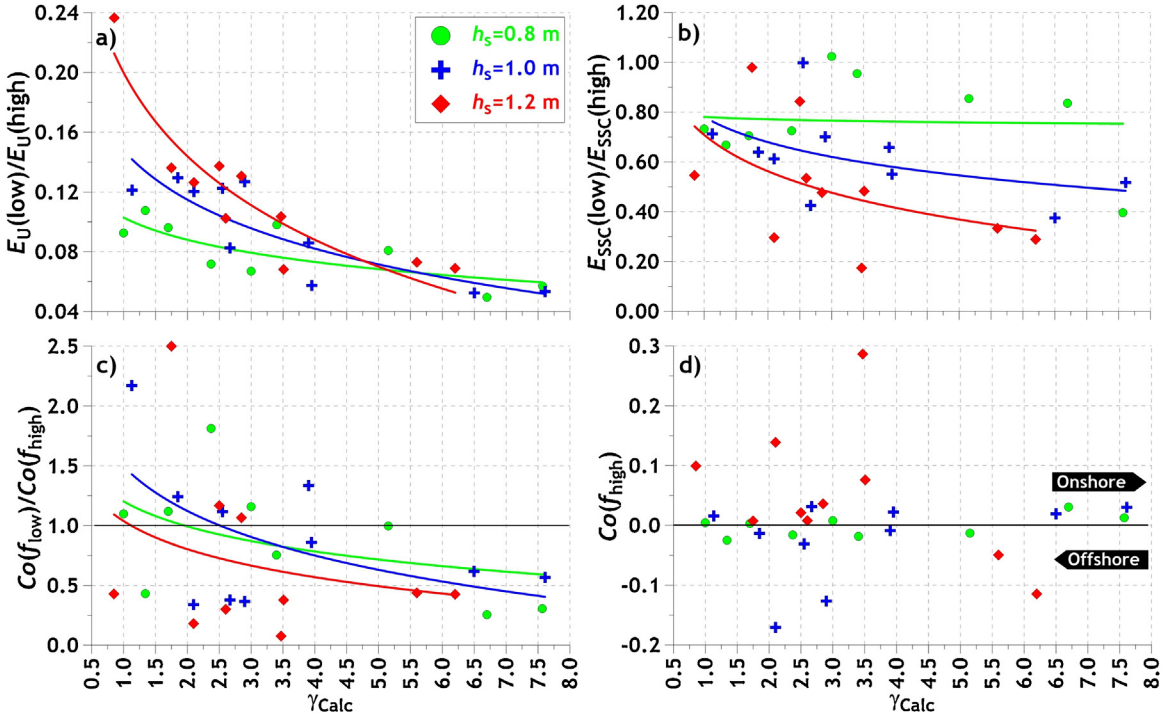

Figure 13 Interrelation of spectral characteristics of synchronous velocity and concentration series with enhancement factors of the surface wave spectrum.

note that regardless of the magnitude of the significant wave heights, for $\gamma < 3.5$ the oscillation energy of concentration fluctuations at low and high frequencies can be comparable ($E_{SSC}(\text{low})/E_{SSC}(\text{high}) \sim 1$).

For $\gamma < 5$, the maximum mutual energy of the synchronous oscillations of the velocity and concentration series can be manifested at both low and high frequencies (Fig. 13c). This is evidenced by the ratio $Co(f_{low})/Co(f_{high})$, which can be either larger or smaller than 1. The dominance of synchronous oscillations in the region of the main maximum of the spectrum is noticeable for $\gamma > 5$, with $Co(f_{low})/Co(f_{high}) \sim 0.5$.

As already noted, the sign of the cospectrum of the flow velocity and concentrations of suspended sediment series determines the direction of transport of the bottom material. For all series of observations, low-frequency oscillations associated with the group structure of waves have a negative sign of the cospectra and thus contribute to the movement of sand from the shore. For oscillations related to the region of the main maximum of the spectrum, no one-to-one dependencies of the sign of the cospectrum on the enhancement factor were observed (Fig. 13d). Obviously, this may be due to the peculiarities of the formation of the bottom surface local microrelief in each particular case.

Thus, for equal integral wave parameters (wave height and period), the features of the spectral structure of surface waves determine the dominance of certain physical scales (of single waves or groups) in suspension processes. As the enhancement factor increases, the vibration energy of the concentration fluctuations at low frequencies decreases, and the energy of the suspension is thus concentrated in the region of the main maximum of the wave spectrum.

4. Conclusions

To analyze the influence of wave energy frequency distribution on the dynamics of the sea-bottom material suspension was the main objective of our research. We found differences in the responses of the eroded sea-bottom to external disturbances presented by irregular surface waves with constant integral characteristics (significant wave height and peak wave period) and variable frequency distribution of the wave energy.

It is worth mentioning that the conducted experiment can hardly be called perfect. Ideally, each series of experiments should be implemented under the same conditions: an even initial bottom and equal depths. In reality, these conditions are practically not feasible. The preliminary blank run of surface waves for, let us say, half an hour, could correct the situation to some extent, but this would require additional resources which was beyond our project.

We posted a simple question: "Does the spectral composition of the wave (with constant wave energy) influence the regularities of suspension?" As follows from the results of the experiment, the answer is rather positive.

We conclude that if the integral characteristics of irregular surface waves are the same (h_s, f_m = const) the wave forcing applied to the sand bottom is determined precisely by the frequency distribution of the wave energy. Wave energy concentration within the spectrum maximum frequency band facilitates the transition from irregular to regular waves, and generally to the regular dynamic forcing applied to the sand bottom. Physically, this leads to the realization of more stable external conditions for the development of the microforms of the sea-bottom topography.

The results presented here are not final but they show that further studies should be related to the analysis of the influence of frequency distribution of surface wave energy on the dynamics of sea-bottom material.

Acknowledgments

This work was initialized by the Russian Science Foundation, project no. 14-17-00547. The processing of experimental data, used for this paper, was supported by the Russian Foundation for Basic Research, project no. 18-05-80035. The computer calculations were supported by the Russian Foundation for Basic Research (Projects no. 17-05-00183 and no. 16-45-230781). Analysis of the results was carried out within the framework of the program 0149-2019-0014.

We greatly thank Prof. Chris Vincent (School of Environmental Sciences, University of East Anglia) for fruitful discussions during preparations of this paper.

References

Davies, A.G., van Rijn, L.C., Damgaard, J.S., van de Graaff, J., Ribberink, J.S., 2002. Intercomparison of research and practical sand transport models. Coast. Eng. 46 (1), 1–23, http://dx.doi.org/10.1016/S0378-3839(02)00042-X.

Divinsky, B.V., 2003. Results of wave measurements near Gelendzhik. In: Kosyan, R.D., Podymov, I.S., Pykhov, N.V. (Eds.), Dynamic Processes in a Coastal Zone. Moscow. 70–91, (in Russian).

Divinsky, B.V., Kos'yan, R.D., Gruene, J., 2014. Influence of the wave spectrum form on the bottom sediment dynamics. Oceanology 54 (2), 132–143, http://dx.doi.org/10.1134/S0001437014020052.

Dohmen-Janssen, C.M., McLean, S.R., Ribberink, J.S., Hanes, D.M., Vincent, C.E., 2000. Sheet flow and suspension under wave groups in a Large Wave Flume (SISTEX99). Eos, Tansactions, AGU Fall meeting Suppl. 81 (48), F642.

Grüne, J., Kos'yan, R., Oumeraci, H., Podymov, I., Schmidt-Koppenhagen, R., Vincent, C.E., 2007. Large-scale laboratory modeling of suspended sand concentration fluctuations under irregular waves. Coastal Sediments 07. ASCE, New Orleans, 248–258, http://dx.doi.org/10.1061/40926(239)19.

Hasselmann, K., Barnett, T.P., Bouws, E., Carlson, H., Cartwright, D. E., Enke, K., Ewing, J.A., Gienapp, H., Hasselmann, D.E., Kruseman, P., Meerburg, A., Müller, P., Olbers, D.J., Richter, K., Sell, W., Walden, H., 1973. Measurements of wind-wave growth and swell decay during the Joint North Sea Wave Project (JONSWAP). In: Erganzungsheft zur Deutschen Hydrographischen Zeitschrift, A (8°), No. 12. Deutsches Hydrograph. Inst., Hamburg, 96 pp.

Kos'yan, R., Grüne, J., Divinskiy, B., Podymov, I., Vincent, C., Ahmari, A., Oumeraci, H., 2010. The dependence of suspended sand concentration on the degree of storm development. Coast. Eng. Proc. 32, 8 pp., http://dx.doi.org/10.9753/icce.v32.sediment.19.

Moate, B.D., Thorne, P.D., 2011. Interpreting acoustic backscatter from suspended sediments of different and mixed mineralogical composition. Cont. Shelf. Res. 46 (1), 67–82, http://dx.doi.org/10.1016/j.csr.2011.10.007.

Thorne, P.D., Hanes, D.M., 2002. A review of acoustic measurement of small-scale sediment processes. Cont. Shelf. Res. 22 (4), 603–632, http://dx.doi.org/10.1016/S0278-4343(01)00101-7.

Thorne, P.D., Meral, R., 2008. Formulations for the scattering properties of suspended sandy sediments for use in the application of acoustics to sediment transport processes. Cont. Shelf. Res. 28 (2), 309—317, http://dx.doi.org/10.1016/j.csr.2007.08.002.

Thorne, P.D., Vincent, C.E., Hardcastle, P.J., Rehman, S., Pearson, N., 1991. Measuring suspended sediment concentrations using acoustic backscatter devices. Mar. Geol. 98 (1), 7—16, http://dx.doi.org/10.1016/0025-3227(91)90031-X.

Vincent, C.E., Hanes, D.M., 2002. The accumulation and decay of nearbed suspended sand concentration due to waves and wave groups. Cont. Shelf. Res. 22 (14), 1987—2000, http://dx.doi.org/10.1016/S0278-4343(02)00051-1.

Oceanologia (2019) 61, 103—113

Available online at www.sciencedirect.com

ScienceDirect

journal homepage: www.journals.elsevier.com/oceanologia/

ORIGINAL RESEARCH ARTICLE

Mixing characteristics of the subarctic front in the Kuroshio-Oyashio confluence region

Zhu Ke-Lan[a,1,*], Chen Xi[b,1], Mao Ke-Feng[b,*], Hu Dong[c], Hong Sen[d], Li Yan[b]

[a] *Army of PLA, Beijing, China*
[b] *College of Meteorology and Oceanography, National University of Defense Technology, Nanjing, China*
[c] *Army of PLA, Beijing, China*
[d] *Army of PLA, Beihai, China*

Received 17 October 2017; accepted 23 July 2018
Available online 11 August 2018

KEYWORDS
Kuroshio—Oyashio confluence region;
Subarctic front;
Mixing;
Turbulent eddy diffusivity;
Thermal diffusivity

Summary This paper analyzes the mixing characteristics of the Subarctic Front (SAF) in the Kuroshio-Oyashio Confluence Region based on temperature, salinity, and current data obtained from surveys and remote sensing in June 2016. The frontal zone of the observed area is at 145°—151°E, 38°—41°N. The front is distributed between 25.5—26.7 σ_θ in a band pattern inclined from north to south and is deeper in the south. The region shallower than 200 m and distributed along the isopycnal of 25.9—26.1 σ_θ has the strongest horizontal temperature and salinity gradients, and the largest of the former can reach over 0.7°C/km. Diapycnal mixing of the SAF is mainly turbulent; it is stronger in the north than in the south. The region with stronger turbulence ($K_\rho > 10^{-3.5}$ m^2/s) is distributed mainly in water layers within and under the front (26.1—26.7 σ_θ), showing that the SAF is shallower in the north and deeper in the south along the front. Symmetric instability may be the main factor causing strong turbulent mixing in the frontal zone. Double diffusion mixing is stronger in the south than in the north; the region with stronger double diffusion ($K_\theta > 10^{-4.5}$ m^2/s) is distributed mainly in water layers within and above the front (25—26.5 σ_θ) on the southern side of the SAF. These water layers are dominated mainly by ``salt-fingering" double diffusion, with only a few water layers dominated by ``diffusive layering" double diffusion mixing in middle and lower waters deeper than 300 m.

* Corresponding author at: College of Meteorology and Oceanography, National University of Defense Technology, Nanjing 211101, China. Tel.: +86 13585119800.
E-mail addresses: 503068020@qq.com (K.-L. Zhu), oceanlgdx@163.com (K.-F. Mao).
[1] These authors are co-first authors and contributed equally to this paper.
Peer review under the responsibility of Institute of Oceanology of the Polish Academy of Sciences.

Production and hosting by Elsevier

https://doi.org/10.1016/j.oceano.2018.07.004

1. Introduction

Ocean fronts, which are the boundaries of different water masses, are distributed along coastal regions and in the open ocean (Nagai et al., 2015a). They appear as sudden changes in ocean water temperature, salinity, density, and velocity. Recent studies have shown that frontal zones are the source of some water masses; for example, the North Pacific Intermediate Water (NPIW) is formed in the Subarctic Front (SAF) region (Hasunuma, 1978). A variety of marine phenomena such as diapycnal mixing (Nagai et al., 2015a), water mass formation and subduction (Nagai et al., 2015a; Pollard and Regier, 1992; Rudnick, 1996), and lateral mixing and cabbeling (Thomas and Shakespeare, 2015) also occur in these regions.

Diapycnal mixing generated from turbulence and double diffusion is of great importance in causing thermohaline intrusions and forming water masses (Pollard and Regier, 1992; Ruddick and Kerr, 2003; Ruddick and Richards, 2003; Stern, 1967), and is also an important mechanism affecting the physical properties of seawater and the intensity of thermohaline circulation (MacKinnon and Gregg, 2003a; Wunsch and Ferrari, 2004). In addition, diapycnal mixing greatly affects the maintenance and variation of ocean fronts (Wang and Li, 2012).

There have been several global studies of mixing at ocean fronts. Some observations have indicated that turbulent dissipation is stronger near the surface and extends deeper at the warm side of the frontal zone (Dewey and Moum, 1990). Nagai et al. (2009, 2012) believe that near-inertial internal waves and front formation strengthen turbulent mixing; from an observation in 2015, they found that the turbulent kinematic dissipation rate of the Kuroshio thermocline is 10—100 times higher than that of a typical thermocline and that it is accompanied by a near-inertial internal wave velocity shear at the isopycnic direction (Nagai et al., 2015b). D'Asaro et al. (2011) believe that strong air-sea interaction in the Kuroshio Extension Region could strengthen turbulent mixing in the upper layer of the frontal zone.

Double diffusion may have a strong influence on the formation of water masses in the frontal zone. Yuan and Talley (1996) believed that the NPIW is related to the "salt-fingering" function of Oyashio water of the mixing layer of SAF in winter. In addition, Nagai et al. (2015a) observed thermohaline intrusions (caused by near-inertial internal waves and sub-inertial flows) under the principal axis of the Kuroshio front and indicated that the sub- and near-inertial motions would strengthen the double diffusion, which then would enhance the diapycnal mixing.

The Kuroshio-Oyashio Confluence Region (KOCR; 142°—160°E, 35°—40°N; Sugimoto and Hanawa, 2011; Sugimoto et al., 2014) is located where the northern branch of the Kuroshio Extension (KE) intersects with the Oyashio Current. The anticyclonic eddy in the southern part of this region takes warm, salty KE water to the north (Itoh and Yasuda, 2010). Thus, the water in the south maintains the characteristics of the KE and the cyclonic eddy in the north brings cold, fresh Oyashio water to this region and forms the SAF (143°—171°E, 37°—43°N; Kitano, 1974; Sugimoto et al., 2014; Uda, 1963) with significant differences in thermohaline characteristics.

Currently, studies on the SAF focus mainly on variations in its characteristics and its response to the atmosphere. Yuan and Talley (1996) discovered that regions, where the horizontal temperature and salinity gradients of the SAF are high, are located mainly at 40°—44°N, with the temperature front in the west stronger than that in the east. Nakamura and Kazmin (2003) indicated that changes in low-frequency sea surface temperatures (SSTs) would result in the SAF changing from north to south and cause the long-term change in a temperature front dominated by a 10-year cycle (Nakamura et al., 1997). In addition, some numerical studies showed that weather- and planetary-scale atmospheric fields could respond to changes in the intensity of the SAF (Kwon and Deser, 2007; Nakamura et al., 2010; Sampe et al., 2010; Taguchi et al., 2009).

However, there are few studies on diapycnal mixing in the SAF, and no explicit conclusions have been drawn regarding its mixing characteristics. Therefore, this paper analyzes the temperature, salinity, current structure, and diapycnal mixing characteristics of the SAF in the KOCR, and discusses the reason for strong turbulence in the SAF region based on observations from a cruise from June 1 to 2, 2016.

This article is organized as follows. In Section 2, we introduce the data and observation information. In Section 3, we analyze the temperature, salinity, and current in the SAF region and the structural characteristics of the SAF. In Section 4, we analyze the mixing characteristics of the SAF region and in Section 5, we discuss the mechanism of strengthening turbulent mixing in the same. Finally, in Section 6, we present our conclusions.

2. Field experiments and data analysis

2.1. Observations of the subarctic front (SAF) in the Kuroshio—Oyashio confluence region (KOCR)

The absolute dynamic topography (ADT), sea surface temperature (SST), and sea surface geostrophic flow system of waters surrounding the SAF from June 1 to 2, 2016, based on satellite altimeter (Archiving Validation and Interpretation of Satellite Oceanographic data, AVISO) and Optimum Interpolation Sea Surface Temperature (OISST) records (Reynolds et al., 2007), are shown in Fig. 1a. Shipboard observations were carried out in the region between 146.75°—148.75°E and 38°—40°N (Fig. 1b). The ADT in this region is high in the south and low in the north; the ADT of the Kuroshio Extension, in the south of the frontal zone, can reach above 1.4 m but that of Oyashio, in the north, is only around 0.3 m. This presents an ADT variation of about 1 m in the frontal zone. The SST in the southern Kuroshio Extension is over 20°C while that of Oyashio is below 10°C, resulting in a temperature gradient of up to 0.1°C/km. There are also many eddies in the surrounding regions; cyclonic eddies are located mainly in the Oyashio area, anticyclonic eddies are located mainly in the sea near the Kuroshio Extension, and there is an obvious anticyclone in the southeastern part of the observed area.

Thus, we organized the cruise into six sections so that we could observe all the structural characteristics of the front. The average length of sections S01—S03 was about 70 km, and that of sections S04—S06 (Fig. 1c) was about 12 km. Fourteen Expendable Conductivity-Temperature-Depth (XCTD) observation stations (XCTD-1, Tsurumi-Seiki Co. Ltd., Japan) with a sampling frequency of 25 Hz and vertical resolution of

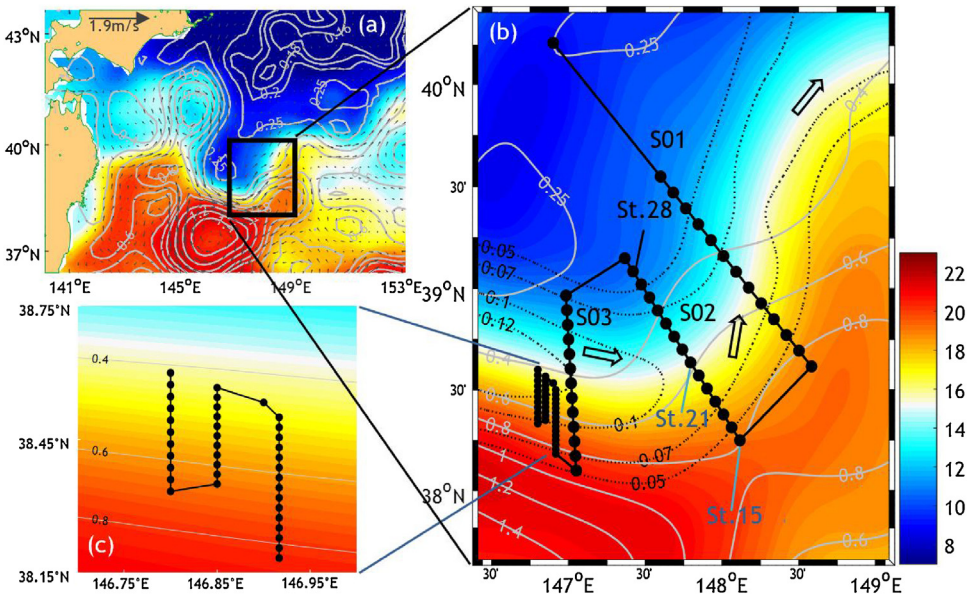

Figure 1 Observations of the Subarctic Front (SAF) on June 1–2, 2016. Distributions of: (a) sea surface temperature (SST) [°C], absolute dynamic topography (ADT) [m], and the sea surface geostrophic flow system (gray text arrow '1.9 m/s' is maximum current velocity) [m/s] in the surrounding regions; (b) tracks of the cruising observations and distribution of the Expendable Conductivity-Temperature-Depth (XCTD) stations; (c) extension of sections for intensive observation. The color map shows SSTs, gray contours indicate ADT, black dots represent XCTD stations, black dotted lines represent the horizontal SST temperature gradient, and black arrows indicate the direction of background current.

0.14 m were deployed along Section S01; fifteen and thirteen of these were deployed, respectively, along Section S02 and Section S03, at horizontal intervals of about 8 km. Further parameters of the XCTD stations are shown in Table 1. For intensive observations within the frontal zone, we deployed 16, 11, and 11 XCTD observation stations along Sections S04–S06, respectively, with horizontal intervals of 3 km. Further details of each section are shown in Table 2.

2.2. Data and methods

2.2.1 Processing the vessel survey data

The XCTDs provided good quality deep temperature and salinity data. However, the temperature profiles also showed distinct spectral spikes at 5 and 10 Hz, which is a common phenomenon in XCTD profiles from subtropical and subpolar waters (Gille et al., 2009). Five-point smoothing was used to

Table 1 Some parameters of the TSK XCTD-1 sensor used in this study.

Parameter	Range	Accuracy
Temperature	−2° to 35°C	0.02°C
Conductivity	0–60 mS/cm	0.03 mS/cm
Depth	0–1000 m	5 m or 2%, whichever is greater

Table 2 Details of sections S01–S06. "Number of stations" refers to the number of Expendable Conductivity-Temperature-Depth stations deployed along each section.

Section	Location	Heading	Number of stations
S01	147.6°–148.58°E, 38.62°–39.55°N	Northwest to southeast	14
S02	147.37°–148.12°E, 38.25°–39.15°N	Southeast to northwest	15
S03	147°E, 38.1°–38.97°N	North to south	13
S04	146.92°E, 38.18°–38.5°N	South to north	16
S05	146.85°E, 38.35°–38.57°N	North to south	11
S06	146.8°E, 38.33°–38.6°N	South to north	11

Table 3 Some parameters of the shipboard acoustic Doppler current profilers (SADCPs) used in this study.

SADCP type	Maximum measured depth (m)	Bin (m)	Frequency (kHz)	Sampling layer
38 kHz	1000	24	0.4	40
150 kHz	400	8	1.5	45

remove this disturbance and retain the authenticity of the data as much as possible according to the method in Gille et al. (2009).

The current data were obtained through observations with 38k and 150k Shipboard Acoustic Doppler Current Profilers (SADCPs) (Teledyne RD Instruments, United States of America; further parameters shown in Table 3) at intervals of 0.16 km and vertical resolutions of 24 m and 8 m. To obtain higher quality flow field data, we merged and processed the data from both SADCPs.

2.2.2 Parameterization

To understand the mixing characteristics of SAF, this paper uses the Thorpe method to calculate turbulent eddy diffusivity (K_ρ) and quantify turbulent mixing; calculates the thermal diffusivity (K_θ) and analyzes the diapycnal mixing characteristics caused by double diffusion with two thermohaline parameterizations; and calculates the Turner Angle (Tu) to analyze the double diffusion characteristics of the frontal zone.

a. Thorpe scale method

The dissipation rate ϵ of turbulent energy is calculated using the Thorpe scale L_T in the formula $\epsilon = c_1 L_T^2 N^3$ (Thorpe, 2005), where L_T is the root mean square of distance moved after formation of stable density profiles due to the rearrangement of sea water mass points on the actual density profile; $c_1 = (L_0/L_T)^2$ where the value of c_1 in this study is 0.64 and L_0 is the Ozmidov scale ($L_o = \langle\epsilon\rangle^{1/2} N^{-3/2}$) (Dillon, 1982); and N^3 is the cubic value of buoyancy frequency given by $N^3 = (-g\ \partial\ \sigma_\theta/\rho_0\ \partial\ z)^{3/2}$.

The resolution of the data also affects the calculation of the Thorpe scale. Galbraith and Kelley (1996) believe that about five sample points are needed to accurately identify turbulence overturns; therefore, turbulence overturns of vertical scale ($H_{\min}$) greater than 5 δ_z (where δ_z is the vertical resolution) are effective. Therefore, $H_{\min} < 5\ \delta_z$ are removed. Galbraith and Kelley (1996) also point out that $H_{\min}$ should be greater than $2\left|\frac{\delta\rho}{\partial\rho/\partial z}\right|$.

These calculations to find ϵ are needed to determine the eddy diffusivity K_ρ, which uses the formula $K_\rho = \Gamma\epsilon/N^2$ (Osborn, 1980) where Γ is a mixing efficiency of 0.2.

b. Thermohaline parameterization

The diapycnal mixing of the SAF caused by double diffusion is quantified by two thermohaline parameterizations used to calculate the thermal diffusivity K_θ: the k-profile parameterization (KPP) scheme (Fedorov, 1988) for the region of the front with a density ratio of $0 < R_\rho < 1$ and the scheme from Radko et al. (2014) for the region of the front with a density ratio of $R_\rho > 1$.

For the former, $K_\theta = 0.909\nu\exp(4.6\exp[-0.54(R_\rho^{-1} - 1)])$ where ν is the molecular viscosity of seawater (1.8×10^{-7} m^2/s in this paper) and R_ρ is the density ratio $\frac{\alpha\Theta_z}{\beta S_z}$ when Θ_z is the vertical potential temperature gradient after smoothing; S_z is the vertical salinity gradient after smoothing; $\alpha\ (-\rho^{-1}\ \partial\ \rho/\partial\ \Theta)$ is the thermal expansion coefficient of seawater; $\beta\ (-\rho^{-1}\ \partial\ \rho/\ \partial\ S)$ is the salinity contraction coefficient; and ρ is the seawater potential density. When $0 < R_\rho < 1$, the thermohaline stratification of the water is favorable for ``diffusive layering" (DL) (Kelley et al., 2003); when $R_\rho > 1$, the thermohaline stratification of the water is favorable for ``salt fingering" (SF) (Stern and Turner, 1969).

In a region with a density ratio $R_\rho > 1 K_\theta = F_s k_t \gamma$, $F_s = a_s(R_\rho - 1)^{-0.5} + b_s$, $\gamma = a_g \exp(-b_g R_\rho) + c_g$, $a_s = 135.7$, $b_s = -62.75$, $a_g = 2.709$, $b_g = 2.513$, and $c_g = 0.5128$.

c. Turner angle

Density ratio R_ρ is not as intuitive as Turner angle Tu [°] although it can also be used to analyze the double diffusion characteristics, thus this paper uses the Tu to analyze the double diffusion characteristics. Tu is calculated using the formula $Tu = \tan^{-1}[(\alpha\Theta_z + \beta S_z),\ (\alpha\Theta_z - \beta S_z)]$, where the parameters are the same as density ratio (R_ρ). When $-90° < Tu < -45°$, conditions are favorable for diffusive layering; when $45° < Tu < 90°$, they are favorable for salt fingering; when $-45° < Tu < 45°$, there will be no double diffusion in the water body; and if Tu gets close to $\pm 90°$, the double diffusion intensity increases.

2.2.3 Diagnosis parameters

The gradient Richardson number (Ri), potential vorticity (q), and effective Coriolis parameter (f_{eff}) are required to measure the Kelvin–Helmholtz instability (KI), symmetric instability (SI), and near-inertial internal waves (NIWs).

a. The gradient Richardson number (Ri)

The Ri is calculated using the formula $Ri = N^2/({u_z}^2 + {ve_z}^2)$, where u_z and v_z represent the vertical shear of zonal and meridional velocity of the SADCP. When $Ri < 0.25$, there is KI in the water; when $0.25 < Ri < 1$, there is SI in the water instead (Stone, 1966).

b. Potential vorticity (q)

q is calculated using the Ertel potential vorticity formula (Hoskins, 1974; Jing et al., 2016), expressed as follows:

$$q = q_v + q_h, \quad q_v = (f + \zeta)N^2, \quad q_h = -|\nabla_h b|^2/f,$$

where q_v and q_h represent the vertical and horizontal components, respectively; f stands for the Coriolis parameter; $\zeta = v_x - u_y$ and represents the relative vorticity; $N^2 = -g\ \partial\ \sigma_\theta/\rho_0\ \partial z$ and is the square of the buoyancy frequency; $b = g\sigma_\theta/\rho_0$ represents buoyancy; g is gravitational acceleration; σ_θ is the potential density after smoothing and ρ_0 is the reference density (=1024 kg/m^3). When $q < 0$, there is SI in the water (D'Asaro et al., 2011).

c. The effective Coriolis parameter (f_{eff})

NIWs can initially be determined using the effective Coriolis parameter (f_{eff}), calculated by Jing et al. (2017) as follows:

$$f_{eff} = \sqrt{\left(f + \frac{\zeta}{2}\right)^2 - \frac{S_n^2 + S_s^2}{4}},$$

where $\zeta = v_x - u_y$ is the relative vorticity (with v_x and u_y still representing the vertical shear of the zonal and meridional velocity of the SADCP) and $S_s = v_x + u_y$ is the shear strain. As the front zone is assumed to be geostrophic, and thus horizontally nondivergent, $S_n = 2u_x = -2v_y$.

Kunze (1985) pointed out that a region of strong positive vorticity ($f_{eff} > f$) can be a barrier to reflect NIWs with inherent frequencies of $\omega < f_{eff}$, while a region with weak effective Coriolis parameter ($f_{eff} < f$) can trap NIWs.

3. Structural characteristics of the SAF

In this section, we use Section S02 as an example with which to understand the structural characteristics of SAF, and analyze the temperature, salinity, and currents in this region based on 65 thermohaline profiles from XCTDs S01–S06 and current data from 38k and 150k SADCPs obtained on a cruise conducted from June 1 to 2, 2016.

3.1. Hydrographic characteristics of SAF waters

The temperature, salinity, and current distributions of the observed area are shown in Fig. 2a, b, c, f. There is cold and fresh Oyashio water in the northern part of the SAF and warm and salty KE water in the south. The former mainly appears in the region less dense than 26.5 σ_θ with the potential temperature of <10°C, but the surface water is warm and fresh with temperatures >11°C and salinity of about 32.5. KE water mainly appears in the region less dense than 26.3 σ_θ with the potential temperature of >15°C and salinity above 34. In addition, there is a clear low saline layer (with a salinity of 33–33.5) between 26.5–26.9 σ_θ that originated from Oyashio; Hasunuma (1978) and Talley (1993) consider that this low saline layer belongs to the NPIW.

The background current in SAF region heads eastwards, which is roughly consistent with the direction of flow in the Kuroshio Extension Region (Fig. 1a). The flow velocity is higher in the southern part of the frontal zone (up to 2 m/s) than in the north (about 0.3 m/s). The weak, shallow (less than 200 m) southward flow at 38.3°N (Section S02, Fig. 2f) is caused by the east wing of an anticyclonic eddy (Fig. 1a) in the southern part of the frontal zone. Section S01 and Sections S03–S06 of the front have structural characteristics similar to Section S02; the difference is that Sections S03–S06 are obvious westward zonal currents caused by the significant effect of the west wing of an anticyclonic eddy (Fig. 1a).

3.2. Structural characteristics of the SAF

The horizontal gradient of the water temperature is shown in Fig. 2d. The front is distributed between 25.5 and 26.7 σ_θ in a band pattern inclined from north to south. As the depth increases, the front moves southwards; the mean horizontal width of the front is about 20 km and it can reach up to 25 km at locations 100 m deep. The narrowest part is only 13 km at a location 50 m deep. In the vertical direction, the front is shallower than 400 m but deepens southward. The region with the highest front intensity (horizontal temperature and salinity gradient) is shallower than 200 m, and the temperature gradient there can reach over 0.7°C/km. The intensity gradually weakens as depth increases. The structural characteristics of the horizontal salinity gradient (Fig. 2e) are consistent with those of temperature gradient (Fig. 2d), but the intensity is only 1/8 that of the temperature gradient. In this text, the term "SAF" refers mainly to the temperature front, and we take a horizontal ship-measured temperature gradient of > 0.2°C/km as the front zone.

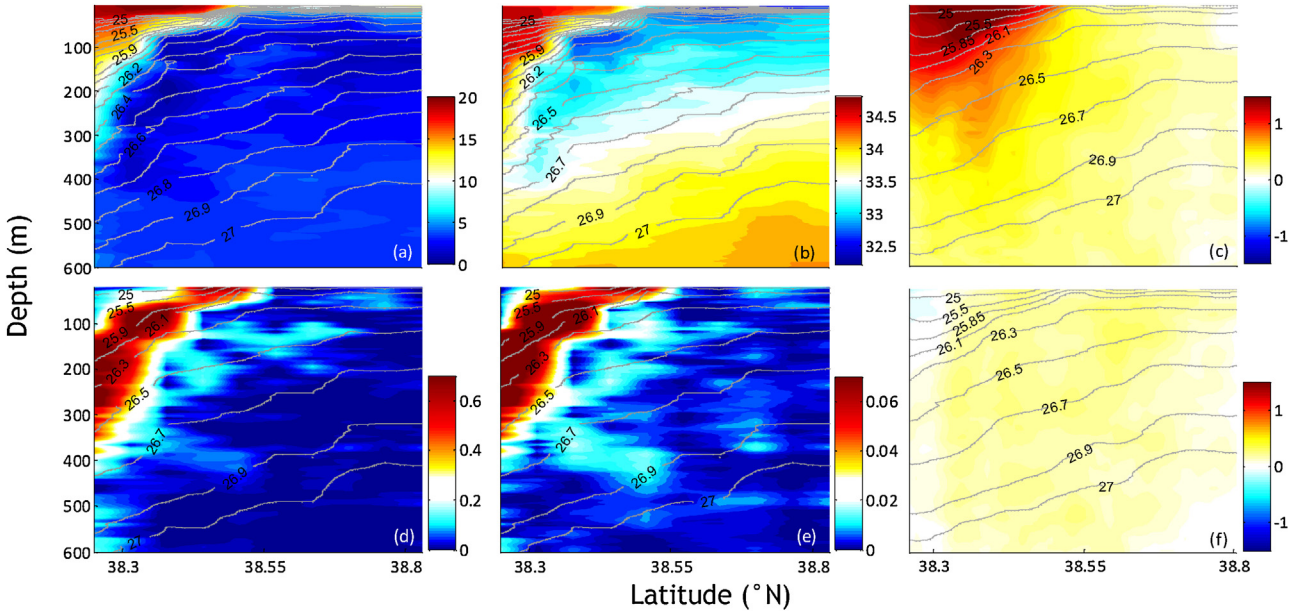

Figure 2 (a) Potential temperature [°C], (b) salinity [PSU], (c) zonal current velocity [m/s], (d) horizontal temperature gradient [°C/km], (e) horizontal salinity gradient [PSU/km], and (f) meridional current velocity [m/s] of Section S02 in which the gray contours are isopycnal (σ_θ). The interval between the potential density lines in (a) and (b) is 0.1 σ_θ.

4. Characteristics of mixing in the SAF region

As shown in Nagai et al. (2009, 2015a, 2015b), there is strong and turbulent mixing and double diffusion in the Kuroshio front. The SAF, which is geographically close to it, has a large temperature gradient; however, there are few studies on its mixing characteristics. Therefore, to understand the mixing characteristics of the SAF, this section takes Section S02 as an example and uses the Thorpe method to calculate the turbulent eddy diffusivity (K_ρ) of the frontal zone, thereby analyzing the turbulent mixing in the region. In this section, we calculate the thermal diffusivity (K_θ) of the frontal zone to analyze the diapycnal mixing characteristics caused by double diffusion with thermohaline parameterizations and use the Turner Angle (Tu) to analyze the double diffusion characteristics of the same area.

4.1. Distribution of turbulence and double diffusion mixing in the frontal zone

4.1.1 Characteristics of turbulent mixing

The characteristics of the distribution of K_ρ in Section S02 are shown in Fig. 3a; K_ρ ranges from 10^{-6}–10^{-3} m^2/s, and is quite low ($<10^{-5}$ m^2/s) for water layers less dense than 26.1 σ_θ. North of 38.4°N, waters with low K_ρ are located mainly in areas shallower than 50 m; south of this latitude, waters with low K_ρ may be as deep as 200 m, possibly related to strong mechanical stirring within the KE region and the shallow sea. These waters can be mixed evenly by mechanical stirring, which could lower the Thorpe displacement and thus result in a small K_ρ value.

There is strong turbulence in water layers below the 26.1 σ_θ, and K_ρ is greater than 10^{-5} m^2/s where the strong turbulent mixing region ($>10^{-3.5}$ m^2/s) is distributed mainly in water layers of 26.1–26.7 σ_θ. South of 38.4°N, the strong turbulent mixing region gradually becomes deeper and can reach up to 400 m at 38.3°N. The strong turbulent mixing region is distributed mainly along the front (Fig. 2d) and, north of 38.4°N, in waters under the front deeper than 50 m. It is located both in and under the front at depths greater than 150 m in the south, And in waters south of 38.3°N, the strong turbulence region can reach 26.9 σ_θ. The characteristics of the distribution of K_ρ in other sections are similar to the ones here.

4.1.2 Characteristics of double diffusion mixing

The characteristics of the distribution of K_θ in S02 are shown in Fig. 3b. The K_θ of the frontal zone is located between 10^{-6} and 10^{-4} m^2/s, which is generally lower than K_ρ. The water layers at 25–26.1 σ_θ have a high K_θ ($>10^{-4.5}$ m^2/s), unlike the upper layer in which the K_ρ value is lower. Waters with K_θ values $>10^{-4.5}$ m^2/s are located mainly in regions less dense than 26.5 σ_θ, both within and above the front (25–26.5 σ_θ), and waters with high K_θ (>10–4.5 m^2/s) are distributed along the front in a manner similar to K_ρ. As the front deepens continuously from north to south, waters with higher K_θ also deepen to up to 400 m. Therefore, diapycnal mixing caused by double diffusion takes place mainly above the front, especially in the upper sea less dense than 26.1 σ_θ.

The distribution of Tu in the frontal zone (Fig. 4) shows that water layers above 26.5 σ_θ with high K_θ values would promote the development of SF-type double diffusion, while those denser than 26.5 σ_θ would promote the development of DL-type double diffusion. Therefore, in areas of the sea that are less dense than 26.5 σ_θ, especially those in the upper sea less dense than 26.1 σ_θ, SF is the key factor causing diapycnal mixing. In water layers denser than 26.5 σ_θ, the "thermohaline staircase" (Schmitt et al., 1987) can be observed although K_θ is quite low at depths greater than 300 m. This indicates that the diapycnal mixing of these layers, which are concentrated mainly in the NPIW layer, is caused by DL-type double diffusion although there are also a few instances of SF-type double diffusion.

4.2. Characteristics of mixing in different regions of the SAF

To further analyze the relationship between turbulent and double diffusion mixing, and the characteristics in different regions of the frontal zone, we select all stations in Section S02 to calculate the mean values of K_ρ and K_θ at 30–560 m, which are about $10^{-4.1}$ m^2/s and $10^{-5.1}$ m^2/s, respectively; from this, we know that the diapycnal mixing of Section S02 is

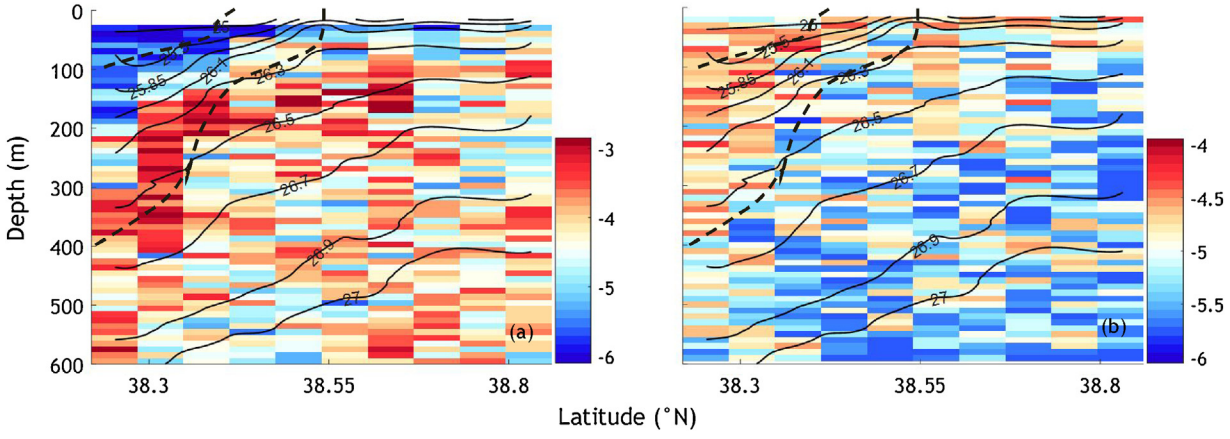

Figure 3 Logarithmic distribution of eddy diffusivity K_ρ (a) and K_θ (b), both [m^2/s] in S02; gray lines are isopycnal contours (σ_θ) and black dashed lines are the locations of the front (horizontal temperature gradient $>$ 0.2°C/km).

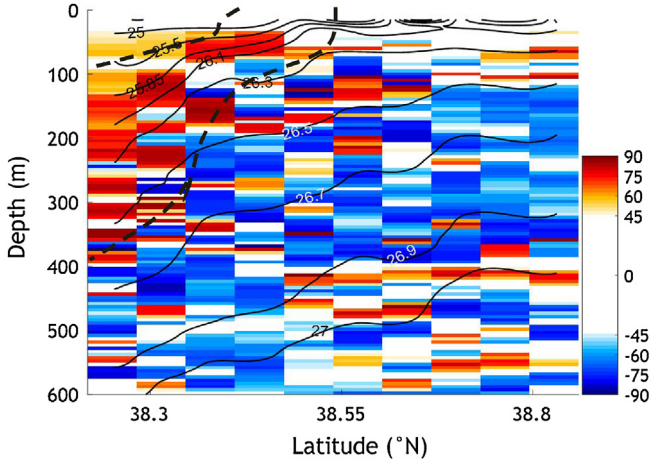

Figure 4 Distribution of the Turner angle (*Tu*) (Ruddick, 1983) of the section S02. The gray contour lines are isopycnal and the black dashed lines represent the location of the front with a horizontal temperature gradient > 0.2°C/km.

generally turbulent. In addition, K_ρ is weak in the south and strong in the north, while K_θ is strong in the south and weak in the north (Fig. 5). This means that in the southern part of the SAF, K_ρ is lower (about $10^{-4.2}$ m^2/s) than in the middle (about $10^{-4.1}$ m^2/s) and in the north (about 10^{-4} m^2/s). Similarly, K_θ is higher (about 10^{-5} m^2/s) in the southern part of the SAF than it is in the middle (about $10^{-5.1}$ m^2/s) and northern (about $10^{-5.2}$ m^2/s) regions. The other regions also show such characteristics.

To understand the mixing characteristics in the southern, middle, and northern regions of the SAF in detail, we select stations 15, 21, and 28 as three typical representative profiles from Section S02. These three stations are located at 148.58°E, 38.25°N; 147.80°E, 38.64°N; and 147.42°E, 39.09°N. We also calculate the buoyancy frequency, *Tu*, and *Ri* for K_θ and K_ρ; all of these are shown in Fig. 6.

Station 15, located in the southern part of the SAF, has a relatively high temperature, salinity, stable stratification, and *Ri* value; its middle and upper layers can promote SF-type double diffusion, while its middle and lower layers can promote DL-type double diffusion. The distribution of K_θ and K_ρ shows that the former is significantly higher than the latter in the waters shallower than 200 m, so diapycnal mixing is caused mainly by SF-type double diffusion. As the depth increases, the K_ρ values gradually increase to 10^{-3} m^2/s in waters deeper than 200 m while K_θ remains at 10^{-5}–10^{-4} m^2/s, indicating that diapycnal mixing is caused mainly by turbulent mixing in waters deeper than 200 m.

Station 21, located in the middle of the frontal zone, has stable stratification and the temperature and salinity fall rapidly with increasing depths due to the effect of Oyashio. The water layer of this station is not conducive to generating SF-type double diffusion, but it is conducive to generating DL-type double diffusion; K_θ is about 10^{-5} m^2/s and K_ρ is between 10^{-5} and 10^{-3} m^2/s. Therefore, diapycnal mixing is caused mainly by turbulent mixing.

Station 28, located in the northern part of the frontal zone, has characteristics similar to Station 21 except for its potential temperature-salinity scatter, which is mainly concentrated in regions cooler than 4°C. The characteristics of *Tu* for this station show that strong turbulent mixing occurs here; there are many water layers not favorable for double diffusion ($-45° < Tu < 45°$). The mean values of K_θ and K_ρ are about 10^{-5} m^2/s and 10^{-4} m^2/s, indicating that the diapycnal mixing is caused mainly by turbulence.

These results show that the characteristics of mixing vary in different regions of the SAF. Although the diapycnal mixing is caused mainly by turbulence, there is obvious double

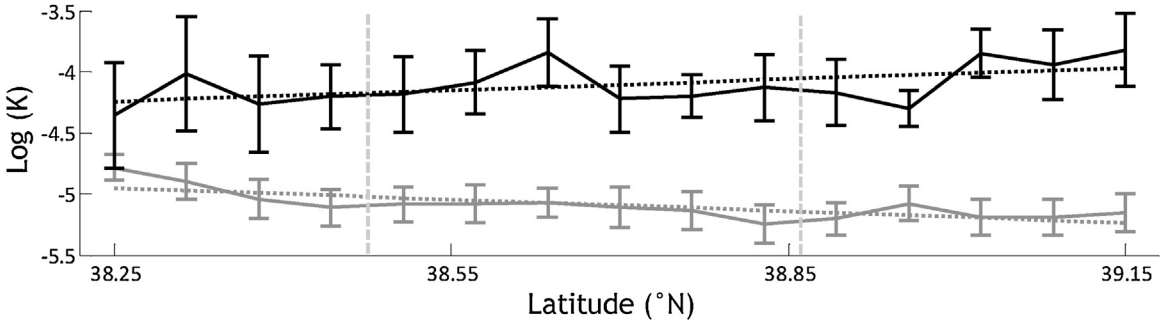

Figure 5 Mean values (30–560 m) and standard deviations of K_ρ (m^2/s, black solid line) and K_θ (m^2/s, gray solid line) of all stations in Section S02. The areas between the vertical gray dotted lines represent the southern, middle, and northern regions of the SAF, respectively (each with a horizontal sea surface temperature gradient < 0.08°C/km). The black and gray dotted lines are the trend lines of the least square fit of K_ρ and K_θ, respectively.

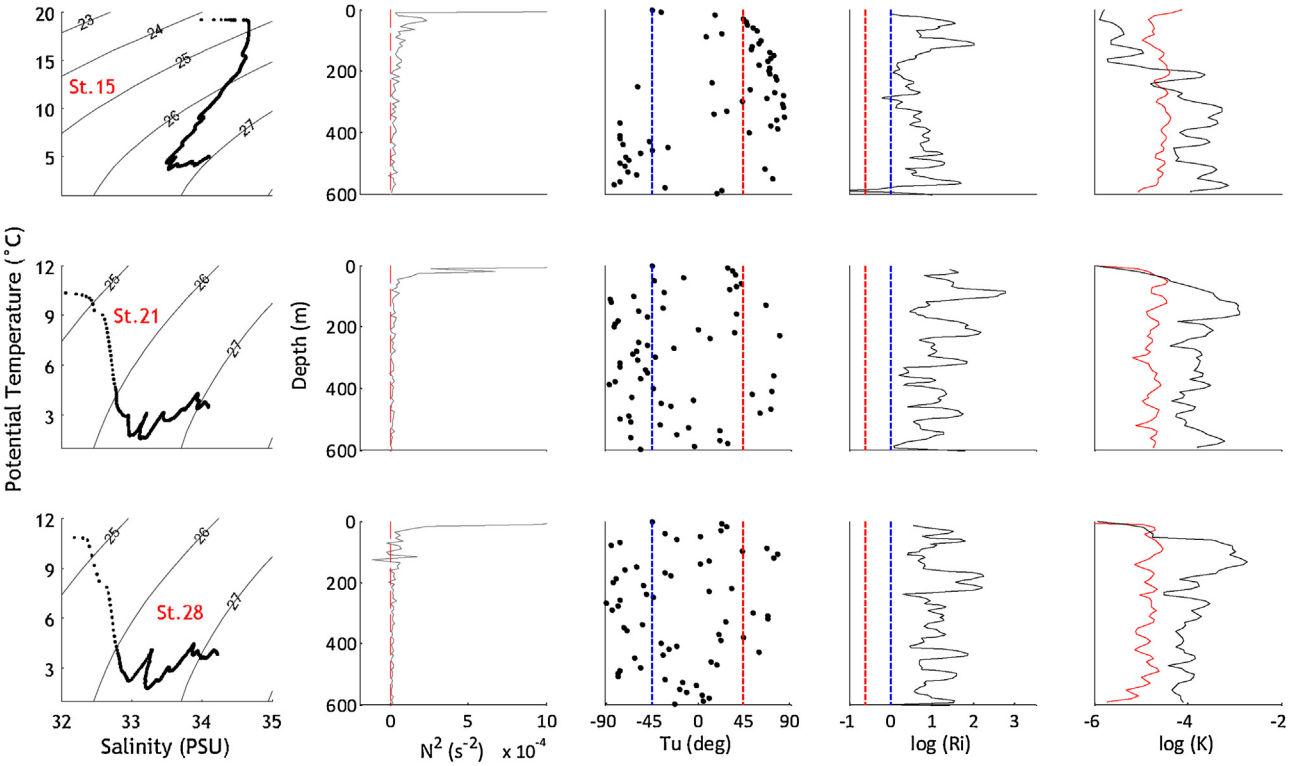

Figure 6 Distribution of temperature-salinity (T-S), N^2, *Tu*, log (*Ri*), log (K_ρ), log (K_θ) for stations 15, 21, and 28, three typical profiles from Section S02, arranged from top to bottom. In the T-S scatterplot, the black and blue contours represent potential density; $N^2 = 0$, as shown with red dotted lines; $Tu = \pm 45^\circ$, as shown by the red and blue dotted lines; *Ri* is shown in logarithmic form, where $Ri = 1$ and 0.25 are the blue and red dotted lines, respectively; and log (K_ρ) and log (K_θ) are presented by black and red solid lines, respectively.

diffusion in the southern part of the SAF. The diapycnal mixing in waters shallower than 200 m is caused mainly by SF-type double diffusion. The depth increases the turbulence functions which are gradually strengthened and diapycnal mixing is caused mainly by turbulence. In the middle and northern part of the SAF, the diapycnal mixing is caused mainly by turbulence; diapycnal mixing caused by double diffusion is weak, making conditions more favorable for the development of DL-type double diffusion.

5. Discussion

By analyzing the mixing characteristics of the SAF, we found that diapycnal mixing is dominated mainly by turbulent mixing in the frontal zone; the K_ρ near the front can reach 10^{-4}–10^{-3} m^2/s, which is 1–2 magnitudes higher than in the open ocean. We use S02 and S03 as examples to discuss the strengthening mechanism of turbulent mixing in the SAF region.

The shear or Kelvin–Helmholtz instability (KI) and symmetric instability (SI) can strengthen turbulent mixing (D'Asaro et al., 2011); the latter can also effectively extract kinetic energy from the geostrophic frontal jet and feed a turbulent cascade to dissipation. Here, we measure this instability using the gradient Richardson number (*Ri*) and potential vorticity (*q*).

The *Ri* and *q* of Section S02 are shown in Fig. 7a and b. The region in which $0.25 < Ri < 1$ basically corresponds to those in which $q < 0$; these are concentrated in the water layers near the front where 25.5–26.7 σ_θ, indicating that SI occurs in these layers. The negative value region of *q* corresponds, simultaneously, to the strong turbulent mixing region; thus, the strong turbulent mixing ($K_\rho \geq 10^{-3.5}$ m^2/s) of water layers near the 26.1–26.7 σ_θ front at Section S02 is closely related to SI. However, there is a large difference between Section S03 (Fig. 7d and e) and Section S02. The values of *q* corresponding to other regions with strong turbulent mixing are basically greater than 0 (Fig. 7e); the exception is the relationship between strong turbulence and SI near 38.15°N and 38.4°N at 26.5–26.7 σ_θ, which indicates that SI is not the main reason for the increased turbulence in Section S03. The horizontal temperature gradient and logarithmic distribution of K_ρ in Section S03 are presented in Fig. 8a and b, respectively.

The characteristics of the *Ri* of Section S03 (Fig. 7d) shows that there are many water layers with KI ($Ri < 0.25$) and that these regions have a high K_ρ ($\geq 10^{-3.5}$ m^2/s), which strengthens the turbulence in this Section. At the same time, there are also several smaller regions of KI in Sections S01 and S02, which also correspond to high K_ρ values ($\geq 10^{-3.5}$ m^2/s). This shows that KI is the main reason for increased turbulence in this region.

In addition, near-inertial internal waves (NIWs) may also strengthen the turbulent mixing (Whitt and Thomas, 2013).

As shown by the characteristics of the effective Coriolis parameter (f_{eff}) in Section S02 (Fig. 7c), the water layers at 25.5–26.7 σ_θ near the front are basically located at the NIWs barrier layers with $f_{eff} > 1.2f$, further indicating that NIWs are not the main factors strengthening the turbulent mixing

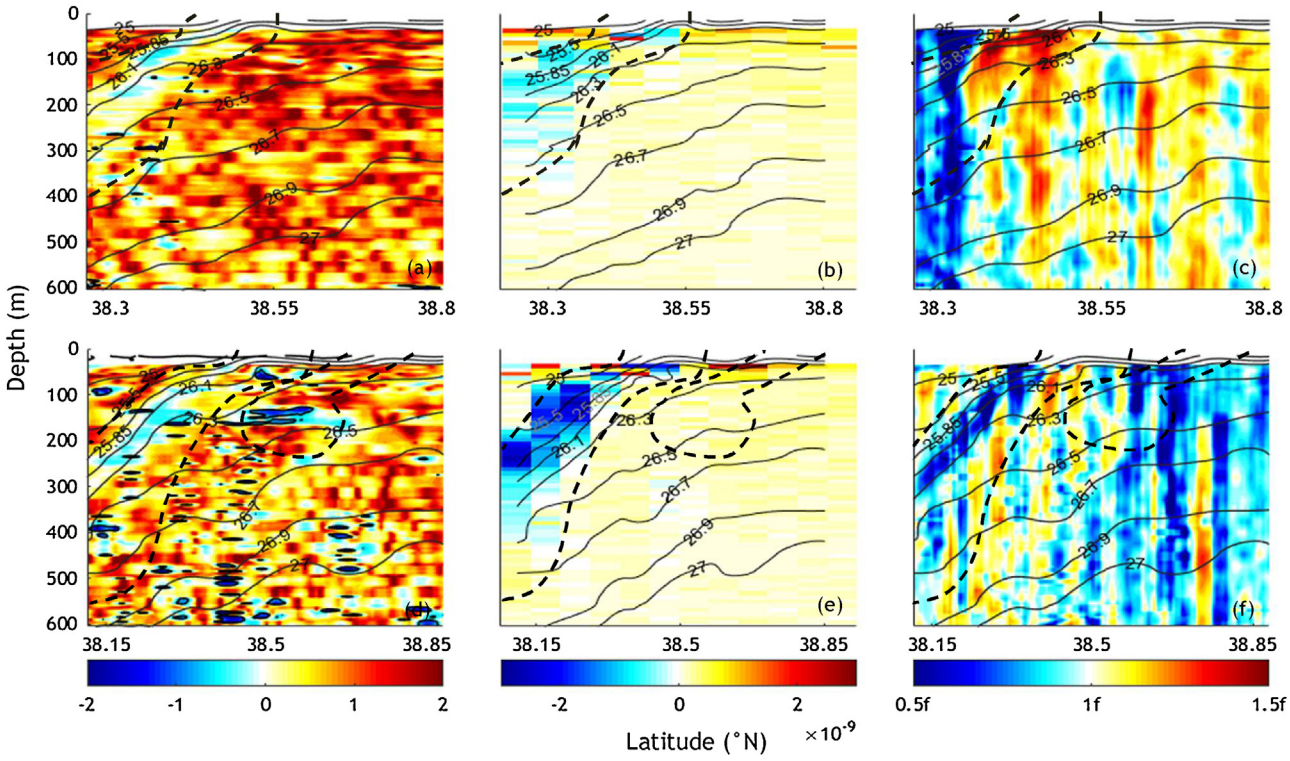

Figure 7 Characteristics of Ri, q (s^{-3}), and f_{eff} (f) in Sections S02 and S03. In (a), the Ri of S02 is given in logarithmic form in the region within the closed black contour lines, (b)–(c) is where $Ri \leq 0.25$, and the q and f_{eff} distribution of S02, respectively, are seen, (d)–(f) illustrate the Ri, q, and f_{eff} distributions of S03, respectively, with the gray lines showing isopycnal contours (σ_θ) and black dashed lines representing the locations of the front (horizontal temperature gradient $>$ 0.2°C/km).

of Section S02, except in areas on the southern side of 38.3°N. Section S01 is similar to Section S02; at the front in Section S03 (Fig. 7f), there is an obviously high K_ρ ($\geq 10^{-3.5}$ m^2/s) and low Ri ($<$0.25) in areas shallower than 200 m north of 38.5°N and deeper than 150 m north of 38.4°N. At the same time, these KI regions have a fine vertical spatial continuity and scale structure, and f_{eff} is generally lower than f. The results suggest that NIWs may be a possible reason for KI, which strengthens turbulence, in these two regions.

Thus, the strong turbulence in the water layers at 26.1–26.7 σ_θ and 26.5–26.7 σ_θ in Sections S02 and S03 near 38.15°N and 38.4°N, respectively, is closely related to SI. The turbulent mixing in Section S03 may be strengthened by KI. In Sections S01 and S02, SI may be the main reason for the strengthened turbulent mixing in the frontal zone. Lastly, NIWs could be the factors causing KI in the front at areas shallower than 200 m north of 38.5°N and deeper than 150 m north of 38.4°N.

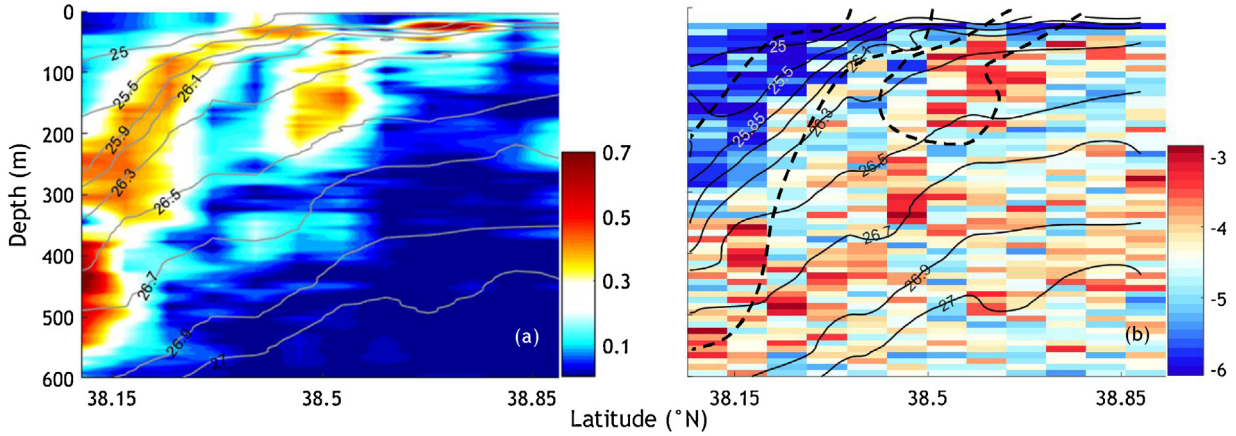

Figure 8 (a) Horizontal temperature gradient [°C/km] and (b) logarithmic distribution of K_ρ [m^2/s] for Section S03; gray lines are isopycnal contours (σ_θ) and the black dashed line in (b) represents the location of the front (horizontal temperature gradient $>$ 0.2°C/km).

6. Conclusion

This paper presents the results of studies on the mixing characteristics of the SAF in the KOCR, and analyzes of the temperature, salinity, current structural characteristics, and mixing characteristics of the SAF. Using data from cruising observations and the AVISO and OISST satellite altimeter datasets to calculate parameters such as the Turner angle (Tu), turbulent eddy diffusivity (K_ρ), thermal diffusivity (K_θ), and gradient Richardson number resulted in the following conclusions:

1. There is cold and fresh Oyashio water in the northern part of the SAF, and warm and salty Kuroshio Extension water in the southern region. The SAF is located between 25.5 and 26.7 σ_θ in a band pattern inclined north to south. As the depth increases, the front moves southward with a gradually weakening intensity. The background current is eastward, with a high and low flow velocity, respectively, in the south and north. There are numerous eddies in the waters around the SAF.
2. Diapycnal mixing in the SAF zone is mainly turbulent, and it is stronger in the north than in the south of the frontal zone. The region with strong turbulence ($K_\rho > 10^{-3.5}$ m^2/s) is distributed mainly in water layers within and under the front (26.1—26.7 σ_θ) and it is shallow in the north and deep in the south. The region with strong double diffusion ($K_\theta > 10^{-4.5}$ m^2/s) is distributed mainly in water layers (25—26.5 σ_θ) within and above the front, in the southern part of the SAF, with a depth gradient similar to that of turbulence. These water layers are dominated mainly by salt-fingering double diffusion, while the middle and lower regions deeper than 300 m also have a few layers dominated by diffusive-layering double diffusion mixing.
3. Symmetric instability may be the main factor strengthening turbulent mixing in the frontal zone, but shear instability causes it in other zones. Shear instability within the front in regions shallower than 200 m north of 38.5°N, and in layers deeper than 150 m north of 38.4°N in Section S03, may be related to near-inertial internal waves.

Acknowledgments

This work was supported by the National Natural Science Foundation of China, No. 11572351 and the Province Natural Science Foundation of Jiangsu, China, No. BK20150711.

We thank all the crew members who participated in the ship cruising observation in May—June 2016.

References

D'Asaro, E., Lee, C., Rainville, L., Harcourt, L., Thomas, L., 2011. Enhanced turbulence and energy dissipation at ocean fronts. Science 332 (6027), 318—322.

Dewey, R.K., Moum, J.N., 1990. Enhancement of fronts by vertical mixing. J. Geophys. Res. 95 (C6), 9433—9445, http://dx.doi.org/10.1029/JC095iC06p09433.

Dillon, T.M., 1982. Vertical overturns: a comparison of Thorpe and Ozmidov length scales. J. Geophys. Res.-Oceans 87 (C12), 9601—9613, http://dx.doi.org/10.1029/JC087iC12p09601.

Fedorov, K.N., 1988. Layer thicknesses and effective diffusivities in "diffusive" thermohaline convection in the ocean. Elsevier Oceanogr. Series vol. 4, 471—479.

Galbraith, P.S., Kelley, D.E., 1996. Identifying overturns in CTD profiles. J. Atmos. Ocean. Tech. 13 (3), 688—702, http://dx.doi.org/10.1175/1520-0426(1996)013%3C0688:IOICP%3E2.0.CO;2.

Gille, S.T., Lombrozo, A., Sprintall, J., Stephenson, G., Scarlet, R., 2009. Anomalous spiking in spectra of XCTD temperature profiles. J. Atmos. Ocean. Tech. 26 (6), 1157—1164, http://dx.doi.org/10.1175/2009JTECHO668.1.

Hasunuma, K., 1978. Formation of the intermediate salinity minimum in the northwestern Pacific Ocean. Bull. Ocean Res. Inst. (Univ. Tokyo) vol. 9, 1—47.

Hoskins, B.J., 1974. The role of potential vorticity in symmetric stability and instability. Q. J. R. Meteorol. Soc. 100 (425), 480—482, http://dx.doi.org/10.1002/qj.49710042520.

Itoh, S., Yasuda, I., 2010. Characteristics of mesoscale eddies in the Kuroshio-Oyashio Extension region detected from the distribution of the sea surface height anomaly. J. Phys. Oceanogr. 40, 1018—1034, http://dx.doi.org/10.1175/2009JPO4265.1.

Jing, Z., Qi, Y., Fox-Kemper, B., Du, Y., Lian, S., 2016. Seasonal thermal fronts on the northern South China Sea shelf: Satellite measurements and three repeated field surveys. J. Geophys. Res.-Oceans 121 (3), 1914—1930, http://dx.doi.org/10.1002/2015JC011222.

Jing, Z., Wu, L., Ma, X., 2017. Energy exchange between the mesoscale oceanic eddies and wind-forced near-inertial oscillations. J. Phys. Oceanogr. 47 (3), 721—733, http://dx.doi.org/10.1175/JPO-D-16-0214.1.

Kelley, D.E., Fernando, H.J.S., Gargett, A.E., Tanny, J., Özsoy, E., 2003. The diffusive regime of double-diffusive convection. Prog. Oceanogr. 56 (3), 461—481, http://dx.doi.org/10.1016/S0079-6611(03)00026-0.

Kitano, K., 1974. Some properties of the warm eddies generated in the confluence zone of the Kuroshio and Oyashio currents. J. Phys. Oceanogr. 5 (5), 245—252, http://dx.doi.org/10.1175/1520-0485(1975)005%3C0245:SPOTWE%3E2.0.CO;2.

Kunze, E., 1985. Near-inertial wave propagation in geostrophic shear. J. Phys. Oceanogr. 15 (5), 544—565, http://dx.doi.org/10.1175/1520-0485(1985)015%3C0544:NIWPIG%3E2.0.CO;2.

Kwon, Y.-O., Deser, C., 2007. North Pacific decadal variability in the Community Climate System Model version 2. J. Climate 20, 2416—2433, http://dx.doi.org/10.1175/JCLI4103.1.

MacKinnon, J.A., Gregg, M.C., 2003a. Shear and baroclinic energy flux on the summer New England shelf. J. Phys. Oceanogr. 33 (7), 1462—1475, http://dx.doi.org/10.1175/15200485(2003)033%3C1462:SA-BEFO%3E2.0.CO;2.

Nagai, T., Tandon, A., Yamazaki, H., Doubell, M.J., 2009. Evidence of enhanced turbulent dissipation in the frontogenetic Kuroshio Front thermocline. Geophys. Res. Lett. 36 (12), 1179, http://dx.doi.org/10.1029/2009GL038832.

Nagai, T., Tandon, A., Yamazaki, H., Doubell, M.J., Gallager, S., 2012. Direct observations of microscale turbulence and thermohaline structure in the Kuroshio Front. J. Geophys. Res.-Oceans 117 (C8), C08013, http://dx.doi.org/10.1029/2011JC00722.

Nagai, T., Inoue, R., Tandon, A., Yamazaki, H., 2015a. Evidence of enhanced double-diffusive convection below the main stream of the Kuroshio Extension. J. Geophys. Res.-Oceans 120 (12), 8402—8421, http://dx.doi.org/10.1002/2015JC011288.

Nagai, T., Tandon, A., Kunze, E., Mahadevan, A., 2015b. Spontaneous generation of near-inertial waves by the Kuroshio Front. J. Phys. Oceanogr. 45 (9), 2381—2406, http://dx.doi.org/10.1175/JPO-D-14-0086.1.

Nakamura, H., Kazmin, A.S., 2003. Decadal changes in the North Pacific oceanic frontal zones as revealed in ship and satellite observations. J. Geophys. Res.-Oceans 108 (C3), 371—376, http://dx.doi.org/10.1029/1999JC000085.

Nakamura, H., Lin, G., Yamagata, T., 1997. Decadal climate variability in the North Pacific during the recent decades. Bull. Am. Meteorol. Soc. 78 (10), 2215—2225, http://dx.doi.org/10.1175/1520-0477(1997)078%3C2215:DCVITN%3E2.0.CO;2.

Nakamura, H., Miyasaka, T., Kosaka, Y., Takaya, K., Honda, M., 2010. Northern hemisphere extratropical tropospheric planetary waves and their low-frequency variability: their vertical structure and interaction with transient eddies and surface thermal contrasts. Geophys. Monogr. Series 189, 149—179, http://dx.doi.org/10.1029/2008GM000789.

Osborn, T.R., 1980. Estimates of the local rate of vertical diffusion from dissipation measurements. J. Phys. Oceanogr. 10 (1), 83—89, http://dx.doi.org/10.1175/15200485(1980)010%3C0083:EOTLRO%3-E2.0.CO;2.

Schmitt, R.W., Perkins, H., Boyd, J.D., Stalcup, M.C., 1987. C-SALT: an investigation of the thermohaline staircase in the western tropical North Atlantic. Deep Sea Res. Part A. Oceanogr. Res. Pap. 34 (10), 1655—1665, http://dx.doi.org/10.1016/0198-0149(87)90014-8.

Pollard, R.T., Regier, L.A., 1992. Vorticity and vertical circulation at an ocean front. J. Phys. Oceanogr. 22 (6), 609—625, http://dx.doi.org/10.1175/15200485(1992)022%3C0609:VAVCAA%3-E2.0.CO;2.

Radko, T., Bulters, A., Flanagan, J.D., Campin, J.M., 2014. Double-diffusive recipes. Part I: Large-scale dynamics of thermohaline staircases. J. Phys. Oceanogr. 44 (5), 1269—1284, http://dx.doi.org/10.1175/JPO-D-13-0155.1.

Reynolds, R.W., Smith, T.M., Liu, C., Chelton, D.B., Casey, K.S., Schlax, M.G., 2007. Daily high-resolution-blended analyses for sea surface temperature. J. Climate 20 (22), 5473—5496, http://dx.doi.org/10.1175/2007JCLI1824.1.

Ruddick, B., 1983. A practical indicator of the stability of the water column to double-diffusive activity. Deep-Sea Res. 30 (10), 1105—1107, http://dx.doi.org/10.1016/0198-0149(83)90063-8.

Ruddick, B., Kerr, O., 2003. Oceanic thermohaline intrusions: theory. Progr. Oceanogr. 56 (3), 483—497, http://dx.doi.org/10.1016/S0079-6611(03)00029-6.

Ruddick, B., Richards, K., 2003. Oceanic thermohaline intrusions: observations. Progr. Oceanogr. 56 (3), 499—527, http://dx.doi.org/10.1016/S0079-6611(03)00028-4.

Rudnick, D.L., 1996. Intensive surveys of the Azores Front: II. Inferring the geostrophic and vertical velocity fields. J. Geophys. Res.-Oceans 101 (C7), 16291—16303, http://dx.doi.org/10.1029/96JC01144.

Sampe, T., Nakamura, H., Goto, A., Ohfuchi, W., 2010. Significance of a midlatitude SST frontal zone in the formation of a storm track and an eddy-driven westerly jet. J. Climate 23, 1793—1814, http://dx.doi.org/10.1175/2009JCLI3163.1.

Stern, M.E., 1967. Lateral mixing of water masses. Deep-Sea Res. 14 (6), 747—753, http://dx.doi.org/10.1016/S0011-7471(67)80011-1.

Stern, M.E., Turner, J.S., 1969. Salt fingers and convecting layers. Deep-Sea Res. 16 (5), 497—511, http://dx.doi.org/10.1016/0011-7471(69)90038-2.

Stone, P.H., 1966. On non-geostrophic baroclinic stability. J. Atmos. Sci. 23 (4), 390—400, http://dx.doi.org/10.1175/1520-0469(1966)023%3C0390:ONGBS%3E2.0.CO;2.

Sugimoto, S., Hanawa, K., 2011. Roles of SST anomalies on the wintertime turbulent heat fluxes in the Kuroshio-Oyashio Confluence Region: influences of warm eddies detached from the Kuroshio Extension. J. Climate 24 (24), 6551—6561, http://dx.doi.org/10.1175/2011JCLI4023.1.

Sugimoto, S., Kobayashi, N., Hanawa, K., 2014. Quasi-decadal variation in intensity of the western part of the winter subarctic SST front in the western north pacific: the influence of Kuroshio extension path state. J. Phys. Oceanogr. 44 (10), 2753—2762, http://dx.doi.org/10.1175/JPO-D-13-0265.1.

Taguchi, B., Nakamura, H., Nonaka, M., Xie, S.-P., 2009. Influences of the Kuroshio/Oyashio Extensions on air-sea heat exchanges and storm-track activity as revealed in regional atmospheric model simulations for the 2003/04 cold season. J. Climate 22, 6536—6560, http://dx.doi.org/10.1175/2009JCLI2910.1.

Talley, L.D., 1993. Distribution and formation of North Pacific Intermediate Water. J. Phys. Oceanogr. 23 (3), 517—538, http://dx.doi.org/10.1175/15200485(1993)023%3C0517:DAFONP%3E-2.0.CO;2.

Thomas, L.N., Shakespeare, C.J., 2015. A new mechanism for mode water formation involving cabbeling and frontogenetic strain at thermohaline fronts. J. Phys. Oceanogr. 45 (9), 2444—2456, http://dx.doi.org/10.1175/JPO-D-15-0007.1.

Thorpe, S.A., 2005. The Turbulent Ocean. Cambridge Univ. Press, Cambridge, UK, 426 pp.

Uda, M., 1963. Oceanography of the subarctic Pacific Ocean. J. Fish. Res. Board. Canada 20 (1), 119—179, http://dx.doi.org/10.1139/f63-011.

Wang, F., Li, Y., 2012. Thermohaline finestructure observed near the northern Philippine coast. Chin. J. Oceanol. Limnol. 30 (6), 1033—1044, http://dx.doi.org/10.1007/s00343-012-1246-0.

Whitt, D.B., Thomas, L.N., 2013. Near-inertial waves in strongly baroclinic currents. J Phys. Oceanogr. 43 (4), 706—725, http://dx.doi.org/10.1175/jpo-d-12-0132.1.

Wunsch, C., Ferrari, R., 2004. Vertical mixing, energy, and the general circulation of the oceans. Annu. Rev. Fluid Mech. 36, 281—314, http://dx.doi.org/10.1146/annurev.fluid.36.050802.122121.

Yuan, X., Talley, L.D., 1996. The subarctic frontal zone in the North Pacific: characteristics of frontal structure from climatological data and synoptic surveys. J. Geophys. Res.-Oceans 101 (C7), 16491—16508, http://dx.doi.org/10.1029/96JC01249.

Oceanologia (2019) 61, 114—130

Available online at www.sciencedirect.com

ScienceDirect

journal homepage: www.journals.elsevier.com/oceanologia/

ORIGINAL RESEARCH ARTICLE

Annual cycle of phytoplankton community through the water column: Study applied to the implementation of bivalve offshore aquaculture in the southeastern Bay of Biscay

Oihane Muñiz [a,*], Marta Revilla [a], José Germán Rodríguez [a], Aitor Laza-Martínez [b], Almudena Fontán [a]

[a] *AZTI-Tecnalia, Marine Research Division, Pasaia, Spain*
[b] *Department of Plant Biology and Ecology, Faculty of Science and Technology, University of the Basque Country, UPV/EHU, Leioa, Spain*

Received 14 March 2018; accepted 2 August 2018
Available online 28 August 2018

KEYWORDS
Phytoplankton abundance;
Taxonomic composition;
Biomass;
Size-fractionated chlorophyll;
Environmental variables

Abstract This study describes, for the first time, the annual variability of phytoplankton community in different layers of the water column in open waters off the Basque coast (southeastern Bay of Biscay). Phytoplankton composition, abundance and biomass, together with size-fractionated chlorophyll *a*, nutrients, and optical and hydrographic conditions were measured in an experimental bivalve culture area from May 2014 to June 2015. Water column conditions showed the typical dynamics previously described for temperate areas, characterised by winter homogeneity and summer stratification. Phytoplankton temporal variability was studied at depths of 3, 17 and 33 m, and was found to be related to those processes. In particular, temperature and nutrients (mostly nitrate and silicate) were the environmental variables which significantly explained most of the variability of chlorophyll concentration, whereas river flow was the main driver of abundance variability. Total chlorophyll was generally low (0.6 $\mu g\ L^{-1}$ on average). Of the 194 registered taxa, 47.4% belonged to dinoflagellates and 35.1% to diatoms. In addition, diatoms showed the highest biomass values, and haptophytes represented the greatest

* Corresponding author at: AZTI-Tecnalia, Marine Research Division, Herrera Kaia Portualdea s/n, E-20110 Pasaia, Spain. Tel.: +34 946 574 000.
E-mail address: omuniz@azti.es (O. Muñiz).

Peer review under the responsibility of Institute of Oceanology of the Polish Academy of Sciences.

ELSEVIER | Production and hosting by Elsevier

https://doi.org/10.1016/j.oceano.2018.08.001

contribution to cell-abundance. This fact, despite the low chlorophyll values indicating low phytoplankton biomass, could favour mussel growth given the high fatty acid content reported for diatoms and haptophytes.

1. Introduction

Phytoplankton constitute an important component of the diet of suspension feeding bivalves (Grant, 1996; MacDonald and Ward, 1994; Petersen et al., 2008; Shumway and Cucci, 1987). In fact, microalgae have long been used as food resource for mollusc bivalves at all growth stages (Brown, 2002). This interaction of mollusc bivalves with phytoplankton as a food source has been studied extensively. For instance, it is known that the quantity and size of the phytoplankton can influence the recruitment of oysters, as well as the survival of bivalve larvae (Bourlès et al., 2009; Robert and Trintignac, 1997). Moreover, phytoplankton blooms have been directly related to the increase of mussel growth and condition index (*i.e.*, the ratio between the dry weight of the meat and the shell) (Blanton et al., 1987; Hickman et al., 1991; van der Veer, 1989). However, not all phytoplankton species are equal in terms of nutritional quality for bivalves. Several bivalves (including mussels) have shown a preferential utilisation of phytoplankton species which depends on both their food value and cell size (Cucci et al., 1985; Kiørboe and Mohlenberg, 1981; Møhlenberg and Riisgård, 1978; Rouillon and Navarro, 2003). In this sense, lipids are the main source of energy for larvae and lipid content of phytoplankton varies depending on the species or group (Marshall et al., 2010; Volkman et al., 1991, 1989). Feeding experiments on *Mytilus galloprovincialis* carried out by Pettersen et al. (2010) showed that alterations in phytoplankton species composition can produce variations in mortality and settlement rates. Also, in field studies, Wall et al. (2013) found that the growth rates of bivalves were more related to the density of certain cellular types than to the total phytoplankton biomass. Therefore, the study of phytoplankton community composition is essential from the standpoint of bivalve nutrition in shellfish production areas.

Currently, there is an increasing interest in developing offshore aquaculture in regions where sheltered coastal areas are scarce or sustain activities incompatible with aquaculture (Azpeitia et al., 2016). This interest prompted the installation of an experimental bivalve farm in open waters off the Basque coast (southeastern Bay of Biscay). However, temporal variability of phytoplankton nutritional attributes and their relationships with environmental conditions needed further investigation. It is widely recognised that both top-down regulation, such as grazing (Burkill et al., 1987), and bottom-up processes driven by meteorological and hydrographic factors play a major role in the control and dynamics of phytoplankton populations (Nogueira et al., 2000; Smayda, 1998).

The Bay of Biscay is located at mid-latitude of the Northeast Atlantic Ocean and thus, here, the annual cycle corresponds to that of temperate sea areas. Winter is characterised by water column mixing, which is generated by a combination of cooling, turbulence and downwelling. This mixing process modifies the properties of the upper waters and leads to great nutrient input from deep waters to the surface. In spring, solar irradiance heats the surface resulting in an increase in the temperature of these waters and a relative stabilisation. However, the stratification of the water column depends also on the relaxation of wind, turbulence and downwelling. Summer is characterised by stratification resulting from greater solar irradiance. Finally, during autumn the surface waters cool down and the southerly and westerly winds prevail, resulting in the mixing of the water column (Fontán et al., 2008; Valencia et al., 2004).

Many studies worldwide have highlighted the seasonal periodicity of phytoplankton assemblages linked to seasonal variations in physical forcing of mixing dynamics, temperature and light regime (Agirbas et al., 2017; Diehl, 2002; Diehl et al., 2002; Leterme et al., 2014; Vajravelu et al., 2017). In the Bay of Biscay in particular, according to the seasonal cycle of hydrographic conditions, phytoplankton biomass shows two main periods related to two main events: winter mixing and summer stratification (Valdés and Moral, 1998; Varela, 1996). On the one hand, the nutrient input caused by the winter mixing leads to favourable conditions for the proliferation of the phytoplankton community and, thus, biomass peaks are usually recorded during late winter and spring. On the other hand, heating of the surface waters during summer leads to a stratified water column. The thermocline acts as a physical barrier that prevents the supply of nutrients, and phytoplankton production and biomass show the lowest values (Calvo-Díaz et al., 2008; Fernandez and Bode, 1991; Varela, 1996).

Although previous studies on phytoplankton communities had been carried out in the southern Bay of Biscay (*e.g.*, Bode and Fernández, 1992; Fernández and Bode, 1994; Varela, 1996) and, in particular, in open waters off the Basque coast (Estrada, 1982; Garmendia et al., 2011; Muñiz et al., 2017), further research was needed. The relevance of the present study is based on the inclusion of novel issues, such as the importance of phytoplankton community composition as a food resource for bivalves in waters off the Basque coast, which was not addressed before, and the variability through the water column, since most of the previous studies were limited to surface waters.

In this context, our study aims to characterize phytoplankton composition and annual variability within an experimental aquaculture farm, in relation with the good growth rates observed in mussels. Recent studies developed in that experi-

mental site indicate that mussels present good growth rates, biometry and nutritional quality (Azpeitia et al., 2016, 2017). Although chlorophyll values in the area are known to be relatively low (Estrada, 1982; Garmendia et al., 2011; Revilla et al., 2009), we hypothesise that the composition and contribution of the different major taxonomic groups could be favourable for bivalve growth. To this end, we examined phytoplankton community composition, abundance and biomass, as well as environmental conditions, through the whole water column from May 2014 to June 2015. Since the period of study covered more than one year, a complete seasonal cycle was investigated.

2. Material and methods

2.1. Study area

The Basque coast extends 100 km along the Cantabrian Sea (southeastern Bay of Biscay) (Fig. 1). The climate of the area is rainy, temperate and oceanic, with moderate winters and warm summers (Fontán et al., 2009). The Basque coast can be described as a littoral coast exposed to waves, mostly formed of cliffs and influenced by 12 short rivers. Although no large coastal plumes are formed (Diez et al., 2000), this freshwater supply modifies the chemical composition of the shelf waters and often leads to increased nutrient levels in inner shelf waters (Ferrer et al., 2009; Valencia et al., 2004).

Field samplings were carried out at a station (43°21,411′N; 2°26,918′W) immediately outside an experimental bivalve farm located at 2 nautical miles off the Basque coast, at a depth of approximately 45 m. The experimental farm used a longline system, based on a subsurface structure, from which bivalve ropes and lanterns were suspended. In particular, the installation consisted of three long lines, occupying a total area of 1 ha. Each longline sustained 100 vertical hanging ropes. The organisms cultured at the farm during the study were mainly mussels (*Mytilus galloprovincialis*) and, to a lesser extent, oysters (*Crassostrea gigas* and *Ostrea edulis*).

2.2. Sampling/laboratory strategy and data acquisition

Samplings took place from May 2014 to June 2015. CTD (conductivity, temperature and depth device) casts and Secchi disk measurements were usually performed twice per month, whereas water samples were collected monthly, except for February when sampling could not be carried out due to meteorological conditions.

In the field, a Seabird25 CTD was employed for the measurement of temperature, salinity, chlorophyll *a* and photosynthetically active radiation (PAR) at every meter of the water column. The Secchi disk depth was measured as an indicator of the water transparency. Water samples were collected using Niskin bottles at six discrete depths through the water column: 3, 10, 17, 24, 33 and 42 m.

Water samples were used for the analysis of nutrients and fractionated chlorophyll *a*, as well as phytoplankton identification and counting. Inorganic nutrients (ammonium, nitrite, nitrate, silicate and phosphate) were measured using a continuous-flow autoanalyser (Bran + Luebbe Autoanalyzer 3, Norderstedt, Germany), according to colorimetric methods described in Grasshoff et al. (1983).

In order to obtain the concentrations of the different chlorophyll *a* fractions, sequential filtrations were performed. Three size fractions were differentiated: smaller than 3 μm, between 3 and 20 μm, and larger than 20 μm, to quantify the chlorophyll contained in the pico-, nano- and microphytoplankton. Whatman Nuclepore track-etched membrane filters (pore size 3 and 20 μm) and Whatman GF/F glass microfiber filters were used, diameter 47 mm. Firstly, approximately 4.5 L of water was filtered through the polycarbonate 20 μm filter to retain the largest fraction. Then, the filtrate was passed through the polycarbonate 3 μm pore size filter to obtain the 3–20 μm fraction. Finally, the smallest fraction (<3 μm) was retained using a Whatman GF/F filter. The nominal pore size of GF/F filters is 0.7 μm, but the effective pore size of the glass-fibre filters is substantially smaller (Sheldon, 1972) and these are routinely used for picophytoplankton (Morán et al., 1999). Pigments were extracted in 10 ml of 90% acetone for 48 h in dark and cold conditions. The absorbance of the extract was measured using a UV–vis spectrophotometer (UV-2401PC Spectrophotometer, Shimadzu Corporation, Kyoto, Japan). The chlorophyll concentration was estimated according to the equations of Jeffrey and Humphrey (1975). The sum of the three fractions was used to determine if the total chlorophyll concentration was above 0.5 μg L^{-1}; this was considered the threshold below which bivalves do not filter (Dolmer, 2000; Riisgård, 2001; Riisgård et al., 2011).

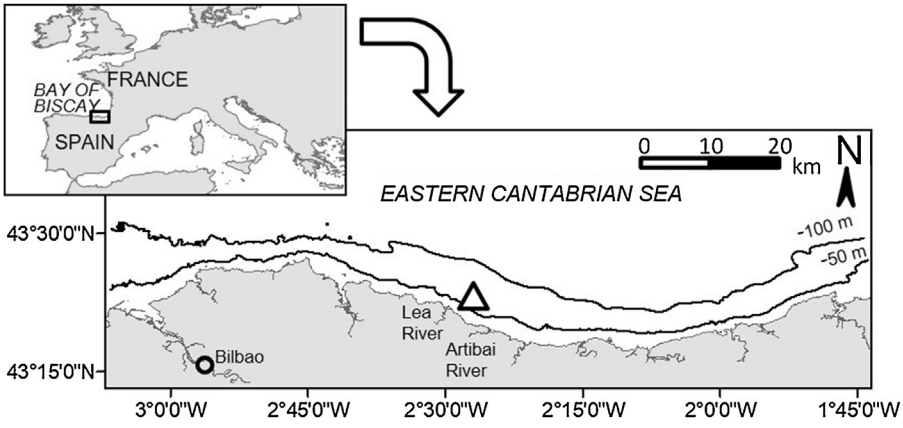

Figure 1 Map of the study area, located in the southeastern Bay of Biscay. The triangle shows the location of the experimental bivalve farm.

Phytoplankton identification and counting were conducted for three depths: 3, 17 and 33 m. Samples were preserved immediately after collection with acidic Lugol's solution (0.4% v/v) and maintained in 125-mL borosilicate bottles under dark and cool conditions (4°C) until analysis. Taxonomic identification and cell counting were performed on subsamples of 50 mL, following the Utermöhl method (Edler and Elbrächter, 2010; Hasle, 1978; Utermöhl, 1958) under a Nikon diaphot TMD inverted microscope. Depending on the organism size, 100× or 400× magnification was used; the detection limit of microscope counts for microplankton organisms was 20 cells L^{-1}. Small nanophytoplankton cells that could not be assigned to any taxonomic group were assigned to a group named "unidentified forms <10 μm". The minimum cell size that could be detected was 2–3 μm; therefore, picophytoplankton could not be identified and counted.

Three variables were used to describe hydrographic conditions: light extinction coefficient, depth of the photic zone and river flow. Light extinction coefficient (k) was estimated from the PAR measured by the CTD using the equation derived from the Beer–Lambert law:

$$I_z = I_f \cdot e^{-kz},$$

where I_z [E m^{-2} d^{-1}] is the radiation received at a specific depth, I_f is the radiation right below the surface, and z is the specific depth [m].

The k was then used to calculate the depth of the photic layer using the following equation: photic zone [m] = 4.605/k. Information on the flow rate of one of the rivers closest to the experimental site, Artibai river (Fig. 1), was obtained from a regional website ("Diputación Foral de Bizkaia", http://www.bizkaia.eus). Information on the other river surrounding the farm, Lea river, was not included due to missing data on the time series. To account for a delay in the influence of river flow on the water column conditions, flow rates were averaged for the seven days prior to the sampling day.

2.3. Data analysis

The variability of temperature and salinity was represented using a temperature-salinity (TS) diagram. The temporal variation of chlorophyll *a* through the water column (up to 45 m depth) was presented as a contour map.

Regarding phytoplankton data, the species list was standardised prior to statistical analysis according to AlgaeBase (Guiry and Guiry, 2015). The phytoplankton community was analysed according to cell concentration [cell L^{-1}] and biomass [μg C L^{-1}]. In order to calculate the latter, the biovolume of each taxon was first calculated from its equivalent spherical diameter (ESD) using the equation of the sphere's volume. Information on phytoplankton cell size was collected from two sources: (i) the ESD measured in phytoplankton species from the northwest Spanish coast by investigators from other institutions (M. Huete from the Spanish Institute of Oceanography – A Coruña Centre, and M. Varela, L. Mene and J. Lorenzo from the University of Vigo) and (ii) the report by Olenina et al. (2006). Then, biomass was determined using the equation reported by Montagnes et al. (1994) for marine phytoplankton: $Biomass = 0.109 \times Volume^{0.991}$, where *Biomass* is expressed in pg C $cell^{-1}$ and *Volume* is expressed in μm^3. For the data analyses, the specific results on abundance and biomass were combined to obtain total data for the following groups: chlorophytes, kleptoplastidic ciliates (*Mesodinium* spp.), cryptophytes, diatoms, dinoflagellates, euglenophytes, haptophytes, ochrophytes (chrysophyceans, dictyochophyceans, raphidophyceans and xanthophyceans), heterotrophic nanoflagellates (including the taxa *Ebria tripartita*, *Katablepharis remigera*, *Leucocryptos* sp. and *Telonema* sp., traditionally considered in phytoplankton studies) and unidentified forms <10 μm. For the description of phytoplankton abundance and biomass, some of these groups were merged into a group called "others". This group was primarily comprised of unidentified forms, but also included the following minority groups (*i.e.* those contributing less than 6.5% to total abundance and biomass): chlorophytes, euglenophytes, ochrophytes and heterotrophic nanoflagellates.

For the study of relationships between the environment and phytoplankton community, exploratory analysis was conducted by means of biplots representing environmental variables against phytoplankton. Correlation matrices (Pearson correlation coefficient, alpha = 0.05) were also performed. Two separate analyses were undertaken: the first one for abundance of phytoplankton groups and the second one for chlorophyll *a* fractions, as a proxy for phytoplankton biomass. The group "unidentified forms" was excluded from the correlation analysis due to its heterogeneity.

Among the environmental variables, only those that *a priori* could be considered most explanatory of phytoplankton variability were included in the analysis, namely Secchi disk depth, light extinction coefficient, temperature, salinity, Artibai river flow and nutrient concentration (ammonium, nitrite, nitrate, phosphate and silicate). Environmental variables were previously transformed in order to attain a distribution close to normal.

Phytoplankton data were processed as follows: prior to analysis, phytoplankton rare taxa, defined here as those occurring in less than 10% of the samples, were removed to avoid noise data (Austin and Greig-Smith, 1968). A total of 78 of the 194 taxa were excluded from the analysis. Phytoplankton abundance data were log-transformed (after adding one to avoid taking the log of zero values) and relationships with environmental variables were studied at depths of 3, 17 and 33 m.

Finally, chlorophyll *a* was also log-transformed prior to analysis and relationships between the three size fractions of chlorophyll and environmental variables were studied at depths of 3, 10, 17, 24, 33 and 42 m.

In ecological research, when multiple statistical tests are undertaken, each at the same significance level (alpha), the probability of achieving at least one significant result is greater than that significance level. In this context, to avoid a "Type I" error, one strategy is to correct the alpha level when performing multiple tests. The most well-known correction is called Bonferroni correction; in this study, Bonferroni sequential correction, described by Holm (1979), was applied. Statgraphics Centurion XVI software was used for the correlation matrices.

3. Results

3.1. Hydrographic, physico-chemical conditions and bulk chlorophyll *a*

The TS diagram shows the prevalence of thermohaline stratification due to spring warming and the presence of waters

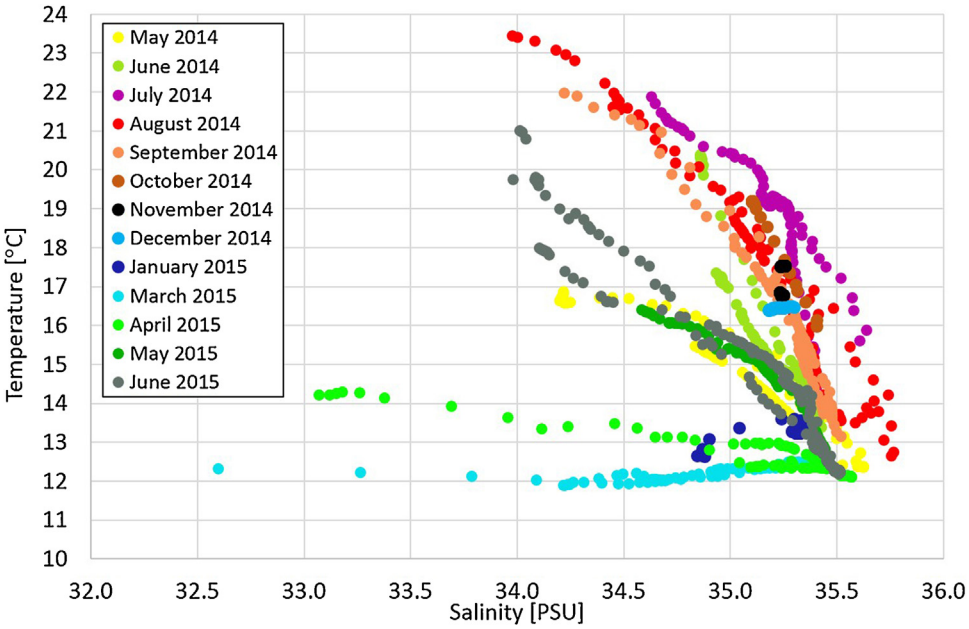

Figure 2 Temperature-Salinity diagram of the waters off the Basque coast, in the SE Bay of Biscay, from May 2014 to June 2015.

of continental origin in May 2014 (Fig. 2). The thermal stratification prevailed from June to October in relation to the progression of the summertime warming. Moreover, more or less extended haline stratification was present throughout this period. In November, a reduction of the vertical gradients of temperature and salinity was observed induced by vertical mixing and cooling. December was characterised by thermohaline homogeneity of the water column and, more importantly, by high water column temperatures (above 16°C) associated with previous warm conditions. Conversely, in January 2015, the entire water column cooled due to extremely cold winter months. This change, together with high precipitation, resulted in the prevalence of haline stratification and thermal inversion in January. The haline stratification was especially enhanced in March and April. Again, the thermal stratification was observed in May and June, induced by an extremely warm spring in 2015. Again, relatively strong haline stratification could be observed in spring 2015.

Overall, thermohaline stratification could be observed throughout the period, with a few exceptions in November–December 2014 and January–April 2015 where homogeneity and haline stratification of the water column prevailed, respectively. Additional information on river flows is included in Fig. 1 of the Supplementary Material.

Chlorophyll *a* (obtained from the fluorescence measured by the CTD) showed several peaks during the studied period (Fig. 3). At the end of May and beginning of June 2014, two deep chlorophyll peaks were observed at depths of 34 and 41 m, respectively, with values between 1.6 and 2.0 μg L^{-1}. Three other sub-surface chlorophyll increases were then detected at the end of July, beginning of August and mid-

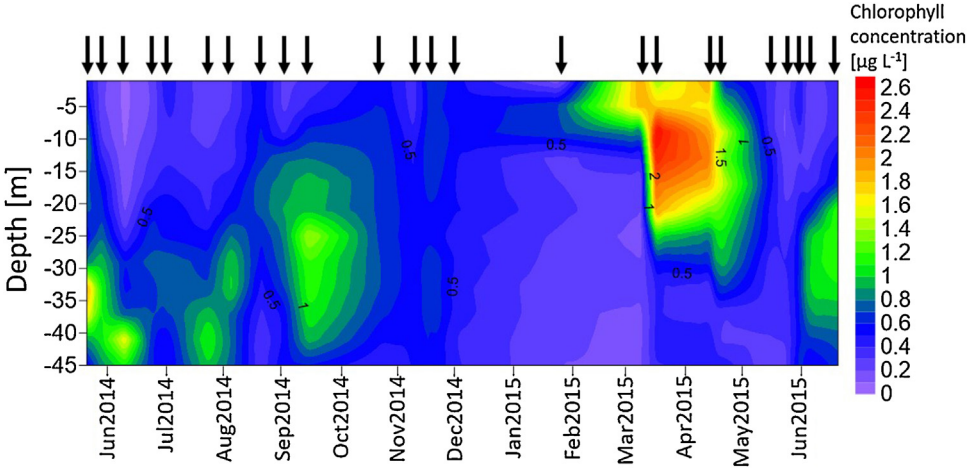

Figure 3 Contour map of chlorophyll *a* in the waters off the Basque coast from the surface to 45 m in depth. The period from May 2014 to June 2015 is represented. Arrows on the top of the plot point the dates of the samplings.

September, ranging from 1.1 to 1.4 μg L^{-1}. These were followed by a period with low values (<0.8 μg L^{-1}) from October to March. The maximum value reported was detected in March at approximately 12 m depth, reaching 2.6 μg L^{-1}. In April, a surface peak was observed (2 μg L^{-1}). Subsequently, chlorophyll concentrations decreased reaching the lowest surface values during spring 2015, although higher concentrations were detected around 20–35 m depth in June.

Table 1 shows the mean values and standard deviations of the parameters relating to the physico-chemical conditions of the study area at the different depths studied and for the whole water column. Secchi disk depth mean value was 11 m. Mean light extinction coefficient (*k*) was 0.1 m^{-1}. Photic layer depth had a mean value of 43.7 m. Mean temperature values for each depth ranged from 17.4 to 14.3°C, showing a decreasing trend from the surface to the deeper waters. In contrast, salinity increased towards the deeper water, with mean values ranging from 34.5 to 35.4. The mean chlorophyll concentrations measured by the CTD were very similar between the six depths, approximately 0.6–0.7 μg L^{-1}. The concentration of several inorganic nutrients did not present great dissimilarities between the mean values of the different sampled depths, showing ranges of 1.4–1.8 μM (ammonium), 0.3–0.4 μM (nitrite), 0.2–0.3 μM (phosphate) and 0.9–1.5 μM (silicate). However, nitrate concentration varied more through the water column, with mean values close to 1 μM within the shallower and intermediate layers (3, 10, 17 and 24 m) to a maximum of 3.0 μM at 42 m depth (additional information on nutrient concentrations is shown in Fig. 2 of the Supplementary Material).

3.2. Phytoplankton composition, abundance and biomass

With regard to phytoplankton richness, a total of 194 phytoplankton taxa were identified during these surveys. Dinoflagellates and diatoms represented the most diverse groups, comprising 47.4% and 35.1% of the total taxa described, respectively.

Phytoplankton total abundance ranged from 3.4×10^4 cells L^{-1} to 5.1×10^6 cells L^{-1}. Differences were found in relation to the different taxonomic groups. Putting aside the group of "unidentified forms", which in several samplings was the most abundant due to its heterogeneity, haptophytes were the most abundant group in 46% of the samples, followed by dinoflagellates (26%), cryptophytes (15%) and diatoms (13%). Table 2 shows the most abundant taxon in each phytoplankton group at the three sampled depths and during the two main seasons (*i.e.*, winter and summer).

The phytoplankton community differed in composition as well as in total cell density between the three sampled depths (Fig. 4). Firstly, at 3 m depth, where the highest abundance values were found, showed a maximum of approximately 5×10^6 cells L^{-1} in May 2014 (Fig. 4a), which was characterised by a large proportion of the group called "others" (mainly, unidentified forms <10 μm). During June and July, the abundance at 3 m depth dropped to just over half of that registered in May, followed by a period of low densities from August 2014 to January 2015, ranging from 1.8×10^5 to 5.0×10^5 cells L^{-1}. The end of the studied period was characterised by a first peak dominated by diatoms, contributing to more than 50% of the total abundance in March 2015, followed by an increase of the haptophyte community representing 60% of the total abundance in April 2015 (maximum abundance of 2.8×10^6 cells L^{-1}).

Similarly, at 17 m depth the highest cell densities were found at the beginning of the study period, from May to July 2014 (Fig. 4b). However, here maximum values were much lower compared to those at the 3 m depth, with the highest value of 1.3×10^6 cells L^{-1} occurring in July. This peak was dominated by the group labelled as "others". Two more increases in abundance were detected in October 2014 and April 2015, with very low values during the intervening period. The three peaks observed at 17 m depth involved an important contribution from the haptophytes, ranging from 40% to 47% of the total abundance. Dinoflagellates gradually raised their contribution within the three peaks.

The greatest depth (33 m) produced the lowest total abundance values, with a maximum of approximately 8.4×10^5 cells L^{-1} (Fig. 4c). The cell density increases

Table 1 Description (mean values and standard deviations) of the water column conditions in a bivalve culture experimental site off the Basque coast for the period May 2014–June 2015. Water-column weighted mean values, as well as the values for the six discrete sampled depths, are shown. *k*: light extinction coefficient; Chl *a* CTD: chlorophyll *a* obtained from the fluorescence measured by the CTD.

Variable	Mean ± SD						
	Water column	3 m	10 m	17 m	24 m	33 m	42 m
Secchi disk depth [m]	11.0 ± 3.5	–	–	–	–	–	–
k [m^{-1}]	0.1 ± 0.0	–	–	–	–	–	–
Photic layer depth [m]	43.7 ± 9.3	–	–	–	–	–	–
Temperature [°C]	15.6 ± 2.6	17.4 ± 3.4	16.8 ± 2.7	16.1 ± 2.4	15.4 ± 2.1	14.7 ± 2.0	14.3 ± 1.7
Salinity	35.1 ± 0.4	34.5 ± 0.5	34.9 ± 0.3	35.1 ± 0.2	35.2 ± 0.1	35.3 ± 0.1	35.4 ± 0.1
Chl *a* CTD [μg L^{-1}]	0.6 ± 0.4	0.6 ± 0.5	0.6 ± 0.6	0.7 ± 0.5	0.7 ± 0.3	0.7 ± 0.4	0.6 ± 0.3
Ammonium [μM]	1.5 ± 0.6	1.4 ± 0.7	1.4 ± 0.7	1.8 ± 0.9	1.7 ± 1.2	1.4 ± 0.5	1.4 ± 0.8
Nitrite [μM]	0.3 ± 0.2	0.3 ± 0.2	0.3 ± 0.2	0.3 ± 0.2	0.4 ± 0.3	0.4 ± 0.2	0.4 ± 0.2
Nitrate [μM]	1.4 ± 1.5	1.0 ± 1.7	0.9 ± 1.6	0.9 ± 1.3	1.1 ± 1.4	1.9 ± 2.2	3.0 ± 2.6
Phosphate [μM]	0.2 ± 0.1	0.2 ± 0.1	0.2 ± 0.1	0.2 ± 0.1	0.2 ± 0.1	0.2 ± 0.1	0.3 ± 0.1
Silicate [μM]	1.1 ± 0.6	1.5 ± 1.1	1.2 ± 0.9	1.0 ± 0.6	0.9 ± 0.5	1.1 ± 0.7	1.5 ± 0.8

Table 2 List of the most abundant taxon in each phytoplankton group at three different sampled depths and during the two main seasons (*i.e.*, winter and summer). The winter season includes two surveys (January and March 2015) and the summer season includes four surveys (July, August and September 2014 and June 2015).

Season	Depth [m]	Group	Taxon	Abundance [cells L^{-1}]
Winter	3	Cryptophytes	*Teleaulax* spp.	1.2×10^5
		Dinoflagellates	*Heterocapsa* sp.	3.1×10^5
		Diatoms	*Thalassiosira* sp.	1.3×10^6
		Haptophytes	Prymnesiales	1.4×10^5
		Ciliates	*Mesodinium* sp.	4.2×10^3
		Others	Unidentified forms	1.9×10^5
	17	Cryptophytes	Cryptophycophyta	1.9×10^4
		Dinoflagellates	*Heterocapsa* sp.	1.2×10^4
		Diatoms	Pennales 10-50 μm	4.2×10^3
		Haptophytes	Prymnesiales	8.5×10^3
		Ciliates	*Mesodinium* sp.	2.2×10^2
		Others	Unidentified forms	2.2×10^4
	33	Cryptophytes	Cryptophycophyta	9.6×10^3
		Dinoflagellates	Gymnodiniales <20 μm	7.8×10^3
		Diatoms	Pennales <10 μm	3.5×10^3
		Haptophytes	Prymnesiales	9.6×10^3
		Ciliates	*Mesodinium* sp.	80
		Others	Unidentified forms	1.5×10^4
Summer	3	Cryptophytes	*Plagioselmis* sp.	4.9×10^4
		Dinoflagellates	Gymnodiniales <20 μm	6.6×10^4
		Diatoms	*Pseudo-nitzschia galaxiae*	2.5×10^5
		Haptophytes	Prymnesiales	9.8×10^5
		Ciliates	*Mesodinium* sp.	1.1×10^3
		Others	Unidentified forms	7.4×10^5
	17	Cryptophytes	*Plagioselmis* sp.	2.5×10^4
		Dinoflagellates	Gymnodiniales <20 μm	8.9×10^4
		Diatoms	*Chaetoceros* sp.	6.8×10^4
		Haptophytes	Prymnesiales	5.4×10^5
		Ciliates	*Mesodinium* sp.	40
		Others	Unidentified forms	6.1×10^5
	33	Cryptophytes	*Plagioselmis* sp.	3.6×10^4
		Dinoflagellates	Gymnodiniales <20 μm	8.5×10^4
		Diatoms	Pennales <10 μm	4.7×10^4
		Haptophytes	Prymnesiales	3.3×10^5
		Ciliates	*Mesodinium* sp.	9.6×10^3
		Others	Unidentified forms	3.1×10^5

observed in July and October 2014 were concurrent with the first two peaks observed at the 17 m depth. Very low abundances were registered from December 2014 to May 2015, between 1.1×10^5 and 1.4×10^5 cells L^{-1}, followed by a six-fold increase in June 2015. As with the intermediate depth (17 m), dinoflagellate abundance slightly increased during the peaks.

The comparison of biomass variability with abundance variability showed that most of the peaks or increases were simultaneous in time and space (Fig. 5). However, the greatest difference was the relative contribution of each group.

The highest biomass values were observed at 3 m, with a maximum of 435 μg C L^{-1}. The contribution of the different phytoplankton groups to the peaks of May and July 2014 was similar compared to abundance values, being dominated by small unidentified forms and haptophytes. Nevertheless, from December 2014 to March 2015 diatoms dominated the community, representing between 54% and 78% of the total biomass (Fig. 5a).

At the intermediate depth (17 m), biomass values were notably lower than at the 3 m depth, ranging from 9 to 104 μg C L^{-1} (Fig. 5b). Similar to the shallower depth studied, diatoms were the dominant group from December 2014 to March 2015 (44–79% of the total biomass). The occasional and significant contribution of ciliates (represented by the genus *Mesodinium*) during the peak of April 2015 was also notable, representing 30% of the total biomass. Dinoflagellates gained importance during the biomass increases, especially in September when they represented 33% of the total biomass.

Finally, the range of biomass values at the 33 m depth was similar to that at 17 m, with the exception of the occurrence of a larger peak which reached 153 μg C L^{-1} in May 2014 (Fig. 5c). Diatoms dominated the community in May and June

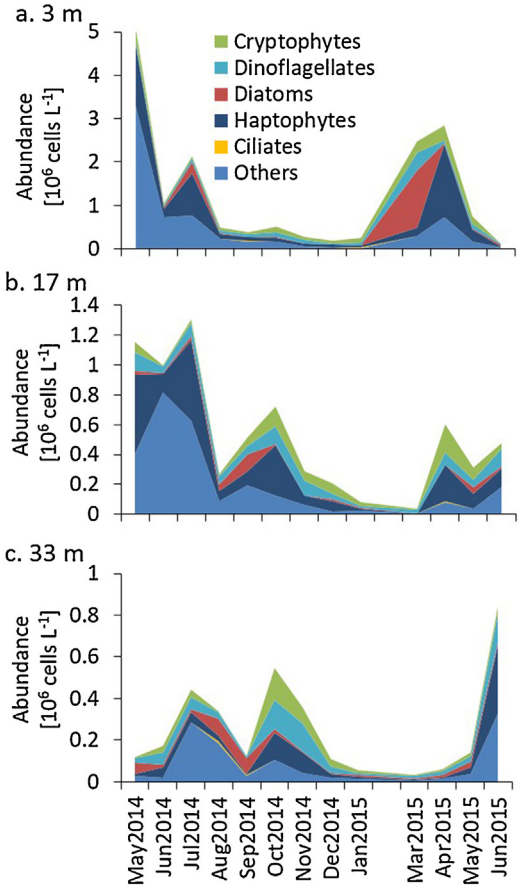

Figure 4 Contribution of each of the major phytoplankton groups to the total abundance per sample at three different depths (3, 17 and 33 m). The group "others" consisted of chlorophytes, euglenophytes, ochrophytes, heterotrophic nanoflagellates and unidentified forms. Note that plots have different scaled y axes.

2014 and from January to May 2015, representing 74—95% of the total biomass. In August 2014, ciliates contributed 44% of the total biomass.

3.3. Size-fractionated chlorophyll *a*

The relative contribution of the three chlorophyll size fractions was studied at six depths (Fig. 6). Overall, the picophytoplankton made the greatest contribution. However, an increase in the nanophytoplankton was observed towards the greatest depths (33 and 42 m). Results for May 2014 at the 33 m depth were remarkable, with 58% of the total chlorophyll provided by the microphytoplankton (Fig. 6e).

Total chlorophyll *a* concentrations, estimated from the sum of the three size fractions studied, showed values lower than 1 $\mu g\ L^{-1}$ in most of the samples. The highest concentrations were observed in March 2015, with approximately 6 $\mu g\ L^{-1}$ at the 3 m depth and 2.5 $\mu g\ L^{-1}$ at the 10 m depth, although values were still low in deeper samples. One month later, in April 2015, secondary peaks were found at depths of 3 to 24 m. Similar peaks were also detected in late spring 2014 at depths of 33 m and 42 m.

Total chlorophyll concentration was above the 0.5 $\mu g\ L^{-1}$ threshold in 62% of the samples. The depth of 42 m showed the highest proportion of values below that value (67% of the samples). Overall, chlorophyll concentrations below 0.5 $\mu g\ L^{-1}$ were found during the summer.

3.4. Relationship between environmental variables and phytoplankton community

Several strong linear relationships were found between some environmental variables and both phytoplankton abundance and chlorophyll *a* measured in the laboratory (as a proxy for phytoplankton biomass).

Firstly, the relationships between environment and abundance of phytoplankton groups at each depth were studied (Table 3). Biplots for each significant correlation are shown in Fig. 3 of the Supplementary Material.

At 3 m, total abundance of phytoplankton was not significantly correlated with any environmental variable. Some of the minor groups, such as chlorophytes and heterotrophic nanoflagellates, showed inverse correlations with different environmental variables. Ciliates (*Mesodinium* spp.) appeared to reach higher abundance at higher values of light extinction coefficient.

Overall, at 17 m depth, some nutrients were the main variables that explained phytoplankton abundance. Ammonium concentration significantly explained the variability of chlorophytes and dinoflagellates, showing a direct correlation. Nitrate showed a strong inverse relationship with total abundance of phytoplankton and, in particular, with dinoflagellates and haptophytes. Finally, silicate partly explained the variability of heterotrophic nanoflagellate abundance (inverse correlation). In addition, Artibai river flow showed inverse correlation with total abundance.

Finally, the greatest number of significant linear correlations was found at a depth of 33 m. However, some of these correlations should be viewed with caution since there were several 'zero' values in the dependent variable. Similar to the pattern observed at the 17 m depth, Artibai river flow showed inverse correlation with total abundance of phytoplankton and, in particular, with diatom abundance. Cryptophytes showed greater abundance at higher temperature and lower salinity.

Similarly, relationships between environment and different chlorophyll size fractions were ascertained at six depths: 3, 10, 17, 24, 33 and 42 m (Table 4). Biplots for each significant correlation are shown in Fig. 4 to Fig. 9 of the Supplementary Material.

At the 3 m depth, temperature, nitrate and silicate concentration were the variables explaining most of the variability of the different chlorophyll fractions: higher chlorophyll values were found at lower temperatures and higher nitrate concentrations. Higher concentrations of the chlorophyll fraction of 3—20 μm were found at lower Secchi disk depths and at higher silicate concentrations. Similar results were obtained at the 10 m depth: higher chlorophyll values were observed at lower temperatures and at higher nitrate and silicate concentrations. In addition, the chlorophyll fraction of 3—20 μm was associated with lower Secchi disk depths, whereas the larger fraction (>20 μm) was directly related to Artibai river flow.

At the 17 m depth, variability of chlorophyll was explained to a lesser extent by environmental variables

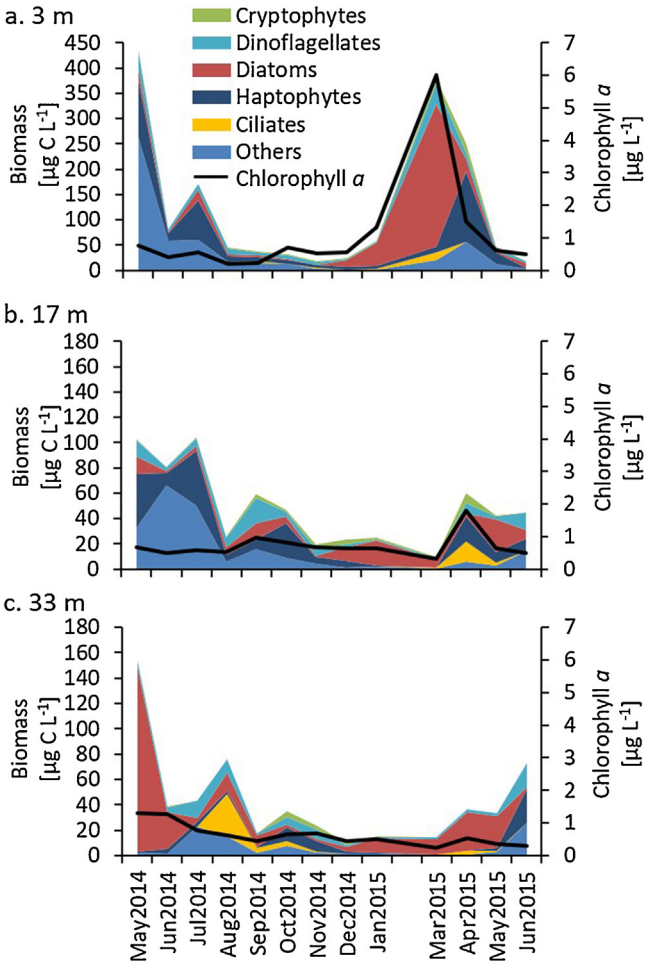

Figure 5 Contribution of each of the major phytoplankton groups to the total biomass per sample at three different depths. The group "others" consisted of chlorophytes, euglenophytes, ochrophytes, heterotrophic nanoflagellates and unidentified forms. The black line represents total chlorophyll *a* concentration [$\mu g\ L^{-1}$] obtained by means of chemical analysis (right axis).

compared to the shallower depths. Only the chlorophyll fraction of 3–20 μm showed significant correlation with the environment, with higher values at lower temperatures and higher silicate concentrations. At the 24 m depth, silicate was the only variable explaining chlorophyll variability: the 3–20 μm fraction was directly correlated with silicate concentration.

At the 33 m depth, temperature, nitrate and silicate concentrations significantly explained the variability of the small chlorophyll fraction, but with the opposite pattern to that observed at 3, 10, 17 and 24 m: higher chlorophyll values were found at higher temperatures and lower nutrient concentrations. The large fraction (>20 μm) was directly related to salinity. Finally, at the 42 m depth, the small (<3 μm) and large (>20 μm) chlorophyll fractions were inversely correlated with silicate concentration. Higher concentrations of the intermediate chlorophyll fraction (3–20 μm) were found at lower Secchi disk depths. In contrast, the large fraction presented lower values as the light extinction coefficient increased.

4. Discussion

The study area showed the typical hydrographic conditions of temperate coastal zones (Mann and Lazier, 1991), previously described for the Bay of Biscay (Valdés and Moral, 1998; Valencia et al., 2004; Varela, 1996). The sea surface appeared stratified during summer months, due to heating by solar irradiation (Varela, 1996). Late autumn and winter were mostly characterised by vertical mixing, which might be generated by a combination of cooling, turbulence and downwelling processes (Valencia and Franco, 2004; Valencia et al., 2004). The low surface salinity values observed in the present study were explained by river discharges mostly during late winter and spring.

Mixing processes are usually accompanied by changes in light and nutrient availability and, thus, growth performance of phytoplankton species within the water column is partly defined by vertical mixing (Diehl, 2002; Huisman et al., 2004). In this study, a well-mixed homogeneous water column was observed in November, December and January, when

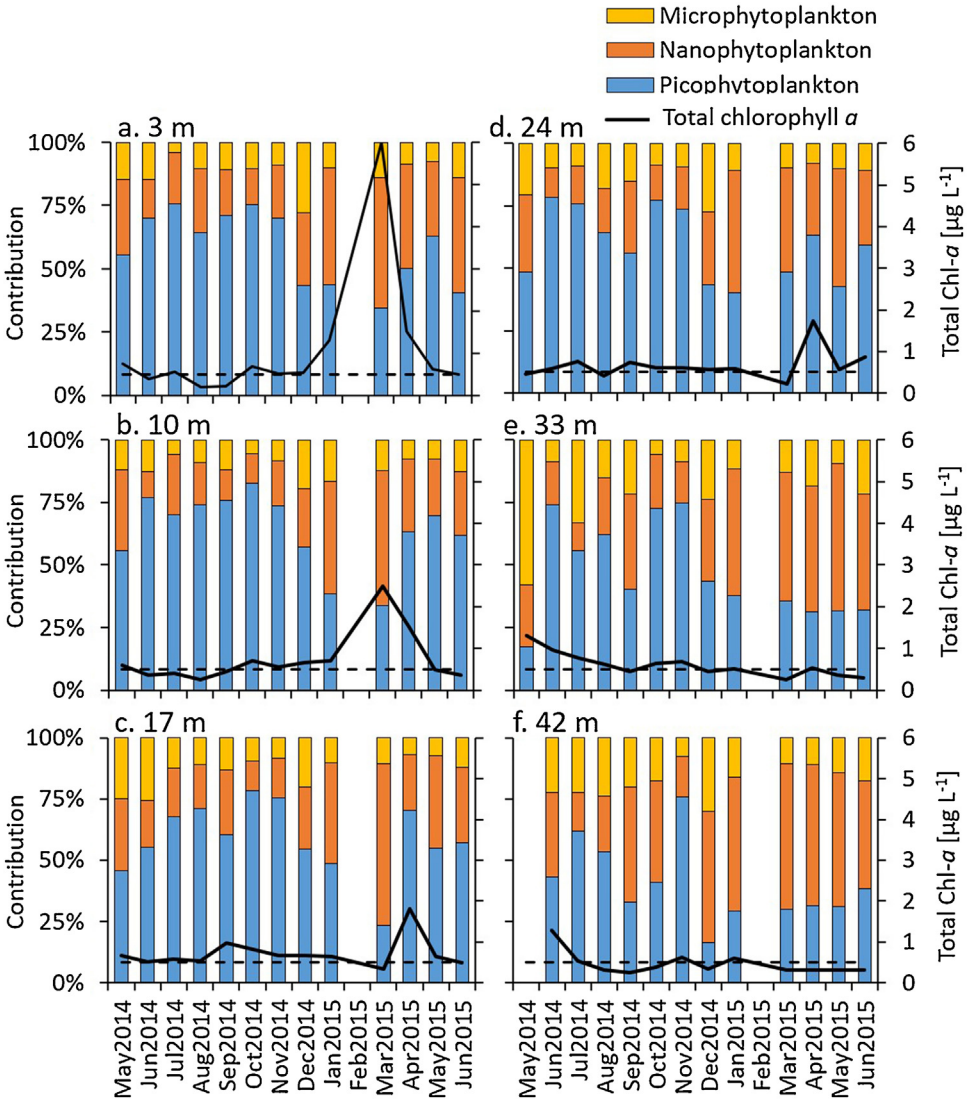

Figure 6 Chlorophyll *a* size fraction (<3 μm, 3–20 μm and >20 μm; *i.e.* pico-, nano- and micro-phytoplankton, respectively) contribution at the six depths for the period May 2014 to June 2015. Total chlorophyll *a* (sum of fractions) is shown on the right axis. The dotted line shows the chlorophyll threshold below which mussels do not filter (Dolmer, 2000; Riisgård, 2001; Riisgård et al., 2011). This threshold should be viewed with caution since it was not developed for open waters (see Section 4).

phytoplankton abundance and biomass showed the lowest values or a decreasing trend. As described by Fernandez and Bode (1991), during this period, although an upward flux of nutrients from deep water layers occurs as a consequence of the mixing, phytoplankton biomass is expected to be low due to limited light. From January onwards, surface phytoplankton abundance and biomass, as well as chlorophyll concentration, started to increase. This increase notably coincided with nutrient input, reaching a maximum in March–April. In particular, these peaks in surface waters were characterised by a high contribution of diatoms, as shown in other late winter blooms previously described in the southern Bay of Biscay (Guillaud et al., 2008; Labry et al., 2001). This fact also agrees with Margalef (1978), who found that strong vertical mixing favours the dominance of diatoms. According to Margalef's mandala, dinoflagellates are expected to be favoured in stratified water columns, where they show competitive advantage over other groups based on their ability to swim to zones rich in light and nutrients (Glibert, 2016; Margalef, 1978; Smayda and Reynolds, 2003). Here, a slight increase in the contribution of dinoflagellates was detected during August–September 2014, when the water column was stratified.

Among the studied environmental variables, temperature and nutrients (mostly nitrate and silicate) seemed to be the variables that explained most of chlorophyll annual variability. The results at depths of 3 m and 10 m coincided with the winter conditions, when deeper cold and nutrient-rich water is mixed with surface waters leading to the increase in phytoplankton biomass (Valdés and Moral, 1998; Varela, 1996). According to this, the observed chlorophyll peak at these depths in March 2015 might be explained by the contemporaneous increase in nitrate and silicate concentrations and low temperatures.

Table 3 Significant correlations (alpha = 0.05, adjusted by sequential Bonferroni correction) between abundance of major phytoplankton groups and environmental variables at depths of 3 m, 17 m and 33 m. The Pearson coefficient (r) and the probability (p) are shown. k: light extinction coefficient estimated for the whole water column. Correlations with an * should be viewed with caution since there were several 'zero' values in the dependent variable.

Depth	Phytoplankton abundance	Environmental variable	r	p
3 m	Chlorophytes	Temperature	−0.553	0.0497
	Ciliates	k	0.686	0.0096*
	Heterotrophic nanoflagellates	Nitrate	−0.745	0.0035
		Phosphate	−0.638	0.0190
17 m	Chlorophytes	Ammonium	0.621	0.0236
	Dinoflagellates	Ammonium	0.658	0.0145
		Nitrate	−0.628	0.0214
	Haptophytes	Nitrate	−0.651	0.0159
	Heterotrophic nanofl.	Silicate	−0.559	0.0471
	Total abundance	Artibai flow	−0.684	0.0099
		Nitrate	−0.749	0.0032
33 m	Chlorophytes	Phosphate	0.749	0.0032*
	Cryptophytes	Temperature	0.688	0.0093
		Salinity	−0.755	0.0028
	Diatoms	Artibai flow	−0.687	0.0095
	Euglenophytes	Nitrite	−0.686	0.0095*
	Heterotrophic nanoflagellates	k	−0.644	0.0175*
		Ammonium	0.705	0.0071*
	Ochrophytes	Secchi disk depth	0.589	0.0340*
	Total abundance	Artibai flow	−0.570	0.0419

In contrast, different results were obtained for phytoplankton abundance. Neither temperature nor silicate explained the variability in total abundance. Among the significant correlations between environmental variables and abundance of phytoplankton groups, the fewest number of correlations was found at the 3 m depth. In fact, previously it had been found that environmental variables explained little about phytoplankton group variability (usually <16%, except in winter when this was 24%) in surface waters off the Basque coast, although the explained variability was higher at the species level (Muñiz et al., 2018). At 17 m, a reduced total abundance coincided with higher river flow and nitrate concentrations. Nitrate has been found to be linked to river discharges into the Basque coastal waters (Borja et al., 2016). This situation would reflect winter conditions, when river flows are high and phytoplankton abundance is low. Indeed, the low abundance of dinoflagellates during winter conditions (and its inverse relation with nitrate) is consistent again with the reported preference of this group for summer stratified waters. Variability in the abundance of dinoflagellates at 17 m was also explained by ammonium concentrations. This observed direct relationship is in accordance with the well-established concept that ammonium is the preferred nitrogen source for marine phytoplankton, with the exception of diatoms, that have shown higher nitrate uptake rates (Heil et al., 2007; Walsh and Dugdale, 1971). Specifically, in the case of dinoflagellates, Li et al. (2010) found the higher acquisition of reduced forms of nitrogen, such as ammonium.

As mentioned before, the variability explained by the environment was different for chlorophyll concentration and for phytoplankton abundance. Although chlorophyll *a* has long been used as a proxy for phytoplankton biomass, it is well known that chlorophyll *a* concentration, phytoplankton biomass (in carbon units) and cell abundance are three different attributes of the phytoplankton community (Domingues et al., 2008). Therefore, different results can be expected from each of them. In the present study, marked differences were found between chlorophyll concentrations and biomass (determined from biovolumes and cell densities). It should be considered that there is an associated error when biomass is calculated from the ESD and the abundance. In addition, the ratio of carbon biomass to chlorophyll in the cell is highly variable, both at intra- and inter-specific levels, and also depending on environmental conditions, mainly light and nutrients (Domingues et al., 2008; Ríos et al., 1998; Taylor et al., 1997).

Overall, chlorophyll values were low compared to adjacent areas, such as the Atlantic French coast with median values from 1.2 to 3.2 $\mu g\ L^{-1}$ (Fariñas et al., 2015); the euhaline zone of Basque estuaries with median values about 2 $\mu g\ L^{-1}$ from spring to autumn (Garmendia et al., 2011), or the Galician Rias with values up to 20 $\mu g\ L^{-1}$ (Varela et al., 2008). For two stations off the Basque coast located at a depth of nearly 50 m, similar to the one studied here, Estrada (1982) found similar results to the ones described above: overall, chlorophyll values ranged between 0 and 1 $\mu g\ L^{-1}$ during the year, showing occasional peaks in the winter. In the present study, during most of the year phytoplankton biomass was dominated by picophytoplankton. However, at the time of maximum biomass, a relative decrease in the contribution of the smallest fraction compared to the larger ones could be noticed. This is in accordance with the findings by Calvo-Díaz et al. (2008) reported for the central Cantabrian Sea.

Similarly, for an eventual estimation of the capacity of the Basque coast for bivalve aquaculture, it is also relevant the

Table 4 Significant correlations (alpha = 0.05, adjusted by sequential Bonferroni correction) between chlorophyll *a* size fractions analysed at the laboratory and environmental variables at depths of 3, 10, 17, 24, 33 and 42 m. The Pearson coefficient (*r*) and the probability (*p*) are shown. *k*: light extinction coefficient estimated for the whole water column.

Depth	Chlorophyll *a*	Environmental variable	*r*	*p*
3 m	Chl <3 μm	Temperature	−0.833	0.0004
		Nitrate	0.621	0.0236
	Chl 3–20 μm	Secchi disk depth	−0.759	0.0026
		Temperature	−0.864	0.0001
		Nitrate	0.783	0.0015
		Silicate	0.839	0.0003
	Chl >20 μm	Temperature	−0.814	0.0007
		Nitrate	0.806	0.0009
		Silicate	0.696	0.0082
10 m	Chl <3 μm	Temperature	−0.654	0.0152
	Chl 3–20 μm	Secchi disk depth	−0.796	0.0011
		Temperature	−0.870	0.0001
		Nitrate	0.785	0.0015
		Silicate	0.899	0.0000
	Chl >20 μm	Temperature	−0.864	0.0001
		Artibai flow	0.687	0.0095
		Nitrate	0.830	0.0004
		Silicate	0.813	0.0007
17 m	Chl 3–20 μm	Temperature	−0.800	0.0010
		Silicate	0.735	0.0042
24 m	Chl 3–20 μm	Silicate	0.714	0.0061
33 m	Chl <3 μm	Temperature	0.677	0.0111
		Nitrate	−0.718	0.0057
		Silicate	−0.895	0.0000
	Chl >20 μm	Salinity	0.633	0.0201
42 m	Chl <3 μm	Silicate	−0.755	0.0045
	Chl 3–20 μm	Secchi disk depth	−0.747	0.0052
	Chl >20 μm	*k*	−0.662	0.0189
		Silicate	−0.648	0.0226

information about the phytoplankton primary production in this area, and how it compares with other coastal areas (*e.g.*, Figueiras et al., 2002). Maps of primary production depicted from recent satellite-based data are available at http://www.bio-oracle.org/explore-data.php (Assis et al., 2018; Tyberghein et al., 2012). These maps show relatively low values in the surface waters of the Basque coast in comparison with other coastal areas within the Bay of Biscay, which is in accordance with the low values of chlorophyll "*a*" found in this study, and previously reported by other authors. As regards for direct measurements of primary production in the marine environment of the Basque Country, these have been undertaken mostly in estuaries and only one study can be cited for open marine waters (Orive et al., 2004; Valencia et al., 1989). An additional study can be considered representative of these waters, as it was conducted in the Cap Ferret Canyon, about 150 km off the Basque coast, on the French shelf (Laborde et al., 1999). The values obtained in surface waters of these two locations resulted lower than those measured in the nearby estuarine environments of Plencia and Urdaibai (Basque Country) and Arcachon Bay (France) (Table 5). However, primary production rates per unit area measured in both studies were of similar magnitude that those obtained, some years later, by Labry et al. (2002) in a northward location influenced by the discharges of the Gironde river, one of the two largest rivers on the French Atlantic coast, and also by Glé et al. (2008) in the mesotrophic Arcachon Bay. The photic layer-integrated production rates can result more similar among those systems due to the occurrence of sub-surface peaks in the offshore waters, as those described by Laborde et al. (1999). In any case, the highest photic layer integrated rates that have been cited for open waters off the Basque coast and for the Cap Ferret Canyon waters are much lower than the maxima cited in the Galician rias, an area of the Iberian coast influenced by upwelling (Bode and Varela, 1998; Cermeño et al., 2006; Figueiras et al., 2002; Tilstone et al., 1999).

In relation to mussel filtration, not all of the seston is available as food for these bivalves. Although controversy still exists, it has been reported by some authors that mussels do not filter below a chlorophyll threshold of around 0.5 μg L^{-1} (Dolmer, 2000; Riisgård, 2001). This threshold should be viewed with caution since it was not developed for open waters. Although on some occasions chlorophyll concentrations were below this limit, the annual average value was slightly above this value. Nevertheless, despite chlorophyll

Table 5 Phytoplankton primary production rates cited for some locations selected within the Bay of Biscay and the northwest coast of the Iberian Peninsula. Most methods involved the ^{14}C incorporation technique. The incubation period has been indicated, as it can affect primary production estimates (Regaudie-de-Gioux et al., 2014).

Geographical area	Environment	Location	Study period	Surface [mg C m^{-3} d^{-1}]	Photic zone integrated rates [mg C m^{-2} d^{-1}]	Method and incubation time	Reference
Bay of Biscay	Open marine waters	Basque coast (43°25′N, 2°W)	April 1986 to April 1987	<1–47[a]	<50–600[a]	^{14}C (2 h)	Valencia et al. (1989)
		Cap Ferret Canyon (44°45′N, 2°W)	Spring, summer and autumn (1989–1991)	4–144	262–1537	^{14}C (2 h)	Laborde et al. (1999)
		Oceanic waters off the Gironde	Early winter to late spring (1998)	–	15–990	^{14}C (8–14 h)	Labry et al. (2002)
		Gironde plume	Early winter to late spring (1998)	–	28–1329	^{14}C (8–14 h)	Labry et al. (2002)
	Euhaline and polyhaline waters in partially enclosed systems	Plencia Bay	February to June (1985)	0.8–153[a]	–	^{14}C (3 h)	Elósegui et al. (1987)
		Urdaibai estuary (lower station)	Annual cycle (1996–1997)	38–387[b]	–	Dark-Light method (24 h)	Revilla et al. (2000)
		Arcachon Bay	Annual cycle (2003)	<50–497	<175–1740[c]	^{14}C (24 h)	Glé et al. (2008)
Northwest Iberian Peninsula	Upwelling-influenced systems	Rías Baixas (Vigo)	Annual cycle (2001–2002)	16.5–1100[a]	224–9950[a]	^{14}C (2 h)	Cermeño et al. (2006)
		Rías Baixas (Vigo)	Spring, summer and autumn (1993)	–	65–3690	^{14}C (2 h)	Tilstone et al. (1999)
		Rías Altas (Ares, Ferrol, La Coruña Bay)	March, August and December (1993)	–	Maximum > 3000	^{14}C (≥2 h)	Bode and Varela (1998)

[a] Original data were expressed in hour units. For comparative purposes, daily rates have been derived assuming a constant photoperiod of 10 h (Cermeño et al., 2006).
[b] Gross oxygen production has been transformed to particulate carbon production using a photosynthetic quotient of 2.2 obtained by Iriarte et al. (1997) in the Urdaibai estuary.
[c] Rates per surface area have been calculated using 3.5 m, the approximate mean depth of Arcachon Bay (Glé et al., 2008).

concentrations being not very high in comparison to other areas where bivalve aquaculture has traditionally developed (Figueiras et al., 2002; Varela et al., 2008), it has previously been reported that mussels from the experimental site off the Basque coast show good growth and biochemical performance, with similar mean chlorophyll values to the ones described here (Azpeitia et al., 2016, 2017).

In addition, the dominance of the diatoms during spring peaks in biomass, together with the relevant contribution of dinoflagellates to the sub-surface abundance and biomass, suggests favourable conditions for mussel culture, since some of the important fatty acids for bivalve growth (EPA, Eicosapentaenoic acid; and DHA, Docosahexaenoic acid) are known to be synthesised by these two groups (*e.g.*, Azpeitia et al. (2016)). Experiments on mussel nutrition, in terms of carbon biomass, have also shown highest retention of diatoms and dinoflagellates, together with ciliates, compared to other phytoplankton groups (Trottet et al., 2008). Moreover, direct correlations have been reported between diatoms and bivalve growth (Beukema and Cadée, 1991; Pernet et al., 2012; Wall et al., 2013; Weiss et al., 2007). Thompson et al. (1993) found that diets containing high levels of saturated fats were more nutritious for oyster larvae. The observed high contribution of haptophytes also suggests favourable conditions for bivalve growth, since they have been reported to contain, on average, the highest proportion of saturated fats (33%), followed by diatoms (27%) (Volkman et al., 1991, 1989). In this study, one genus of ciliates (*Mesodinium* spp.) and four taxa of heterotrophic nanoflagellates (*Ebria tripartita*, *Katablepharis remigera*, *Leucocryptos* sp. and *Telonema* sp.) were taken into account. However, for future studies it would be of interest to account for all the nanoheterotrophs and ciliates, given their significant role as a food source for mussels (Trottet et al., 2008).

Some of the observed results from the water column, such as the higher phytoplankton abundance and biomass registered at shallower depths in comparison to the greater depths, suggest that bivalves would grow better in shallower waters. Furthermore, abundance and biomass of diatoms, dinoflagellates and haptophytes (*i.e.* the groups with the highest fatty acid content) were lower at the 33 m depth. In contrast, some subsurface chlorophyll maxima were found during the summer. Also, as previously mentioned, the chlorophyll size fractions above 3 μm (corresponding to nano- and micro-phytoplankton) appeared to increase slightly towards the greatest depths that were sampled. These size fractions are the ones of interest for the correct growth of bivalves as, although there is still considerable controversy, the majority of the studies indicate that the minimum particle size for efficient retention is 4 μm (Jørgensen, 1990; Møhlenberg and Riisgård, 1978; Riisgard, 1988). Azpeitia et al. (2016) analysed mussels from the same experimental site to compare whether there were differences between two culture depths. They found significant differences between mussels cultured at 5 m and at 15 m in terms of dry weight, length, shell shape and density, but not for any of the biochemical parameters analysed, such as fatty acid content. Nevertheless, they concluded that these differences might not lessen the quality of the final product.

In summary, the water column conditions in open waters off the Basque coast were characterised by the classical seasonal cycle of temperate areas at mid-latitudes of the Northeast Atlantic. These hydrographic and environmental conditions influenced to a great extent the vertical distribution and temporal variability of the phytoplankton community. The overall phytoplankton community found through the water column in the experimental site seemed to be suitable for bivalve aquaculture, based on the dominance of diatoms, dinoflagellates and haptophytes, and a chlorophyll concentration that was above the reported threshold for bivalve filtration in most of the samples collected. Composition and contribution of the major groups were in accordance with the reported requirements for mussel growth. Although chlorophyll values were found to be relatively low during some periods, this may not be a problem for the good performance of mussels, as other authors who found very similar average chlorophyll values have previously reported good growth and biochemical composition in mussels from the experimental site.

Acknowledgements

This work was supported by the projects “IM13OSTREA”, “IM16SIMMA” and “IM17MUSSELS”, funded by the Department of Economic Development and Competitiveness of the Basque Government. O. Muñiz was funded by a grant from the same Department (BOPV núm. 201; 2013/4467). Useful suggestions and comments by two anonymous reviewers greatly improved the manuscript. We thank Proof-Reading-Service for their great professional proof reading and editing service. This paper is contribution 872 from AZTI-Tecnalia (Marine Research Division).

Appendix A. Supplementary data

Supplementary material related to this article can be found, in the online version, at doi:https://doi.org/10.1016/j.oceano.2018.08.001.

References

Agirbas, E., Koca, L., Aytan, U., 2017. Spatio-temporal pattern of phytoplankton and pigment composition in surface waters of south-eastern Black Sea. Oceanologia 59 (3), 283—299, http://dx.doi.org/10.1016/j.oceano.2017.03.004.

Assis, J., Tyberghein, L., Bosch, S., Verbruggen, H., Serrao, E.A., De Clerck, O., 2018. Bio-ORACLE v2.0: extending marine data layers for bioclimatic modelling. Glob. Ecol. Biogeogr. 27 (3), 277—284, http://dx.doi.org/10.1111/geb.12693.

Austin, M.P., Greig-Smith, P., 1968. The application of quantitative methods to vegetation survey: II. Some methodological problems of data from rain forest. J. Ecol. 56 (3), 827—844, http://dx.doi.org/10.2307/2258109.

Azpeitia, K., Ferrer, L., Revilla, M., Pagaldai, J., Mendiola, D., 2016. Growth, biochemical profile, and fatty acid composition of mussel (*Mytilus galloprovincialis* Lmk.) cultured in the open ocean of the Bay of Biscay (northern Spain). Aquaculture 454, 95—108, http://dx.doi.org/10.1016/j.aquaculture.2015.12.022.

Azpeitia, K., Ríos, Y., Garcia, I., Pagaldai, J., Mendiola, D., 2017. A sensory and nutritional validation of open ocean mussels (*Mytilus galloprovincialis* Lmk.) cultured in SE Bay of Biscay (Basque Country) compared to their commercial counterparts from Galician Rías (Spain). Int. Aquat. Res. 9 (2), 1—18, http://dx.doi.org/10.1007/s40071-017-0159-0.

Beukema, J., Cadée, G., 1991. Growth rates of the bivalve *Macoma balthica* in the Wadden Sea during a period of eutrophication: relationships with concentrations of pelagic diatoms and flagellates. Mar. Ecol. Prog. Ser. 68 (3), 249—256, http://dx.doi.org/10.3354/meps068249.

Blanton, J.O., Tenore, K.R., Castillejo, F., Atkinson, L.P., Schwing, F. B., Lavin, A., 1987. The relationship of upwelling to mussel production in the rias on the western coast of Spain. J. Mar. Res. 45 (2), 497—511, http://dx.doi.org/10.1357/002224087788401115.

Bode, A., Fernández, E., 1992. Influence of water-column stability on phytoplankton size and biomass succession patterns in the central Cantabrian Sea (Bay of Biscay). J. Plankton Res. 14 (6), 885—902, http://dx.doi.org/10.1093/plankt/14.6.885.

Bode, A., Varela, M., 1998. Primary production and phytoplankton in three Galician Rias Altas (NW Spain): seasonal and spatial variability. Sci. Mar. 62 (4), 319—330.

Borja, A., Chust, G., Rodríguez, J.G., Bald, J., Belzunce-Segarra, M. J., Franco, J., Garmendia, J.M., Larreta, J., Menchaca, I., Muxika, I., Solaun, O., Revilla, M., Uriarte, A., Valencia, V., Zorita, I., 2016. 'The past is the future of the present': learning from long-time series of marine monitoring. Sci. Total Environ. 566—567, 698—711, http://dx.doi.org/10.1016/j.scitotenv.2016.05.111.

Bourlès, Y., Alunno-Bruscia, M., Pouvreau, S., Tollu, G., Leguay, D., Arnaud, C., Goulletquer, P., Kooijman, S., 2009. Modelling growth and reproduction of the Pacific oyster *Crassostrea gigas*: advances in the oyster-DEB model through application to a coastal pond. J. Sea Res. 62 (2), 62—71, http://dx.doi.org/10.1016/j.seares.2009.03.002.

Brown, M.R., 2002. Nutritional value and use of microalgae in aquaculture. In: Cruz Suárez, L.E., Ricque Marie, D., Tapia Salazar, M., Gaxiola Cortés, M.G., Simoes, N. (Eds.), Avances en Nutrición Acuícola VI. Memorias del VI Simposium Internacional de Nutrición Acuícola. 3 al 6 de Septiembre de 2002. Cancún, Quintana Roo, México. Universidad Autónoma de Nuevo Léon, Monterrey, 281—292.

Burkill, P., Mantoura, R., Llewellyn, C., Owens, N., 1987. Microzooplankton grazing and selectivity of phytoplankton in coastal waters. Mar. Biol. 93 (4), 581—590, http://dx.doi.org/10.1007/BF00392796.

Calvo-Díaz, A., Morán, X.A.G., Suárez, L.Á., 2008. Seasonality of picophytoplankton chlorophyll *a* and biomass in the central Cantabrian Sea, southern Bay of Biscay. J. Mar. Syst. 72 (1), 271—281, http://dx.doi.org/10.1016/j.jmarsys.2007.03.008.

Cermeño, P., Marañón, E., Pérez, V., Serret, P., Fernández, E., Castro, C.G., 2006. Phytoplankton size structure and primary production in a highly dynamic coastal ecosystem (Ría de Vigo, NW-Spain): seasonal and short-time scale variability. Estuar. Coast. Shelf Sci. 67 (1—2), 251—266, http://dx.doi.org/10.1016/j.ecss.2005.11.027.

Cucci, T.L., Shumway, S.E., Newell, R.C., Selvin, R., Guillard, R.R., Yentsch, C.M., 1985. Flow cytometry: a new method for characterization of differential ingestion, digestion and egestion by suspension feeders. Mar. Ecol. Prog. Ser. 24, 201—204, http://dx.doi.org/10.3354/meps024201.

Diehl, S., 2002. Phytoplankton, light, and nutrients in a gradient of mixing depths: theory. Ecology 83 (2), 386—398, http://dx.doi.org/10.1890/0012-9658(2002)083[0386:PLANIA]2.0.CO;2.

Diehl, S., Berger, S., Ptacnik, R., Wild, A., 2002. Phytoplankton, light, and nutrients in a gradient of mixing depths: field experiments. Ecology 83 (2), 399—411, http://dx.doi.org/10.1890/0012-9658(2002)083[0399:PLANIA]2.0.CO;2.

Diez, I., Secilla, A., Santolaria, A., Gorostiaga, J.M., 2000. The north coast of Spain. In: Sheppard, C. (Ed.), Seas at the Millennium: An Environmental Evaluation. Pergamon Press of Elsevier Science, Oxford, 135—150.

Dolmer, P., 2000. Feeding activity of mussels *Mytilus edulis* related to near-bed currents and phytoplankton biomass. J. Sea Res. 44 (3), 221—231, http://dx.doi.org/10.1016/S1385-1101(00)00052-6.

Domingues, R.B., Barbosa, A., Galvão, H., 2008. Constraints on the use of phytoplankton as a biological quality element within the Water Framework Directive in Portuguese waters. Mar. Pollut. Bull. 56 (8), 1389—1395.

Edler, L., Elbrächter, M., 2010. The Utermöhl method for quantitative phytoplankton analysis. In: Karlson, B., Cusack, C., Bresnan, E. (Eds.), Microscopic and Molecular Methods for Quantitative Phytoplankton Analysis. Intergovernmental Oceanographic Commission of UNESCO, Paris, 13—20.

Elósegui, A., Pozo, J., Orive, E., 1987. Plankton pulses in a temperate coastal embayment during the winter-spring transition. Estuar. Coast. Shelf Sci. 24 (6), 751—764, http://dx.doi.org/10.1016/0272-7714(87)90150-8.

Estrada, M., 1982. Ciclo anual del fitoplancton en la zona costera frente a Punta Endata (golfo de Vizcaya). Investigación Pesquera 46, 469—491.

Fariñas, T.H., Bacher, C., Soudant, D., Belin, C., Barillé, L., 2015. Assessing phytoplankton realized niches using a French national phytoplankton monitoring network. Estuar. Coast. Shelf Sci. 159, 15—27, http://dx.doi.org/10.1016/j.ecss.2015.03.010.

Fernandez, E., Bode, A., 1991. Seasonal patterns of primary production in the Central Cantabrian Sea (Bay of Biscay). Sci. Mar. 55, 629—636.

Fernández, E., Bode, A., 1994. Succession of phytoplankton assemblages in relation to the hydrography in the southern Bay of Biscay: a multivariate approach. Sci. Mar. 58 (3), 191—205.

Ferrer, L., Fontán, A., Mader, J., Chust, G., González, M., Valencia, V., Uriarte, A., Collins, M., 2009. Low-salinity plumes in the oceanic region of the Basque Country. Cont. Shelf Res. 29 (8), 970—984, http://dx.doi.org/10.1016/j.csr.2008.12.014.

Figueiras, F.G., Labarta, U., Reiriz, M.F., 2002. Coastal upwelling, primary production and mussel growth in the Rías Baixas of Galicia. Hydrobiologia 484 (1—3), 121—131, http://dx.doi.org/10.1023/A:1021309222459.

Fontán, A., Valencia, V., Borja, Á., Goikoetxea, N., 2008. Oceanometeorological conditions and coupling in the southeastern Bay of Biscay, for the period 2001—2005: a comparison with the past two decades. J. Mar. Syst. 72 (1—4), 167—177, http://dx.doi.org/10.1016/j.jmarsys.2007.08.003.

Fontán, A., González, M., Wells, N., Collins, M., Mader, J., Ferrer, L., Esnaola, G., Uriarte, A., 2009. Tidal and wind-induced circulation within the Southeastern limit of the Bay of Biscay: Pasaia Bay, Basque Coast. Cont. Shelf Res. 29 (8), 998—1007, http://dx.doi.org/10.1016/j.csr.2008.12.013.

Garmendia, M., Revilla, M., Bald, J., Franco, J., Laza-Martínez, A., Orive, E., Seoane, S., Valencia, V., Borja, Á., 2011. Phytoplankton communities and biomass size structure (fractionated chlorophyll "*a*"), along trophic gradients of the Basque coast (northern Spain). Biogeochemistry 106 (2), 243—263, http://dx.doi.org/10.1007/s10533-010-9445-2.

Glé, C., Del Amo, Y., Sautour, B., Laborde, P., Chardy, P., 2008. Variability of nutrients and phytoplankton primary production in a shallow macrotidal coastal ecosystem (Arcachon Bay, France). Estuar. Coastal Shelf Sci. 76 (3), 642—656, http://dx.doi.org/10.1016/j.ecss.2007.07.043.

Glibert, P.M., 2016. Margalef revisited: a new phytoplankton mandala incorporating twelve dimensions, including nutritional physiology. Harmful Algae 55, 25—30, http://dx.doi.org/10.1016/j.hal.2016.01.008.

Grant, J., 1996. The relationship of bioenergetics and the environment to the field growth of cultured bivalves. J. Exp. Mar. Biol. Ecol. 200 (1), 239—256, http://dx.doi.org/10.1016/S0022-0981(96)02660-3.

Grasshoff, K., Ehrhardt, M., Kremling, K., 1983. Methods of Seawater Analyses. Verlag Chemie, Weinheim, 419 pp.

Guillaud, J.-F., Aminot, A., Delmas, D., Gohin, F., Lunven, M., Labry, C., Herbland, A., 2008. Seasonal variation of riverine nutrient inputs in the northern Bay of Biscay (France), and patterns of marine phytoplankton response. J. Mar. Syst. 72 (1), 309—319, http://dx.doi.org/10.1016/j.jmarsys.2007.03.010.

Guiry, M.D., Guiry, G.M., 2015. AlgaeBase. World-wide Electronic Publication, National University of Ireland, Galway, http://www.algaebase.org.

Hasle, G.R., 1978. The inverted-microscope methods. In: Sournia, A. (Ed.), Phytoplankton Manual. UNESCO, Paris, 88—96.

Heil, C.A., Revilla, M., Glibert, P.M., Murasko, S., 2007. Nutrient quality drives differential phytoplankton community composition on the southwest Florida shelf. Limnol. Oceanogr. 52 (3), 1067—1078, http://dx.doi.org/10.4319/lo.2007.52.3.1067.

Hickman, R.W., Waite, R.P., Illingworth, J., Meredyth-Young, J.L., Payne, G., 1991. The relationship between farmed mussels, *Perna canaliculus*, and available food in Pelorus-Kenepuru Sound, New Zealand, 1983—1985. Aquaculture 99 (1), 49—68, http://dx.doi.org/10.1016/0044-8486(91)90287-H.

Holm, S., 1979. A simple sequentially rejective multiple test procedure. Scand. J. Stat. 6 (2), 65—70.

Huisman, J., Sharples, J., Stroom, J.M., Visser, P.M., Kardinaal, W.E.A., Verspagen, J.M.H., Sommeijer, B., 2004. Changes in turbulent mixing shift competition for light between phytoplankton species. Ecology 85 (11), 2960—2970, http://dx.doi.org/10.1890/03-0763.

Iriarte, A., de Madariaga, I., Diez Garagarza, F., Revilla, M., Orive, E., 1997. Primary plankton production, respiration and nitrification in a shallow temperate estuary during summer. J. Exp. Mar. Biol. Ecol. 208 (1—2), 127—151, http://dx.doi.org/10.1016/s0022-0981(96)02672-x.

Jeffrey, S.W., Humphrey, G.F., 1975. New spectrophotometric equations for determining chlorophylls *a*, *b*, c_1 and c_2 in higher plants, algae and natural phytoplankton. Biochemie und Physiologie der Pflanzen 167 (2), 191—194.

Jørgensen, C.B., 1990. Functional morphology of bivalve feeding. In: Jørgensen, C.B. (Ed.), Bivalve Filter Feeding: Hydrodynamics, Bioenergetics, Physiology and Ecology. Olsen & Olsen, Fredensborg, 4—10.

Kiørboe, T., Mohlenberg, F., 1981. Particle selection in suspension-feeding bivalves. Mar. Ecol. Prog. Ser. 5, 291—296, http://dx.doi.org/10.3354/meps005291.

Laborde, P., Urrutia, J., Valencia, V., 1999. Seasonal variability of primary production in the Cap-Ferret Canyon area (Bay of Biscay) during the ECOFER cruises. Deep Sea Res. Pt. II 46 (10), 2057—2079, http://dx.doi.org/10.1016/s0967-0645(99)00055-7.

Labry, C., Herbland, A., Delmas, D., Laborde, P., Lazure, P., Froidefond, J., Jegou, A.-M., Sautour, B., 2001. Initiation of winter phytoplankton blooms within the Gironde plume waters in the Bay of Biscay. Mar. Ecol. Prog. Ser. 212, 117—130, http://dx.doi.org/10.3354/meps212117.

Labry, C., Herbland, A., Delmas, D., 2002. The role of phosphorus on planktonic production of the Gironde plume waters in the Bay of Biscay. J. Plankton Res. 24 (2), 97—117, http://dx.doi.org/10.1093/plankt/24.2.97.

Leterme, S.C., Jendyk, J.-G., Ellis, A.V., Brown, M.H., Kildea, T., 2014. Annual phytoplankton dynamics in the gulf saint Vincent, south Australia, in 2011. Oceanologia 56 (4), 757—778, http://dx.doi.org/10.5697/oc.56-4.757.

Li, J., Glibert, P.M., Zhou, M., 2010. Temporal and spatial variability in nitrogen uptake kinetics during harmful dinoflagellate blooms in the East China Sea. Harmful Algae 9 (6), 531—539, http://dx.doi.org/10.1016/j.hal.2010.03.007.

MacDonald, B.A., Ward, J.E., 1994. Variation in food quality and particle selectivity in the sea scallop *Placopecten magellanicus* (Mollusca: Bivalvia). Mar. Ecol. Prog. Ser. 108, 251—264, http://dx.doi.org/10.3354/meps108251.

Mann, K.H., Lazier, J.R.N., 1991. Dynamical of Marine Ecosystems, Biological—Physical Interactions in the Oceans. Blackwell Sci. Publ., Oxford, 466 pp.

Margalef, R., 1978. Life-forms of phytoplankton as survival alternatives in an unstable environment. Oceanol. Acta 1 (4), 493—509.

Marshall, R., McKinley, S., Pearce, C.M., 2010. Effects of nutrition on larval growth and survival in bivalves. Rev. Aquacult. 2 (1), 33—55, http://dx.doi.org/10.1111/j.1753-5131.2010.01022.x.

Møhlenberg, F., Riisgård, H.U., 1978. Efficiency of particle retention in 13 species of suspension feeding bivalves. Ophelia 17 (2), 239—246, http://dx.doi.org/10.1080/00785326.1978.10425487.

Montagnes, D.J.S., Berges, J.A., Harrison, P.J., Taylor, F.J.R.L., 1994. Estimating carbon, nitrogen, protein, and chlorophyll *a* from volume in marine phytoplankton. Limnol. Oceanogr. 39 (5), 1044—1060, http://dx.doi.org/10.4319/lo.1994.39.5.1044.

Morán, X.A.G., Gasol, J.M., Arin, L., Estrada, M., 1999. A comparison between glass fiber and membrane filters for the estimation of phytoplankton POC and DOC production. Mar. Ecol. Prog. Ser. 187, 31—41, http://dx.doi.org/10.3354/meps187031.

Muñiz, O., Revilla, M., Rodríguez, J.G., Laza-Martínez, A., Seoane, S., Franco, J., Orive, E., 2017. Evaluation of phytoplankton quality and toxicity risk based on a long-term time series previous to the implementation of a bivalve farm (Basque coast as a case study). Reg. Stud. Mar. Sci. 10, 10—19, http://dx.doi.org/10.1016/j.rsma.2016.12.012.

Muñiz, O., Rodríguez, J.G., Revilla, M., Laza-Martínez, A., Seoane, S., Franco, J., 2018. Seasonal variations of phytoplankton community in relation to environmental factors in an oligotrophic area of the European Atlantic coast (southeastern Bay of Biscay). Reg. Stud. Mar. Sci. 17, 59—72, http://dx.doi.org/10.1016/j.rsma.2017.11.011.

Nogueira, E., Ibanez, F., Figueiras, F.G., 2000. Effect of meteorological and hydrographic disturbances on the microplankton community structure in the Ría de Vigo (NW Spain). Mar. Ecol. Prog. Ser. 203, 23—45, http://dx.doi.org/10.3354/meps203023.

Olenina, I., Hajdu, S., Edler, L., Andersson, A., Wasmund, N., Busch, S., Göbel, J., Gromisz, S., Huseby, S., Huttunen, M., Jaanus, A., Kokkonen, P., Ledaine, I., Niemkiewicz, E., 2006. Biovolumes and size-classes of phytoplankton in the Baltic Sea. Helsinki Commission. Baltic Marine Environ. Prot. Comm., 144 pp.

Orive, E., Franco, J., de Madariaga, I., Revilla, M., 2004. Chapter 15 — Bacterioplankton and phytoplankton communities. In: Borja, Á., Collins, M. (Eds.), Oceanography and Marine Environment of the Basque Country. Elsevier, Amsterdam, 367—393.

Pernet, F., Malet, N., Pastoureaud, A., Vaquer, A., Quéré, C., Dubroca, L., 2012. Marine diatoms sustain growth of bivalves in a Mediterranean lagoon. J. Sea Res. 68, 20—32, http://dx.doi.org/10.1016/j.seares.2011.11.004.

Petersen, J.K., Nielsen, T.G., Van Duren, L., Maar, M., 2008. Depletion of plankton in a raft culture of *Mytilus galloprovincialis* in Ría de Vigo, NW Spain. I. Phytoplankton. Aquat. Biol. 4, 113—125, http://dx.doi.org/10.3354/ab00124.

Pettersen, A.K., Turchini, G.M., Jahangard, S., Ingram, B.A., Sherman, C.D., 2010. Effects of different dietary microalgae on survival, growth, settlement and fatty acid composition of blue mussel (*Mytilus galloprovincialis*) larvae. Aquaculture 309 (1), 115—124, http://dx.doi.org/10.1016/j.aquaculture.2010.09.024.

Regaudie-de-Gioux, A., Lasternas, S., Agustí, S., Duarte, C.M., 2014. Comparing marine primary production estimates through different methods and development of conversion equations. Front. Mar. Sci. 1 (19), 1—14, http://dx.doi.org/10.3389/fmars.2014.00019.

Revilla, M., Iriarte, A., Madariaga, I., Orive, E., 2000. Bacterial and phytoplankton dynamics along a trophic gradient in a shallow temperate estuary. Estuar. Coast. Shelf Sci. 50 (3), 297—313, http://dx.doi.org/10.1006/ecss.1999.0576.

Revilla, M., Franco, J., Bald, J., Borja, Á., Laza, A., Seoane, S., Valencia, V., 2009. Assessment of the phytoplankton ecological

status in the Basque coast (northern Spain) according to the European Water Framework Directive. J. Sea Res. 61 (1—2), 60—67, http://dx.doi.org/10.1016/j.seares.2008.05.009.

Riisgard, H.U., 1988. Efficiency of particle retention and filtration rate in 6 species of Northeast American bivalves. Mar. Ecol. Prog. Ser. 45, 217—223, http://dx.doi.org/10.3354/meps211275.

Riisgård, H.U., 2001. On measurement of filtration rates in bivalves—the stony road to reliable data: review and interpretation. Mar. Ecol. Prog. Ser. 211, 275—291, http://dx.doi.org/10.3354/meps211275.

Riisgård, H.U., Egede, P.P., Barreiro Saavedra, I., 2011. Feeding behaviour of the mussel, *Mytilus edulis*: new observations, with a minireview of current knowledge. J. Mar. Biol. 2011, Art Id. 312459, 13 pp., http://dx.doi.org/10.1155/2011/312459.

Ríos, A.F., Fraga, F., Pérez, F.F., Figueiras, F.G., 1998. Chemical composition of phytoplankton and particulate organic matter in the Ría de Vigo (NW Spain). Sci. Mar. 62 (3), 257—271.

Robert, R., Trintignac, P., 1997. Substitutes for live microalgae in mariculture: a review. Aquat. Living Resour. 10 (5), 315—327, http://dx.doi.org/10.1051/alr:1997035.

Rouillon, G., Navarro, E., 2003. Differential utilization of species of phytoplankton by the mussel *Mytilus edulis*. Acta Oecol. 24 (S1), S299—S305, http://dx.doi.org/10.1016/S1146-609X(03)00029-8.

Sheldon, R.W., 1972. Size separation of marine seston by membrane and glass-fiber filters. Limnol. Oceanogr. 17 (3), 494—498, http://dx.doi.org/10.4319/lo.1972.17.3.0494.

Shumway, S.E., Cucci, T.L., 1987. The effects of the toxic dinoflagellate *Protogonyaulax tamarensis* on the feeding and behaviour of bivalve molluscs. Aquat. Toxicol. 10 (1), 9—27, http://dx.doi.org/10.1016/0166-445X(87)90024-5.

Smayda, T.J., 1998. Patterns of variability characterizing marine phytoplankton, with examples from Narragansett Bay. ICES J. Mar. Sci. 55 (4), 562—573, http://dx.doi.org/10.1006/jmsc.1998.0385.

Smayda, T.J., Reynolds, C.S., 2003. Strategies of marine dinoflagellate survival and some rules of assembly. J. Sea Res. 49 (2), 95—106, http://dx.doi.org/10.1016/s1385-1101(02)00219-8.

Taylor, A.H., Geider, R.J., Gilbert, F.J.H., 1997. Seasonal and latitudinal dependencies of phytoplankton carbon-to-chlorophyll *a* ratios: results of a modelling study. Mar. Ecol. Prog. Ser. 152 (1), 51—66, http://dx.doi.org/10.3354/meps152051.

Thompson, P.A., Guo, M., Harrison, P.J., 1993. The influence of irradiance on the biochemical composition of three phytoplankton species and their nutritional value for larvae of the Pacific oyster (*Crassostrea gigas*). Mar. Biol. 117 (2), 259—268, http://dx.doi.org/10.1007/BF00345671.

Tilstone, G.H., Figueiras, F.G., Fermin, E.G., Arbones, B., 1999. Significance of nanophytoplankton photosynthesis and primary production in a coastal upwelling system (Ria de Vigo, NW Spain). Mar. Ecol. Prog. Ser. 183, 13—27, http://dx.doi.org/10.3354/meps183013.

Trottet, A., Roy, S., Tamigneaux, E., Lovejoy, C., Tremblay, R., 2008. Impact of suspended mussels (*Mytilus edulis* L.) on plankton communities in a Magdalen Islands lagoon (Québec, Canada): a mesocosm approach. J. Exp. Mar. Biol. Ecol. 365 (2), 103—115, http://dx.doi.org/10.1016/j.jembe.2008.08.001.

Tyberghein, L., Verbruggen, H., Pauly, K., Troupin, C., Mineur, F., De Clerck, O., 2012. Bio-ORACLE: a global environmental dataset for marine species distribution modelling. Glob. Ecol. Biogeogr. 21 (2), 272—281, http://dx.doi.org/10.1111/j.1466-8238.2011.00656.x.

Utermöhl, H., 1958. Zur vervollkommnung der quantitativen phytoplankton-methodik. Mitteilungen der Internationale Vereinigung fuür Theoretische und Angewandte Limnologie 9, 1—38.

Vajravelu, M., Martin, Y., Ayyappan, S., Mayakrishnan, M., 2017. Seasonal influence of physico-chemical parameters on phytoplankton diversity, community structure and abundance at Parangipettai coastal waters, Bay of Bengal, South East Coast of India. Oceanologia 60 (2), 114—127, http://dx.doi.org/10.1016/j.oceano.2017.08.003.

Valdés, L., Moral, M., 1998. Time-series analysis of copepod diversity and species richness in the southern Bay of Biscay off Santander, Spain, in relation to environmental conditions. ICES J. Mar. Sci. 55 (4), 783—792, http://dx.doi.org/10.1006/jmsc.1998.0386.

Valencia, V., Franco, J., 2004. Chapter 8 — Main characteristics of the water masses. In: Borja, Á., Collins, M. (Eds.), Oceanography and Marine Environment of the Basque Country. Elsevier, Amsterdam, 197—232.

Valencia, V., Motos, L., Urrutia, J., 1989. Estudio de la variación temporal de hidrografía y el plancton en la zona nerítica frente a San Sebastián. Resultados abril 1986 — diciembre 1987. Servicio central de publicaciones del Gobierno Vasco, Vitoria-Gasteiz, 81 pp.

Valencia, V., Franco, J., Borja, Á., Fontán, A., 2004. Chapter 7 — Hydrography of the southeastern Bay of Biscay. In: Borja, Á., Collins, M. (Eds.), Oceanography and Marine Environment of the Basque Country. Elsevier, Amsterdam, 159—194.

van der Veer, H.W., 1989. Eutrophication and mussel culture in the western Dutch Wadden Sea: impact on the benthic ecosystem; a hypothesis. Helgol. Meeresunter. 43 (3—4), 517—527.

Varela, M., 1996. Phytoplankton ecology in the Bay of Biscay. Sci. Mar. 60, 45—53.

Varela, M., Prego, R., Pazos, Y., 2008. Spatial and temporal variability of phytoplankton biomass, primary production and community structure in the Pontevedra Ria (NW Iberian Peninsula): oceanographic periods and possible response to environmental changes. Mar. Biol. 154 (3), 483—499, http://dx.doi.org/10.1007/s00227-008-0943-x.

Volkman, J.K., Jeffrey, S.W., Nichols, P.D., Rogers, G.I., Garland, C. D., 1989. Fatty acid and lipid composition of 10 species of microalgae used in mariculture. J. Exp. Mar. Biol. Ecol. 128 (3), 219—240, http://dx.doi.org/10.1016/0022-0981(89)90029-4.

Volkman, J.K., Dunstan, G.A., Jeffrey, S.W., Kearney, P.S., 1991. Fatty acids from microalgae of the genus Pavlova. Phytochemistry 30 (6), 1855—1859, http://dx.doi.org/10.1016/0031-9422(91)85028-X.

Wall, C.C., Gobler, C.J., Peterson, B.J., Ward, J.E., 2013. Contrasting growth patterns of suspension-feeding molluscs (*Mercenaria mercenaria*, *Crassostrea virginica*, *Argopecten irradians*, and *Crepidula fornicata*) across a eutrophication gradient in the Peconic Estuary, NY, USA. Estuar. Coast. 36 (6), 1274—1291, http://dx.doi.org/10.1007/s12237-013-9632-1.

Walsh, J.J., Dugdale, R.C., 1971. A simulation model of the nitrogen flow in the Peruvian upwelling system. Investigación Pesquera 35 (1), 309—330.

Weiss, M.B., Curran, P.B., Peterson, B.J., Gobler, C.J., 2007. The influence of plankton composition and water quality on hard clam (*Mercenaria mercenaria* L.) populations across Long Island's south shore lagoon estuaries (New York, USA). J. Exp. Mar. Biol. Ecol. 345 (1), 12—25, http://dx.doi.org/10.1016/j.jembe.2006.12.025.

Oceanologia (2019) 61, 131—142

Available online at www.sciencedirect.com

ScienceDirect

journal homepage: www.journals.elsevier.com/oceanologia/

ORIGINAL RESEARCH ARTICLE

Random forest assessment of correlation between environmental factors and genetic differentiation of populations: Case of marine mussels *Mytilus*

Tomasz Kijewski [a], Malgorzata Zbawicka [a], Jakob Strand [b], Hans Kautsky [c], Jonne Kotta [d], Merli Rätsep [d], Roman Wenne [a,*]

[a] *Institute of Oceanology, Polish Academy of Sciences, Sopot, Poland*
[b] *Arctic Research Centre, Department of Bioscience, Aarhus University, Aarhus, Denmark*
[c] *Department of Ecology, Environment and Plant Sciences, Stockholm University, Sweden*
[d] *Estonian Marine Institute, University of Tartu, Tallinn, Estonia*

Received 29 April 2018; accepted 15 August 2018
Available online 30 August 2018

KEYWORDS
Marine environment;
Spatial distribution;
Seascape genetics;
Nuclear DNA markers EFbis, Glu-5′, ITS, M7 and Single Nucleotide Polymorphism;
Baltic Sea

Summary The novel machine learning technique Random Forest (RF) was used to test if the genetic differentiation of populations of marine species may be related to any of the key environmental variables known to shape species distributions. The study was performed in North and Baltic Sea characterized by strong gradients of environmental factors and almost continuous distributions of *Mytilus* mussel populations. Assessment of the species identity was performed using four nuclear DNA markers, and previously published single nucleotide polymorphism (SNP) data. A general pattern of cline variation was observed with increasing *Mytilus trossulus* share towards the eastern Baltic Sea. Average allele share rose to 61% in Höga Kusten, Gulf of Bothnia. All Baltic Sea samples revealed a strong introgression of *Mytilus edulis* and a limited introgression of *M. trossulus* through the Danish Straits.

The studied environmental variables described 67 and 68% of the variability in the allele frequencies of *M. edulis* and *M. trossulus*. Salinity defined over 50% of the variability in the gene frequencies of the studied *Mytilus* spp. populations. Changes along this environmental gradient were not gradual but instead a significant shift from gene dominance was found at a salinity of 12 PSU. Water temperature and the trophic status of the sea area had only moderate association with the gene frequencies. The

* Corresponding author at: Institute of Oceanology, Polish Academy of Sciences, Powstańców Warszawy 55, 81-712 Sopot, Poland. Tel.: +48 58 7311763; fax: +48 58 5512130.
E-mail address: rwenne@iopan.gda.pl (R. Wenne).
Peer review under the responsibility of Institute of Oceanology of the Polish Academy of Sciences.

Production and hosting by Elsevier

https://doi.org/10.1016/j.oceano.2018.08.002

obtained results showed that the novel machine learning technique can be successfully used for finding correlations between genetic differentiation of populations and environmental variables and for defining the functional form of these linkages.

1. Introduction

Global climate changes and human economic activities, such as aquaculture and maritime transport, influence geographic distribution of marine species (Bach et al., 2018; Bosch et al., 2018; Gardner et al., 2016; Wenne, 2018). Extending knowledge on processes shaping species distribution will enable elaboration of adequate models for future forecasting. Changes to biodiversity and species distribution can be caused by biological or environmental factors, e.g. food availability, alterations in temperature, salinity, oxygen content in water, ocean circulation or depth (Banks et al., 2010; Silliman et al., 2011; Watson et al., 2011). Population genetic methods are tools for quantification of the genetic component of biodiversity. Studies of correlations between genetic diversity and spatial differentiation of factors along a broad range of environmental gradients can extend our understanding of species distribution changes (Riddle et al., 2008). This can be achieved through analyses of the linkage between these environmental variables and frequencies of genes in populations.

In comparison with other parts of the Atlantic Ocean, the Baltic Sea is a semi-enclosed reservoir characterized by marginal environments (Johannesson and André, 2006; Pocwierz-Kotus et al., 2014). Its salinity decreases in the North-East direction and strongly influences distribution and diversity of pelagic and benthic assemblages (Grabowska et al., 2015; Kijewska et al., 2009, 2016; Malachowicz et al., 2015; Vuorinen et al., 2015). Fauna of the Baltic is a mixture of fresh-water and marine species including *Mytilus* (Wennerström et al., 2013). *Mytilus* mussels have widely been used as an indicator of environmental quality and recently for monitoring of global climate changes (Dowd and Somero, 2013; Lesser, 2016; Li et al., 2015; Michaelidis et al., 2014). Morphologically similar species of *Mytilus* can hybridize in areas where their populations merge (Larraín et al., 2018; Wenne et al., 2016; Zbawicka et al., 2018). This impeded an identification of *Mytilus* species, their hybrids and backcross progenies, using classic methodology and justified using molecular markers. In the Baltic, *Mytilus* mussels have been used to study the effects of water acidification (Thomsen and Melzner, 2010), genotoxicity induced by oil spills (Barsiene et al., 2012), accumulation, the effects of pharmaceuticals (Ericson et al., 2010), and the accumulation of a variety of other chemical compounds and metals (Albalat et al., 2002; Bjork and Gilek, 1997; Dabrowska et al., 2017; Hoher et al., 2012; Kopecka et al., 2006; Larsson et al., 2018; Nyberg et al., 2015; Pempkowiak et al., 2006; Piwoni-Piórewicz et al., 2017; Potrykus et al., 2003; Protasowicki et al., 2008; Szefer et al., 2002; Szefer and Szefer, 1990; Szefer and Wenne, 1987; Szymczak-Zyla et al., 2006). *Mytilus* spp. have several ecologically important features including water filtration and providing a link between the benthos and the pelagic zones by cycling nutrients and organic matter (Kautsky and Evans, 1987). In the Baltic, mussel farms have been set up for the purpose of mitigating eutrophication processes (Ozoliņa, 2017; Petersen et al., 2014). Commercial mussel farming and harvesting for human consumption operate in Limfjörd, Denmark, Sweden and in Kiel Bight, Germany (Bergström et al., 2017; Larsen and Riisgård, 2016; Utermann et al., 2018). Therefore, knowledge of the genetic composition of local populations of *Mytilus* can be useful not only for monitoring but also for the mariculture industry.

Mytilus populations in the Baltic have been studied with allozymes, nuclear DNA markers and sequences of mitochondrial (mt) DNA (Larsson et al., 2017; Rawson and Hilbish, 1998; Väinölä and Hvilsom, 1991; Zbawicka et al., 2007, 2014b). MtDNA of *Mytilus* is characterized by doubly uniparental inheritance, recombination and length polymorphism in the Baltic populations, which makes surveys of population differentiation more complex (Filipowicz et al., 2008; Zbawicka et al., 2003a,b). In the case of some nuclear DNA markers, polymorphism identified with, for example, e.g. PCR Amplified Fragment Length Polymorphism depends on reaction conditions and is not always reproducible (Cuéllar-Pinzón et al., 2016). New markers based on single nucleotide polymorphisms have been discovered by Zbawicka et al. (2012, 2014a). The reported studies highlighted the hybrid status of the Baltic *Mytilus* spp. populations with differential introgression power of selected genetic features. The Baltic populations of *Mytilus* spp. were established after the glaciation period during the Holocene and have retained unique characteristics compared to populations from other geographic areas (Kijewski et al., 2006; Smietanka et al., 2013; Väinölä and Strelkov, 2011; Wennerström et al., 2013). A steep salinity gradient was expected to act as a barrier between the North and Baltic Seas and result in an elevated mortality of larvae passing this barrier by means of currents (Gilg and Hilbish, 2003). Nonetheless, the influence of water circulation has been found to shape the genetic composition of the *Mytilus* spp. populations within the Baltic Sea and between the North and Baltic Seas (Larsson et al., 2017). Besides oceanographic connectivity and larval drift, local environmental conditions were expected to account for local adaptation and population differentiation (Valladares et al., 2014). A large array of environmental variables such as water temperature, flow velocity, food availability, either separately or interactively were considered as factors shaping the distribution and potential differentiation patterns of *Mytilus* spp. populations (Kotta et al., 2015). Salinity has been reported as an environmental factor significantly influ-

encing *Mytilus* shell variation across European and Arctic coasts (Telesca et al., 2018).

Commonly used statistical modelling may not be the most successful way to understand relationships between environmental variables and population genetics, as it starts by assuming an appropriate data model, and model parameters are then estimated from the data. Due to the lack of a solid understanding of how the external environment shapes the genetic composition of the *Mytilus* spp. populations being modelled, the predictive performance of these models would be expected to be moderate. Machine learning could provide a novel theoretical framework where modelling is seen as a sophisticated tool to improve our understanding of the relationship between environment and biota. In contrast, machine learning avoids starting with a data model, and rather uses an algorithm to learn the relationship between the response and its predictors (Hastie et al., 2009).

As with machine learning, the Random Forest (RF) method copes with different non-linear relationships, which are common in ecological data but difficult to analyse using more classic methods. The RF generates a large number of regression trees, each calibrated on a bootstrap sample of the original data (Breiman, 2001). Each node is split using a subset of randomly selected predictors and the tree is grown to the largest possible extent without pre-running. For predicting the value of a new data point, the data are run through each of the trees in the forest and each tree provides a value. The model prediction is then calculated as the average value over the predictions of all the trees in the forest. Recently, the RF has been applied to assignment analysis from population genetic data (Sylvester et al., 2018). There are other effective machine learning techniques such as Boosted Regression Trees and Maximum Entropy (Elith et al., 2006, 2008). All these methods belong to the same family of statistical models and therefore yield more or less similar results. The RF modelling is very efficient with a small sample size and this property makes this technique highly suitable for the current study.

The aim of this paper was to use random forest (RF) as the modelling algorithm to assess the relative contribution of natural environmental drivers in the allele frequencies in populations of marine species. North and Baltic Sea transects were used as an example because of known strong environmental gradients and almost continuous geographic distributions of *Mytilus* populations. Assessment of the species identity was made using four nuclear DNA markers in conjunction with already published single nucleotide polymorphism (SNP) data specific to the *Mytilus* species.

2. Material and methods

2.1. Environmental variables

The environmental layers used in the modelling (see below the section of statistical analyses) were produced from simulations of a coupled physical-biogeochemical model of the Baltic Sea (Meier et al., 2012). The model produced physical, chemical and biological data layers: annual average of salinity and current velocity, summer average of temperature and chlorophyll-*a*, winter average of nitrate (NO_3) and phosphate (PO_4). Annual and seasonal means were calculated for the periods 1978–2007. In addition to the RCO-SCOBI data layers, depth and wave exposure (simplified wave model) data were also used as modelling input variables. Depth data were acquired from the Baltic Sea Bathymetry Database (Baltic Sea Hydrographic Commission 2013). The simplified wave model is a surface wave exposure model that incorporates shoreline topography, fetch and wind data together with empirically derived algorithms to mimic diffraction (Isæus, 2004).

2.2. Sampling

Mytilus spp. samples consisting of 1466 individuals in total were collected from 32 sites in a transition from the south-eastern North Sea to the northeastern Baltic Sea mostly in 2008–2009 (Fig. 1 and Table 1). Three samples were collected in 2007, 2 in 2010 and 1 in 2011. The studied individuals varied in size from 1.5 to 8 cm. Prior to DNA extraction, mussels were frozen at −70°C or preserved in 96% ethanol.

2.3. Molecular methods

For DNA extraction, pieces of gill tissue ∼3 mm × 3 mm were dissected and processed with the CTAB method of Hoarau et al. (2002). After precipitation in isopropyl alcohol, total DNA was suspended in deionized water. Four nuclear DNA markers, which tentatively diagnostically differentiate the *Mytilus* taxa in their North Atlantic and North Pacific range were analysed. A segment of gene coding an adhesive protein of byssus (Glu-5′) has been characterized by diagnostic PCR products length differences among three studied taxa: *M. edulis*, *M. trossulus* and *M. galloprovincialis* (Inoue et al., 1995; Kijewski et al., 2009). Diagnostic differences between *M. trossulus* and the other two taxa in the internal transcribed spacer (ITS) regions between the 18S and 28S rDNA genes were detected with the restriction enzyme *Hha*I digestion (Heath et al., 1995; Kijewski et al., 2009). The EFbis marker is an intron in the elongation factor 1 α (Bierne et al., 2003) with double digestion RFLP variation diagnostic between *M. trossulus*, *M. edulis* and *M. galloprovincialis* (Kijewski et al., 2009, 2006). A taxonomic discrepancy in a sequence of acrosomal sperm protein (Riginos et al., 2006) was exposed using a set of 5 primers in PCR reaction as marker M7 (Kijewski et al., 2009). Amplicons and restriction fragments (*Hha*I digestion of ITS, *Hha*I + *Rsa*I digestion of EFbis) were separated by electrophoresis in 3% NuSieve GTG agarose gels in TBE buffer and visualized with ethidium bromide.

2.4. Statistical analyses

Nuclear markers were scored for each individual and taxon-specific allele composition was described for each sample. Deviations from the random association of alleles within loci (Hardy–Weinberg equilibrium, HWE) were computed with the use of Arlequin 3.5.2.2 (Excoffier et al., 2005). The statistical significance of disequilibria was tested with the Markov chain. Genetic structure was analysed primarily by Structure 2.3 software (Pritchard et al., 2000), where Bayesian algorithm estimates the most plausible number of genetic clusters by 4 runs for *K* range from 1 to 10 with a length of the burn-in period of 500 000 and 15M MCMC

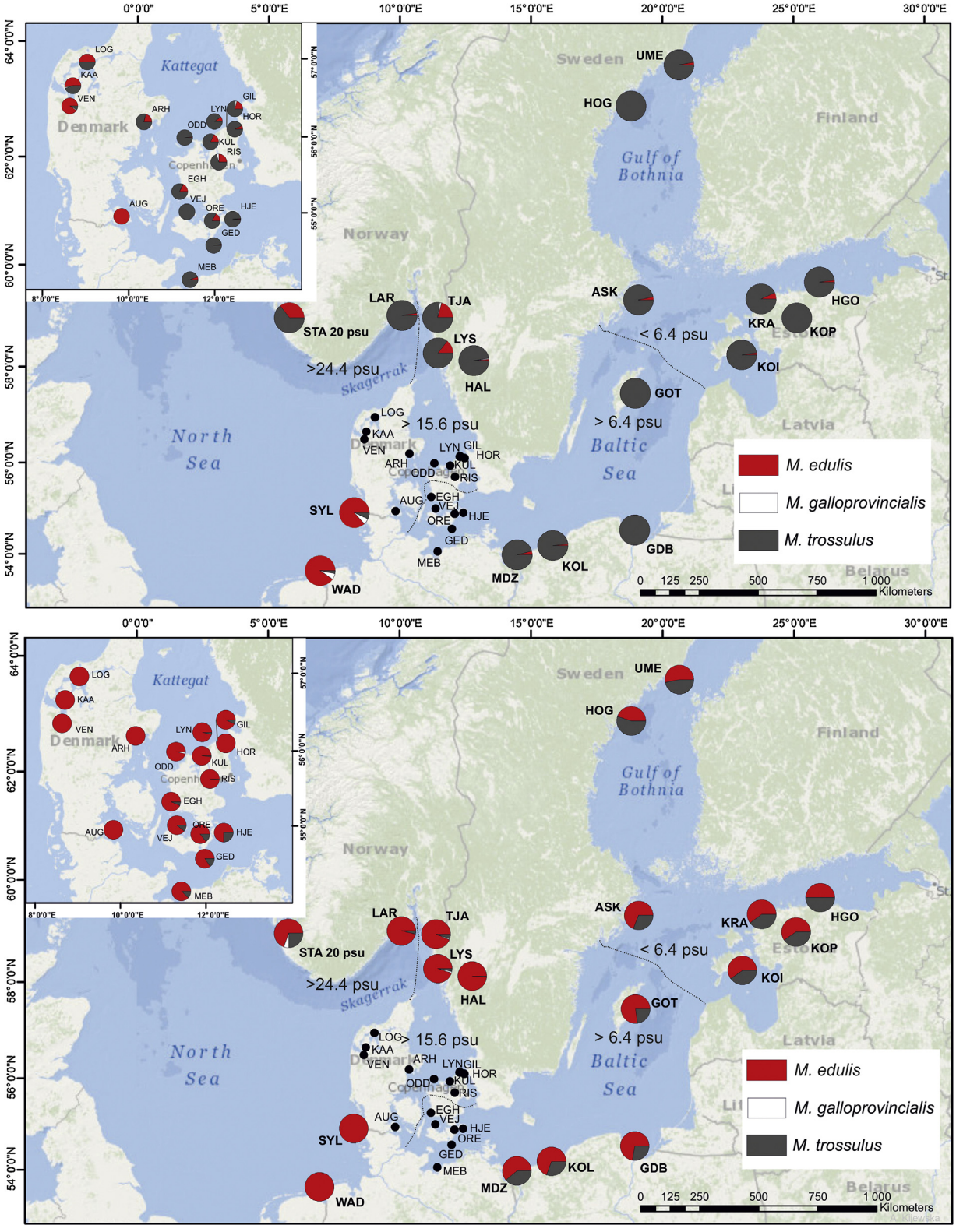

Figure 1 Map showing locations of sampling sites and genetic composition of the studied populations of *Mytilus* mussels. The pie charts visualise the frequency of taxon-specific alleles identified with 2 nuclear DNA markers: EFbis (a) and Glu-5′ (b) and 26 SNPs (c).

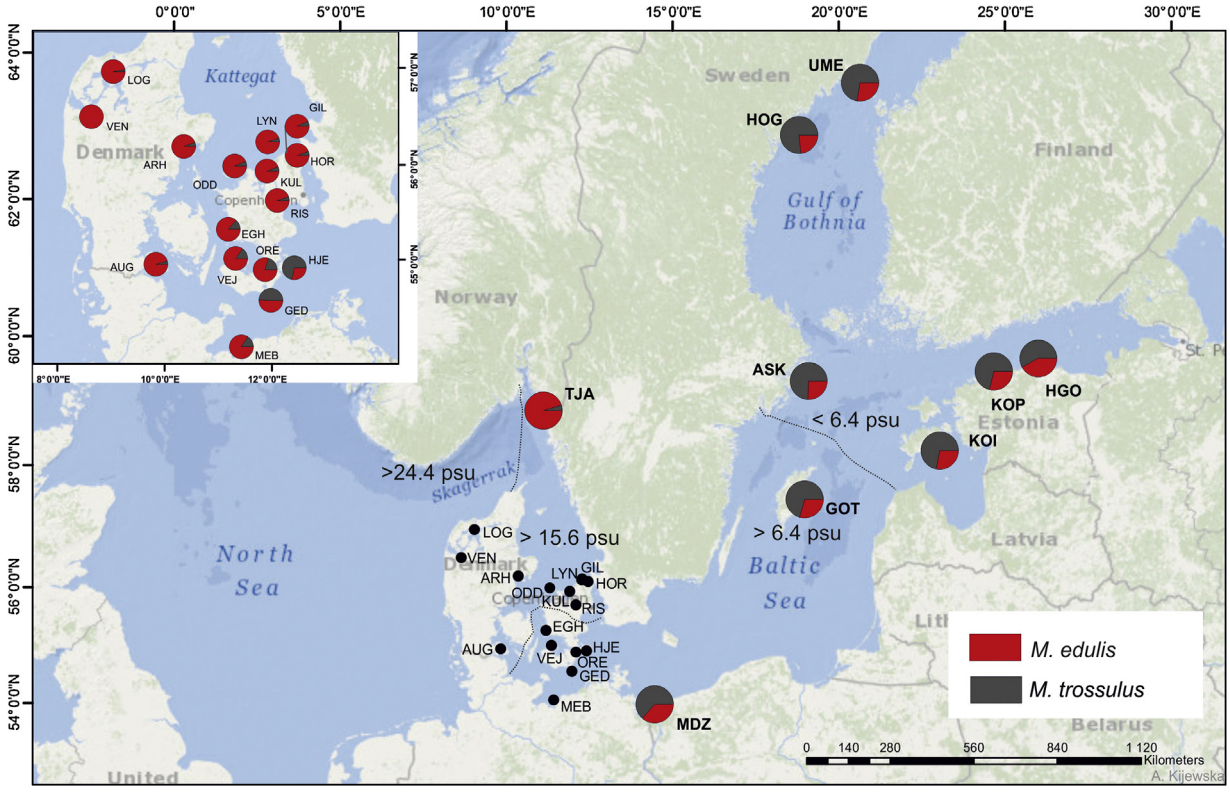

Figure 1 (*Continued*).

iterations after burn-in. The Evanno method highlights which number of clusters is the most probable by estimating the maximum value of ΔK (Evanno et al., 2005). The results of each run were compiled with the use of Structure Harvester v0.6.94 (Earl and vonHoldt, 2012). The different runs of the selected K were averaged in CLUMPP version 1.1.2 (Jakobsson and Rosenberg, 2007). Principal Coordinate Analysis (PCoA) was performed using the procedure implemented in GenAlEx 6.502 on the matrix of individual genotypes (Peakall and Smouse, 2012). The M7 reads were removed from this analysis due to lack of genotyping results for KOL, MDZ and MEB samples and the PCoA was conducted for three markers only. Two structure assessments obtained with Structure and PCoA were tested further by hierarchical φ-/F-statistics using the AMOVA program Arlequin 3.5.2.2 (Excoffier et al., 2005) with fixation indices estimated overall (F_{ST}), between groups of populations (F_{CT}), within groups (F_{SC}) and F_{ST} pairwise. Significance was assessed by 9999 permutations of the original data matrix.

The package "randomForest" (Breiman and Cutler, 2015) was used to run RF models in the statistical software R 3.2.2 (The R Foundation for Statistical Computing 2015). Two main parameters can be set in RF models: the number of predictor variables to be randomly selected at each node (mtry) and the number of trees in a forest (ntree). The parameter mtry was set to the square root of the number of predictor variables as suggested by Liaw and Wiener (2002) for the classification model, and ntree was set to 1000, as 500 trees usually yield stable results. The importance of predictor variables in the model was assessed using the internal method of the package "randomForest" (mean decrease in accuracy) using 10 permutations (Breiman and Cutler, 2015). Partial dependence plots (sensu Friedman, 2001) were produced using partialPlot function in "randomForest" to illustrate the dependence of model predictions on individual covariates. In general, a regression function will depend on many predictor variables. Partial dependence is the dependence of the probability of presence on one predictor variable after averaging out the effects of the other predictor variables in the model. The *y*-axis represents the modelled marginal effect on a response variable. Negative values (in the *y*-axis) mean that the positive class is less likely for that value of the independent variable (*x*-axis) according to the model. Positive values mean that the positive class is more likely for that value of the independent variable. Zero implies no average impact on class probability according to the model. In this study, allele frequencies of the *M. edulis*, *M. trossulus* and *M. galloprovincialis* specific nuclear markers were modelled along key environmental variables. Additionally, the frequency of twenty-six outlier SNP markers characteristic to *M. trossulus*, based on the already published results by Zbawicka et al. (2014a), were included in the analysis (Table S1). Eighty-four SNPs were genotyped in 630 specimens from the Baltic Sea, Belt Sea, Kattegat and North Sea using the Sequenom MassARRAY iPLEX genotyping platform. Sixty SNPs were polymorphic. Based on F_{ST} outlier analysis, 26 SNPs were significantly involved in the differentiation between the Baltic Sea and Danish Straits (Zbawicka et al., 2014a). Separate RF models were built for each *Mytilus* species.

Multicollinearity can be an issue with the RF modelling when answering if and when environmental variables are of

Table 1 Geographic localization of sampling sites. Allelic share of *Mytilus edulis*, *Mytilus galloprovincialis* and *Mytilus trossulus* for the studied genetic markers: Glu-5, Ef-bis, M7 and ITS. Samples marked with an asterisk were genotyped only with Glu-5, EF-bis and ITS markers by Kijewski et al. (2011). Frequencies of *M. trossulus* genes were used in RF model.

Sample		Coordinates		Salinity		Average allelic share over loci		
Name	Localization	N	E	ppt	*n*	*M. edulis*	*M. galloprovincialis*	*M. trossulus*
WAD	Wadden Sea	53°37′8.92″N	6°56′25.49″E	29.48	48	0.98	0.01	0.01
AUG	Augustenborg	54°57′2.00″N	9°50′0.00″E	17.44	39	0.97	0	0.03
VEN	Venø Bight	56°29′54.00″N	8°38′1.00″E	32.67	48	0.94	0.05	0.01
SYL	Sylt	54°54′55.14″N	8°14′43.63″E	31.23	15	0.92	0.06	0.02
KAA	Kaas Breding	56°39′32.00″N	8°42′15.00″E	32.31	48	0.89	0	0.11
LOG	Løgstør Breding	56°57′37.00″N	9°2′17.00″E	24.31	48	0.83	0	0.17
RIS	Riso	55°42′1.44″N	12°5′32.11″E	17.63	45	0.81	0.01	0.18
ARH	Århus	56°11′33.00″N	10°21′12.00″E	20.88	48	0.8	0	0.2
GIL	Gileleje	56°7′43.00″N	12°16′13.00″E	15.66	48	0.78	0.01	0.22
LYN	Lynetten	56°8′30.00″N	12°16′60.00″E	15.62	48	0.77	0	0.23
HOR	Hornbæk	56°5′54.90″N	12°27′49.09″E	15.79	47	0.76	0	0.24
TJA	Tjarnö	58°51′34.65″N	11°6′43.29″E	24.10	48	0.76	0.01	0.23
KUL	Kulhuse	55°56′5.00″N	11°54′10.00″E	17.27	48	0.75	0.02	0.22
ODD	Odden	55°59′17.00″N	11°18′2.00″E	15.90	47	0.75	0.01	0.24
HAL	Halse Fjord	58°7′1.48″N	11°49′46.34″E	22.82	40	0.75	0	0.25
LAR	Larvik Fjord	59°0′54.59″N	10°3′48.18″E	34.48	40	0.74	0	0.26
LYS	Lysekill	58°16′4.38″N	11°26′43.36″E	23.54	48	0.73	0.04	0.22
EGH	Egholm	55°15′49.42″N	11°11′1.77″E	13.67	48	0.71	0.04	0.25
GDB	Zatoka Gdańska	54°31′49.88″N	18°56′35.67″E	6.58	45	0.71	0.01	0.28
STA	Stavanger	58°58′9.98″N	5°45′58.15″E	20.00	48	0.71	0.01	0.28
VEJ	Vejrø	55°0′43.60″N	11°21′1.74″E	13.42	47	0.7	0.02	0.28
ORE	Ore	54°53′34.00″N	12°4′50.00″E	10.13	68	0.69	0.03	0.28
GED	Gedser	54°33′45.00″N	11°58′27.00″E	9.58	48	0.62	0.01	0.38
MEB*	Mecklemburg	54°3′32.04″N	11°25′28.92″E	11.80	63	0.6	0	0.4
HJE	Hjelm	54°54′47.99″N	12°24′45.29″E	8.16	48	0.56	0	0.44
KOI	Kõiguste Bay	58°13′59.24″N	23°2′7.83″E	5.21	47	0.55	0	0.45
KOP	Kopli Bay	59°28′0.61″N	24°40′1.74″E	4.23	47	0.54	0.02	0.44
GOT	Gotland	57°27′1.25″N	18°58′15.32″E	6.40	48	0.52	0.01	0.47
HGO	Hgona	59°39′49.91″N	26°0′8.72″E	3.34	48	0.49	0	0.51
KRA	Krassi shallow	59°20′23.34″N	23°46′20.79″E	4.50	47	0.49	0	0.51
KOL*	Kołobrzeg	54°11′19.92″N	15°33′41.81″E	7.24	41	0.49	0	0.51
ASK	Askö	59°19′5.62″N	19°5′31.29″E	5.29	48	0.48	0	0.52
UME	Umeå	63°36′15.62″N	20°38′23.66″E	2.97	48	0.45	0	0.55
MDZ*	Międzyzdroje	53°58′36.84″N	14°27′36.00″E	6.70	51	0.44	0	0.56
HOG	Höga Kusten	62°53′39.97″N	18°48′20.49″E	4.10	28	0.39	0	0.61

ecological interest. Thus, prior to modelling, the Pearson correlation analysis between all environmental variables was run in order to avoid situations of including highly correlated variables into the modelling. The correlation analysis showed that most variables were only weakly intercorrelated at $r < 0.5$. However, winter average nitrate and current velocity were positively correlated ($r = 0.73$, $p < 0.001$). Nevertheless, these values were far below the critical threshold when collinearity begins to severely distort model estimation and subsequent prediction (Dormann et al., 2013).

3. Results and discussion

Mussels from 32 samples from the Baltic Sea, Sound, Great Belt, Little Belt, Kattegat, Limfjord, Skagerrak, North Sea and Wadden Sea (salinity gradient ranging from 3 to 34 PSU) were assayed for nuclear markers Glu-5′, ITS, EFbis and M7 (Fig. 1 and Table 1). Already published results of the genotyping of 3 samples collected in 1995 from the southern Baltic (KOL, MDZ and MEB) for Glu-5′, ITS and EFbis markers were also included in further analyses (Kijewski et al., 2006, 2011). These 4 markers differed in sensitivity of *Mytilus* spp. discrimination. None of the samples was identified as pure *M. edulis* or *M. trossulus* with all markers, however for three samples (Wadden Sea, Augustenborg and Halse Fjord) genetic composition across all the studied loci was over 95% *M. edulis*. A general pattern of cline variation was observed, with increasing *M. trossulus* share towards the eastern Baltic Sea, but average allele share rose to 61% in Höga Kusten (Bothnian Sea). All Baltic Sea samples revealed a strong introgression of *M. edulis* and a limited introgression of *M. trossulus* through the Danish Straits. A higher frequency of *M. trossulus* genes was reported in populations from the Gulf of Finland and Bothnian Sea as identified using an 8-locus allozyme character set (Väinölä and Strelkov, 2011). SNP analysis revealed

up to 76% of *M. trossulus* characteristic alleles in Höga Kusten (Zbawicka et al., 2014a), which was used in this study.

The frequency of *M. edulis* allele at the codominant Glu-5′ locus varied across populations from 1 in the Wadden Sea, Jutland Peninsula to 0.45 in the Bothnian Bay (Table S2A). The *M. trossulus* specific alleles at EFbis marker were distributed across all analysed samples except Augustenborg sample where 100% of *M. edulis* alleles were observed. Average share of *M. trossulus* alleles over all samples was 77% and 5 populations from inner Baltic (Gdańsk Bay, Gotland, Höga Kusten, Kopli Bay) and Vejrø in Smålandsfarvandet, the Great Belt, were monomorphic with *M. trossulus* alleles (Table S2B). The acrosomal sperm protein M7 in this study displays moderate *M. edulis* specific alleles share with maximum (100%) in the northern entrance to the Sound (Hornbæk, Gileleje) and Limfjord (Kås Bredning). Minimum *M. edulis* allele frequency (40%) was noted with this marker in Askö in the central Baltic Sea (Table S2C).

Introgression of *M. edulis* alleles in the Baltic Sea was strong for the ITS marker. Most populations from the Danish coast and Tjärnö were monomorphic with *M. edulis*. The minimum frequency of *M. edulis* was observed in Kõiguste Bay, Estonia (66%) (Table S2D). Clinal differentiation in allele frequencies at Glu-5′, EFbis, M7 and ITS loci have been also reported in populations of *Mytilus* from Sounds and South-Western Baltic by Kijewski et al. (2006), Stuckas et al. (2009, 2017) and Väinölä and Strelkov(2011). The higher percentage of *M. edulis* characteristic alleles in sample GDB in comparison with populations from the central Baltic Sea in the present study and from the shallow site in the Gdańsk Bay presented in Kijewski et al. (2011) can be explained by the different origin of mussels from a deeper site (50 m).

The Bayesian clustering implemented in STRUCTURE for 3 and 4 markers identified two genetic clusters ($K = 2$) corresponding to *M. edulis* and *M. trossulus*, as expected. Three groups of samples could be distinguished. The first group (6 samples) with q values above 0.7 for *M. edulis* cluster (North Sea and northern Danish Straits), The second (18 samples) with values from about 0.6 to 0.2, indicating a high gene admixture (mainly in the Danish Straits), and the last group (11 samples) with *q* values below 0.2 covering the southern and central Baltic. The result reflects the geographical structure of sampling, with a barrier south to Zeland Island, this being similar to results based on SNP (Zbawicka et al., 2014a). The inner Baltic group consisted of samples representing 11 populations, including Gedser and Hjelm from Lolland, Falster and Møn Islands. The PCoA analysis reveals a similar split of populations into three groups along the 1st axis, confirmed with the AMOVA analysis (Fig. 2).

The large-scale patterns of *Mytilus* spp. populations are highly complex and driven by multiple environmental factors. Earlier studies have suggested that direct environmental and resource gradients define the large-scale distribution pattern of *Mytilus* spp. (e.g. Kotta et al., 2015). Direct environmental gradients represent features that have a direct physiological impact on growth but are not consumed, whereas resource gradients are substances being consumed. The most important direct environmental gradients for *Myti-*

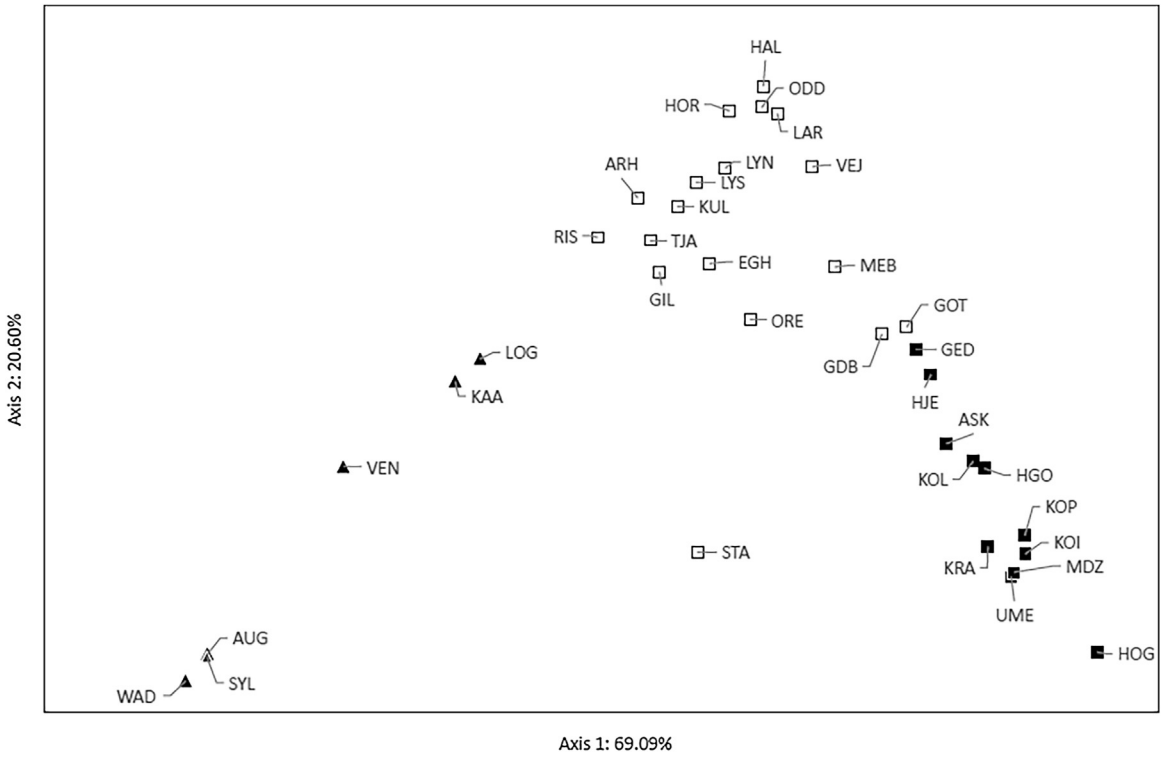

Figure 2 Scatterplot of samples constructed for 3 nuclear DNA markers (EFbis, Glu-5′and ITS). The axes represent the contribution of inertia of the data matrix as an analogue of the total variance in allelic frequencies. Filled triangles — samples from the North Sea (high share of *Mytilus edulis* genes), open squares — samples from transition zone, filled squares — samples from inner and eastern Baltic with higher *Mytilus trossulus* share.

lus spp. are salinity and water exchange and within a favourable distribution range of these direct environmental variables, resource gradients in interaction with direct environmental factors are expected to modulate the patterns of populations. The RF modelling of the allele frequencies of *M. edulis* and *M. trossulus* along environmental gradients described 67 and 68% of the variability in the respective gene frequencies. The model of *M. galloprovincialis* was insignificant and explained only 5% of its allele frequency. The analysis identified strong variability of allele frequencies of *Mytilus* spp. populations along the studied environmental gradients. The most significant source of variation was salinity and to a lesser degree, temperature. The responses of salinity and temperature were not gradual but a clear discontinuity in the allele frequencies was observed at salinity 12 PSU and temperature 16°C (around the eastern islands of Falster and Moen) (Fig. 3). It is important to note that the current statistical analyses involved only arithmetic means of environmental variables and these threshold limits only infer that variability in both salinity and temperature may be behind the current allele frequencies of *Mytilus* spp. The ecological meaning of the observed relationships between environmental variables and the biota is not always obvious and it is as plausible that local salinity and/or temperature minima define the observed patterns of allele frequencies. However, due to high covariation of natural gradients of the minima, means and maxima, their individual effects cannot be separated. Similarly, twenty-six SNP included in the RF analysis were significantly involved in the differentiation between mussels from the North Sea and Baltic area, showing very sharp differences in frequencies forming clines at the Baltic Sea entrance (Zbawicka et al., 2014a). These SNPs based on F_{ST} outlier analysis have been identified as outliers and could be under selection of salinity stress.

Water nutrients, exposure to waves and chlorophyll-*a*, all contributed to the models but their effects were notably lower compared to the effects of salinity and temperature. As salinity and temperature were not intercorrelated with the other studied environmental variables then the observed high contributions of salinity and temperature in the RF models suggest their significance in shaping the allele frequencies of *Mytilus* spp. in the North and Baltic Seas. The existing salinity gradient is much more stable compared to the patterns of factors such as wind and food availability resulting in a strong selection pressure over a centennial-scale. Moreover, as opposed to other environmental gradients (such as exposure to waves and food availability) salinity values are always suboptimal for *Mytilus* spp. in the Baltic Sea basin. The situation may change in the near future as salinity values are expected to be dramatically changed by current climate change influences (BACC, 2015).

This study characterized the geographical distribution pattern of *Mytilus* mussels in the Baltic Sea, Danish Straits and eastern shore of North Sea in terms of PCR species-specific markers. The blue mussels in the Baltic Sea appeared as an established hybrid swarm containing relics of boreal *M. trossulus* under a strong introgression of Atlantic *M. edulis*

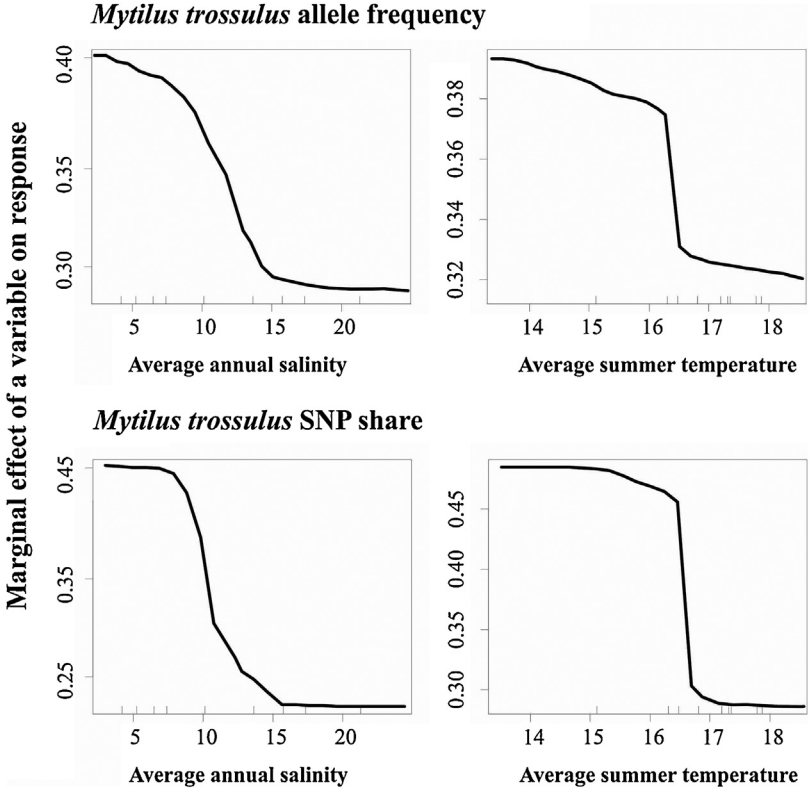

Figure 3 The plots computed in the Random Forest show the relative logit contribution of the variable on the class probability from the perspective of the model. Marginal effect of a variable on response, based on salinity gradient and average frequency of taxon-specific (*Mytilus trossulus*) alleles for EFbis, Glu-5′, ITS and M7 markers and 26 SNPs.

(Väinölä and Strelkov, 2011). The genetic structure of the *Mytilus* spp. transition zone in the Danish Straits is maintained by water currents and also larvae dispersal and water salinity (Larsson et al., 2017; Stuckas et al., 2017; Väinölä and Strelkov, 2011). Our data analysis with Bayesian clustering method STRUCTURE displays a prevalent barrier to gene flow in Falster and Lolland Islands. However PCoA analysis displayed a pattern with distinct samples from the North Sea, and another group split into group east — north from Gotland, and from Gdansk Bay to Stavanger. These spatial positions reflect the main division into the Baltic area and the Danish Straits and larval dispersal pattern across the transition zone (Fraïsse et al., 2016; Stuckas et al., 2017). Salinity and temperature are critical aspects in the marginal habitat of the Baltic Sea, setting the limits for the distribution of various species (Bonsdorff and Pearson, 1999). This study demonstrated multigene clines at the Baltic Sea entrance and the main barrier to gene flow in *Mytilus* populations in the area of the south Danish Islands Falster and Lolland.

The generic result of this study is that salinity appeared to define over 50% of the variability in the gene frequencies of the studied *Mytilus* spp. populations. Changes along this environmental gradient are not gradual but instead, a significant shift from gene dominance was found at a salinity of 12 PSU. Other environmental gradients involved water temperature and trophic status of the sea area but these environmental gradients had only moderate linkage with the gene frequencies. Surprisingly, the gradients that define the availability of food resources (e.g. water chlorophyll-*a* and exposure to waves) were nearly insignificant. However, causalities remain to be determined as the observed gene frequencies along the studied environmental gradients were based on correlations, and multiple possible mechanisms not involved with the current study may have influenced these frequencies. Despite these limitations, the results presented here have helped to understand how the gene frequencies of *Mytilus* spp. were distributed along environmental gradients on a regional scale. As the study involved the most important environmental gradients known to shape distribution of *Mytilus* spp. populations at large scales, the results may have pointed to potential reasoning for causation. The study identified strong interregional variability and showed that patterns of gene frequencies of *Mytilus* spp. were primarily a function of water salinity. However, *M. trossulus* is known to be tolerant to lowered salinity (Qiu et al., 2002; Yaroslavtseva and Sergeeva, 2005), the responsible genetic background still remains unclear (Lockwood and Somero, 2011).

4. Conclusions

This study demonstrated that the novel machine learning technique random forest can be successfully used for finding correlation between genetic differentiation of populations and environmental variables. Populations of the mussels *Mytilus* in the Baltic Sea were used as a model. The genetic differentiation of populations was assayed using 4 known *Mytilus* taxa-specific nuclear DNA markers and published single nucleotide polymorphism markers. Strong genetic differentiation in allele frequencies was correlated with environmental factors along the North Sea — inner Baltic transect. Environmental gradients explained large variability in the studied allele frequencies with salinity contributing the most to observed genetic differences.

Conflict of interest

The authors declare no conflict of interests.

Acknowledgements

This study was partially funded by the BaltGene Bonus Plus, 03/BONUS/2009 SPB, 2011/01/B/NZ9/04352 NCN project to R.W. and Statutory topic IV.1 in the IO PAN. J.K. and M.R. were supported by the Estonian Research Council, Institutional research funding, IUT02-20. The authors thank Dr Agnieszka Kijewska for assistance in figure preparation.

Appendix A. Supplementary data

Supplementary material related to this article can be found, in the online version, at https://doi.org/10.1016/j.oceano.2018.08.002.

References

Albalat, A., Potrykus, J., Pempkowiak, J., Porte, C., 2002. Assessment of organotin pollution along the Polish coast (Baltic Sea) by using mussels and fish as sentinel organisms. Chemosphere 47 (2), 165—171, http://dx.doi.org/10.1016/S0045-6535(01)00294-6.

BACC Author Team, 2015.In: II Second Assessment of Climate Change for the Baltic Sea Basin. Springer-Open, Cham, Heidelberg, New York, Dordrecht, London, 501 pp.

Bach, L., Zbawicka, M., Strand, J., Wenne, R., 2018. *Mytilus trossulus* in NW Greenland is genetically more similar to North Pacific than NW Atlantic populations of the species. Mar. Biodivers., 7 pp., http://dx.doi.org/10.1007/s12526-018-0870-0.

Banks, S.C., Ling, S.D., Johnson, C.R., Piggott, M.P., Williamson, J. E., Beheregaray, L.B., 2010. Genetic structure of a recent climate change-driven range extension. Mol. Ecol. 19 (10), 2011—2024, http://dx.doi.org/10.1111/j.1365-294X.2010.04627.x.

Barsiene, J., Rybakovas, A., Garnaga, G., Andreikenaite, L., 2012. Environmental genotoxicity and cytotoxicity studies in mussels before and after an oil spill at the marine oil terminal in the Baltic Sea. Environ. Monit. Assess. 184 (4), 2067—2078, http://dx.doi.org/10.1007/s10661-011-2100-0.

Bergström, P., Carlsson, M.S., Lindegarth, M., Petersen, J.K., Lindegarth, S., Holmer, M., 2017. Testing the potential for improving quality of sediments impacted by mussel farms using bioturbating polychaete worms. Aquacult. Res. 48 (1), 161—176, http://dx.doi.org/10.1111/are.12870.

Bierne, N., Bonhomme, F., David, P., 2003. Habitat preference and the marine-speciation paradox. Proc. R. Soc. Lond. B 270 (1522), 1399—1406, http://dx.doi.org/10.1098/rspb.2003.2404.

Bjork, M., Gilek, M., 1997. Bioaccumulation kinetics of PCB 31, 49 and 153 in the blue mussel, *Mytilus edulis* L as a function of algal food concentration. Aquat. Toxicol. 38 (1—3), 101—123, http://dx.doi.org/10.1016/S0166-445X(96)00837-5.

Bonsdorff, E., Pearson, T.H., 1999. Variation in the sublittoral macrozoobenthos of the Baltic Sea along environmental gradients: a functional-group approach. Austral. J. Ecol. 24 (4), 312—326, http://dx.doi.org/10.1046/j.1442-9993.1999.00986.x.

Bosch, S., Tyberghein, L., Deneudt, K., Hernandez, F., De Clerck, O., Syphard, A., 2018. In search of relevant predictors for marine species distribution modelling using the MarineSPEED benchmark dataset. Divers. Distrib. 24 (2), 144–157, http://dx.doi.org/10.1111/ddi.12668.

Breiman, L., 2001. Random Forests. Mach. Learn. 45 (1), 5–32, http://dx.doi.org/10.1023/A:1010933404324.

Breiman, L., Cutler, A., 2015. Package 'randomForest'. https://cran.r-project.org/web/packages/randomForest/randomForest.pdf.

Cuéllar-Pinzón, J., Presa, P., Hawkins, S.J., Pita, A., 2016. Genetic markers in marine fisheries: types, tasks and trends. Fish. Res. 173, 194–205, http://dx.doi.org/10.1016/j.fishres.2015.10.019.

Dabrowska, H., Kopko, O., Lehtonen, K.K., Lang, T., Waszak, I., Balode, M., Strode, E., 2017. An integrated assessment of pollution and biological effects in flounder, mussels and sediment in the southern Baltic Sea coastal area. Environ. Sci. Pollut. Res. 24 (4), 3626–3639, http://dx.doi.org/10.1007/s11356-016-8117-8.

Dormann, C.F., Elith, J., Bacher, S., Buchmann, C., Carl, G., Carré, G., Marquez, J.R.G., Gruber, B., Lafourcade, B., Leitao, P.J., Munkemuller, T., McClean, C., Osborne, P.E., Reineking, B., Schroder, B., Skidmore, A.K., Zurell, D., Lautenbach, S., 2013. Collinearity: a review of methods to deal with it and a simulation study evaluating their performance. Ecography 36 (1), 27–46, http://dx.doi.org/10.1111/j.1600-0587.2012.07348.x.

Dowd, W.W., Somero, G.N., 2013. Behavior and survival of *Mytilus* congeners following episodes of elevated body temperature in air and seawater. J. Exp. Biol. 216 (3), 502–514, http://dx.doi.org/10.1242/jeb.076620.

Earl, D.A., vonHoldt, B.M., 2012. STRUCTURE HARVESTER: a website and program for visualizing STRUCTURE output and implementing the Evanno method. Conserv. Genet. Resour. 4 (2), 359–361, http://dx.doi.org/10.1007/s12686-011-9548-7.

Elith, J., Graham, C.H., Anderson, R.P., Dudík, M., Ferrier, S., Guisan, A., Hijmans, R.J., Huettmann, F., Leathwick, J.R., Lehmann, A., Li, J., Lohmann, L.G., Loiselle, B.A., Manion, G., Moritz, C., Nakamura, M., Nakazawa, Y., Overton, Jacob, McC, Peterson, A.T., Phillips, S.J., Richardson, K., Scachetti-Pereira, R., Schapire, R.E., Soberón, J., Williams, S., Wisz, M.S., Zimmermann, N.E., 2006. Novel methods improve prediction of species' distributions from occurrence data. Ecography 29 (2), 129–151, http://dx.doi.org/10.1111/j.2006.0906-7590.04596.x.

Elith, J., Leathwick, J.R., Hastie, T., 2008. A working guide to boosted regression trees. J. Anim. Ecol. 77 (4), 802–813, http://dx.doi.org/10.1111/j.1365-2656.2008.01390.x.

Ericson, H., Thorsen, G., Kumblad, L., 2010. Physiological effects of diclofenac, ibuprofen and propranolol on Baltic Sea blue mussels. Aquat. Toxicol. 99 (2), 223–231, http://dx.doi.org/10.1016/j.aquatox.2010.04.017.

Evanno, G., Regnaut, S., Goudet, J., 2005. Detecting the number of clusters of individuals using the software STRUCTURE: a simulation study. Mol. Ecol. 14 (8), 2611–2620, http://dx.doi.org/10.1111/j.1365-294X.2005.02553.x.

Excoffier, L., Laval, G., Schneider, S., 2005. Arlequin (version 3.0): an integrated software package for population genetics data Analysis. Evol. Bioinform. Online 1, 47–50.

Filipowicz, M., Burzynski, A., Smietanka, B., Wenne, R., 2008. Recombination in mitochondrial DNA of European mussels *Mytilus*. J. Mol. Evol. 67 (4), 377–388, http://dx.doi.org/10.1007/s00239-008-9157-6.

Fraïsse, C., Belkhir, K., Welch, J.J., Bierne, N., 2016. Local interspecies introgression is the main cause of extreme levels of intraspecific differentiation in mussels. Mol. Ecol. 25 (1), 269–286, http://dx.doi.org/10.1111/mec.13299.

Friedman, J.H., 2001. Greedy function approximation: a gradient boosting machine. Ann. Stat. 29 (1), 1189–1232, http://dx.doi.org/10.1111/mec.13299.

Gardner, J.P., Zbawicka, M., Westfall, K.M., Wenne, R., 2016. Invasive blue mussels threaten regional scale genetic diversity in mainland and remote offshore locations: the need for baseline data and enhanced protection in the Southern Ocean. Glob. Change Biol. 22 (9), 3182–3195, http://dx.doi.org/10.1111/gcb.13332.

Gilg, M.R., Hilbish, T.J., 2003. The geography of marine larval dispersal: coupling genetics with fine-scale physical oceanography. Ecology 84 (11), 2989–2998, http://dx.doi.org/10.1890/02-0498.

Grabowska, M., Grzelak, K., Kukliński, P., 2015. Rock encrusting assemblages: structure and distribution along the Baltic Sea. J. Sea Res. 103, 24–31, http://dx.doi.org/10.1016/j.seares.2015.05.003.

Hastie, T., Tibshirani, R., Friedman, J.H., 2009. The Elements of Statistical Learning: Data Mining, Inference, and Prediction. Springer-Verlag, New York, 744 pp.

Heath, D.D., Rawson, P.D., Hilbish, T.J., 1995. PCR-based nuclear markers identify alien blue mussel (*Mytilus spp.*) genotypes on the west coast of Canada. Can. J. Fish. Aquat. Sci. 52 (12), 2621–2627, http://dx.doi.org/10.1139/f95-851.

Hoarau, G., Rijnsdorp, A.D., Van Der Veer, H.W., Stam, W.T., Olsen, J. L., 2002. Population structure of plaice (*Pleuronectes platessa* L.) in northern Europe: microsatellites revealed large-scale spatial and temporal homogeneity. Mol. Ecol. 11 (7), 1165–1176, http://dx.doi.org/10.1046/j.1365-294X.2002.01515.x.

Hoher, N., Kohler, A., Strand, J., Broeg, K., 2012. Effects of various pollutant mixtures on immune responses of the blue mussel (*Mytilus edulis*) collected at a salinity gradient in Danish coastal waters. Mar. Environ. Res. 75 (SI), 35–44, http://dx.doi.org/10.1016/j.marenvres.2011.11.003.

Inoue, K., Waite, J.H., Matsuoka, M., Odo, S., Harayama, S., 1995. Interspecific variations in adhesive protein sequences of *Mytilus edulis*, *M. galloprovincialis*, and *M. trossulus*. Biol. Bull. 189 (3), 370–375, http://dx.doi.org/10.2307/1542155.

Isæus, M., 2004. Factors structuring *Fucus* communities at open and complex coastlines in the Baltic Sea. University of Stockholm Print Center, Stockholm, Frescati, 40 pp.

Jakobsson, M., Rosenberg, N.A., 2007. CLUMPP: a cluster matching and permutation program for dealing with label switching and multimodality in analysis of population structure. Bioinformatics 23 (14), 1801–1806, http://dx.doi.org/10.1093/bioinformatics/btm233.

Johannesson, K., André, C., 2006. INVITED REVIEW: life on the margin: genetic isolation and diversity loss in a peripheral marine ecosystem, the Baltic Sea. Mol. Ecol. 15 (8), 2013–2029, http://dx.doi.org/10.1111/j.1365-294X.2006.02919.x.

Kautsky, N., Evans, S., 1987. Role of biodeposition by *Mytilus edulis* in the circulation of matter and nutrients in a Baltic coastal ecosystem. Mar. Ecol. Prog. Ser. 38 (3), 201–212, http://dx.doi.org/10.3354/meps038201.

Kijewska, A., Burzynski, A., Wenne, R., 2009. Molecular identification of European flounder (*Platichthys flesus*) and its hybrids with European plaice (*Pleuronectes platessa*). ICES J. Mar. Sci. 66 (5), 902–906, http://dx.doi.org/10.1093/icesjms/fsp110.

Kijewska, A., Kalamarz-Kubiak, H., Arciszewski, B., Guellard, T., Petereit, C., Wenne, R., 2016. Adaptation to salinity in Atlantic cod from different regions of the Baltic Sea. J. Exp. Mar. Biol. Ecol. 478, 62–67, http://dx.doi.org/10.1016/j.jembe.2016.02.003.

Kijewski, T., Śmietanka, B., Zbawicka, M., Gosling, E., Hummel, H., Wenne, R., 2011. Distribution of *Mytilus* taxa in European coastal areas as inferred from molecular markers. J. Sea Res. 65 (2), 224–234, http://dx.doi.org/10.1016/j.seares.2010.10.004.

Kijewski, T., Wijsman, J.W.M., Hummel, H., Wenne, R., 2009. Genetic composition of cultured and wild mussels *Mytilus* from The Netherlands and transfers from Ireland and Great Britain. Aquaculture 287 (3–4), 292–296, http://dx.doi.org/10.1016/j.aquaculture.2008.10.048.

Kijewski, T.K., Zbawicka, M., Väinölä, R., Wenne, R., 2006. Introgression and mitochondrial DNA heteroplasmy in the Baltic populations of mussels *Mytilus trossulus* and *M. edulis*. Mar. Biol. 149 (6), 1371–1385, http://dx.doi.org/10.1007/s00227-006-0316-2.

Kopecka, J., Lehtonen, K.K., Barsiene, J., Broeg, K., Vuorinen, P.J., Gercken, J., Pempkowiak, J., 2006. Measurements of biomarker levels in flounder (*Platichthys flesus*) and blue mussel (*Mytilus trossulus*) from the Gulf of Gdansk (southern Baltic). Mar. Pollut. Bull. 53 (8—9), 406—421, http://dx.doi.org/10.1016/j.marpolbul.2006.03.008.

Kotta, J., Oganjan, K., Lauringson, V., Parnoja, M., Kaasik, A., Rohtla, L., Kotta, I., Orav-Kotta, H., 2015. Establishing functional relationships between abiotic environment, macrophyte coverage, resource gradients and the distribution of *Mytilus trossulus* in a brackish non-tidal environment. PLOS ONE 10 (8), e0136949, http://dx.doi.org/10.1371/journal.pone.0136949.

Larraín, M.A., Zbawicka, M., Araneda, C., Gardner, J.P.A., Wenne, R., 2018. Native and invasive taxa on the Pacific coast of South America: impacts on aquaculture, traceability and biodiversity of blue mussels (*Mytilus* spp.). Evol. Appl. 11 (3), 298—311, http://dx.doi.org/10.1111/eva.12553.

Larsen, P., Riisgård, H., 2016. Growth-prediction model for blue mussels (*Mytilus edulis*) on future optimally thinned farm-ropes in Great Belt (Denmark). J. Mar. Sci. Eng. 4 (3), 42, http://dx.doi.org/10.3390/jmse4030042.

Larsson, J., Lind, E.E., Corell, H., Grahn, M., Smolarz, K., Lönn, M., 2017. Regional genetic differentiation in the blue mussel from the Baltic Sea area. Estuar. Coast. Shelf Sci. 195, 98—109, http://dx.doi.org/10.1016/j.ecss.2016.06.016.

Larsson, J., Smolarz, K., Świeżak, J., Turower, M., Czerniawska, N., Grahn, M., 2018. Multi biomarker analysis of pollution effect on resident populations of blue mussels from the Baltic Sea. Aquat. Toxicol. 198, 240—256, http://dx.doi.org/10.1016/j.aquatox.2018.02.024.

Lesser, M.P., 2016. Climate change stressors cause metabolic depression in the blue mussel, *Mytilus edulis*, from the Gulf of Maine. Limnol. Oceanogr. 61 (5), 1705—1717, http://dx.doi.org/10.1002/lno.10326.

Li, S.G., Liu, C., Huang, J.L., Liu, Y.J., Zheng, G.L., Xie, L.P., Zhang, R.Q., 2015. Interactive effects of seawater acidification and elevated temperature on biomineralization and amino acid metabolism in the mussel *Mytilus edulis*. J. Exp. Biol. 218 (22), 3623—3631, http://dx.doi.org/10.1242/jeb.126748.

Liaw, A., Wiener, M., 2002. Classification and regression by Random Forest. R. News 2/3, 18—22.

Lockwood, B.L., Somero, G.N., 2011. Transcriptomic responses to salinity stress in invasive and native blue mussels (genus *Mytilus*). Mol. Ecol. 20 (3), 517—529, http://dx.doi.org/10.1111/j.1365-294X.2010.04973.x.

Malachowicz, M., Kijewska, A., Wenne, R., 2015. Transcriptome analysis of gill tissue of Atlantic cod *Gadus morhua* L. from the Baltic Sea. Mar. Genomics 23, 37—40, http://dx.doi.org/10.1016/j.margen.2015.04.005.

Meier, H.E.M., Hordoir, R., Andersson, H.C., Dieterich, C., Eilola, K., Gustafsson, B.G., Höglund, A., Schimanke, S., 2012. Modeling the combined impact of changing climate and changing nutrient loads on the Baltic Sea environment in an ensemble of transient simulations for 1961—2099. Climate Dyn. 39 (9—10), 2421—2441, http://dx.doi.org/10.1007/s00382-012-1339-7.

Michaelidis, B., Portner, H.O., Sokolova, I., Tomanek, L., 2014. Advances in predicting the impacts of global warming on the mussels *Mytilus galloprovincialis* in the Mediterranean Sea. In: Goffredo, S., Dubinsky, Z. (Eds.), Mediterranean Sea: Its History and Present Challenges. Springer-Verlag, Berlin, 319—339, http://dx.doi.org/10.1007/978-94-007-6704-1_18.

Nyberg, E., Faxneld, S., Danielsson, S., Eriksson, U., Miller, A., Bignert, A., 2015. Temporal and spatial trends of PCBs, DDTs, HCHs, and HCB in Swedish marine biota 1969—2012. Ambio 44 (Suppl. 3, SI), S484—S497, http://dx.doi.org/10.1007/s13280-015-0673-5.

Ozoliņa, Z., 2017. Mussel farming and its potential in the Baltic Sea. Econ. Bus. 30 (1), 40—50, http://dx.doi.org/10.1515/eb-2017-0004.

Peakall, R., Smouse, P.E., 2012. GenAlEx 6.5: genetic analysis in Excel. Population genetic software for teaching and research — an update. Bioinformatics 28 (19), 2537—2539, http://dx.doi.org/10.1093/bioinformatics/bts460.

Pempkowiak, J., Pazdro, K., Kopecka, J., Perez, E., Sole, M., 2006. Toxicants accumulation rates and effects in *Mytilus trossulus* and *Nereis diversicolor* exposed separately or together to cadmium and PAHs. J. Environ. Sci. Health Part A: Toxic/Hazard. Subst. Environ. Eng. 41 (11), 2571—2586, http://dx.doi.org/10.1080/10934520600927963.

Petersen, J.K., Hasler, B., Timmermann, K., Nielsen, P., Tørring, D. B., Larsen, M.M., Holmer, M., 2014. Mussels as a tool for mitigation of nutrients in the marine environment. Mar. Pollut. Bull. 82 (1—2), 137—143, http://dx.doi.org/10.1016/j.marpolbul.2014.03.006.

Piwoni-Piórewicz, A., Kuklinski, P., Strekopytov, S., Humphreys-Williams, E., Najorka, J., Iglikowska, A., 2017. Size effect on the mineralogy and chemistry of *Mytilus trossulus* shells from the southern Baltic Sea: implications for environmental monitoring. Environ. Monit. Assess. 189 (4), 197, http://dx.doi.org/10.1007/s10661-017-5901-y.

Pocwierz-Kotus, A., Bernas, R., Debowski, P., Kent, M.P., Lien, S., Kesler, M., Titov, S., Leliuna, E., Jespersen, H., Drywa, A., Wenne, R., 2014. Genetic differentiation of southeast Baltic populations of sea trout inferred from single nucleotide polymorphisms. Anim. Genet. 45 (1), 96—104, http://dx.doi.org/10.1111/age.12095.

Potrykus, J., Albalat, A., Pempkowiak, J., Porte, C., 2003. Content and pattern of organic pollutants (PAHs, PCBs and DDT) in blue mussels (*Mytilus trossulus*) from the southern Baltic Sea. Oceanologia 45 (2), 337—355.

Pritchard, J.K., Stephens, M., Donnelly, P., 2000. Inference of population structure using multilocus genotype data. Genetics 155 (2), 945—959.

Protasowicki, M., Dural, M., Jaremek, J., 2008. Trace metals in the shells of blue mussels (*Mytilus edulis*) from the Poland coast of Baltic sea. Environ. Monit. Assess. 141 (1—3), 329—337, http://dx.doi.org/10.1007/s10661-007-9899-4.

Qiu, J.-W., Tremblay, R., Bourget, E., 2002. Ontogenetic changes in hyposaline tolerance in the mussels *Mytilus edulis* and *M. trossulus*: implications for distribution. Mar. Ecol. Prog. Ser. 228, 143—152, http://dx.doi.org/10.3354/meps228143.

Rawson, P.D., Hilbish, T.J., 1998. Asymmetric introgression of mitochondrial DNA among European populations of blue mussels (*Mytilus* spp.). Evolution 52 (1), 100—108, http://dx.doi.org/10.1111/j.1558-5646.1998.tb05142.x.

Riddle, B.R., Dawson, M.N., Hadly, E.A., Hafner, D.J., Hickerson, M. J., Mantooth, S.J., Yoder, A.D., 2008. The role of molecular genetics in sculpting the future of integrative biogeography. Prog. Phys. Geogr. 32 (2), 173—202, http://dx.doi.org/10.1177/0309133308093822.

Riginos, C., Wang, D., Abrams, A.J., 2006. Geographic variation and positive selection on M7 lysin, an acrosomal sperm protein in mussels (*Mytilus* spp.). Mol. Biol. Evol. 23 (10), 1952—1965, http://dx.doi.org/10.1093/molbev/msl062.

Silliman, B.R., Bertness, M.D., Altieri, A.H., Griffin, J.N., Bazterrica, M.C., Hidalgo, F.J., Crain, C.M., Reyna, M.V., 2011. Whole-community facilitation regulates biodiversity on Patagonian rocky shores. PLOS One 6 (10), e24502, http://dx.doi.org/10.1371/journal.pone.0024502.

Smietanka, B., Zbawicka, M., Sanko, T., Wenne, R., Burzynski, A., 2013. Molecular population genetics of male and female mitochondrial genomes in subarctic *Mytilus trossulus*. Mar. Biol. 160 (7), 1709—1721, http://dx.doi.org/10.1007/s00227-013-2223-7.

Stuckas, H., Knobel, L., Schade, H., Breusing, C., Hinrichsen, H.H., Bartel, M., Langguth, K., Melzner, F., 2017. Combining hydrodynamic modelling with genetics: can passive larval drift shape the

genetic structure of Baltic *Mytilus* populations? Mol. Ecol. 26 (10), 2765—2782, http://dx.doi.org/10.1111/mec.14075.

Stuckas, H., Stoof, K., Quesada, H., Tiedemann, R., 2009. Evolutionary implications of discordant clines across the Baltic Mytilus hybrid zone (*Mytilus edulis* and *Mytilus trossulus*). Heredity 103 (2), 146—156, http://dx.doi.org/10.1038/hdy.2009.37.

Sylvester, E.V.A., Bentzen, P., Bradbury, I.R., Clement, M., Pearce, J., Horne, J., Beiko, R.G., 2018. Applications of random forest feature selection for fine-scale genetic population assignment. Evol. Appl. 11 (2), 153—165, http://dx.doi.org/10.1111/eva.12524.

Szefer, P., Frelek, K., Szefer, K., Lee, C.B., Kim, B.S., Warzocha, J., Zdrojewska, I., Ciesielski, T., 2002. Distribution and relationships of trace metals in soft tissue, byssus and shells of *Mytilus edulis trossulus* from the southern Baltic. Environ. Pollut. 120 (2), 423—444, http://dx.doi.org/10.1016/S0269-7491(02)00111-2.

Szefer, P., Szefer, K., 1990. Metals in molluscs and associated bottom sediments of the Southern Baltic. Helgolander Meeresun. 44 (3—4), 411—424, http://dx.doi.org/10.1007/BF02365477.

Szefer, P., Wenne, R., 1987. Concentration of uranium and thorium in molluscs inhabiting Gdańsk Bay, Baltic Sea. Sci. Total Environ. 65, 191—202, http://dx.doi.org/10.1016/0048-9697(87)90172-0.

Szymczak-Zyla, M., Wawrzyniak-Wydrowska, B., Kowalewska, G., 2006. Products of chlorophyll a transformation by selected benthic organisms in the Odra Estuary (southern Baltic Sea). Hydrobiologia 554, 155—164, http://dx.doi.org/10.1007/s10750-005-1016-5.

Telesca, L., Michalek, K., Sanders, T., Peck, L.S., Thyrring, J., Harper, E.M., 2018. Blue mussel shell shape plasticity and natural environments: a quantitative approach. Sci. Rep. 8, Art. No. 2865, 15 pp., http://dx.doi.org/10.1038/s41598-018-20122-9.

Thomsen, J., Melzner, F., 2010. Moderate seawater acidification does not elicit long-term metabolic depression in the blue mussel *Mytilus edulis*. Mar. Biol. 157 (12), 2667—2676, http://dx.doi.org/10.1007/s00227-010-1527-0.

Utermann, C., Parrot, D., Breusing, C., Stuckas, H., Staufenberger, T., Blumel, M., Labes, A., Tasdemir, D., 2018. Combined genotyping, microbial diversity and metabolite profiling studies on farmed *Mytilus* spp. from Kiel Fjord. Sci. Rep. 8, Art No. 7983, 13 pp., http://dx.doi.org/10.1038/s41598-018-26177-y.

Väinölä, R., Hvilsom, M.M., 1991. Genetic divergence and a hybrid zone between Baltic and North Sea *Mytilus* populations (Mytilidae: Mollusca). Biol. J. Linn. Soc. 43 (2), 127—148, http://dx.doi.org/10.1111/j.1095-8312.1991.tb00589.x.

Väinölä, R., Strelkov, P., 2011. *Mytilus trossulus* in Northern Europe. Mar. Biol. 158 (4), 817—833, http://dx.doi.org/10.1007/s00227-010-1609-z.

Valladares, F., Matesanz, S., Guilhaumon, F., Araujo, M.B., Balaguer, L., Benito-Garzon, M., Cornwell, W., Gianoli, E., van Kleunen, M., Naya, D.E., Nicotra, A.B., Poorter, H., Zavala, M.A., 2014. The effects of phenotypic plasticity and local adaptation on forecasts of species range shifts under climate change. Ecol. Lett. 17 (11), 1351—1364, http://dx.doi.org/10.1111/ele.12348.

Vuorinen, I., Hänninen, J., Rajasilta, M., Laine, P., Eklund, J., Montesino-Pouzols, F., Corona, F., Junker, K., Meier, H.E.M., Dippner, J.W., 2015. Scenario simulations of future salinity and ecological consequences in the Baltic Sea and adjacent North Sea areas — implications for environmental monitoring. Ecol. Indic. 50, 196—205, http://dx.doi.org/10.1016/j.ecolind.2014.10.019.

Watson, J.R., Hays, C.G., Raimondi, P.T., Mitarai, S., Dong, C., McWilliams, J.C., Blanchette, C.A., Caselle, J.E., Siegel, D.A., 2011. Currents connecting communities: nearshore community similarity and ocean circulation. Ecology 92 (6), 1193—1200, http://dx.doi.org/10.1890/10-1436.1.

Wenne, R., 2018. Single nucleotide polymorphism markers with applications in aquaculture and assessment of its impact on natural populations. Aquat. Living Resour. 31, Art No. 2, 17 pp., http://dx.doi.org/10.1051/alr/2017043.

Wenne, R., Bach, L., Zbawicka, M., Strand, J., McDonald, J.H., 2016. A first report on coexistence and hybridization of *Mytilus trossulus* and *M. edulis* mussels in Greenland. Polar Biol. 39, 343—355, http://dx.doi.org/10.1007/s00300-015-1785-x.

Wennerström, L., Laikre, L., Ryman, N., Utter, F.M., Ab Ghani, N.I., André, C., DeFaveri, J., Johansson, D., Kautsky, L., Merilä, J., Mikhailova, N., Pereyra, R., Sandström, A., Teacher, A.G.F., Wenne, R., Vasemägi, A., Zbawicka, M., Johannesson, K., Primmer, C.R., 2013. Genetic biodiversity in the Baltic Sea: species-specific patterns challenge management. Biodiv. Conserv. 22 (13—14), 3045—3065, http://dx.doi.org/10.1007/s10531-013-0570-9.

Yaroslavtseva, L.M., Sergeeva, E.P., 2005. Adaptivity of the bivalve *Mytilus trossulus* larvae to short and long-term changes in water temperature and salinity. Rus. J. Mar. Biol. 32 (2), 82—87, http://dx.doi.org/10.1134/S1063074006020027.

Zbawicka, M., Burzynski, A., Wenne, R., 2007. Complete sequences of mitochondrial genomes from the Baltic mussel *Mytilus trossulus*. Gene 406, 191—198, http://dx.doi.org/10.1016/j.gene.2007.10.003.

Zbawicka, M., Drywa, A., Śmietanka, B., Wenne, R., 2012. Identification and validation of novel SNP markers in European populations of marine *Mytilus* mussels. Mar. Biol. 159 (6), 1347—1362, http://dx.doi.org/10.1007/s00227-012-1915-8.

Zbawicka, M., Sańko, T., Strand, J., Wenne, R., 2014a. New SNP markers reveal largely concordant clinal variation across the hybrid zone between *Mytilus* spp. in the Baltic Sea. Aquat. Biol. 21 (21), 25—36, http://dx.doi.org/10.3354/ab00566.

Zbawicka, M., Skibinski, D., Wenne, R., 2003a. Doubly uniparental transmission of mitochondrial DNA length variants in the mussel *Mytilus trossulus*. Mar. Biol. 142 (3), 455—460, http://dx.doi.org/10.1007/s00227-002-0969-4.

Zbawicka, M., Trucco, M.I., Wenne, R., 2018. Single nucleotide polymorphisms in native South American Atlantic coast populations of smooth shelled mussels: hybridization with invasive European *Mytilus galloprovincialis*. Genet. Sel. Evol. 50, Art. No. 5, 14 pp., http://dx.doi.org/10.1186/s12711-018-0376-z.

Zbawicka, M., Wenne, R., Burzynski, A., 2014b. Mitogenomics of recombinant mitochondrial genomes of Baltic Sea *Mytilus* mussels. Mol. Genet. Genomics: MGG 289 (6), 1275—1287, http://dx.doi.org/10.1007/s00438-014-0888-3.

Zbawicka, M., Wenne, R., Skibinski, D.O.F., 2003b. Mitochondrial DNA variation in populations of the mussel *Mytilus trossulus* from the Southern Baltic. Hydrobiologia 499, 1—12, http://dx.doi.org/10.1023/A:1026356603105.

Oceanologia (2019) 61, 143—169

Available online at www.sciencedirect.com

ScienceDirect

journal homepage: www.journals.elsevier.com/oceanologia/

ORIGINAL RESEARCH ARTICLE

Average nutrient and chlorophyll distributions in the western Mediterranean: RADMED project

María del Carmen García-Martínez [a,*], Manuel Vargas-Yáñez [a], Francina Moya [a], Rocío Santiago [b], María Muñoz [c], Andreas Reul [c], Teodoro Ramírez [a], Rosa Balbín [b]

[a] *Instituto Español de Oceanografía, C.O. Málaga (Fuengirola), Spain*
[b] *Instituto Español de Oceanografía, C.O. Baleares, Spain*
[c] *Universidad de Málaga. Departamento de Ecología, Spain*

Received 31 May 2018; accepted 16 August 2018
Available online 2 September 2018

KEYWORDS
Inorganic nutrients;
Chlorophyll;
Western Mediterranean;
Climatological values;
Time series;
Climate change

Abstract Because of its reduced dimensions and its location, surrounded by three continents, the Mediterranean Sea could be especially vulnerable to climate change effects. An increase of the water column stratification could inhibit winter mixing and reduce the frequency and intensity of convection processes which inject nutrients into the photic layer and are responsible for the ventilation of deep waters. In this context, the long-term monitoring of the Mediterranean waters is a basic task. The RADMED project is a monitoring program that covers the waters from the eastern side of the Gibraltar Strait to the Catalan and Balearic Seas. This project was initiated in 2007, merging some previous programs, some of them initiated in 1992. The main objective of this project is to establish average distributions, ranges of variability and long-term trends for physical, and biochemical variables which could be considered as indicative of the environmental state of the sea. The present work analyses nutrient, chlorophyll and oxygen time series from 2007 to 2015 in some cases and from 1992 in other cases. The current analyses show a clear trophic gradient in the RADMED area. Nutrient and chlorophyll concentrations and the intensity of the deep chlorophyll maximum decrease northeastward. The deep chlorophyll maximum depth increases to the northeast. The Balearic and Catalan Seas show a clear seasonal pattern with maximum surface concentrations for nutrients and chlorophyll in winter/spring, associated with winter mixing. On the contrary, the Alboran Sea does not show such a clear seasonal cycle,

* Corresponding author at: Instituto Español de Oceanografía, Centro Oceanográfico de Málaga (Fuengirola), n/n, 29640 Fuengirola (Málaga), Spain.
E-mail address: mcarmen.garcia@ieo.es (M.d.C. García-Martínez).
Peer review under the responsibility of Institute of Oceanology of the Polish Academy of Sciences.

Production and hosting by Elsevier

https://doi.org/10.1016/j.oceano.2018.08.003

probably because of the existence of permanent upwelling processes acting along the whole year. The Atlantic Water occupying the upper part of the water column shows a Redfield N:P ratio close to or lower than 16, indicating no phosphorus limitation. Finally, chlorophyll concentrations seem to have increased from 1992 to 2015 in the Alboran Sea, while no long-term changes could be established for the rest of the variables and geographical areas.

1. Introduction

The Mediterranean Sea is characterized by an anti-estuarine circulation with fresh Atlantic Water (AW) flowing at the surface into the Mediterranean, and saltier Mediterranean Water outflowing at depth to the Atlantic. The surface AW has low nutrient concentrations while the Mediterranean Water (MW) shows higher values. The result is a net nutrient transport from the Mediterranean to the Atlantic and, as a consequence, the oligotrophic character of the Mediterranean Sea (Bethoux et al., 1998, 2002; D'Ortenzio and Ribera d'Alcala, 2009; Powley et al., 2017; Schroeder et al., 2010). This oligotrophy increases from west to east at the same time that phytoplanktonic biomass and the *f* ratio (new to total primary production) decrease (Bethoux et al., 1998; Estrada, 1996; Lavigne et al., 2015). This nutrient deficit is compensated by river runoff, atmospheric depositions and nitrogen-fixing organisms (Bethoux et al., 1998; Macías et al., 2014, 2018).

In spite of this general oligotrophy, the Mediterranean Sea is able to sustain moderate levels of primary production. This fact has been known as the "Mediterranean paradox" (Estrada, 1996; Sournia, 1973). The explanation seems to be a high regenerated production and the existence of several fertilizing mechanisms acting at some specific locations within the Mediterranean. These processes are: frontal and mesoscales structures responsible for an important vertical circulation, winter mixing (intermediate and deep convection) and nutrient inputs from such rivers as the Nile, Rhone, Po and Ebro. Furthermore, the AW flowing into the Western Mediterranean (WMED) is not as impoverished as previously thought. Intense current shear, internal tides and the upward displacement of the Atlantic-Mediterranean interface, from southwest to northeast at the Strait of Gibraltar, are able to inject nitrate and phosphate into the upper layer of the WMED (Echevarría et al., 2002; Gómez et al., 2000, Gómez, 2003; Huertas et al., 2012). These mechanisms would account for the difference between the oligotrophy of the WMED and the ultra-oligotrophy of the Eastern Mediterranean (EMED, Powley et al., 2017). The result of these different mechanisms is the existence of a complex distribution of trophic regimes, with some areas showing a behavior similar to that of sub-tropical regions and other ones closer to temperate zones (D'Ortenzio and Ribera d'Alcala, 2009).

As already commented, the distributions of nutrients, chlorophyll and dissolved oxygen (DO) are modulated by several processes and therefore can differ across the Mediterranean Sea. Nevertheless, some common features can be established. In the case of the WMED, nutrient concentrations at surface layers are very low during the stratified period (late spring to autumn) and increase to maximum values at the depth of the Levantine Intermediate Water (LIW, 200—400 m) with concentrations around 9.5 μM and 0.45 μM for nitrate and phosphate respectively. These concentrations then slightly decrease to the sea bottom (8.5 μM and 0.4 μM). Silicate concentrations simply increase with depth without any maximum at intermediate levels. This fact has been attributed to lower remineralization rates. An almost ubiquitous Deep Chlorophyll Maximum (DCM) is also observed for the stratified period at depths increasing from west to east. During the mixing period (late autumn to winter), surface nutrient concentrations increase and the position of the DCM is shallower or even disappears, being the maximum chlorophyll concentrations at the sea surface (Lavigne et al., 2015). DO is at saturation levels at the sea surface increasing to a maximum value linked to photosynthetic activity at the depth of the DCM or above it. The nutrient maxima at the LIW depth are also accompanied by a DO minimum. DO values increase to the sea bottom, as deep waters are well ventilated by winter deep convection processes occurring in the Northwestern Mediterranean.

The Mediterranean Sea has been considered as a sea "under siege" (Coll et al., 2011). Several anthropogenic stressors such as an increasing population at the coast or the increase of agriculture, industrial and tourism activities seem to threaten marine ecosystems enhancing phenomena such as eutrophication at some coastal areas (Macías et al., 2018). It has also been suggested that climate change could increase the vertical thermal stratification and/or increase the stratified period, decreasing the nutrient supply to the photic layer (Calvo et al., 2011). A similar effect would be expected from a reduction in the intensity and frequency of intermediate and deep convection which is responsible for the ventilation of deep waters and the injection of nutrients at the upper part of the water column. Some areas of the world ocean have already evidenced a reduction of the DO content associated with the solubility decrease of warming waters and the lower ventilation rates (Schmidtko et al., 2017).

Within this context, the monitoring of the biogeochemical properties of the Mediterranean waters becomes a basic task. Climatological values, variability ranges and the detection of possible trends is of prime importance for the detection and quantification of climate change and other anthropogenic effects. Beside this, routine time series of variables such as nutrients, chlorophyll-*a*, phyto- and zooplankton abundance, *etc*. could be beneficial for operational services (www.emodnet.eu, www.copernicus.eu). Nevertheless, oceanographic stations with periodic *in situ* sampling of biochemical variables are scarce. For the case of the WMED, one of the

longest open sea periodic stations is the Dyfamed station at the Ligurian Sea (Marty and Chiavérini, 2002, 2010; Pasqueron de Fommervault et al., 2015). Examples of coastal oceanographic stations are the Blanes Bay Microbial Observatory in the Catalan coast (see for instance Gasol et al., 2016) or those in the Italian RITMARE network (Ravaioli et al., 2018). General descriptions of the vertical and horizontal distributions of nutrient and chlorophyll-*a* concentrations have been obtained from the compilation of *in situ* measurements from oceanographic surveys (Manca et al., 2004) or from the analysis and inter-calibration of fluorescence profiles (Lavigne et al., 2015). Nevertheless, the information is scarce and unevenly distributed not allowing to obtain seasonal climatological profiles for some areas and some variables such as chlorophyll-*a* (Manca et al., 2004). In other cases, our knowledge about the seasonal dynamics of nutrients and phytoplankton communities do not derive from long-term time series, but from research projects covering just one seasonal cycle. Although very valuable information has been obtained, it seems to be unevenly distributed. A good example is the westernmost part of the Mediterranean Sea. A large amount of information is available for the continental shelf and slope of the Catalan Sea and the frontal zone at the Catalan shelf break (Estrada et al., 2014; Gasol et al., 2016; Latasa et al., 2010; 2016; Segura-Noguera et al., 2016). Similarly, a large number of surveys have described the nutrient, chlorophyll, phyto- and zooplankton communities and the primary production in the Alboran Sea (L'Helguen et al., 2002; Morán and Estrada, 2001; Ramírez et al., 2005; Reul et al., 2005), paying special attention to the upwelling areas in the Northwestern Alboran Sea and the Almería-Orán front. On the contrary, biogeochemical information from the Balearic Sea, the Balearic front, and mainly the eastern coast of the Spanish Mediterranean, from the north of Cape Gata to Valencia Gulf is very sparse.

One attempt to fill these gaps corresponds to the RADMED program from the Instituto Español de Oceanografía (Spanish Institute for Oceanography). This project is devoted to the implementation and maintenance of a monitoring system around the continental shelf and slope, including some deep stations (>2000 m) around the Spanish Mediterranean (López-Jurado et al., 2015; Tel et al., 2016). It is aimed at the study of the seasonal and long-term variability of the westernmost Mediterranean waters from a multidisciplinary point of view. Oceanographic stations are visited on a seasonal basis since 1992 in some cases and since 2007 in the case of the stations most recently included in the RADMED project. Garcia-Martinez et al. (2018), Vargas-Yáñez et al. (2017) have shown that temperature and salinity data from the RADMED project can be merged with historical data in order to construct long time series. These works updated temperature and salinity time series by extending the previous ones to 2015 (inclusive). The goal of the present work is to complete the hydrological information presented in previous works with nutrient, chlorophyll and DO distributions along the RADMED area. In some cases, the length of the time series will allow us to establish climatological profiles and ranges of variability as well as linear trends which could be used as a reference for future works and operational services. In other cases, the oceanographic stations have been initiated very recently and they will simply be used as a first attempt to estimate the average seasonal cycles of nutrient, chlorophyll and DO concentrations, relating them to the physical forcing and general circulation of the WMED. Section 2 presents the data set, Section 3 shows the main results, and a discussion and summary are presented in Section 4.

2. Data and methods

The RADMED project is a monitoring program funded by the Instituto Español de Oceanografía. This program was launched in 2007, unifying and extending previous monitoring programs: ECOMÁLAGA, initiated in 1992 in the area of the Málaga Bay, ECOBALEARES, initiated in 1994 to the south of Mallorca Island, and ECOMURCIA and CIRBAL to the south of Cape Palos and in the Balearic Channels respectively, initiated in 1996 (Fig. 1). The stations are distributed in transects perpendicular to the coast, covering the continental shelf and slope and in some cases some deep stations (>2000 m). Stations are named by a letter corresponding to each transect and a number increasing from the coast to the open sea. In the Alboran Sea, the westernmost transects are Cape Pino (P in Fig. 1), Málaga (M) and Vélez (V). For instance, the closest station to the coast in Cape Pino transect is named as P1, and the most offshore station is P4. Sacratif transect extends from Cape Sacratif in the central part of the Alborán Sea, and Cape Gata transect (CG) is on its eastern limit. Those transects extending from the eastern Spanish coast are Cape Palos (CP), Tarragona (T) and Barcelona (BNA). Two more transects are located in the Balearic Islands, one of them to the south of Mallorca Island (B) and another one extending in a northeast direction from Menorca Island (MH). 37 oceanographic stations forming two triangles cover the Balearic channels: The Ibiza channel between the peninsula and Ibiza Island and the Mallorca channel between Ibiza and Mallorca. These stations are labelled as C. Finally a deep station (>2200 m) is located to the south of Cabrera Island (EPC). All the stations are visited three-monthly, that is, once per season, unless weather conditions or technical problems prevent the sampling.

CTD profiles are obtained in all the stations. The hydrographic sampling is done using CTDs, mainly model SBE 911 and as spare instruments, the models SBE 25 or SBE 19+, installed in a carousel water sampler SBE 32. CTDs are equipped with a Dissolved Oxygen SBE 43 sensor. DO and conductivity sensors are calibrated using water samples for selected depths of the water column at least once for a campaign, when it lasts less than a week, and at least at the beginning and at the end of the campaign, when it is longer. The DO determinations to calibrate the SBE 43 sensor are performed by the Winkler titration method (Strickland and Parsons, 1972) and by direct spectrophotometry of total iodine at 456 nm (Labasque et al., 2004; Pai et al., 1993). The salinity calibrations are done using a Guildline 8400 Autosal.

Water samples for the determination of nutrients and chlorophyll-*a* are taken at all the stations. Water samples for nutrient determinations are taken at 0, 10, 20, 50, 75, 100, 200, 300, 500, 700, 1000 m, and sea bottom for deep stations while sampling is limited to the station depth for the shallower ones. Nutrient samples are collected using 12 ml vials that are kept frozen at −20°C until they are analyzed in the laboratory. Nitrate, nitrite and silicate concentrations

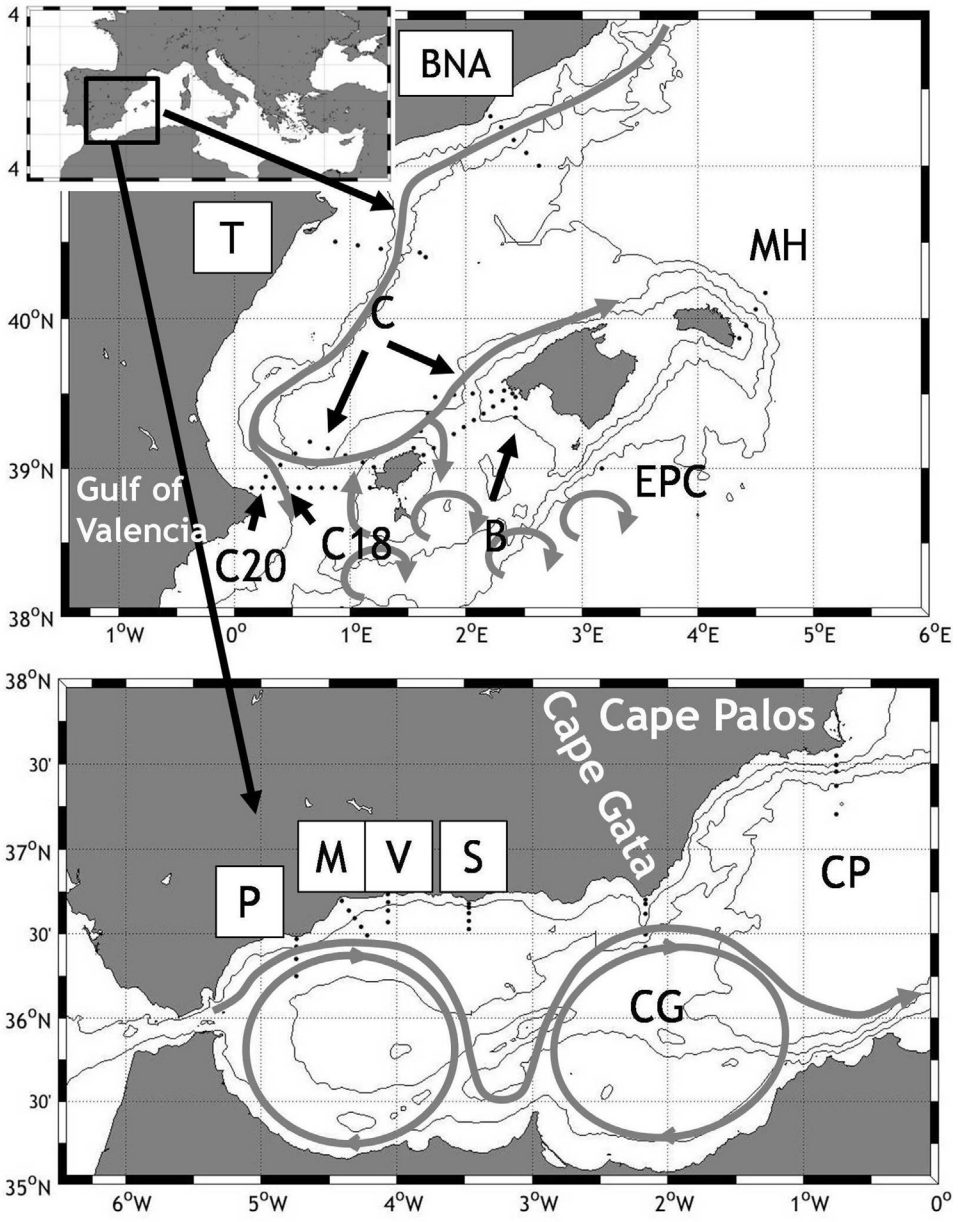

Fig. 1 RADMED area within the Western Mediterranean. The upper map shows the northern RADMED stations. The lower map shows the Alboran Sea and Cape Palos RADMED stations. The labels for each transect are included. Stations C20 (continental shelf) and C18 (continental slope) from the Ibiza Channel are also indicated. 200, 500 and 1000 m isobaths have been included. The grey line shows a schematic of the AW circulation.

are determined according to the methods in Grasshof et al. (1983). Phosphate concentrations are determined by the method of Treguer and Le Corre (1975). All these methods are adapted to oligotrophic waters and analyses are performed with a Technicon Autoanalyzer AAIII and QuAAtro Marine of SEAL 25 Analytical. Samples for chlorophyll-*a* determinations are limited to the upper 100 m of the water column (0, 10, 20, 50, 75 and 100 m), or to the maximum depth for shallower stations. 1 l samples are filtered and kept frozen at −20°C until they are analyzed by fluorometry (Holm-Hansen et al., 1965) using a Turner 10 AU spectrofluorometer previously calibrated with pure chlorophyll-*a*.

For each transect, stations labelled as 2 are considered as representative of the continental shelf conditions and stations 4 represent the continental slope. Stations 2 are located over a bottom depth ranging from 75 to 295 m with most of the stations over 75 m depth. Stations labelled as 4 are at the continental slope with bottom depths ranging from 300 to 2500 m. For the triangles covering the Balearic Channels, stations C20 and C18 were chosen as representative of the peninsular continental shelf and slope conditions respectively (see Fig. 1). Table 1 shows the position, initial time, depth and sampling depths of stations labelled as 2 and 4. Protocols and further details about the sampling and data analysis can be

Table 1 Columns 1—4 show the positions for the stations labelled as 2 (continental shelf) and 4 (continental slope). Column 5 and 6 are the station name and depths respectively. Column 7 is the year when the sampling was initiated and column 8 shows the discrete depths where nutrients and chlorophyll is sampled.

Longitude (degrees)	Longitude (minutes)	Latitude (degrees)	Latitude (minutes)	Station	Depth	Initial year	Sampling depths
1	2	3	4	5	6	7	8
−4	−44.4960	36	25.4280	P2	130	1992	0-10-20-50-75-100-bottom
−4	−44.4960	36	15.0000	P4	870	2007	0-10-20-50-75-100-200-300-500-bottom
−4	−21.2160	36	38.3160	M2	75	1992	0-10-20-50-75
−4	−15.8280	36	32.5380	M4	350	2000	0-10-20-50-75-100-200-bottom
−4	−3.8460	36	41.2500	V2	75	1992	0-10-20-50-75
−4	−3.9000	36	34.2000	V4	490	2000	0-10-20-50-75-100-200-300-bottom
−3	−28.0920	36	39.3480	S2	300	2007	0-10-20-50-75-100-200-300
−3	−28.0920	36	34.6140	S4	650	2007	0-10-20-50-75-100-200-300-500-bottom
−2	−9.9120		40.6500	CG2	75	2007	0-10-20-50-75
−2	−9.9120	36	29.8260	CG4	700	2007	0-10-20-50-75-100-200-300-500-700
0	−45.4500	37	29.7900	CP2	75	2007	0-10-20-50-75
0	−45.4500	37	22.3680	CP4	2100	2003	0-10-20-50-75-100-200-300-500-700-1000-bottom
2	25.6020	39	28.6020	B1	75	1994	0-25-50-75
2	25.6020	39	24.1020	B2	100	1994	0-25-50-75-100
2	25.6020	39	20.5020	B3	200	1994	0-25-50-75-100-200
0	27.0000	38	52.2000	C18	300	1999	0-25-50-75-100-200-300
0	14.5980	38	52.2000	C20	95	2002	0-25-50-75-bottom
4	25.0020	39	57.0000	Mh2	180	2007	0-25-50-75-100-bottom
4	34.9620	40	10.0020	Mh4	2500	2007	0-25-50-75-100-200-300-500-700-1000-1500-bottom
1	3.8820	40	28.7700	T2	75	2007	0-10-20-50-75
1	36.0000	40	25.9020	T4	950	2007	0-10-20-50-75-100-200-300-500-700-bottom
2	18.1320	41	15.0000	BNA2	295	2007	0-10-20-50-75-100-200-bottom
2	31.1700	41	4.9980	BNA4	1320	2007	0-10-20-50-75-100-200-300-500-700-1000-bottom

seen in López-Jurado et al. (2015) or in www.repositorio.ieo.es/e-ieo/handle/10508/1762. The present work will be mainly focused on the analysis of stations 2 and 4. Additionally, stations P3, M3, V3 and CP3 over the shelf break will be analyzed because of its length and good temporal coverage.

All the individual profiles (four per year when there were no missing values) were grouped by seasons: winter (January—March), spring (April—June), summer (July—September) and autumn (October—December). Average profiles were calculated for each season for potential temperature, salinity, nitrate, nitrite, phosphate, silicate, DO and chlorophyll-*a*. Notice that nutrient and chlorophyll-*a* profiles were calculated at discrete depths.

The mixed layer depth (MLD) was calculated for each individual profile using both the maximum curvature criterion (Lorbacher et al., 2006) and the threshold method (De Boyer Montégut et al., 2004). After comparison of both methods, the latter was selected. The MLD was considered as that where the temperature was 0.3°C lower than a reference value that was considered as the temperature at 10 m depth. Once the MLD was determined for each temperature profile, the values were seasonally grouped and the average MLD was obtained for each season. A similar calculation was carried out for the nutricline which was considered as the depth where nitrate plus nitrite exceeded 1 μM (Macias et al., 2008). Secchi disk measurements were also obtained at stations 2 and 4 for each transect. Values for each station were also grouped by season and the average seasonal cycle was obtained.

The seasonal cycle for all the variables analyzed is made of four values corresponding to the winter, spring, summer and autumn mean values. These seasonal cycles were subtracted to the initial time series for obtaining time series of residuals or deviations. Such residuals time series were used for the estimation of decadal changes.

3. Results

3.1. Distribution of water masses

Fig. 2A shows the potential temperature-salinity (θS) diagrams for the Gulf of Cadiz, close to the Strait of Gibraltar and the θS diagrams for the continental shelf (Fig. 2B, C) and continental slope stations (Fig. 2D, E) in the RAMED area (hereafter it will always be written temperature for brevity but potential temperature is always used). The θS diagram for the Gulf of Cadiz shows the water mass flowing into the Mediterranean Sea. This figure is included in order to show the continuous modification of the waters occupying the upper layer (0—150 m) of the Mediterranean Sea. Differences between the θS diagrams in the RADMED stations and the properties of the water masses in the Gulf of Cadiz provide information about the degree of mixing with the underlying Mediterranean waters. The winter inflow corresponds to the upper part of the North Atlantic Central Water (NACW). The maximum depth of Camarinal Sill in the Strait of Gibraltar

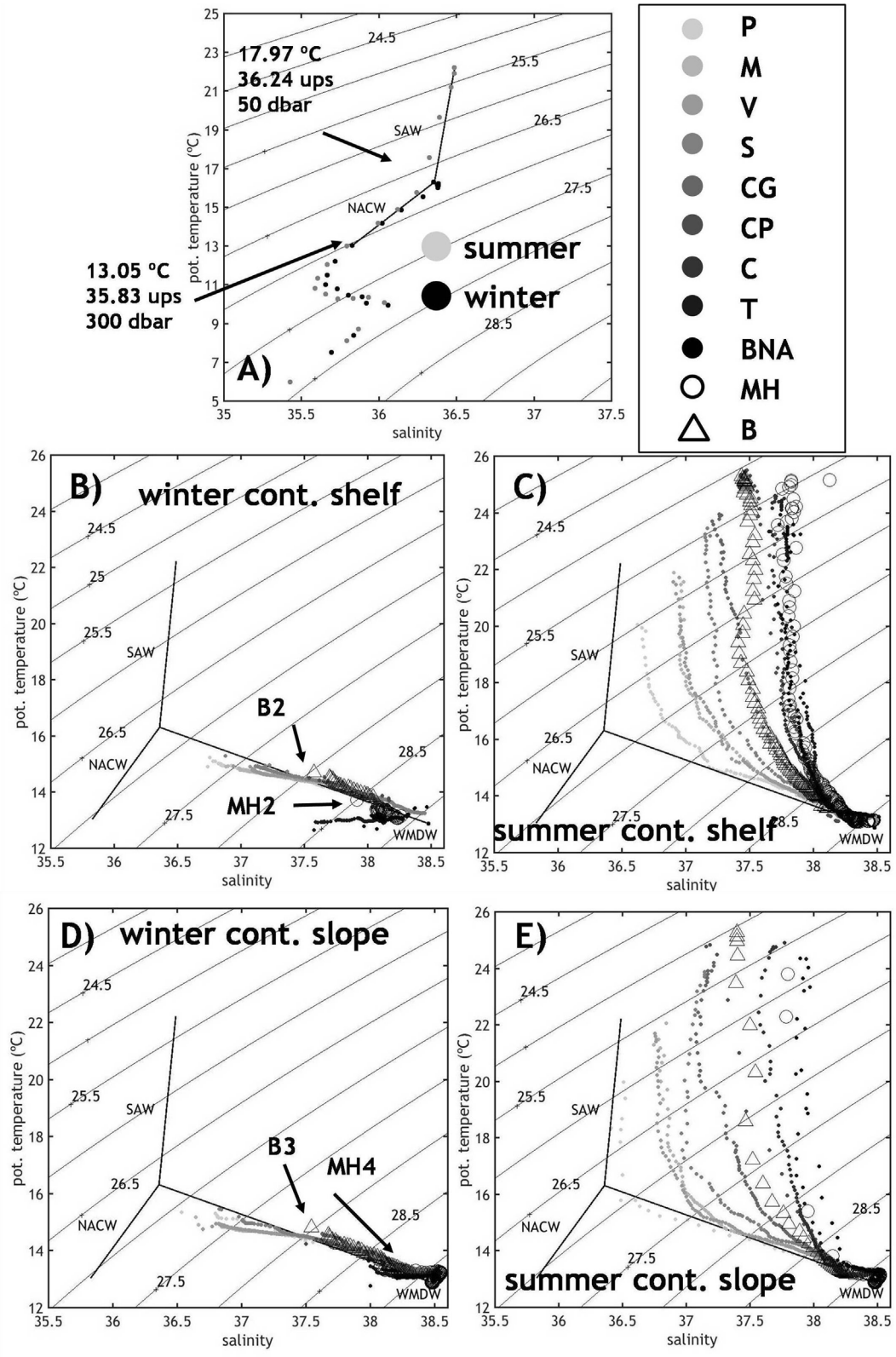

Fig. 2 Figure A shows the θS diagram for summer and winter in the Gulf of Cádiz, close to the eastern side of the Gibraltar Strait. Light grey dots are for summer and black ones for winter. Strait lines show the North Atlantic Central Water from the depth where summer heating is observed to 300 m, which is the maximum depth of the sill at Gibraltar. Waters above the NACW are labeled as Surface

limits the depth of the water column which is suitable for feeding the Atlantic current. This depth is around 300 m. The upper 300 m of the NACW is indicated at Fig. 2A as a continuous line. Fig. 2B to E use the same colour criterion. Grey dots are darker as the stations are further from Gibraltar. That is, light grey is used for stations close to the Strait of Gibraltar and black dots are used for the Barcelona stations (BNA). Winter diagrams (Fig. 2B and D) simply reflect that the water masses along the water column relay along the mixing line between the NACW and the Mediterranean Waters (Western Mediterranean Deep Water, WMDW and Levantine Intermediate Water, LIW). As the distance from Gibraltar increases (darker dots) the surface temperature and salinity are more different from the Atlantic values, indicating a higher percentage of Mediterranean waters. In all the stations this percentage increases with depth. Summer θS values (Fig. 2C, E) are similar to those for winter with the exception of the warming of the upper part of the water column, which is reflected in the almost vertical part of the diagram. Insular stations (MH and B) to the northeast of Menorca Island and to the south of Mallorca Island are represented by open circles and triangles respectively. The temperature and salinity values to the south of Mallorca seem to be similar to those of the peninsular side of the Ibiza Channel (stations C20, C18) at the same latitude, while Mahon (MH) properties resemble those of the northern stations T and BNA (Tarragona and Barcelona). The initial part (sea surface) of the B and MH θS diagrams are marked in Fig. 2 for the clarity of the plot. It is interesting to notice the low temperatures during winter in Barcelona continental shelf ($<13^{\circ}C$) with salinity values around 37.5 at the sea surface. This fact is the consequence of intense winter cooling and the possible influence of continental waters. These values suggest the Western Intermediate Water (WIW) formation in the Catalan shelf (López-Jurado et al., 1995; Vargas-Yáñez et al., 2012). Continental slope stations for Barcelona, Tarragona and Mahon (BNA, T and MH) show winter, spring (not shown) and summer temperatures below 13°C above the LIW temperature and salinity maxima. This indicates the presence of WIW. In summary, the net of oceanographic stations in the present work reflects the Atlantic-Mediterranean gradient of water masses within the WMED and some of the winter convection process occurring in the Northwestern Mediterranean.

3.2. Nutrients, dissolved oxygen and chlorophyll-*a* profiles

Chlorophyll-*a*, nutrient and DO average vertical profiles showed some common features for the whole sampling area, as well as some important differences. Figs. 3—8 show these average seasonal profiles for some selected stations. Confidence limits have not been included in these figures for the clarity of the plot. Nevertheless, one of the goals of this work is to provide mean values and ranges of variability which could be used as a reference for future works. Because of the huge amount of information, tables showing the average values, the standard deviations and the number of data used for the calculations are presented in the supplementary material (Table S1). Among the most recurrent features, it can be established that surface nitrate and phosphate concentrations are maxima in winter and/or spring and decrease for the summer season. For all the seasons, nitrate and phosphate concentrations increase with depth to a maximum located between 200 and 500 m, coinciding with the LIW depth level (see Figs. 4 and 6) and then slightly decrease with depth to the sea bottom. Chlorophyll-*a* concentrations reach maximum values in winter/spring when the surface waters have higher nutrient concentrations. Chlorophyll concentrations decrease during the stratified seasons, mainly summer and autumn. The depth where such a maximum is reached also increases from winter/spring, when it can be situated at the sea surface or at a sub-surface position (10—20 m), to summer and autumn, when the maximum chlorophyll concentrations deepen to 50—75 m, developing a Deep Chlorophyll Maximum (DCM) at some stations. Nitrite concentrations show an almost ubiquitous deep maximum usually found at or below the DCM. This maximum is usually referred to as Primary Nitrite Maximum (PNM, Lomas and Lipschultz, 2006). DO is at saturation at the sea surface increasing below the surface to a maximum at or above the DCM. When the maximum chlorophyll concentrations are at the sea surface, the highest DO values are also found at the sea surface (see Figs. 3 and 5A). DO decreases to a minimum at the LIW level and then increases to the sea bottom (Figs. 4 and 6).

In spite of these common features, the RADMED data show also important differences from the southwest to the northeast of the sampling area, and also between peninsular and insular waters. In the Alboran Sea, the highest chlorophyll concentrations are observed in winter in most of the Western Alboran Sea stations (P, M and V2) while such maximum values are advanced to autumn is the Eastern Alboran Sea (stations V4, S and CG, see Figs. 4A and 5D, 6D or chlorophyll concentrations at P2, P4, M2, M4, V2 and V4, S4, CG2, CG4 in Table S1). When the maximum chlorophyll concentrations correspond to winter, the lowest ones are observed in summer (western sector, P, M and V2) while, when maximum values correspond to autumn, the weakest chlorophyll concentrations are also moved forward to spring (eastern stations, S4, CG, Figs. 5 and 6). The maximum values of chlorophyll concentrations in the Western Alboran Sea occur at the sea surface or at 10—20 m depth (Tables 2—5). Therefore it is not properly a Deep Chlorophyll Maximum and the term sub-surface chlorophyll maximum is a more appropriate one. The intensity of the DCM (or sub-surface in the case of the Western Alboran Sea) also exhibits a SW-NE gradient. The highest DCM values are always higher than 1 mg/m^3 in the P, M, V and S stations. The chlorophyll concentrations within the weakest DCM of the year are higher than 0.5 mg/m^3. From CG transect to the east and north, the highest DCM values never exceed

Atlantic Water. Figures B and C show the θS diagrams for the continental shelf stations (labelled as 2 in each transect). Dots correspond to the peninsular continental shelf. A grey scale is used with the lightest grey for the P2 station, and darker grey as the distance to the Strait of Gibraltar is increased. Black dots correspond to BNA station. Open circles and triangles are for the MH and B stations respectively. Figures D, E are the same as figures B, C, but for the continental slope stations (labelled as 4).

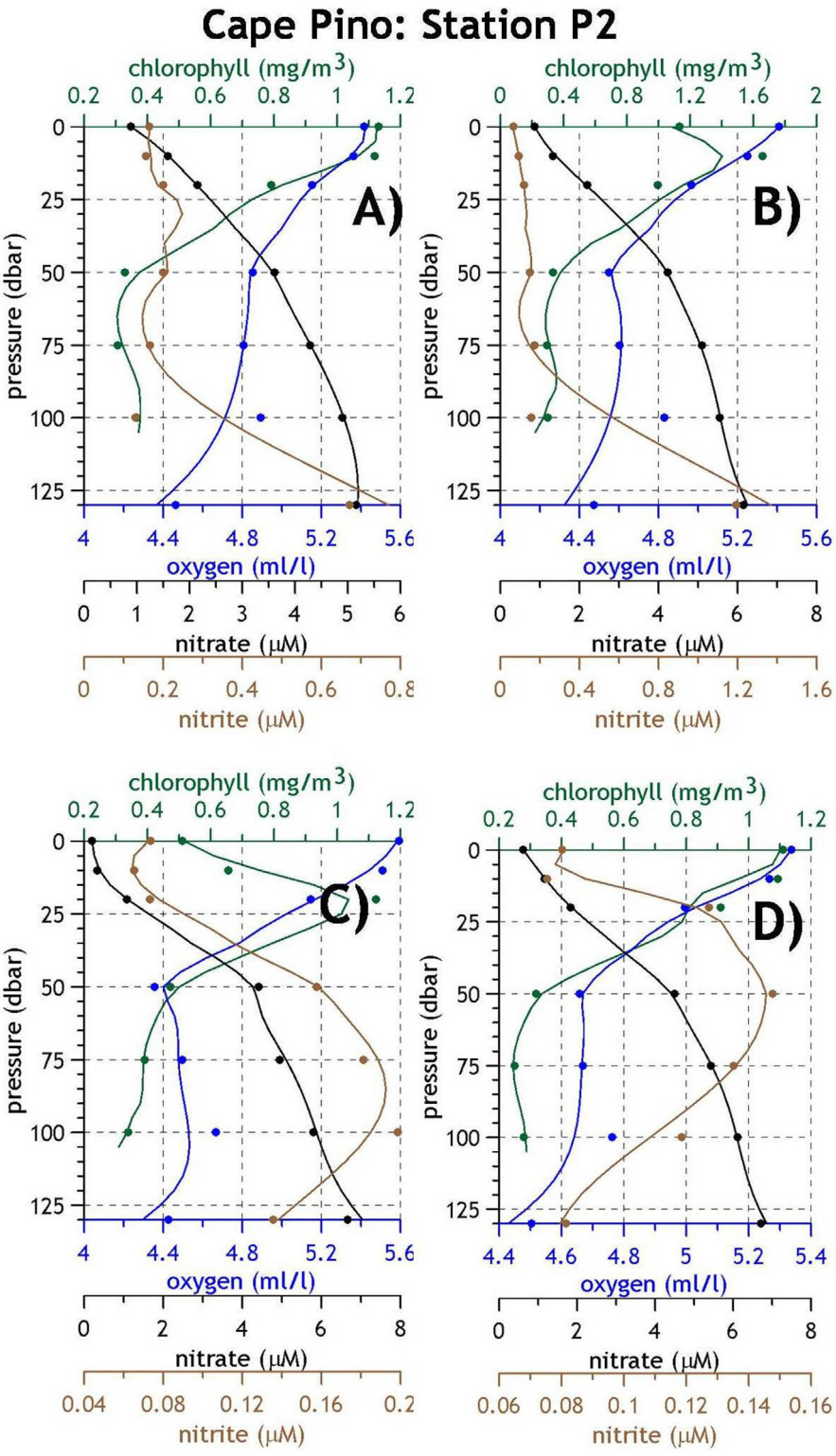

Fig. 3 Station P2, Cape Pino transect. Chlorophyll-*a*, nitrate, nitrite and DO average seasonal profiles. (A) Winter, (B) Spring, (C) Summer, (D) Autumn.

1 mg/m^3. Furthermore, the maximum DCM for CG, Cape Palos (CP) and Mallorca transect (B) is lower than 0.5 mg/m^3, that is, the maximum DCM is lower than the minimum ones in the Western Alboran Sea. The highest and lowest values of the DCM are reached in autumn and spring respectively in CG and CP. For the rest of the stations to the north of Cape Palos (C, T, BNA, B and MH), the highest values occur in winter/spring (Tables 2 and 3) and the lowest ones in summer/autumn (Tables 4 and 5). Another difference is observed for the depth of the DCM. For the case of the

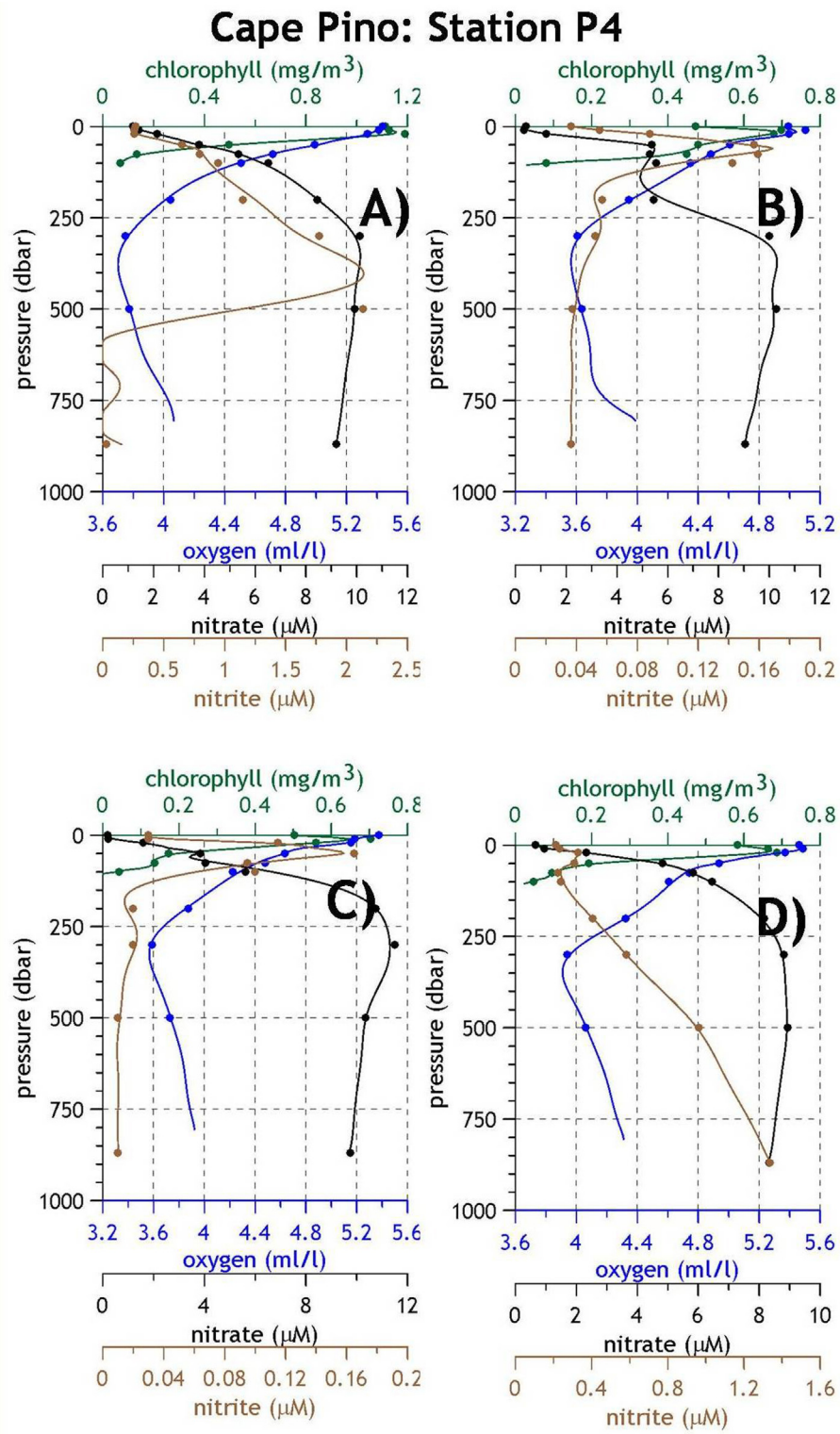

Fig. 4 Station P4, Cape Pino transect. Chlorophyll-*a*, nitrate, nitrite and DO average seasonal profiles. (A) Winter, (B) Spring, (C) Summer, (D) Autumn.

Western Alboran Sea (P, M and V) the highest chlorophyll concentrations are always at the upper 20 m of the water column. From S and CG (Alboran Sea) to the north, the DCM is at the upper 20—25 m when the highest concentrations are observed (mainly winter and spring) and it deepens to 50—75 m for the weakest summer and autumn values and even deeper (100 m) in the Mallorca transect (B2). Figs. 3 and 4 (stations P2 and P4) are shown as an example

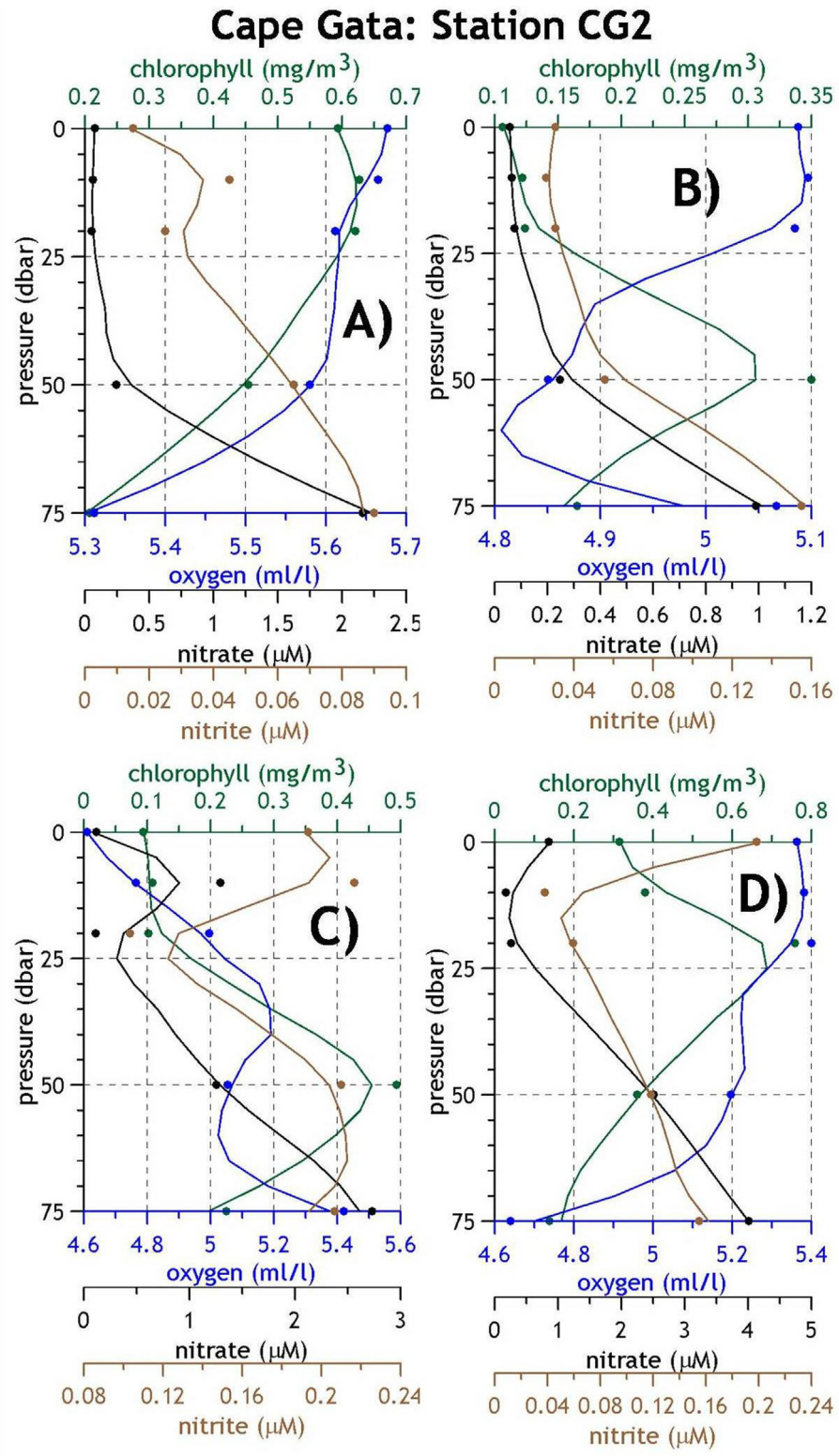

Fig. 5 Station CG2, Cape Gata transect. Chlorophyll-*a*, nitrate, nitrite and DO average seasonal profiles. (A) Winter, (B) Spring, (C) Summer, (D) Autumn.

of those stations within the Alboran Sea with high chlorophyll values during the whole year and maximum chlorophyll values at shallow waters or even at the sea surface. Figs. 5 and 6 (GC2 and CG4) are used as an example of weak and deeper DCM, and Figs. 7 and 8 are representative of very low chlorophyll concentrations with maximum values lower than 0.5 mg/m^3 (the autumn DCM is only 0.3 mg/m^3 at the B transect, Table 4).

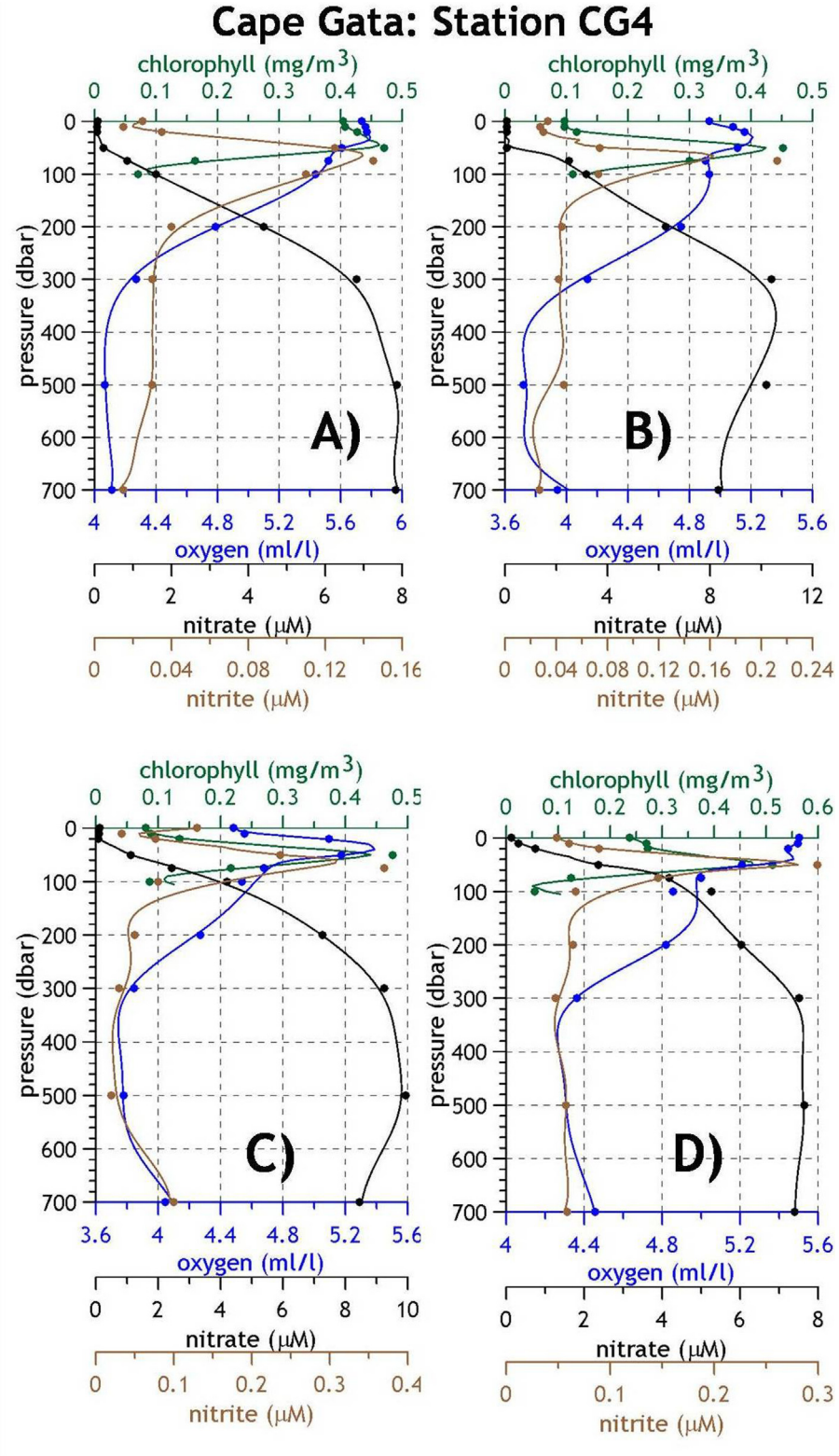

Fig. 6 Station CG4, Cape Gata transect. Chlorophyll-*a*, nitrate, nitrite and dissolved oxygen average seasonal profiles. (A) Winter, (B) Spring, (C) Summer, (D) Autumn.

Surface DO concentrations exhibit a clear seasonal cycle with minimum values in summer, when the temperature is higher and the solubility decreases. Nevertheless, stations P2, P4 and M2 are exceptions to this general behavior. The lowest DO concentrations associated to the nutrient maxima are at 300 m for the westernmost station P4. For M and V transects the minimum of DO is at the sea bottom as these stations

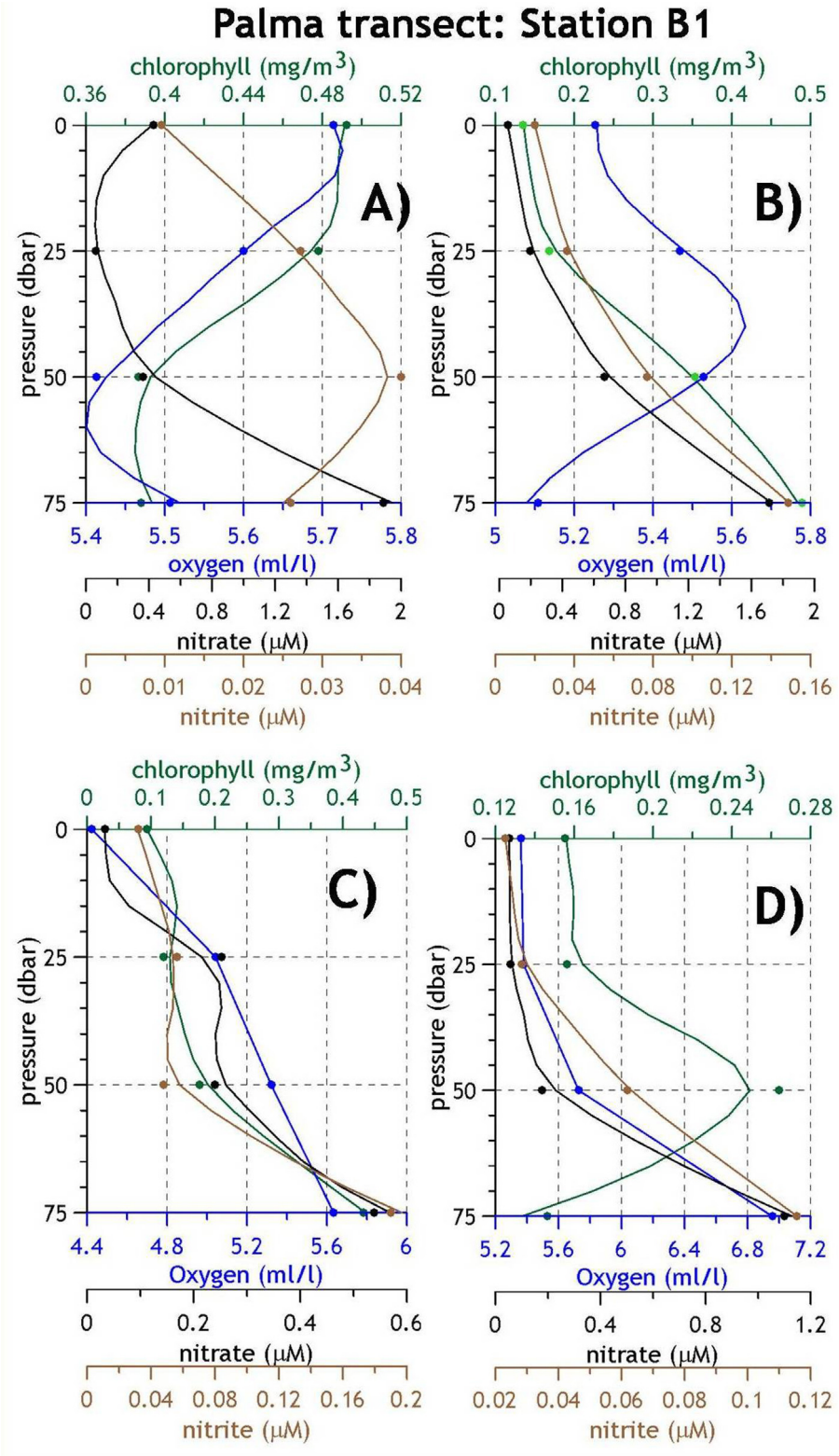

Fig. 7 Station B1, Mallorca transect. Chlorophyll-*a*, nitrate, nitrite and dissolved oxygen average seasonal profiles. (A) Winter, (B) Spring, (C) Summer, (D) Autumn.

are shallower than 500 m. For the peninsular and insular continental slope, from the S transect in the central Alboran Sea to the North, the DO minimum is almost always located at 500 m depth when the stations are deeper than this level. The DO minimum level is lower than 4 ml/l in the Alboran Sea with values close to 3.6 ml/l in the north of Cape Gata (Table S1).

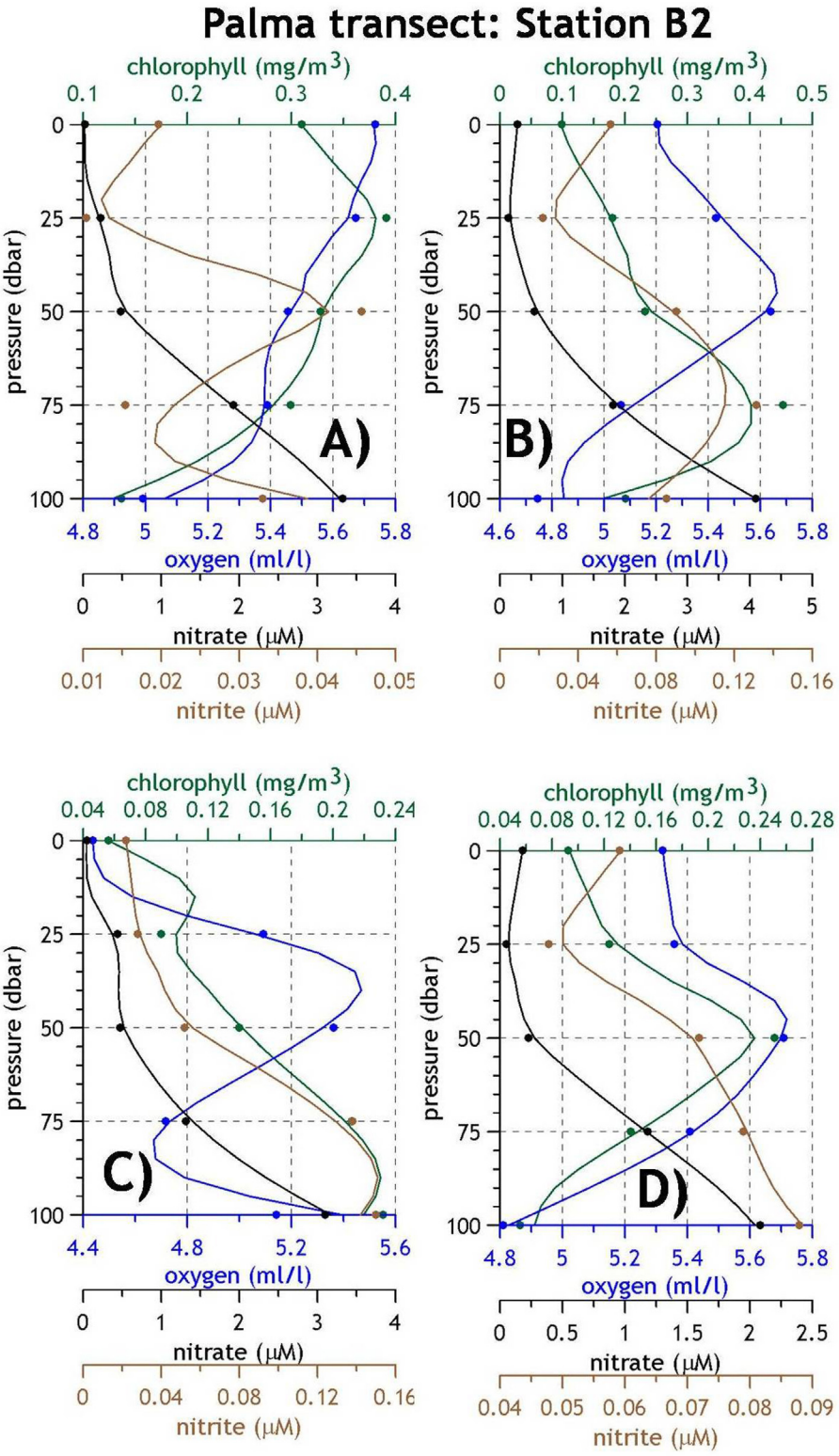

Fig. 8 Station B2, Mallorca transect. Chlorophyll-*a*, nitrate, nitrite and dissolved oxygen average seasonal profiles. (A) Winter, (B) Spring, (C) Summer, (D) Autumn.

Table 2 WINTER. Mixed layer depth (MLD), nutricline depth, integrated nitrogen (nitrate + nitrite), phosphate and silicate, integrated Dissolved Oxygen and chlorophyll, Deep Chlorophyll Maximum (DCM) concentration and depth and Secchi disk depth.

Winter	MLD (m)	Nut. Depth (m)	Int. N. (mmol/m)	Int. P. (mmol/m^2)	Int. Si. (mmol/m^2)	Int.DO. (L/m^2)	Int. Chl. (mg/m^2)	DCM (mg/m^3)	DCM Depth (m)	Secchi (m)
P2	56	13	291	19	223	495	53	1.4	6	14
P3	50	14	313	21	229	421	44	1.5	17	
P4	84	5	395	20	238	499	58	1.5	5	16
M2	58	14	160	12	138	380	58	1.4	15	13
M3	75	26	199	18	179	440	53	1.4	15	
M4	64	17	238	9	200	508	88	2.1	13	13
V2	52	16	176	12	140	382	59	1.5	20	13
V3	50	18	223	18	194	440	57	1.5	12	
V4	56	22	221	12	188	517	79	1.8	24	16
S2	40	0	315	20	229	504	60	1.1	22	18
S4	52	0	199	12	176	508	59	1.1	18	16
CG2	67	60	40	4	74	411	33	0.6	23	14
CG4	62	78	59	4	101	563	31	0.7	30	16
CP2	53	27	80	3	85	393	23	0.4	28	19
CP3	57	60	118	6	130	540	22	0.6	34	
CP4	84	34	197	7	132	483	33	0.7	33	16
C20	59	40	95	5	60	525	35	0.5	39	15
C18	153	41	148	6	128	553	28	0.4	36	19
T2	49	20	108	6	108	429	38	0.8	14	16
T4	190	55	109	4	156	558	38	0.5	32	18
BNA2	219	43	96	3	89	563	49	0.7	21	16
BNA4	870	0	184	5	175	526	39	0.7	31	18
B1	54	57	42	1	93	395	33	0.7	41	23
B2	56	58	122	1	138	509	31	0.6	42	23
B3	69	56	126	1	141	530	25	0.5	53	22
MH2	158	5	173	4	171	540	33	0.7	25	17
MH4	268	0	247	7	186	545	32	0.7	20	15

3.3. Mixed layer depth and nutricline. Integrated nutrients, chlorophyll-*a* and dissolved oxygen

MLD, nutricline depth, DCM concentration and depth, and chlorophyll-*a*, nitrogen (nitrate + nitrite), phosphate and silicate integrated concentrations from the surface to 100 m depth were calculated. The seasonal average values for all the RADMED stations are presented in Tables 2—5. In addition, Secchi disk depths have been included (see Table S2 for the complete statistics of the Secchi disk). Figs. 9A, B to 11A, B show the MLD (dashed black line), the DCM depth (continuous black line), DCM concentration (purple line) and integrated chlorophyll-*a* (dark green bars). Figs. 9C, D to 11C, D show the nutricline depth (dashed black line), integrated nitrate (white bars), integrated silicate (continuous black line) and integrated phosphate (dark brown bars). Figs. 9E, F to 11E, F show the integrated DO (dark blue bars), depth of the DO maximum (continuous black line), DO maximum concentration (continuous light blue line), depth of the DO minimum (dashed black line) and the DO minimum concentration (dashed light blue line).

P2 and P4 stations at the westernmost section of the RADMED area show a MLD (dashed line in Fig. 9A, B) which is maximum in winter (60 and 80 m respectively) and minimum in summer when the water column has a stronger stratification (~10 m). At station P4, Chlorophyll-*a* integrated for the upper 100 m of the water column is maximum for the same season when the MLD reaches its highest value and then decreases as the MLD becomes shallower. The behavior of the chlorophyll concentration at the DCM also follows that of the MLD at station P4. On the contrary, this relationship is not so clear in station P2 where weak values of the DCM concentration are coincident with high integrated chlorophyll values in winter. The depth of the nutricline (dashed lines in Figs. 9C, D to 11C, D), shows the lowest values (shallowest position) in winter at stations P2 and P4 (Fig. 9) while it is at the deepest levels (maximum values) during summer. Therefore MLD and nutricline show opposite seasonal patterns. Nitrogen (nitrate plus nitrite), phosphate and silicate concentrations integrated for the upper 100 m of the water column do not seem to follow the mixed layer and nutricline patterns, with the only exception of station P4 (Fig. 9D). Integrated DO seems to respond to the MLD and nutricline seasonal patterns with lowest values in summer when the MLD is shallower and the nutricline is at its deepest level.

Although the seasonal cycle of integrated variables does not show a common pattern, it can be observed the southwest-northeast gradient already described for the surface nutrient concentrations and the strength and depth of the DCM. The integrated chlorophyll is higher at the Alboran Sea with values ranging at stations P2 and P4 between 30 and 60 mg/m^2 (Tables 2—5). These values are even higher at the

Table 3 SPRING. Mixed layer depth (MLD), nutricline depth, integrated nitrogen (nitrate + nitrite), phosphate and silicate, integrated Dissolved Oxygen and chlorophyll, Deep Chlorophyll Maximum (DCM) concentration and depth and Secchi disk depth.

Spring	MLD (m)	Nut. Depth (m)	Int. N. (mmol/m^2)	Int. P. (mmol/m^2)	Int. Si. (mmol/m^2)	Int.DO. (L/m^2)	Int. Chl. (mg/m^2)	DCM (mg/m^3)	DCM depth (m)	Secchi (m)
P2	17	13	404	24	240	478	58	2.3	13	13
P3	22	19	344	22	216	386	43	1.5	21	
P4	25	13	514	42	236	468	48	1.2	36	18
M2	16	20	202	13	125	363	49	1.6	30	13
M3	18	27	299	18	231	393	29	1.2	32	
M4	18	30	291	15	120	477	57	1.4	33	16
V2	17	24	215	12	148	369	51	1.8	29	14
V3	17	20	341	20	218	399	46	1.7	21	
V4	19	33	319	21	158	486	53	1.2	42	16
S2	14	20	400	18	212	483	33	0.7	32	17
S4	20	28	359	18	196	480	47	1.3	38	17
CG2	21		10	8	51	352	14	0.4	55	15
CG4	19	60	162	19	172	504	25	0.6	55	23
CP2	16	50	86	7	94	399	28	0.7	44	20
CP3	19	78	78	9	104	544	13	0.4	53	
CP4	20	35	123	8	127	503	21	0.4	54	24
C20	15	34	152	7	135	473	27	0.5	46	19
C18	15	44	148	7	115	527	25	0.5	44	24
T2	30	45	57	5	35	409	21	0.4	45	22
T4	19					538	21	0.3	48	19
BNA2	53	67	94	2	111	526	23	0.4	50	23
BNA4	39	43	110	3	201	517	35	0.8	57	20
B1	17	51	55	2	82	383	21	0.6	64	26
B2	19	49	118	3	118	513	25	0.6	63	28
B3	20	61	123	3	134	533	18	0.4	57	28
MH2	33	48	151	6	185	541	23	0.6	40	24
MH4	24	33	151	6	175	527	28	0.5	53	25

M transect where 88 mg/m^2 are reached (Table 2). From Cape Gata transect to the north (CG, CP, C, B and MH transects) the minimum integrated values are observed, ranging along the seasonal cycle between 10 and 35 mg/m^2 (CG2 in Fig. 10), or even between 12 and 25 mg/m^2 in station B3 (Tables 2—5 and Fig. 11 for similar values at the B1 and B2 stations). Nutrient concentrations resemble the chlorophyll gradient with nitrate + nitrite integrated values ranging from 300 to 450 mmol/m^2 in P transect (Fig. 9) and similar values at the other Alboran stations from transect P to S, and then a clear decrease from CG transect (Fig. 10) to CP, C, B and MH transects where integrated nitrogen rarely exceeds 150 mmol/m^2. Integrated phosphate concentrations can reach values as high as 42 mmol/m^2 in the Alboran Sea, from Cape Pino (P, Fig. 9) to Sacratif (S). CG section shows integrated phosphate concentrations ranging between 4 and 19 mmol/m^2 (Fig. 10) and even lower values at sections CP, C, B (Fig. 11) and MH where concentrations are around 5 mmol/m^2. Nitrate + nitrite integrated concentrations in the northern transects BNA and MH are slightly higher than those from Cape Gata to the Balearic channels (transects C and B) with values reaching 247 mmol/m^2 at MH4 station and 184 mmol/m^2 in BNA4. On the contrary, integrated phosphates remain at very low values around 5 mmol/m^2 in the transects T, BNA and MH.

Secchi disk depth is maximum in summer when the integrated chlorophyll is lower, the nutricline is deeper and the MLD is shallower. The minimum Secchi disk depths are found in the P transect where the chlorophyll concentrations are highest (around 15 m). There are no significant differences between winter and summer values coinciding with the lack of a clear seasonal pattern for chlorophyll and nutrient concentrations. The summer maximum Secchi disk depth increases at section M (20 m) and V4 (25 m). S and CG transects show minimum values around 15 in winter and maximum values close to 25 m in summer. Similar values are observed in C, T and BNA transects. The clearest waters are found in CP4 where the summer Secchi disk depth reaches 30 m, and in the B and MH transects, with summer values higher than 30 m (Table S2).

3.4. Redfield ratios

For the calculation of the N:Si:P ratios, the RADMED stations were grouped into three different areas: Alboran (P, M, V, S and CG transects), peninsular eastern coast (CP, C, T and BNA transects) and Balearic Islands (B and MH transects). Nitrogen (Nitrate + nitrite), phosphate and silicate concentrations were also divided into two layers. The upper one extended from the surface to 75 m depth, representing the AW flowing in the upper layer of the Mediterranean Sea. The lower layer extended from 100 m to the bottom and represents waters with a higher percentage of Mediterranean water masses. N *versus* P data are presented in Figs. 12—14 for the three areas and the two layers considered. Following Pujo-Pay et al. (2011), the Redfield

Table 4 SUMMER. Mixed layer depth (MLD), nutricline depth, integrated nitrogen (nitrate + nitrite), phosphate and silicate, integrated Dissolved Oxygen and chlorophyll, Deep Chlorophyll Maximum (DCM) concentration and depth and Secchi disk depth.

Summer	MLD (m)	Nut. Depth (m)	Int. N. ($mmol/m^2$)	Int. P. ($mmol/m^2$)	Int. Si. ($mmol/m^2$)	Int.DO. (L/m^2)	Int. Chl. (mg/m^2)	DCM (mg/m^3)	DCM depth (m)	Secchi (m)
P2	13	29	351	21	257	471	57	1.5	24	15
P3	14	16	392	23	266	364	42	1.8	14	
P4	11	23	322	19	200	471	29	0.8	13	19
M2	14	32	180	13	129	352	38	1.4	29	17
M3	13	32	288	19	195	390	28	1.0	30	
M4	12	34	314	18	210	457	65	2.0	21	20
V2	14	30	173	11	129	368	35	1.0	38	20
V3	14	35	272	16	199	394	23	0.9	34	
V4	12	40	279	22	187	461	42	1.1	31	25
S2	13	35	216	9	155	473	31	0.8	50	26
S4	11	45	233	6	148	470	21	0.4	50	27
CG2	17	35	98	5	86	356	21	0.6	60	24
CG4	13	48	166	6	116	491	24	0.5	49	25
CP2	16	63	38	3	74	373	13	0.3	63	25
CP3	16	68	131	9	124	516	23	1.1	53	
CP4	14	63	87	4	88	458	19	0.4	63	30
C20	15	63	71	3	116	438	15	0.4	75	21
C18	17	73	91	5	100	506	21	0.4	67	24
T2	17	65	38	7	58	385	16	0.7	75	22
T4	13	65	65	3	107	479	18	0.4	75	26
BNA2	13	80	55	4	82	514	20	0.4	67	25
BNA4	15	63	137	9	133	512	19	0.4	50	23
B1	21	70	23	4	59	353	15	0.5	63	31
B2	20	64	99	3	106	459	15	0.3	68	33
B3	20	60	147	7	130	493	13	0.3	58	32
MH2	14	78	69	3	101	526	15	0.4	88	29
MH4	17	68	109	6	137	513	19	0.4	75	32

ratios were calculated using two different methods. For the first one, the Redfield ratio was estimated as the slope of the regression line fitted to the N:P and Si:P data (see Figs. 12—14). For the second one, mean N, Si and P concentrations were calculated for each area and layer and then the corresponding ratio was calculated. In both cases, 95% confidence intervals were estimated using a *t*-student distribution for the slope of the regression line and for the mean nutrient concentrations (see for instance Zar, 1984). Errors for the ratios were derived from the mean concentration confidence intervals using the error propagation formulae for the quotient. The Redfield ratios estimated using both methods, including the confidence limits at the 95% confidence level have been included in Figs. 12—14. Upper numbers correspond to the slope of the linear fit and the lower numbers correspond to the ratio of the mean N and P concentrations.

Different results were obtained depending on the calculation method used. Nevertheless, if the 95% confidence intervals are considered, both results (regression and ratio between mean concentrations) overlap. For the upper layer of the Alboran Sea, N:P ratios are higher than the theoretical 16 value when the regression line is considered while the values are 16 or lower if the mean N and P concentrations are divided. Notice that if the lower limit is considered, the regression line also would yield ratios close to 16. Si:P ratios (not shown) for the upper Alboran Sea were lower than the 15 theoretical value in all the cases. More contradictory results were obtained for the lower layer (100 m—bottom). If the slope of the regression line was considered, values ranging from 10 to 20 were obtained, depending on the season. On the contrary, if mean concentrations were divided, the N:P ratio ranged from 17 (autumn) to 24 (summer). Considering the uncertainty in the calculations, Si:P ratios varied along the seasonal cycle around the 15 value.

For the peninsular eastern coast, the upper layer N:P values showed a very large dispersion with some unrealistic results such as the 2 ± 5 value for the summer season. N:P ratios based on mean concentrations oscillate between 23 ± 9 for winter and 11 ± 7 for summer. Notice that the lower limit for the winter interval would be 14. This ratio is close to 16 if an average value is calculated for the whole year. Once again very low values are obtained for the lower layer if the first method is applied (see Fig. 13), while values ranging from 19 to 22 are obtained for the second one. Similar results are observed when the Si:P ratio is analyzed, with very low values for the regression line in both the upper and lower layer and higher values for the ratio between mean concentrations. For the latter case, the Si:P ratio is above 15 for most of the cases.

3.5. Decadal changes

Chlorophyll and nutrient time series in the Malaga Bay and Cape Palos regions were initiated under the umbrella of previous projects: ECOMALAGA and ECOMURCIA in

Table 5 AUTUMN. Mixed layer depth (MLD), nutricline depth, integrated nitrogen (nitrate + nitrite), phosphate and silicate, integrated Dissolved Oxygen and chlorophyll, Deep Chlorophyll Maximum (DCM) concentration and depth and Secchi disk depth.

Autumn	MLD (m)	Nut. Depth (m)	Int. N. (mmol/m^2)	Int. P. (mmol/m^2)	Int. Si. (mmol/m^2)	Int.DO. (L/m^2)	Int. Chl. (mg/m^2)	DCM (mg/m^3)	DCM depth (m)	Secchi (m)
P2	19	23	401	24	262	483	47	1.5	16	16
P3	16	11	433	27	289	379	23	0.9	10	
P4	28	18	458	30	317	499	32	0.8	15	18
M2	17	27	216	15	157	367	41	1.1	24	17
M3	20	23	376	22	252	377	28	1.0	24	
M4	18	30	375	21	238	486	33	0.9	18	18
V2	17	30	197	14	144	358	31	1.0	18	18
V3	20	31	326	21	203	389	26	1.0	18	
V4	18	24	417	26	265	490	58	2.3	23	18
S2	30	26	418	21	323	494	23	0.8	22	20
S4	28	23	414	22	256	504	44	1.6	25	21
CG2	29	35	138	8	105	386	32	0.8	38	21
CG4	28	33	269	14	174	524	27	0.6	40	23
CP2	38	18	147	9	99	383	25	0.7	22	20
CP3	39	55	175	8	136	508	17	0.5	30	
CP4	33	36	193	12	127	484	31	0.9	30	24
C20	54	43	86	5	153	417	19	0.3	44	20
C18	38	88	76	3	111	548	21	0.3	56	22
T2	34	60	37	4	87	412	10	0.1	35	24
T4	35	50	175	8	185	528	14	0.3	33	22
BNA2	51	65	103	4	127	559	17	0.3	27	17
BNA4	42	69	60	3	117	561	16	0.2	16	21
B1	39	63	25	2	64	353	14	0.3	50	26
B2	42	61	72	4	99	520	15	0.3	50	27
B3	41	62	85	3	87	540	17	0.3	50	27
MH2	42					506	15	0.3	50	23
MH4	40	100	35	4	79	514	14	0.2	28	26

1992 and 1996 respectively. Beside the existence of some gaps caused by bad weather conditions, instrument failures, and vessel availability, data obtained from these projects and the present RADMED program provide 20 year-long time series for chlorophyll-*a*, nutrient and DO concentrations. Stations P3, M3 and V3 are the longest and best sampled time series in the Malaga Bay area. CP3 is the best-sampled station at Cape Palos transect. Once the seasonal cycle was subtracted for each data point, residuals or deviations from the seasonal cycle were obtained. Residuals time series for P3, M3, V3 and CP3 are presented in Fig. 15. For each station, the left plot shows the nutricline depth (black line) and the integrated nitrogen (light brown) and integrated phosphate concentrations (dark brown). The right plot shows the DCM depth (black line), the chlorophyll concentration at the DCM (purple) and the integrated chlorophyll concentration (dark green).

For the P3 case, the only variables which showed a significant trend (at the 0.05 significance level) were the integrated chlorophyll, which increased along the considered period at a rate of 1.3 ± 1.1 mg m^{-2}/yr and the integrated DO (not shown) which increased at a rate of 3.0 ± 1.6 lm^{-2}/yr. Similarly, integrated chlorophyll and DO also increased in a significant way at M3 station with trends of 1.3 ± 0.8 mg m^{-2}/yr and 1.9 ± 1.7 lm^{-2}/yr. This chlorophyll and DO increase at M3 was accompanied by nitrogen and phosphate negative trends of -5.4 ± 5.3 and -0.5 ± 0.3 mmol m^{-2}/yr respectively. Once again integrated chlorophyll and DO showed positive trends for V3 (1.4 mg m^{-2}/yr and 2.1 ± 1.5 lm^{-2}/yr), while nutrient trends were not significant. No clear results were obtained for the MLD trends which were not significant in most of the cases and showed positive and negative values. Finally, trends in CP3 station were not significant with the only exception of the integrated DO which decreased at a rate of -2.1 ± 1.8 lm^{-2}/yr.

4. Discussion and conclusions

RADMED stations cover an area with important oceanographic differences. The westernmost stations in the Alboran Sea are close to the Strait of Gibraltar (mainly P and M transects) and therefore are subject to the direct influence of the AW. The northernmost stations, (T and BNA transects) receive AW severely modified after recirculation along the whole Western Mediterranean (northern current). The AW continues its pathway southward and partially flows along the Ibiza Channel, while another branch of this current turns to the north of the Balearic Islands feeding the Balearic current (see Fig. 1 and Pinot et al., 1995; Pinot and Ganachaud, 1999). MH transect would be affected by this current while the C20 and C18 stations would be under the influence of the southward extension of the northern current. According to this simplified circulation scheme, the AW reaching the MH and C

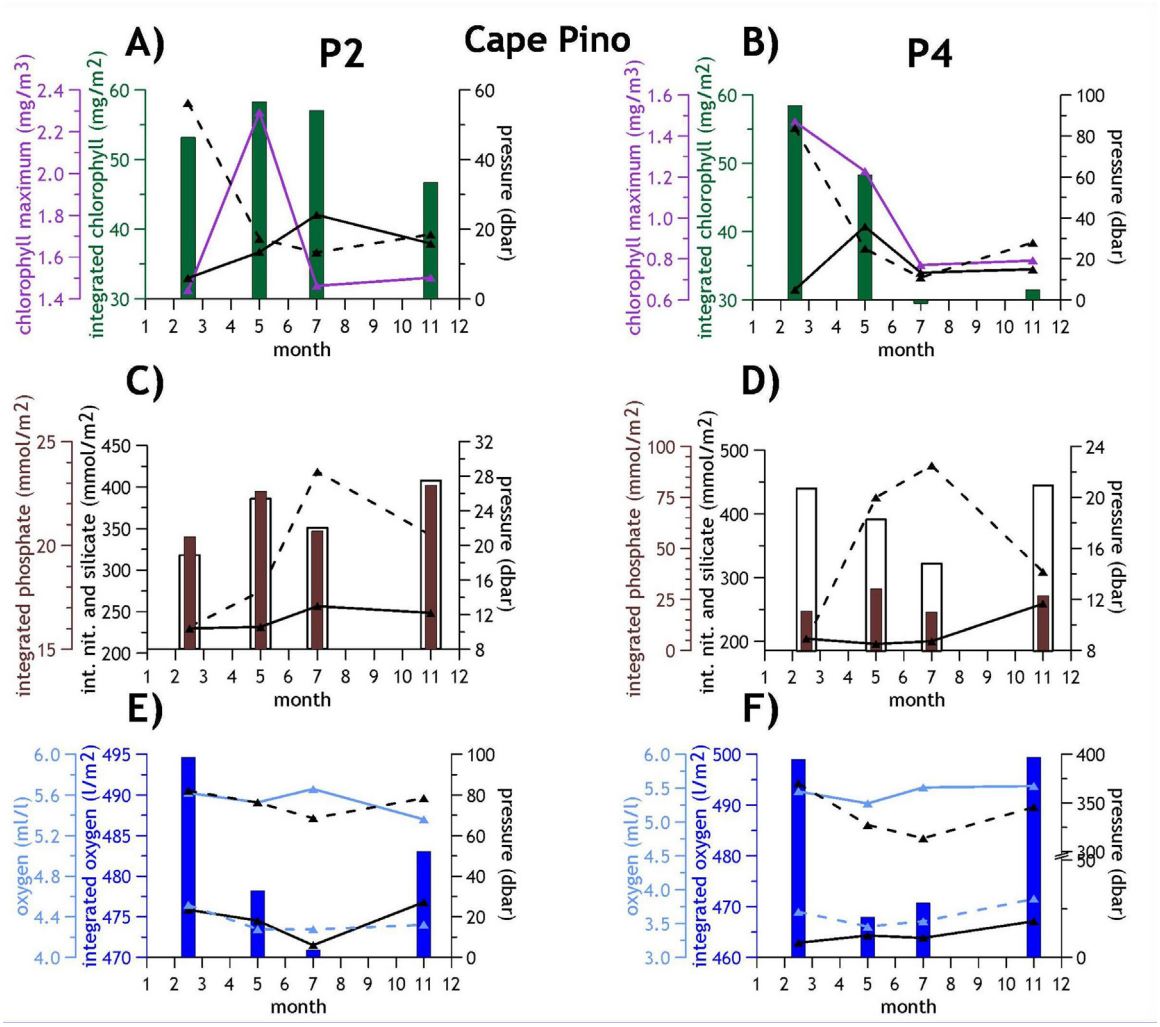

Fig. 9 Stations P2 and P4, Cape Pino transect. (A) and (B) Mixed layer depth (MLD, black dashed line), DCM depth (black solid line), chlorophyll-*a* maximum concentration (purple), integrated chlorophyll-*a* (dark green). (C) and (D) integrated phosphate (dark brown bars), integrated nitrate (white bars), integrated silicate (continuous black line) and nutricline depth (dashed black line). (E) and (F) maximum Dissolved Oxygen concentration (light blue solid line) and depth (black solid line) minimum Dissolved Oxygen concentration (light blue dashed line) and depth (black dashed line) and integrated Dissolved Oxygen (dark blue bar). (For interpretation of the references to colour in this figure legend, the reader is referred to the web version of this article.)

transects would be modified after a residence time within the WMED longer than the one corresponding to the T and BNA stations. Nevertheless, the Balearic Channels are a transition zone between the AW recently advected into the Mediterranean Sea through the Strait of Gibraltar and the AW to the north, modified by evaporation and mixing with Mediterranean waters. According to Millot (1999) and Pinot et al. (1995, 1999), AW trapped in anticyclonic gyres would detach from the Algerian current and cross northward the Balearic Channels. These traits of the AW circulation within the WMED are reflected in the θS distributions presented in Fig. 2. There is a clear salinity gradient from Cape Pino stations to BNA transect with the Balearic Islands showing intermediate θS properties between the Alboran Sea and the Catalan Sea stations. Another interesting feature observed in the average θS diagrams is the low potential temperature (<13°C) observed in winter in BNA stations. This is an indication of WIW formation and therefore intermediate convection that could account for the mixing of the upper 200–300 m in the Catalan continental shelf and slope and the winter nutrient injection to the photic layer. These cold waters above the LIW are also observed in spring, summer and autumn in BNA and MH transects, but in this case, this would only reflect the arrival of WIW formed to the north (Gulf of Lions) during the previous winter. θS values for all the stations lie on the mixing line between the NACW and the LIW (200–600 m), characterized by a salinity maximum, and the WMDW from 600 m to the bottom in the deep stations.

The distribution of water masses and their circulation have a clear influence on the nutrient and DO concentrations along the Spanish Mediterranean waters. First, the highest nitrate concentrations are observed in the westernmost Alboran Sea decreasing eastwards to Cape Gata during all the seasons. Low nitrate concentrations (compared with the

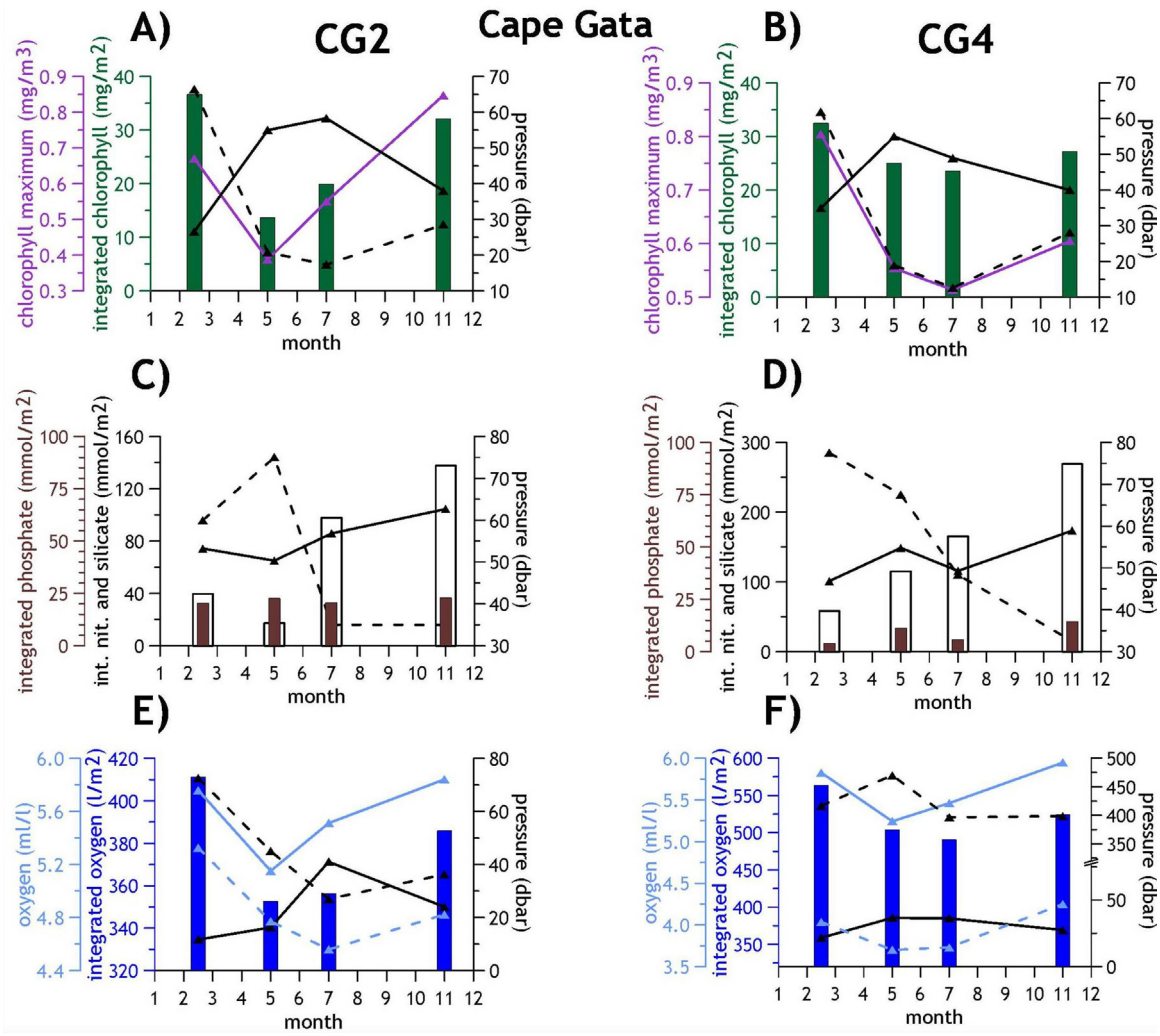

Fig. 10 The same as in Fig. 9, but for CG2 and CG4 stations in Cape Gata transect.

Alboran Sea) are observed for all the stations to the north of Cape Gata (Tables 2—5). This difference is even clearer for the phosphate concentrations which can reach 42 mmol/m^2 in spring at P4 station, while they are around 2 or 3 mmol/m^2 in BNA and B transects. Maximum surface nitrate concentrations are frequently found in winter or spring (see Table S1), although some stations present surface maxima in autumn (CG2, CP2, B2, B3). In most of the cases, the nutricline is at its deepest level in summer (Figs. 9—11) when the MLD is at its shallowest position. Nitrate and phosphate increase with the depth reaching a maximum between 200 and 500 m, which is clearly observable in those stations deeper than 500 m (see for instance Figs. 4 and 6). These nutrient maxima are associated to the LIW. This water mass is formed in the Eastern Mediterranean and flows into the WMED through the Strait of Sicily. This water mass describes a cyclonic circuit within the WMED similar to that followed by the AW (see for instance Millot, 1999). Remineralization of organic matter sunk during the LIW formation and from the photic layer above is responsible for the nutrient increase in the LIW. The same reason would explain the DO minimum at the same depth level (Figs. 4 and 6). LIW flows along the northern part of the WMED following the northern current, then flows southward through the Ibiza Channel and finally turns to the west in the Alboran Sea towards the Strait of Gibraltar. For this reason, the P, M and V transects are the last ones to receive the LIW. Organic matter oxidation during this long time could be responsible for the lower values of the DO minimum which is between 3.6 ml/l and 3.9 ml/l in the Alboran Sea and above 4 ml/l for those stations to the east and north of Cape Gata. Another explanation for the lower values of the DO minimum in the Alboran Sea would be the DO extra-minimum described by Minas et al. (1991). Notice that P3, P4, V3 and S2 stations show DO concentrations ranging between 3.6 and 3.8 ml/l at 300 m. According to Minas et al. (1991), the high primary production at the eastern side of the Strait of Gibraltar and the Northwestern Alboran Sea, and the oxidation of the organic matter exported below the photic layer would be responsible for the existence of this DO extra minimum lower than the one associated to the LIW.

The high primary production at the Northwestern Alboran Sea has been related to the enrichment of surface waters at the Strait of Gibraltar as a consequence of internal tide mixing and the upward movement of the AW flowing through Gibraltar (Echevarría et al., 2002; Gómez et al., 2000; Gómez, 2003; Huertas et al., 2012; Reul et al., 2005). The

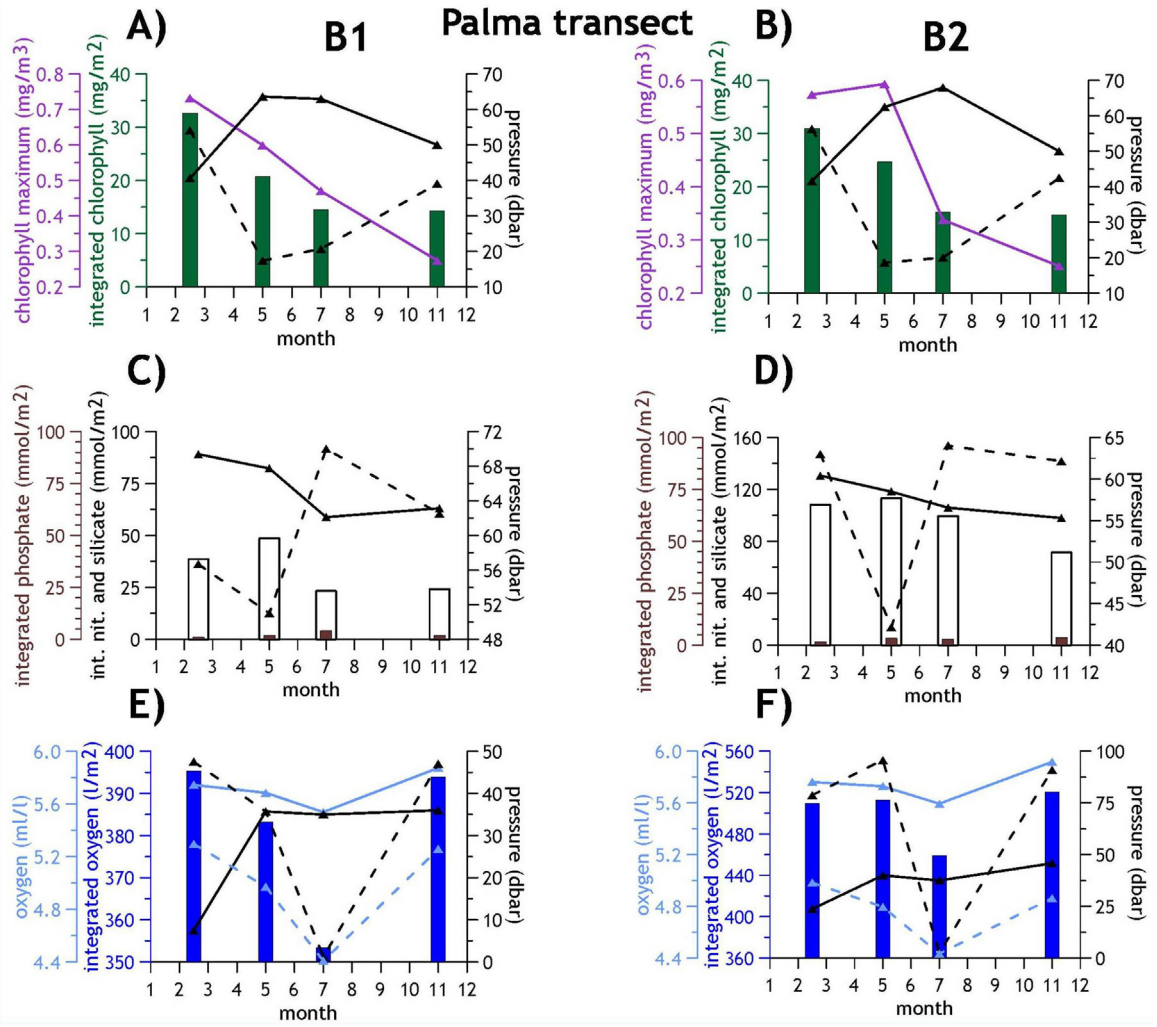

Fig. 11 The same as in Figs. 9 and 10, but for B1 and B2 stations in Mallorca transect.

high chlorophyll concentrations observed in the northern sector of the Alboran Sea and mainly along the Atlantic Jet which surrounds the Western Alboran gyre would be partially produced by the phytoplankton uptake of nutrients upwelled at the northeastern side of Gibraltar (Ruiz et al., 2001). On the other hand, cyclonic circulation cells between Punta Europa (Strait of Gibraltar) and Cape Pino, and in front of Malaga Bay would also be responsible for high primary production rates (Reul et al., 2005; Sarhan et al.,2000). These circulation patterns would be reflected in the high surface and integrated chlorophyll concentrations in the P, M and V transects. Notice that integrated chlorophyll concentrations do not show a clear seasonal pattern at these stations as high values are observed during the stratified season: summer and autumn (65 mg/m^2 in summer at M4 station and 47 mg/m^2 at P2 in autumn). Beside this, the DCM (or subsurface chlorophyll maximum) is always at the upper 20 m of the water column (Tables 2—5). All these facts suggest the high influence of permanent upwelling mechanisms operating in the Western Alboran Sea throughout the whole year.

Tables 2—5 show clearly the SW-NE trophic gradient in the RADMED area. The chlorophyll concentration at the DCM decreases clearly from the top of the table (Alboran Sea) to the bottom (Balearic stations). At the same time, the depth of the DCM increases in the same direction. Nevertheless, high nutrient and chlorophyll concentrations are observed in winter in BNA4 and MH4 stations. These results are coincident with the existence of very low winter temperatures which could indicate the influence of strong winter mixing and intermediate convection on the fertilization of these areas.

Redfield ratios have been calculated for three geographical areas: the Alboran Sea, the peninsular part of the Eastern Spanish coast and the Balearic Islands. Two different approaches were used. For the first one, all nitrate + nitrite values and all the phosphate values from the upper layer (0—75 m) were chosen and the same was done for the lower layer (100 m—bottom). A regression line was fitted to the nitrogen-phosphate data and the slope was considered as the N:P Redfield ratio. The same procedure was followed for the Si:P ratio. The results from this method seem to be very dispersed with confidence intervals exceeding the ratio value. The second method consisted in the estimation of the nitrogen (nitrate + nitrite), phosphate and silicate mean concentrations for each layer and then the calculation of the corresponding ratios: N:P and Si:P. This second approach seemed to yield more coherent results in the case of the Alboran Sea and the peninsular eastern coast. For the Alboran

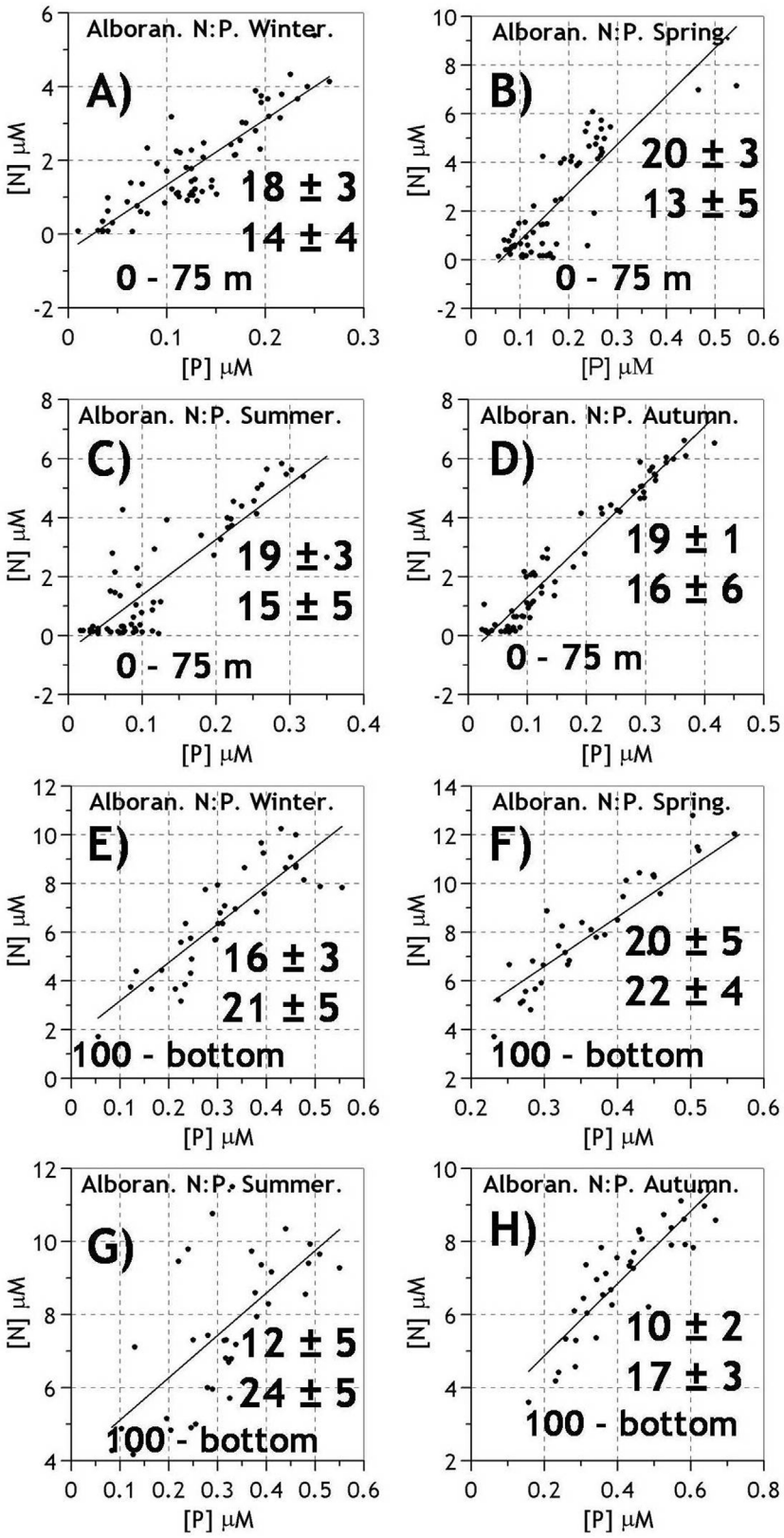

Fig. 12 Redfield N:P ratios for the 0—75 m layer for the Alboran Sea. Fig. 12A is for winter, 12B for spring, 12C for summer and 12D for autumn. Figs. 12E, F, G and H are the same for the 100 m-bottom layer.

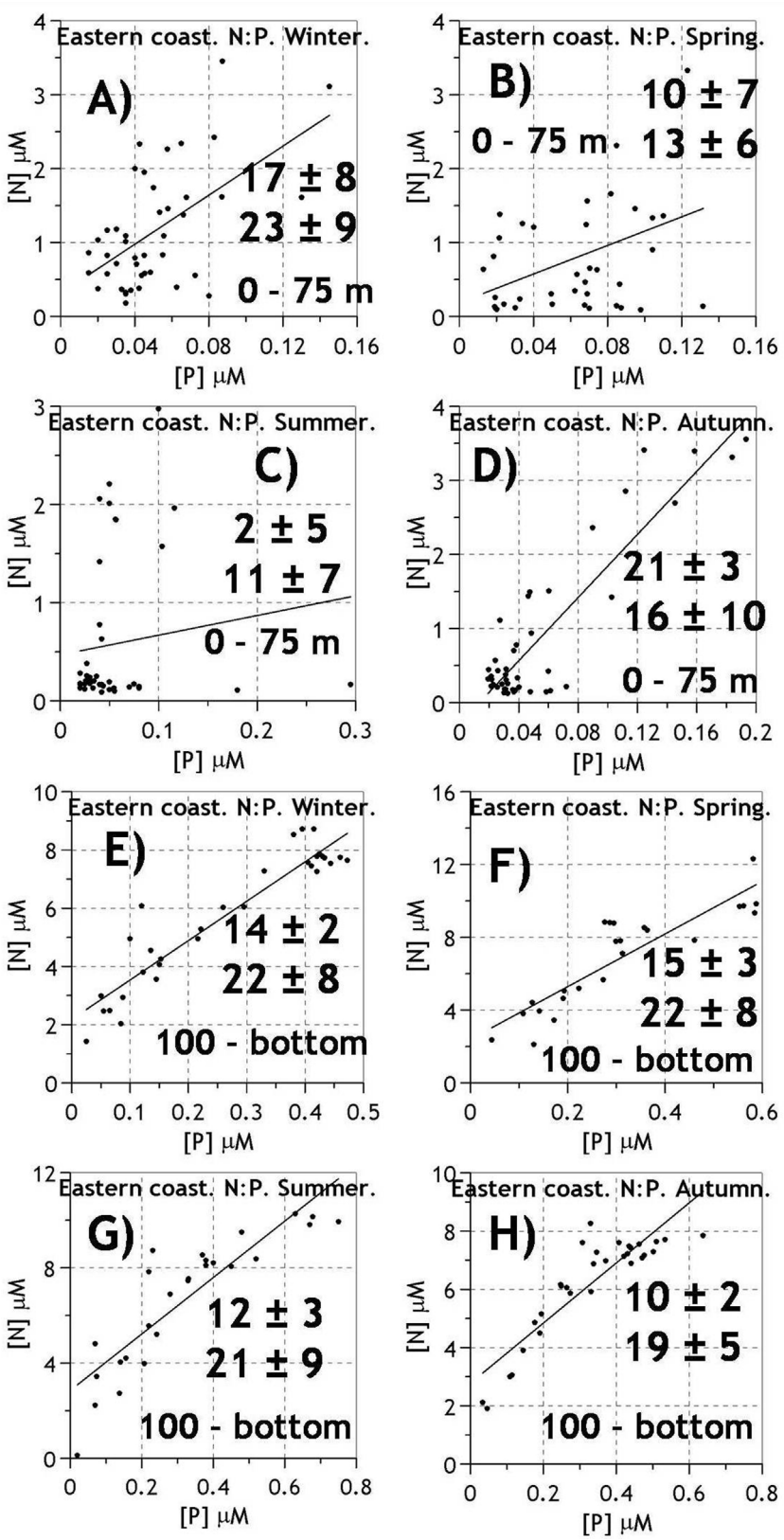

Fig. 13 The same as in Fig. 12, but for the peninsular eastern Spanish Mediterranean.

Sea, N:P ratios for the upper layer changed with the season between 13 and 16 with an annual mean value of 15. For the deep layer the values ranged between 17 and 24 with an annual mean value of 21. Very similar results were obtained for the peninsular eastern coast with N:P ratios of 16 and 22 for the upper and lower layers respectively. The Redfield ratios estimated for the Balearic Islands were very dispersed, very likely as a consequence of the data scarcity. Taking into

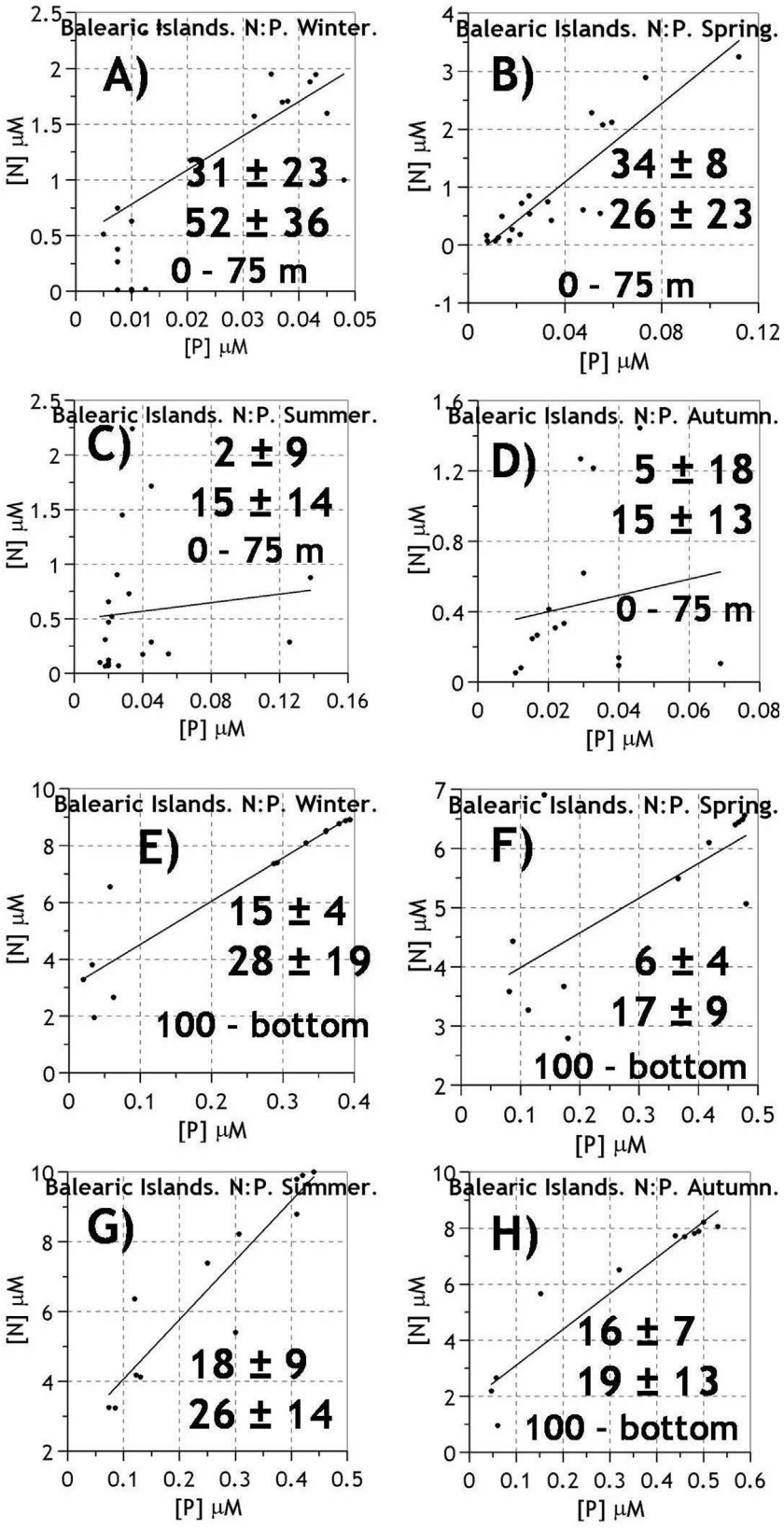

Fig. 14 The same as in Figs. 12 and 13, but for the Balearic Islands.

account the Alboran Sea and eastern coast results, it can be established that the upper layer follows the theoretical ratio 16, while the ratio for the deep layer clearly exceeds this value as already reported in previous works. This result would suggest that there is no phosphorus limitation for the AW within the westernmost sector of the Mediterranean Sea,

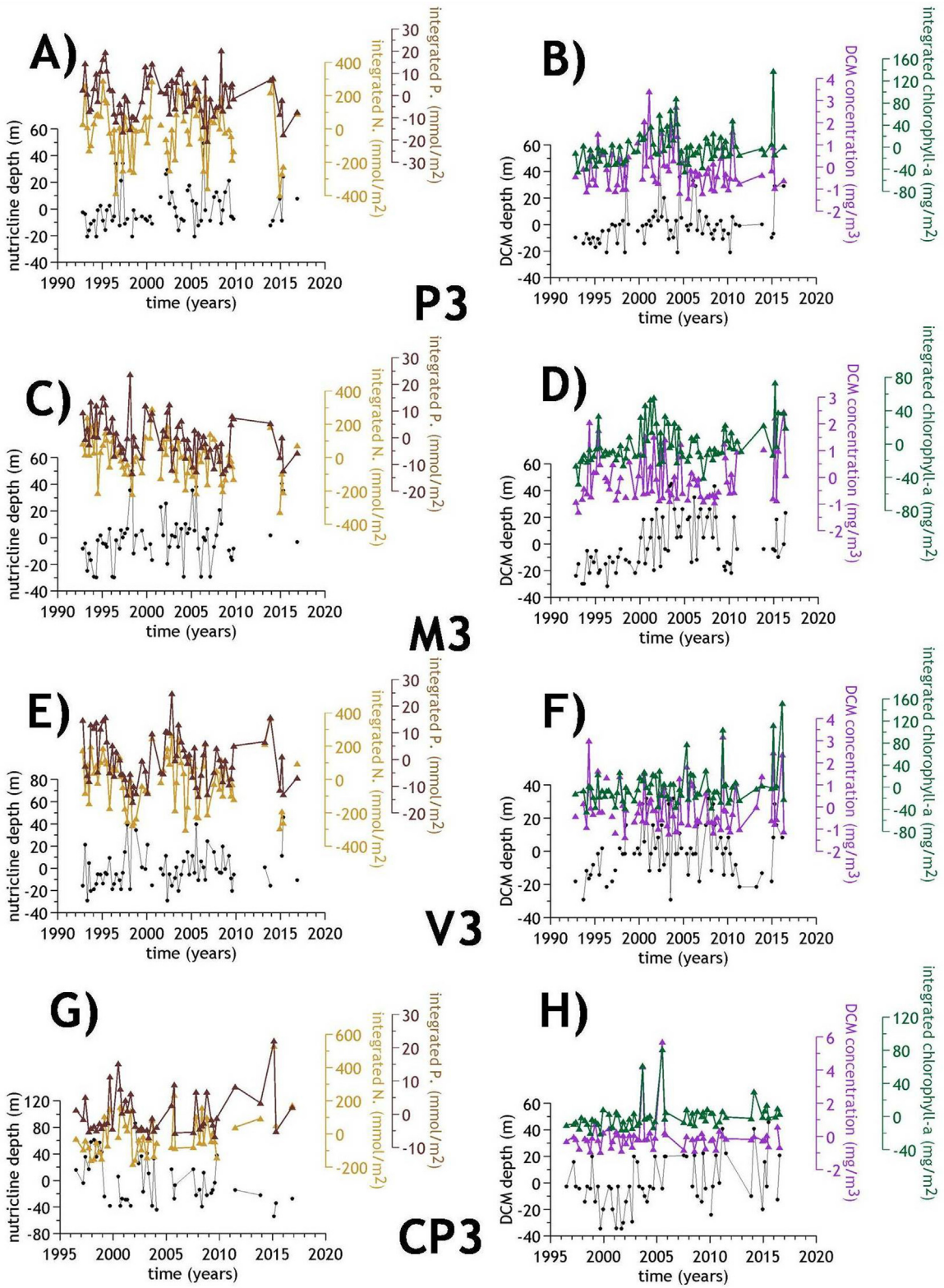

Fig. 15 Figures A, B show the residuals time series (deviations from the seasonal cycle) for the P3 station. Fig. 15A shows the nutricline depth (black line), the nitrate concentration integrated to the 100 m depth (light brown) and the integrated phosphate concentrations (dark brown). Fig. 15 B shows the residuals for the DCM (black line), the chlorophyll concentration at the DCM (purple) and the integrated chlorophyll (dark green). Fig. 15 C, D are the same for the M3 station, Fig. 15 E, F are the same for V3 station and Fig. 15 G, H for CP3 station. (For interpretation of the references to colour in this figure legend, the reader is referred to the web version of this article.)

while this limitation exists for the eastern basin (Thingstad et al., 2005) where LIW is formed. Notice that this water mass occupies the 150—600 m layer within the WMED and is also a main contributor to the WMDW formation.

Finally, the lengths of the present time series do not allow us to estimate long-term changes. Nevertheless, time series at the Malaga Bay area (P, M and V transects) and the Cape Palos area (CP) are suitable for the estimation of the decadal variability from the beginning of the 1990s to 2015. Linear trends for integrated nutrient concentrations, integrated chlorophyll-*a* and DO, nutricline depth and MLD, DCM chlorophyll concentration and DCM depth were estimated for these transects. Most of the trends obtained were not statistically significant at the 0.05 significance level. One of the threats on the Mediterranean Sea and the global ocean is the increase of the water column stratification as a consequence of the upper layer warming. This warming and stratification would produce the decrease of the DO solubility, lower ventilation rates for the intermediate and deep layers and the decrease of the nutrient injection into the photic layer. More stratified waters would require a higher kinetic energy to be mixed during autumn, winter and early spring. Therefore the MLD could be considered as a good indicator of these processes. Time series from 1992 to 2015 in the Malaga Bay area and from 1996 to 2015 in the Cape Palos transect did not show significant changes in the MLD. The only significant trends were obtained in M2 station with a positive trend of 0.28 ± 0.26 m/yr (deepening of the MLD) and at V3, with a negative trend of -0.29 ± 0.26 m/yr. The results were not significant for the other stations and therefore it cannot be concluded the existence of changes in the MLD in these two regions. The only significant trends were those obtained for the integrated chlorophyll and DO in the P3, M3 and V3 stations. Both variables increased for the 1992—2015 period indicating a possible increase in the primary production in the Western Alboran Sea.

In summary, the RADMED monitoring program has allowed us to establish a clear trophic gradient from the southwest to the northeast in the Spanish Mediterranean waters as well as the main traits of the nutrient, DO and chlorophyll distributions. Nitrate concentrations at the upper layers of the water column reach maximum values during winter mixing. Nevertheless some exceptions are observed in S and CG transects (Eastern Alboran Sea) and in B2 and B3 stations in Mallorca transect. In these cases, the surface nitrate maximum is advanced to autumn when stormy conditions usually begin. Notice that the autumn nitrate estimations are based on 4 autumn cruises for the case of S and CG transects and 7 cruises for the case of B transect. Phosphate concentrations at the upper layer seem to be more homogeneous along the year without a clear seasonal cycle. The nitrate surface injection decreases from the southwest to the northeast. The only exceptions are BNA4 station and the MH transect with surface winter nitrate concentrations close to or higher than 1 μM. Notice that these stations are located in areas of intermediate winter convection (Vargas-Yáñez et al., 2012). The intensity of the DCM decreases and its depth increases from the Alboran Sea to the northeast. The DCM is accompanied by a DO maximum at the same depth or above it and a nitrite maximum which has been attributed to incomplete assimilatory reduction of nitrate by phytoplankton. Redfield ratios seem to indicate phosphorus limitation for the intermediate and deep layers, but not for the AW occupying the 0—75 m layer of the water column. The longest time series are those corresponding to P, M and V transects in the Western Alboran Sea and CP to the south of Cape Palos. The only significant trends observed show an increase of the chlorophyll and DO content in the P, M and V transects. Nevertheless, the length of these time series precludes us from considering that these decadal changes could be considered as the long-term trend.

Finally, some of the seasonal estimations presented in the present work are based on more than 15 or 20 data per season and therefore mean values and variability ranges could be provided (see Table S1). Mean values and standard deviations obtained in this way could be used as a reference for future works or operational services providing reference values and ranges of variability. On the other hand, transects recently included in the monitoring program and the frequent difficulties such as bad weather conditions, instrument failures and vessel availability do not allow us to present robust statistics in some cases. These estimations, although based on very scarce data are presented for the completeness of the work and for showing the importance of such monitoring programs for base line setting and trend detection in the context of global change scenario.

Acknowledgements

The RADMED monitoring program is funded by the Instituto Español de Oceanografìa, and has been partially funded by the DESMMON project (PN I+D+I CTM2008-05695-C02-01), the PERSEUS project (FP7-287600), the IRIS-SES project (DG ENV GA-07.0335/2013/659540/SUB/C2.), the ActionMed project (DG-ENVGA-11.0661/2015/12631/SUB/ENVC.2) ATHAPOC project (PN I+D+I CTM2014-54374-R).

Appendix A. Supplementary data

Supplementary material related to this article can be found, in the online version, at https://doi.org/10.1016/j.oceano.2018.08.003.

References

Bethoux, J.P., Morin, P., Chaumery, C., Connan, O., Gentili, B., Ruiz-Pino, D., 1998. Nutrients in the Mediterranean Sea, mass balance and statistical analysis of concentrations with respect to environmental change. Mar. Chem. 63 (1—2), 155—169, http://dx.doi.org/10.1016/S0304-4203(98)00059-0.

Bethoux, J.P., Morin, P., Ruiz-Pino, D.P., 2002. Temporal trends in nutrient ratios: chemical evidence of Mediterranean ecosystem changes driven by human activity. Deep-Sea Res. Pt. II 49 (11), 2007—2015, http://dx.doi.org/10.1016/S0967-0645(02)00024-3.

Calvo, E., Simó, R., Coma, R., Ribes, M., Pacual, J., Sabatés, A., Gili, J.M., Pelejero, C., 2011. Effects of climate change on Mediterranean marine ecosystems: the case of the Catalan Sea. Clim. Res. 50 (1), 1—26, http://dx.doi.org/10.3354/cr01040.

Coll, M., Piroddi, C., Albouy, C., Rais Lasram, F.B., Cheung, W.W.L., Christensen, V., Karpouzi, V.S., Guilhaumon, F., Mouillot, D., Paleczny, M., Palomeras, M.L., Steenbeek, J., Trujillo, P., Watson, R., Pauly, D., 2011. The Mediterranean Sea under siege: spatial overlap between marine biodiversity, cumulative threats and

marine reserves. Glob. Ecol. Biogeogr. 21 (4), 465—480, http://dx.doi.org/10.1111/j.1466-8238.2011.00697.x.

De Boyer Montégut, C., Madec, G., Fischer, A.S., Lazar, A., Iudicone, D., 2004. Mixed layer depth over the global ocean: an examination of profile data and a profile-based climatology. J. Geophys. Res. 109 (C12), C12003, http://dx.doi.org/10.1029/2004JC002378.

D'Ortenzio, F., Ribera d'Alcala, M., 2009. On the trophic regimes of the Mediterranean Sea: a satellite analysis. Biogeosciences 6 (2), 139—148, http://dx.doi.org/10.5194/bg-6-139-2009.

Echevarría, F., García-Lafuente, J., Bruno, M., Gorsky, G., Goutx, M., Gonzalez, N., García, C.M., Gómez, F., Vargas, J.M., Picheral, M., Striby, L., Varela, M., Alondo, J.J., Reul, A., Cózar, A., Prieto, L., Sarhan, T., Plaza, F., Jiménez-Gómez, F., 2002. Physical—biological coupling in the Strait of Gibraltar. Deep-Sea Res. II 49, 4115—4130, http://dx.doi.org/10.1016/S0967-0645(02)00145-5.

Estrada, M., Latasa, M., Emelianov, M., Gutiérrez-Rodríguez, A., Fernández-Castro, B., Isern-Fontanet, J., Mouriño-Carballido, B., Salat, J., Vidal, M., 2014. Seasonal and mesoscale variability of primary production in the deep winter-mixing region of the NW Mediterranean. Deep-Sea Res. Pt. I 94, 45—61, http://dx.doi.org/10.1016/j.dsr.2014.08.003.

Estrada, M., 1996. Primary production in the northwestern Mediterranean. Sci. Mar. 60 (Suppl. 2), 55—64.

Garcia-Martinez, M.C., Vargas-Yañez, M., Moya, F., Zunino, P., Bautista, B., 2018. The effects of climate change and rivers damming in the Mediterranean Sea during the twentieth century. Int. J. Environ. Sci. Nat. Res. 8 (4), 555741, http://dx.doi.org/10.19080/IJESNR.2018.08.555741.

Gasol, J.M., Cardelús, C., Anxelu, X., Morán, G., Balagué, V., Forn, I., Marrasé, C., Massana, R., Pedrós-Alió, C., Montserrat Sala, M., Simó, R., Vaqué, D., Estrada, M., 2016. Seasonal patterns in phytoplankton photosynthetic parameters and primary production at a coastal NW Mediterranean site. Sci. Mar. 80 (S1), 63—77, http://dx.doi.org/10.3989/scimar.04480.06E.

Gómez, F., 2003. The role of the exchanges through the Strait of Gibraltar on the budgets of elements in the Western Mediterranean Sea: consequences of human-induced modifications. Mar. Pollut. Bull. 46 (6), 685—694, http://dx.doi.org/10.1016/S0025-326X(03)00123-1.

Gómez, F., González, N., Echevarría, F., García, C.M., 2000. Distribution and fluxes of dissolved nutrients in the Strait of Gibraltar and its relation to microphytoplankton biomass. Estuar. Coast. Shelf Sci. 51 (4), 439—449, http://dx.doi.org/10.1006/ecss.2000.0689.

Grasshof, K., Erhardt, M., Kremling, K., 1983. Methods of Seawater Analysis, 2nd edn. Verlag Chemie, Weinheim, 419 pp.

Holm-Hansen, O., Lorenzen, C.J., Holmes, R.W., Strickland, J.D., 1965. Fluorometric determination of chlorophyll. J. Mar. Sci. 30 (1), 3—15, http://dx.doi.org/10.1093/icesjms/30.1.3.

Huertas, I.E., Ríos, A.F., García-Lafuente, J., Navarro, G., Makaoui, A., Sánchez-Román, A., Rodríguez-Gálvez, S., Orbi, A., Ruiz, J., Pérez, F.F., 2012. Atlantic forcing of the Mediterranean oligotrophy. Global Biogeochem. Cycle 26 (2), GB2022, http://dx.doi.org/10.1029/2011GB004167.

Labasque, T., Chaumery, C., Aminot, A., Kergoat, G., 2004. Spectrophotometric Winkler determination of DO: re-examination of critical factors and reliability. Mar. Chem. 88 (1—2), 53—60, http://dx.doi.org/10.1016/j.marchem.2004.03.004.

Latasa, M., Gutiérrez-Rodríguez, A., Cabello, A.M., Scharek, R., 2016. Influence of light and nutrients on the vertical distribution of marine phytoplankton groups in the deep chlorophyll maximum. Sci. Mar. 80 (S1), 57—62, http://dx.doi.org/10.3989/scimar.04316.01A.

Latasa, M., Scharek, R., Vidal, M., Vila-Reixach, G., Gutiérrez-Rodríguez, A., Emelianov, M., Gasol, J.M., 2010. Preferences of phytoplankton groups for waters of different trophic status in the northwestern Mediterranean Sea. Mar. Ecol. Prog. Ser. 407, 27—42, http://dx.doi.org/10.3354/meps08559.

Lavigne, H., D'Ortenzio, F., Ribera D'Alcalá, M., Claustre, H., Sauzède, R., Gacic, M., 2015. On the vertical distribution of the chlorophyll-*a* concentration in the Mediterranean Sea: a basin-scale and seasonal approach. Biogeosciences 12 (16), 5021—5039, http://dx.doi.org/10.5194/bg-12-5021-2015.

L'Helguen, S., Le Corre, P., Madec, C., Morin, P., 2002. New and regenerated production in the Almería-Orán front area, eastern Alboran Sea. Deep-Sea Res. Pt. I 49 (1), 83—99, http://dx.doi.org/10.1016/S0967-0637(01)00044-9.

Lomas, M.W., Lipschultz, F., 2006. Forming the primary nitrite maximum: nitrifyers or phytoplankton? Limnol. Oceanogr. 5 (15), 2453—2467, http://dx.doi.org/10.4319/lo.2006.51.5.2453.

López-Jurado, J.L., Balbín, R., Amengual, B., Aparicio-González, A., Fernández de Puelles, M.L., García-Martínez, M.C., Gaza, M., Jansá, J., Morillas-Kieffer, A., Moya, F., Santiago, R., Serra, M., Vargas-Yáñez, M., Vicente, L., 2015. The RADMED monitoring program: towards an ecosystem approach. Ocean. Sci. 11 (6), 645—671, http://dx.doi.org/10.5194/osd-12-645-2015.

López-Jurado, J.L., García-Lafuente, J., Cano Lucaya, N., 1995. Hydrographic conditions of the Ibiza Channel during November 1990, March 1991 and July 1992. Oceanol. Acta 18 (2), 235—243.

Lorbacher, K., Dommenget, D., Niiler, P.P., Köhl, A., 2006. Ocean mixed layer depth: a subsurface proxy of ocean-atmosphere variability. J. Geophys. Res. 111 (C7), C07010, http://dx.doi.org/10.1029/2003JC002157.

Macias, D., Bruno, M., Echevarnia, F., Vazquez, A., Garcia, C.M., 2008. Meteorologically-induced mesoscale variability of the North-western Alboran Sea (southern Spain) and related biological patterns. Estuar. Coast. Shelf Sci. 78 (2), 250—266, http://dx.doi.org/10.1016/j.ecss.2007.12.008.

Macías, D., García-Gorriz, E., Piroddi, C., Stips, A., 2014. Biogeochemical control of marine productivity in the Mediterranean Sea during the last 50 years. Global Biogechem. Cy. 28 (8), 897—907, http://dx.doi.org/10.1002/2014GB004846.

Macías, D., García-Gorriz, E., Stips, A., 2018. Major fertilization mechanisms for Mediterranean Sea coastal ecosystems. Limnol. Oceanogr. 63 (2), 897—914, http://dx.doi.org/10.1002/lno.10677.

Manca, B., Burca, M., Giorgetti, A., Coatanoan, C., García, M.J., Iona, A., 2004. Physical and biological averaged vertical profiles in the Mediterranean regions. An important tool to trace the climatology of water masses and to validate incoming data from operational oceanography. J. Mar. Syst. 48 (1—4), 83—116, http://dx.doi.org/10.1016/j.jmarsys.2003.11.025.

Marty, J.C., Chiavérini, J., 2010. Hydrological changes in the Ligurian Sea (NW Mediterranean, DYFAMED site) during 1995—2007 and biogeochemical consequences. Biogeosciences 7 (7), 2117—2128, http://dx.doi.org/10.5194/bg-7-2117-2010.

Marty, J.C., Chiavérini, J., 2002. Seasonal and interannual variations in phytoplankton production at DYFAMED time-series station, northwestern Mediterranean Sea. Deep Sea Res. Pt. II 49 (11), 2017—2030, http://dx.doi.org/10.1016/S0967-0645(02)00025-5.

Millot, C., 1999. Circulation in the Western Mediterranean Sea. J. Mar. Syst. 20 (1—4), 423—442, http://dx.doi.org/10.1016/S0924-7963(98)00078-5.

Minas, H.J., Coste, B., Le Corre, P., Minas, M., Raimbault, P., 1991. Biological and geochemical signatures associated with the wáter circulation through the Starit of Gibraltar and the Western Alboran Sea. J. Geophys. Res. 96 (C5), 8755—8771.

Morán, X.A., Estrada, M., 2001. Short-term variability of photosynthetic parameters and particulate and dissolved primary production in the Alboran Sea (SW Mediterranean). Mar. Ecol. Prog. Ser. 212, 53—67, http://www.jstor.org/stable/24864175.

Pai, S.-C., Gong, G.-C., Liu, K.-K., 1993. Determination of dissolved oxygen in seawater by direct spectrophotometry of total iodine.

Mar. Chem. 41 (4), 343—351, http://dx.doi.org/10.1016/0304-4203(93)90266-Q.

Pasqueron de Fommervault, O., Migon, C., D'Ortenzio, F., Ribera d'Alcalà, M., Coppola, L., 2015. Temporal variability of nutrient concentrations in the northwestern Mediterranean sea (DYFAMED time-series station). Deep-Sea Res. Pt. I 100, 1—12, http://dx.doi.org/10.1016/j.dsr.2015.02.006.

Pinot, J.M., Ganachaud, A., 1999. The role of winter intermediate waters in spring-summer circulation of the Balearic Sea: 1. Hydrography and inverse modeling. J. Geophys. Res. 104 (C12), 29843—29864, http://dx.doi.org/10.1029/1999JC900071.

Pinot, J.M., Tintoré, J., Gomis, D., 1995. Multivariate analysis of the surface circulation in the Balearic Sea. Prog. Oceanogr. 36 (4), 345—376, http://dx.doi.org/10.1016/0079-6611(96)00003-1.

Powley, H.R., Cappellen, P.V., Krom, M.D., 2017. Nutrient cycling in the Mediterranean Sea: the key to understanding how the unique marine ecosystem functions and responds to anthropogenic pressures. In: Fuerst-Bjeliš, B. (Ed.), Mediterranean Identities — Environment, Society, Culture. InTech, 47—77, http://dx.doi.org/10.5772/intechopen.70878.

Pujo-Pay, M., Conan, P., Oriol, L., Cornet-Barthaux, V., Falco, C., Ghiglione, J.F., Goyet, C., Moutin, T., Prieur, L., 2011. Integrated survey of elemental stoichiometry (C, N, P) from the western to eastern Mediterranean Sea. Biogeosciences 8 (4), 883—899, http://dx.doi.org/10.5194/bg-8-883-2011.

Ramírez, T., Cortés, D., Mercado, J.M., Vargas-Yáñez, M., Sebastián, M., Liger, E., 2005. Seasonal dynamics of inorganic nutrients and phytoplankton biomass in the NW Alboran Sea. Estuar. Coast. Shelf Sci. 65 (4), 654—670, http://dx.doi.org/10.1016/j.ecss.2005.07.012.

Ravaioli, M., Bergami, C., Riminucci, F., Langone, L., Cardin, V., Di Sarra, A., Aracri, S., Bastianini, M., Bensi, M., Bergamasco, A., Bommarito, C., Borghini, M., Bortoluzzi, G., Bozzano, R., Cantoni, C., Chiggiato, J., Crisafi, E., D'Adamo, R., Durante, S., Fanara, C., Grilli, F., Lipizer, M., Marini, M., Miserocchi, S., Paschini, E., Penna, P., Pensieri, S., Pugnetti, A., Raicich, F., Schroeder, K., Siena, G., Specchiulli, A., Stanghellini, G., Vetrano, A., Crise, A., 2018. The RITMARE Italian fixed-point observatory network (IFON) for marine environmental monitoring: a case study. J. Oper. Oceanogr. 9 (Suppl. 1), s202—s214, http://dx.doi.org/10.1080/1755876X.2015.1114806.

Reul, A., Rodríguez, V., Jiménez-Gómez, F., Blanco, J.M., Bautista, B., Sarhan, T., Guerrero, F., Ruiz, J., García-Lafuente, J., 2005. Variability in the spatio-temporal distribution and size-structure of phytoplankton across an upwelling area in the NW-Alboran Sea (W-Mediterranean). Cont. Shelf Res. 25 (5—6), 589—608, http://dx.doi.org/10.1016/j.csr.2004.09.016.

Ruiz, J., Echevarría, F., Font, J., Ruiz, S., García, E., Blanco, J.M., Jiménez-Gómez, F., Prieto, L., González-Alaminos, A., García, C. M., Cipollini, P., Snaith, H., Bartual, A., Reul, A., Rodríguez, V., 2001. Surface distribution of chlorophyll, particles and gelbstoff in the Atlantic jet of the Alborán Sea: from submesoscale to subinertial scales of variability. J. Mar. Syst. 29 (1—4), 277—292, http://dx.doi.org/10.1016/S0924-7963(01)00020-3.

Sarhan, T., Garcia-Lafuente, J., Vargas, M., Vargas, J.M., Plaza, F., 2000. Upwelling mechanisms in the northwestern Alboran Sea. J. Mar. Syst. 23 (4), 317—331, http://dx.doi.org/10.1016/S0924-7963(99)00068-8.

Schmidtko, S., Stramma, L., Visbeck, M., 2017. Decline in global oceanic content during the past five decades. Nature 542, 335—339, http://dx.doi.org/10.1038/nature21399.

Schroeder, K., Gasparini, G.P., Borghini, M., Cerrati, G., Delfanti, R., 2010. Biogeochemical tracers and fluxes in the Western Mediterranean Sea, spring 2005. J. Mar. Syst. 80 (1—2), 8—24, http://dx.doi.org/10.1016/j.jmarsys.2009.08.002.

Segura-Noguera, M., Cruzado, A., Blasco, D., 2016. The biogeochemistry of nutrients, dissolved oxygen and chlorophyll-*a* in the Catalan Sea (NW Mediterranean Sea). Sci. Mar. 80 (S1), 39—56, http://dx.doi.org/10.3989/scimar.04309.20A.

Sournia, A., 1973. La production primaire planctonique en Méditerranée: Essai de mise à jour. Bulletin de l'Etude en commun de la Méditerranée 5—128.

Strickland, J.D.H., Parsons, T., 1972. A practical handbook of seawater analysis. B. Fish. Res. Board Can. 167, 310 pp., http://dx.doi.org/10.1002/iroh.19700550118.

Tel, E., Balbín, R., Cabanas, J.M., García, M.J., García-Martínez, M. C., González-Pola, C., Lavín, A., López-Jurado, J.L., Rodríguez, C., Ruiz-Villareal, M., Sánchez-Leal, R.F., Vargas-Yáñez, M., Vélez-Belchi, P., 2016. IEOOS: The Spanish Institute of Oceanography Observing System. Ocean Sci. 12 (2), 345—353, http://dx.doi.org/10.5194/os-12-345-2016.

Thingstad, T.F., Krom, M.D., Mantoura, R.F.C., Flaten, G.A.F., Groom, S., Herut, B., Kress, N., Law, C.S., Pasternak, A., Pitta, P., Psarra, S., Rassoulzadegan, F., Tanaka, T., Tselepides, A., Wassmann, P., Woodward, E.M.S., Wexels Riser, C., Zodiatis, G., Zohary, T., 2005. Nature of phosphorus limitation in the ultraoligotrophic Eastern Mediterranean. Science 309, 1068—1071, http://dx.doi.org/10.1126/science.1112632.

Treguer, P., Le Corre, P., 1975. Manuel d'analyse des sels nutritifs dans l'eau de mer, Utilisation de l'AutoAnalyser II Technicon, Occidentale, Vol. 5. Univ. Bretagne, Laboratoire de Chimie Marine, Brest, France, 110 pp.

Vargas-Yáñez, M., García-Martínez, M.C., Moya, F., Balbín, R., López-Jurado, J.L., Serra, M., Zunino, P., Pascual, J., Salat, J., 2017. Updating temperature and salinity mean values and trends in The Western Mediterranean: The RADMED Project. Prog. Oceanogr. 157, 27—46, http://dx.doi.org/10.1016/j.pocean.2017.09.004.

Vargas-Yáñez, M., Zunino, P., Schroeder, K., López-Jurado, J.L., Plaza, F., Serra, M., Castro, C., García-Martínez, M.C., Moya, F., Salat, J., 2012. Extreme western intermediate water formation in winter 2010. J. Mar. Syst. 105—108, 52—59, http://dx.doi.org/10.1016/j.jmarsys.2012.05.010.

Zar, J.H., 1984. Biostatistical Analysis, 2nd ed. Prentice-Hall, Inc., Englewood Cliffs, 718 pp.

Oceanologia (2019) 61, 170—177

Available online at www.sciencedirect.com

ScienceDirect

journal homepage: www.journals.elsevier.com/oceanologia/

SHORT COMMUNICATION

Spatiotemporal variation of alkaline phosphatase activity in coastal waters off Trivandrum

Mamatha S. Shivaramu *, Amruta K. Randive, Ritu Kumari, Manguesh Gauns, LokaBharathi A. Ponnapakkam

Biological Oceanography Division, CSIR-National Institute of Oceanography, Goa, India

Received 16 February 2018; accepted 13 June 2018
Available online 3 July 2018

KEYWORDS
Phosphorus;
Alkaline phosphatase activity;
Chlorophyll;
Phytoplankton;
Bacteria

Summary Phosphatase is an extracellular enzyme which releases inorganic phosphate (Pi) from dissolved organic phosphate and indirectly organic carbon as nutrients for aquatic communities. Here, we have examined spatiotemporal variation in total alkaline phosphatase activity (APA) over a short period off Trivandrum, SW India. Sampling was at 50 m water depth at 5, 15, 25 and 45 m for 5 consecutive days at 6 h intervals during post-monsoon season. Total APA and phosphatase producing bacteria (PPB) were estimated along with pertinent environmental parameters. APA increased with depth up to 3.98 μM P h^{-1} at 45 m. Increase in pigment concentration with depth is responsible for an increase in APA and Pi uptake. There is a marginal increase in APA towards 18—24 h suggesting feeding activities of secondary producers. On the whole, chlorophyll and phaeophytin were responsible for nearly 45 and 55% variation in APA ($p < 0.01$, $p < 0.001$, $n = 16$), respectively. Total bacterial count (TBC) was responsible for 32% ($p < 0.05$, $n = 16$) and total viable direct counts-aerobic (TVCa) for 24% ($p < 0.05$, $n = 16$) APA variation. About 38% ($p < 0.01$, $n = 20$) variation of APA was linked to chlorophyll at noon and 22% ($p < 0.001$, $n = 20$) to PPB at dawn. Thus, it is possible that bacteria and chlorophyll/phytoplankton could be responsible for variation in APA, with the latter contribution greater than the former at noon. Such studies would help to profile the fertility of coastal waters in terms of bioavailable Pi. Laboratory experiments are underway to help us discern the extent of light-dependent contribution of chlorophyll/phytoplankton to APA and light independent participation of bacteria to the process.

* Corresponding author at: Biological Oceanography Division, CSIR-National Institute of Oceanography, Dona Paula 403004, Goa, India. Tel.: +91 832 2450 254; fax: +91 832 2450 606.
E-mail address: mamatha@nio.org (M.S. Shivaramu).
Peer review under the responsibility of Institute of Oceanology of the Polish Academy of Sciences.

ELSEVIER Production and hosting by Elsevier

https://doi.org/10.1016/j.oceano.2018.06.004

The availability of organic carbon and inorganic nutrients in water limits the biological productivity of aquatic environments. Of the essential elements involved in the biogeochemical cycle of the marine environment, phosphorus and nitrogen are most often considered as limiting factors. Dissolved and dead organic matter unusable by other organisms is subjected to microbial decomposition. Hence, the 'microbial loop' is important for recycling of phosphate and nitrogen in both water and sediment (Azam et al., 1983, 1995). The extensive number of microbial ectoenzyme activities detected in the water column has been noticed. Also the importance of heterotrophic bacteria and phytoplankton in biochemical/chemical processing and biogeochemical cycling in the ocean has been reported (Benitez-Nelson, 2000; Dyhrman et al., 2006). Hydrolytic enzymes include alkaline phosphatase, chitinase, lipase, protease, aminopeptidase, glucosidase, and others. These enzymes convert organic matter to more labile form and thus influence the growth dynamics of different microbes and phytoplankton (Azam et al., 1995; Chrost, 1991; Martinez et al., 1996). Phytoplankton and bacteria can satisfy their phosphorus (P) requirements by producing hydrolytic enzymes such as alkaline phosphatase (AP) to access Pi from organic P. Pi gets limited in coastal areas with high nitrogen availability or in oceans where there is high rates of nitrogen fixation (Ammerman et al., 2003; Labry et al., 2005; Vidal et al., 2003; Yucel, 2018).

Alkaline phosphatases have a broad range of organic substrate specificities, and therefore hydrolyze a wide variety of organic phosphomonoesters (Ammerman, 1991). These enzymes are attached to cell surface or, are freely dissolved in the water column resulting from the cell lysis or excretion (Hoppe, 2003; Jansson et al., 1988; Li et al., 1998). Upon enzyme hydrolysis, phosphomonoesters release inorganic P (Pi) into the water, along with their organic moiety, thereby increasing Pi availability for planktonic, as well as benthic organisms in shallow marine systems (Dyhrman and Ruttenberg, 2006; Koch et al., 2009). APA has been identified and associated with major groups of algae, cyanobacteria (Dyhrman and Ruttenberg, 2006; Martinez et al., 1996) and heterotrophic bacteria (De Souza et al., 2000) and also studied in seawater (Koch et al., 2009; Mamatha et al., 2012) and sediment (Taga and Kobori, 1978). Generally, it is reported that APA gets expressed when P is limiting and suppressed when P level is replete. It is presumed that APA promotes organic P mineralization and recycling within P-limited systems (Ammerman et al., 2003; Koch et al., 2009; Labry et al., 2005; Mamatha et al., 2015; Sebastian et al., 2012; Vidal et al., 2003).

The concentration of P in coastal waters could be increased by either land runoff or by upwelling process. In the rainy season (June–September), strong south-west monsoonal winds cause coastal upwelling in the Arabian Sea, which is one of the most productive areas in the world (Naqvi et al., 2010; Prell et al., 1991). However, upwelling weakens in the southernmost part of the west coast of India by October, and as a result, the high concentrations of nutrients available at the surface water get exhausted due to autotrophic production (Peetersa et al., 2002). During the post-monsoon season, the weaker north-east monsoon winds result in deeply stratified water and deeper euphotic zone (Peetersa et al., 2002; Pillai et al., 2000). Based on this information, we have examined the spatiotemporal variation in APA along with other environmental parameters over a short period off Trivandrum to appreciate the extent of changes in fertility as shown by the variation in APA. Previously, Mamatha et al. (2015) have noticed that low APA could be indicative of P sufficiency in coastal waters and higher activity suggestive of deficiency in off-shore waters off Trivandrum during upwelling season. In this communication on spatiotemporal variation during post upwelling, there is an increase in APA with depth due to increase in pigment and also Pi utilization without any temporal changes. The paper discusses these remarkable aspects.

The study station was off Trivandrum coast, south-west of India (8°26.04′N, 76°30′E) in the eastern Arabian Sea. Seawater samples were collected onboard FORV "Sagar Sampada" (cruise No. 282) during a post-monsoon season (November 2010) at lat. 08°27.742′N and long. 76°46.709′E at the maximum water depth of 50 m. The sampling was done at 4 depths i.e. 5, 15, 25 and 45 m bss (below sea surface) at 6 hourly intervals for 5 days. The sampling hours were 0 (24), 6, 12 and 18 where 6 and 18 h were designated as dawn and dusk and 12 and 24 h as noon and midnight, respectively. The data with time intervals 6, 12, 18 and 24 h for 5 days were averaged to discern the spatiotemporal variation (supplementary Table S1). Each data point is derived from triplicates.

Samples for dissolved oxygen (DO) were collected in 125 mL stoppered glass bottles avoiding air bubbles and were immediately fixed with Winkler's reagents. Fixed samples were stored in the dark until analysis (Strickland and Parsons, 1965). Sub-samples were taken for analysis of various parameters like total APA, chlorophyll *a*, phaeopigment, phosphate and other nutrients. Seawater sub-samples for the total bacterial count (TBC) were collected in sterile containers immediately after retrieval and fixed with buffered formalin. Seawater sub-samples for other microbiological analyses were similarly collected and stored at 4°C till analysis.

Salinity and temperature were derived from the Sea Bird CTD connected to the rosette Niskin sampler that operated vertically all the time. The pH was checked onboard using pH meter.

Winkler's titrimetric method (Strickland and Parsons, 1965) was used for estimating the dissolved oxygen (DO) concentration onboard using a Dosimeter (Metrohm 785 DMP Titrino). Nutrients were also analyzed on board by SKALAR auto analyzer as described by Wurl (2009).

Chlorophyll *a* (Chl*a*) and phaeophytin (phaeo) concentrations were determined fluorometrically (Turner Designs, USA) by filtering 1 L water samples from each depth with GF/F filters and extracting with 10 mL of 90% acetone in the dark for 24 h under refrigeration. The extract was measured following UNESCO (1994) protocol. The readings were measured before and after acidification using Turner Design (10 AU) fluorometer and then both Chl*a* and phaeo concentrations were calculated.

Total bacterial abundance (TBC) was counted using epifluorescence microscopy (Olympus Fluorescent Microscope Model BX61) by acridine orange direct count (AODC) method (Hobbie et al., 1977) and expressed as numbers per litre (nos L^{-1}). Total direct viable counts (TVC), were estimated as outlined by Kogure et al. (1980) using a mixture of piromedic, pipemedic, nalidixic acid and yeast extract.

Table 1 Range and average of physico-chemical and biological parameters in whole water column (5 days, 4-time interval, 4 depths; $n = 80$).

Parameter	Range	Mean
Temperature [°C]	27.2–28.7	28 ± 0.57
Salinity	33.07–35.46	34.9 ± 0.57
pH	8.19–8.35	8.31 ± 0.04
DO [ml L^{-1}]	1.19–4.68	3.47 ± 0.64
NO_2^-N [μM]	ndl–0.795	0.16 ± 0.21
NO_3^-N [μM]	0.681–20.026	5.32 ± 4.68
PO_4^-P [μM]	0.093–2.37	0.27 ± 0.29
Chl*a* [μg L^{-1}]	0.71–2.90	1.39 ± 0.5
Phaeo [μg L^{-1}]	0.15–1.29	0.5 ± 0.3
TBC [cells L^{-1}]	2.48×10^8–1.54×10^{10}	$5 \times 10^9 \pm 2.85 \times 10^9$
TVC [cells L^{-1}]	6.37×10^8–8.16×10^9	$3.3 \times 10^9 \pm 2 \times 10^9$
PPB-MPN [cells L^{-1}]	ndl–1.5×10^6	$0.27 \times 10^6 \pm 0.46 \times 10^6$
APA [μM P h^{-1}]	ndl–13.79	2.34 ± 2.71

DO – dissolved oxygen; Chl*a* – chlorophyll *a*; Phaeo – pheaophytin TBC – total bacterial count; TVCa – total viable bacteria; PPB – phosphatase producing bacteria; APA – alkaline phosphatase activity; ndl – non detectable level.

The end point dilution method (MPN – Most Probable Number) is based on a series of dilutions prepared from a sample, where selected liquid media are inoculated with each dilution using 3 parallels. After the incubation period, estimation of the microbial count was done, using statistical tables based on the number of positive wells (showing colour formation i.e. colourless to yellow colour). Three tube method was suitably adopted for microtiter plate method. Phosphatase producing bacteria (PPB) were enumerated by most probable numbers (PPB-MPN) by microtitre plate method using para-nitrophenol phosphate (pNPP) as substrate (1 mM) (Fig. 1s). The hydrolysis of phosphate was indicated by the release of colored para-nitrophenol (pNP) from colourless para-nitrophenol phosphate (pNPP) in proportion to the Pi released. The samples were incubated in the dark at room temperature (28 ± 2°C) for scoring positive and negative growth/reactions. Scoring/calculations were done using McCrady's table (Rodina, 1972). It is assumed that the color development is attributed only to bacteria and free enzymes in the diluted inoculum.

The alkaline phosphatase activity (APA, EC 3.1.3.1) was estimated using the method of Taga and Kobori (1978) and Mamatha et al. (2015). Measurements were run against a control containing an equivalent volume of the seawater samples previously autoclaved. The results represent the average of triplicates corrected for controls. Experimental values were calculated against a standard (para-nitrophenol, pNP) curve prepared to cover concentrations from 10 nM to 1000 nM.

Microbiological data were log(x+1) transformed for statistical analysis. Inter-relationships between biological and environmental parameters were examined using Statistica ver. 6.0 and analysis tool pack in Microsoft Excel. Analysis of variance (ANOVA) was carried out to find out significant spatiotemporal variations in pertinent parameters.

In the present study, there is little variation in salinity with the minimum of 33.07 and maximum of 35.46. The increase of salinity from the surface to bottom is evident but it is not statistically significant. Variation in temperature and pH were also minimal as shown in Table 1. The dissolved oxygen in the water column ranged between 1.19 ml L^{-1} in 45 m depth to 4.42 ml L^{-1} in 5 m layer (Table 1). There was significant variation in vertical distribution with depth and time in temperature and DO ($p < 0.05$). Higher concentration of nitrate (20.02 μM) was measured at 45 m while nitrite (1.55 μM) was measured at surface waters (Table 1). Nitrate and nitrite showed significant variation with depth but not with time. The average concentration of phosphate over the study period was 0.268 ± 0.246 μM ($n = 80$) and it ranged from 0.08–2.37 μM. Phosphate concentration was higher at 25 m depth (2.37 μM) than at the 5 m depth (0.08 μM). However, the spatial and temporal variation was not statistically significant.

The Chl*a* and bacterial numbers can effectively represent algal and bacterial biomass. Chl*a* concentration varied from 0.71–2.90 μg L^{-1} with an average 1.39 ± 0.50 μg L^{-1} (Table 1). Surprisingly, it was high at 45 m depth (2.9 μg L^{-1}) at all time intervals except noon when it is uniform throughout (Fig. 1a). Like Chl*a*, phaeopigment also follows the same trend in distribution (Fig. 1b).

TBC ranged from 2.4×10^8 to 1.54×10^{10} cells L^{-1} (av. $5 \times 10^9 \pm 3 \times 10^9$ cells L^{-1}) with the maximum at the 45 m, waters showing one order higher than the other depths (Table 1). TVCa was one order less than the TBC and was marginally higher at 45 m where it varied from 6.37×10^8–8.16×10^9 cells L^{-1} (av. $3.7 \times 10^9 \pm 2 \times 10^9$ cells L^{-1}). PPB-MPN ranged from ndl–1.5×10^6 cells L^{-1} (av. $0.27 \times 10^6 \pm 0.46 \times 10^6$ cells L^{-1}). Though there are large standard deviations in the average values of the bacterial parameters, ANOVA showed that there was no significant variation in distribution with depth and time (Fig. 2).

Total APA of the whole water column ranged from ndl to 13.79 μM P h^{-1} ($n = 80$) (Table 1). It increased with depth to a maximum of 3.98 μM P h^{-1} ($n = 16$, Fig. 3) at 45 m ($p < 0.05$) corresponding to increase in Chl*a* and phaeo concentration. There is not much variation with time, however, marginal increase towards 18 to 24 h was discernible. Two way ANOVA showed that depth variation is stronger ($p < 0.05$) than the temporal variation in APA.

On the whole, APA is positively related to depth ($r = 0.63$, $p < 0.05$, $n = 80$), and negatively with DO ($r = -0.594$, $p < 0.05$, $n = 16$). Nitrate influenced 41% ($r = 0.637$, $p < 0.01$)

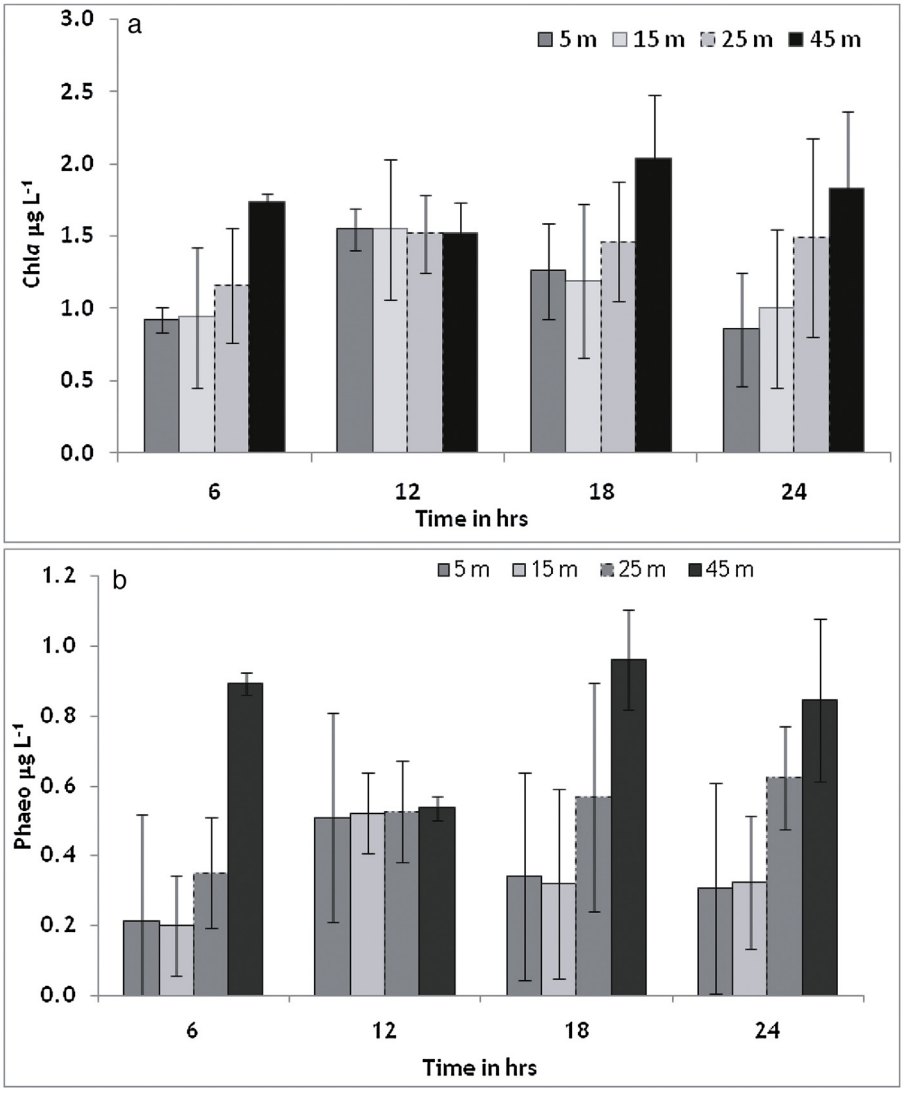

Figure 1 Spatio-temporal variations in (a) chlorophyll and (b) phaeophytin off Trivandrum.

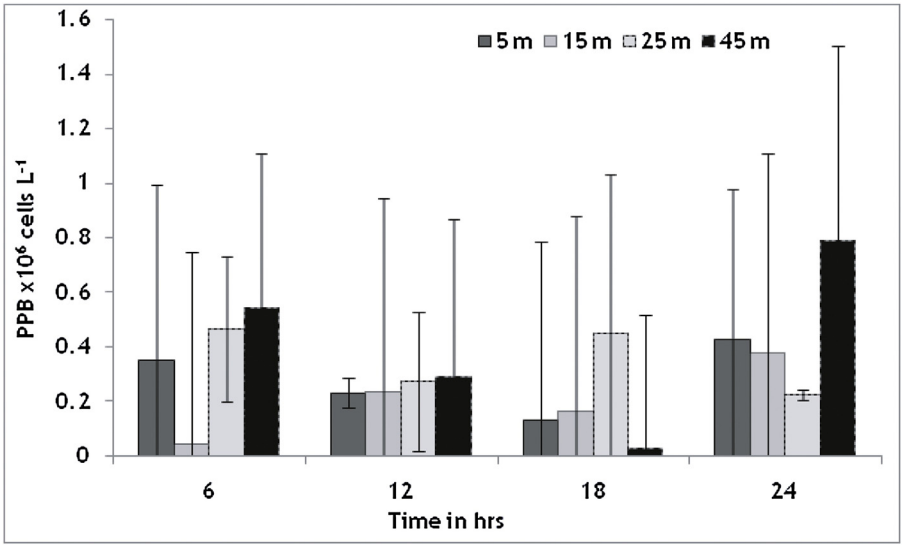

Figure 2 Spatio-temporal variations in phosphatase producing bacteria (PPB-MPN) off Trivandrum.

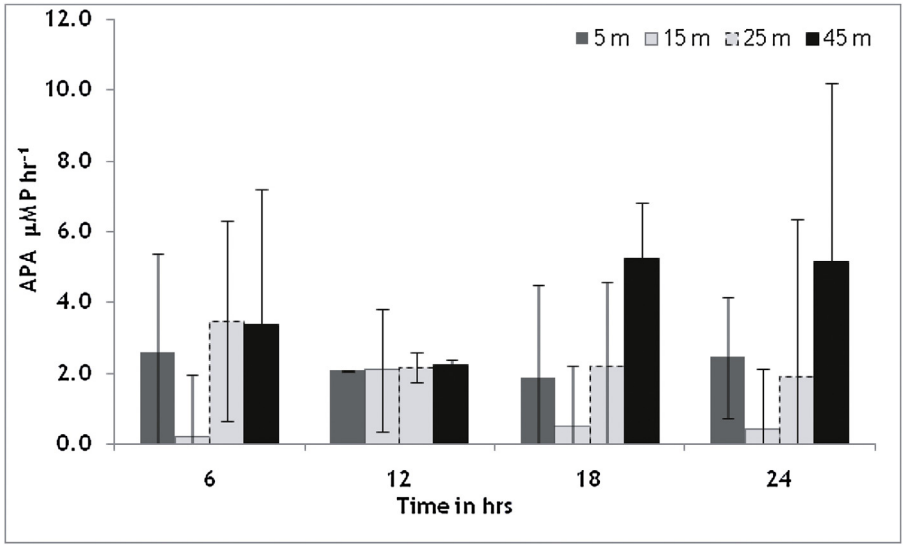

Figure 3 Spatio-temporal variations in alkaline phosphatase activity (APA) off Trivandrum.

Table 2 Relationships of alkaline phosphatase activity (APA) with environmental parameters.

	Whole water (n = 16)	6 h (n = 20)	12 h (n = 20)	18 h (n = 20)	24 h (n = 20)
Depth	0.616[b]	–	0.631[b]	–	0.468[c]
DO	−0.547[c]	–	−0.608[b]	–	–
NO_3-N	0.637[b]	–	–	0.625[b]	–
Chl*a*	0.670[b]	–	0.619[b]	–	–
Phaeo	0.740[c]	–	0.638[b]	–	0.491[c]
TBC	0.561[a]	–	–	–	–
TVC	0.491[a]	–	–	–	–
PPB-MPN	–	0.465[c]	–	–	–

Superscripts denote different significant levels; [a]$p < 0.05$; [b]$p < 0.01$ and [c]$p < 0.001$. DO – dissolved oxygen; Temp. – temperature; Chl – chlorophyll *a*; Phaeo – pheaophytin; TBC – total bacterial count; TVC – total viable count; PPB – phosphatase producing bacteria; APA – alkaline phosphatase activity.

variation in APA. Chl*a* and phaeo were responsible for 45 and 55% variation in APA, respectively ($p < 0.05$, $p < 0.001$, n = 16) (Table 2). Bacterial fractions examined contributed to the changes in APA with the TBC being responsible for nearly 32% ($p < 0.05$, n = 16) and TVCa for 24% ($p < 0.05$, n = 16). Time dependent study showed that 38% ($p < 0.01$, n = 20) variation of APA at noon was linked to Chl*a* and 22% ($p < 0.001$, n = 20) variation in APA to PPB-MPN at dawn (Table 2).

The spatial variation (depth) is discernible in these waters (Nyadjro et al., 2012). The variation with temperature and DO confirms that there is stratification in these shallow coastal waters during this season but restricted to physico-chemical parameters. The higher concentration of nitrate at the bottom suggests that the source could be from sediment. Chl*a* and phaeo were also high at 45 m all the time, suggesting that the settling of the pigments was high throughout the observation. The Chl*a* maxima were observed at noon at all the depths. This peaking could be a reflection of the penetration of PAR (photosynthetically active radiation) up to 45 m depth. However, the depth of the euphotic zone could vary in different waters. Qasim (1982) reported that euphotic zone in the southern Arabian Sea was 60 m and in the northern part it was 40 m. Pillai et al. (2000) also found that the average depth of the euphotic zone in the west coast is 60 m during post-monsoon season. Lack of significant variation in the different bacterial parameters with depth and time suggests that this could be due to their stronger association with phytoplankton (Riemann et al., 1999; Rooney-Varga et al., 2004). A rise in bacterial population at the bottom may be a consequence of nocturnal feeding and excretion by benthic organisms. Nandakumar and Damodaran (1998) found that there is a diurnal variation in the feeding intensity of speckled shrimps at Kochi. They feed more in the night than day. This benthic activity may enrich the bottom area with essential nutrients subsequently allowing bacteria including PPB to proliferate rapidly. Thus there is less heterogeneity in the microbial distribution in the coastal waters, suggesting that the representative sampling can be at any depth.

In the present study, APA peaks were observed from dusk to dawn (1/4 observations – dusk, 1/4 – midnight and 2/4 – dawn) (Fig. 3). These APA peaks could be linked to prolonged grazing by zooplankton. Their sloppy feeding generally leads

to release of phytoplankton exudates (Fouilland et al., 2014; Lignell, 1990; Yucel, 2018). Besides, higher APA at 45 m layer could also be a reflection of higher phosphatase producing bacterial population from sediments below (Ayyakkannu and Chandramohan, 1970, 1971; Barik et al., 2001). Increased expression of APA with depth is noticeable in spite of the same level of Pi. Hence, it is inferred that uptake rate could also be high with depth. On the other hand, Kobori and Taga (1979) found that APA was high at the surface layer and decreased with increasing depth at Tokyo Bay. This difference could be because the water is shallower in the present study than Tokyo Bay. Experimentally, Ivancić et al. (2010) and Lin et al. (2011, 2012) have shown that bacterial contribution to APA could also be as important as phytoplankton. This inference could be particularly true for coastal waters.

The relation of APA with DO and nitrate are indirectly related to depth. APA relates with both pigments and bacterial parameters. The variation of Chl*a* and phaeo with nitrate could be partly due to their requirement of this nutrient and also because nitrate and Chl*a* co-vary with depth. The relationships between APA and biological parameters are discernible in scatter plots (Fig. 2s(a–d)). Thus, it is possible that both bacteria (r = 0.561, $p < 0.05$) and Chl*a* (r = 0.670, $p < 0.01$) could be responsible for variation in APA, with Chl*a* (r = 0.619, $p < 0.01$) contribution being prominent at noon. Kwon et al. (2011) in the northern part of Gamak Bay, Korea and Hino (1988) in Lake Barato, Japan also found a strong linear relation between APA and Chl*a*. Thus, it could be inferred that major part of APA might have been induced by phytoplankton during the daytime. Chrost and Overbeck (1987) also observed that phytoplankton were major APA producers in the photic zone of the lake plusee of East Holstain (North Germany). During summer or winter, phytoplankton APA constituted, on an average, 49% of the total APA in the plusee water but bacteria were the dominant APA producers in winter (41.3–44.9%). Increased phaeo is indicative of degradation of Chl*a*. When Chl*a* degrades, dissolved phosphate gets released into the environment and may indirectly supply the Pi requirement to phytoplankton and microbial communities. Dissolved AP can also be liberated into the environment through the lysis of dead phytoplankton cells (Chrost, 1991). Taga and Kobori (1978) found a positive relationship between phosphatase and Pi in the eutrophic seawater samples in Tokyo Bay. In our study, the phosphate concentration was similar over time and depth (ca 0.2 μM). This lack of variation could be attributed to the balance between uptake and release of this nutrient by the water column community. Induction of APA by phytoplankton may be ecologically significant, allowing dominance by these organisms under phosphate limiting conditions (Kwon et al., 2011; Ly et al., 2014). Thus, the synchronization between the APA-Chl*a* and APA-TBC (n = 16) during the whole time series suggests that both bacteria and phytoplankton contribute to total APA.

We, therefore, conclude that there is a positive synchronization of APA with biotic variables like Chl*a*, phaeo and bacterial abundance (Fig. 2s(a–d)). Phytoplankton contribution to variation in total APA is more pronounced at noon, while bacteria contributes during dawn (r = 0.465, $p < 0.001$). Like phytoplankton, bacteria also have a major role in continuously making this important nutrient, phosphate, bioavailable to the surrounding waters, especially in the sub euphotic layers. Continuing the observation for the longer time will strengthen our inference about the extent of contribution by primary producers and bacteria to APA in the coastal system. Such studies will help us to understand the changes in productivity of coastal waters in space and time.

Acknowledgements

The authors are grateful to Directors, CSIR-National Institute of Oceanography for the facilities provided. They also express their gratitude to Ministry of Earth Science and Director, CMLRE, Kochi, India for providing FORV “Sagar Sampada” for the above study. The authors also thank all the participants, Captain and crew members of “Sagar Sampada” cruise No. 282 for their constant support during sample collection and analyses onboard. This work was carried out under “Supra institutional (SIP 1301)” and “PSC 0206” projects of Council of Scientific and Industrial Research, India. This is NIO contribution No. 6241.

Appendix A. Supplementary data

Supplementary material related to this article can be found, in the online version, at https://doi.org/10.1016/j.oceano.2018.06.004.

References

Ammerman, J.W., 1991. Role of ecto-phosphohydrolases in phosphorus regeneration in estuarine and coastal ecosystems. In: Chrost, R.J. (Ed.), Microbial Enzymes in Aquatic Environments. Springer-Verlag, New York, 165–186, http://dx.doi.org/10.1007/978.1.4612.3090.8.10.

Ammerman, J.W., Hood, R.R., Case, D.A., Cotner, J.B., 2003. Phosphorus deficiency in the Atlantic: an emerging paradigm in oceanography. Eos Trans. Am. Geophys. Union 84 (18), 165–170, http://dx.doi.org/10.1029.2003/EO180001.

Ayyakkannu, K., Chandramohan, D., 1970. On the occurrence and distribution of phosphobacteria in the marine environment at Porto-Novo. Curr. Sci. 39, 398–399.

Ayyakkannu, K., Chandramohan, D., 1971. Occurrence and distribution of phosphate solubilizing bacteria and phosphatase in marine sediments at Porto Novo. Mar. Biol. 11 (3), 201–205, http://dx.doi.org/10.1007/BF00401268.

Azam, F., Fenchel, T., Field, J.G., Gray, J.S., Meyer-Reil, L.A., Thingstad, F., 1983. The ecological role of water-column microbes in the sea. Mar. Ecol. Prog. Ser. 10, 257–263, http://dx.doi.org/10.3354/meps010257.

Azam, F., Smith, D.C., Long, R.A., Steward, G.F., 1995. Bacteria in oceanic carbon cycling as a molecular problem. In: Joint, I (Ed.), Molecular Ecology of Aquatic Microbes, NATO ASI Series, vol. 38. Springer-Verlag, Berlin, 39–54, http://dx.doi.org/10.1007/978.3.642.79923.5.3.

Barik, S.K., Purushothaman, C.S., Mohanty, A.N., 2001. Phosphatase activity with reference to bacteria and phosphorus in tropical freshwater aquaculture pond systems. Aquacult. Res. 32, 819–832, http://dx.doi.org/10.1046/j.1355-557x.2001.00619.x.

Benitez-Nelson, C.R., 2000. The biogeochemical cycling of phosphorus in marine systems. Earth Sci. Rev. 51, 109–135, http://dx.doi.org/10.1016/S0012-8252(00)00018-0.

Chrost, R.J., Overbeck, J., 1987. Kinetics of alkaline phosphatase activity and phosphorus availability for phytoplankton and bacterioplankton in lake plusee (North German Eutrophic Lake).

Microb. Ecol. 13 (3), 229–248, http://dx.doi.org/10.1007/BF02025000.

Chrost, R.J., 1991. Environmental control of the synthesis and activity of aquatic microbial ectoenzymes. In: Chrost, R.J. (Ed.), Microbial Enzymes in Aquatic Environments. Springer-Verlag, New York Inc., 29–59, http://dx.doi.org/10.1007/978-1-4612-3090-8_3.

De Souza, M.J.B.D., Nair, S., Chandramohan, D., 2000. Phosphate solubilizing bacteria around the Indian Peninsula. Indian J. Mar. Sci. 29, 48–51.

Dyhrman, S.T., Ammerman, W.J., Van Mooy, B.A.S., 2006. Microbes and the marine phosphorus cycle, microbes and major elemental cycles. Oceanography 20 (2), 196–199, http://dx.doi.org/10.5670/oceanog.2007.54.

Dyhrman, S.T., Ruttenberg, K.C., 2006. Presence and regulation of alkaline phosphatase activity in eukaryotic phytoplankton from the coastal ocean: Implications for dissolved organic phosphorus remineralization. Limnol. Oceanogr. 51 (3), 1381–1390, http://dx.doi.org/10.4319/lo.2006.51.3.1381.

Fouilland, E., Tolosa, I., Bonnet, D., Bouvier, C., et al., 2014. Bacterial carbon dependence on freshly produced phytoplankton exudates under different nutrient availability and grazing pressure conditions in coastal marine waters. FEMS Microbiol. Ecol. 87 (3), 757–769, http://dx.doi.org/10.1111/1574-6941.12262.

Hino, S., 1988. Fluctuation of algal alkaline phosphatase activity and the possible mechanisms of hydrolysis of dissolved organic phosphorus in Lake Barato. Hydrobiology 157 (1), 77–84, http://dx.doi.org/10.1007/BF00008812.

Hobbie, J.E., Daley, R.J., Jasper, S., 1977. Use of nuclepore filters for counting bacteria by fluorescence microscopy. Appl. Environ. Microbiol. 33 (5), 1225–1228.

Hoppe, H.G., 2003. Phosphatase activity in the sea. Hydrobiology 493 (1/3), 187–200, http://dx.doi.org/10.1023/A:1025453918247.

Ivancić, I., Fuks, D., Radić, T., Lyons, D.M., Šilović, T., Kraus, R., Precali, R., 2009. Phytoplankton and bacteria alkaline phosphatase activity in the northern adriatic sea. Mar. Environ. Res. 69 (2), 85–94, http://dx.doi.org/10.1016/j.marenvres.2009.08.004.

Jansson, M., Olsson, H., Pettersson, K., 1988. Phosphatases; origin, characteristics and function in lakes. Hydrobiology 170 (1), 157–175, http://dx.doi.org/10.1007/BF00024903.

Kobori, H., Taga, N., 1979. Phosphatase activity and its role in the mineralization of organic phosphorus in coastal sea water. J. Exp. Mar. Biol. Ecol. 36 (1), 23–39, http://dx.doi.org/10.1016/0022-0981(79)90098-4.

Kogure, K., Simidu, U., Taga, N., 1980. Distribution of viable marine bacteria in neritic seawater around Japan. Can. J. Microbiol. 26 (3), 318–323, http://dx.doi.org/10.1139/m80.052.

Koch, M.S., Kletou, D.C., Tursi, R., 2009. Alkaline phosphatase activity of water column fractions and seagrass in a tropical carbonate estuary, Florida Bay. Estuar. Coast. Shelf Sci. 83, 403–413, http://dx.doi.org/10.1016/j.ecss.2009.04.007.

Kwon, H.K., Oh, S.J., Yang, H.S., 2011. Ecological significance of alkaline phosphatase activity and phosphatase-hydrolyzed phosphorus in the northern part of Gamak Bay, Korea. Mar. Pollut. Bull. 62 (11), 2476–2482, http://dx.doi.org/10.1016/j.marpolbul.2011.07.027.

Labry, C., Delmas, D., Herbland, A., 2005. Phytoplankton and bacterial alkaline phosphatase activities in relation to phosphate and DOP availability within the Gironde plume waters. J. Exp. Mar. Biol. Ecol. 318, 213–225, http://dx.doi.org/10.1016/j.jembe.2004.12.017.

Li, H., Veldhuis, M.J.W., Post, A.F., 1998. Alkaline phosphatase activities among planktonic communities in the northern Red Sea. Mar. Ecol. Prog. Ser. 173, 107–115.

Lignell, R., 1990. Excretion of organic carbon by phytoplankton: its relation to algal biomass, primary productivity and bacterial secondary productivity in the Baltic Sea. Mar. Ecol. Prog. Ser. 68 (1–2), 85–99, http://dx.doi.org/10.3354/meps068085.

Lin, X., Zhang, H., Huang, B., Lin, S., 2011. Alkaline phosphatase gene sequence and transcriptional regulation by phosphate limitation in *Amphidinium carterae* (Dinophyceae). J. Phycol. 47, 1110–1120, http://dx.doi.org/10.1111/j.1529-8817.2011.01038.x.

Lin, X., Zhang, H., Huang, B., Lin, S., 2012. Alkaline phosphatase gene sequence characteristics and transcriptional regulation by phosphate limitation in *Karenia brevis* (Dinophyceae). Harmful Algae 17, 14–24, http://dx.doi.org/10.1016/j.hal.2012.02.005.

Ly, S.J., Philippart, C.J.M., Kromkamp, J.C., 2014. Phosphorus limitation during a phytoplankton spring bloom in the western Dutch Wadden. Quaternary Res. 88, 109–120, http://dx.doi.org/10.1016/j.seares.2013.12.010.

Mamatha, S.S., Gobika, A., Janani, S., 2012. Phosphate solubilizing bacteria and alkaline phosphatase activity in coastal waters off Trivandrum. J. Coast. Environ. 3 (1), 89–100.

Mamatha, S.S., Malik, A., Varik, S., Paravthi, V., Jineesh, V.K., Gauns, M.U., LokaBharathi, P.A., 2015. Alkaline phosphatase activity at the southwest coast of India: a comparison of locations differently affected by upwelling. J. Sea Res. 95, 196–205, http://dx.doi.org/10.1016/j.seares.2014.06.002.

Martinez, J., Smith, D.C., Steward, G.F., Azam, F., 1996. Variability in ectohydrolytic enzyme activities of pelagic marine bacteria and its significance for substrate processing in the sea. Aquat. Microb. Ecol. 10 (3), 223–230, http://dx.doi.org/10.3354/ame010223.

Nandakumar, G., Damodaran, R., 1998. Food and feeding habits of the speckled shrimp *Metapenaeus monoceros* (fabricius). J. Mar. Biol. Ass. India 40 (1–2), 30–43.

Naqvi, S.W.A., Moffett, J.W., Gauns, M.U., Narvekar, P.V., Pratihary, A.K., Naik, H., Shenoy, D.M., Jayakumar, D.A., Goepfert, T.J., Patra, P.K., Al-Azri, A., Ahmed, S.I., 2010. The Arabian Sea as a high-nutrient, low-chlorophyll region during the late Southwest Monsoon. Biogeosciences 7, 2091–2100, http://dx.doi.org/10.5194/bg.7.2091.2010.

Nyadjro, E.S., Subrahmanyam, B., Murty, V.S.N., Shriver, J.F., 2012. The role of salinity on the dynamics of the Arabian Sea mini warm pool. J. Geophys. Res. 117 (C09002), 1–12, http://dx.doi.org/10.1029/2012.JC.007978.

Peetersa, F.J.C., Brummera, G.J.A., Ganssen, G., 2002. The effect of upwelling on the distribution and stable isotope composition of *Globigerina bulloides* and *Globigerinoides ruber* (planktic foraminifera) in modern surface waters of the NW Arabian Sea. Global Planet. Change 34 (3), 269–291, http://dx.doi.org/10.1016/S0921-8181(02)00120-0.

Pillai, V.N., Pillai, V.K., Gopinathan, C.P., Nandakumar, A., 2000. Seasonal variations in the physico-chemical and biological characteristics of the eastern Arabian Sea. J. Mar. Biol. Ass. India 42 (1–2), 1–20.

Prell, W.L., Niitsuma, N., et al., 1991. Proceedings of the Ocean Drilling Program. Sci. Results 117, 257–267.

Qasim, S.Z., 1982. Oceanography of the northern Arabian Sea. Deep Sea Res. Pt. A 29 (9), 1041–1068, http://dx.doi.org/10.1016/0198-0149(82)90027-9.

Riemann, L., Steward, G.F., Fandino, L.B., Campbell, L., Landry, M. R., Azam, F., 1999. Bacterial community composition during two consecutive NE monsoon periods in the Arabian Sea studied by denaturing gradient gel electrophoresis (DGGE) of rRNA genes. Deep Sea Res. Pt. II 46 (8–9), 1791–1811, http://dx.doi.org/10.1016/S0967-0645(99)00044-2.

Rodina, A.G., 1972. In: Colwell, R.R., Zambruski, M.S. (Eds.), Methods in Aquatics Microbiology. Univ. Park Press, Baltimore–London–Tokyo, 461 pp.

Rooney-Varga, J.N., Giewat, M.W., Savin, M.C., Sood, S., LeGresley, M., Martin, J.L., 2004. Links between phytoplankton and bacterial community dynamics in a coastal marine environment. Mar. Ecol. 49 (1), 163–175, http://dx.doi.org/10.1007/s00248.003.1057.0.

Sebastian, M., Pitta, P., Gonzalez, J.M., Thingstad, T.F., Gasol, J.M., 2012. Bacterioplankton groups involved in the uptake of phosphate and dissolved organic phosphorus in a mesocosm experiment with P-starved Mediterranean waters. Environ. Microbiol. 14 (9), 2334—2347, http://dx.doi.org/10.1111/j.1462-2920.2012.02772.x.

Strickland, J.D.H., Parsons, T.R., 1965. A manual of sea water analysis. In: Stevenson, J.C. (Ed.), Fisheries Research Board of Canada, No. 125. second ed. Roger Duhamel FRSC, Ottawa, Canada, 37—86.

Taga, N., Kobori, H., 1978. Phosphatase activity in eutrophic Tokyo Bay. Mar. Biol. 49 (3), 223—229, http://dx.doi.org/10.1007/BF00391134.

UNESCO, 1994. Protocols for the Joint Global Ocean Flux Study (JGOFS) Core Measurements. Manual and Guides No. 29. 97—100.

Vidal, M., Duarte, C.M., Agusti, S., Gasol, J.M., Vaque, D., 2003. Alkaline phosphatase activities in the central Atlantic Ocean indicate large areas with phosphorus deficiency. Mar. Ecol. Prog. Ser. 262, 43—53, http://dx.doi.org/10.3354/meps.262043.

Wurl, O., 2009. Boca Raton. In: Practical guidelines for the analysis of sea water. CRC Press, 143—178.

Yucel, N., 2018. Spatio-temporal variability of the size fractionated primary production and chlorophyll in the Levantine Basin (north-eastern Mediterranean). Oceanologia 60 (3), 288—304, http://dx.doi.org/10.1016/0022-0981(79)90098-4.